

Copyright
by
Jonathan Larkin Poole
2007

**The Dissertation Committee for Jonathan Larkin Poole Certifies that this is the
approved version of the following dissertation:**

Modeling Temperature Sensitivity and Heat Evolution of Concrete

Committee:

Kevin J. Folliard, Supervisor

Maria C. G. Juenger, Co-Supervisor

David W. Fowler

Anton K. Schindler

Harovel G. Wheat

Modeling Temperature Sensitivity and Heat Evolution of Concrete

by

Jonathan Larkin Poole, B.S.E., M.S.E.

Dissertation

Presented to the Faculty of the Graduate School of

The University of Texas at Austin

in Partial Fulfillment

of the Requirements

for the Degree of

Doctor of Philosophy

The University of Texas at Austin

May 2007

Dedication

To my wife, Stephanie, for her endless patience and love, and to Mom, Dad, and Daniel.

Acknowledgements

I would like to thank all of the people that helped make this dissertation a reality. First, I would like to thank Dr. Maria Juenger, Dr. Anton Schindler, and Dr. Kevin Folliard for their guidance with the technical content of this dissertation. Their advice, guidance, and mentoring was unparalleled, and I am sincerely grateful to them. Ralph Browne at TxDOT also deserves a debt of gratitude for his vision and support of this project.

I am further indebted to Kyle Riding, whose technical insight, creativeness, and ability to manage ten hour drives to El Paso were most important. He has been a great partner on this project, and he certainly challenged me to be a better graduate student. I would also like to thank my fellow PhD students Tyler Ley, John Hema, Ryan Chancy, Eric Kohler, Thanos Drimalas, and Jason Ideker. Also, I'd like to thank Rachael Lute for her excellent work with the isothermal calorimetry in this dissertation. Finally, Cuyler Smith, Paul Warfield, Sam Slatnik, Arnaud Thibonnier have been most helpful with the project. Next, I would like to thank Mike Rung, Kerry Rothenbach, Dave Whitney, and Sherian Williams for their invaluable help.

Finally, I would like to thank my dad, Toy, for his support, advice, and discussions about cement chemistry; my mom, Marian, for her encouragement and kind ear; my brother Daniel for his patience and for the comfortable floor, and my wife Stephanie for her unconditional support and love.

Modeling Temperature Sensitivity and Heat Evolution of Concrete

Publication No. _____

Jonathan Larkin Poole, Ph.D.

The University of Texas at Austin, 2007

Supervisors: Kevin J. Folliard and Maria C. G. Juenger

The hydration of cement in concrete is exothermic, which means it gives off heat. In large elements, the heat caused by hydration can dissipate at the surface, but is trapped in the interior, resulting in potentially large thermal gradients. The thermal expansion of concrete is greater at higher temperatures, so if the temperature differential between the surface and the interior becomes too great, the interior will expand more than the exterior. When the thermal stress from this mis-matched expansion exceeds the tensile strength of the material, the concrete will crack. This phenomenon is referred to as thermal cracking. Accurate characterization of the progress of hydration of a concrete mixture is necessary to predict temperature gradients, maximum concrete temperature, thermal stresses, and relevant mechanical properties of concrete that will influence the thermal cracking risk of concrete.

Calorimetry is the most direct test method to quantify the heat evolution from a concrete mixture. There is currently no model, based solely on calorimetry, which

completely describes the effects of mixture proportions, cement and SCM chemistry, and chemical admixture dosages on the temperature sensitivity and adiabatic temperature rise of concrete. The objective of this study is to develop a comprehensive model to describe these effects. First, the temperature sensitivity of the hydration reaction (described with activation energy, E_a) is needed to accurately predict the behavior of concrete under a variety of temperature conditions. A multivariate regression model is from isothermal calorimetry testing to describe the effects of water-cementitious materials ratio, cement chemistry, supplementary cementing materials, and chemical admixtures on the E_a of portland cement pastes. Next, a multivariate regression model is developed from semi-adiabatic calorimetry testing that predicts the temperature development of concrete mixtures based on mixture proportions, cement and SCM chemistry, and chemical admixture dosages. The results of the models are validated using data from literature. The final model provides a useful tool to assess the temperature development of concrete mixtures, and thereby reduce the thermal cracking risk of the concrete structure.

Table of Contents

Chapter 1.	Introduction.....	1
1.1.	References.....	5
Chapter 2.	The Effects of Cement Chemistry and Water-Cement Ratio on Activation Energy	6
2.1.	Introduction.....	6
2.2.	Research Significance.....	9
2.3.	Literature Review.....	9
2.4.	Test methods	10
2.4.1.	Materials	10
2.4.2.	Experimental Program	11
2.4.3.	E_a Calculation Procedure	12
2.5.	Results and Discussion	15
2.6.	Effects of Cement Chemistry and Water-Cement Ratio on E_a	15
2.6.1.	Effect of Cement Chemistry and Alkalis.....	15
2.6.2.	Effect of Water-Cement Ratio	16
2.6.3.	E_a Prediction Models	16
2.6.4.	Comparison Between E_a from Lerch and Ford Data and Calorimeter Data	19
2.7.	Variability of Results	21
2.7.1.	Variability of Three-Parameter Model Values	21
2.7.2.	Comparison of Results to Variability Reported by Nordtest.....	23
2.7.3.	Confidence Limits of E_a Results.....	24
2.8.	Conclusions.....	25

2.9. References.....	27
Chapter 3. The Effects of Chemical Admixtures on Activation Energy of Cementitious Materials	38
3.1. Introduction.....	38
3.2. Review of Chemical Admixture Mechanisms	40
3.2.1. Low-Range Water-Reducing and Retarding Admixtures.....	40
3.2.2. High-Range Water-reducing Admixtures	41
3.2.3. Calcium Nitrate-Based Accelerators.....	42
3.3. Experimental Program	42
3.4. Results and Discussion	43
3.4.1. Effects of Water Reducing and Retarding Admixtures on Heat of Hydration	44
3.4.2. Effects of Water Reducing and Retarding Admixtures on E_a	48
3.4.3. Effects of High-Range Water-Reducing Admixtures on Heat of Hydration	49
3.4.4. Effects of High-Range Water Reducing Admixtures on E_a	50
3.4.5. Effects of Calcium Nitrate-Based Accelerating Admixtures on Heat of Hydration	51
3.4.6. Effects of Calcium Nitrate-Based Accelerating Admixtures on E_a	52
3.4.7. Effects of Air-Entraining Admixtures on Hydration and E_a	53
3.5. Conclusions.....	53
3.6. References.....	54
Chapter 4. The Effects of Supplementary Cementing Materials on Activation Energy.....	69
4.1. Introduction.....	69

4.2. Research Significance.....	71
4.3. Experimental Program	72
4.4. Results and Discussion	73
4.4.1. Effects of Class F Fly Ash on Heat Evolution and E_a	75
4.4.2. Effects of Class C Fly Ash on Heat Evolution and E_a	77
4.4.3. Effects of GGBF Slag on Heat Evolution and E_a	78
4.4.4. Effects of Alkali Content on Heat Evolution and E_a in Pastes with SCM.....	79
4.4.5. Retardation of Hydration with Class C Fly Ash and GGBF Slag.....	80
4.4.6. Effects of Silica Fume and Ultra-Fine Fly Ash (UFFA) on E_a and the Rate of Heat Evolution.....	83
4.4.7. Summary of Trends.....	85
4.5. Conclusions.....	86
4.6. References.....	87
Chapter 5. A Model for Estimating the Activation Energy of Cementitious Systems.....	109
5.1. Introduction.....	109
5.1.1. Summary of E_a Trends.....	111
5.2. Research Significance.....	114
5.3. Experimental Methods for E_a Determination.....	114
5.3.1. Materials	114
5.4. E_a Model development Process.....	115
5.4.1. Variable Selection.....	115
5.4.2. Multivariate Regression Analysis	116
5.4.3. Application of Arrhenius Theory to E_a Regression Analysis	116
5.4.4. Independent Variable Selection	118

5.4.5.	Model Selection	119
5.5.	Activation Energy (E_a) Model	120
5.5.1.	Effects of Cement Chemistry and Fineness on E_a	123
5.5.2.	Effects of SCMs on E_a	124
5.5.3.	Effects of Chemical Admixture on E_a	125
5.5.4.	Other Variables Investigated.....	126
5.6.	Conclusions.....	126
5.7.	References.....	128
Chapter 6.	Hydration Study of Cementitious Materials Using Semi-Adiabatic Calorimetry.....	141
6.1.	Introduction.....	141
6.1.1.	Background	143
6.1.2.	Variability in Semi-Adiabatic Calorimetry.....	147
6.1.3.	Experimental Work.....	148
6.1.4.	Calculation of Fully Adiabatic Temperature Rise	149
6.1.5.	Calibration Procedure	151
6.2.	Results and Discussion	152
6.2.1.	Variation from Conduction Model.....	152
6.2.2.	Variability in Heat Capacity of Calorimeter	153
6.2.3.	Instrument Precision	154
6.2.4.	Confidence Limits for Semi-Adiabatic Calorimetry.....	155
6.3.	Trends in Hydration Behavior	155
6.3.1.	Effects of Water-to-Cementitious Materials Ratio on Hydration	156
6.3.2.	Effects of Cement Content on Hydration.....	157
6.3.3.	Effects of Aggregate Type on Hydration.....	157
6.3.4.	Effects of Placement Temperature on Hydration.....	158

6.3.5.	Effects of Cement Type on Hydration	158
6.3.6.	Effects of SCMs on Hydration.....	160
6.4.	Conclusions.....	161
6.5.	References.....	162
Chapter 7.	Study of the Effects of Chemical Admixtures on Hydration	172
7.1.	Introduction.....	172
7.2.	Research Significance.....	174
7.3.	Background	174
7.3.1.	Calculation of E_a	178
7.4.	Experimental Program	179
7.4.1.	Test Methods.....	179
7.4.2.	Materials	179
7.4.3.	Comparison between Isothermal and Semi-Adiabatic Calorimetry	181
7.5.	Results and Discussion	182
7.5.1.	Effects of Low-Range Water Reducing/Retarding Admixtures on Mixtures with 100% Cement	183
7.5.2.	Effects of Low-Range Water Reducing/Retarding Admixtures on Mixtures with Fly Ash	184
7.5.3.	Effects of Mid-Range and High-Range Water Reducing Admixtures on Hydration and Temperature Rise	186
7.5.4.	Effects of Accelerating and Air Entraining Admixture on Hydration and Temperature Rise	187
7.6.	Summary of Hydration Trends	187
7.6.1.	Effects of Low-Range Water Reducing and Retarding Admixtures on Hydration Parameters.....	188

7.6.2. Effects of Accelerating and Air Entraining Admixture on Hydration Parameters.....	190
7.6.3. Effects of Mid-Range and High-Range Water Reducing Admixtures on Hydration Parameters.....	190
7.7. Conclusions.....	191
7.8. References.....	192
Chapter 8. Study of the Hydration of Supplementary Cementing Materials Using Semi-Adiabatic Calorimetry	216
8.1. Introduction.....	216
8.2. Research Significance.....	218
8.3. Background	219
8.3.1. Calculation of E_d	223
8.4. Experimental Program	224
8.4.1. Test Methods.....	224
8.4.2. Materials	224
8.5. Analysis of Results	225
8.5.1. Effects of Class F Fly Ash on Rate of Heat Evolution	226
8.5.2. Effects of Class C Fly Ash on Rate of Heat Evolution.....	227
8.5.3. Effects of Ground Granulated Blast-Furnace Slag on Rate of Heat Evolution.....	228
8.5.4. Effects of Silica Fume on Rate of Heat Evolution.....	229
8.5.5. Effects of SCMs and Cement on Hydration Parameters.....	229
8.5.6. Retardation with Cement and Reactive SCMs.....	232
8.5.7. Effects of SCMs on Adiabatic Temperature Rise.....	233
8.5.8. Comparison Between Isothermal and Semi-Adiabatic Calorimetry.....	234
8.5.9. Limitations of Semi-Adiabatic Calorimetry with SCMs	234

8.6. Conclusions.....	236
8.7. References.....	237
Chapter 9. Modeling the Hydration of Cementitious Systems	258
9.1. Abstract.....	258
9.2. Introduction.....	258
9.2.1. Challenges with Regression Analysis and Material Characterization ..	261
9.3. Research Significance.....	263
9.4. Summary OF Hydration Trends.....	263
9.4.1. Effects of SCMs on Hydration.....	264
9.4.2. Effects of Chemical Admixtures on Hydration	266
9.5. Suggested Modifications to Heat of Hydration Values of Cementitious Materials	266
9.5.1. Analysis of Heat of Hydration Data.....	267
9.5.2. Results.....	267
9.5.3. Challenges with Degree of Hydration (α_u) Modeling	268
9.6. Analytical Methods for Hydration Model.....	269
9.6.1. Model Selection	269
9.6.2. Variable Selection Procedure.....	270
9.6.3. Non-Linear Regression Analysis	272
9.7. Regression Analysis Results.....	273
9.8. Sensitivity Analysis of Hydration Model	276
9.8.1. Modeled Response of the Behavior of Supplementary Cementing Materials	276
9.8.2. Modeled Response of the Behavior of Water-Cementitious Materials Ratio (w/cm)	277

9.8.3. Modeled Response of the Behavior of Chemical Admixtures.....	277
9.8.4. Modeled Response of the Behavior of Cement Chemistry.....	278
9.9. Validation of Model Using Calibration Dataset	279
9.10. Conclusions.....	280
9.11. References.....	282
Appendix A. Additional Isothermal Results for Chapter 2.....	299
A.1. Effects of w/cm on Rate of Heat Evolution of 100% Cement Pastes	299
A.2. Effects of Alkali Addition on Rate of Heat Evolution.....	304
Appendix B. Additional Isothermal Results for Chapter 3.....	313
B.1. Effects of Chemical Admixtures on Rate of Heat Evolution of 100% Cement Pastes.....	313
B.2. Effects of Accelerators and AEA on Pastes with 100% Cement	322
B.3. Effects of HRWR on Mixtures with 100% Cement.....	325
B.4. Effects of WRRET and ACCL on Mixtures with SCMs	336
Appendix C. Additional Isothermal Calorimetry Results for Chapter 4.....	354
C.1. Effects of Fly Ash FF1 on Rate of Heat Evolution of Pastes.....	354
C.2. Effects of Fly Ash FF2 on Rate of Heat Evolution of Pastes.....	359
C.3. Effects of Fly Ash FC1 on Rate of Heat Evolution of Pastes	365
C.4. Effects of Fly Ash FC2 on Rate of Heat Evolution of Pastes	370
C.5. Effects of GGBF Slag on Rate of Heat Evolution of Pastes	376
C.6. Effects of Silica Fume on Rate of Heat Evolution of Pastes.....	382
C.7. Effects of Alkalies Increases on Rate of Heat Evolution of Pastes with Fly Ash	

FF1 and FC2	393
Appendix D. Additional Discussion of Multivariate Regression Modeling of E_a for Chapter 5.....	399
D.1. Multivariate Regression Analysis	399
D.2. Independent Variable Selection Procedure using PROC RSQUARE	400
D.3. Independent Variables in Study	401
D.4. Number of Variables	405
D.5. Analysis of Variance (ANOVA) using PROC GLM.....	406
D.6. GLM Results	407
D.7. PROC NLIN.....	408
D.8. Application of Arrhenius Theory to E_a Regression Analysis	409
D.9. NLIN Results	410
D.10. E_a Model Based on Bogue Calculations	411
D.11. E_a Model Based on Rietveld Analysis of Cement Phases	412
D.12. Sensitivity Analysis.....	413
D.13. Residuals	414
D.14. REFERENCES.....	414
D.15. SAS Code (v. 9.1.3) – Bogue Calculations.....	441
D.16. SAS Code (v. 9.1.3) – Rietveld Analysis.....	443
Appendix E. Additional Semi-Adiabatic Test Results for Chapter 7.....	446
E.1. Effects of MRWR and HRWR on Hydration.....	446
E.2. Additional Comparisons of Effects of ACCL and AEA on Hydration and	

Adiabatic Temperature Rise	446
E.3. Effects of Chemical Admixtures on τ and β	447
E.4. Effects of Admixtures on α_u	448
Appendix F. Additional Semi-Adiabatic Calorimeter Results for Chapter 8	465
F.1. Adiabatic Temperature Rise of Mixtures with Class F Fly Ash.....	465
F.2. Adiabatic Temperature Rise of Mixtures with Class C Fly Ash	468
F.3. Adiabatic Temperature Rise of Mixtures GGBF Slag – S1	470
F.4. Adiabatic Temperature Rise of Mixtures with Silica Fume	472
F.5. Rate of Heat Evolution for Mixtures with Cement C6 and Fly Ash	475
F.6. Rate of Heat Evolution Normalized by Cement Content	476
F.7. Rate of Heat Evolution for Mixtures with Silica Fume.....	480
F.8. Effect of Limiting α_u to 1.0	483
Appendix G. Additional Discussion of Multivariate Regression Modeling of Exponential Model Parameters for Chapter 9.....	489
G.1. Independent Variables in Study	489
G.2. Number of Variables.....	495
G.3. ANOVA	495
G.4. Notes for Non-Linear Analysis	496
G.5. Notes for Sensitivity Analysis.....	497
G.6. SAS 9.1.3 Code – Bogue Model	498
G.7. SAS 9.1.3 Code – Rietveld Model.....	501
References.....	566

Vita.....	577
-----------	-----

List of Figures

Figure 1-1: Isothermal Calorimeter (Left) and Semi-Adiabatic Calorimeter with Concrete Sample (Right)	3
Figure 2-1: Effects of $\text{Na}_2\text{O}_{\text{eq}}$ on Rate of Heat Evolution for Different Cements	35
Figure 2-2: Activation Energy v. $\text{Na}_2\text{O}_{\text{eq}}$	35
Figure 2-3: Effects of w/c on Rate of Heat Evolution per Gram of Cement for Cement C2	36
Figure 2-4: Activation Energy v. w/c	36
Figure 2-5: Comparison Between Regression Analysis Results for Equation 2-7 and Equation 2-8.....	37
Figure 3-1: Rate of Heat Evolution (Per Gram of Cementitious Material) for 100% Cement C1 (Paste) with Different Dosages of WRRET at 23°C (73°F)	60
Figure 3-2: Rate of Heat Evolution (Per Gram of Cementitious Material) for 100% Cement C1 (Paste) with Different Dosages of LRWR at 23°C (73°F)	60
Figure 3-3: Rate of Heat Evolution (Per Gram of Cementitious Material) for 100% Cement C2 (Paste) with Different Dosages of WRRET at 23°C (73°F)	61
Figure 3-4: Changes in Time Parameter (τ) with LRWR, WRRET, ACCL, and PCHRWR	61
Figure 3-5: Changes in Slope Parameter (β) with LRWR, WRRET, ACCL, and PCHRWR.....	62

Figure 3-6: Rate of Heat Evolution (Per Gram of Cementitious Material) for Paste Mixtures with WRRET and Cement C2 at 23 °C (73 °F)	62
Figure 3-7: Rate of Heat Evolution (Per Gram of Cementitious Material) for Paste Mixtures of 50% Cements C2 and C6 with 50% GGBF Slag	63
Figure 3-8: Comparison Between Isothermal and Semi-Adiabatic Calorimetry for Mixture 40 and 41 (y-axis on the left is for the semi-adiabatic data and on the right is for the isothermal data).....	63
Figure 3-9: E_a v. LRWR and WRRET Dose, 100% Cement.....	64
Figure 3-10: E_a v. WRRET with Various % SCM	64
Figure 3-11: Rate of Heat Evolution (Per Gram of Cementitious Material) for Paste Mixtures of 100% Cement C6 with NHRWR at 23 °C (73 °F).....	65
Figure 3-12: Rate of Heat Evolution (Per Gram of Cementitious Material) for 100% Cement C6 with PCHRWR at 23 °C (73 °F).....	65
Figure 3-13: Rate of Heat Evolution (Per Gram of Cementitious Material) for Paste Mixtures of 100% Cement C8 with NHRWR and PCHRWR at 23 °C (73 °F) ...	66
Figure 3-14: E_a v. NHRWR and PCHRWR Dose, 100% Type I Cement (Cement C2 and C6).....	66
Figure 3-15: E_a v. NHRWR and PCHRWR Dose, 100% Type III Cement (Cement C7 and C8).....	67
Figure 3-16: Effects of ACCL and WRRET on Cement C2 with Fly Ash FF2 and FC1 (Paste) at 23 °C (73 °F).....	67

Figure 3-17: Effects of ACCL on Cement C6 with Fly Ash FF2 and FC1 (Paste) at 23 °C (73 °F)	68
Figure 3-18: E_a v. ACCL Dose, Various % SCM.....	68
Figure 4-1: Rate of Heat Evolution (Per Gram of Cementitious Material) for Cements..	94
Figure 4-2: Rate of Heat Evolution (Per Gram of Cementitious Material) for Cement C2 with Different Replacements of FF1 (0.7% CaO) at 23 °C (73.4 °F).....	94
Figure 4-3: Rate of Heat Evolution (Per Gram of Cementitious Material) for Cement C3 with Different Replacements of FF1 (0.7% CaO) at 23 °C (73.4 °F).....	95
Figure 4-4: Rate of Heat Evolution (Per Gram of Cementitious Material) for Cement C6 with Different Replacements of FF1 (0.7% CaO) at 23 °C (73.4 °F).....	95
Figure 4-5: Cement C2 with Different Replacements of FF2 (13.1% CaO) at 23 °C (73.4 °F)	96
Figure 4-6: Rate of Heat Evolution (Per Gram of Cementitious Material) for Cement C6 with Different Replacements of FF2 (13.1% CaO) at 23 °C (73.4 °F).....	96
Figure 4-7: Summary of E_a Trends for Class F Fly Ash FF1 (0.7% CaO).....	97
Figure 4-8: Summary of E_a Trends for Class F Fly Ash FF2 (13.1% CaO).....	97
Figure 4-9: Rate of Heat Evolution (Per Gram of Cementitious Material) for Cement C2 with Different Replacements of FC1 (23.1% CaO) at 23 °C (73.4 °F)	98
Figure 4-10: Rate of Heat Evolution (Per Gram of Cementitious Material) for Cement C6 with Different Replacements of FC1 (23.1% CaO) at 23 °C (73.4 °F)	98
Figure 4-11: Rate of Heat Evolution (Per Gram of Cementitious Material) for Cement C2	

with Different Replacements of FC2 (28.9% CaO) at 23 °C (73.4 °F)	99
Figure 4-12: Rate of Heat Evolution (Per Gram of Cementitious Material) for Cement C6	
with Different Replacements of FC2 (28.9% CaO) at 23 °C (73.4 °F)	99
Figure 4-13: Summary of E_a Trends for Class C Fly Ash FC1 (23.1% CaO)	100
Figure 4-14: Summary of E_a Trends for Class C Fly Ash FC2 (28.9% CaO)	100
Figure 4-15: Rate of Heat Evolution (Per Gram of Cementitious Material) for Cement C2	
with Different Replacements of GGBF Slag (S1) at 23 °C (73.4 °F).....	101
Figure 4-16: Rate of Heat Evolution (Per Gram of Cementitious Material) for Cement C6	
with Different Replacements of GGBF Slag (S1) at 23 °C (73.4 °F).....	101
Figure 4-17: Rate of Heat Evolution (Per Gram of Cementitious Material) for Cement C2	
with Different Replacements of GGBF Slag (S1) at 60 °C (140 °F).....	102
Figure 4-18: Rate of Heat Evolution (Per Gram of Cementitious Material) for Cement C6	
with Different Replacements of GGBF Slag (S1) at 60 °C (140 °F).....	102
Figure 4-19: Summary of E_a Trends for GGBF Slag (S1).....	103
Figure 4-20: Effects of Alkalis on Hydration of FF1 and FC2 (28.9% CaO)	103
Figure 4-21: Time Parameter τ with Cement C2 and Different SCMs.....	104
Figure 4-22: Time Parameter τ with Cement C3 and Different SCMs.....	104
Figure 4-23: Time Parameter τ with Cement C6 and Different SCMs.....	105
Figure 4-24: Rate of Heat Evolution (Per Gram of Cementitious Material) for Cement C3	
with 30% FC2 (28.9% CaO) at 23 °C (73.4 °F)	105
Figure 4-25: Cements C2 and C6 with Different Replacements of Silica Fume.....	106

Figure 4-26: Cement C2 with Silica Fume and 20% Replacement by Mass of FF1 (CaO=0.7%)	106
Figure 4-27: Cement C2 with Silica Fume, 30%, and 35% Replacement by Mass of FC2 (CaO=28.9%)	107
Figure 4-28: Cement C6 with Silica Fume and 30% Replacement by Mass of FC2 (CaO=28.9%)	107
Figure 4-29: Cement C6 with UFFA and FF2 (CaO=13.1%)	108
Figure 4-30: Summary of E_a Trends for Mixtures with Silica Fume	108
Figure 5-1: Predicted E_a v. Measured E_a for Non-Linear Model in Equation 5-5	133
Figure 5-2: Residual Plot for Non-Linear E_a Model in Equation 5-5	134
Figure 5-3: 70% Cement C2, 30% SCM-C1, 0.35% WRRET (Mix 44); Lines are predicted values; discrete points are measured values.....	134
Figure 5-4: 100% Cement C1, 0.35% LRWR (Mix 342); Lines are predicted values; discrete points are measured values.....	135
Figure 5-5: Sensitivity of Proposed E_a Model to Gypsum ($C\hat{S}H_2$) Percentage in Cementitious System	135
Figure 5-6: Sensitivity of Proposed E_a Model to $(C_3A+C_4AF)\times C\hat{S}H_2$ in Cementitious System.....	136
Figure 5-7: Sensitivity of Proposed E_a Model to Blaine Fineness.....	136
Figure 5-8: Sensitivity of Proposed E_a Model to Total Equivalent Alkalis in Cement ..	137
Figure 5-9: Sensitivity of Proposed E_a Model to Fly Ash CaO and Replacement	

Percentage	137
Figure 5-10: Sensitivity of Proposed E_a Model to GGBFS Replacement Percentage....	138
Figure 5-11: Sensitivity of Proposed E_a Model to Silica Fume Replacement Percentage	138
Figure 5-12: Sensitivity of Proposed E_a Model to WRRET Dosage	139
Figure 5-13: Sensitivity of Proposed E_a Model to ACCL Dosage	140
Figure 6-1: Comparison of Adiabatic Temperature Rise Calculations.....	168
Figure 6-2: Water Calibration Results for Calorimeters Used in Study	168
Figure 6-3: Effects of W/CM on Hydration Behavior	169
Figure 6-4: Effects of Cementitious Content on Hydration Behavior	169
Figure 6-5: Effects of Aggregate Type and Admixture Type on Hydration Behavior...	170
Figure 6-6: Effects of Placement Temperature on Calculated Adiabatic Temperature Rise for 100% Cement C1 (Mixtures 4, 5, and 6) and 30% FF2, 70% Cement C1 (Mixtures 15, 16, and 17).....	170
Figure 6-7: Effects of Cement Type on Adiabatic Temperature (Mixtures 9-13).....	171
Figure 6-8: Effects of SCMs on Adiabatic Temperature Rise (Mixtures 10, 13, 14, 19 and 20)	171
Figure 7-1: Comparison Between Isothermal Calorimetry Results and Semi-Adiabatic Calorimetry Results for Mixtures with Cement C1 and Different Water Reducing Admixtures.....	199
Figure 7-2: Effects of Type B&D WRRET on Rate of Heat Evolution of Cements C1,	

C2, C6, and C9.....	200
Figure 7-3: Effects of Type B&D WRRET on Adiabatic Temperature Rise of Cements C1, C2, C6, and C9.....	201
Figure 7-4: Effects of Type A LRWR and Type B&D WRRET on Hydration of a Mixture of 70% Cement C1 and 30% FF2	202
Figure 7-5: Effects of Type A LRWR and Type B&D WRRET on Hydration of a Mixture of 70% Cement C1 and 30% FC1	203
Figure 7-6: Effects of Type A LRWR and Type B&D WRRET on Hydration of a Mixture of 70% Cement C1 and 30% FC2.....	203
Figure 7-7: Effects of Type A LRWR and Type B&D WRRET on Adiabatic Temperature Rise of a Mixture of 70% Cement C1 and 30% FF2	204
Figure 7-8: Effects of Type A LRWR and Type B&D WRRET on Rate of Heat Evolution of a Mixture of 70% Cement C1 and 30% FC1.....	204
Figure 7-9: Effects of Type A LRWR and Type B&D WRRET on Adiabatic Temperature Rise of a Mixture of 70% Cement C1 and 30% FC2.....	205
Figure 7-10: Effects of Naphthalene-Based HRWR on Rate of Heat Evolution of Cement C2, C6, C10, and C12	206
Figure 7-11: Effects of Polycarboxylate-Based HRWR on Rate of Heat Evolution of Cement C1, C2, C10, and C12.....	207
Figure 7-12: Effects of MRWR on Rate of Heat Evolution of Mixtures of 100% Cement C2, 100% C9, and 70% C6 with 30% FF2	208

Figure 7-13: Effects of Type C Non-Chloride Accelerator on Hydration of a Mixture of 100% Cement C2	209
Figure 7-14: Effects of Type C Non-Chloride Accelerator on Hydration of a Mixture of 100% Cement C2	209
Figure 7-15: Effects of Type C ACCL and Type B&D WRRET on Rate of Heat Evolution of a Mixture of 70% Cement C2 and 30% FC1	210
Figure 7-16: Effects of Type A LRWR on Time Parameter (τ)	210
Figure 7-17: Effects of Type A LRWR on Slope Parameter (β)	211
Figure 7-18: Effects of Type B&D WRRET on Time Parameter (τ)	211
Figure 7-19: Effects of Type B&D WRRET on Slope Parameter (β)	212
Figure 7-20: Effects of Type B&D WRRET on Degree of Hydration Parameter (α_u) ..	212
Figure 7-21: Effects of Type C ACCL on Time Parameter (τ)	213
Figure 7-22: Effects of Type C ACCL on Slope Parameter (β)	213
Figure 7-23: Effects of NHRWR, PCHRWR, and MRWR on Time Parameter (τ)	214
Figure 7-24: Effects of Type F HRWR (N-Naphthalene, PC-Polycarboxylate, M-Mid- Range) on Slope Parameter (β)	214
Figure 7-25: Effects of Type F HRWR (N-Naphthalene, PC-Polycarboxylate) on Degree of Hydration Parameter (α_u)	215
Figure 8-1: Rate of Heat Evolution per Kilogram of Cementitious Material for Concrete Mixtures with Different Dosages of FF1 (CaO = 0.7%)	246
Figure 8-2: Rate of Heat Evolution per Kilogram of Cementitious Material for Concrete	

Mixtures with Different Dosages of FF2 (CaO = 13.1%)	246
Figure 8-3: Rate of Heat Evolution per Kilogram of Cementitious Material for Concrete	
Mixtures with Different Dosages of FC1 (CaO = 23.1%)	247
Figure 8-4: Rate of Heat Evolution per Kilogram of Cementitious Material for Concrete	
Mixtures with Different Dosages of SCM FC2 (CaO = 28.9%)	247
Figure 8-5: Rate of Heat Evolution per Kilogram of Cementitious Material for Mixtures	
with 30% SCM FC1 and Cement C2 or C6	248
Figure 8-6: Rate of Heat Evolution per Kilogram of Cementitious Material for Mixtures	
with Cement C2 and Different Dosages of S1	248
Figure 8-7: Rate of Heat Evolution per Kilogram of Cementitious Material for Mixtures	
with a.) Cement C2, b.) Cement C2, 20% FF1, c.) Cement C2, 30% FC2, and d.)	
Cement C6	249
Figure 8-8: Effect of SCM Type and Dosage on τ - Cement C2	249
Figure 8-9: Effect of SCM Type and Dosage on τ - Cement C6	250
Figure 8-10: Effect of SCM Type and Dosage on τ - Cement C9	250
Figure 8-11: Effect of SCM Type and Dosage on β - Cement C2	251
Figure 8-12: Effect of SCM Type and Dosage on β - Cement C6	251
Figure 8-13: Effect of SCM Type and Dosage on β - Cement C9	252
Figure 8-14: Effect of SCM Type and Dosage on α - Cement C2	252
Figure 8-15: Effect of SCM Type and Dosage on α - Cement C6	253
Figure 8-16: Effect of SCM Type and Dosage on α_u - Cement C9	254

Figure 8-17: Effect of Silica Fume on α_u	254
Figure 8-18: Effect of C ₃ A Content of Cementitious Material on τ with 30% Class C Fly Ash (FC1 and FC2) and 50% GGBF Slag (S1)	255
Figure 8-19: Adiabatic Temperature Rise of Mixtures with 100% Cement C2, 70% Cement C2 with 30% FF1, FF2, FC1, FC2, and 50% Cement C2 and 50% S1.	256
Figure 8-20: Adiabatic Temperature Rise of Mixtures with 100% Cement C6, 70% Cement C6 with 30% FF1, FF2, FC1, FC2, and 50% Cement C6 and 50% S1.	256
Figure 8-21: Comparison Between Isothermal Calorimetry Results and Semi-Adiabatic Calorimetry Results for Mixtures with Cement C2 and Different Replacement Percentages of FC2 (28.9% CaO).....	257
Figure 9-1: Rate of Heat Evolution (per gram of Cement) for a Control Mixture, and a Mixture with 40% GGBF Slag	287
Figure 9-2: Effects of Type B&D WRRET on Time Parameter (τ)	287
Figure 9-3: Effects of Type B&D WRRET on Slope Parameter (β).....	288
Figure 9-4: Regression Analysis Results for a Mixture of 70% Type I Cement and 30% Class F Fly Ash.....	288
Figure 9-5: Predicted Versus Measured Degree of Hydration for Bogue Model	289
Figure 9-6: Effect of % Fly Ash and % CaO in Fly Ash on Time Parameter, τ	290
Figure 9-7: Effect of Fly Ash % CaO on Degree of Hydration	291
Figure 9-8: Effect of % GGBF Slag on τ and β	291
Figure 9-9: Effect of %GGBF Slag on Degree of Hydration	292

Figure 9-10: Effect of w/cm on Degree of Hydration.....	292
Figure 9-11: Effect of Type B&D WRRET on Time (τ) and Slope Parameter (β).....	293
Figure 9-12: Effect of Type B&D WRRET Dosage on Degree of Hydration.....	293
Figure 9-13: Effect of Type C ACCL Dosage on Degree of Hydration.....	294
Figure 9-14: Effect of Various Water Reducers on the Slope Parameter, β	294
Figure 9-15: Effect of ASTM Type A LRWR on Degree of Hydration.....	295
Figure 9-16: Effect of C ₃ A on Degree of Hydration Parameter (α_u) and C ₄ AF on Slope Parameter (β)	295
Figure 9-17: Effect of C ₃ A/C ₄ AF on Degree of Hydration	296
Figure 9-18: Effect of %Na ₂ O _{eq} on Degree of Hydration Parameter (α_u) and %Na ₂ O on Time Parameter (τ)	296
Figure 9-19: Effect of %Na ₂ O _{eq} on Degree of Hydration.....	297
Figure 9-20: Predicted Versus Measured Degree of Hydration for Validation Dataset – Bogue Model.....	297

List of Tables

Table 2-1: Chemical and Physical Properties of Cement	32
Table 2-2: Three-Parameter Curve Fit Values for All Mixtures.....	33
Table 2-3: Batch-to-Batch Variability for Three-Parameter-Model Values.....	33
Table 2-4: Within-Batch Variability for Three-Parameter-Model Values	34
Table 2-5: Summary of Isothermal Calorimeter Round Robin Study ¹⁴	34
Table 2-6: Comparison of Confidence Limits of Wadsö ¹⁴ and Present Study	34
Table 3-1: Chemical and Physical Properties of Cement and SCMs	57
Table 3-2: Three-Parameter Curve Fit Values for All Mixtures.....	58
Table 3-3: Three-Parameter Curve Fit Values for Mixtures with SCMs.....	59
Table 4-1: Chemical and Physical Properties of Cement	91
Table 4-2: Three-Parameter Curve Fit Values for Mixtures with Fly Ash.....	92
Table 4-3: Three-Parameter Curve Fit Values for Mixtures with GGBF Slag, Silica Fume, and Ternary Blends	93
Table 5-1: Summary of Variables that Affect E_a	131
Table 5-2: Chemical and Physical Properties of Cement	132
Table 5-3: Chemical and physical properties of SCMs	133
Table 6-1: Chemical and physical properties of cement.....	166
Table 6-2: Summary Statistics for Semi-Calorimetry Variation	166
Table 6-3: Summary of Semi-Adiabatic Test Results	167
Table 7-1: Chemical and Physical Properties of Cementitious Materials	196

Table 7-2: Summary of Three-Parameter Model Parameters for Mixtures with 100% Cement	197
Table 7-3: Summary of Mixtures with SCMs.....	198
Table 8-1: Chemical and physical properties of cement.....	242
Table 8-2: Curve Fit Parameters for Mixtures with 100% Cement or Class F Fly Ash Replacement.....	243
Table 8-3: Curve Fit Parameters for Mixtures with Class C Fly Ash.....	244
Table 8-4: Curve Fit Parameters for Silica Fume, GGBF Slag, and Ternary Blends.....	245
Table 9-1: Effect of Different Mixture Characteristics on Exponential Model Hydration Parameters ^{2,3,4}	286

CHAPTER 1. INTRODUCTION

The hydration of cement in concrete is exothermic, which means it gives off heat. For thin elements, this heat dissipates quickly from the element, temperature differentials are small, and the thermal stresses result only from large environmental temperature shifts. In large elements, the heat caused by hydration can dissipate at the surface, but is trapped in the interior, resulting in potentially large thermal gradients. The thermal expansion of concrete is greater at higher temperatures, so if the temperature differential between the surface and the interior becomes too great, the interior will expand more than the exterior. When the thermal stress from this mis-matched expansion exceeds the tensile strength of the material, the concrete will crack. This phenomenon is referred to as thermal cracking.

Cracking in massive concrete structures due to temperature-induced stresses is a problem almost as old as concrete itself. However, thermal cracking in mass concrete elements has only been recognized since the beginning of the twentieth century, when it was first discovered in dams¹. Thermal gradients in bridge elements have historically been ignored in the U.S. However, as element size increases for structural, traffic, or aesthetic reasons, thermal gradients and thermal cracking have become serious concerns for bridge engineers. Owners and engineers in other parts of the world, such as Europe, have been dealing with these problems for a long time. Large jobs in Europe (such as the Chunnel from England to France) conduct extensive analysis and laboratory testing prior to construction of a project.

While in-depth analysis of thermal gradients is not typically done on highway projects in the U.S., many mass concrete projects rely on a 35 °F (20 °C) temperature differential, and some maximum internal temperature (usually 160 °F) to control thermal cracking and delayed ettringite formation (DEF), respectively². Contractors are required to prove that any concrete deemed “mass concrete” meets these specifications. Unfortunately, even though the premise behind the specification is well understood, the research behind the 35 °F specification is ambiguous. Verification of temperature differentials is also poor, since guidelines for instrumentation are vague, and measurement of thermal gradients is difficult. As a result, most thermal analysis of “smaller” mass concrete elements, like bridge structures, is inadequate. A better method is needed to estimate the temperature development in mass concrete elements. A model for concrete hydration would give engineers a cost-effective tool to estimate the in-place temperature development of different concrete mixtures in structures prior to placement, which would help lower the risk of thermal cracking.

Calorimetry is the most direct test method to quantify the heat evolution from a concrete mixture. Mortar cubes strengths are used in ASTM C 1074³, “Standard Practice for Estimating Concrete Strength by the Maturity Method,” because they roughly correlate with the amount of heat evolved, but they are not sufficiently accurate for the purposes of the present study. There is currently no model, based solely on calorimetry, which completely describes the effects of mixture proportions, cement and SCM chemistry, and chemical admixture dosages on the temperature sensitivity and adiabatic temperature rise of concrete.

Heat evolution of concrete or cement paste is commonly measured with a calorimeter. Calorimeters can be classified in three ways: Adiabatic (no heat loss or gain through system), Semi-adiabatic (known heat loss through system), and isothermal (constant temperature in system). Figure 1-1 shows the isothermal and semi-adiabatic calorimeters used in the present study. Typically, adiabatic and semi-adiabatic calorimetry is run on concrete samples, while isothermal calorimetry is run on cement pastes.



Figure 1-1: Isothermal Calorimeter (Left) and Semi-Adiabatic Calorimeter with Concrete Sample (Right)

The objective of this study is to develop a comprehensive model to describe the effects of mixture proportions, cement and SCM chemistry, and chemical admixture dosages on the temperature sensitivity and adiabatic temperature rise of concrete. First, the temperature sensitivity of the hydration reaction (described with activation energy, E_a) is needed to accurately predict the behavior of concrete under a variety of temperature

conditions. A multivariate regression model from isothermal calorimetry testing is developed to describe the effects of water-cementitious materials ratio, cement chemistry, supplementary cementing materials, and chemical admixtures on the E_a of portland cement pastes. Next, a multivariate regression model is developed from semi-adiabatic calorimetry testing that predicts the temperature development of concrete mixtures based on mixture proportions, cement and SCM chemistry, and chemical admixture dosages. The results of the semi-adiabatic models are validated using data from literature. The final model provides a useful tool to assess the temperature development of concrete mixtures, and thereby reduce the thermal cracking risk of the concrete structure.

This dissertation is divided into eight chapters. Each chapter is intended to be able to stand-alone, with only minimal references to the previous chapters. Chapter 2 examines the effects of cement chemistry and water-cement ratio (w/c) on E_a . A statistical analysis of the results is presented to identify the important variables and to quantify the variability of the test method. Chapter 3 studies the mechanisms by which accelerating, retarding, and water reducing admixtures affect E_a . Chapter 4 examines the effects of different supplementary cementing materials (SCMs) and ternary blends on E_a . Chapter 5 uses the results from Chapter 2, 3, and 4 to construct a model using multivariate statistics that predicts E_a . The model accounts for the effects of cement chemistry, supplementary cementing materials, and chemical admixtures on E_a .

The model from Chapter 5 is then used to calculate E_a for concrete mixtures. This allows the adiabatic temperature rise for a concrete mixture to be calculated from semi-adiabatic calorimeter results. Chapter 6 investigates the effects of cement type,

cementitious content, water-cementitious material ratio, coarse aggregate type (siliceous river gravel and limestone), and mixture placement temperature on semi-adiabatic results. Chapter 7 studies the effects of chemical admixtures on semi-adiabatic test results, and Chapter 8 compares the effects of different supplementary cementing materials (SCMs) and cements on the hydration behavior of typical concrete mixtures as determined by semi-adiabatic calorimetry. Finally, Chapter 9 presents a multivariate regression model for hydration that may be used to predict heat evolution and temperature rise of most concrete mixtures.

1.1. REFERENCES

1. ACI Committee 207, “Guide to Mass Concrete”, ACI 207.1R-05, American Concrete Institute, Farmington Hills, Michigan, 2005.
2. Chini, A.R., L.C. Muszynski, L. Acquaye, and S. Tarkhan, Determination of the Maximum Placement and Curing Temperatures in Mass Concrete to Avoid Durability Problems and DEF, FDOT Contract BC 354-29. Comp. Lucy Acquaye, et al. Vers. Final Report. Feb. 2003.
3. ASTM C 1074, “Standard Practice for Estimating Concrete Strength by the Maturity Method,” ASTM International, West Conshohocken, PA, 1998, 8 pp.

CHAPTER 2. THE EFFECTS OF CEMENT CHEMISTRY AND WATER-CEMENT RATIO ON ACTIVATION ENERGY

Accurate characterization of the progress of hydration is necessary to predict temperature gradients, maximum concrete temperature, thermal stresses, and relevant mechanical properties of concrete. An accurate estimate of the activation energy (E_a) of the hydration reactions is required to define the temperature sensitivity of the reactions and characterize the progress of hydration. Isothermal calorimetry is generally considered to be the most accurate method for measuring E_a ; however, the effects of many variables on E_a , including cement type, have not been thoroughly investigated. Also, the variability of results has not been analyzed. This chapter examines the effects of cement chemistry and water-cement ratio (w/c) on E_a . A statistical analysis of the results is presented to identify the important variables and to quantify the variability of the test method.

2.1. INTRODUCTION

Accurate estimation of the hydration of concrete is necessary to predict temperature gradients, maximum concrete temperature, thermal stresses, and relevant mechanical properties. This prediction of concrete hydration requires estimates of the heat of hydration and temperature sensitivity of the hydration reaction for given cementitious materials. The temperature sensitivity of hydration is best described by the Arrhenius equation and the concept of activation energy (E_a), as shown in Equation 2-1¹:

$$k = A \cdot e^{\frac{-E_a}{RT}} \quad \text{Equation 2-1}$$

where R = natural gas constant (8.314 J/mol/K), T = temperature (K) at which reaction occurs, k = rate of heat evolution (W), A = proportionality constant (same units as k), and E_a = activation energy (J/mol). Glasstone¹ defines the experimental (or apparent) activation energy (E_a) as the activation energy obtained experimentally by plotting the natural log of reaction rate versus the inverse of the reaction temperature. E_a may be determined by multiplying the negative of the slope of the best-fit line through $\ln(k)$ versus $1/T$ by R . This interpretation of E_a is typically used to characterize the reaction rate of cementitious materials at various temperatures.

A wide range of values for activation energy of cement has been reported in literature². In order to better understand the variation in E_a , Schindler investigated the effects of cement chemistry on E_a values using data from cements from the 1940's. The data Schindler used² relied on a combination of heat of solution and conduction calorimetry measurements to estimate the reaction rates needed for activation energy calculation. These results suggested that E_a varied greatly depending on the chemistry of the cement. However, modern cements are much more reactive, are ground more finely, and tend to have a higher heat of hydration, so Schindler's findings may not be appropriate for modern cements^{3,4,5}. It is important to know if E_a values from cements produced 60 years ago are similar to those for cements today, because many of the models used to quantify temperature distribution in a concrete element rely on these older data to determine E_a . Inaccurate characterization of E_a will lead to errors in models used

for estimating the temperature rise, thermal stresses, and mechanical properties of concrete elements.

There are other factors besides cement composition that may affect E_a . For example, the water-cement ratio (w/c) of a mixture is known to strongly affect the rate of hydration⁶. When more water is available to solubilize and react with the cement, the rate of heat evolution generally increases in the first week or so of hydration⁷. It is not known whether an increase in w/c will lead to a decrease in the amount of energy required to start the reaction, and a corresponding decrease in E_a . An estimate of the magnitude of this effect is needed to accurately model temperature in mixtures with different w/c.

Finally, the variability of test methods used to measure reaction rate is important. For cementitious materials, E_a is typically calculated by measuring the reaction rate of cement hydration at different temperatures using either isothermal calorimetry data from cement pastes or compressive strength data from mortar cubes. To measure reaction rates for the purpose of temperature prediction, isothermal calorimetry is the most appropriate test method⁴. Several researchers^{8,9,10} have reported values for E_a obtained using isothermal calorimetry. However, the confidence limits of the results are not generally reported. The precision of activation energy values obtained from this test method has not been quantified and is needed in order to draw significant conclusions about the test results.

As part of a larger study on the hydration behavior of concrete, 116 E_a values were measured. A subset of 20 results is presented in this chapter to examine the effects

of cement chemistry and w/c of modern cements on E_a . The variability of the calculation of hydration parameters using isothermal calorimeter is also presented. The confidence limits are calculated for the E_a results, which then permits a comparison to results in existing literature^{8,11}.

2.2. RESEARCH SIGNIFICANCE

Large thermal gradients at early ages can lead to cracking in concrete elements. Computational models for the prediction of temperature gradients are useful for identifying concrete mixtures that will be susceptible to thermal cracking. A more robust model for activation energy (E_a) is needed for accurate prediction of thermal gradients in concrete elements. Cement type and w/c are known to strongly influence the hydration behavior of concrete mixtures, and this difference can be seen in calorimetric curves. However, the effect of these variables on E_a has not been thoroughly or accurately examined using isothermal calorimetry. In addition, the variability of E_a has not been determined. This chapter presents results examining the effects of cement chemistry and w/c on E_a using isothermal calorimetry. A number of tests are repeated to measure the confidence limits of E_a .

2.3. LITERATURE REVIEW

Several aspects of cement chemistry have been reported to influence activation energy, including C_3A , C_4AF , C_3S , and Blaine fineness. However, the methods with which activation energy values were determined varied considerably. Maekawa, Chaube, and Kishi¹² suggest independent fractional contributions of each of the cementitious

materials. They suggest that E_a of C_3A , C_3S , C_4AF , and C_2S are approximately 54,000, 42,000, 32,000, and 21,000 J/mol, respectively. In a numerical simulation of heat of hydration development, D'Aloia and Chanvillard⁹ use values of 33,000 J/mol for C_3S , 39,000-43,000 J/mol for C_3A conversion to ettringite, and 25,000-29,000 J/mol for ettringite conversion to monosulfate. However, all of these values are numerical fits of heat of hydration data from calorimeter results and were not based on direct measurement of reaction rates for the individual reactions.

Barnett et al.¹³ found that E_a (determined using ASTM C 1074 and mortar cubes) did not change for mixtures with w/cm of 0.25 to 0.60. Schindler² developed a model for E_a , using values based on heat of solution tests, which depended on C_3A , C_4AF , and Blaine fineness. No published research has examined the effects of alkalis on E_a .

All of the previous research has correlated Bogue compounds with E_a . None have looked at the phases as calculated by Rietveld¹⁴ analysis, which is a much more accurate technique for determining the crystalline phases in cement. Therefore, the sensitivity of E_a models to the choice of cement analysis needs to be assessed. The present study will use a large number of calorimetric test result to evaluate the effects of cement chemistry (as determined by both Bogue calculations and Rietveld analysis) on E_a .

2.4. TEST METHODS

2.4.1. MATERIALS

The following cements conforming to ASTM C 150¹⁵ were used: one low-alkali Type I cement (C1), two high-alkali Type I cements (C2 and C3), three low-alkali Type I/II cements (C4, C5, and C6), two low-alkali Type III cements (C7 and C8), and one

Type V cement (C9). De-ionized water was used for mixing. Cement phases were calculated from x-ray fluorescence data using the Bogue calculations per ASTM C 150¹⁵. In addition, Rietveld analysis¹⁴ was used to estimate the amount of each crystalline phase in each cement. Chemical and physical properties of the materials are summarized in Table 2-1.

2.4.2. EXPERIMENTAL PROGRAM

During this study, isothermal calorimetry was performed on various cementitious pastes at 5 °C, 15 °C, 23 °C, 38 °C, and 60 °C using an eight channel isothermal conduction calorimeter. The calorimeter was kept in a temperature-controlled room at 21 ± 3 °C. Cement pastes were proportioned using a variety of water-to-cement ratios, and using 250 grams of cementitious material. Prior to mixing, materials were kept as close as possible to room temperature. Pastes were mixed in a kitchen blender for approximately three minutes. At higher w/c, the mixture was re-agitated immediately preceding sample introduction into the ampoule so that the bleeding would not alter the w/c of the paste in the ampoule. Eight tests were run simultaneously in the isothermal calorimeter. Each test sample had a mass of approximately 20 grams. Test durations ranged from 44 hours for those at 60 °C to over 100 hours for those at 5 °C.

Several variables were tested as part of this program. First, several cements were examined in order to determine the effects of cement chemistry on E_a . Next, the effect of cement alkali content was examined by artificially changing the alkali content ($\text{Na}_2\text{O} + 0.658 \times \text{K}_2\text{O}$) of three cements to 0.85% by adding the appropriate amount of a dilute solution of NaOH to de-ionized mixing water. The alkali content of a cement

affects the pH of the cementitious solution. Alkalies in cement are usually present as alkali sulfates¹⁶, or may be incorporated in the crystalline phases of the cement¹⁷. OH⁻ ions balance the Na⁺ and K⁺ ions when they go into solution. This increase in pH increases the dissolution of the various phases of the cement. In this study, the addition of alkalies to the mixing water is intended to imitate a cement with a higher alkali content. This was done in order to examine the effects of alkalies while holding all other cement chemistry variables constant. This is an imperfect approach, because the alkalies in cement are often bound in the various crystalline phases, and may increase the solubility of these particular phases. Therefore, the addition of alkalies as NaOH to the paste may model more the effects of a boost in pore solution pH, rather than the effects of a cement with a higher alkali content. The addition of NaOH may also dissolve the gypsum in the cement, rather than actually boosting the alkalies¹⁹. Despite these imperfections, the addition of NaOH to the paste appears to be a reasonable and practical way to test the variation of pore solution chemistry on E_a . Finally, w/c of 0.40, 0.44, 0.50, 0.55, and 0.68 were tested using two different cements to examine the effects w/c on E_a .

2.4.3. E_a CALCULATION PROCEDURE

The following section discusses the calculation procedure for E_a . This procedure is a modification of the ASTM C1074 method⁴. The concept of “equivalent age”²⁰ is necessary to calculate E_a and to predict hydration behavior at various curing temperatures. Equation 2-2, proposed by Friesleben Hansen and Pedersen²⁰, is the most common expression used to compute equivalent age, and is used in the remainder of this chapter to model the effects of time and temperature on hydration:

$$t_e(T_r) = \sum_0^t e^{-\frac{E_a}{R}(\frac{1}{T_c} - \frac{1}{T_r})} \cdot \Delta t \quad \text{Equation 2-2}$$

where $t_e(T_r)$ = equivalent age at reference temperature ($T_r(^{\circ}\text{K})$), T_c = temperature of the concrete ($^{\circ}\text{K}$), and E_a and R are as defined previously.

Note that in this derivation, E_a is assumed to be independent of temperature, which is consistent with the Arrhenius theory for rate processes. This is a reasonable approximation, given the relatively small temperature range concrete experiences in most situations.

The progress of the hydration of portland cement may be quantified by the degree of hydration (α), which varies from 0 to 1, with a value of 1 indicating complete hydration. For this study, degree of hydration is taken as the ratio of heat evolved at time, t , to the total amount of heat available, as shown in Equation 2-3:^{21,22,23,24,25,26}

$$\alpha = \frac{H(t)}{H_u} \quad \text{Equation 2-3}$$

where α = degree of hydration at time t , $H(t)$ = heat evolved from time 0 to time t (J/gram), and H_u = total heat available for reaction (J/gram). The maximum heat of hydration (H_u) was calculated for the cements in this study using Equation 2-4¹¹.

$$H_{cem} = 500 \cdot p_{C_3S} + 260 \cdot p_{C_2S} + 866 \cdot p_{C_3A} + 420 \cdot p_{C_4AF} + 624 \cdot p_{SO_3} + 1186 \cdot p_{FreeCa} + 850 \cdot p_{MgO} \quad \text{Equation 2-4}$$

where H_{cem} = total heat of hydration of portland cement (J/gram) at $\alpha = 1.0$, and p_i = mass of i-th component to total cement content ratio.

A mathematical relationship may be used to model the degree of hydration development. A number of researchers^{11,27} have suggested an exponential function to characterize cement hydration based on degree of hydration data. The most commonly used relationship is a three-parameter model defined in Equation 2-5:

$$\alpha(t_e) = \alpha_u \cdot e^{-\left[\frac{\tau}{t_e}\right]^\beta} \quad \text{Equation 2-5}$$

The following equation can be used to calculate E_a ²:

$$E_a = -\frac{\ln\left(\frac{\tau_{ref}}{\tau_c}\right)}{\left(\frac{1}{T_{ref}} - \frac{1}{T_c}\right)} \cdot R \quad \text{Equation 2-6}$$

where E_a , t , T_{ref} , T_c , and R are as defined previously.

E_a is calculated as follows:

- Time and heat evolution data from isothermal calorimeter tests are collected for the sample at different temperatures: 5, 15, 23, 38, and 60 °C (41, 59, 73, 100, and 140 °F) for this study.
- The data are fit to Equation 2-5 at each temperature by solving for α_u , τ , and β using a least squares fit of the exponential function.
- α_u and β are presumed independent of the test temperature.
- $\ln(\tau)$ versus $1/\text{Temperature (°K)}$ is plotted. E_a is the slope of the best fit line times the negative of the natural gas constant, R , as defined in Equation 2-6.

2.5. RESULTS AND DISCUSSION

E_a values for twenty different mixtures were calculated using the modified ASTM 1074 method of analysis⁴. The results are summarized in Table 2-2. H_u for the cements is summarized in Table 2-1, and the curve fit parameters (α_u , τ , and β) are summarized for all twenty mixtures in Table 2-2. The effects of w/c, alkali content, fineness, and cement chemistry on E_a are discussed next. Also, the variability of the test method for E_a are presented. Results for 5, 15, 38, and 60 °C (41, 59, 100, and 140 °F) different temperatures may be found in Appendix A.

2.6. EFFECTS OF CEMENT CHEMISTRY AND WATER-CEMENT RATIO ON E_A

2.6.1. EFFECT OF CEMENT CHEMISTRY AND ALKALIS

The percentages of crystalline phases in the cement and the cement fineness should have some effect on E_a , based on previous research. The effects of cement chemistry were not easily observable from heat of hydration and E_a results. There was no simple, direct correlation between the crystalline phases or the fineness of the cement and E_a . Therefore, multivariate regression analysis will be used in a following section to look for trends in the data.

The alkali content of mixtures with cements C2, C4, and C9 was boosted to 0.85% $\text{Na}_2\text{O}_{\text{eq}}$ with NaOH. The effect of boosting alkalis on the rate of hydration at 23 °C is shown in Figure 2-1, and the effect on E_a is shown in Figure 2-2. The addition of NaOH to the mixture increases the rate of hydration, but does not significantly affect the E_a of either cement. This is an interesting result; the hydration process is clearly affected

by the addition of alkalis, yet the activation energy is unchanged. However, this result does not necessarily rule out the possibility that cement alkalis affect E_a . As mentioned previously, adding NaOH is not an ideal method for testing an increase in alkalis. Since alkali content cannot be easily varied in a given cement, keeping all other compositional variables constant, multivariate analysis of several cements is necessary to determine if alkalis truly have any significant effect on E_a .

2.6.2. EFFECT OF WATER-CEMENT RATIO

Mixtures of Cement C2 and Cement C6 (Table 2-2) were tested at different water to cement ratios (w/c) to examine the sensitivity of E_a to w/c. There is a slight increase in the maximum rate of heat evolution when the w/c is increased, as shown in Figure 2-3. Figure 2-4 shows that raising the w/c slightly lowers E_a for both cements. This result is logical, because more water is available to solubilize the cement particles, and to permit more complete hydration. However the reductions in E_a presented here are quite small in relation to the confidence limits which will be presented subsequently. The variations shown here may be within the error of the test method.

2.6.3. E_a PREDICTION MODELS

Multivariate regression analysis of the E_a results is necessary to determine the variables that have the greatest effect on activation energy, and to validate previous studies on the subject. The first step involves evaluating the goodness of fit of different combinations of independent variables (predictor variables) that could have an effect on the dependent variable (or response variable), E_a . The procedure analyzes a specified

number of combinations of the independent variables and ranks them according to the coefficient of determination (R^2). The procedure also provides a matrix of the correlation coefficients of each variable combination. Next, an analysis of variance (ANOVA) for Type I and III errors is performed on each potential variable combination. A Type I error measures the probability that the model shows a relationship between an independent variable and the dependent variable (in this case, E_a) when there is really no relationship²⁸. A Type III error evaluates the probability that the choice of independent variables shows a statistical correlation, but that a wrong direction or variable has been chosen. A Type III error would lead one to believe that either the incorrect variable affects the dependent variable, or that the independent variable affects the dependent variable in the wrong way²⁹. Variables with a probability greater than 5% of Type I or III errors are not included in the model. Finally, non-linear regression analysis is used to select a model that best fits all of the data. To use least squares regression analysis, it is necessary to break the data into discrete points. This requires several steps. First, Equation 2-2 is solved for different time steps, which gives discrete points that quantify the equivalent age at each point of hydration. Then, the degree of hydration is calculated at each time and temperature using Equation 2-5.

Using this method, Schindler² suggested an activation energy model that depended on C_3A , C_4AF , and the Blaine fineness of the cement, as shown in Equation 2-7. The model was based on a 1940's data set generated by Lerch and Ford³⁴, as discussed previously.

$$E_a = 22,100 \cdot p_{C_3A}^{0.30} \cdot p_{C_4AF}^{0.25} \cdot Blaine^{0.35} \quad \text{Equation 2-7}$$

To evaluate Schindler's model, the measured E_a values from this study were compared to the values predicted by Equation 2-7². Next, multivariate regression analysis was performed on the data collected in the present study using C_3A , C_4AF , gypsum content, and Blaine fineness as dependent variables. The form of Equation 2-7 was used as a basis for the model because it provides a good model for the changes in E_a . However, the variables and coefficients were changed to give a best fit of the model to the data. The result of this analysis is shown in Equation 2-8.

$$E_a = 31,400 \cdot ((p_{C_3A} + p_{C_4AF}) \cdot p_{Gypsum})^{0.13} \cdot Blaine^{-0.07} \cdot w/c^{-0.05} \quad \text{Equation 2-8}$$

Where p_{C_3A} = % C_3A in cement; p_{C_4AF} = % C_4AF in cement; p_{Gypsum} = % gypsum in cement ($1.7 \times \%SO_3$); $Blaine$ = Blaine fineness of cement (m^2/kg); and w/c = water-cement ratio of paste. An R^2 of 0.999 was obtained (compared to 0.981 from Schindler²). When Rietveld analysis is used to determine the cement phases, the best fit of the data is as follows:

$$E_a = 37,800 \cdot ((p_{C_3A}) \cdot (CaSO_4 \cdot xH_2O + K_2SO_4))^{0.05} \cdot Blaine^{-0.03} \cdot w/c^{-0.04} \quad \text{Equation 2-9}$$

Where $CaSO_4 \cdot xH_2O$ = Sum of % by mass of gypsum, hemihydrate, and anhydrite, K_2SO_4 = % by mass of arcanite, and p_{C_3A} = % C_3A in cement, as determined by Rietveld analysis.

There are several differences between the model from Schindler² (Equation 2-7) and Equation 2-8 and Equation 2-9. The new models for E_a take into account the soluble sulfate content of the mixture. The alkalis in the cement and the amount of sulfate in

solution are known to affect the reaction rate of the aluminate phases³³. In the new models, an increase in either the C_3A or the soluble sulfates will increase E_a , which is also the trend in Equation 2-7, although it only takes into account C_3A . Equation 2-8 includes C_4AF , while Equation 2-9 does not. Though the form of the equations is similar, this suggests that the use of Bogue compounds and sulfate content of a mixture may miss some of the subtleties in the reaction between the aluminates and the sulfates. The new equations also suggest that the magnitude of the effects of C_3A and soluble sulfates on E_a are relatively similar. Finally, the effect of Blaine fineness is reversed from the old model. This stands to reason because an increase in the fineness of the cement should facilitate the hydration reaction and reduce E_a .

2.6.4. COMPARISON BETWEEN E_A FROM LERCH AND FORD DATA AND CALORIMETER DATA

Figure 2-4 compares the measured E_a of the cements in this study versus E_a predicted from both Equation 2-7² (labeled “Schindler 2004”) and Equation 8 (labeled “New Model”). The solid line represents a 1-to-1 correlation, indicating a perfect relationship between measured and predicted values. The results of this comparison are discussed next.

Equation 7² predicts a much greater range of E_a values than the current experimental data suggest, based on the range of dependent variables investigated; this is clearly apparent in Figure 2-5. This difference could be due to the different chemistries of cements examined in the two experimental databases. The range of experimentally measured E_a values in the present study is surprisingly small. Schindler reported a range

of measured E_a values from 36,132 J/mol to 54,467 J/mol for 1940's cements, while this study reports a range of measured E_a values from 35,223 to 41,323 J/mol. As a result, the coefficients in Equation 2-8 are smaller than the coefficients in Equation 2-7.

There are two possible reasons for this difference. First, it is likely that this difference is a result of the different cement chemistries represented in the present study. The average Blaine finenesses of the Type I/II, III, and V cements tested here were 386, 546, and 409 m²/kg, respectively. The average finenesses for the same cements in the Lerch and Ford dataset were 333, 535, and 367 m²/kg. The average C₂S content for modern cements is 14.0 %, versus 29.5 % for Lerch and Ford³⁴. These differences are reflected in the parameters from Equation 2-5. They provide an indication of the hydration behavior of the mixture. An increase in the time parameter (τ) correlates with an increase in the amount of retardation of a mixture, and an increase in the slope parameter (β) correlates with an increase in the reaction rate of the mixtures. The range of time parameters (τ) is greater for the Lerch and Ford³⁴ data set than the data presented here. For Type I cements, the range of τ values reported in Lerch and Ford² was 17.8 to 33.5 at 21.1 °C (70 °F). For Type III cements, the range of τ values reported² was 11.1 to 15.4 at 21.1 °C (70 °F). Also, the calculated slope parameters (β) were typically lower for the Lerch and Ford data ($\beta = 0.369$ to 0.537) compared to this data ($\beta = 0.750$ to 1.108). This indicates that the cements from sixty years ago were slower reacting than cements produced today.

The results presented here support the assertion that modern cements are much more homogenous than older cements. However, the test methods from the Lerch and Ford dataset and the present dataset are different. The dataset from which Equation 2-7 was developed was based on a combination of conduction calorimeter and heat of solution data, rather than isothermal calorimeter data. The variability of the rate constants (τ) determined from each of these two methods may affect the results for E_a . The rate constant (τ) for the Lerch and Ford dataset was determined using seven conduction calorimeter tests and four heat of solution tests. ASTM C 186³⁶ states the single operator standard deviation for the heat of hydration and heat of solution tests as 14.5 and 12.2 J/gram, respectively. The results of any two tests should not differ by more than 42 and 34 J/gram for the heat of hydration and heat of solution tests. The rate constants for the research presented here are based on isothermal calorimetry. The methods used in the Lerch and Ford study are believed to be comparable to isothermal calorimetry for individual measurements. Given the small range of predicted values in the current study, it is possible that the differences between the previous model and the current model for E_a are due to experimental error. Therefore, the variability of the modified ASTM C 1074 test method with isothermal calorimetry should be quantified.

2.7. VARIABILITY OF RESULTS

2.7.1. VARIABILITY OF THREE-PARAMETER MODEL VALUES

To investigate the effects of calorimeter variability on curve-fit parameters from Equation 2-5, isothermal tests were replicated for mixtures 3, 4, 8, and 13. Batch-to-

batch average, standard deviation, and standard error values are summarized in Table 2-3. The number of tests (n), within batch average, standard deviation, and standard error values are summarized in Table 2-4. These results were combined to give an overall measure of the variability of the test method. To quantify variability, the pooled weighted mean and standard deviation for α_u , τ , and β are useful for estimating the confidence limits of the E_a calculations. The **pooled weighted mean** $\{\bar{x}\}_w$ for α_u , τ , and β may be calculated using Equation 2-10, and the **pooled weighted standard deviation** $\{S_x\}_w$ may be calculated using Equation 2-11 and Equation 2-12²⁸.

$$\{\bar{x}\}_w = \frac{\sum_{j=1}^M N_j \bar{x}_j}{\sum_{j=1}^M N_j} \quad \text{Equation 2-10}$$

where N = physical parameter of experiment, M = number of replicate experiments, \bar{x} = average of each experiment.

$$\{S_x\}_w = \sqrt{\frac{v_1 S_{x_1}^2 + v_2 S_{x_2}^2 + \dots + v_M S_{x_M}^2}{v}}, \quad \text{Equation 2-11}$$

where S_x^2 = variance of \bar{x} , and v = degrees of freedom as follows:

$$v = \sum_{j=1}^M v_j = \sum_{j=1}^M (N_j - 1). \quad \text{Equation 2-12}$$

The pooled weighted mean for the degree of hydration constant (α_u) for all tests used to quantify batch to batch variation was 0.692, and the standard deviation (S_{α_u}) was 0.040. The pooled weighted mean for the degree of hydration constant (α_u) for all tests used to quantify within batch variation was 0.708 and the standard deviation (S_{α_u}) was

0.010. The pooled weighted mean for the rate constant (τ) for all tests used to quantify batch to batch variation was 21.418, and the standard deviation (S_τ) was 1.292. The pooled weighted mean for the rate constant (τ) for all tests used to quantify within batch variation was 17.941 and the standard deviation (S_τ) was 0.258. The pooled weighted mean for the slope constant (β) for all tests used to quantify batch-to-batch variation was 0.878, and the standard deviation (S_β) was 0.016. The average for the rate constant (β) for all tests used to quantify within batch variation was 0.958 and the standard deviation (S_β) was 0.015. With this information, a pooled t-test may be used to determine the confidence intervals for α_u , τ , and β . The 95%, 90%, and 80% confidence intervals for α_u , τ , and β are shown in Table 2-6, and will be compared to a previous study on the variability of the test method in the next section.

2.7.2. COMPARISON OF RESULTS TO VARIABILITY REPORTED BY NORDTEST

Wadsö³⁵ compared 7-day heat of hydration tests determined using the same isothermal calorimeter used in this present study. Three labs tested two different cements as part of a round robin study. A summary of the results presented by Wadsö³⁵ for cement pastes are presented in Table 2-5. The 95%, 90%, and 80% confidence intervals for 7-day heat of hydration are shown in Table 2-6. These results give an estimate of the variability of degree of hydration results at room temperature. The variability of results may increase at higher or lower temperatures depending on sample size, frequency of calibration, room temperature fluctuation, and low signal-to-noise ratios³⁵.

The confidence limits for 7-day heat of hydration are roughly equivalent to the results for α_u in the present study. Within-batch 95% confidence limits in the present study were similar to the within-batch variation reported by Wadsö³⁵ (6.0% v. 4.2%). However, the batch-to-batch confidence limits in the present study were higher than those reported previously (23.6% v. 4.2%). This difference is likely due to the greater range of temperatures tested here. For example, the total amount of heat evolved for Mixture 3 (100% cement C2) at 90 hours was 176 J/gram for tests at 5°C (41°F), and was 287 J/gram for tests at 23°C (73°F). The standard deviation of α_u was 0.094 at 5°C (41°F), and was 0.015 at 23°C (73°F). Tests run at lower temperatures may experience more variability because the signal-to-noise ratio is lower than it is for tests run at higher temperatures. Also, tests run at temperatures that are significantly different than the ambient temperature may be more sensitive to calibration errors or changes in ambient conditions. Finally, the standard deviation of τ and β show less dependence on test temperature than α_u .

2.7.3. CONFIDENCE LIMITS OF E_A RESULTS

The variability in the τ parameter will influence E_a . The 95% confidence interval for τ was approximately 25%, which indicates that the 95% confidence limits for E_a will be very high. However, the confidence interval of τ does not translate directly to the confidence interval for E_a . The confidence interval for E_a is improved substantially by using isothermal calorimeter tests at five temperatures, because these tests essentially serve as repeated tests. The 95% confidence limits using 5 temperatures were

approximately ± 780 J/mol ($\pm 2.0\%$). Confidence limits of E_a results grew to ± 1980 J/mol ($\pm 5.1\%$) when 4 temperatures were used.

The variability of the degree of hydration parameter (α_u) in the present study is less than the variability of heat of solution testing, and are comparable to other studies on isothermal calorimetry³⁵, which suggests that the results in the present research are more accurate than the results from the Lerch and Ford³⁴ dataset. This also suggests that the differences in E_a between Lerch and Ford³⁴ and the present study may be due to the choice of test methods, rather than any inherent difference in cements.

2.8. CONCLUSIONS

This chapter presents revised models for E_a which utilize an improved calorimetric technique. These models can use either Bogue calculations or Rietveld analysis to determine E_a . The range of the model results for E_a is less than previously believed. However, this is probably due to differences in the reliability of the test methods, and due to the changes in cement chemistry from sixty years ago to the present. Further study is necessary to determine the effects of cement type with supplementary cementing materials (SCMs) and chemical admixtures on E_a . Nevertheless, the results presented in this chapter improve the ability to properly compare calorimetry results and show that E_a results from isothermal calorimetry are repeatable.

This study examined the effects of cement chemistry and w/c on the activation energy (E_a). E_a was compared to the crystalline phases in the cement determined from both Bogue calculations and Rietveld analysis. The predicted E_a was not significantly

affect by the choice of analysis methods. The differences in E_a for cements tested here was smaller than previously determined for cements produced in the 1940's. E_a ranged from 35,200 to 40,000 J/mol. Raising the w/c of a paste from 0.40 to 0.68 increased the maximum rate of heat evolution slightly, and reduced E_a by approximately 2,000 J/mol, which is close to the error of the test method. Artificially boosting alkalis to 0.85% $\text{Na}_2\text{O}_{\text{eq}}$ using NaOH also increased the maximum rate of heat evolution, but had little effect on E_a . The Blaine fineness of the cement reduced E_a . Furthermore, the combination of the aluminate content and the soluble sulfate content of the cement had a significant effect on E_a .

To compare the results of this study with previous work, the confidence limits of the three parameter hydration model variables (α_u , τ , β) and E_a (determined from isothermal calorimetry tests) were determined. The 95% confidence limits for batch-to-batch variation for α_u , τ , and β were $\pm 23.6\%$, $\pm 24.7\%$, and $\pm 7.3\%$, respectively. The 95% confidence limits for within-batch variation for α_u , τ , and β were $\pm 6.0\%$, $\pm 6.6\%$, and $\pm 6.0\%$, respectively. The 95% confidence limits for E_a were 2.0% when five different temperatures were used to calculate E_a , and were 5% when 4 tests were used. The single operator variability is less than the variability of heat of solution testing, which suggests that the results in the present research are more accurate than the results from the Lerch and Ford dataset.

2.9. REFERENCES

1. Glasstone, S., K.J. Laidler, and H. Eyring, *The Theory of Rate Processes: The Kinetics of Chemical Reactions, Viscosity, Diffusion, and Electrochemical Phenomena*. McGraw-Hill Book Company, Inc. New York, 1941, 611 pp.
2. Schindler, A.K., "Effect of Temperature on Hydration of Cementitious Materials", *ACI Materials Journal*, V. 101, No. 1, Jan.-Feb., 2004, pp. 72-81.
3. Poole, J.L., "Hydration Study of Cementitious Materials Using Semi-Adiabatic Calorimetry," PhD Dissertation, Chapter 6, The University of Texas at Austin, Austin, TX, 2007, pp 141-171.
4. Poole, J.L., K.A. Riding, K.J. Folliard, M.G.C. Juenger, and A.K. Schindler "Methods of Activation Energy Calculation for Portland Cement," *ACI Materials Journal*, V. 104, No. 1, Jan.-Feb., 2007, pp. 303-311.
5. Poole, T.S., "Changes in ASTM Type II Portland Cement from 1940 to 1994", *Cement and Concrete Aggregates*, CCAGDP, Vol. 20, No. 1, June 1998, pp. 157-162.
6. Mills, R.H. "Factors Influencing Cessation of hydration in Water Cured Cement Pastes." Special Report 90: Symposium on Structure of Portland Cement Paste and Concrete. Washington, D.C.: Highway Research Board, 1966. 406-424.
7. Taylor, H.F.W., Cement Chemistry, 1st ed. Academic Press Limited, London, 1990.
8. Ma, W., D. Sample, R. Martin, and P.W. Brown, "Calorimetric Study of Cement Blends Containing Fly Ash, Silica Fume, and Slag at Elevated Temperatures." *Cement, Concrete, and Aggregates*, V. 16, 1994, pp. 93-99.

9. D'Aloia, L., and G. Chanvillard, "Determining the "Apparent" Activation Energy of Concrete; E_a – Numerical Simulations of the Heat of Hydration of Cement," *Cement and Concrete Research*, V. 32, 2002, pp. 1277-1289.
10. Kada-Benameur, H., E. Wirquin, and B. Duthoit, "Determination of Apparent Activation Energy of Concrete by Isothermal Calorimetry," *Cement and Concrete Research*, V. 30, 2000, pp. 301-305.
11. Schindler, A.K., and K.J. Folliard, "Heat of Hydration Models for Cementitious Materials", *ACI Materials Journal*, V. 102, No. 1, Jan.-Feb., 2005, pp. 24-33.
12. Maekawa, K., R. Chaube, and T. Kishi, *Modelling of Concrete Performance: Hydration, Microstructure Formation, and Mass Transport*, E&FN Spon, London, 1999.
13. Barnett, S.J., M.N. Soustos, S.G. Millard, and J.H. Bungey, "Strength Development of Mortars Containing Ground Granulated Blast Furnace Slag: Effect of Curing Temperature and Determination of Apparent Activation Energies" *Cement and Concrete Research*, V. 36, 2005, pp. 434-440.
14. Scrivener, K.L., T. Füllmann, E. Gallucci, G. Walenta, and E. Bermejo, "Quantitative Study of Portland Cement Hydration by X-Ray Diffraction/Rietveld Analysis and Independent Methods", *Cement and Concrete Research*, V. 34, 2004, pp 1541-1547.
15. ASTM C 150, "Standard Specification for Portland Cement," Annual Book of ASTM Standards, Vol 04.01., ASTM International, West Conshohocken, PA., 2002, 8 pp.

16. Jackson, P.J., "Portland Cement: Classification and Manufacture" Lea's Chemistry of Cement and Concrete, 4th ed., ed. P.C. Hewlett, Arnold Publishers, New York, 1998, p 25-94.
17. Lawrence, C.D., "The Constitution and Specification of Portland Cements" Lea's Chemistry of Cement and Concrete, 4th ed., ed. P.C. Hewlett, Arnold Publishers, New York, 1998, p 131-193.
18. Haider, A., "The Benefits of Installing an Online Free Lime Analyzer to Control the Clinkering Process," PCA Fall Technical Session, Oak Brook, IL, September 1999.
19. Diamond, S., "Alkali-Silica Reactions – Some Paradoxes," *Cement and Concrete Composites*, V.19, 1997, pp. 391-401.
20. Freiesleben Hansen, P., and E.J. Pedersen, "Maturity computer for controlling curing and hardening of concrete," *Nordisk Betong*, V. 1, No. 19, 1977, pp. 21-25.
21. Van Breugel, K., "Prediction of Temperature Development in Hardening Concrete", *Prevention of Thermal Cracking in Concrete at Early Ages*, RILEM Report 15, E & FN Spon, London 1998.
22. D'Aloia, L., and G. Chanvillard, "Determining the "Apparent" Activation Energy of Concrete; E_a – Numerical Simulations of the Heat of Hydration of Cement," *Cement and Concrete Research*, V. 32, 2002, pp. 1277-1289.
23. Kada-Benameur, H., E. Wirquin, and B. Duthoit, "Determination of Apparent Activation Energy of Concrete by Isothermal Calorimetry," *Cement and Concrete Research*, V. 30, 2000, pp. 301-305.

24. Copeland, L.E., Kantro, D.L., Verbeck, G., “Part IV-3 Chemistry of Hydration of Portland Cement,” 4th International Symposium of the Chemistry of Cement, Washington, D.C., 1960, pp. 429-465.
25. De Schutter, G., and Taerwe, L., “Degree of Hydration-Based Description of Mechanical Properties of Early-Age Concrete,” *Materials and Structures*, Vol. 29, No. 7, 1996, pp. 335-344.
26. Verbeck, G., and Forster, C.W. “Long-Time Study of Cement Performance in Concrete. Chapter 6 – The Heats of Hydration of the Cement,” *Proceedings of the American Society for Testing Materials*, Vol. 50, 1950, pp. 1235-1262.
27. Pane, I., and W. Hansen, “Concrete Hydration and Mechanical Properties under Nonisothermal Conditions,” *ACI Materials Journal*, V. 99, No. 6, Nov.-Dec, 2002, pp. 534-542.
28. Devore, Jay L., *Probability and Statistics for Engineering and the Sciences*, 4th ed. Duxbury Press, New York, 743 p, 1995.
29. Hsu, J.C. *Multiple Comparisons, Theory and Methods*, 1st ed. Chapman & Hall/CRC, Boca Raton, FL, 1996
30. Lerch, W., and R.H. Bogue, “The Heat of Hydration of Portland Cement” Portland Cement Association Fellowship, National Bureau of Standards, Paper no. 26, May, 1934 30 pp.
31. ASTM C 114, “Standard Test Methods for Chemical Analysis of Hydraulic Cement” *Annual Book of ASTM Standards*, Vol 04.01., ASTM International, West Conshohocken, PA., 2005, 31 pp.

32. Hewlett, P. C., Lea's Chemistry of Cement and Concrete, 4th ed. Arnold Publishers, New York, 1998.
33. Lerch, W., "The Influence of Gypsum on the Hydration and Properties of Portland Cement Paste," Proceedings of the American Society for Testing Materials, V. 46, 1946.
34. Lerch, W. and Ford, C. L., "Long-Term Study of Cement Performance in Concrete: Chapter 3 – Chemical and Physical Tests of the Cements," *ACI Journal*, Proceedings V. 44, No. 8, 1948, pp. 745-795.
35. Wadsö, L., "An Experimental Comparison Between Isothermal Calorimetry, Semi-Adiabatic Calorimetry and Solution Calorimetry for the Study of Cement Hydration." Nordtest Report TR 522, Nordtest, Espoo, Finland, 2003.
36. ASTM C 186, "Standard Test Method for Heat of Hydration of Hydraulic Cement" Annual Book of ASTM Standards, Vol 04.01., ASTM International, West Conshohocken, PA., 2005, 7 pp.

Table 2-1: Chemical and Physical Properties of Cement

	Ty I LA	Ty I	Ty I	Ty I/II LA	Ty I/II LA	Ty I/II LA	Ty III LA	Ty III LA	Ty V
Cement	C1	C2	C3	C4	C5	C6	C7	C8	C9
SiO ₂ (%)	20.45	19.18	19.27	21.29	20.6	20.77	19.72	20.3	21.63
Al ₂ O ₃ (%)	5.43	5.34	5.08	4.88	4.8	3.88	5.27	4.85	4.04
Fe ₂ O ₃ (%)	2.01	2.3	3.08	2.92	3.2	3.73	2.02	3.56	5.29
CaO (%)	64.51	63.17	61.45	63.31	64.3	64.5	64.08	63.94	63.07
MgO (%)	1.15	1.09	2.64	1.23	1.5	1.01	1.22	0.82	0.77
Na ₂ O (%)	0.14	0.12	0.24	0.28	0.18	0.18	0.13	0.07	0.27
K ₂ O (%)	0.56	0.95	0.93	0.4	0.37	0.6	0.52	0.66	0.23
Na ₂ O Equiv. (%)	0.51	0.75	0.85	0.543	0.423	0.575	0.472	0.504	0.42
SO ₃ (%)	3.35	3.2	4.19	2.63	2.8	2.38	4.4	3.44	2.74
LOI (%)	1.80	4.1	2.41	2.43	1.2	2.67	1.95	1.71	1.55
Insoluble Residue (%)	-	0.63	0.3	-	0.18	0.25	-	-	1.43
Free CaO (%)	1.66	4	2.34	0.91	1.9	2.8	1.33	1.89	3.8
CaO (%)**	0.0	0.0	0.7	0.0	0.0	0.0	0.0	0.0	0.0
C ₃ S (%)*	58.29	63.11	53.23	51.47	60.40	66.54	60.16	58.54	49.85
C ₃ S (%)**	61.2	61	57.2	56.6	55.5	55.7	64.6	54.0	49.0
C ₂ S (%)*	14.65	7.38	15.09	22.21	13.50	9.35	11.16	14.04	24.41
C ₂ S (%)**	16.0	15.6	15.1	18.6	17.4	21.1	11.8	21.7	26.4
C ₃ A (%)*	10.99	10.26	8.25	7.99	7.31	3.97	10.55	6.83	1.76
C ₃ A (%)**	13.1	9.6	5.3	6.4	6.8	4.0	12.4	5.7	4.4
C ₄ AF (%)*	6.12	7.00	9.37	8.80	9.74	11.35	6.15	10.83	16.10
C ₄ AF (%)**	3.5	6.0	9.6	8.6	10.7	10.7	4.0	10.2	12.1
Gypsum (%)*	5.70	5.44	7.12	4.47	4.76	4.05	7.48	5.85	4.66
C \bar{S} H ₂ (%)**	1.4	0.4	6.6	3.1	0.9	0.0	2.4	0.0	2.3
C \bar{S} H _{0.5} (%)**	1.5	1.2	0.8	1.3	1.9	2.5	2.4	3.7	2.0
C \bar{S} (%)**	0.6	0.7	0.4	0.6	0.9	0.7	0.6	0.6	0.4
K ₂ SO ₄ (%)**	1.5	1	1.6	0.8	0.5	0.7	0.8	1.3	0.9
CaCO ₃ (%)**	0.8	3.6	1.7	3.4	2.5	3.2	0.7	1.5	2.5
Blaine fineness (m ² /kg)	350.0	390.9	388.9	413.2	404.9	365.4	552.0	539.0	409.0
H _{cem} (J/g)	501	530	461	458	494	496	501	493	464
H _{cem} *** (J/g)	481	482	473	447	471	463	485	474	419

* Bogue Calculations, ** Rietveld Analysis ***Free CaO Determined from Rietveld Analysis

Table 2-2: Three-Parameter Curve Fit Values for All Mixtures

Mix	Cement	w/c	Na ₂ O _{eq}	α_u	β	τ (hours)					E_a (J/mol)
			%			5°C	15°C	23°C	38°C	60°C	
1	C1	0.44	0.51	0.764	0.988	53.06	25.12	14.27	6.77	3.25	38,950
2	C2	0.40	0.75	0.656	0.888	56.44	26.62	16.66	7.41	2.87	41,323
3	C2	0.44	0.75	0.648	0.968	57.06	28.07	16.52	6.74	3.25	40,540
4	C2	0.50	0.75	0.685	0.939	60.20	29.51	14.72	7.56	3.36	40,223
5	C2	0.55	0.75	0.690	0.915	56.68	28.23	15.92	7.74	3.27	39,715
6	C2	0.68	0.75	0.710	0.909	60.45	30.13	15.31	7.96	3.68	39,022
7	C2	0.44	0.85	0.637	0.986	58.19	25.22	15.19	6.35	3.29	40,146
8	C3	0.44	0.85	0.736	1.016	55.19	27.01	15.16	6.93	3.48	38,845
9	C4	0.44	0.54	0.789	0.896	54.51	28.25	15.28	7.18	3.87	37,447
10	C4	0.44	0.85	0.686	1.108	39.81	18.45	10.79	5.69	2.61	37,450
11	C5	0.44	0.42	0.714	0.807	64.40	32.27	20.35	8.78	4.31	38,069
12	C6	0.40	0.58	0.630	0.865	33.42	17.77	11.17	5.40	2.34	37,126
13	C6	0.44	0.58	0.684	0.819	35.93	18.80	11.71	6.35	2.42	37,100
14	C6	0.50	0.58	0.710	0.750	41.49	21.71	12.94	6.29	3.06	36,563
15	C6	0.55	0.58	0.665	0.801	40.32	20.84	13.78	7.13	3.08	35,497
16	C6	0.68	0.58	0.602	0.826	39.66	20.69	13.34	7.37	3.04	35,223
17	C7	0.44	0.47	0.843	1.013	46.75	21.92	12.28	5.88	2.62	40,056
18	C8	0.40	0.50	0.732	0.829	32.90	17.12	9.81	6.30	2.08	37,347
19	C9	0.44	0.42	0.716	0.827	75.03	34.93	24.11	8.48	4.66	39,536
20	C9	0.44	0.85	0.634	0.985	54.58	23.65	18.48	6.53	3.42	38,861

Table 2-3: Batch-to-Batch Variability for Three-Parameter-Model Values

Mix	Temp. (°C)	n	α_u			β			τ (hours)		
			Avg.	Std. Dev	Std. Error	Avg.	Std. Dev	Std. Error	Avg.	Std. Dev	Std. Error
3	5	4	0.754	0.094	0.047	0.747	0.086	0.043	68.433	6.599	3.299
3	15	3	0.690	0.035	0.020	0.895	0.014	0.008	27.873	2.273	1.312
13	15	2	0.677	0.040	0.029	0.811	0.099	0.070	16.778	0.964	0.682
3	23	5	0.691	0.015	0.007	0.874	0.030	0.013	17.299	0.656	0.294
4	23	2	0.706	0.001	0.001	0.929	0.047	0.033	16.176	0.173	0.122
13	23	3	0.695	0.018	0.010	0.828	0.016	0.009	12.340	0.798	0.461
3	38	2	0.622	0.016	0.011	1.207	0.110	0.078	6.957	0.156	0.110
3	60	2	0.633	0.013	0.009	0.877	0.003	0.002	3.585	0.152	0.107
13	60	2	0.674	0.007	0.005	0.877	0.003	0.002	2.554	0.004	0.003

Table 2-4: Within-Batch Variability for Three-Parameter-Model Values

Mix	Temp. (°C)	n	α_u			β			τ (hours)		
			Avg. α_u	Std. Dev	Std. Error	Avg. β	Std. Dev	Std. Error	Avg. τ (hrs)	Std. Dev	Std. Error
8	5	2	0.689	0.004	0.003	0.874	0.006	0.005	48.422	0.370	0.262
8	15	2	0.738	0.019	0.013	0.918	0.051	0.036	26.340	0.754	0.533
3	23	8	0.694	0.005	0.002	0.834	0.014	0.005	18.367	0.190	0.067
3	23	4	0.697	0.008	0.004	0.857	0.009	0.004	17.254	0.266	0.133
4	23	7	0.726	0.016	0.006	0.896	0.010	0.004	16.315	0.242	0.092
4	23	2	0.705	0.002	0.001	0.963	0.001	0.001	16.054	0.035	0.025
13	23	2	0.693	0.001	0.001	0.814	0.006	0.004	12.073	0.032	0.023
8	23	2	0.746	0.004	0.003	1.078	0.004	0.003	16.378	0.104	0.073
8	38	2	0.710	0.000	0.000	1.376	0.006	0.005	7.732	0.053	0.038
8	60	2	0.688	0.003	0.002	1.602	0.022	0.016	3.945	0.002	0.001

Table 2-5: Summary of Isothermal Calorimeter Round Robin Study³⁵

Cement	Location	Temp (°C)	Mixes	Tests/ Mix	Avg. (J/g)	Std.Dev. (J/g)	C.V.
A	BML-Lund	20	4	2	284	4	1.41%
A	BML-Lund	20	1	7	270	6	2.22%
A	SP-Borås	20	2	2	284	4	1.41%
A	Grace-Boston	22	1	4	272	5	1.84%
B	BML-Lund	20	4	2	363	6	1.65%
B	BML-Lund	20	1	7	354	7	1.98%
B	SP-Borås	20	2	2	357	3	0.84%
B	Grace-Boston	22	1	4	351	3	0.85%

Table 2-6: Comparison of Confidence Limits of Wadsö³⁵ and Present Study

Confidence Interval		7-day HOH	α_u	τ	β
95%	Single Batch	±3.5%	±6.0%	±6.0%	±6.6%
90%	Single Batch	±2.9%	±4.9%	±4.9%	±5.5%
80%	Single Batch	±2.2%	±3.8%	±3.8%	±4.2%
95%	Multiple Batch	±4.2%	±23.6%	±24.7%	±7.3%
90%	Multiple Batch	±3.4%	±19.3%	±20.3%	±6.0%
80%	Multiple Batch	±2.5%	±14.9%	±15.6%	±4.6%

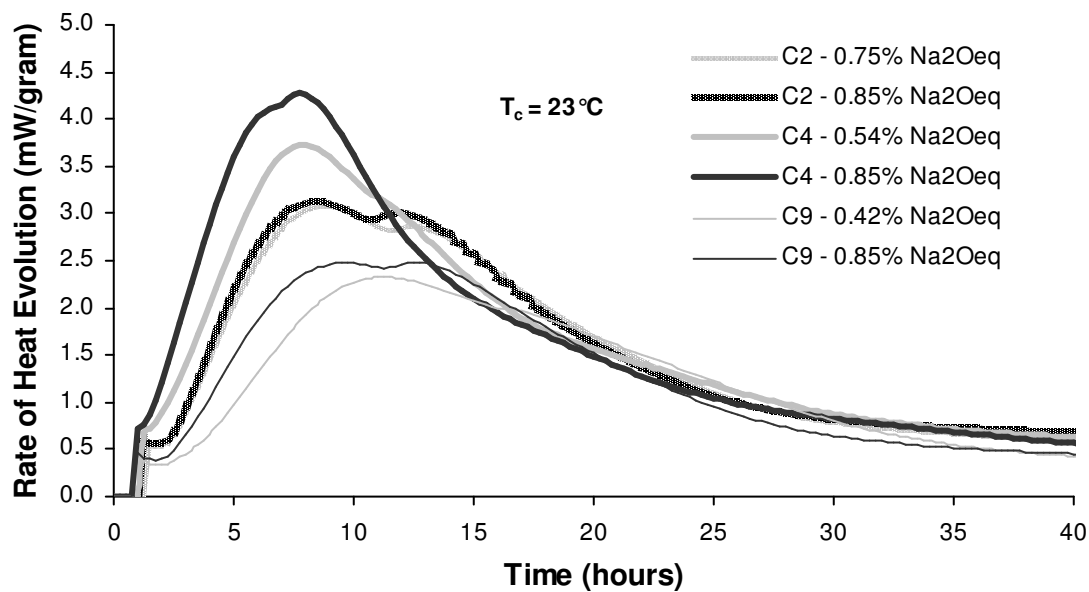


Figure 2-1: Effects of Na_2O_{eq} on Rate of Heat Evolution for Different Cements

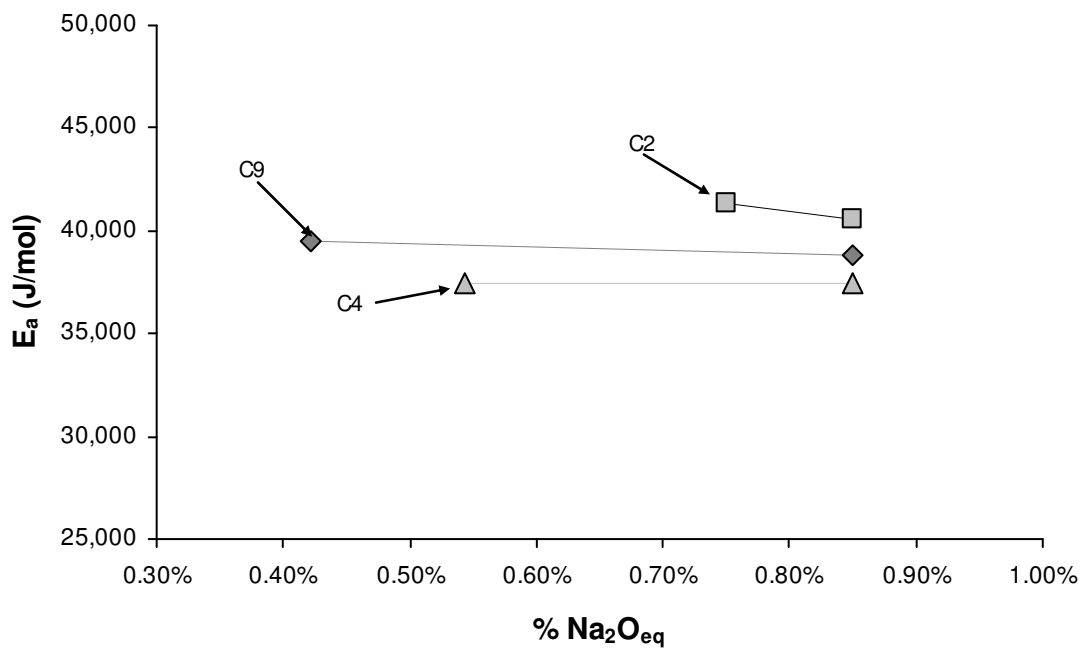


Figure 2-2: Activation Energy v. Na_2O_{eq}

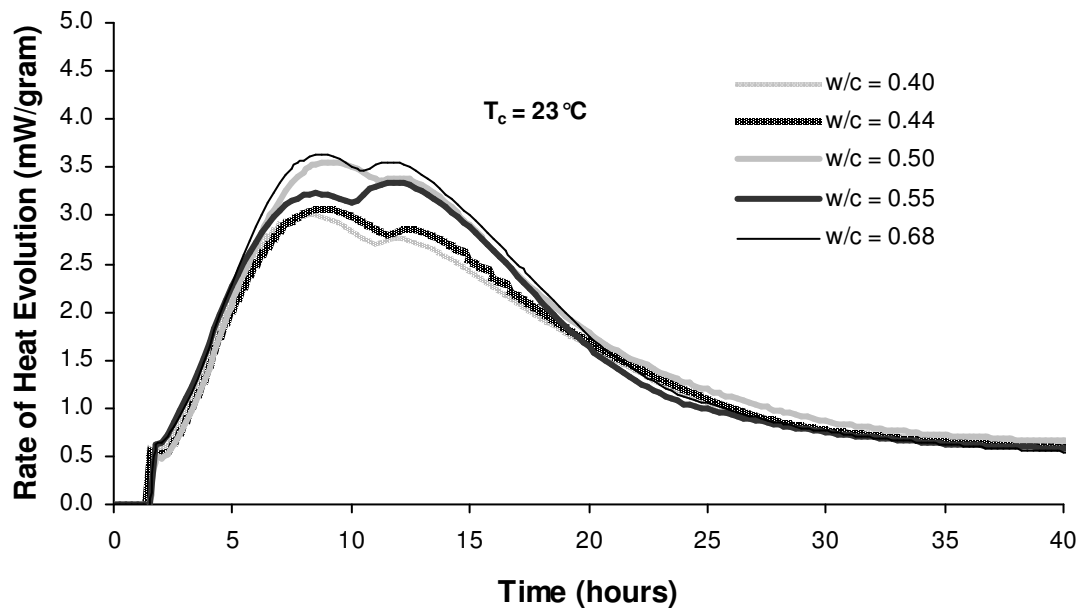


Figure 2-3: Effects of w/c on Rate of Heat Evolution per Gram of Cement for Cement C2

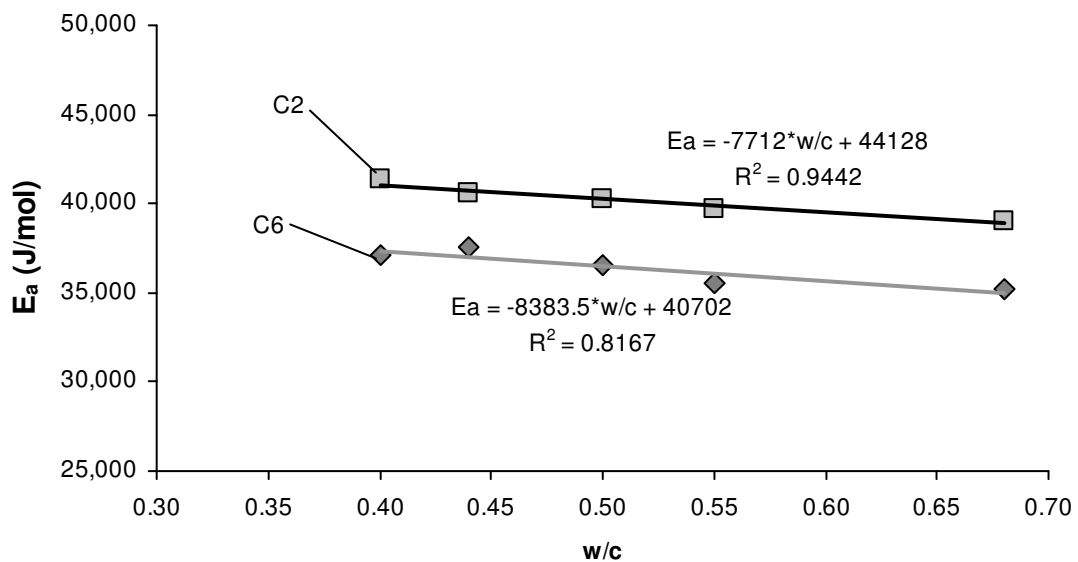


Figure 2-4: Activation Energy v. w/c

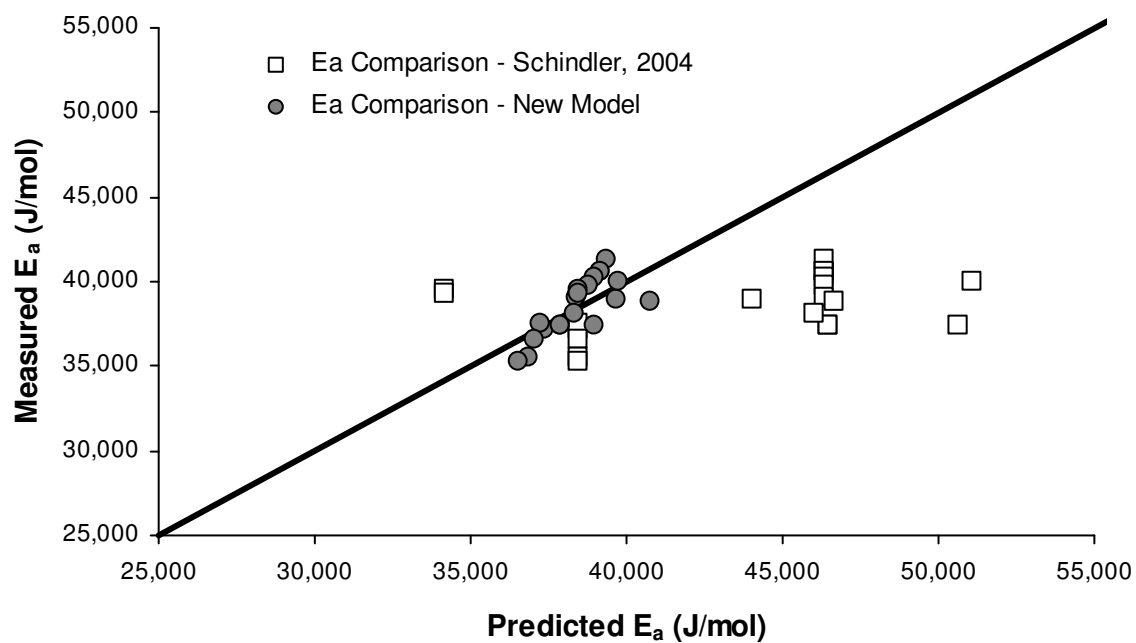


Figure 2-5: Comparison Between Regression Analysis Results for Equation 2-7 and Equation 2-8

CHAPTER 3. THE EFFECTS OF CHEMICAL ADMIXTURES ON ACTIVATION ENERGY OF CEMENTITIOUS MATERIALS

Accurate characterization of the progress of hydration is necessary to predict temperature gradients, maximum concrete temperature, thermal stresses, and relevant mechanical properties of concrete. An accurate estimate of the activation energy (E_a) is required to define the temperature sensitivity of the reaction. The effects of chemical admixtures on E_a of concrete mixtures have not been thoroughly investigated. This chapter will examine the mechanisms by which accelerating, retarding, and water reducing admixtures affect E_a . The results show that low- and high-range water reducing admixtures slightly lower E_a of a mixture, and retarding and accelerating admixtures lower E_a more significantly.

3.1. INTRODUCTION

Chemical admixtures are commonly used in a concrete mixture to improve the workability and strength, reduce water content (and sometimes the cementitious materials content), delay or accelerate hydration, entrain air, improve durability, or to modify other relevant concrete properties. Accelerators, retarders, and water reducers (low-, mid-, and high-range) are present in most concrete mixtures used today. As a result, the effects of these admixtures on the hydration, strength, permeability, durability, workability, and other concrete properties have been extensively investigated. However, the temperature sensitivity of mixtures with different admixtures has not been thoroughly studied.

In order to properly model the progress of hydration, the temperature sensitivity of concrete hydration must be characterized. Previous studies^{1,2,3} have shown the usefulness of the Arrhenius equation⁴ (Equation 3-1) to describe the temperature sensitivity of hydration:

$$k = A \cdot e^{\frac{-E_a}{RT}} \quad \text{Equation 3-1}$$

where R = natural gas constant (8.314 J/mol/K), T = temperature (K) at which reaction occurs, k = rate of heat evolution (W), A = proportionality constant (same units as k), and E_a = activation energy (J/mol).

The activation energy (E_a) gives a measure of temperature sensitivity of a reaction. Glasstone⁴ defines the experimental (or apparent) activation energy (E_a) as the activation energy obtained experimentally by plotting the natural log of reaction rate versus the inverse of the reaction temperature. E_a may be determined by multiplying the negative of the slope of the best-fit line through $\ln(k)$ versus $1/T$ by R . This interpretation of E_a is used to characterize the reaction rate of cementitious materials at various temperatures.

The methods to determine E_a from isothermal calorimeter results³, the variability of the test method³, and the effects of different cement types^{2,3} on E_a have been reported previously. However, the effects of different chemical admixtures on E_a have not been studied. A thorough investigation of the chemical admixtures that can affect E_a is warranted. The results will provide the basis for a future mechanistic-empirical model for E_a in concrete. This study examines the effects of accelerators, retarders, and water

reducers on the hydration of a concrete mixture. The results from isothermal calorimetry will be used to assess the effect of each of these admixtures on the E_a of the cementitious system.

3.2. REVIEW OF CHEMICAL ADMIXTURE MECHANISMS

3.2.1. LOW-RANGE WATER-REDUCING AND RETARDING ADMIXTURES

ASTM C 494⁵ Type A and D low-range water reducing admixtures (LRWR) and water-reducing and retarding admixtures (WRRET) are commonly used in concrete to provide a minimum of 5% water reduction and some delay in set time to the mixture (typically 1-3.5 hours)⁵. These admixtures are commonly composed of lignosulfonates, sugars, hydroxycarboxylic acids, and calcium and sodium salts⁶. Typical dosages range from 0.15%-0.60% of the total cementitious content of the concrete mixture. Water reducing admixtures are hydrophilic surfactants which, when dissolved in water, deflocculate and disperse particles of cement. The molecules of these admixtures tend to be adsorbed to the surface of cement particles so that a negatively charged end group of the molecule is thrust into solution. These admixtures make the surface of the cement particles hydrophilic, which helps with dispersion^{6,7}. Dispersion of particles leads to an increase in the reaction rate of certain phases in the cement, since more surface area is available to react. In addition, the molecules in these admixtures (lignosulfonates, sugars, etc.) typically retard the hydration to some degree.

The type, molecular composition, and amount of the chemicals in these admixtures determine the amount of dispersion of the cementitious material, and the

degree of retardation of the system. Taylor⁷ reports that organic retarders (such as those investigated here) are readily adsorbed on the surfaces of growing particles of hydration products. However, there is some disagreement as to the mechanism of retardation. Some suggest that retarders either bond to the surface of cement particles so they cannot react⁸, or they poison the surface of the hydration products so they cannot grow⁹. Sugars, the most effective retarders, may alter the formation process, surface area, and density of C-S-H¹⁰.

3.2.2. HIGH-RANGE WATER-REDUCING ADMIXTURES

ASTM C 494 Type F high-range water-reducing admixtures, or superplasticizers, provide a 12%-40% water reduction in a mixture. They are long-chain polymers that are strongly adsorbed on the surface of the cement particles⁶. The two main classes of high-range water-reducing admixtures are sulfonated melamine or naphthalene-formaldehyde condensates (NHRWR) and polycarboxylates (PCHRWR). Melamine and naphthalene-based high-range water-reducing admixtures work by a mechanism similar to the low-range water-reducing admixtures (dispersion and ionic repulsion). Polycarboxylate high-range water-reducing admixtures also disperse cement particles, but additionally use the mechanism of steric repulsion¹¹. The effect of high-range water-reducing admixtures on the heat of hydration of cement is mainly due to physical factors, such as dispersion, rather than chemical interaction⁶ such as changes in solubility of the various components of the cementitious system.

3.2.3. CALCIUM NITRATE-BASED ACCELERATORS

Accelerators for setting and hardening are often used during cold weather placements, or where high early strength is desired. They are typically added in dosages of 1–3% (0.3-2.3% by mass of admixture solids) by mass of cementitious material. These admixtures tend to accelerate the hydration rate of the alite (C_3S) phase of cement⁶. Bhatt¹ showed that calcium chloride, calcium formate, and calcium nitrate all accelerated the C_3S hydration. The addition of calcium chloride to a mixture of C_3S may produce C-S-H that is less dense, which facilitates the diffusion of ions through the initial, outer C-S-H layer¹². It has also been reported that calcium nitrite-based accelerators speed up the reaction of the aluminates¹³. However, the specific mechanism of this acceleration is unknown.

3.3. EXPERIMENTAL PROGRAM

During this study, isothermal calorimetry was performed on various cementitious pastes at 5, 15, 23, 38, and 60 °C (41, 59, 73, 100, and 140 °F) using an eight channel isothermal conduction calorimeter. The calorimeter was kept in a temperature-controlled room at 21 ± 3 °C. Cement pastes were proportioned using a variety of water-to-cementitious materials ratios (w/cm), and using 250 g of cementitious material. Prior to mixing, materials were kept as close as possible to the room temperature. Pastes were mixed in a kitchen blender for approximately three minutes. Eight tests were run simultaneously in the isothermal calorimeter. Each test sample had a mass of approximately 20 grams. Tests were conducted for durations varying from 44 hours at 60 °C to more than 100 hours at 5 °C.

The following cements conforming to ASTM C150¹⁴ were used: one low-alkali Type I cement (C1), one high alkali Type I cement (C2), one low-alkali Type I/II cement (C6), and two low-alkali Type III cements (C7 and C8). The following supplementary cementing materials (SCM) were used: two ASTM Class F fly ashes¹⁵ (labeled FF1 and FF2 for this study), one ASTM Class C fly ash¹⁵ (labeled FC1 for this study), and one ASTM Grade 120¹⁶ ground granulated blast furnace (GGBF) slag (labeled S1 for this study). Chemical and physical properties of the cementitious materials are summarized in Table 3-1. Cement phases were calculated from x-ray fluorescence data using the Bogue calculations per ASTM C 150¹⁴. The cement phases were also calculated using Rietveld analysis¹⁷.

The following water reducers conforming to ASTM C 494⁵ were used: a Type A glucose-based water-reducer (LRWR), a Type B and D lignosulfonate-based water-reducer/retarder (WRRET), a Type F naphthalene-sulfonate-based HRWR admixture (NHRWR), and a Type F polycarboxylate-based HRWR admixture (PCHRWR). The accelerator used was an ASTM C 494⁵, Type C calcium nitrate-based accelerator. De-ionized water was used for mixing.

3.4. RESULTS AND DISCUSSION

The shape of the hydration curve of the mixtures in the present study is represented by the parameters in the three-parameter model defined in Equation 3-2^{18,19}:

$$\alpha(t_e) = \alpha_u \cdot e^{-\left[\frac{\tau}{t_e}\right]^\beta} \quad \text{Equation 3-2}$$

where $\alpha(t_e)$ = degree of hydration at equivalent age t_e , τ = hydration time parameter (hours), β = hydration shape parameter, and α_u = ultimate degree of hydration. The parameters of the model, α_u , τ , and β , relate to the shape of the hydration curve, and are used to capture the effects of different mixture constituents on the amount of acceleration, retardation, rate of hydration, and degree of hydration of a mixture. α_u correlates with the total amount of heat evolved of a mixture. τ corresponds to the timing of the accelerating portion of the hydration curve. β provides an indication of the rate of hydration. The procedure for determining the parameters in Equation 3-2 have been discussed previously⁴. The results of the calorimetry testing on mixtures with 100% portland cement are shown in Table 3-2, and the mixtures with SCMs and admixtures are shown in Table 3-3. Admixtures dosages are listed as percent solids by mass per of cementitious material. The mixtures are numbered sequentially 1-54. The following sections will examine the effects of various chemical admixtures on these hydration parameters.

3.4.1. EFFECTS OF WATER REDUCING AND RETARDING ADMIXTURES ON HEAT OF HYDRATION

Figure 3-1 shows the effects of different lignosulfonate-based WRRET dosages on the rate of hydration of a mixture of 100% Cement C1. Figure 3-2 shows the effects of different glucose-based LRWR dosages on the rate of hydration of the same mixture. As the dosage of admixture increases, the LRWR slightly extends the dormant period of the hydration. The WRRET extends the dormant period more than the LRWR. The extension of the dormant period with the WRRET is even more pronounced with

Cements C2 and C6, as shown in Figure 3-3 for Cement C2 (Cement C6 not shown). Both admixtures cause the second hydration peak to increase with increasing dosage. The second peak is believed to be caused by the hydration of the C_3A or some other aluminate phase in the system.

The time parameter (τ) and slope parameter (β) from Equation 3-2 can also be used to show the increased delay with WRRET compared to LRWR. τ increases with increasing dosages of WRRET (especially with Cement C2), as shown in Figure 3-4. β increases because the maximum rate of heat evolution increases, or because of a delay in the onset of the accelerating portion of the hydration curve. These trends are shown in Figure 3-5. Note that an increase in β without an increase in τ suggests that the maximum rate of hydration is increasing, as is the case with Cement C2 and PCHRWR. When an increase in β is accompanied by an increase in τ , this means that there is a delay in the onset of the accelerating portion of the hydration curve. This is the case for Cement C1 and C2 with WRRET.

There are two mechanisms responsible for the increase in the height of the second peak, generally associated with C_3A hydration, in the presence of LRWR and WRRET. First, the LRWR is known to have triethanolamine (TEA) as a component. Edmeades and Hewlett⁶ state that triethanolamine will accelerate the hydration of C_3A , and accelerate the formation of ettringite, as well as retard the hydration of C_3S . Second, certain water reducers may slow down the dissolution of anhydrite in the mixture, which results in less SO_4^{2-} available to retard the hydration of C_3A .

The latter effect may also be seen by comparing a mixture with the addition of a Class F and Class C fly ash. FC1 is a Class C fly ash with some reactive aluminate phases and FF2 is a Class F fly ash with little to no reactive aluminate phases. Figure 3-6 shows the effect dosages of WRRET on a mixture of 70% Cement C2 and 30% FC1 and FF2. The addition of WRRET to the mixture with FC1 extends the dormant period and increases the size of the second peak relative to the first peak. When the same treatment is applied to the mixture with FF2, which has no reactive aluminate phases, the dormant period is also extended to a similar degree, but the second hydration peak does not grow as much in relation to the first peak. The increase in the second peak height relative to the first peak is thus related to the combination of reactive aluminate phases and WRRET in a mixture.

The relative changes in the peak height are minor effects compared to the retardation caused by the WRRET. Figure 3-6 and Figure 3-7 show that high dosages of WRRET cause delays that will overshadow other phenomenon in the hydration curve. However, the delay is not consistent across all combinations of cements and SCMs, as can be seen in the following comparison. Figure 3-1 shows that the addition of 0.32% WRRET to cement C1 will cause approximately four hours of delay in the dormant period. The delay for a dosage of 0.35% WRRET and cement C2 is approximately 20 hours, as shown in Figure 3-3. This delay is approximately 24 hours for a mixture of 70% cement C2 and 30% fly ash FC1 with 0.35% WRRET, as shown in Figure 3-6.

In concrete mixtures, the delay associated with a dosage of 0.35% of WRRET should be less than the 16-20 hours shown in Figure 3-6⁵. The extension of the dormant

period is associated with a delay in setting in concrete, which should only be on the order of a few hours at this dosage⁵. This suggests that the extension of the dormant period seen in pastes in isothermal calorimetry with WRRET may be exaggerated. However, Figure 3-8 shows that the dormant period of a concrete (tested in a semi adiabatic calorimeter) is somewhat similar to the paste tested in an isothermal calorimeter; the end of the dormant period in this plot is marked by the point when the concrete temperature begins to rise sharply. The concrete was made using the proportions from Mixture 42 (70% C2, 30% FC1, 0.35% WRRET), with a cementitious materials content of 325 kg/m³ (564 lb/yd³). The semi-adiabatic results presented in Figure 3-8 are corrected for equivalent age, which accounts for the difference in temperature history between the tests. Since the delays in the isothermal calorimeter tests are the same magnitude as delays seen in actual concrete, the activation energies calculated for the admixtures in this study should correlate well with the behavior of these admixtures in concrete.

The mechanisms that control the amount of retardation caused by a WRRET are complex. They depend on the amount of reactive aluminate phases in the cement and SCM, the amount of soluble SO_4^{2-} available to retard these aluminates, the effect of alkalis on the SO_4^{2-} solubility, and the overall effect of a water reducer on the solubility and hydration of the various phases¹³. In spite of these complexities, the effect of a water reducer/retarder on the activation energy of a mixture is relatively straightforward, as discussed in the next section.

3.4.2. EFFECTS OF WATER REDUCING AND RETARDING ADMIXTURES ON E_a

The results of Mixtures 2 to 7, 9, 11, 12, and 20 are shown in Figure 3-9, and can be evaluated to determine the effects of different LRWR and WRRET dosages on different cements. Mixtures 39, 41, 42, 44, 45 and 52 test the effects of WRRET on mixtures with different types of SCMs, and the results are shown in Figure 3-10. Several trends are apparent.

First, increasing the dosage of a LRWR/WRRET decreases the E_a of the system for all mixtures. The glucose-based LRWR reduces E_a less than the lignosulfonate-based WRRET. Part of this reduction is due to the water-reducing properties of the admixtures, and part is due to the retarding properties of the admixture. For example, increasing the w/cm of a mixture has been shown to slightly reduce E_a ²⁰ because the cement is more dispersed and solubilizes more easily. Therefore, some of the reduction in E_a with LRWR and WRRET may be attributed to the increased dispersion with these admixtures. However, WRRET reduces E_a more than LRWR, which indicates that there are additional mechanisms contributing to the reduction in E_a . For example, WRRET reduces E_a from 41,300 J/mol to approximately 25,400 J/mol, while LRWR reduces E_a from 39,000 J/mol to 37,600 J/mol. This is likely due to the amount of retarder in the WRRET.

E_a may approach a lower bound as admixture dosage increases. For example, Figure 3-9 shows E_a of cement C2 with different dosages of WRRET. In this case, E_a levels out at approximately 25,000 J/mol with addition of WRRET above 0.35% by mass. This phenomenon may also be seen in Figure 3-10 for the same mixture with 30%

replacement by mass of FC1. The lower bound for E_a may indicate an excessive dosage of WRRET. This effect was only seen with this cement/admixture combination and remains to be verified for the others at higher admixtures dosages.

Finally, the combination of cement and SCM used in a mixture plays a significant role in the amount of reduction in E_a with a water reducer/retarder. These effects may be seen in the following example. Figure 3-10 shows data for mixtures containing WRRET with 50% GGBF slag (S1) and 50% Cement C2, as well as those containing WRRET with 50% GGBF slag (S1) and 50% Cement C6. The reduction in E_a with increasing admixture dosage is much greater for Cement C6 than Cement C2. Figure 3-7 shows that the dosage of 0.35% of WRRET seems to cause excessive delay in the hydration the mixtures with GGBF slag for cement pastes.

3.4.3. EFFECTS OF HIGH-RANGE WATER-REDUCING ADMIXTURES ON HEAT OF HYDRATION

The addition of a naphthalene-based high-range water-reducing admixture (NHRWR) to a mixture of 100% Cement C6 causes very little retardation, as shown in Figure 3-11. However, the magnitude of the hydration peak increases somewhat with increasing NHRWR dosage. The addition of a polycarboxylate-based high-range water-reducing admixture (PCHRWR) to a mixture of 100% Cement C6 has a similar effect on peak height, but causes slightly more retardation than NHRWR at a dosage of 0.34%, as shown in Figure 3-12. Figure 3-13 shows that the addition of NHRWR or PCHRWR to Type III cement, C8, has virtually the same effect on the rate of hydration as for Type I/II cement, C6. Therefore, the addition of a NHRWR or PCHRWR to a mixture will

generally increase the maximum rate of hydration, but this will not substantially affect the timing of the accelerating portion of the hydration curve. This increase in maximum rate of hydration may be due to the increased dispersion of the cement particles. Like low-range water reducing admixtures, high-range water reducing admixtures (HRWR) improve workability by dispersing the cement particles, but they do not substantially retard the cementitious system (at least when used at normal dosages).

3.4.4. EFFECTS OF HIGH-RANGE WATER REDUCING ADMIXTURES ON E_a

Adding a HRWR to a mixture will slightly reduce E_a with a Type I and Type III cement, as shown in Figure 3-14 and Figure 3-15, respectively. The reduction in E_a due to an increase in HRWR is relatively small (2,000-5,000 J/mol) compared to the reduction associated with a WRRET, and is likely associated with increased dispersion of the cement caused by the HRWR. NHRWR and PCHRWR reduce E_a by roughly the same amount. The exception is Cement C2 with the addition of PCHRWR; in this combination E_a is reduced much more with increasing dosage of admixture.

The effects of fly ash with HRWR on E_a are not plotted, but can be seen in Table 3. Mixture 53 tests the effects of a polycarboxylate-based HRWR on Type III cement (C8). Mixtures 54 and 55 test the same, but with a Class F fly ash (FF2) and Class C fly ash (FC1), respectively, replacing a portion of the cement. The E_a data in Table 3 show that a Class F fly ash slightly lowers E_a , and a Class C fly ash slightly raises E_a , which is in agreement with other research²¹.

NHRWR and PCHRWR appear to alter the hydration of a mixture primarily by dispersion of the cement particles, which is similar to the effect of increasing the w/cm^{20} . These admixtures tend to slightly reduce E_a , which is again similar to the reduction in E_a caused by raising the w/cm^{20} . The effects of high-range water reducers are relatively consistent for mixtures with and without SCMs.

3.4.5. EFFECTS OF CALCIUM NITRATE-BASED ACCELERATING ADMIXTURES ON HEAT OF HYDRATION

The mechanism by which a calcium nitrate-based accelerating admixture promotes the hydration of the cement is poorly understood. Figure 3-16 shows the effects of the addition of a calcium nitrate-based accelerating admixture (ACCL) on a mixture with Cement C2, with C2 and 30% FC1, and with C2 and 20% FF2. ACCL significantly magnifies height of the second peak, which is believed to be due to the aluminate phase. In this example, ACCL actually delays the accelerating portion of the hydration curve when SCMs are used. Figure 3-17 shows the effects of ACCL on mixtures with Cement C6, FF2, and FC1. The behavior is totally different than with Cement C2. First, only the mixture with Cement C2 and FC1 shows some increase in the size of the aluminate peak with the addition of ACCL. And unlike Cement C2, ACCL actually accelerates hydration with Cement C6, shifting the both the calcium silicate and aluminate peaks earlier.

Calcium nitrate-based accelerating admixtures are believed to function by upsetting the dissolution and reaction between C_3A and gypsum⁶. Therefore, the amount

of aluminate, available SO_3 , and the amount of ACCL seem to play a large role in the timing of the hydration of the aluminate peak. The aluminate peak is also accelerated by the addition of the WRRET (a lignosulfonate-based water reducer/retarder), as discussed earlier. The growth in the second peak with the WRRET is believed to be due to the acceleration of the C_3A hydration due to the dispersion of the cement particles, and by the presence of triethanolamine. It is possible that the mechanisms of the WRRET and calcium nitrate-based accelerating admixtures are related. Clearly the mechanisms of accelerators are more complex than can be explained purely from calorimeter testing. Fortunately, the effects of ACCL on E_a are fairly consistent, even if the precise mechanism of reaction is poorly understood.

3.4.6. EFFECTS OF CALCIUM NITRATE-BASED ACCELERATING ADMIXTURES ON E_a

The addition of a calcium nitrate-based accelerator (ACCL) to a mixture will generally reduce E_a , as shown in Figure 3-18. Samples of 100% Cement C2, 80% Cement C2 with 20% FF2, and 70% Cement C2 with 30% FC1 all show a decrease in E_a with the addition of 0.74% by mass of cementitious material of ACCL. The addition of the same amount of ACCL to a mixture of 80% Cement C6 with 20% FF2, and 70% Cement C6 with 30% FC1 very slightly decreases in E_a . An increase in the dosage of ACCL from 0.74% to 1.30% lowers E_a slightly more. This trend suggests that the magnitude of the change in E_a depends on the type of cement and SCM in the mixture, and the dosage of ACCL. More testing would be needed to determine the precise shape of the trend with increasing ACCL dosage because the interactions between admixture,

cement, and SCM appear to be more complex than can be covered with seven tests. However, the present data provide enough information to suggest that ACCL generally lowers E_a .

3.4.7. EFFECTS OF AIR-ENTRAINING ADMIXTURES ON HYDRATION AND E_A

Air-entraining admixtures (AEA) are typically added to concrete mixtures at dosages of 0.04-0.20% by mass of cementitious materials. Mixtures with 0.19% air entraining admixture (AEA), 100% cement C2, and 100% cement C6 were tested to determine the effects of AEA on the heat of hydration and E_a . The heat of hydration and E_a were not significantly altered by the addition of AEA. These results are shown in Appendix B.

3.5. CONCLUSIONS

In this chapter the effect that chemical admixtures have on the activation energy (E_a) of concrete mixtures is evaluated. Isothermal calorimeter tests were performed on 55 paste samples at 5, 15, 23, 38, and 60 °C. Several trends were identified. Low-range water reducers, high-range water reducers, accelerators, and retarders tend to reduce E_a of a mixture. Air-entraining admixture (AEA) has little effect on E_a . E_a varies with the chemistry of the cementitious phases, and this affects the impact of particular admixtures. However, the changes in E_a due to cement-admixture interactions are minor compared to the effects of the chemical admixtures themselves. For example, glucose-based LRWR, polycarboxylate-based HRWR, and naphthalene-sulfonate-based HRWR slightly lower E_a . ACCL and lignosulfonate-based WRRET lower E_a more significantly. E_a drops as

the dosage of water reducing admixture increases, and as the dosage of retarding or accelerating admixture increases. LRWR, PCHRWR, and NHRWR reduce E_a for mixtures with and without SCMs. The order of magnitude of the reduction in E_a is comparable to the effects of lowering the w/cm of the mixture.

3.6. REFERENCES

1. Bhatti, J.I., "A Review of the Application of Thermal Analysis to Cement-Admixture Systems," *Thermochimica Acta*, V. 189, 1991, pp. 313-350.
2. Schindler, A.K., "Effect of Temperature on Hydration of Cementitious Materials", *ACI Materials Journal*, V. 101, No. 1, Jan.-Feb., 2004, pp. 72-81.
3. Poole, J.L., K.A. Riding, K.J. Folliard, M.G.C. Juenger, and A.K. Schindler "Methods of Activation Energy Calculation for Portland Cement," *ACI Materials Journal*, V. 104, No. 1, Jan.-Feb., 2007, pp. 303-311.
4. Glasstone, S., K.J. Laidler, and H. Eyring, *The Theory of Rate Processes: The Kinetics of Chemical Reactions, Viscosity, Diffusion, and Electrochemical Phenomena*. McGraw-Hill Book Company, Inc. New York, 1941, 611 pp.
5. ASTM C 494, "Standard Specification for Chemical Admixtures for Concrete," Annual Book of ASTM Standards, V. 04.01., ASTM International, West Conshohocken, PA., 2005, 10 pp.
6. Edmeades, R.M. and P.C. Hewlett, "Cement Admixtures," Lea's Chemistry of Cement and Concrete, 4th ed., ed. P.C. Hewlett, Arnold Publishers, New York, 1998, p 837-901.

7. Taylor, H.F.W., Cement Chemistry, 1st ed. Academic Press Limited, London, 1990, 475 pp.
8. Young, J.F. “A Review of the Mechanisms of Set Retardation in Portland Cement Pastes Containing Organic Admixtures”, *Cement and Concrete Research*, V. 2, No. 4, 1972, pp. 415-433.
9. Thomas, N.L. and J.D. Birchall, “The Retardation Action of Sugars on Cement Hydration,” *Cement and Concrete Research*, V. 13, No. 6, 1983, pp. 830-842.
10. Juenger, M.C.G. and H.M. Jennings, “New Insights into the Effects of Sugar on the Hydration and Microstructure of Cement Pastes,” *Cement and Concrete Research*, V. 32, 2002, pp 393-399.
11. Uchikawa, H., S. Hanehara, and D. Sawaki, “The Role of Steric Repulsive Force in the Dispersion of Cement Particles in Fresh Paste Prepared with Organic Admixture” *Cement and Concrete Research*, V. 27, No. 1, 1997, pp. 37-50.
12. Juenger, M.C.G., P.J.M. Monteiro, E.M. Gartner, and G.P. Denbeaux, “A Soft X-Ray Microscope Investigation Into the Effects of Calcium Chloride on Tricalcium Silicate Hydration,” *Cement and Concrete Research*, V. 35, 2005, pp 19-25.
13. Sandberg, P. and Roberts, L., “Cement-Admixture Interactions Related to Aluminate Control”, *Journal of ASTM International*, V. 2, No. 6, June 2005, pp.6-13.
14. ASTM C 150, “Standard Specification for Portland Cement,” *Annual Book of ASTM Standards*, V. 04.01., ASTM International, West Conshohocken, PA., 2002, 8 pp.

15. ASTM C 618, “Standard Specification for Coal Ash and Raw or Calcined Natural Pozzolans for Use in Concrete,” Annual Book of ASTM Standards, V. 04.01., ASTM International, West Conshohocken, PA., 2003, 3 pp.
16. ASTM C 989, “Standard Specification for Ground Granulated Blast-Furnace Slag for Use in Concrete and Mortars,” Annual Book of ASTM Standards, V. 04.01., ASTM International, West Conshohocken, PA., 2005, 5 pp.
17. Scrivener, K.L., T. Füllmann, E. Gallucci, G. Walenta, and E. Bermejo, “Quantitative Study of Portland Cement Hydration by X-Ray Diffraction/Rietveld Analysis and Independent Methods”, *Cement and Concrete Research*, V. 34, 2004, pp 1541-1547.
18. Pane, I., and W. Hansen, “Concrete Hydration and Mechanical Properties under Nonisothermal Conditions,” *ACI Materials Journal*, V. 99, No. 6, Nov.-Dec, 2002, pp. 534-542.
19. Schindler, A.K., and K.J. Folliard, “Heat of Hydration Models for Cementitious Materials”, *ACI Materials Journal*, V. 102, No. 1, Jan.-Feb., 2005, pp. 24-33.
20. Poole, J.L., “The Effects of Cement Chemistry and Water-Cement Ratio on Activation Energy,” PhD Dissertation, Chapter 2, The University of Texas at Austin, Austin, TX, 2007, pp 6-37.
21. Poole, J.L., “The Effects of Supplementary Cementing Materials on Activation Energy,” PhD Dissertation, Chapter 4, The University of Texas at Austin, Austin, TX, 2007, pp 69-108.

Table 3-1: Chemical and Physical Properties of Cement and SCMs

	Cements					Fly Ash			GGBFS
	C1	C2	C6	C7	C8	FF1	FF2	FC1	S1
SiO ₂ (%)	20.45	19.18	20.77	19.72	20.3	51.69	51.69	37.83	34.48
Al ₂ O ₃ (%)	5.43	5.34	3.88	5.27	4.85	24.81	24.81	19.83	11.35
Fe ₂ O ₃ (%)	2.01	2.3	3.73	2.02	3.56	4.22	4.22	6.17	0.67
CaO (%)	64.51	63.17	64.5	64.08	63.94	13.12	13.12	23.13	41.73
MgO (%)	1.15	1.09	1.01	1.22	0.82	2.29	2.29	4.62	7.32
Na ₂ O (%)	0.14	0.12	0.18	0.13	0.07	0.18	0.18	1.74	0.14
K ₂ O (%)	0.56	0.95	0.6	0.52	0.66	0.84	0.84	0.057	0.38
Na ₂ O Eq. (%)	0.51	0.75	0.575	0.472	0.504	0.733	0.733	1.778	0.390
SO ₃ (%)	3.35	3.2	2.38	4.4	3.44	0.46	0.46	1.50	1.88
LOI (%)	1.80	4.1	2.67	1.95	1.71	0.23	0.23	0.67	0.83
Free CaO (%)	1.66	4.0	2.8	1.33	1.89	-	-	-	-
CaO (%)**	0.0	0.0	0.0	0.0	0.0	-	-	-	-
C ₃ S (%)*	58.29	63.1	66.5	60.2	58.5	-	-	-	-
C ₃ S (%)**	61.2	61.0	55.7	64.6	54.0	-	-	-	-
C ₂ S (%)*	14.65	7.4	9.4	11.2	14.0	-	-	-	-
C ₂ S (%)**	16	15.6	21.1	11.8	21.7	-	-	-	-
C ₃ A (%)*	10.99	10.3	4.0	10.6	6.8	-	-	-	-
C ₃ A (%)**	13.1	9.6	4.0	12.4	5.7	-	-	-	-
C ₄ AF (%)*	6.12	7.0	11.4	6.2	10.8	-	-	-	-
C ₄ AF (%)**	3.5	6.0	10.7	4.0	10.2	-	-	-	-
Gypsum(%)*	5.7	5.44	4.76	7.48	5.85				
C $\bar{\text{S}}$ H ₂ (%)**	1.4	0.4	0.0	2.4	0.0	-	-	-	-
C $\bar{\text{S}}$ H _{0.5} (%)**	1.5	1.2	2.7	2.4	3.7	-	-	-	-
C $\bar{\text{S}}$ (%)**	0.6	0.7	0.7	0.6	0.6	-	-	-	-
K ₂ SO ₄ (%)**	1.4	1.0	0.7	0.8	1.3				
CaCO ₃ (%)**	0.8	3.6	2.5	0.7	1.5				
Blaine Fineness ¹	350	391	365	552	539	147	166	348	332

* = Bogue Calculations, ** = Rietveld Analysis, ¹ m²/kg

Table 3-2: Three-Parameter Curve Fit Values for All Mixtures

Mix/ Cement	w/cm	Admix. (ASTM)	Dose by Mass	α_u	β	τ (hours)					H_u (J/g)	E_a (J/mol)
						5°C	15°C	23°C	38°C	60°C		
1-C1	0.44	-	0.00%	0.796	0.988	53.06	25.12	14.27	6.77	3.25	481	38,950
2-C1	0.44	Ty A	0.07%	0.817	0.972	54.10	26.73	14.94	7.07	2.99	481	40,450
3-C1	0.44	Ty A	0.15%	0.805	1.004	53.78	26.34	14.29	7.36	3.41	481	38,350
4-C1	0.44	Ty A	0.30%	0.817	1.021	55.55	29.15	15.49	8.32	3.75	481	37,550
5-C1	0.44	Ty B&D	0.08%	0.797	0.997	51.09	25.50	14.75	6.98	3.27	481	38,450
6-C1	0.44	Ty B&D	0.16%	0.816	0.999	52.89	27.35	15.81	8.66	4.01	481	35,700
7-C1	0.44	Ty B&D	0.32%	0.815	1.071	64.23	32.39	20.01	14.95	5.95	481	31,450
8-C2	0.40	-	0.00%	0.656	0.888	56.44	26.62	16.66	7.41	2.87	482	41,300
9-C2	0.40	Ty B&D	0.35%	0.637	2.059	65.78	49.68	33.08	17.99	11.43	482	25,650
10-C2	0.40	Ty B&D	0.52%	0.655	2.367	89.67	70.94	46.11	24.23	16.33	482	25,400
11-C2	0.44	-	0.00%	0.648	0.968	57.06	28.07	16.52	6.74	3.25	482	40,550
12-C2	0.44	Ty B&D	0.35%	0.617	2.227	69.34	55.81	32.62	18.59	10.18	482	28,150
13-C2	0.44	Ty F-PC	0.18%	0.634	1.111	52.69	24.60	14.03	7.62	3.49	482	37,250
14-C2	0.44	Ty F-PC	0.34%	0.618	1.289	51.22	28.43	14.91	8.01	4.55	482	34,250
15-C2	0.44	Ty F-N	0.78%	0.655	1.175	52.98	27.19	16.11	7.73	3.69	482	37,300
16-C2	0.44	Ty F-N	1.25%	0.643	1.174	60.40	29.03	16.84	9.13	3.69	482	38,350
17-C2	0.44	Ty C	0.74%	0.680	0.970	49.93	26.66	14.49	7.24	3.97	482	35,750
18-C2	0.44	AEA	0.19%	0.734	0.867	57.06	27.03	15.02	7.05	2.87	482	41,550
19-C6	0.44	-	0.00%	0.741	0.826	36.27	19.43	12.22	5.21	2.57	463	37,550
20-C6	0.44	Ty B&D	0.35%	0.734	1.269	52.56	28.45	23.68	13.19	8.65	463	24,750
21-C6	0.44	Ty F-PC	0.18%	0.711	0.940	33.87	17.15	10.55	5.17	2.53	463	36,150
22-C6	0.44	Ty F-PC	0.34%	0.690	1.025	35.45	18.47	11.13	6.61	2.63	463	35,550
23-C6	0.44	Ty F-NS	0.78%	0.716	0.924	31.90	16.27	10.15	6.06	2.69	463	33,700
24-C6	0.44	Ty F-NS	1.25%	0.723	0.917	33.36	17.25	10.85	5.91	2.52	463	35,500
25-C6	0.44	AEA	0.19%	0.696	0.864	34.41	17.25	10.14	6.22	2.59	463	35,150
26-C7	0.40	-	0.00%	0.744	0.829	32.90	17.12	9.81	6.30	2.08	485	37,350
27-C7	0.32	Ty F-PC	0.55%	0.639	1.025	33.20	15.40	9.32	5.62	2.30	485	36,050
28-C7	0.32	Ty F-NS	0.94%	0.659	0.898	29.38	13.58	8.15	4.73	2.11	485	35,750
29-C7	0.32	Ty F-NS	0.94%	0.705	0.816	34.09	16.53	10.55	5.32	3.23	485	32,800
		Ty B&D	0.16%									
30-C8	0.44	-	0.00%	0.891	1.013	46.75	21.92	12.28	5.88	2.62	474	40,050
31-C8	0.32	Ty F-PC	0.55%	0.726	1.054	35.50	19.28	10.95	5.90	1.96	474	40,000
32-C8	0.32	Ty F-NS	0.94%	0.694	1.054	30.73	15.36	9.24	4.49	2.24	474	36,550
33-C8	0.32	Ty F-N	0.94%	0.713	1.004	34.47	18.72	11.26	5.05	2.59	474	36,750
		Ty B&D	0.16%									

PC-Polycarboxylate-based HRWR; N – Naphthalene Sulfonate-based HRWR;
AEA – Air-Entraining Admixture

Table 3-3: Three-Parameter Curve Fit Values for Mixtures with SCMs

Mix/ Cement	w/cm	Admix. / SCM	Dose by Mass	α_u	β	τ	τ	τ	τ	τ	H_u J/g	E_a (J/mol)
						5°C	15°C	23°C	38°C	60°C		
34-C2	0.44	FF2	20%	0.748	0.909	74.33	28.17	16.88	8.409	4.48	433	38,200
35-C2	0.44	FF2	30%	0.746	0.783	53.38	28.04	19.39	9.19	4.71	410	33,950
36-C2	0.44	FC1	30%	0.755	0.962	64.75	33.40	19.27	9.495	5.63	462	34,450
37-C2	0.44	S1	50%	0.793	0.650	86.97	53.28	26.88	13.42	5.23	472	39,100
38-C2	0.44	Ty C	1.76%	0.777	0.979	57.59	26.83	19.92	10.68	5.21	433	32,550
		FF2	20%									
39-C2	0.44	Ty B&D	0.16%	0.728	1.799	111.6	52.66	42.14	23.02	9.02	433	33,750
		FF2	30%									
40-C2	0.44	Ty C	0.74%	0.842	0.920	63.09	33.92	25.43	14.03	7.07	462	30,050
		FC1	30%									
41-C2	0.44	Ty B&D	0.16%	0.682	1.485	85.01	47.31	34.14	18.36	11.38	462	28,050
		FC1	30%									
42-C2	0.44	Ty B&D	0.35%	0.744	1.592	106.2	70.71	47.34	25.93	13.73	462	29,100
		C1	30%									
43-C2	0.44	Ty C	0.74%	1.032	0.546	122.1	74.71	46.57	16.58	7.82	472	40,100
		S1	50%									
44-C2	0.44	Ty B&D	0.08%	0.743	0.715	101.0	49.81	29.80	12.64	5.44	472	41,050
		S1	50%									
45-C2	0.44	Ty B&D	0.35%	0.730	1.431	125.1	73.42	56.87	23.12	10.21	472	35,600
		S1	50%									
46-C6	0.44	FF2	20%	0.742	0.768	44.95	31.67	14.10	7.39	3.54	417	36,950
47-C6	0.44	FC1	30%	0.743	0.780	59.93	28.54	21.30	10.11	4.34	449	36,050
48-C6	0.44	S1	50%	0.810	0.650	86.97	53.28	26.88	13.42	5.23	462	39,100
49-C6	0.44	Ty C	0.74%	0.800	0.703	45.59	24.38	14.50	7.37	3.37	417	36,400
		FF2	20%									
50-C6	0.44	Ty C	0.74%	1.110	0.497	113.7	56.50	37.07	17.93	8.81	449	35,550
		FC1	30%									
51-C6	0.44	Ty C	1.30%	1.164	0.508	99.29	48.92	28.89	15.22	8.05	417	34,850
		FF2	20%									
52-C6	0.44	Ty B&D	0.35%	1.773	0.501	258.1	214.1	170.0	101.2	44.95	462	25,000
		S1	50%									
53-C8	0.32	Ty F-PC	0.55%	0.654	0.943	56.08	26.72	17.76	8.63	3.63	470	37,650
54-C8	0.32	Ty F-PC	0.55%	0.678	1.098	39.89	19.52	12.05	6.08	3.00	426	35,850
		FF2	20%									
55-C8	0.32	Ty F-PC	0.55%	1.068	0.546	122.1	74.71	46.57	16.58	7.82	456	40,100
		FC1	30%									

PC-Polycarboxylate-based HRWR; N – Naphthalene Sulfonate-based HRWR

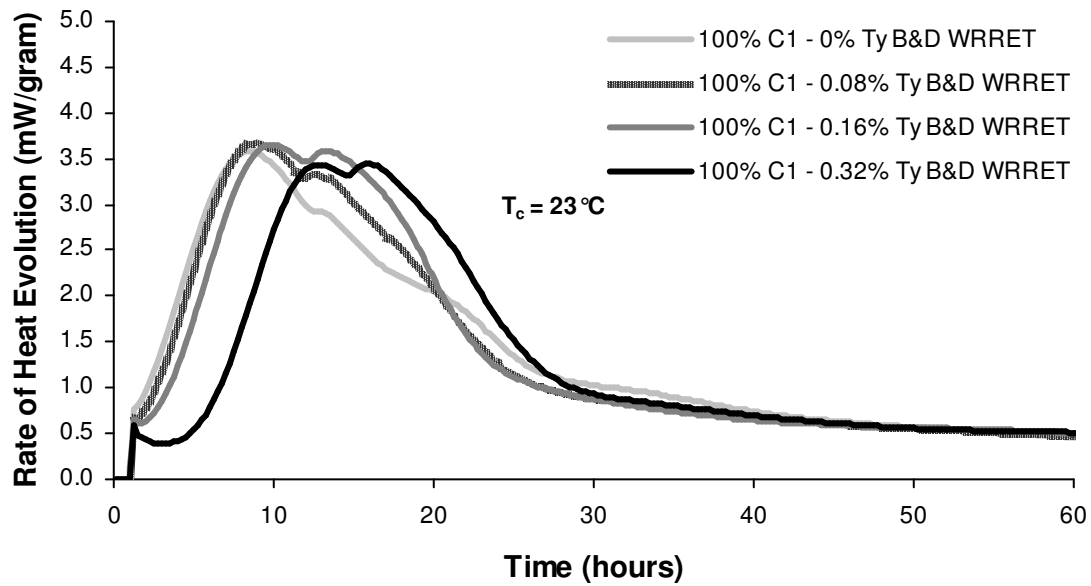


Figure 3-1: Rate of Heat Evolution (Per Gram of Cementitious Material) for 100% Cement C1 (Paste) with Different Dosages of WRRET at 23°C (73°F)

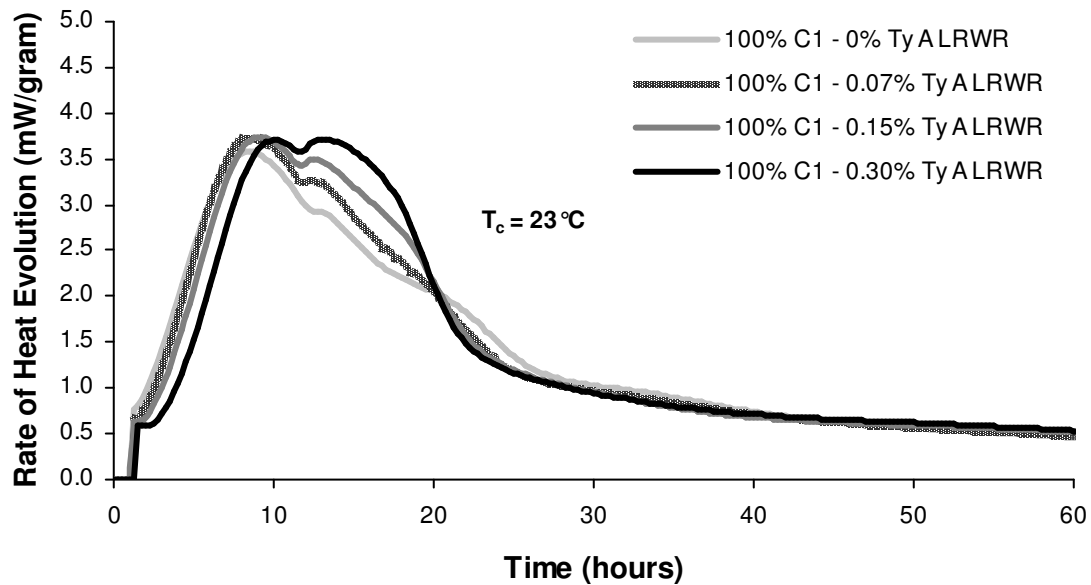


Figure 3-2: Rate of Heat Evolution (Per Gram of Cementitious Material) for 100% Cement C1 (Paste) with Different Dosages of LRWR at 23°C (73°F)

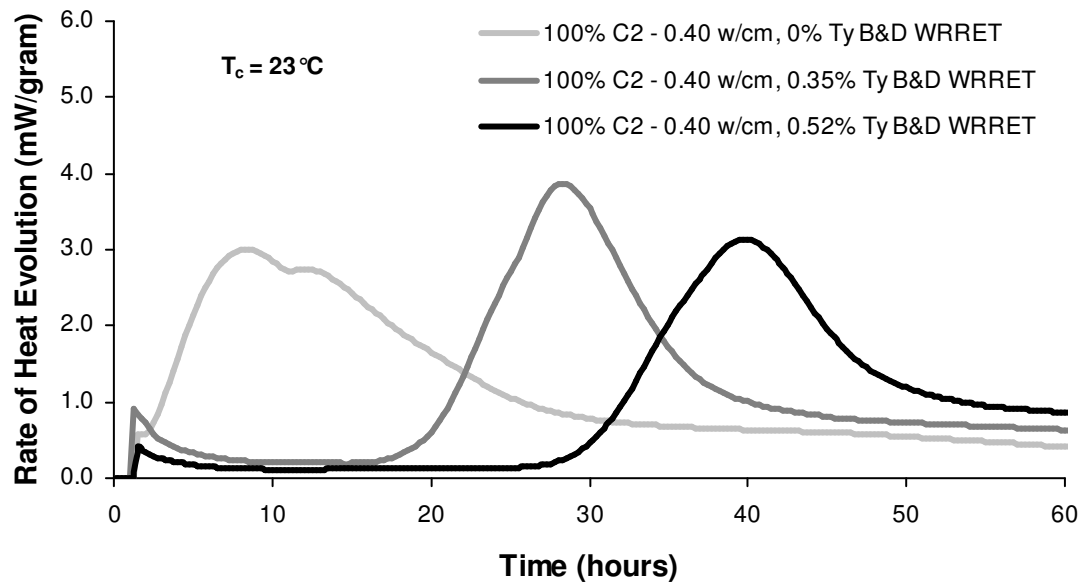


Figure 3-3: Rate of Heat Evolution (Per Gram of Cementitious Material) for 100% Cement C2 (Paste) with Different Dosages of WRRET at 23°C (73°F)

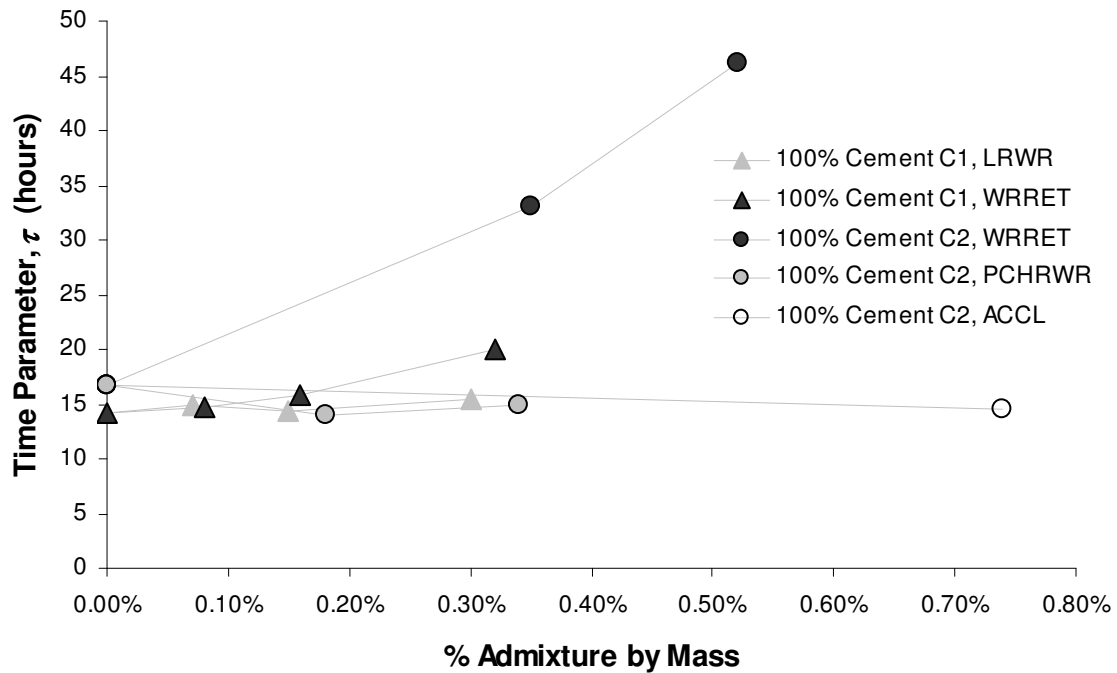


Figure 3-4: Changes in Time Parameter (τ) with LRWR, WRRET, ACCL, and PCHRWR

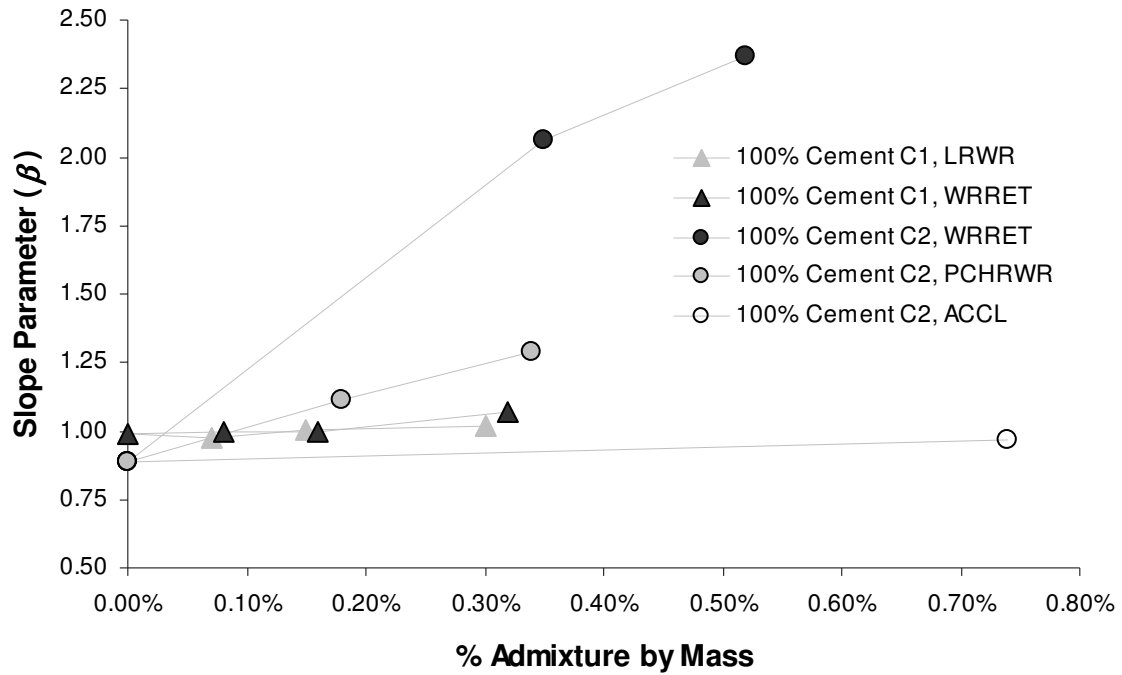


Figure 3-5: Changes in Slope Parameter (β) with LRWR, WRRET, ACCL, and PCHRWR

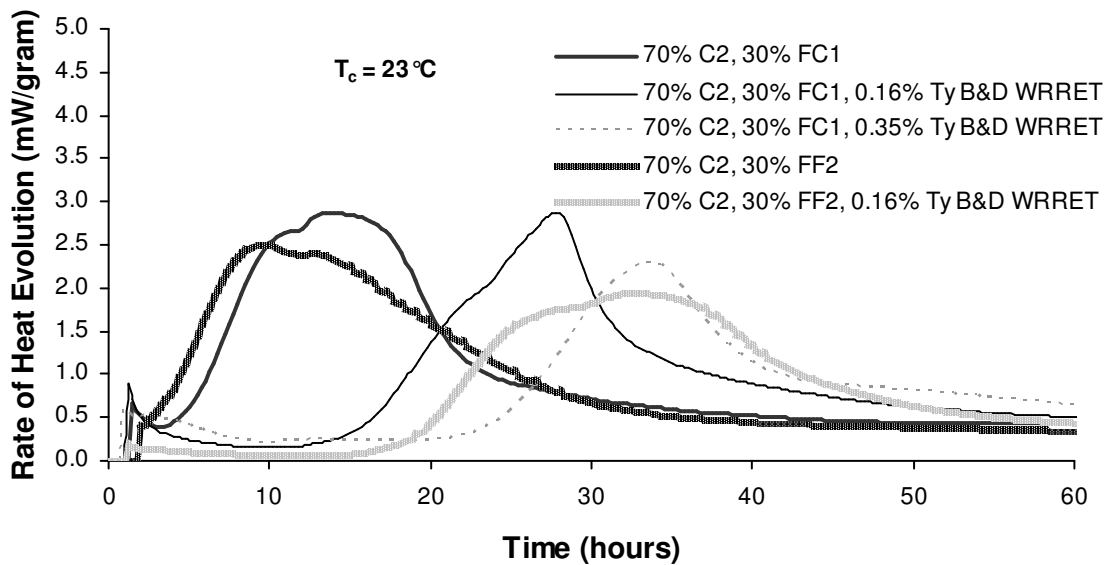


Figure 3-6: Rate of Heat Evolution (Per Gram of Cementitious Material) for Paste Mixtures with WRRET and Cement C2 at 23 °C (73 °F)

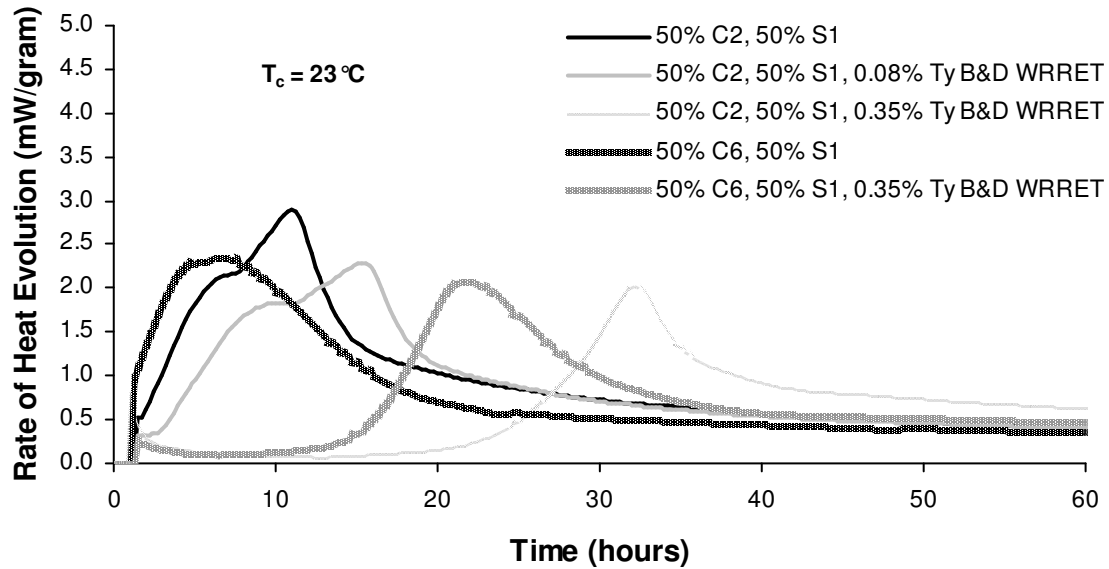


Figure 3-7: Rate of Heat Evolution (Per Gram of Cementitious Material) for Paste Mixtures of 50% Cements C2 and C6 with 50% GGBF Slag

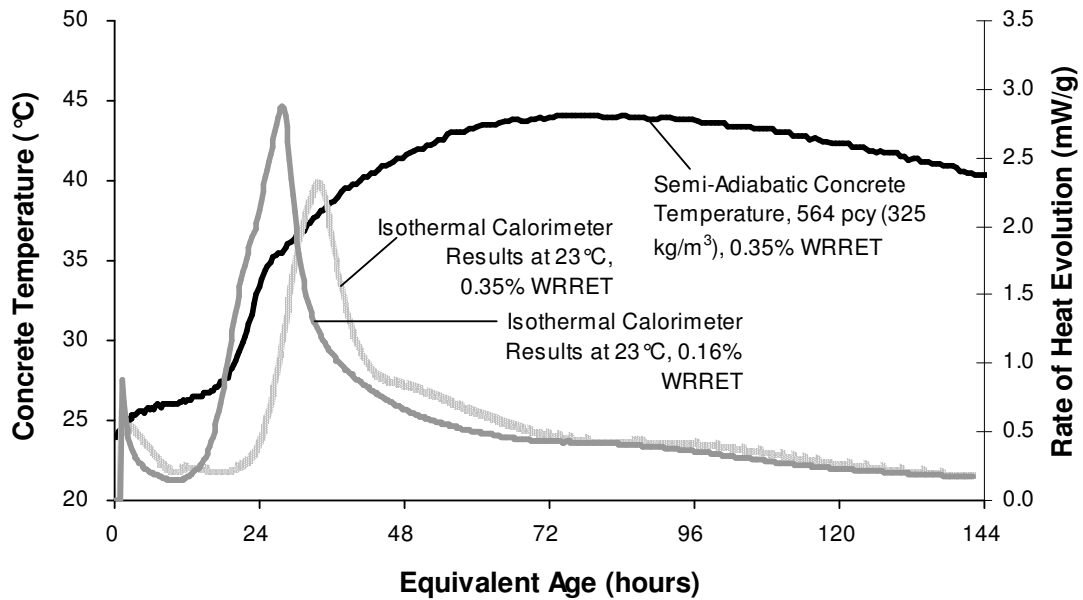


Figure 3-8: Comparison Between Isothermal and Semi-Adiabatic Calorimetry for Mixture 40 and 41 (y-axis on the left is for the semi-adiabatic data and on the right is for the isothermal data)

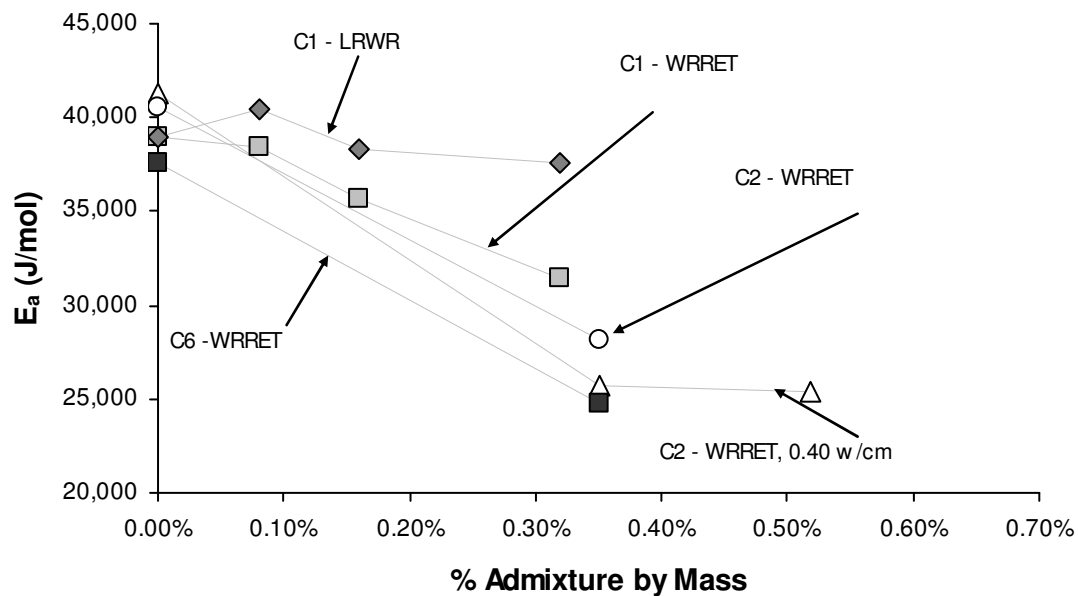


Figure 3-9: E_a v. LRWR and WRRET Dose, 100% Cement

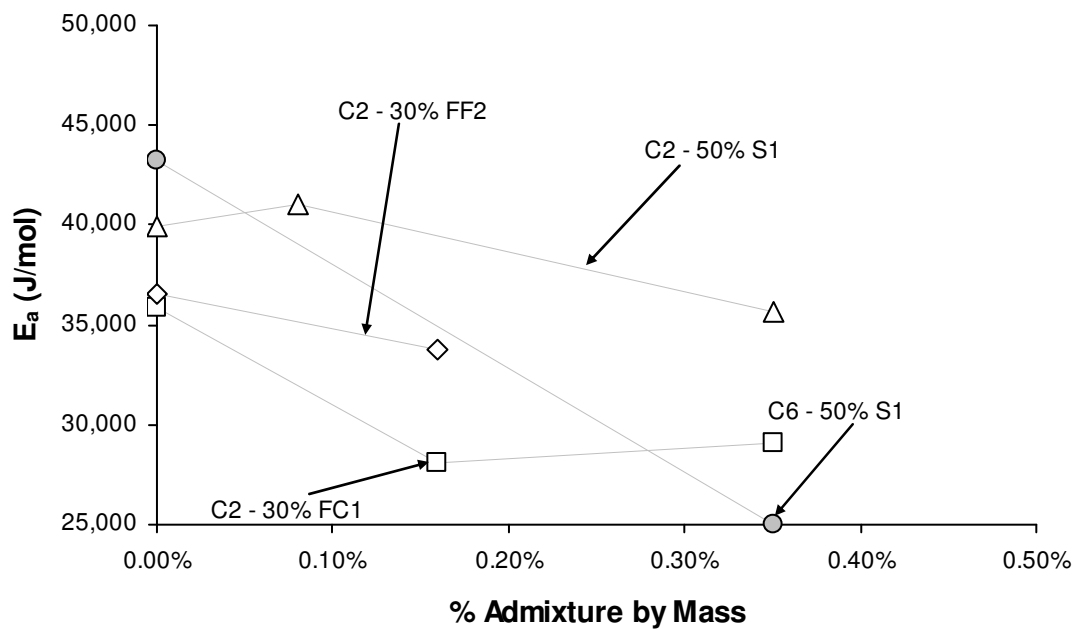


Figure 3-10: E_a v. WRRET with Various % SCM

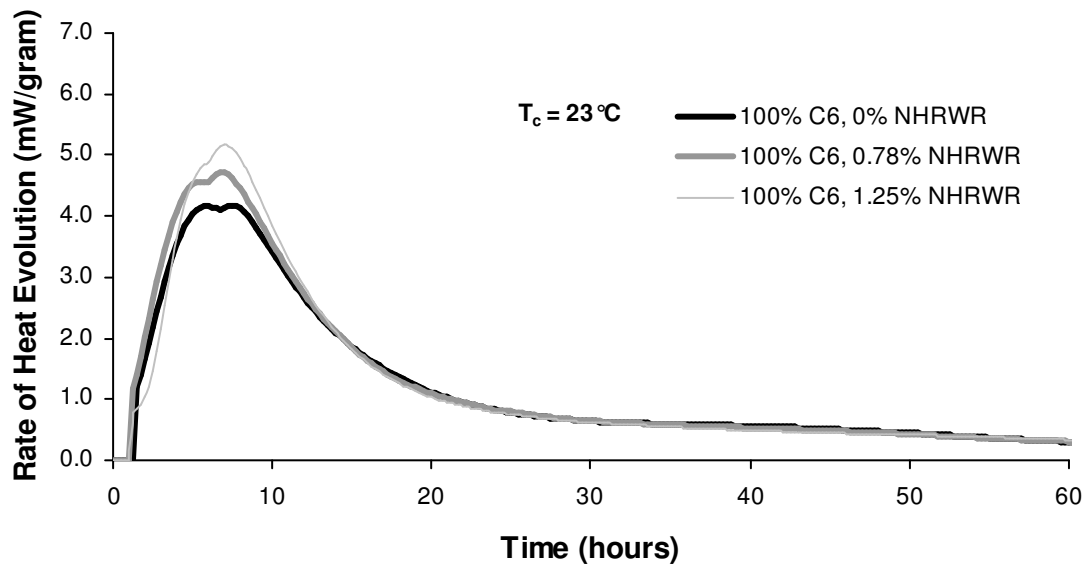


Figure 3-11: Rate of Heat Evolution (Per Gram of Cementitious Material) for Paste Mixtures of 100% Cement C6 with NHRWR at 23 °C (73 °F)

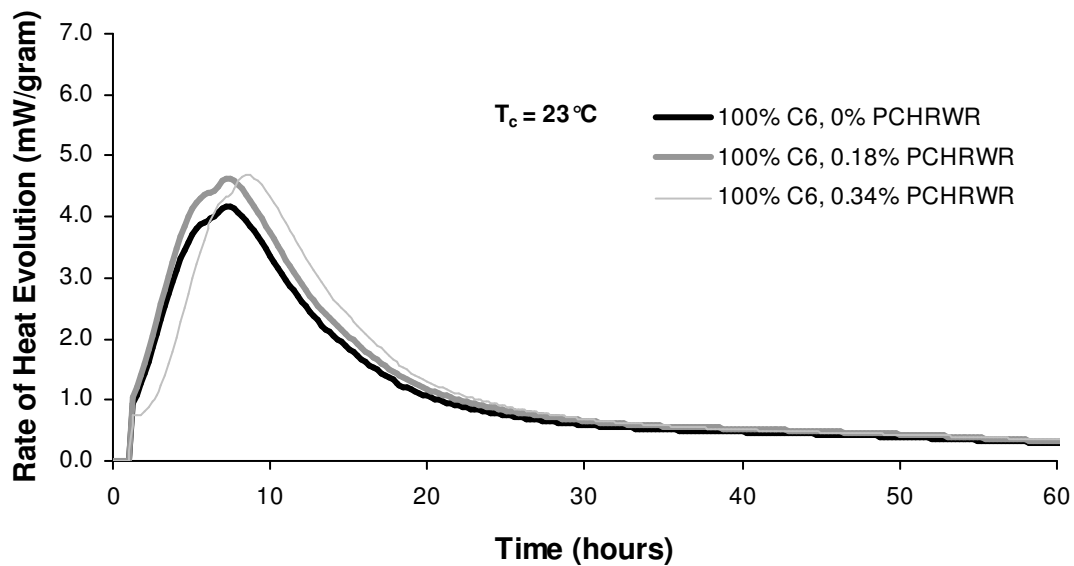


Figure 3-12: Rate of Heat Evolution (Per Gram of Cementitious Material) for 100% Cement C6 with PCHRWR at 23 °C (73 °F)

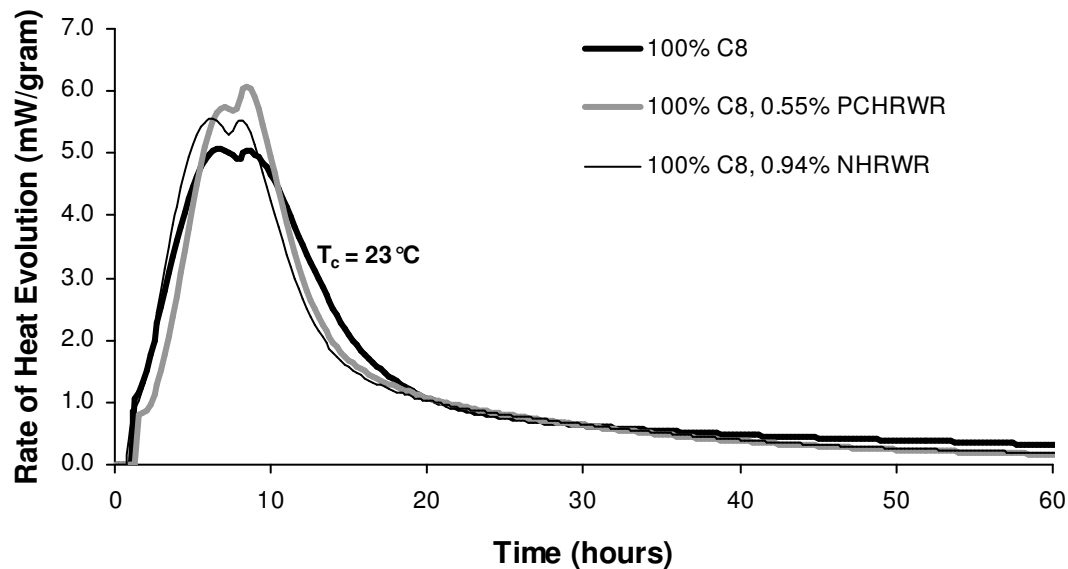


Figure 3-13: Rate of Heat Evolution (Per Gram of Cementitious Material) for Paste Mixtures of 100% Cement C8 with NHRWR and PCHRWR at 23 °C (73 °F)

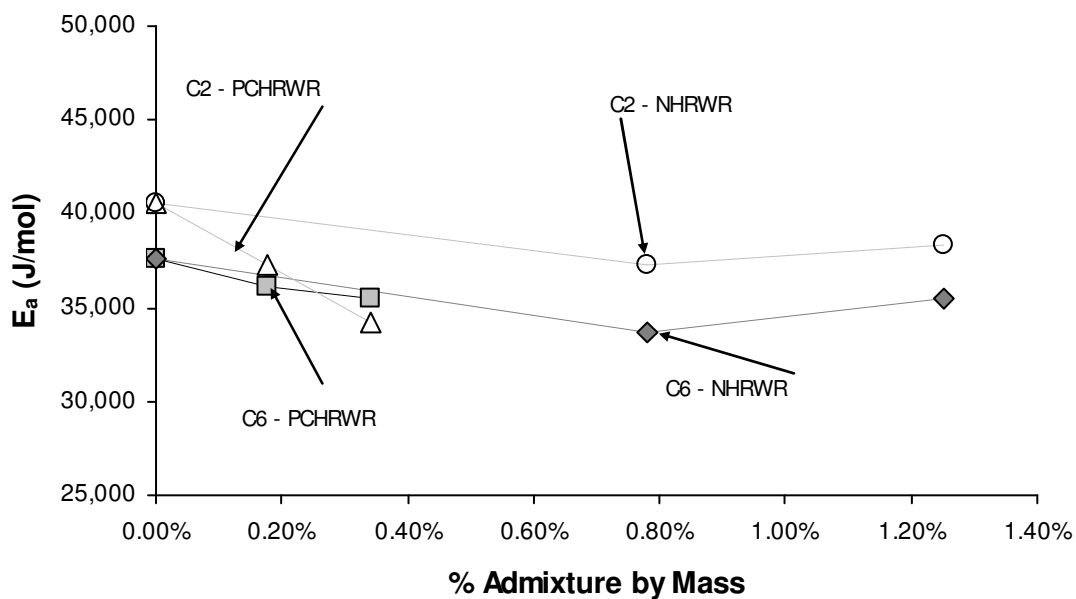


Figure 3-14: E_a v. NHRWR and PCHRWR Dose, 100% Type I Cement (Cement C2 and C6)

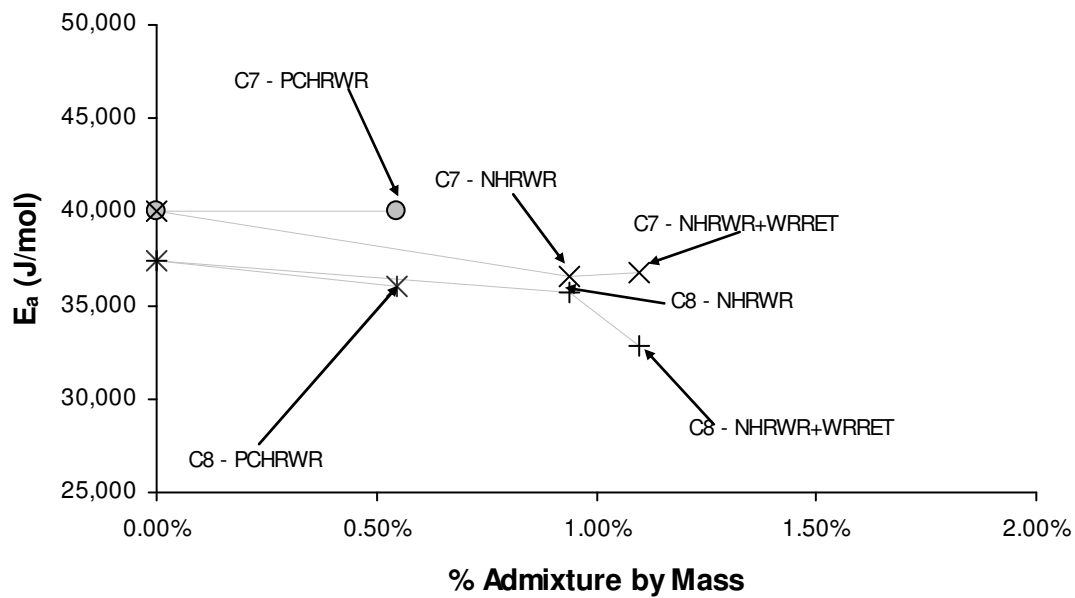


Figure 3-15: E_a v. NHRWR and PCHRWR Dose, 100% Type III Cement (Cement C7 and C8)

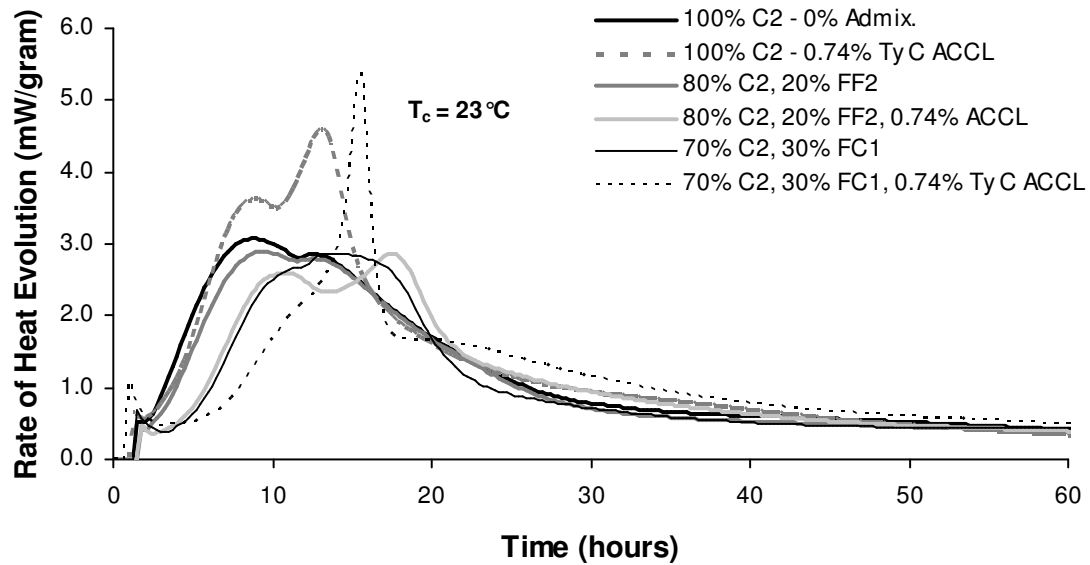


Figure 3-16: Effects of ACCL and WRRET on Cement C2 with Fly Ash FF2 and FC1 (Paste) at 23 °C (73 °F)

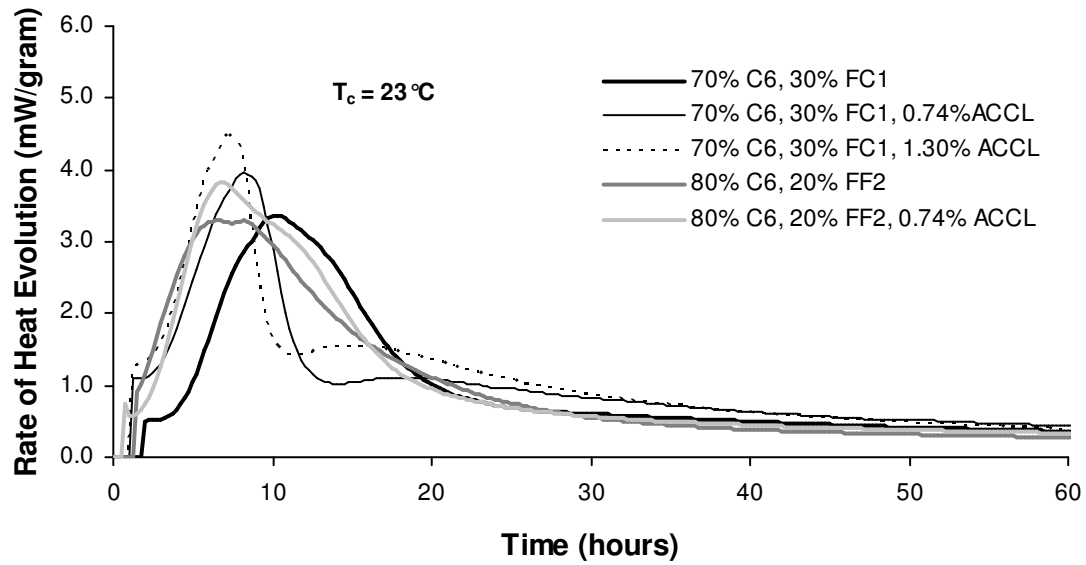


Figure 3-17: Effects of ACCL on Cement C6 with Fly Ash FF2 and FC1 (Paste) at 23 °C (73 °F)

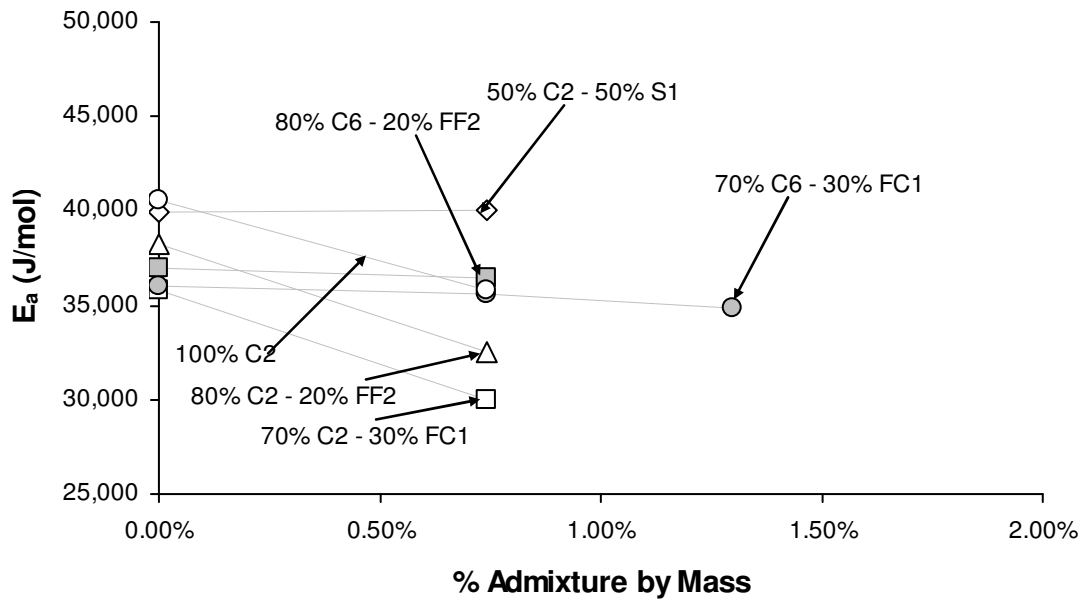


Figure 3-18: E_a v. ACCL Dose, Various % SCM

CHAPTER 4. THE EFFECTS OF SUPPLEMENTARY CEMENTING MATERIALS ON ACTIVATION ENERGY

Previous research has shown the validity of the Arrhenius equation to accurately characterize the progress of hydration of cement. In the Arrhenius equation, the selection of an activation energy (E_a) is required to define the temperature sensitivity of the reaction. This chapter will examine the effects of different supplementary cementing materials (SCMs) and ternary blends on E_a . The study examines four fly ashes, one ultra-fine fly ash, one silica fume, and one ground-granulated blast-furnace (GGBF) slag with several different cements. Also, the hydration of mixtures with SCMs and additional alkalis are tested. The results are compared to existing values in literature and are used to select the appropriate mechanisms to best describe the effects of SCMs on E_a . GGBF slag and high-CaO fly ashes generally raise E_a , and low-CaO fly ashes and silica fume generally lower E_a . The type of cement in the mixture also affects E_a of a mixture. The results generally confirm the trends seen in previous research, but provide more insight into the mechanisms responsible for these differences in behavior.

4.1. INTRODUCTION

Supplementary cementing materials (SCMs) such as fly ash, ground-granulated blast-furnace (GGBF) slag, and silica fume are an integral part of most concrete mixtures for a variety of reasons. They may lower the heat produced by the mixture, improve the workability, increase strength, and improve resistance to alkali-silica reaction (ASR), sulfate attack, and delayed ettringite formation (DEF). Accurate characterization of the

temperature sensitivity of cement- SCM combinations is important to determine the progress of hydration, and hence the rate of development of temperature and mechanical properties. The temperature sensitivity of hydration is best described by the Arrhenius equation and the concept of activation energy (E_a), as shown in Equation 4-1¹:

$$k = A \cdot e^{\frac{-E_a}{RT}} \quad \text{Equation 4-1}$$

where R = natural gas constant (8.314 J/mol/K), T = temperature (K) at which reaction occurs, k = rate of heat evolution (W), A = proportionality constant (same units as k), and E_a = activation energy (J/mol).

The effects of SCMs on the mechanical properties of concrete are well known. These include benefits in mechanical properties due to the pozzolanic reactions of fly ash, slag, and silica fume. The addition of SCMs to a mixture should affect the rate of heat evolution and E_a , depending on the dosage, physical properties, and chemical properties of the SCM. Class F fly ash and silica fume are not expected to greatly alter the rate of heat evolution, other than through dilution of cement. However, the addition of a Class C fly ash or GGBF slag may alter the rate of heat evolution more significantly, since these materials have a significant amount of reactive aluminate phases. The temperature sensitivity of these SCM in a concrete mixture has been the subject of limited research. Much of the research in this area^{2,3,4} has relied on E_a values derived from ASTM C 1074, which uses mortar cube strength as an index of the rate of hydration. Few results for E_a determined from calorimetry have been presented, and isothermal calorimetry has been shown to be a better method than mortar strength for determining E_a ⁶. Ma and Brown⁷

reported E_a values determined from isothermal calorimetry for mixtures of a Type I cement and a low CaO fly ash, GGBF slag, and silica fume. E_a was 26,700 J/mol for a mixture of 83% Type I cement and 17% Class F fly ash (CaO=3.57%), 30,400 J/mol for a mixture of 92.5% Type I cement and 7.5% silica fume, and 49,300 J/mol for a mixture of Type I cement and GGBF slag. In a literature review of the subject, Moranville-Regourd⁵ reported a value of 49,100 J/mol for a mixture of 50% GGBF slag and 50% cement, and a value of 56,000 for a mixture of 70% GGBF slag and 30% CEM III/B cement. Other calorimetry research^{8,9} focused on the computational procedures for determining E_a . However, a systematic study to determine the mechanisms by which SCMs affect E_a has not been undertaken.

This research presents results from 51 mixtures that compare the E_a values of cement pastes with replacements of fly ash, GGBF slag, fly ash with silica fume, and fly ash with ultra-fine fly ash. Also, several mixtures are tested with the addition of alkalis to the paste as NaOH. Seventeen of these results were presented as part of a study⁸ on the appropriate computational procedure to determine E_a , and are provided again here for continuity. The results provide a large dataset for E_a of mixtures with SCMs published to date, and are used to identify the mechanisms that best explain the variations in E_a values when SCMs are used.

4.2. RESEARCH SIGNIFICANCE

Accurate characterization of the progress of hydration is necessary to predict temperature gradients, maximum concrete temperature, thermal stresses, and relevant

mechanical properties of concrete. An accurate estimate of the activation energy (E_a) is required to define the temperature sensitivity of the reaction. Supplementary cementing materials (SCMs) are commonly used in concrete mixtures. However, E_a , as determined by isothermal calorimetry for mixtures containing SCMs has not been adequately examined. This chapter presents a comprehensive set of E_a results for cement pastes with different supplementary cementing materials. The results are used to identify the mechanisms that describe the temperature sensitivity of mixtures with SCMs.

4.3. EXPERIMENTAL PROGRAM

During this study, isothermal calorimetry was performed on various cementitious pastes at 5, 15, 23, 38, and 60 °C (41, 59, 73, 100, and 140 °F) using an eight channel isothermal conduction calorimeter. The calorimeter was kept in a temperature-controlled room at 21 ± 3 °C. Cement pastes were proportioned using a water-to-cementitious materials ratio (w/cm) of 0.44, and using 250 g of cementitious material. Prior to mixing, materials were kept as close as possible to the room temperature. Pastes were mixed in a kitchen blender for approximately three minutes. Eight tests were run simultaneously in the isothermal calorimeter. Each test sample had a mass of approximately 20 grams. Duration of the tests ranged from 44 hours at 60 °C to over 100 hours at 5 °C. The isothermal calorimeter test procedure and the computational procedure for determining E_a have been discussed previously⁸. The same methods are used to determine the E_a values for each mixture in this test program.

Two Type I cements (C2 and C3) and one low-alkali Type I/II cement (C6) conforming to ASTM C150¹⁰ were used. The following SCMs were used: two ASTM C 618 Class F fly ashes¹¹ (FF1 and FF2), two ASTM C 618 Class C fly ashes¹¹ (FC1 and FC2), one ultra-fine fly ash (UFFA), one ASTM C 989 Grade 120 ground-granulated blast-furnace slag¹² (S1), and one silica fume (SF). De-ionized water was used for mixing. NaOH was added to the mixing water of several mixtures to increase the equivalent alkali content to 0.85%. Chemical and physical properties of the materials are summarized in Table 4-1. Cement phases were calculated from x-ray fluorescence data using the Bogue calculations per ASTM C 150¹⁰. Cement phases were also calculated from quantitative x-ray diffraction (QXRD) data using Rietveld analysis¹³.

The shape of the hydration curve of the mixtures in the present study is represented by the parameters in the three-parameter model defined in Equation 4-2^{14,15}:

$$\alpha(t_e) = \alpha_u \cdot e^{-\left[\frac{\tau}{t_e}\right]^\beta} \quad \text{Equation 4-2}$$

where $\alpha(t_e)$ = degree of hydration at equivalent age t_e , τ = hydration time parameter (hours), β = hydration shape parameter, and α_u = ultimate degree of hydration. The procedure for determining the parameters in Equation 4-2 have been discussed previously^{4,8}.

4.4. RESULTS AND DISCUSSION

The curve fit parameters (α_u , τ , and β), H_u , and E_a are summarized for 51 mixtures in Table 4-2 and Table 4-3. The maximum heat of hydration (H_u) was

calculated for the mixtures in this study using relationships developed in previous research¹⁴. Table 4-2 shows the results for mixtures with Class F and Class C fly ash, and Table 4-3 shows the results for mixtures with GGBF slag, ultra-fine fly ash, silica fume, and ternary blends. Several tests are marked with an asterisk (*) to indicate that NaOH was added to increase the equivalent alkali content of the mixture to 0.85%. H_u was calculated based on an independent, fractional model for heat of hydration of cementitious materials from previously published research.¹⁴ Results at 23 °C are presented in this chapter, and tests at 5 °C, 15 °C, 38 °C, and 60 °C are included in Appendix C.

The chemistry of the cement was found to have an effect on E_a independent of the presence of SCM¹⁶. Cements C2 and C6 were chosen for investigation because of the differences quantities of aluminate phases in each cement. Cement C2 has a higher C_3A content (9.6%) than Cement C6 (4.0%), while Cement C6 has a higher C_4AF content (10.7% versus 6.0%). Cement C3 was chosen for investigation because of its inherently high alkali content (0.86% Na_2O_{eq}). Figure 4-1 shows the heat evolution curves of each of the control mixtures with 100% cement (Mixtures 1-3). The differences in cement chemistry clearly affect the shape of the hydration curve for each the cements For example, Cement C2 has a lower maximum rate of heat evolution, and the accelerating portion of the hydration curve is delayed, while Cement C6 has a higher maximum rate of heat evolution, and the accelerating portion of the hydration curve is not delayed. Cements C2 and C6 have two clearly distinguishable peaks (corresponding to the C_3S and C_3A hydration); these two peaks overlap more for cement C3. The size and timing of

these peaks are important to consider when evaluating the effects of SCMs on the heat of hydration. In spite of significant differences in the shape of the heat evolution curves, the E_a for these three cements are very similar (Table 4-2). As discussed in Chapter 2¹⁶, cement chemistry alone does not have a strong effect on E_a with modern cements. However, the next sections will show that the weighted percentage of reactive phases, total alkalis, and type of sulfate (anhydrite, hemihydrate, or gypsum) present in the total cementitious system may have a larger effect on E_a , especially when SCMs are involved.

4.4.1. EFFECTS OF CLASS F FLY ASH ON HEAT EVOLUTION AND E_A

Figure 4-2, Figure 4-3 and Figure 4-4 show the effect of different replacement percentages of FF1 on the heat evolution of mixtures with Cement C2, C3, and C6 respectively. The figures show that the addition of a low-CaO fly ash uniformly reduces the heat of hydration of the mixture as the dosage of fly ash is increased. The shape of the hydration curve remains the same with the addition of FF1 for all cements. The same dilution effect on heat evolution that is seen with FF1 may also be seen with FF2 in Figure 4-5 and Figure 4-6 with Cements C2 and C6, respectively. Several trends are exhibited by FF1 and FF2. First, the accelerating period of hydration is delayed slightly with higher additions of both fly ashes (i.e. a longer induction period). The delay is roughly the same for all cements and fly ashes. Next, there is a difference in the relative heights of the hydration peaks between FF1 and FF2. FF2 appears to affect the shape of the heat evolution curve more than FF1. The second peak seems to be slightly larger with Cement C2 at 30% and 40% replacement with FF2 compared to the control with

100% cement C2 (Figure 4-5). While there are clearly differences in the heat evolution with FF2, differences in the shape of the hydration curve will be much more significant with the addition of Class C fly ash and GGBF slag since these have more hydraulic reactivity than Class F fly ashes.

Figure 4-7 compares the E_a of mixtures with different replacement percentages of FF1 (CaO = 0.7%) with three different cements (C2, C3, and C6). The results are shown in Table 4-2 as Mixtures 4 to 7 and 9 to 12. The addition of FF1 reduces E_a for all of the cements. The change in E_a is approximately the same for all of the cements. The reduction in E_a with FF1 is similar in magnitude (3,000-7,000 J/mol) to reductions seen with increases in w/cm¹⁶. This evidence suggests that dilution of cement may be the primary mechanism for the reduction in E_a with fly ash FF1.

Figure 4-8 compares the effects of different replacement percentages of FF2 (CaO = 13.1%) with two different cements (C2 and C6) on E_a . The results are shown in Table 4-2 as Mixtures 13 to 18. As with FF1, the addition of FF2 reduces E_a for Cement C2. However, the addition of FF2 to Cement C6 has no effect on E_a . For both cements, the change in E_a from FF2 is less than the change in E_a from FF1. Like FF1, FF2 reduces E_a predominately through dilution of the cement. However, FF2 has a higher CaO content than FF1. The small amount of growth in the second hydration peak confirms that the FF2 is slightly more reactive than FF1. This may explain the differences in E_a trends.

4.4.2. EFFECTS OF CLASS C FLY ASH ON HEAT EVOLUTION AND E_a

Figure 4-9 and Figure 4-10 show the effects of different replacement percentages of FC1 on the heat evolution of mixtures with Cement C2 and C6, respectively. The results are shown in Table 4-2 as mixtures 25 to 27 and 29 to 32. Several trends may be seen in the graphs. First, increasing replacement of FC1 and FC2 causes a delay in the onset of the accelerating stage of hydration with both cements. Next, Figure 4-9 shows an increase in the height of the second hydration peak with the addition of FC1 (a high-CaO fly ash) to Cement C2. This increase is much less noticeable for Cement C6, shown in Figure 4-10. The second peak is believed to be due to the hydration of the aluminate phases in the mixture.

Figure 4-11 and Figure 4-12 show the effects of different replacement percentages of FC2 on the heat evolution of mixtures with Cement C2 and C6. The height of the second peak is much greater for Cement C2 than for Cement C6 for this fly ash. However, with 30-40% replacement of Cement C6 with FC2, the height of the second peak relative to the first peak increases similar to mixtures with FC1

Figure 4-13 compares E_a with different replacement percentages of FC1 (CaO = 23.1%) and two different cements (C2 and C6). The results are shown in Table 4-2 as Mixtures 19 to 24. The addition of FC1 reduces E_a for cement C2 at a 20% replacement. The same addition of FC1 to cement C6 causes no change in E_a .

Figure 4-14 compares E_a with different replacement percentages of FC2 (CaO=28.9%) with Cement C2, C3, and C6. The results are shown in Table 4-2 as Mixtures 25 to 27 and 29 to 32. The addition of FC2 to cement C2 reduces E_a .

Interestingly, E_a is lower at 20% replacement than at 30 and 40% replacement. 30% FC2 with Cement C3 causes no change to E_a . The same fly ash with cement C6 causes E_a to slightly increase as replacement percentage increases.

4.4.3. EFFECTS OF GGBF SLAG ON HEAT EVOLUTION AND E_A

Figure 4-15 and Figure 4-16 show the effects of GGBF slag (S1) on the heat evolution of mixtures with Cement C2 and C6. The onset of the accelerating portion of the hydration curve is not delayed with the addition of S1 to Cement C2 or C6. The first peak height is reduced in proportion to the replacement percentage of S1. The second peak is very clearly defined for Cement C2 and is very poorly defined for cement C6. The timing of the sharp peak (presumably the aluminate hydration^{17,18} switches places with the smoother peak at 60 °C (140 °F) for Cement C2, as shown in Figure 4-17. The smoother peak at 60 °C (presumably the silicate hydration) grows as S1 replacement percentage increases. Unlike Cement C2, the addition of S1 to Cement C6 does not magnify the aluminate peak at 23 °C (73 °F) (Figure 4-16). However, the aluminate peak does become more pronounced with Cement C6 at 60 °C (140 °F), as shown in Figure 4-18.

Figure 4-19 compares E_a of mixtures with different replacement percentages of S1 with Cement C2 and C6. The results are shown in Table 4-3 as Mixtures 33 to 42. S1 decreases E_a at 30 and 40% replacement only but has no effect at higher replacement levels. S1 significantly increases E_a with Cement C6.

4.4.4. EFFECTS OF ALKALI CONTENT ON HEAT EVOLUTION AND E_a IN PASTES WITH SCM

The addition of NaOH to a paste is intended to approximate the effects of a cement with higher alkali content. However, this is an imperfect treatment, because the alkalis in cement are often bound in the various crystalline phases, and may increase the solubility of these phases; adding NaOH in the mixing water may not have the same effect¹⁶. This treatment, in essence, tests the effects of increased pore solution pH on hydration rather than testing the effects of a cement with a higher internal alkali content. However, it may have the consequence of also testing the effects of dissolving the gypsum in the cement. This has been shown previously for cements without SCM¹⁶.

Mixtures 6, 8, 26, and 28 show the effects of alkali content on heat of hydration and E_a for mixtures with Class F and Class C fly ash. The addition of alkalis as NaOH reduces the height of both peaks in the rate of heat evolution curve for the mixture with FF1, but the timing is relatively unchanged as shown in Figure 4-20. Adding alkalis as NaOH shifts the timing of both peaks slightly earlier for the mixture with FC2, also shown in Figure 4-20. The difference is fairly small, but, as further examination will show, it suggests that the addition of NaOH affects the dissolution of gypsum, and does not truly test the effects of pore solution alkalinity on E_a .

E_a increases slightly as alkali content is increased with the addition of NaOH, as shown in Table 4-2 for Mixtures 6, 8, 26, and 28. NaOH may affect the dissolution of gypsum, rather than an increase in the pore solution pH¹⁹. Figure 4-20 supports this hypothesis, so this may be the mechanism by which NaOH alters E_a . Further testing is necessary to isolate the effects on E_a of alkalis on the solubility of the crystalline phases

of the cement and SCM. However, these results suggest that the interaction between the NaOH, gypsum, and aluminates will affect E_a of a mixture. The next section will explain these interactions further.

4.4.5. RETARDATION OF HYDRATION WITH CLASS C FLY ASH AND GGBF SLAG

Changes in the shape of the hydration curve and changes in E_a with Class C fly ash and GGBF slag are likely related. Mechanisms for the shape of the hydration curve will likely apply to trends in E_a . Previous sections showed that Cement C2 behaved differently than Cement C6 with Class C fly ash. For example, cement C2 with Class C fly ash had a large increase in hydration peak height, and E_a was not affected. Cement C6 did not have such large increase in peak height with Class C fly ashes, but E_a increased with increasing replacement percentage. The following section addresses these differences.

The amount of acceleration or retardation of a mixture is quantified in Equation 4-2 as the time parameter τ . This parameter will be used to examine the delays in heat evolution seen with Class C fly ash and GGBF slag. τ for Cement C2, C3, and C6 was measured with different combinations of SCM type and replacement percentage. Figure 4-21, Figure 4-22, and Figure 4-23 show the variation in τ with Cement C2, C3, and C6, respectively, for isothermal tests at 23 °C. The figures show that τ increases with replacement percentage, and increases with increasing reactivity of the SCM. S1 gives the largest increase in τ . The increases in τ for Cement C2 and C3 are similar to each

other, and Cement C6 has the largest increase in τ . This suggests that retardation due to SCM replacement is increased in cement C6 compared to Cement C2 and C3.

The shape of the hydration curve often gives an indication of the causes of retardation. Figure 4-24 compares the rate of heat evolution of mixtures with cements C2, C3, and C6 with 30% FC2. The second hydration peak, associated with the aluminate phase, is higher with Cement C2 and C3 than with Cement C6. This suggests that the crystalline aluminate phases in this fly ash (FC2) seem to react more readily with Cement C2 and C3 than C6.

It is also interesting to note that the hydration peak in Figure 4-24 is sharpest for Cement C2, less sharp with Cement C3, and smooth for Cement C6. This difference is likely due to the differences in alkali, SO_4^{2-} , and C_3A contents of the cements. Cement C2 is a high alkali (0.75% $\text{Na}_2\text{O}_{\text{eq}}$), high C_3A cement (9.6%), C3 is a very high alkali (0.86% $\text{Na}_2\text{O}_{\text{eq}}$), low C_3A cement (5.3%) and cement C6 is a low alkali (0.57% $\text{Na}_2\text{O}_{\text{eq}}$), low C_3A (4.0%) cement. Table 4-1 shows the amount of soluble SO_4^{2-} (gypsum - $\text{CaSO}_4 \cdot 2\text{H}_2\text{O}$, hemihydrate - $\text{CaSO}_4 \cdot 0.5\text{H}_2\text{O}$, anhydrite - CaSO_4 , and arcanite - K_2SO_4) content of the cements (calculated using Rietveld analysis). Cement C2 has 3.3% soluble SO_4^{2-} , C3 has 9.4% soluble SO_4^{2-} , and Cement C6 has 5.6% soluble SO_4^{2-} . It is assumed that the reactive phase in the SCMs is some sort of aluminate phase (e.g., C_3A , $\text{C}_4\text{A}_3\hat{\text{S}}$) and will thus be sensitive to the gypsum content of the cement. These differences in cement chemistry may explain why FC2 behaves differently with different cements, and will be discussed next.

The alkali content, gypsum content, and amount of reactive aluminates play a key role in the shape of the hydration curve. It is known that cements with high aluminate contents require more gypsum than cements with low aluminate contents, so one would expect that Cement C2 needs more gypsum than C3 and C6. Lerch¹⁷ reported that for cements with equal aluminate contents, those with higher alkali contents tended to consume gypsum more rapidly than those with low alkali contents, so Cement C2 should need more gypsum than C6; however, it actually has the lowest soluble SO_4^{2-} content of these three cements. Since reactive SCMs provide additional reactive aluminates to the system, they increase the soluble sulfate requirement. Therefore, it is possible that C2 will not have enough SO_4^{2-} available to properly retard any additional aluminates contributed by the SCMs. This is why SCMs retard hydration more with Cement C6.

These results indicate that the soluble sulfate content of the mixture combined with the alkali content of the mixture dictates the degree to which the hydration of the aluminate phases is delayed. Lerch¹⁷ showed the presence of a sharp hydration peak with high C_3A cements (with no SCMs), and a smooth curve with low C_3A cements, similar to the cements in Figure 4-24. SO_4^{2-} (typically added as gypsum) was shown to affect the timing and rate of this sharp peak in similar manner to the effect of increasing the dosage and reactivity of the SCM. These trends have also been reported by Sandberg and Roberts¹⁸ in mixtures with SCMs. It has also been observed that the presence of alkali sulfates will affect the timing of the hydration peaks in the system,^{18,20} and that²¹ the type

of alkali bound in the crystalline lattice of C_3A may affect the rate of solubility of the phase.

Clearly, the amount and solubility of the SO_4^{2-} in the cement will affect the rate of hydration and E_a . The alkalis in the cement will affect the hydration as well. To fully understand this interaction, accurate information is needed on the quantity, solubility and reactivity of the crystalline and glassy phases in the SCMs. Unfortunately, CaO is the only index readily available to measure reactivity of the fly ash, and little information is available for slag and silica fume. Further study is needed to determine the precise nature of the interactions between cement chemistry, SCM chemistry, and retardation of hydration. In spite of this, given the ranges of E_a reported here (32,800-41,100 J/mol), the CaO content of fly ash is actually a useful index of the changes in E_a with different fly ashes and different cement chemistries. Fly ashes with low CaO contents tend to lower E_a , and fly ashes with high CaO contents tend to raise E_a .

4.4.6. EFFECTS OF SILICA FUME AND ULTRA-FINE FLY ASH (UFFA) ON E_A AND THE RATE OF HEAT EVOLUTION

Silica fume and ultra-fine fly ash (UFFA) are very small particles and are often used to produce concrete with very low permeability and very high strength. However, their hydration behavior and effects on E_a differ significantly. Previous research²² suggests that the addition of silica fume to a mixture will promote the hydration of C_3S by providing preferential nucleation sites for C-S-H. Silica fume may also adsorb Ca^{2+} ions from the pore solution and may lower the SO_4^{2-} content, which can accelerate the hydration of C_3A and C_4AF ²³. Figure 4-25 through Figure 4-28 show the heat evolution

for cement and fly ash mixtures at 23 °C (73 °F) with and without silica fume (Mixtures 45 to 51). The addition of silica fume increases the slope of the accelerating portion of the hydration curve of the binary mixtures. Also, silica fume increases the height of the first peak of the hydration curve for all of the mixtures. Silica fume also changes the second peak height with cements C2 and C6, as shown in Figure 4-25. The second peak height increases more with cement C2 than C6, and appears to be proportional to the amount of C_3A in the cement.

The maximum rate of heat evolution will increase slightly with silica fume in a ternary blend, which is similar to the behavior of a mixture with cement alone. Figure 4-26 shows an increase in height of both peaks with a ternary blend of fly ash FF1 and silica fume. Figure 4-27 shows that the aluminate peak increases in height in a mixture with Cement C2, FC2, and silica fume. This trend is also seen with Cement C6 in Figure 4-28.

The effect of UFFA on hydration is very similar to Class F fly ash. Figure 4-29 compares the effects of fly ash FF2 and ultra-fine fly ash (UFFA) on the rate of heat evolution. Fly ash FF2 is the parent fly ash of the UFFA; that is, UFFA represents the smaller size fraction from FF2. The heat of hydration curves for UFFA and FF2 are nearly identical.

Figure 4-30 shows the effects of silica fume on E_a with cement and cement/fly ash combinations. Silica fume reduces E_a in all cases. This reduction is likely due to the acceleration of the C_3S hydration with silica fume, as well as the reduction in SO_4^{2-} available to regulate the hydration of C_3A .

Mixture 43 was composed of 85% cement C6 and 15% UFFA (by mass), and mixture 44 was composed of 70% cement C6, 15% UFFA, and 15% FF2 (by mass). Mixture 43 had an E_a of 37,200 J/mol, and mixture 44 had an E_a of 38,700 J/mol, effectively the same. Mixture 23 had 70% cement C6 and 30% FF2 and had an E_a of 38,600 J/mol, the same as the mixture with UFFA (44) and similar to the control (43). UFFA, like its parent Class F fly ash, thus has no effect on E_a . UFFA mirrors the effects of the parent ash FF2 because the effects of these SCMs on pore solution chemistry are likely similar.

4.4.7. SUMMARY OF TRENDS

The calorimeter results presented here show that SCMs have a large effect on the rate of heat evolution of a cementitious system. First, an increase in the reactivity of the SCM results in a noticeable hydration peak, which is presumed to be a result of the reactive aluminate phases in the SCM. Class C fly ash and GGBF slag affect hydration more than Class F fly ash. Silica fume will generally promote the hydration of the C_3A and C_3S . UFFA affects hydration similar to its parent Class F fly ash. Next, the addition of alkalis as NaOH in the mixing water to the cementitious system will slightly shorten the time to the onset of the accelerating portion of the hydration curve. The cement chemistry, particularly the amount of aluminates, form and type of SO_4^{2-} , and alkalis, clearly plays a large role in the shape and retardation of the heat of hydration curve of mixtures with SCMs. However, the effects of the fly ash, GGBF slag, and silica fume on the rate of hydration are largely unknown because the availability of SO_4^{2-} and alkalis is

unknown, and the precise nature of the crystalline and reactive amorphous phases are poorly understood.

The effect of SCMs on E_a is relatively easy to quantify. Class F fly ash will generally reduce E_a , while Class C fly ash may either lower or raise E_a , depending on the C_3A and SO_4^{2-} content of the cement that is paired with the fly ash. The amount of change in E_a roughly correlates with the CaO content of the fly ash. GGBF slag will generally raise E_a , and silica fume will lower E_a . The addition of GGBF slag raises E_a more than Class C fly ash. UFFA affects E_a like its parent Class F fly ash. The addition of SCMs to cement C2 lowers E_a more than the addition of SCMs to cement C6, which is likely related to the different alkali contents of the cements. The effect of alkalis on E_a of the cementitious system is inconclusive, but is likely related to its effects on the availability of SO_4^{2-} required to retard the aluminates. Precise mechanistic explanation of these changes in E_a is difficult, since numerous reactions are occurring simultaneously, and E_a is merely a blended representation of the temperature sensitivity of these reactions.

4.5. CONCLUSIONS

Isothermal calorimetry was performed on 51 mixtures to test the effects of fly ash, GGBF slag, silica fume, and ultra-fine fly ash on the activation energy (E_a) of these mixtures. Several trends may be seen in the results presented here. First, SCMs that are largely inert tend to reduce E_a . For example, the addition of low CaO fly ash to a mixture tends to reduce the activation energy, as does the addition of silica fume. This effect is the result of the SCM diluting the amount of reactive phase (cement) in the paste.

Second, SCMs that have a reactive component to them, such as Class C fly ash or GGBF slag, alter E_a in a more complex way. The change in E_a depends greatly on the type of cement that the SCM is paired with. For example, a highly hydraulic fly ash paired with low-aluminate cement will have a higher E_a than the same fly ash paired with a high-aluminate cement. The interaction between the aluminate phases and SO_4^{2-} , the solubility of these components, and changes in alkali content of the cement clearly play some role in the progression of hydration, and the associated E_a . However, the precise nature of the relationship is difficult to ascertain because an accurate measure of glassy phase composition of the SCMs in this study was not available. E_a values ranged from 30,500 – 47,900 J/mol for all mixtures. Within this range, the type and dosage rate of SCM and CaO content of fly ash are useful indices to describe the effects of SCMs on E_a .

4.6. REFERENCES

1. Glasstone, S., K.J. Laidler, and H. Eyring, *The Theory of Rate Processes: The Kinetics of Chemical Reactions, Viscosity, Diffusion, and Electrochemical Phenomena*. McGraw-Hill Book Company, Inc. New York, 1941, 611 pp.
2. Tank, R.C., and N.J. Carino, “Rate Constant Functions for Strength Development of Concrete” *ACI Materials Journal*, V. 88, No. 1, Jan.-Feb., 1991, pp. 74-83.
3. Kjellsen, K.O., and R.J. Detwiler, “Later-Age Strength Prediction by a Modified Maturity Model,” *ACI Materials Journal*, V. 90, No. 3, May-June, 1993, pp. 220-227.

4. RILEM 119-TCE, "Adiabatic and Semi-Adiabatic Calorimetry to Determine the Temperature Increase in Concrete due to Hydration Heat of Cement," RILEM Report 15, R. Springenschmid, ed., E&FN Spon, London, 1999, pp. 315-330.
5. Moranville – Regourd, M., "Cements Made From Blastfurnace Slag," Lea's Chemistry of Cement and Concrete, 4th ed., ed. P.C. Hewlett, Arnold Publishers, New York, 1998, p 633-674.
6. Schindler, A.K., "Effect of Temperature on Hydration of Cementitious Materials", *ACI Materials Journal*, V. 101, No. 1, Jan.-Feb., 2004, pp. 72-81.
7. Ma, W., D. Sample, R. Martin, and P.W. Brown, "Calorimetric Study of Cement Blends Containing Fly Ash, Silica Fume, and Slag at Elevated Temperatures." *Cement, Concrete, and Aggregates*, V. 16, 1994, pp. 93-99.
8. Poole, J.L., K.A. Riding, K.J. Folliard, M.G.C. Juenger, and A.K. Schindler "Methods of Activation Energy Calculation for Portland Cement," *ACI Materials Journal*, V. 104, No. 1, Jan.-Feb., 2007, pp. 303-311.
9. D'Aloia, L., and G. Chanvillard, "Determining the "Apparent" Activation Energy of Concrete; E_a – Numerical Simulations of the Heat of Hydration of Cement," *Cement and Concrete Research*, V. 32, 2002, pp. 1277-1289.
10. ASTM C 150, "Standard Specification for Portland Cement," Annual Book of ASTM Standards, Vol 04.01., ASTM International, West Conshohocken, PA., 2002, 8 pp.

11. ASTM C 618, “Standard Specification for Coal Ash and Raw or Calcined Natural Pozzolans for Use in Concrete,” Annual Book of ASTM Standards, V. 04.01., ASTM International, West Conshohocken, PA., 2003, 3 pp.
12. ASTM C 989, “Standard Specification for Ground Granulated Blast-Furnace Slag for Use in Concrete and Mortars,” Annual Book of ASTM Standards, V. 04.01., ASTM International, West Conshohocken, PA., 2005, 5 pp.
13. Scrivener, K.L., T. Füllmann, E. Gallucci, G. Walenta, and E. Bermejo, “Quantitative Study of Portland Cement Hydration by X-Ray Diffraction/Rietveld Analysis and Independent Methods”, *Cement and Concrete Research*, V. 34, 2004, pp 1541-1547.
14. Schindler, A.K., and K.J. Folliard, “Heat of Hydration Models for Cementitious Materials”, *ACI Materials Journal*, V. 102, No. 1, Jan.-Feb., 2005, pp. 24-33.
15. Pane, I., and W. Hansen, “Concrete Hydration and Mechanical Properties under Nonisothermal Conditions,” *ACI Materials Journal*, V. 99, No. 6, Nov.-Dec, 2002, pp. 534-542.
16. Poole, J.L., “The Effects of Cement Chemistry and Water-Cement Ratio on Activation Energy,” PhD Dissertation, Chapter 2, The University of Texas at Austin, Austin, TX, 2007, pp 6-37.
17. Lerch, W., “The Influence of Gypsum on the Hydration and Properties of Portland Cement Paste,” *Proceedings of the American Society for Testing Materials*, V. 46, 1946.

18. Sandberg, P. and Roberts, L., "Cement-Admixture Interactions Related to Aluminate Control", *Journal of ASTM International*, V. 2, No. 6 June 2005, pp. 6-13.
19. Diamond, S., "Alkali-Silica Reactions – Some Paradoxes," *Cement and Concrete Composites*, V.19, 1997, pp. 391-401.
20. Samet, B. and S.L. Sarkar, "The Influence of Calcium Sulfate Form on the Initial Hydration of Clinkers Containing Different Alkali Combinations", *Cement and Concrete Research*, V. 27, No. 3, 1997, pp. 369-380.
21. Odler, I., and R. Wonnemann, "Effect of Alkalis on Portland Cement Hydration: I. Alkali Oxides Incorporated into the Crystalline Lattice of Clinker Minerals," *Cement and Concrete Research*, V. 13, No. 4, 1983, pp 477-482.
22. Ogawa, K, H. Uchikawa, K. Takemoto, and I. Yasui, "The Mechanism of the Hydration in the System C_3S Pozzolanas" *Cement and Concrete Research*, V. 10, No. 5, 1980, pp 683-696.
23. Chandra, S., "Properties of Concrete with Mineral and Chemical Admixtures", *Structure and Performance of Cements*, 2nd ed., J. Bensted and P. Barnes, eds, 2002, pp 140-185
24. Poole, J.L., "The Effects of Chemical Admixtures on Activation Energy of Cementitious Materials," PhD Dissertation, Chapter 3, The University of Texas at Austin, Austin, TX, 2007, pp 38-68.

Table 4-1: Chemical and Physical Properties of Cement

	Cements			Fly Ashes					Other SCMs	
	C2	C3	C6	FF1	FF2	FC1	FC2	UFFA	S1	S.F.
SiO ₂ (%)	19.18	20.25	20.77	56.63	51.69	37.83	33.31	50.65	34.48	94.28
Al ₂ O ₃ (%)	5.34	5.27	3.88	30.68	24.81	19.83	18.39	26.64	11.35	0.04
Fe ₂ O ₃ (%)	2.3	3.14	3.73	4.94	4.22	6.17	5.40	4.66	0.67	0.06
CaO (%)	63.17	61.86	64.5	0.69	13.12	23.13	28.91	10.85	41.73	0.51
MgO (%)	1.09	2.68	1.01	0.73	2.29	4.62	5.25	2.23	7.32	0.57
Na ₂ O (%)	0.12	0.27	0.18	0.12	0.18	1.74	1.64	0.41	0.14	0.06
K ₂ O (%)	0.95	0.90	0.60	2.26	0.84	0.06	0.35	1.02	0.38	0.99
Na ₂ O Eq. (%)	0.75	0.862	0.575	1.607	0.733	1.778	1.870	1.081	0.390	0.71
SO ₃ (%)	3.20	4.17	2.38	0.00	0.46	1.50	2.27	1.00	1.88	0.16
LOI (%)	4.10	0.73	2.67	2.10	0.23	0.67	0.34	0.39	0.83	3.10
Insoluble Residue (%)	0.63	0.30	0.25	-	-	-	-	-	-	-
CaO (%)**	0.0	0.7	0.0	-	-	-	-	-	-	-
C ₃ S (%)*	63.1	46.2	66.5	-	-	-	-	-	-	-
C ₃ S (%)**	61.0	57.2	55.7	-	-	-	-	-	-	-
C ₂ S (%)*	7.4	23.2	9.4	-	-	-	-	-	-	-
C ₂ S (%)**	15.6	15.1	21.1	-	-	-	-	-	-	-
C ₃ A (%)*	10.3	8.7	4.0	-	-	-	-	-	-	-
C ₃ A (%)**	9.6	5.3	4.0	-	-	-	-	-	-	-
C ₄ AF (%)*	7.0	9.6	11.4	-	-	-	-	-	-	-
C ₄ AF (%)**	6.0	9.6	10.7	-	-	-	-	-	-	-
C \hat{S} H ₂ (%)**	0.4	6.6	3.1	-	-	-	-	-	-	-
C \hat{S} H _{0.5} (%)**	1.2	0.8	1.3	-	-	-	-	-	-	-
C \hat{S} (%)**	0.7	0.4	0.6	-	-	-	-	-	-	-
K ₂ SO ₄ (%)**	1.0	1.6	0.7	-	-	-	-	-	-	-
CaCO ₃ (%)**	3.6	1.7	2.5	-	-	-	-	-	-	-
Blaine fineness (m ² /kg)	391	389	365	147	166	348	300	394	332	20000

* = Bogue Calculations, ** = Rietveld Analysis

Table 4-2: Three-Parameter Curve Fit Values for Mixtures with Fly Ash

Mix/ Cement	SCM	% by Mass	% CaO	α_u	β	τ (hours)					H_u (J/g)	E_a J/mol
						5°C	15°C	23°C	38°C	60°C		
1-C2	-	0%	-	0.713	0.968	57.06	28.07	16.52	6.740	3.250	530	40,550
2-C3	-	0%	-	0.783	1.016	55.18	27.01	15.16	6.933	3.479	464	38,850
3-C6	-	0%	-	0.741	0.826	36.27	19.43	12.22	5.210	2.570	496	37,550
4-C2	FF1	17%	0.7	0.775	0.898	44.61	22.26	17.49	7.290	3.370	442	36,050
5-C2	FF1	20%	0.7	0.838	0.831	50.52	25.68	16.31	8.144	4.710	426	33,150
6-C2	FF1	30%	0.7	0.897	0.783	53.38	28.04	19.39	9.188	4.706	374	33,950
7-C2	FF1	40%	0.7	0.909	0.813	52.55	27.62	18.26	8.982	5.056	323	32,800
8-C2*	FF1	30%	0.7	0.826	0.876	59.48	28.98	18.41	8.830	4.555	374	35,750
9-C3	FF1	30%	0.7	0.893	1.022	58.79	28.66	16.59	9.119	4.684	328	34,900
10-C6	FF1	20%	0.7	0.780	0.776	38.23	18.85	12.05	6.569	3.302	399	33,400
11-C6	FF1	30%	0.7	0.814	0.780	38.73	21.18	13.59	7.115	3.291	351	34,300
12-C6	FF1	40%	0.7	0.900	0.707	43.81	23.39	16.54	8.626	3.799	302	33,750
13-C2	FF2	20%	13.1	0.748	0.909	74.33	28.17	16.88	8.409	4.478	471	38,200
14-C2	FF2	30%	13.1	0.742	0.895	65.41	30.59	18.72	9.058	4.709	442	36,500
15-C2	FF2	40%	13.1	0.665	1.031	69.33	29.82	18.03	8.582	4.879	412	36,700
16-C6	FF2	20%	13.1	0.742	0.768	44.95	31.67	14.10	7.389	3.540	444	36,950
17-C6	FF2	30%	13.1	0.745	0.762	52.13	34.33	15.60	8.233	3.532	418	38,550
18-C6	FF2	40%	13.1	0.778	0.672	59.55	44.52	18.73	10.49	4.143	392	38,550
19-C2	FC1	20%	23.1	0.744	0.962	64.75	33.40	19.27	9.495	5.629	507	34,450
20-C2	FC1	30%	23.1	0.731	0.950	66.86	42.23	21.92	11.61	5.410	496	35,850
21-C2	FC1	40%	23.1	0.720	0.938	77.20	47.77	25.37	13.07	5.828	484	36,750
22-C6	FC1	20%	23.1	0.736	0.793	48.08	23.19	17.12	8.361	3.482	480	35,950
23-C6	FC1	30%	23.1	0.743	0.780	59.93	28.54	21.30	10.11	4.337	472	36,050
24-C6	FC1	40%	23.1	0.783	0.701	80.18	42.08	29.50	13.19	5.132	464	38,300
25-C2	FC2	20%	28.9	0.708	0.993	52.39	26.21	18.79	8.934	5.067	528	32,550
26-C2	FC2	30%	28.9	0.713	0.989	63.65	32.38	21.55	12.63	5.386	527	33,550
27-C2	FC2	40%	28.9	0.745	0.874	77.05	42.71	27.67	13.15	5.251	526	37,600
28-C2*	FC2	30%	28.9	0.802	0.761	86.86	43.10	29.45	11.57	4.969	527	40,250
29-C3	FC2	30%	28.9	0.715	1.048	67.26	36.72	20.37	10.06	4.468	464	38,150
30-C6	FC2	20%	28.9	0.755	0.707	53.26	28.83	18.10	8.309	3.587	501	37,900
31-C6	FC2	30%	28.9	0.756	0.702	68.16	37.30	23.59	9.932	4.114	503	39,750
32-C6	FC2	40%	28.9	0.795	0.647	95.15	51.93	35.55	14.14	5.161	506	41,150

* - 0.85% Na₂O_{eq}

Table 4-3: Three-Parameter Curve Fit Values for Mixtures with GGBF Slag, Silica Fume, and Ternary Blends

Mix/ Cement	SCM	% by Mass	% CaO	α_u	β	τ (hours)					H_u (J/g)	E_a (J/mol)
						5°C	15°C	23°C	38°C	60°C		
33-C2	Slag	30%	-	0.729	0.817	58.49	28.64	17.55	9.262	3.939	509	37,100
34-C2	Slag	40%	-	0.749	0.734	68.04	33.83	21.23	11.35	4.608	502	36,950
35-C2	Slag	50%	-	0.793	0.650	86.97	53.28	26.88	13.42	5.231	495	39,100
36-C2	Slag	65%	-	0.691	0.621	99.85	54.40	31.59	13.94	5.900	485	40,050
37-C2	Slag	70%	-	0.587	0.683	83.72	47.53	28.12	11.49	4.984	482	40,350
38-C6	Slag	30%	-	0.828	0.536	62.86	34.05	21.96	11.57	3.320	485	40,350
39-C6	Slag	40%	-	0.920	0.471	98.15	55.92	29.49	12.88	4.823	482	42,800
40-C6	Slag	50%	-	1.027	0.412	156.9	94.79	56.88	18.48	8.143	478	43,250
41-C6	Slag	65%	-	1.011	0.413	232.1	134.8	68.31	23.82	9.144	473	46,850
42-C6	Slag	70%	-	0.994	0.414	264.7	154.9	88.18	29.48	9.520	471	47,900
43-C6	UFFA	15%	10.8	0.812	0.787	46.04	24.29	14.22	6.312	3.360	451	37,200
44-C6	FF2	15%	13.1	0.806	0.804	54.91	27.80	17.84	7.406	3.550	412	38,650
	UFFA	15%	10.8									
45-C2	S.F.	7.5%	-	0.742	1.064	32.28	19.88	12.75	5.940	3.570	490	31,800
46-C6	S.F.	5%	-	0.753	0.831	35.45	16.48	11.42	5.873	2.718	471	35,050
47-C6	S.F.	7.5%	-	0.738	0.856	33.26	17.85	9.907	4.843	2.975	456	34,300
48-C2	FF1	20%	0.7	0.834	0.838	36.90	23.43	15.66	8.177	4.309	400	30,500
	S.F.	5%	-									
49-C2	FC2	30%	28.9	0.827	0.777	83.40	45.18	23.97	14.78	6.709	500	34,750
	S.F.	5%	-									
50-C2	FC2	35%	28.9	0.788	0.817	77.12	45.62	25.42	16.81	6.878	500	33,200
	S.F.	5%	-									
51-C6	FC2	30%	28.9	0.765	0.751	67.27	35.57	16.94	9.039	4.577	478	37,800
	S.F.	5%	-									

* - Previously Presented⁴

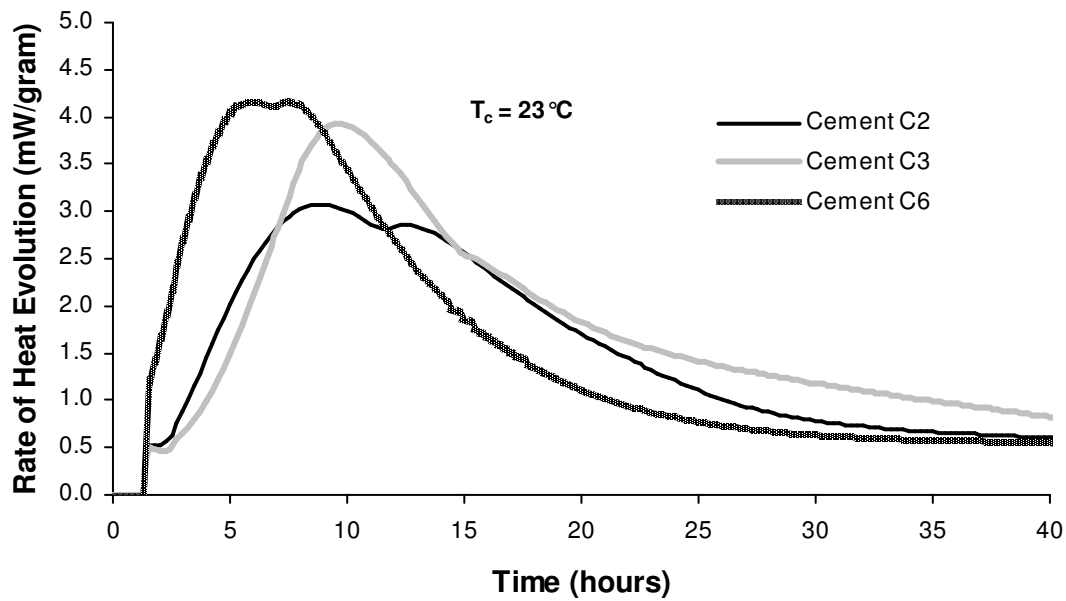


Figure 4-1: Rate of Heat Evolution (Per Gram of Cementitious Material) for Cements

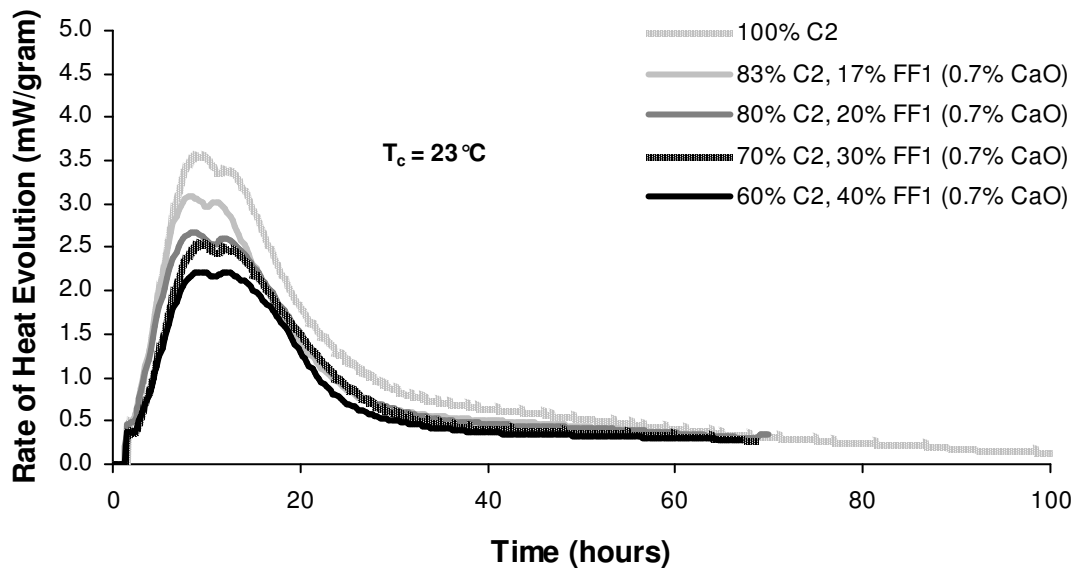


Figure 4-2: Rate of Heat Evolution (Per Gram of Cementitious Material) for Cement C2 with Different Replacements of FF1 (0.7% CaO) at 23°C (73.4°F)

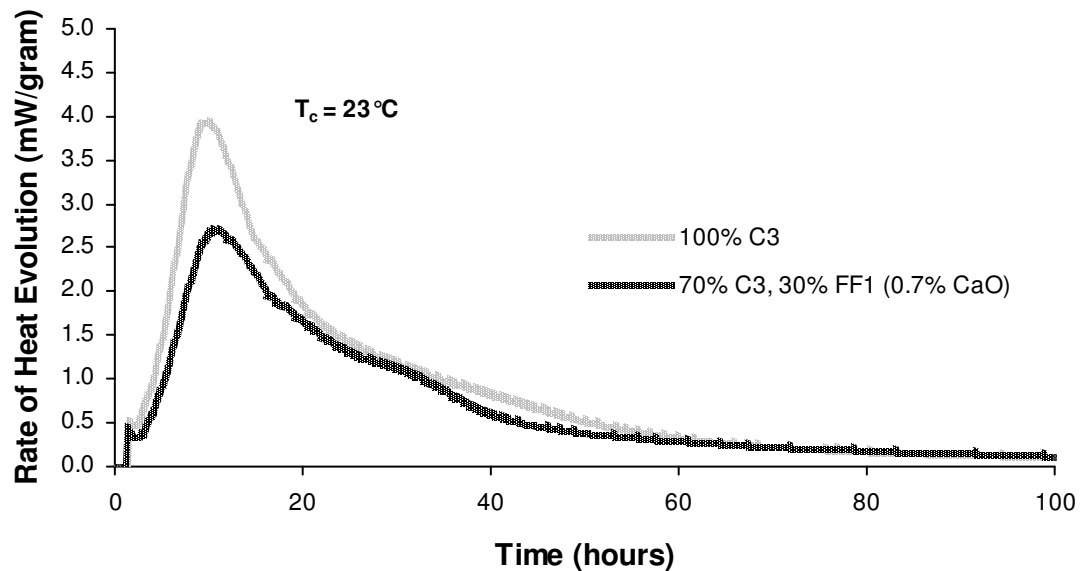


Figure 4-3: Rate of Heat Evolution (Per Gram of Cementitious Material) for Cement C3 with Different Replacements of FF1 (0.7% CaO) at 23°C (73.4°F)

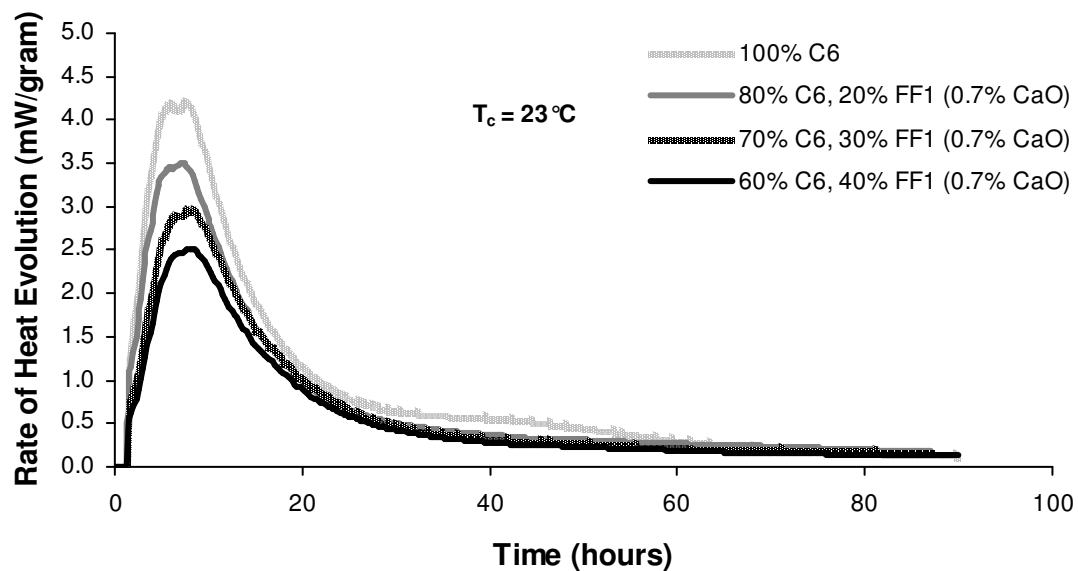


Figure 4-4: Rate of Heat Evolution (Per Gram of Cementitious Material) for Cement C6 with Different Replacements of FF1 (0.7% CaO) at 23°C (73.4°F)

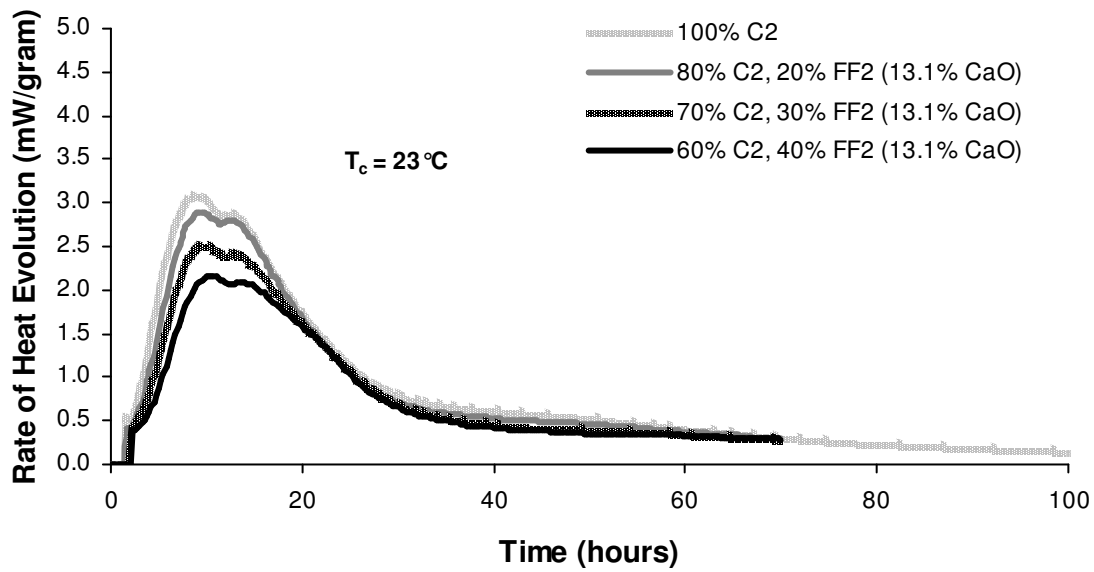


Figure 4-5: Cement C2 with Different Replacements of FF2 (13.1% CaO) at 23 °C (73.4 °F)

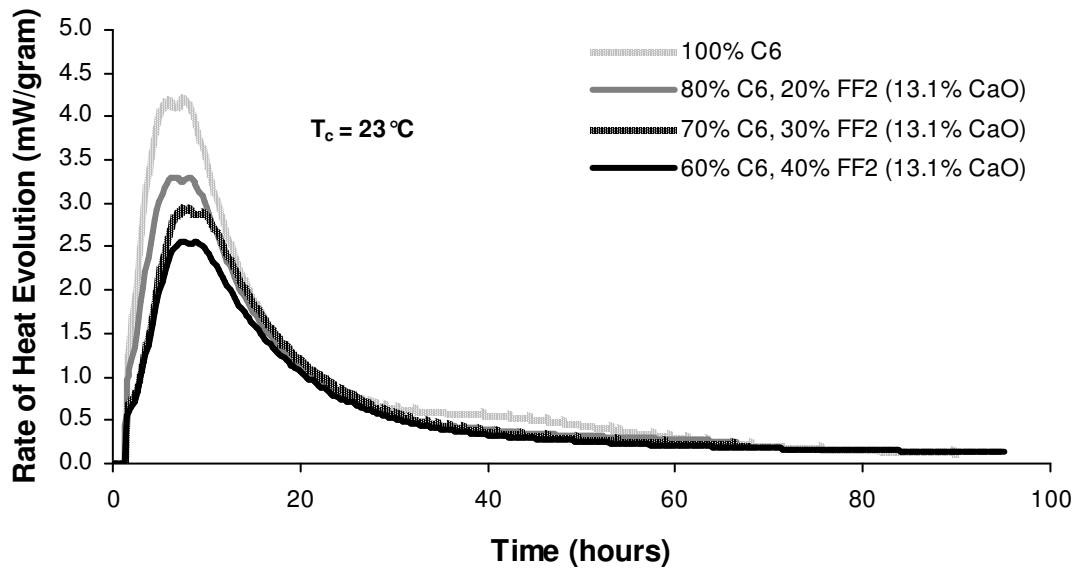


Figure 4-6: Rate of Heat Evolution (Per Gram of Cementitious Material) for Cement C6 with Different Replacements of FF2 (13.1% CaO) at 23 °C (73.4 °F)

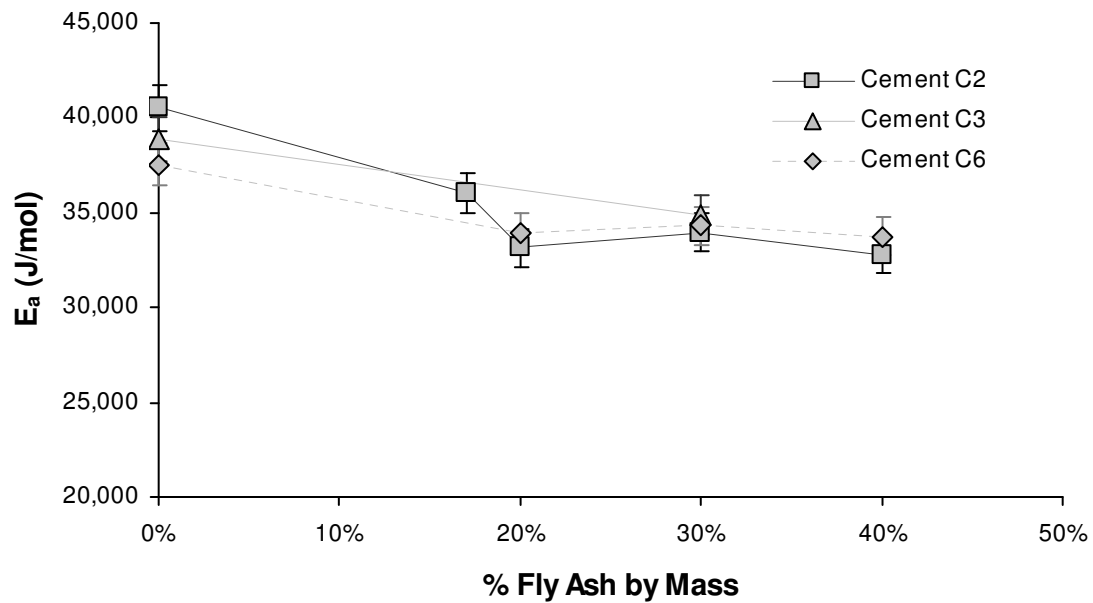


Figure 4-7: Summary of E_a Trends for Class F Fly Ash FF1 (0.7% CaO)

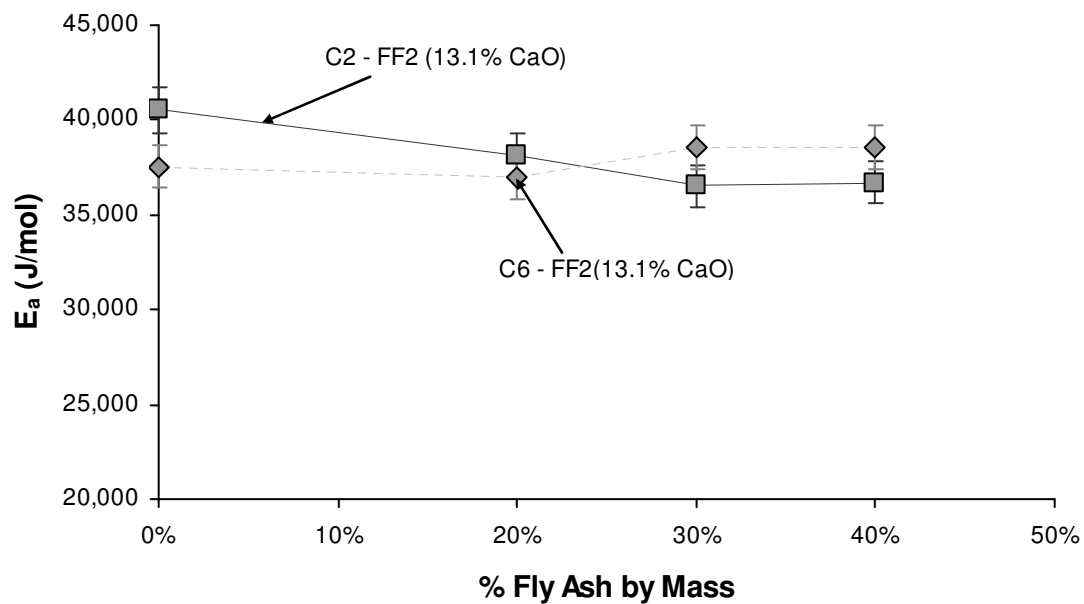


Figure 4-8: Summary of E_a Trends for Class F Fly Ash FF2 (13.1% CaO)

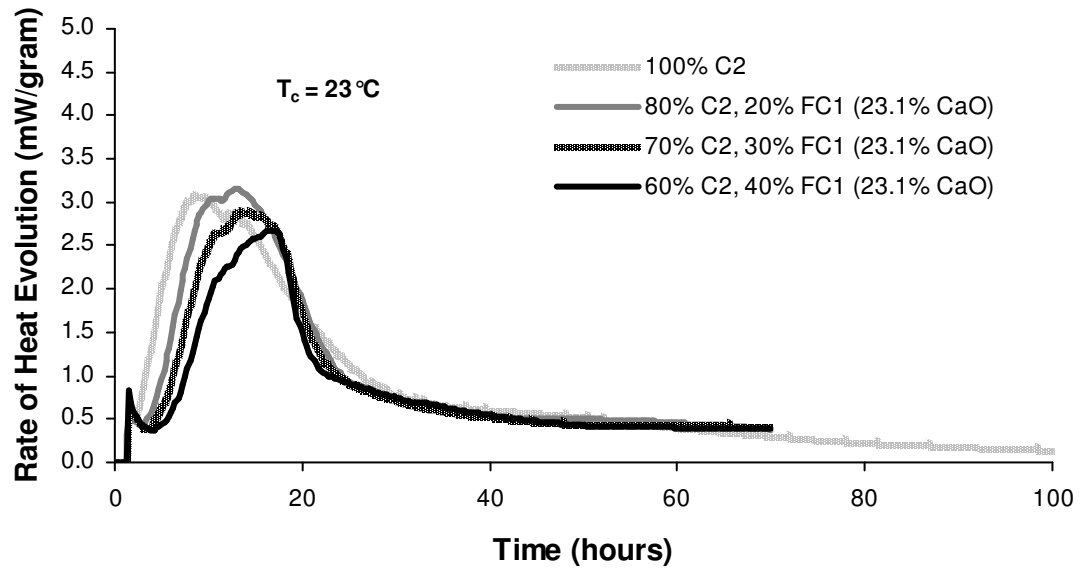


Figure 4-9: Rate of Heat Evolution (Per Gram of Cementitious Material) for Cement C2 with Different Replacements of FC1 (23.1% CaO) at 23 °C (73.4 °F)

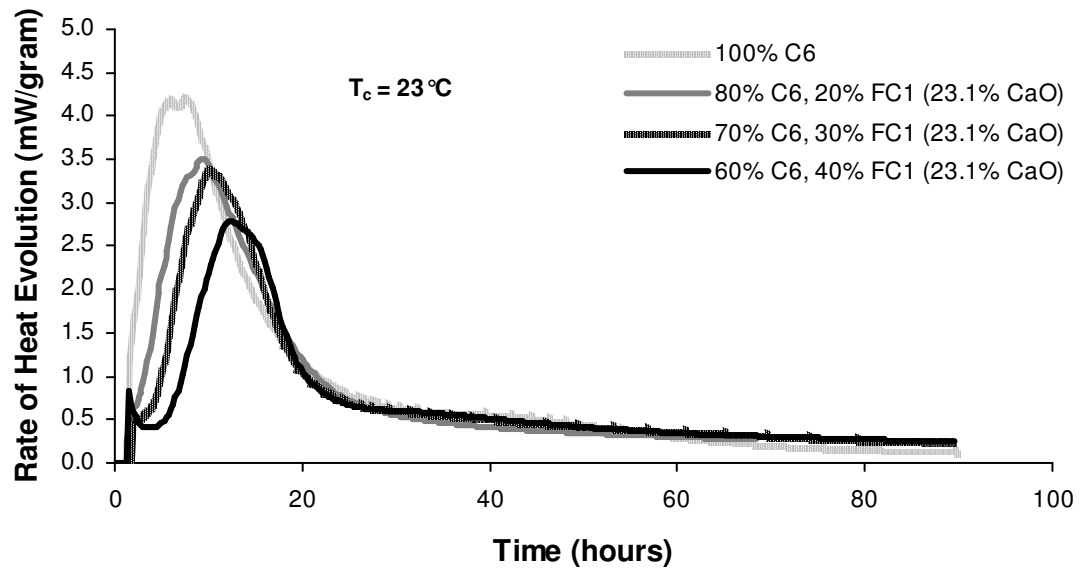


Figure 4-10: Rate of Heat Evolution (Per Gram of Cementitious Material) for Cement C6 with Different Replacements of FC1 (23.1% CaO) at 23 °C (73.4 °F)

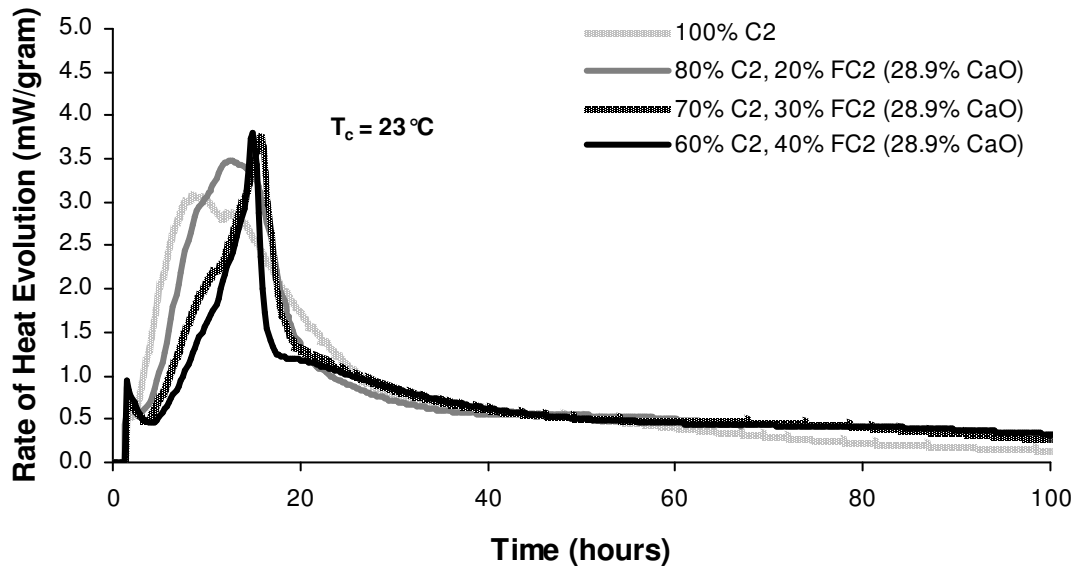


Figure 4-11: Rate of Heat Evolution (Per Gram of Cementitious Material) for Cement C2 with Different Replacements of FC2 (28.9% CaO) at 23 °C (73.4 °F)

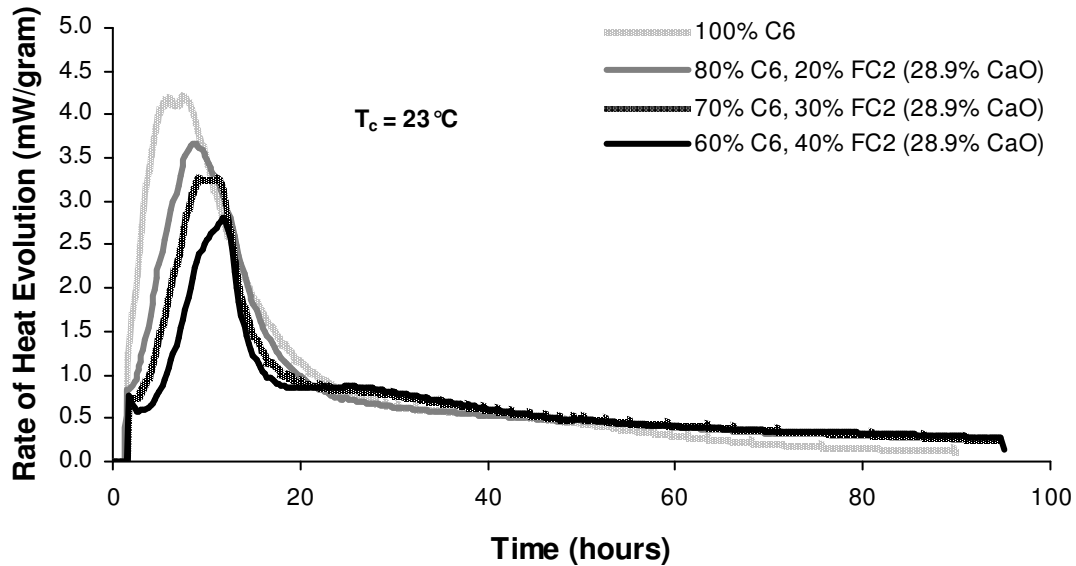


Figure 4-12: Rate of Heat Evolution (Per Gram of Cementitious Material) for Cement C6 with Different Replacements of FC2 (28.9% CaO) at 23 °C (73.4 °F)

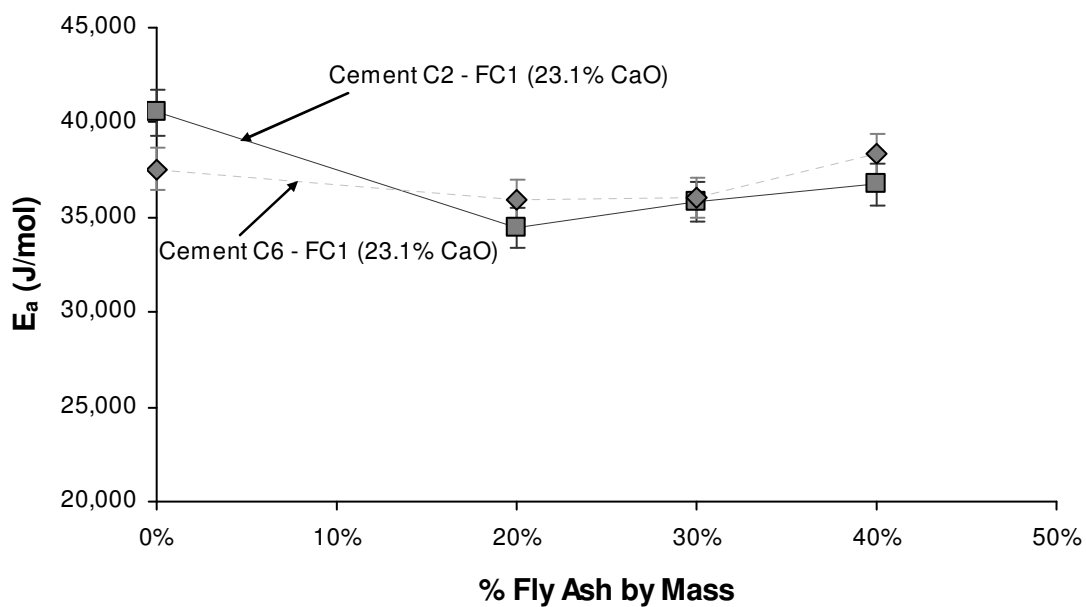


Figure 4-13: Summary of E_a Trends for Class C Fly Ash FC1 (23.1% CaO)

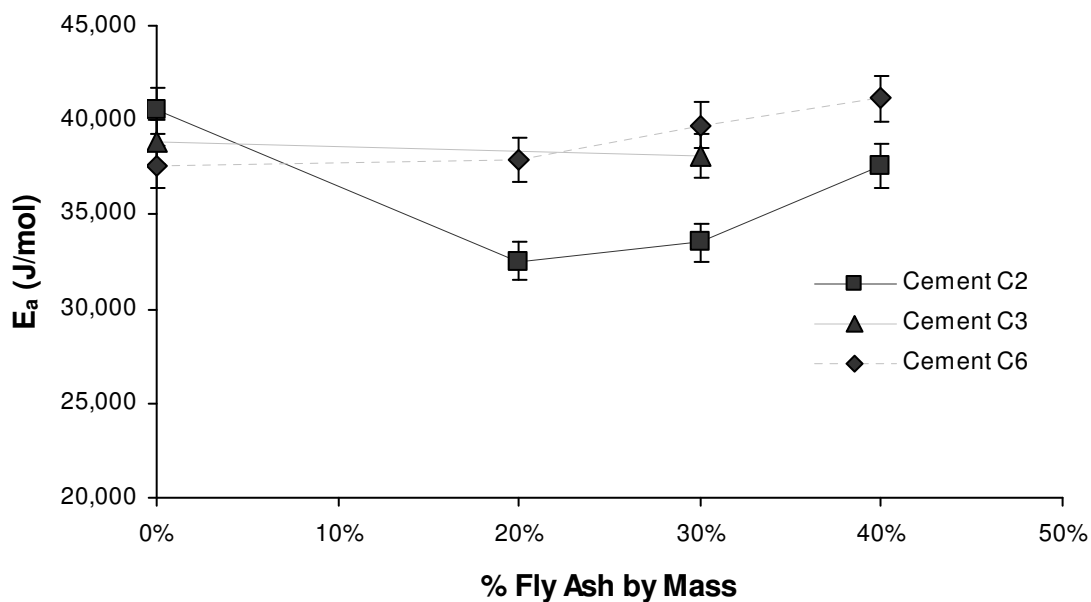


Figure 4-14: Summary of E_a Trends for Class C Fly Ash FC2 (28.9% CaO)

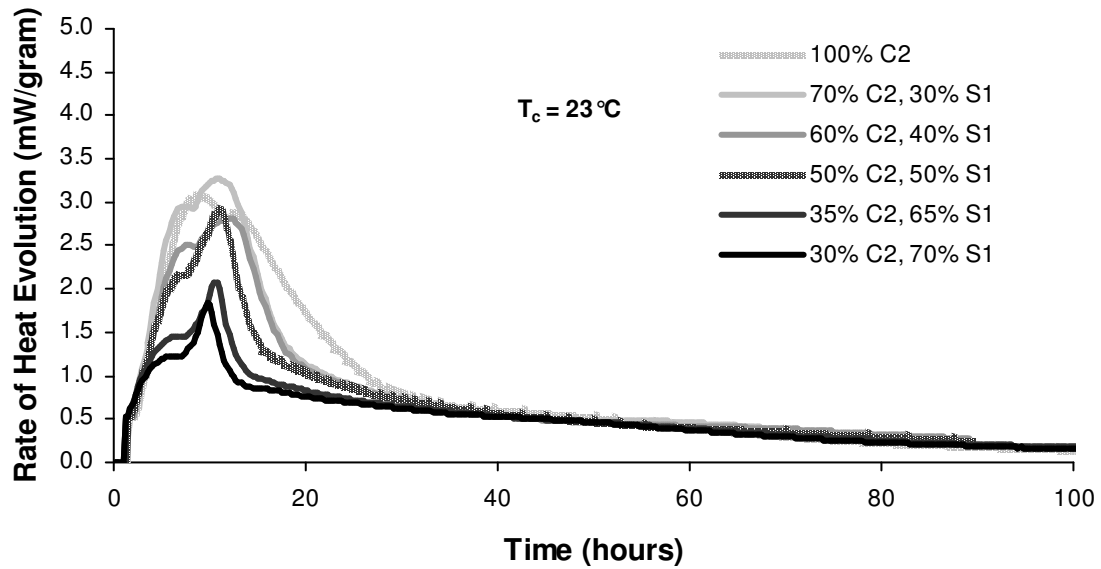


Figure 4-15: Rate of Heat Evolution (Per Gram of Cementitious Material) for Cement C2 with Different Replacements of GGBF Slag (S1) at 23 °C (73.4 °F)

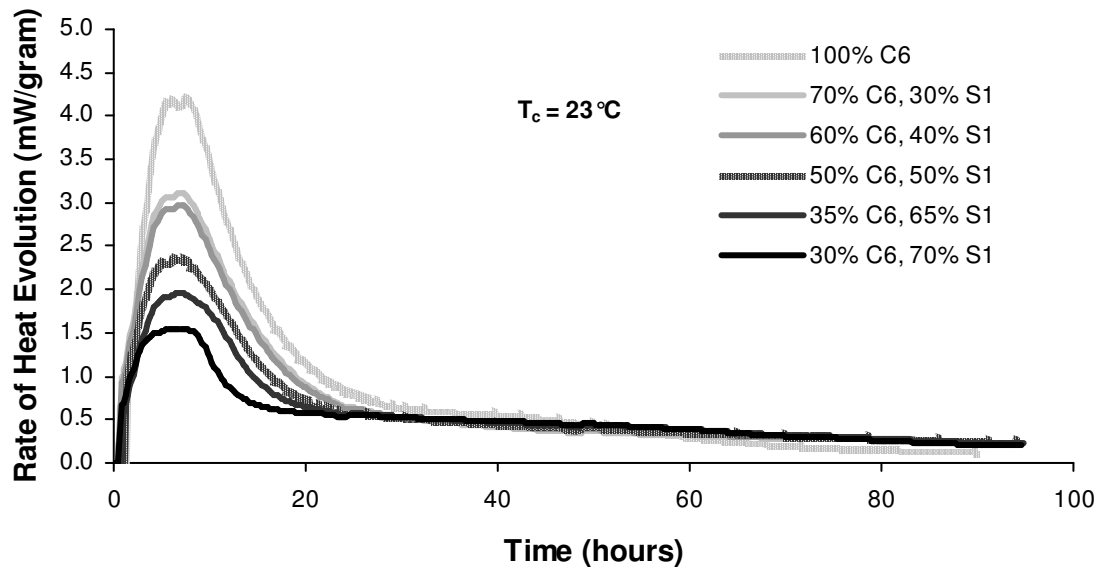


Figure 4-16: Rate of Heat Evolution (Per Gram of Cementitious Material) for Cement C6 with Different Replacements of GGBF Slag (S1) at 23 °C (73.4 °F)

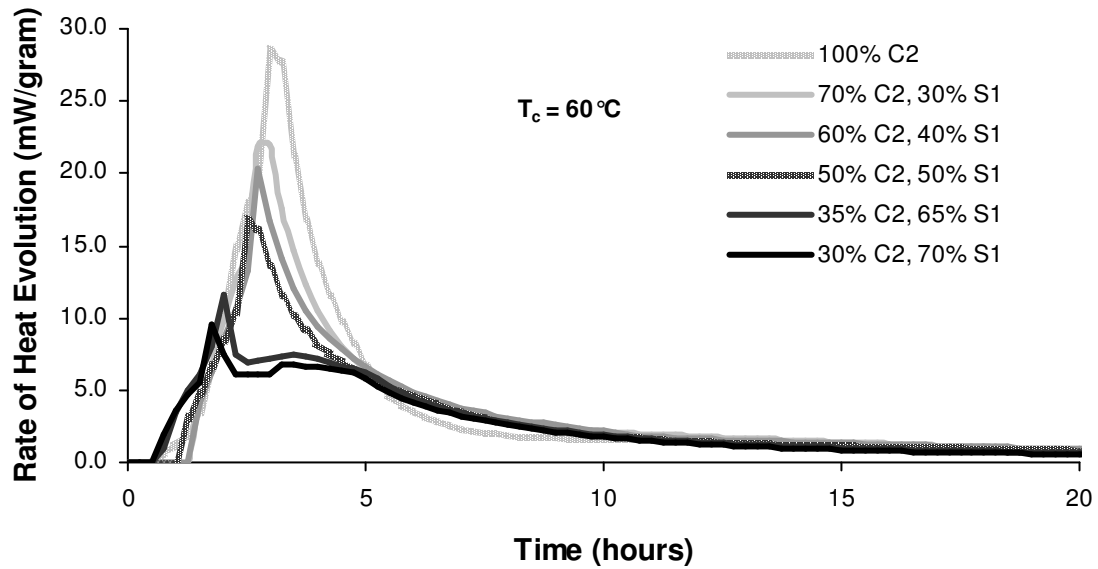


Figure 4-17: Rate of Heat Evolution (Per Gram of Cementitious Material) for Cement C2 with Different Replacements of GGBF Slag (S1) at 60 °C (140 °F)

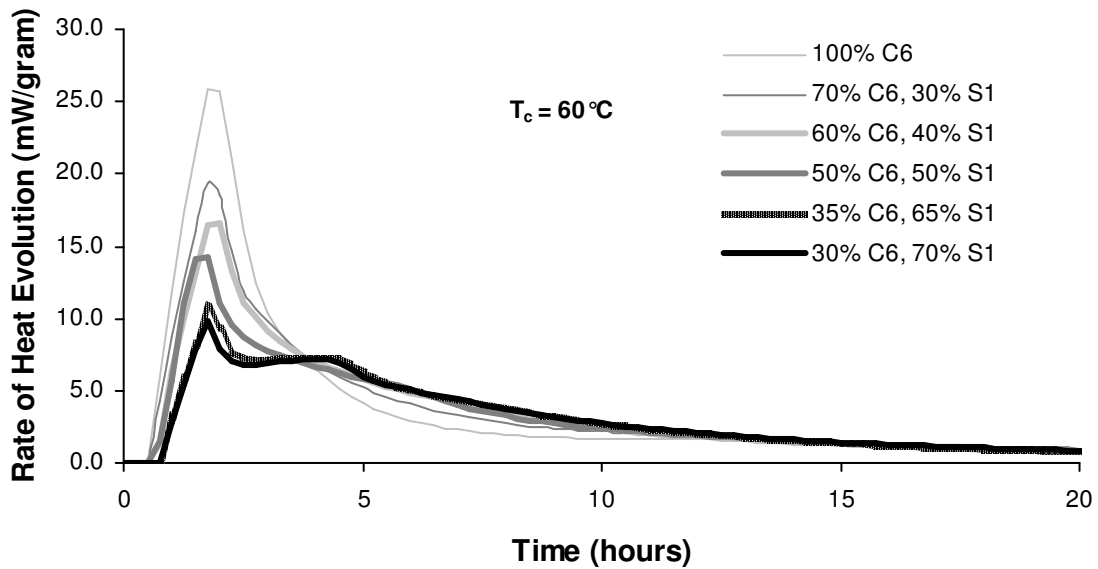


Figure 4-18: Rate of Heat Evolution (Per Gram of Cementitious Material) for Cement C6 with Different Replacements of GGBF Slag (S1) at 60 °C (140 °F)

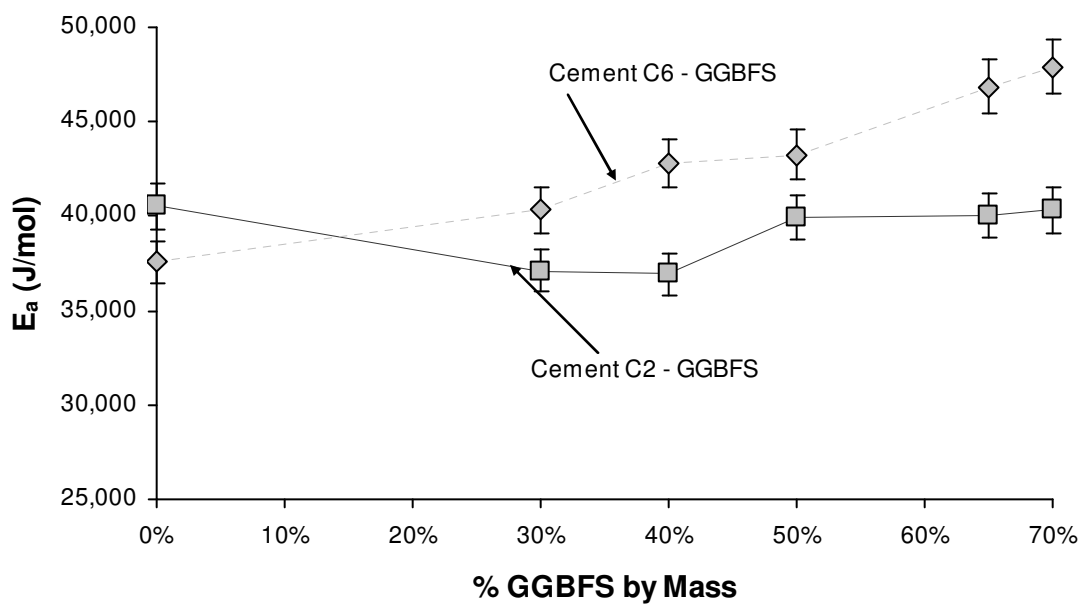


Figure 4-19: Summary of E_a Trends for GGBF Slag (S1)

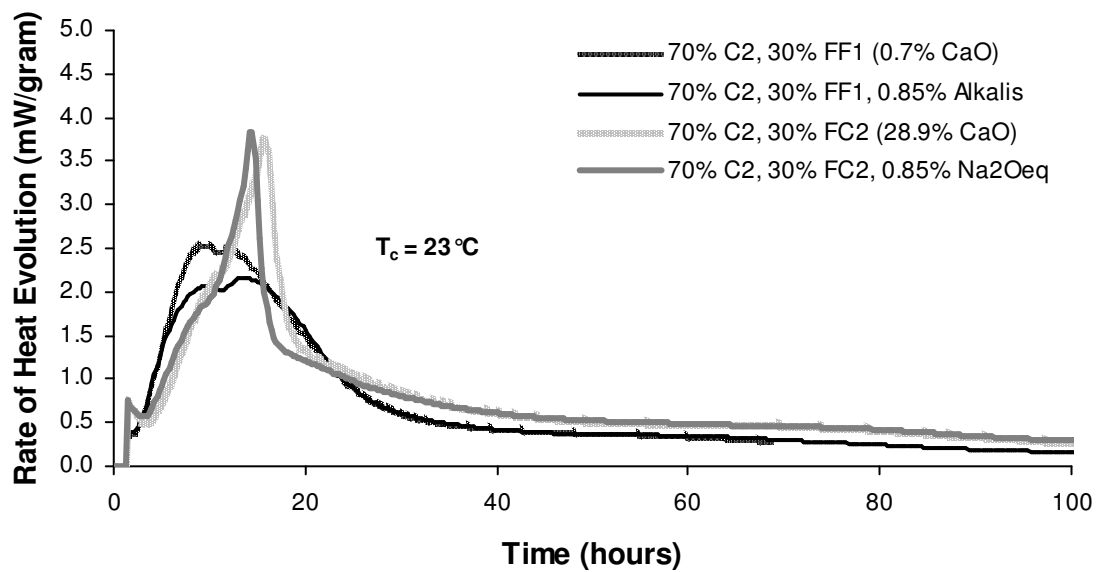


Figure 4-20: Effects of Alkalis on Hydration of FF1 and FC2 (28.9% CaO)

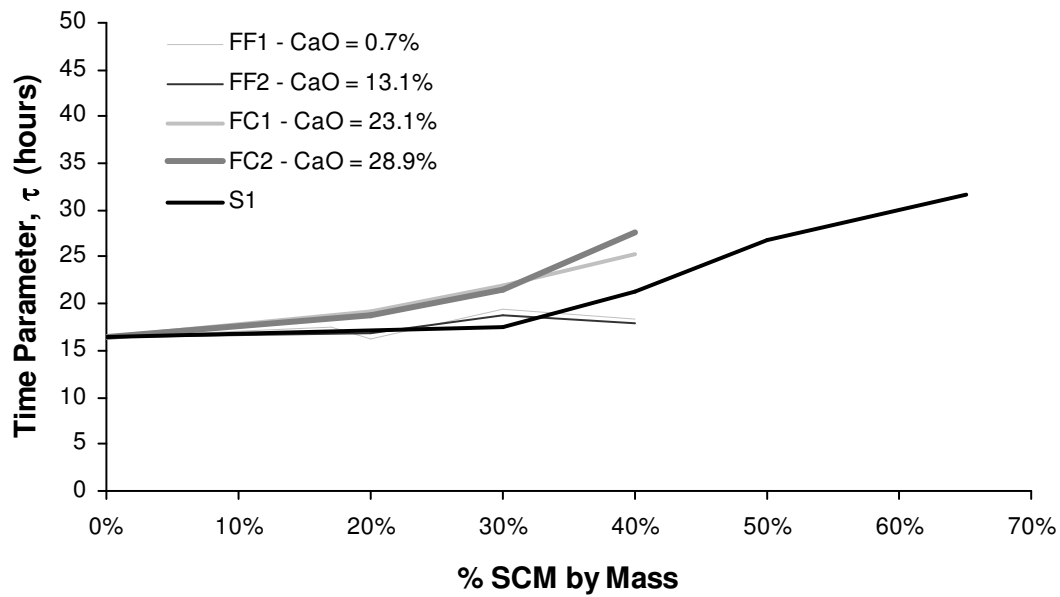


Figure 4-21: Time Parameter τ with Cement C2 and Different SCMs

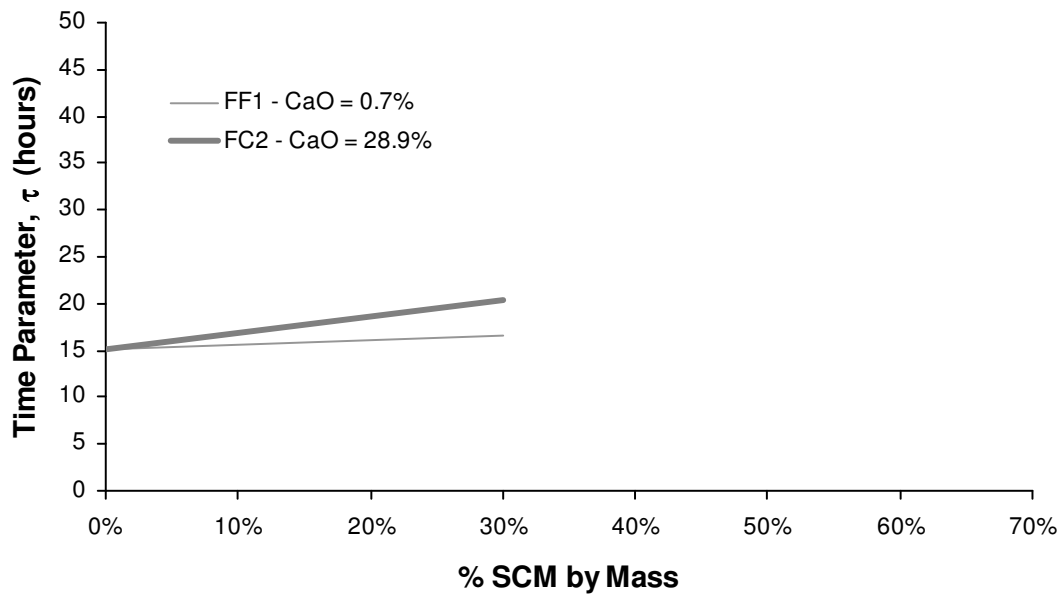


Figure 4-22: Time Parameter τ with Cement C3 and Different SCMs

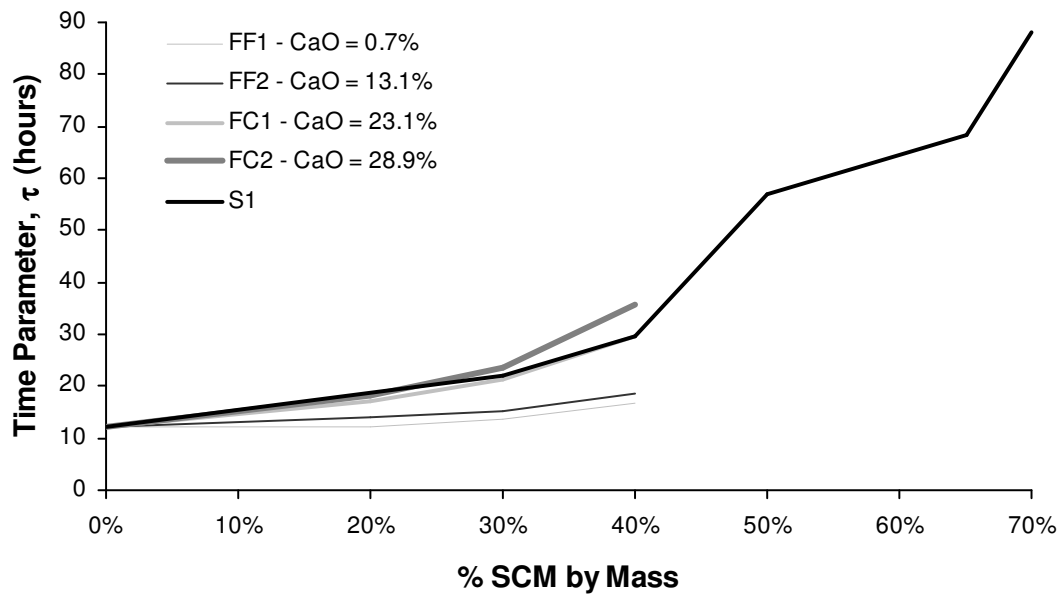


Figure 4-23: Time Parameter τ with Cement C6 and Different SCMs

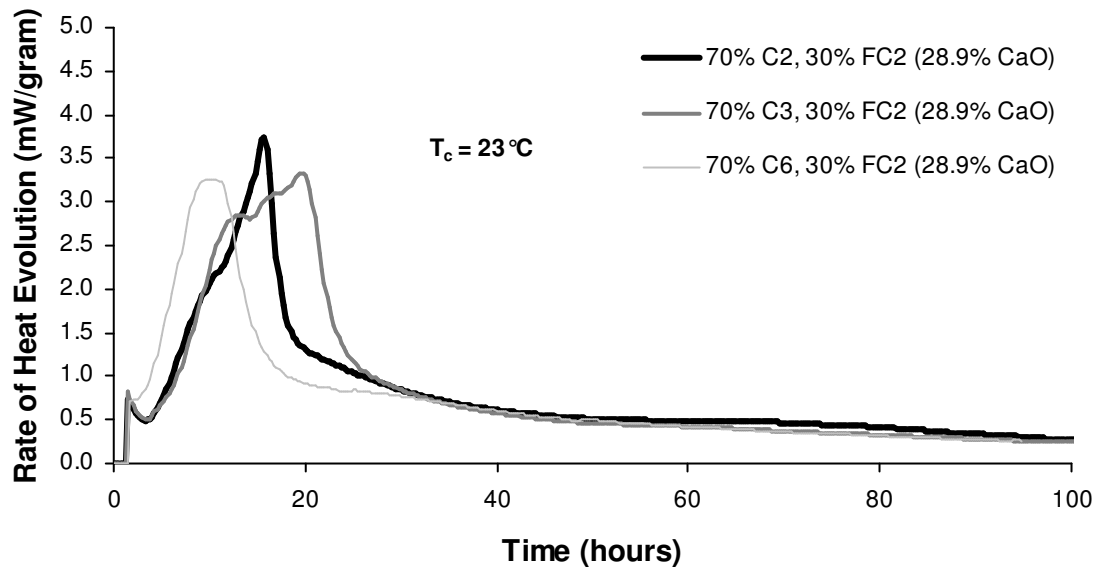


Figure 4-24: Rate of Heat Evolution (Per Gram of Cementitious Material) for Cement C3 with 30% FC2 (28.9% CaO) at 23 °C (73.4 °F)

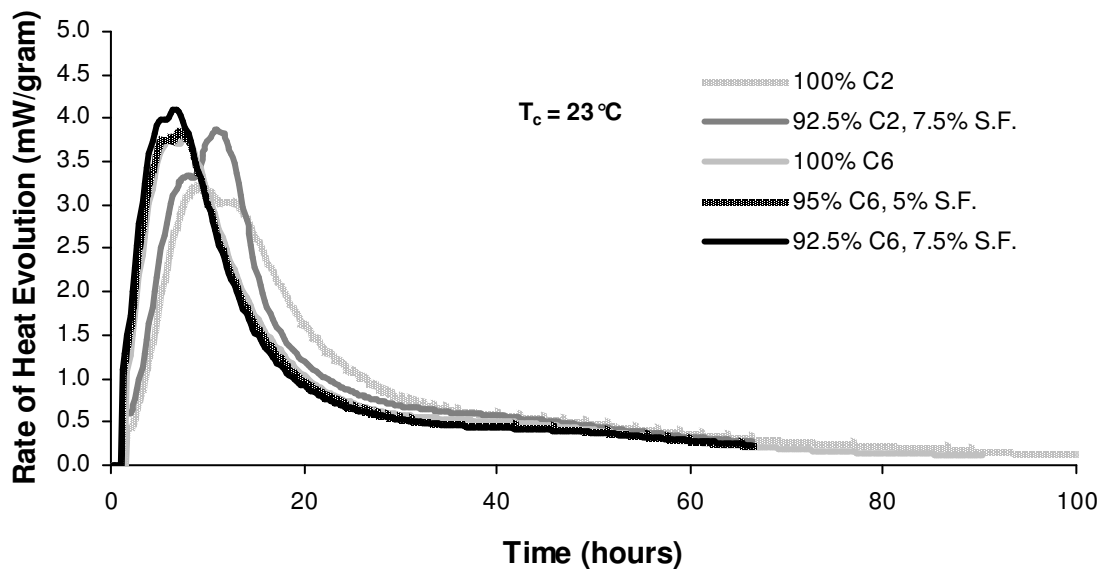


Figure 4-25: Cements C2 and C6 with Different Replacements of Silica Fume

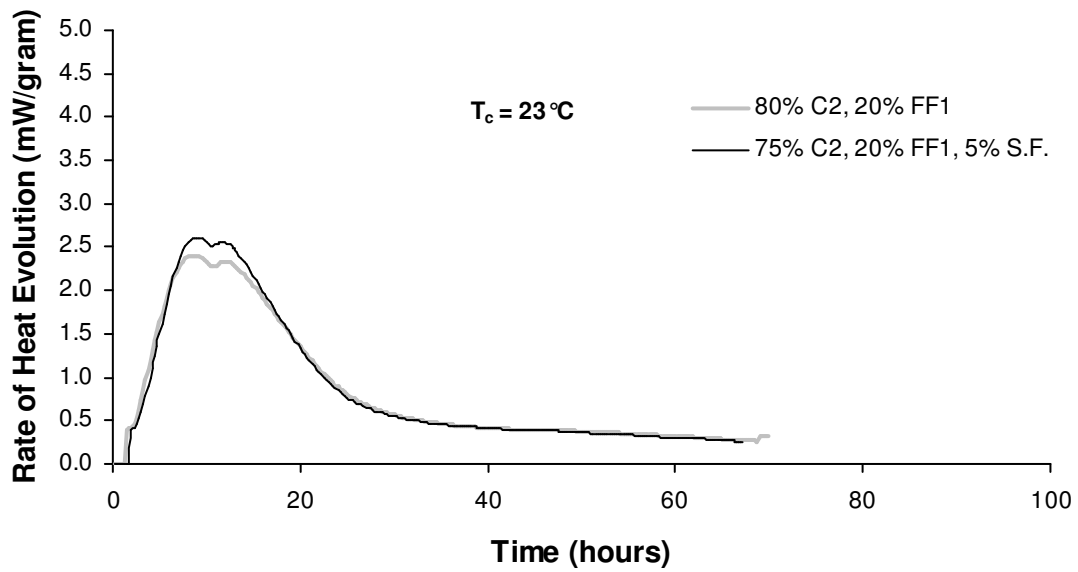


Figure 4-26: Cement C2 with Silica Fume and 20% Replacement by Mass of FF1 (CaO=0.7%)

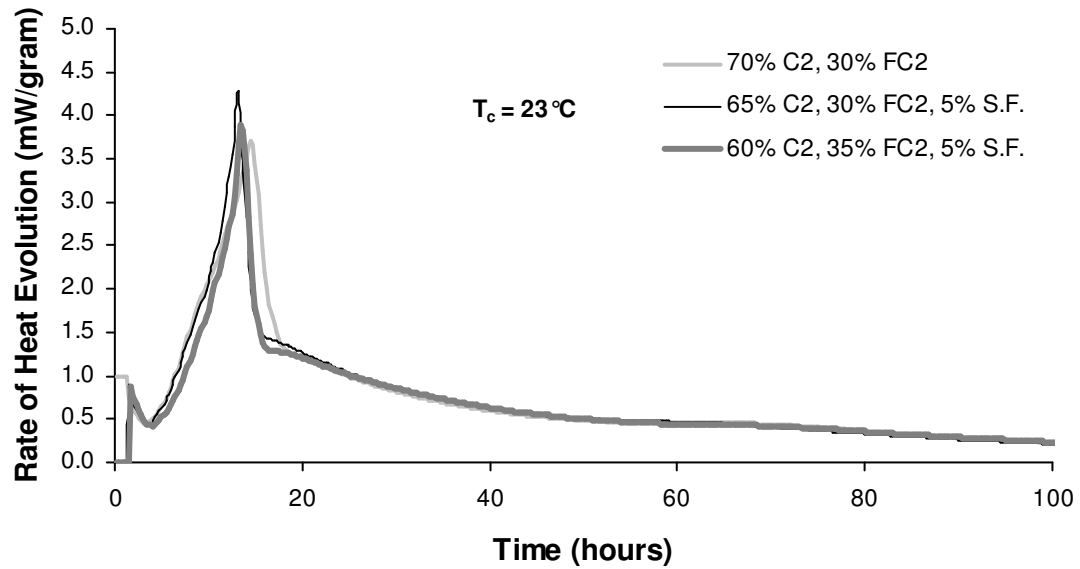


Figure 4-27: Cement C2 with Silica Fume, 30%, and 35% Replacement by Mass of FC2 (CaO=28.9%)

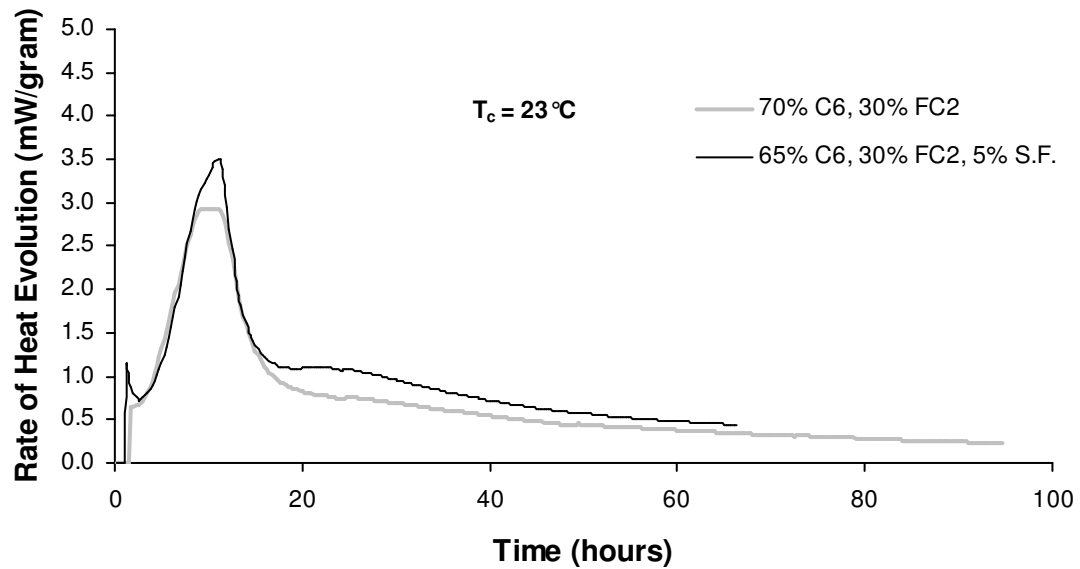


Figure 4-28: Cement C6 with Silica Fume and 30% Replacement by Mass of FC2 (CaO=28.9%)

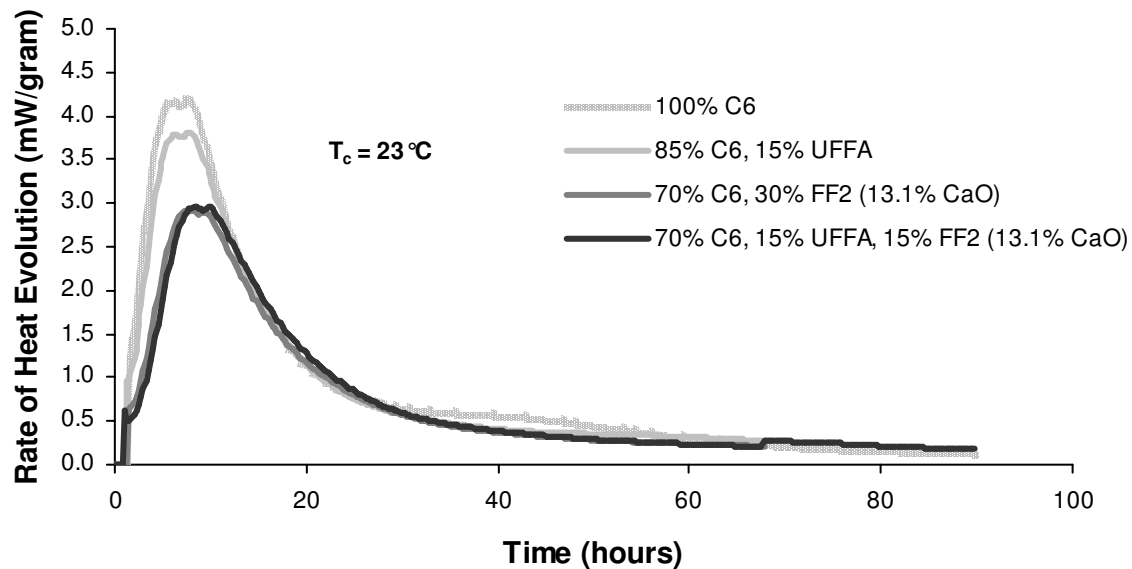


Figure 4-29: Cement C6 with UFFA and FF2 (CaO=13.1%)

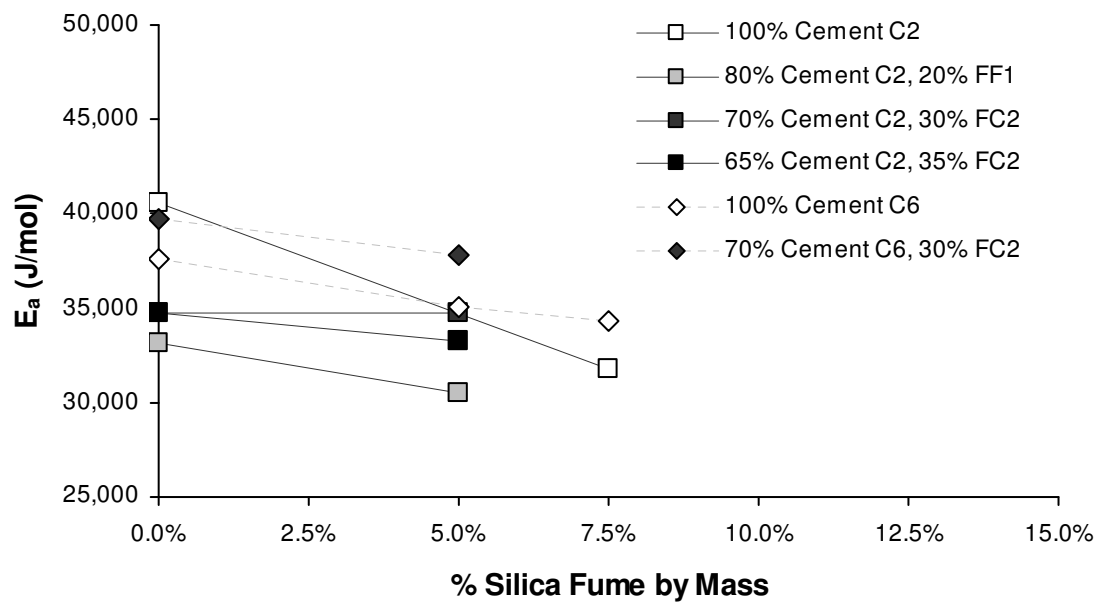


Figure 4-30: Summary of E_a Trends for Mixtures with Silica Fume

CHAPTER 5. A MODEL FOR ESTIMATING THE ACTIVATION ENERGY OF CEMENTITIOUS SYSTEMS

Previous research has demonstrated the validity of the Arrhenius equation to accurately characterize the progress of hydration of cement. Application of the Arrhenius equation requires the selection of an activation energy (E_a) to define the temperature sensitivity of the reaction. A model that predicts E_a taking into account the variable chemistry of cementitious systems is needed. This chapter will describe a model for E_a developed using multivariate statistics on experimental hydration data. The model accounts for the effects of cement chemistry, supplementary cementing materials, and chemical admixtures.

5.1. INTRODUCTION

The heat of hydration of cementitious materials has been well studied. Cement hydration and the mechanisms behind most chemical admixtures (such as retarders and superplasticizers) are relatively well understood, while the mechanisms of certain supplementary cementing materials (SCMs) such as Class C fly ash and ground-granulated blast-furnace (GGBF) slag are less well understood. Various models have been developed to model the heat of hydration of a cementitious system^{1,2}. These models are generally based on the Arrhenius equation, which models the temperature sensitivity of a reaction, as shown in Equation 5-1:

$$k = A \cdot e^{\frac{-E_a}{RT}} \quad \text{Equation 5-1}$$

where R = natural gas constant (8.314 J/mol/K), T = temperature (K) at which reaction occurs, k = rate of heat evolution (W), A = proportionality constant (same units as k), and E_a = activation energy (J/mol).

Activation energy has been shown to be a useful measure of the early age temperature sensitivity of a concrete mixture^{1,2}. Measurements of E_a in cementitious systems represent a blended temperature sensitivity of the mixture because isolation of the individual constituent reactions is very difficult. The underlying mechanisms that affect E_a have not been well understood. As a result, a parametric study, combined with multivariate regression analysis is needed to develop a model for E_a . The results of such a model should complement existing theories of hydration, rather than introduce any new mechanisms.

Previous research^{3,4,5} has presented several distinct hydration trends in E_a . Some of these trends are clearly visible in two-variable (one dependent and one independent variable) analyses of the test data. For example, the addition of SCMs (independent variable) to a mixture alters E_a (dependent variable) in proportion to the reactivity of the SCM (insert reference). E_a will be lower with the addition of a Class F fly ash, but will tend to be higher with a Class C fly ash or slag⁵. Also, the addition of an accelerator, retarder, water reducer, or HRWR admixture will reduce E_a , generally in proportion to the effect of the chemical admixture on the hydration of C_3S and C_3A , and the amount of retardation that the admixture imparts⁴.

Other trends in E_a are less clear. For example, an increase in the w/cm may decrease E_a , but the effect is very slight. Second, alkalis and sulfates in the cementitious system have some effect on E_a . Lerch⁶ showed that the amount, phase, and solubility of alkalis and sulfates present in the cementitious system will significantly alter the hydration of cement. These variables will affect the rate and timing of the C_3A hydration. This, in turn, may alter the activation energy (E_a) of the system. Variables

such as amount of C_3A phase, amount of alkali phase and its solubility, and amount of sulfate phase and its solubility are difficult to isolate for testing, so multivariate regression analysis is a useful method to determine the effects of each of these variables.

This study examines the results from 116 calculated E_a values using multivariate regression analysis. A statistical model for E_a based on the cement chemistry, SCM type and dosage, and chemical admixture type and dosage is developed, and is compared to established hydration mechanisms and existing experimental data from the literature. The model reflects existing theories about the hydration mechanisms of cementitious systems.

5.1.1. SUMMARY OF E_A TRENDS

The first step in developing a model for E_a is to identify the trends that are visible without multivariate regression analysis. The results from the isothermal calorimetry used to calculate E_a were presented previously, and selected results will be discussed here to highlight several of the important trends that are apparent in the data. The following trends were visible without regression analysis. The trends are summarized in Table 5-1.

The C_3A and gypsum content of the cement will influence E_a . Increasing the C_3A or gypsum content of the cement will increase E_a ³. In general, gypsum is added to cement to regulate the hydration of C_3A . Also, increased Blaine fineness will decrease E_a ³. This is because smaller particle size allows easier dissolution of the cement. Increasing w/cm slightly lowers E_a ³. The decrease is likely the result of dilution, since the increase in water content should promote the dissolution and hydration of the crystalline phases in the cement. A similar effect is seen with the addition of a low-CaO fly ash⁵, since the reduction in reactive cement content in the system also effectively dilutes it with

respect to water. It is also possible that the fly ash provides some preferential nucleation sites for C-S-H, increasing reactivity and thereby lowering E_a . However, the heat-of-hydration curves strongly suggest dilution as the primary mechanism.

The addition of reactive SCMs will affect E_a in more complex manner than low-CaO fly ash does. Much of the sensitivity in E_a values when SCMs are used depends on the cement used in the system, i.e. trends that hold true for one cement may not be the same for another. For some cements, the addition of ground-granulated blast-furnace (GGBF) slag or high-CaO fly ash will raise E_a significantly, while for other cements, these SCMs will have little effect². Silica fume reduces E_a fairly significantly. It is likely that the addition of silica fume to a mixture will promote the hydration of C_3S by providing preferential nucleation sites for C-S-H⁷.

The specific effects of cement and SCM chemistry variables on E_a are difficult to parse. However, the ease with which the aluminate phase reacts seems crucial. Sulfate content and availability, and alkalis strongly affect the hydration of the aluminates. E_a seems to be related to the total reactive aluminate phase in the system and its interaction with SCMs and chemical admixtures. SCMs or chemical admixtures that increase the height of the aluminate peak generally reduce E_a . Also, E_a seems to rise when the addition of highly reactive SCMs to the mixture does not substantially increase the height of the aluminate peak. Unfortunately, oxide analysis of the cement and SCMs only provides a part of the puzzle. Information on the availability of soluble sulfate, the phases in which the alkalis are present, and the reactivity of phases in the fly ash and GGBFS is not readily available, but is important for a full understanding the hydration process.

Chemical admixtures have a variety of different effects on E_a , as would be expected given their different effects on concrete performance. The addition of low-range water reducer (LRWR), water-reducer/retarder (WRRET), high-range water reducers (NHRWR and PCHRWR), and calcium nitrate-based accelerators (ACCL) reduce E_a to some degree⁴. The addition of a retarder (WRRET) and an accelerator (ACCL) reduce E_a more than the other admixtures, and higher dosages of WRRET reduce E_a to a threshold value⁴. LRWR, HRWR and PCHRWR act by dispersing and deflocculating cementitious particles (either ionic or steric repulsion). This facilitates the dissolution of the crystalline phases of the cement and tends to slightly reduce E_a . WRRET and ACCL affect the reaction rate and timing of the C_3S and C_3A in the cement, and tend to more greatly reduce E_a .

The data collected in this study suggest that the relationship between *WRRET* and E_a is nonlinear. With cement C2 it was seen that E_a drops as *WRRET* dosage increases up to some limit of dosage. From previous research⁴, dosages of *WRRET* over 0.35% by mass tend to excessively retard the cement paste. When *WRRET* is overdosed, E_a ceases to drop. This type of relationship could be modeled by using a nonlinear equation. However, the dosage at which E_a ceases to drop may vary depending on the cement and SCM percentages in the mixture. Therefore, in the case of a very high dosage of admixture, a lower bound should be placed on the calculated value for E_a . It is suggested that a lower bound of 25,000 J/mol is appropriate until further testing can confirm the behavior of cementitious systems at extreme admixture dosages.

5.2. RESEARCH SIGNIFICANCE

This chapter presents a comprehensive multivariate statistical model of E_a for cement pastes with different chemistries, supplementary cementing materials, and chemical admixtures. The model reflects relatively well known hydration behavior that has been observed in cementitious systems. The results provide a predictive tool to model the temperature dependency of concrete mixtures in the first week of hydration. The model improves the ability to predict temperature gradients, maximum concrete temperatures, and thermal stresses in concrete.

5.3. EXPERIMENTAL METHODS FOR E_a DETERMINATION

In previous research^{3,4,5}, a total of 116 calculated activation energy (E_a) values were presented. E_a was determined from isothermal calorimetry, which was performed on cementitious pastes at 5, 15, 23, 38, and 60 °C (41, 59, 73, 100, and 140 °F) using an eight-channel isothermal conduction calorimeter. The tests examined the effects of cement chemistry, supplementary cementing materials (SCMs), and chemical admixtures, and interactions between the SCMs and chemical admixtures on E_a . Details of the calculation methods used to determine E_a have been presented previously⁸. The following sections highlight the materials that were investigated, and discuss the procedure for determining the variables that will model E_a .

5.3.1. MATERIALS

Three Type I cements (C1, C2 and C3), three Type I/II cements (C4, C5, and C6), two Type III cements (C7 and C8), and one Type V cement (C9) conforming to ASTM C150¹⁵ were used. The following SCMs were used: two ASTM C 618¹⁰ Class F fly ashes (FF1 and FF2), two ASTM 618¹⁰ Class C fly ashes (FC1 and FC2), one ultra-fine fly ash

(UFFA), one ASTM C 989¹¹ Grade 120 ground-granulated blast-furnace slag¹¹ (S1), and one silica fume (SF). De-ionized water was used for mixing. The following water reducers conforming to ASTM C 494¹² were used: a Type A glucose-based low-range water reducing admixture (LRWR), a Type B and D lignosulfonate-based water reducing and retarding admixture (WRRET), a Type F naphthalene-sulfonate-based high-range water-reducing admixture (NHRWR), and a Type F polycarboxylate-based high-range water-reducing admixture (PCHRWR). The accelerator used was an ASTM C 494¹², Type C calcium nitrate-based accelerator.

Chemical and physical properties of the cements are summarized in Table 5-2, and for the SCMs are summarized in Table 5-3. Cement phases were calculated from x-ray fluorescence data using the Bogue calculations per ASTM C 150⁹. Cement phases were also calculated from quantitative x-ray diffraction (QXRD) data using Rietveld analysis¹³.

5.4. E_A MODEL DEVELOPMENT PROCESS

5.4.1. VARIABLE SELECTION

Based on the observations in the previous section, several variables are likely to have an effect on E_a . These include the aluminate content of the cement, the fineness of the cement, water-cementitious materials ratio, the amount and type of chemical admixtures, the replacement percentage and reactivity (as measured by CaO content) of SCM, the total alkalis in the cement or in the system, and the amount of sulfate in the system. Possible interactions that should be investigated include the relationships between the following variables: water reducing admixtures, retarding admixtures, and reactive SCMs (Class C fly ash and GGBF slag), water reducers/retarders and aluminates,

accelerators and aluminates, and Class C fly ash, aluminates, gypsum, and total alkalis. The combined effect of each of these variables on E_a is unknown. Several statistical techniques will be used in the following section to isolate the variables and interactions of greatest importance.

5.4.2. MULTIVARIATE REGRESSION ANALYSIS

In order to model the combined effects of these trends, multivariate regression analysis was performed to identify the critical variables. The results were used to develop a statistical model that describes the combined effects of different independent variables on E_a . There are several steps to develop a model for E_a . The sequence of procedures used here to analyze the results has been used in previous research¹⁴. First, the results and variables from the isothermal testing are summarized in a database. Next, the independent variables that have the greatest effect on E_a are determined. The trends from previous studies are summarized in Table 5-1 . However, a systematic analysis of the variables is needed to isolate the important variables. Once the independent variables are chosen, an estimate of their statistical significance is needed. An analysis of variance (ANOVA) is performed on the selected variables. Finally, a model is developed that estimates the contribution of each variable to E_a . The following procedure was followed to evaluate the results.

5.4.3. APPLICATION OF ARRHENIUS THEORY TO E_A REGRESSION ANALYSIS

A framework is necessary to evaluate a model for E_a . Therefore, Equation 5-2, Equation 5-3, and Equation 5-5 are used to assess the accuracy of the E_a model that is ultimately developed. The concept of “equivalent age” is necessary to utilize E_a to

predict hydration behavior at various curing temperatures. Equation 5-2, proposed by Friesleben Hansen and Pederson², is the most common expression used to compute equivalent age, and is used in the remainder of the chapter to model the effects of time and temperature on hydration:

$$t_e(T_r) = \sum_0^t e^{-\frac{E_a}{R}(\frac{1}{T_c} - \frac{1}{T_r})} \cdot \Delta t \quad \text{Equation 5-2}$$

where $t_e(T_r)$ = equivalent age at reference temperature (T_r (°K)), T_c = temperature of the concrete (°K), and E_a and R are as defined previously.

The progress of the hydration of portland cement may be quantified by the degree of hydration (α), which varies from 0 to 1, with a value of 1 indicating complete hydration. For this study, degree of hydration is taken as the ratio of heat evolved at time, t , to the total amount of heat available, as shown in Equation 5-3^{15,16,17,18,19}:

$$\alpha = \frac{H(t)}{H_u} \quad \text{Equation 5-3}$$

where α = degree of hydration at time t , $H(t)$ = heat evolved from time 0 to time t (J/gram), and H_u = total heat available for reaction (J/gram).

A mathematical relationship may be used to model the degree of hydration development. A number of researchers^{1,20} have suggested an exponential function to characterize cement hydration based on degree of hydration data. The most commonly used relationship is a three-parameter model defined in Equation 5-4:

$$\alpha(t_e) = \alpha_u \cdot e^{-\left[\frac{\tau}{t_e}\right]^\beta} \quad \text{Equation 5-4}$$

where $\alpha(t_e)$ = degree of hydration at equivalent age t_e , t_e = equivalent age determined from Equation 5-2 (hours), τ = hydration time parameter (hours), β = hydration shape parameter, and α_u = ultimate degree of hydration.

Equation 5-2 through Equation 5-4 will be used to help develop and evaluate the E_a model. To use least squares regression analysis, it is necessary to break the data into discrete points. This requires several steps. First, Equation 5-2 is solved for different time steps at 5, 15, 23, 38, and 60 °C (41, 59, 73, 100, and 140 °F). This gives discrete points that quantify the equivalent age at each time and temperature. Then, the degree of hydration is calculated at each time and temperature using Equation 5-4. Equation 5-4 uses curve fit parameters (α_u , β , and τ) generated experimentally from the isothermal tests performed at different temperatures. The result of the calculations is a discrete estimate of the degree of hydration at different equivalent ages. The experimental results may then be compared to the model created from non-linear regression analysis. E_a values (116) were calculated using isothermal results from five different isothermal temperatures. The degree of hydration was calculated for each test at 18 different times. This combination of data gives a total of 10,440 data points to evaluate the E_a model.

5.4.4. INDEPENDENT VARIABLE SELECTION

A statistical procedure using multivariate regression was used to isolate the independent variables (regressors or predictor variables) that could have an effect on the dependent variable (or response variable) E_a . The procedure analyzes a specified number of combinations of the independent variables and ranks them according to the coefficient of determination (R^2). A comparison of R^2 versus a number of combinations of variables provides a method to screen different combinations of independent variables. The

procedure also provides a matrix of the correlation coefficients of each variable combination. Next, an ANOVA (ANalysis Of Variance Analysis) of Type I and Type III errors, analysis of covariance, and a non-linear multivariate regression analysis were performed on each potential combination of variables. Computational procedures and regression output are included in Appendix D.

5.4.5. MODEL SELECTION

The multivariate regression analysis has several steps. First, E_a and the independent variables from the E_a test results are summarized in a database. Next, a specified number of combinations of the independent variables are analyzed and ranked according to their coefficient of determination (R^2). The model for E_a should describe as much of the variability as possible with as few independent variables as possible. A complex model with a large number of independent variables may show incremental gains in accuracy compared simpler a model, but these gains may be negated by poor predictive ability of the model. Based on prior studies on activation energy^{3,4,5}, several possible variables were considered highly likely to have an effect on E_a . These variables were w/cm, dosage of WRRET, HRWR, ACCL, and PCHRWR, % Silica Fume, % Fly Ash, % CaO of fly ash, % GGBFS, % Gypsum or soluble SO_4^{2-} , % C_3S , % C_2S , % C_3A , % C_4AF , and Blaine fineness of cementitious material.

Additionally, the correlation coefficient, $Corr(x_1, x_2)$, between each of the variables (x_1 and x_2) is calculated to ensure that the variables are truly independent. For the purposes of this study, $Corr(x_1, x_2) < 0.65$ was chosen as a sufficiently weak correlation between two variables to allow both to be included in the model for E_a . The combination of variables that has the highest R^2 and a correlation coefficient for any two

variables less than 0.65 is considered a candidate for the model. Next, an analysis of variance (ANOVA) for Type I and Type III errors is performed on each potential variable combination. A Type I error measures the probability that the model shows a relationship between an independent variable and the dependent variable (in this case, E_a) when there is really no relationship²¹. A Type III evaluates the probability that the choice of independent variables shows a statistical correlation, but that wrong direction or variable has been chosen²¹. Variables with a probability greater than 5% of Type I or III errors are not included in the model. These errors are substantially reduced by selecting variables that have been clearly shown to affect hydration, such as those presented in Table 5-1.

For this study, linear and non-linear models for E_a are investigated, since the exact effects of the independent variables on E_a are unknown. Schindler¹ used a non-linear model to describe E_a . A non-linear model was reported to provide a better estimate of the behavior of E_a ¹. However, a linear model is more straightforward. Therefore, both linear and non-linear models will be included in the analysis. Based on the results presented previously^{3,4,5}, the relationship between E_a and most of the independent variables appears to be linear. A linear expression for E_a will be used since the R^2 for a linear model was similar to the non-linear model. A lower bound of 25,000 J/mol should be set for cases where an over dosage of chemical admixture occurs.

5.5. ACTIVATION ENERGY (E_A) MODEL

Based on the non-linear regression analysis presented above, two linear models were developed to describe the effects of different SCMs, admixtures, and cement properties. The strongest correlations with E_a were found with WRRET ($R^2=0.36$) and %

GGBFS ($R^2=0.14$). Two models are presented to account for the differences in calculation methods of cement phases. The final form of the first model, based on phase analysis of the cement using Bogue calculations, is shown in Equation 5-5.

$$\begin{aligned}
 E_a = & 41,230 + 1,416,000 \cdot [(C_3A + C_4AF) \cdot p_{Cement} \cdot SO_3 \cdot p_{Cement}] \\
 & - 347,000 \cdot Na_2O_{eq} - 19.8 \cdot Blaine \\
 & + 29,600 \cdot p_{FlyAsh} \cdot p_{CaO-FlyAsh} + 16,200 \cdot p_{GGBFS} - 51,600 \cdot p_{SF} \\
 & - 3,090,000 \cdot WRRET - 345,000 \cdot ACCL
 \end{aligned}
 \tag{Equation 5-5}$$

where p_{cement} = % cement in mixture; p_{FlyAsh} = % fly ash in mixture; $p_{CaO-FlyAsh}$ = % CaO in fly ash; p_{GGBFS} = % GGBFS in mixture; p_{SF} = % silica fume in mixture; $Blaine$ = Blaine fineness of cement; Na_2O_{eq} = % Na_2O_{eq} in cement ($0.658 \times \%K_2O + \%Na_2O$); C_3A = % C_3A in cement; C_4AF = % C_4AF in cement; SO_3 = % SO_3 in cement; $WRRET$ = ASTM Type A&D water reducer/retarder, % solids per gram of cementitious material; $ACCL$ = ASTM Type C calcium-nitrate based accelerator, % solids per gram of cementitious material.

The final form of the second model, based on phase analyses of the cement using Rietveld analysis, is shown in Equation 5-6

$$\begin{aligned}
 E_a = & 39,200 + 1,069,000 \cdot [(C_3A) \cdot p_{Cement} \cdot (CaSO_4 \cdot xH_2O + K_2SO_4) \cdot p_{Cement}] \\
 & - 12.2 \cdot Blaine + 12,400 \cdot p_{FlyAsh} \cdot p_{CaO-FlyAsh} + 12,000 \cdot p_{GGBFS} - 53,300 \cdot p_{SF} \\
 & - 3,020,000 \cdot WRRET - 343,000 \cdot ACCL
 \end{aligned}
 \tag{Equation 5-6}$$

Where $CaSO_4 \cdot xH_2O$ = Sum of % by mass of gypsum, hemihydrate, and anhydrite, K_2SO_4 = % by mass of arcanite, and C_3A = % C_3A in cement, and all other variables the same as for Equation 5-5.

The results of Equation 5-5 and Equation 5-6 are very similar. The equations differ in the way they account for the effects of gypsum and aluminates on E_a . Equation 5-5 is based on Bogue calculations of the crystalline phases in cement, and uses

$[(C_3A+C_4AF)\times C\hat{S}H_2]$ to model E_a . Equation 5-6 is based on Rietveld analysis of the crystalline phases in cement, and models E_a using $(C_3A)\times(C\hat{S}H_2+C\hat{S}H_{0.5}+C\hat{S}H+K_2SO_4)$. The other independent variables are the same, and the coefficients are relatively the same magnitude. A plot of the predicted E_a value, using Equation 5-5, versus the measured E_a value for the 116 combinations tested in this study is shown in Figure 5-1. The plot of the residuals for the same analysis is shown in Figure 5-2. The residual plot appears random, which indicates that the linear model of E_a captures the behavior fairly well. The residual plot also shows which tests could potentially be outliers. These potential outliers are generally tests that had fairly high dosages of low-range water-reducer/retarder, and that had large replacement percentages of GGBF slag or Class C fly ash. Figure 5-3 and Figure 5-4 compare the measured degree of hydration to the degree of hydration predicted from the model in Equation 5-5 for two example mixtures. These figures show that even for the outliers, the model provides acceptable results for the measured degree of hydration at all ages.

When the error from the regression analysis (residuals) is plotted versus each of the independent variables, the distribution of error should be random. All of the variables chosen for the E_a model have a random distribution of error. The plot of the residuals for the independent variables is shown in Appendix D. Also, the sensitivity of the model to each of the independent variables on E_a is shown in Figure 5-5 through Figure 5-13. These figures show the sensitivity of the model to changes in each independent variable. 95% confidence intervals are given for each variable. Several trends are apparent, and will be discussed below.

5.5.1. EFFECTS OF CEMENT CHEMISTRY AND FINENESS ON E_a

Phases in the cement will generally be determined by one of two methods: Bogue calculations or Rietveld analysis. When Bogue calculations are used, Equation 5-5 shows that an increase in the aluminate, ferrite, or gypsum content in the cement will raise E_a . When Rietveld analysis is used, Equation 5-6 shows that an increase in the aluminate or total soluble sulfate ($\text{C}\hat{\text{S}}\text{H}_2 + \text{C}\hat{\text{S}}\text{H}_{0.5} + \text{C}\hat{\text{S}}\text{H} + \text{K}_2\text{SO}_4$) content will raise E_a . $\text{C}\hat{\text{S}}\text{H}_2$ is added to cement to retard the hydration of the aluminates. If the aluminate content in the cement (especially C_3A) rises, the $\text{C}\hat{\text{S}}\text{H}_2$ content will typically rise as well. In the model presented here, this will result in a higher E_a . This relationship is shown in Figure 5-5 and Figure 5-6.

Also, Blaine fineness will have an effect on E_a . A higher Blaine fineness corresponds to a finer particle size distribution of the cement. Finer cement allows a greater surface area to be available for dissolution and reaction. Since increasing Blaine fineness allows the cement to react more readily, higher Blaine fineness lowers E_a in this model. This relationship is shown in Figure 5-7.

Finally, the total alkali content will influence E_a in Equation 5-5 (Bogue calculations). This is because the total alkali content in the cement will affect the pH of the cementitious system. Alkalis in cement are usually present as alkali sulfates²², or may be incorporated in the crystalline phases of the cement²³. Hydroxyl ions will balance the Na^+ and K^+ ions in solution. This allows an easier dissolution of the various phases of the cement and SCMs, and may affect the solubility of $\text{C}\hat{\text{S}}\text{H}_2$. However, the effect of alkalis in the SCMs is unknown, since the rate of their solubility and phase composition is unknown with Bogue calculations. Therefore, only the alkalis in the cement will be

considered in the model. The relationship between the equivalent alkali content and E_a is shown in Figure 5-8.

If Rietveld analysis is done, an estimate of the alkali sulfates (arcanite (K_2SO_4) and thenardite (Na_2SO_4)) may be obtained. However, the equivalent alkali content of the cement from oxide analysis does not factor into the model based on Rietveld analysis (Equation 5-6). Instead, arcanite is the only independent variable that accounts for alkalis.

5.5.2. EFFECTS OF SCMS ON E_A

The type and percentage replacement of an SCM in the cementitious system has a large effect on E_a . Fly ash raises and lowers E_a in proportion to the CaO content of the fly ash. Low-CaO fly ashes will lower E_a of the cementitious system, while higher CaO ashes will raise E_a slightly, as shown in Figure 5-9. Also, E_a tends to rise with increasing dosage of GGBF slag, as shown in Figure 5-10. This agrees with existing research^{23,24,25} which supports the higher temperature sensitivity of GGBF slag. Third, silica fume tends to reduce E_a , which again correlates well with literature²⁴. The sensitivity of the model is shown in Figure 5-11.

The relationship between the shape of the heat evolution curve for each mixture and the class of fly ash is certainly dependent on more than CaO and replacement percentage. Also, only one type of GGBF slag was investigated (Grade 120). It is quite possible that different grades or sources of GGBF slag will have a different effect on E_a . However, more detailed information about the phase composition and reactivity requires that Rietveld analysis be performed and this is not commonly done for SCMs. In addition, an incremental improvement in model accuracy is probably possible with a

more detailed phase analysis, but is not practical given the information available on most SCMs. Accurate and universal characterization of the reactivity and solubility of the phases in fly ash and slag is not yet common. A model that incorporates more information than is readily available to most engineers is not very useful to practitioners. Therefore, the model variables for this study are limited to SCM type, replacement percentage, and CaO of fly ash.

5.5.3. EFFECTS OF CHEMICAL ADMIXTURE ON E_A

Chemical admixtures alter E_a significantly. Both low-range water reducers and retarders (WRRET) and accelerators (ACCL) tend to lower E_a . For WRRET, this is likely due to a combination of dispersion, retardation of the C_3S phases, and acceleration of the aluminate phases. For ACCL, the change in E_a is believed to be due to acceleration of the C_3A hydration⁴. Figure 5-12 and Figure 5-13 show the effects of WRRET and ACCL on E_a , as modeled in Equation 5-5. For the WRRET, 4 oz/100 lbs (2.61 mL/kg) cementitious material should be considered the upper end of admixture dosage (based on manufacturer's recommended dosage). This is a typical dosage of WRRET. However, the results presented previously show that a cement paste (no aggregate) with this dosage of WRRET is most likely overdosed. Therefore, for modeling purposes, 1 oz/100 lbs cementitious (0.65 mL/kg) should be considered low, 2 oz/100 lbs. (1.30 mL/kg) considered medium, and 3-4 oz/100 lbs (1.96-2.61 mL/kg) considered a high dosage of WRRET.

The admixture portion of the model has several limitations. First, a particular dosage of chemical admixture may behave one way in a concrete mixture and a different way in a cement paste. For example, water reducers may improve workability more with

pastes than with concrete, because the coarse and fine aggregate are left out of the mixture. Therefore, the activation energy determined for a particular admixture dosage from isothermal calorimetry may be somewhat inaccurate. However, previous research has shown that isothermal calorimeter results on paste reasonably approximate the hydration of concrete in semi-adiabatic calorimetry⁴. As a result, the sensitivity of the E_a model to admixture dosage should be reasonably accurate in this respect. Another limitation is that the model is based on a limited number of chemical admixtures. Also, the ingredients in the chemical admixtures are not always known. For example, some water reducers may have unknown dosages of an accelerator or a retarder, which can result. Therefore, inaccuracies in the prediction of E_a could result if an admixture is used that is markedly different than the ones presented here.

5.5.4. OTHER VARIABLES INVESTIGATED

The effects of water-to-cementitious materials ratio, air-entraining admixture (AEA), and various naphthalene and polycarboxylate-based high-range water-reducing admixtures (HRWR) were investigated. Each of these variables seemed to have some effect on E_a . However, their influence was small compared to the variables included in the model. Water-cementitious materials ratio had a minor effect on E_a . When the compounding effects of the different independent variables were considered, the effects that AEA and HRWR have on E_a were not large enough to warrant their inclusion in the model.

5.6. CONCLUSIONS

This chapter presents a model for activation energy (E_a) of cementitious systems that accounts for cement chemistry, fineness, SCMs, and chemical admixtures. The

results of the model are presented in Equation 5-5 and Equation 5-6, based on Bogue calculations and Rietveld analysis of cement phases, respectively. Equation 5-5 and Equation 5-6 are the models that best fit the activation energy results, while using variables that meet the requirements for statistical significance. Models from regression analyses (as opposed to purely mechanistic models) are inherently limited by the range of variables in the empirical data set. The models presented here are similarly limited. However, by focusing on the most important variables and ensuring that the results of the models confirm experimental tests of E_a , the results should be broadly applicable.

The first model (Equation 5-5) uses independent variables that are readily available on mill certifications for cement, fly ash, slag, and silica fume. An analysis using Bogue compounds has inherent limitations. For example, the phases determined from Bogue calculations can be very inaccurate¹³, especially when calculating C_3A . However, more complex phase analysis is often not available. If Rietveld analysis is available, the second model (Equation 5-6) is appropriate for the prediction of E_a , since it incorporates more accurate information about the aluminate and sulfate phases. With respect to SCMs, both models can only account for the SCM type, replacement percentage, and CaO content of fly ash because of the scarcity of more detailed and relevant information about the SCMs. Finally, the models are limited in the composition of the chemical admixtures tested. Nevertheless, the models presented in this chapter take into account more variables than any previous model and provide a very good estimate of the effects of chemical admixtures on E_a .

5.7. REFERENCES

1. Schindler, A.K., and K.J. Folliard, "Heat of Hydration Models for Cementitious Materials", *ACI Materials Journal*, V. 102, No. 1, Jan.-Feb., 2005, pp. 24-33.
2. Freiesleben Hansen, P., and E.J. Pedersen, "Maturity computer for controlling curing and hardening of concrete," *Nordisk Betong*, V. 1, No. 19, 1977, pp. 21-25.
3. Poole, J.L., "The Effects of Cement Chemistry and Water-Cement Ratio on Activation Energy," PhD Dissertation, Chapter 2, The University of Texas at Austin, Austin, TX, 2007, pp 6-37.
4. Poole, J.L., "The Effects of Chemical Admixtures on Activation Energy of Cementitious Materials," PhD Dissertation, Chapter 3, The University of Texas at Austin, Austin, TX, 2007, pp 38-68.
5. Poole, J.L., "The Effects of Supplementary Cementing Materials on Activation Energy of SCMs," PhD Dissertation, Chapter 4, The University of Texas at Austin, Austin, TX, 2007, pp 69-108.
6. Lerch, W., "The Influence of Gypsum on the Hydration and Properties of Portland Cement Paste," *Proceedings of the American Society for Testing Materials*, V. 46, 1946.
7. Massazza, F., "Pozzolana and Pozzolanic Cements" Lea's Chemistry of Cement and Concrete, 4th ed., ed. P.C. Hewlett, Arnold Publishers, New York, 1998, p 471-631.
8. Poole, J.L., K.A. Riding, K.J. Folliard, M.G.C. Juenger, and A.K. Schindler "Methods of Activation Energy Calculation for Portland Cement," *ACI Materials Journal*, V. 104, No. 1, Jan.-Feb., 2007, pp. 303-311.

9. ASTM C 150, "Standard Specification for Portland Cement," Annual Book of ASTM Standards, Vol 04.01., ASTM International, West Conshohocken, PA., 2002, 8 pp.
10. ASTM C 618, "Standard Specification for Coal Ash and Raw or Calcined Natural Pozzolans for Use in Concrete," Annual Book of ASTM Standards, V. 04.01., ASTM International, West Conshohocken, PA., 2003, 3 pp.
11. ASTM C 989, "Standard Specification for Ground Granulated Blast-Furnace Slag for Use in Concrete and Mortars," Annual Book of ASTM Standards, V. 04.01., ASTM International, West Conshohocken, PA., 2005, 5 pp.
12. ASTM C 494, "Standard Specification for Chemical Admixtures for Concrete," Annual Book of ASTM Standards, V. 04.01., ASTM International, West Conshohocken, PA., 2005, 10 pp.
13. Scrivener, K.L., T. Füllmann, E. Gallucci, G. Walenta, and E. Bermejo, "Quantitative Study of Portland Cement Hydration by X-Ray Diffraction/Rietveld Analysis and Independent Methods", *Cement and Concrete Research*, V. 34, 2004, pp 1541-1547.
14. Schindler, A.K., "Concrete Hydration, Temperature Development, and Setting at Early-Ages," Ph.D. Dissertation, University of Texas at Austin, Austin, TX, 531 pp.
15. Van Breugel, K., "Prediction of Temperature Development in Hardening Concrete", *Prevention of Thermal Cracking in Concrete at Early Ages*, RILEM Report 15, E & FN Spon, London 1998.

16. D'Aloia, L., and G. Chanvillard, "Determining the "Apparent" Activation Energy of Concrete; E_a – Numerical Simulations of the Heat of Hydration of Cement," *Cement and Concrete Research*, V. 32, 2002, pp. 1277-1289.
17. Kada-Benameur, H., E. Wirquin, and B. Duthoit, "Determination of Apparent Activation Energy of Concrete by Isothermal Calorimetry," *Cement and Concrete Research*, V. 30, 2000, pp. 301-305.
18. Copeland, L.E., Kantro, D.L., Verbeck, G., "Part IV-3 Chemistry of Hydration of Portland Cement," 4th International Symposium of the Chemistry of Cement, Washington, D.C., 1960, pp. 429-465.
19. De Schutter, G., and Taerwe, L., "Degree of Hydration-Based Description of Mechanical Properties of Early-Age Concrete," *Materials and Structures*, Vol. 29, No. 7, 1996, pp. 335-344.
20. Pane, I., and W. Hansen, "Concrete Hydration and Mechanical Properties under Nonisothermal Conditions," *ACI Materials Journal*, V. 99, No. 6, Nov.-Dec, 2002, pp. 534-542.
21. Devore, Jay L., *Probability and Statistics for Engineering and the Sciences*, 4th ed. Duxbury Press, New York, 743 p, 1995
22. Jackson, P.J., "Portland Cement: Classification and Manufacture" Lea's Chemistry of Cement and Concrete, 4th ed., ed. P.C. Hewlett, Arnold Publishers, New York, 1998, p 25-94.
23. Lawrence, C.D., "The Constitution and Specification of Portland Cements" Lea's Chemistry of Cement and Concrete, 4th ed., ed. P.C. Hewlett, Arnold Publishers, New York, 1998, p 131-193.

24. Ma, W., D. Sample, R. Martin, and P.W. Brown, "Calorimetric Study of Cement Blends Containing Fly Ash, Silica Fume, and Slag at Elevated Temperatures." *Cement, Concrete, and Aggregates*, V. 16, 1994, pp. 93-99.
25. Moranville – Regourd, M., "Cements Made From Blastfurnace Slag," Lea's Chemistry of Cement and Concrete, 4th ed., ed. P.C. Hewlett, Arnold Publishers, New York, 1998, p 633-674.

Table 5-1: Summary of Variables that Affect E_a

Action	Effect on E_a	Proposed Mechanism
<i>Class F Fly Ash Replacement</i> (\uparrow)	\downarrow	Dilution of cement with SCM ⁵
<i>Class C Fly Ash Replacement</i> (\uparrow)	\leftrightarrow for high C_3A , high Na_2O_{eq} cement; \uparrow for low C_3A , low Na_2O_{eq} cement	Combination of SO_4^{2-} available to retard the aluminates and alkalis available to solubilize the SCM ⁵
<i>GGBFS Replacement</i> (\uparrow)	\leftrightarrow for High C_3A , high Na_2O_{eq} cement; \uparrow for Low C_3A , low Na_2O_{eq} cement	Combination of SO_4^{2-} available to retard the aluminates and alkalis available to solubilize the SCM ⁵
<i>Silica Fume Replacement</i> (\uparrow)	\downarrow for cement mixtures; \downarrow for mixtures with fly ash	Dilution from SCM, nucleation sites for C_3S ⁵
<i>Higher w/cm</i>	\downarrow	Dispersion of cement from w/cm ³
<i>Add LRWR</i>	\downarrow	Dispersion of cement LRWR ⁴
<i>Add HRWR</i>	\downarrow	Dispersion of cement HRWR ⁴
<i>Add WRRET</i>	\downarrow	Retardation of C_3S and acceleration of C_3A from WRRET ⁴
<i>Add ACCL</i>	\downarrow for cement mixtures; \downarrow with fly ash replacement; \leftrightarrow with GGBFS replacement	Acceleration of C_3A and C_3S from ACCL ⁴
<i>Add Alkalis to 0.85% Na_2O_{eq}</i>	\leftrightarrow for cement mixtures; \uparrow with fly ash replacement	Solubility of reactive phases of fly ash goes up, which requires more SO_4^{2-} to regulate hydration. ³

Table 5-2: Chemical and Physical Properties of Cement

	Ty I LA	Ty I	Ty I	Ty I/II LA	Ty I/II LA	Ty I/II LA	Ty III LA	Ty III LA	Ty V
Cement	C1	C2	C3	C4	C5	C6	C7	C8	C9
SiO ₂ (%)	20.45	19.18	19.27	21.29	20.6	20.77	19.72	20.3	21.63
Al ₂ O ₃ (%)	5.43	5.34	5.08	4.88	4.8	3.88	5.27	4.85	4.04
Fe ₂ O ₃ (%)	2.01	2.3	3.08	2.92	3.2	3.73	2.02	3.56	5.29
CaO (%)	64.51	63.17	61.45	63.31	64.3	64.5	64.08	63.94	63.07
MgO (%)	1.15	1.09	2.64	1.23	1.5	1.01	1.22	0.82	0.77
Na ₂ O (%)	0.14	0.12	0.24	0.28	0.18	0.18	0.13	0.07	0.27
K ₂ O (%)	0.56	0.95	0.93	0.4	0.37	0.6	0.52	0.66	0.23
Na ₂ O Equiv. (%)	0.51	0.75	0.85	0.543	0.423	0.575	0.472	0.504	0.42
SO ₃ (%)	3.35	3.2	4.19	2.63	2.8	2.38	4.4	3.44	2.74
LOI (%)	1.80	4.1	2.41	2.43	1.2	2.67	1.95	1.71	1.55
Insoluble Residue (%)	-	0.63	0.3	-	0.18	0.25	-	-	1.43
CaO (%)**	0.0	0.0	0.7	0.0	0.0	0.0	0.0	0.0	0.0
C ₃ S (%)*	58.29	63.11	53.23	51.47	60.40	66.54	60.16	58.54	49.85
C ₃ S (%)**	61.2	61	57.2	56.6	55.5	55.7	64.6	54.0	49.0
C ₂ S (%)*	14.65	7.38	15.09	22.21	13.50	9.35	11.16	14.04	24.41
C ₂ S (%)**	16.0	15.6	15.1	18.6	17.4	21.1	11.8	21.7	26.4
C ₃ A (%)*	10.99	10.26	8.25	7.99	7.31	3.97	10.55	6.83	1.76
C ₃ A (%)**	13.1	9.6	5.3	6.4	6.8	4.0	12.4	5.7	4.4
C ₄ AF (%)*	3.5	6.0	9.6	8.6	9.74	10.7	4.0	10.2	12.1
C ₄ AF (%)**	5.70	5.44	7.12	4.47	10.7	4.05	7.48	5.85	4.66
Gypsum(%)*	1.4	0.4	6.6	3.1	4.76	0.0	2.4	0.0	2.3
C \hat{S} H ₂ (%)**	1.5	1.2	0.8	1.3	0.9	2.5	2.4	3.7	2.0
C \hat{S} H _{0.5} (%)**	0.6	0.7	0.4	0.6	1.9	0.7	0.6	0.6	0.4
C \hat{S} (%)**	1.5	1	1.6	0.8	0.9	0.7	0.8	1.3	0.9
K ₂ SO ₄ (%)**					0.5				
CaCO ₃ (%)**	0.8	3.6	1.7	3.4	2.5	3.2	0.7	1.5	2.5
Blaine fineness (m ² /kg)	350.0	390.9	388.9	413.2	404.9	365.4	552.0	539.0	409.0
H _{cem} (J/g)	501	530	461	458	494	496	501	493	464
H _{cem} *** (J/g)	481	482	473	447	471	463	485	474	419

*** Bogue Calculations, ** Rietveld Analysis ***Free CaO Determined from Rietveld Analysis**

Table 5-3: Chemical and physical properties of SCMs

	Fly Ashes					Other SCMs	
	FF1	FF2	FC1	FC2	UFFA	S1	S.F.
SiO ₂ (%)	56.63	51.69	37.83	33.31	50.65	34.48	94.28
Al ₂ O ₃ (%)	30.68	24.81	19.83	18.39	26.64	11.35	0.04
Fe ₂ O ₃ (%)	4.94	4.22	6.17	5.40	4.66	0.67	0.06
CaO (%)	0.69	13.12	23.13	28.91	10.85	41.73	0.51
MgO (%)	0.73	2.29	4.62	5.25	2.23	7.32	0.57
Na ₂ O (%)	0.12	0.18	1.74	1.64	0.41	0.14	0.06
K ₂ O (%)	2.26	0.84	0.06	0.35	1.02	0.38	0.99
Na ₂ O Eq. (%)	1.607	0.733	1.778	1.870	1.081	0.390	0.71
SO ₃ (%)	0.00	0.46	1.50	2.27	1.00	1.88	0.16
LOI (%)	2.10	0.23	0.67	0.34	0.39	0.83	3.10
Blaine fineness (m ² /kg)	147	166	348	300	394	332	20000

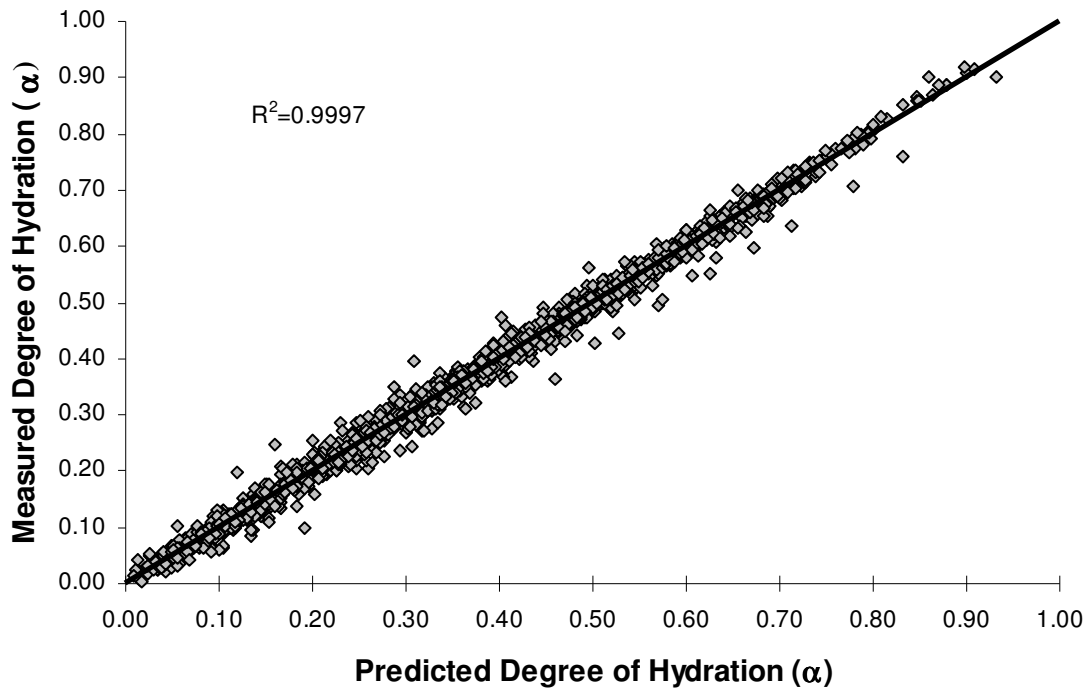


Figure 5-1: Predicted E_a v. Measured E_a for Non-Linear Model in Equation 5-5

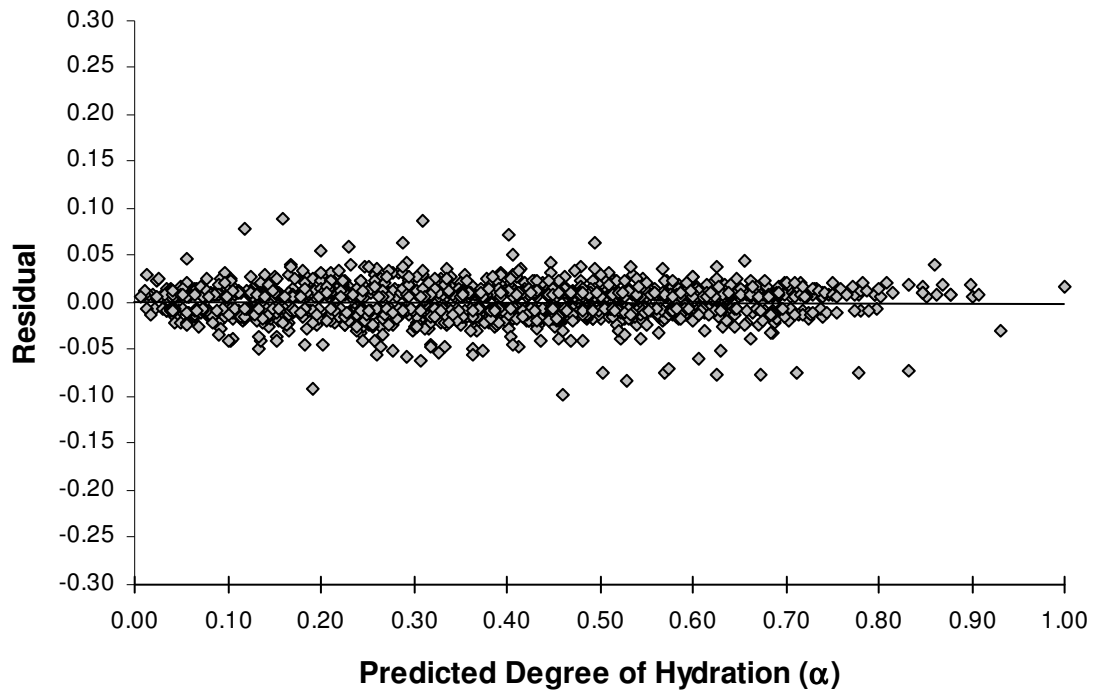


Figure 5-2: Residual Plot for Non-Linear E_a Model in Equation 5-5

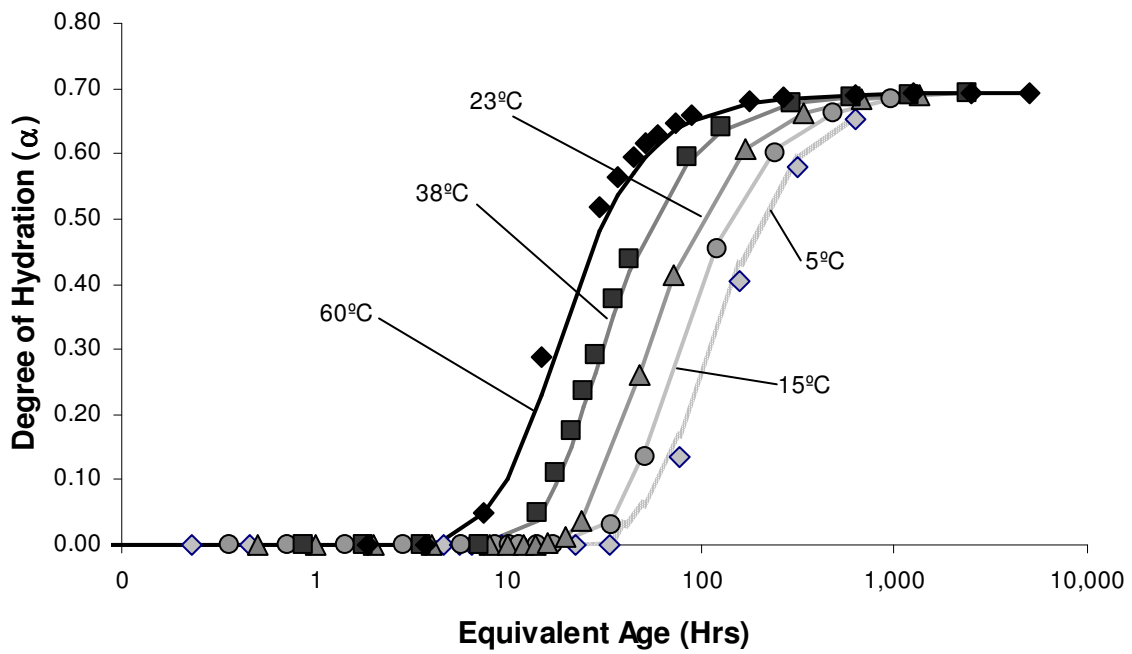


Figure 5-3: 70% Cement C2, 30% SCM-C1, 0.35% WRRET (Mix 44); Lines are predicted values; discrete points are measured values.

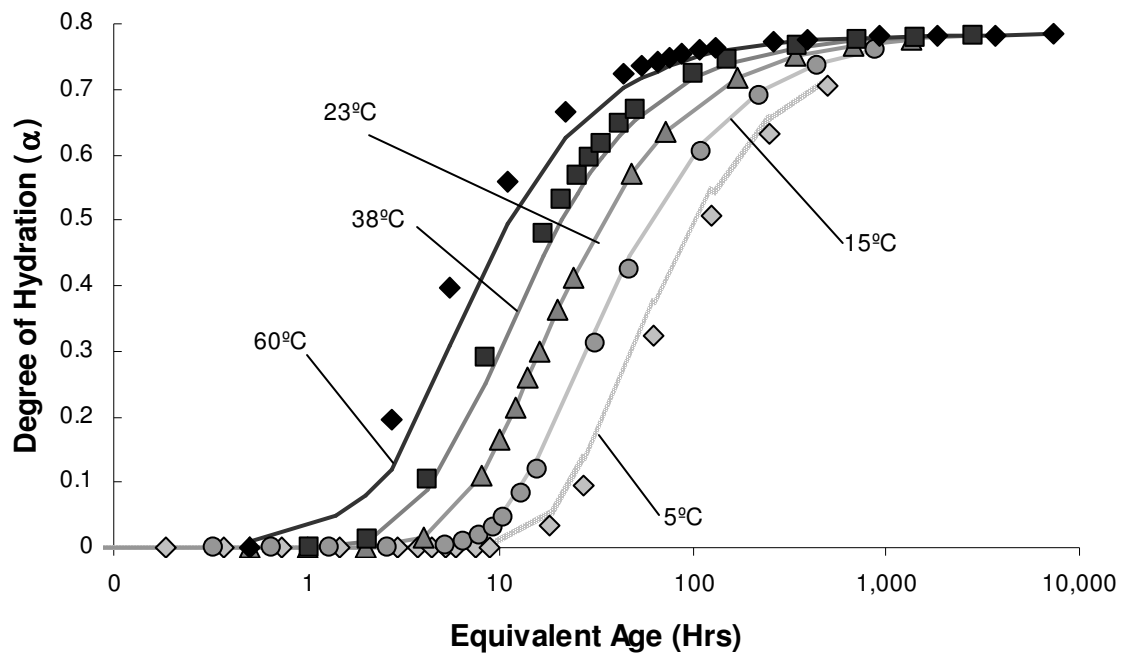


Figure 5-4: 100% Cement C1, 0.35% LRWR (Mix 342); Lines are predicted values; discrete points are measured values.

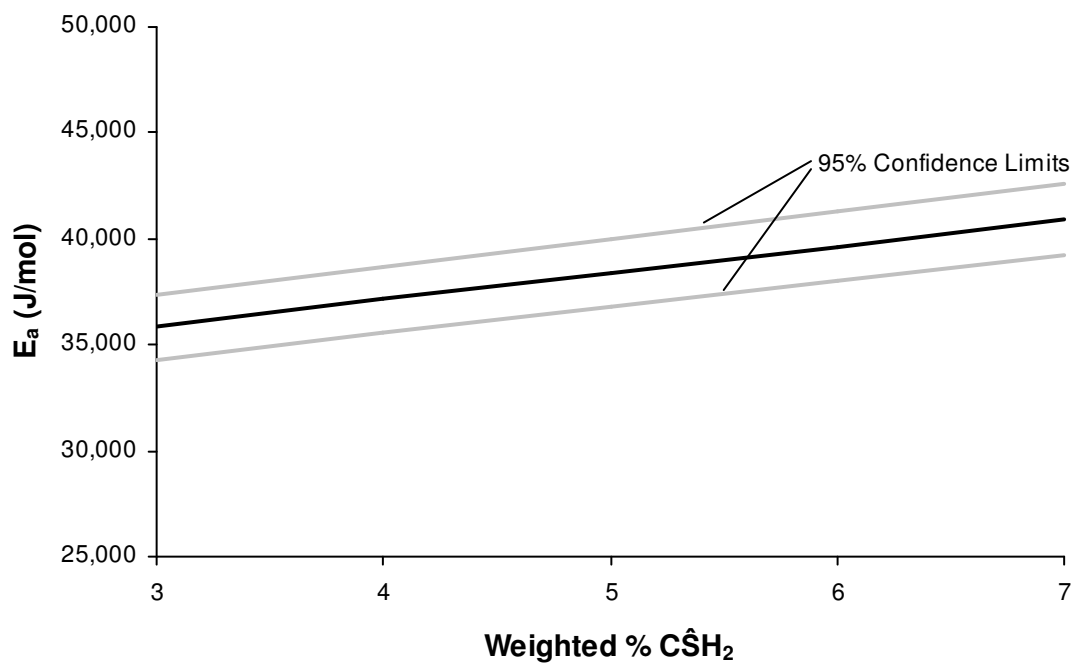


Figure 5-5: Sensitivity of Proposed E_a Model to Gypsum ($C\hat{S}H_2$) Percentage in Cementitious System

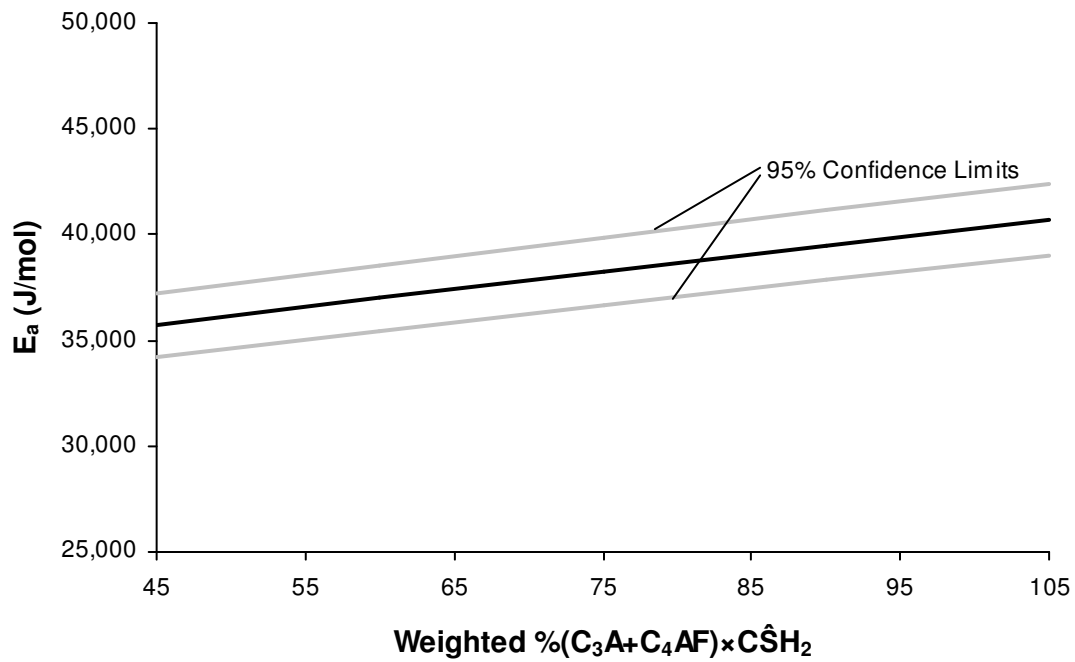


Figure 5-6: Sensitivity of Proposed E_a Model to $(C_3A + C_4AF) \times C\hat{S}H_2$ in Cementitious System

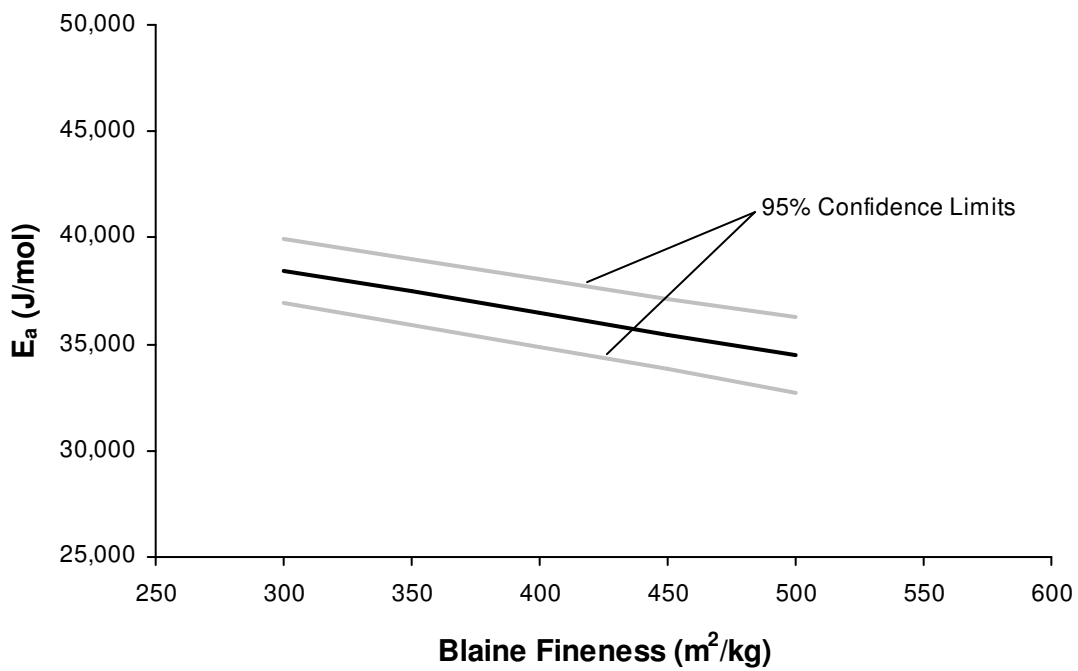


Figure 5-7: Sensitivity of Proposed E_a Model to Blaine Fineness

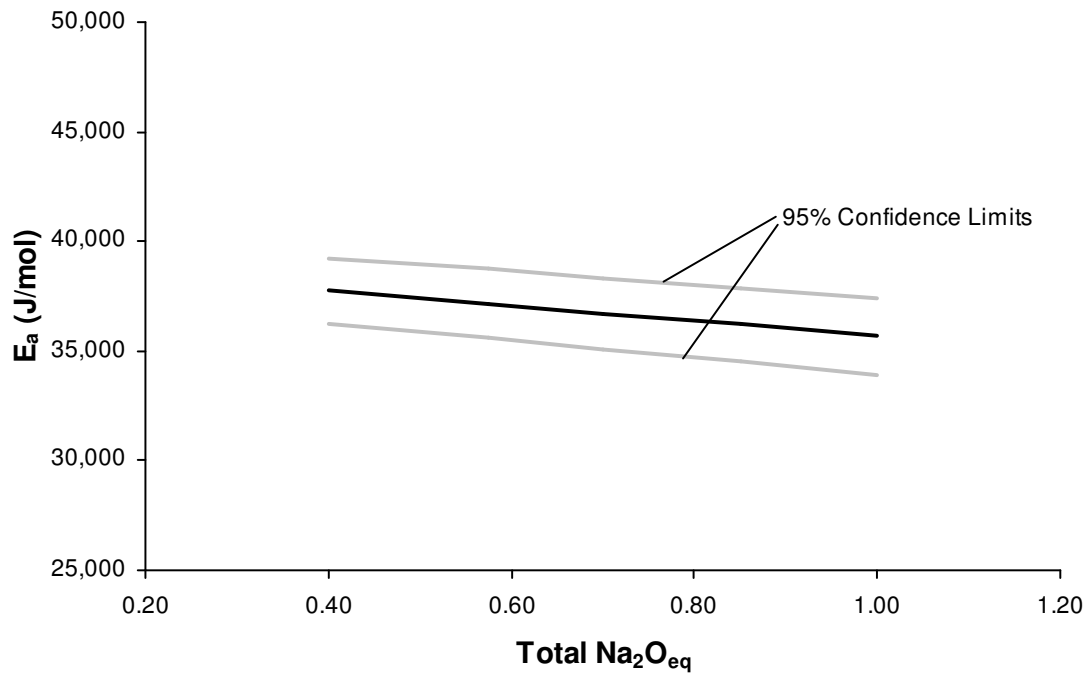


Figure 5-8: Sensitivity of Proposed E_a Model to Total Equivalent Alkalies in Cement

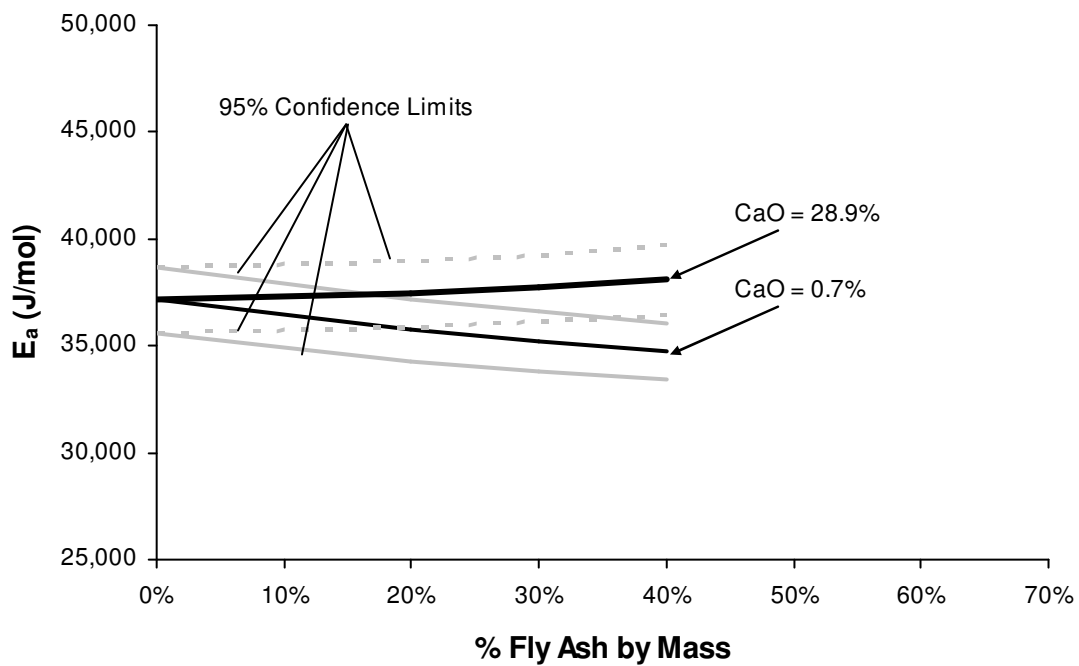


Figure 5-9: Sensitivity of Proposed E_a Model to Fly Ash CaO and Replacement Percentage

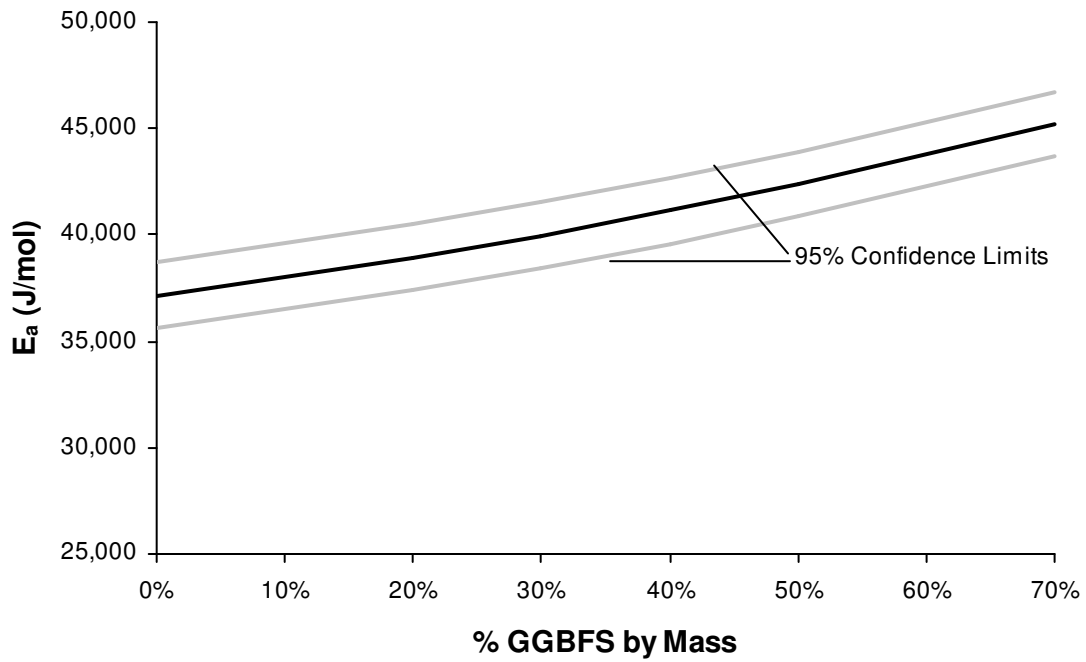


Figure 5-10: Sensitivity of Proposed E_a Model to GGBFS Replacement Percentage

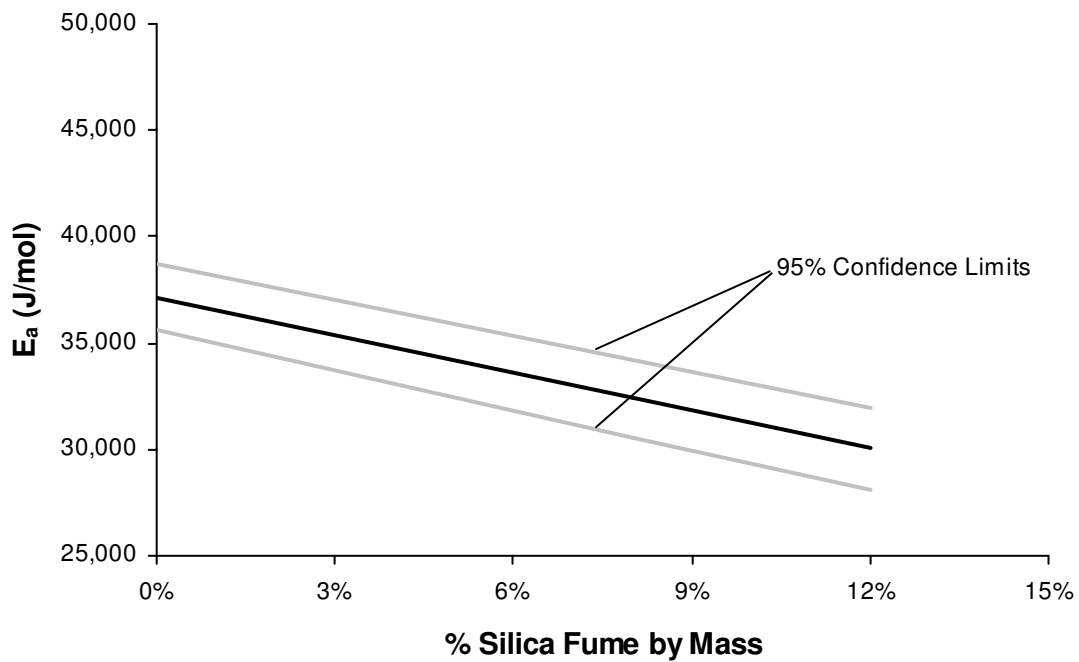


Figure 5-11: Sensitivity of Proposed E_a Model to Silica Fume Replacement Percentage

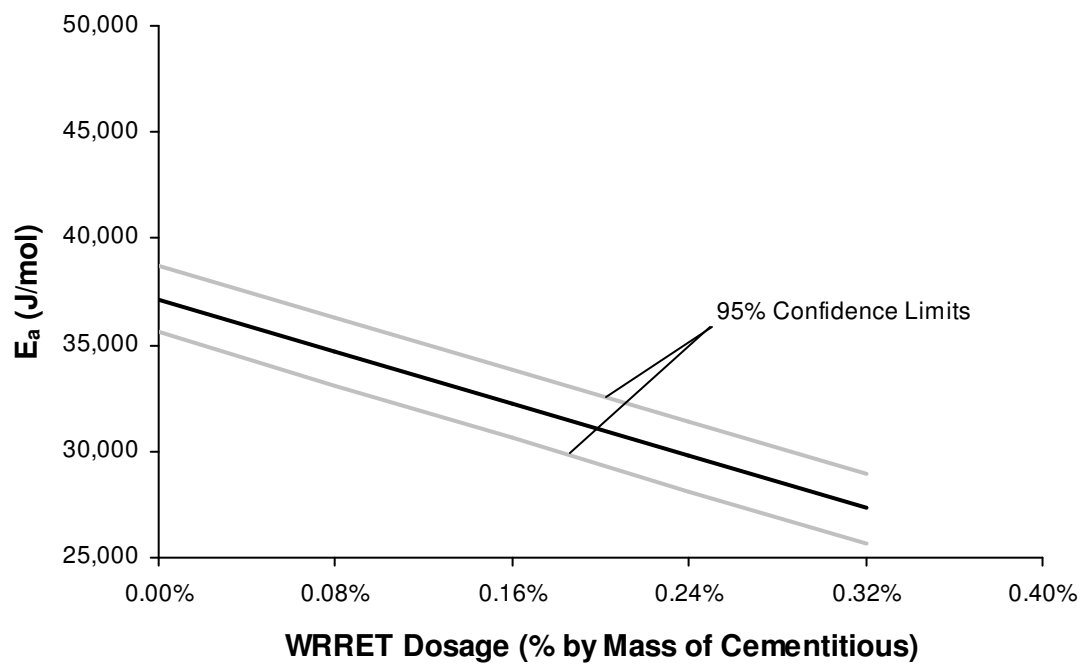


Figure 5-12: Sensitivity of Proposed E_a Model to WRRET Dosage

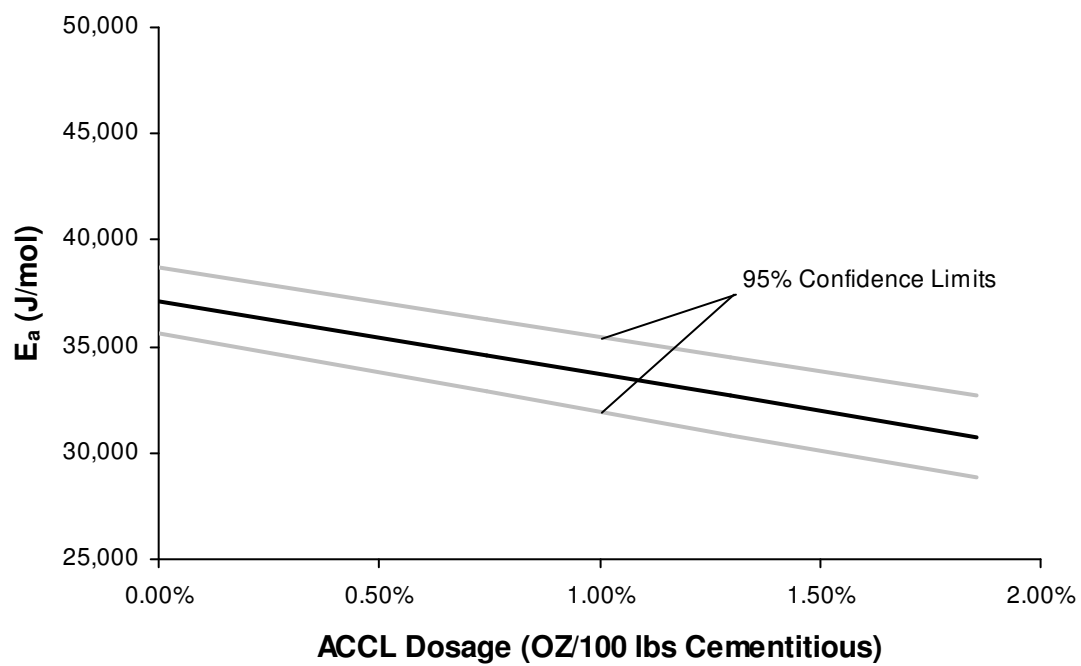


Figure 5-13: Sensitivity of Proposed E_a Model to ACCL Dosage

CHAPTER 6. HYDRATION STUDY OF CEMENTITIOUS MATERIALS USING SEMI-ADIABATIC CALORIMETRY

Accurate characterization of the temperature rise in a concrete element requires an estimate of the adiabatic temperature rise of the concrete mixture. Semi-adiabatic calorimetry is commonly used to provide an estimate of the heat generation characteristics of a concrete mixture because of the relative simplicity of the test. This study examines the sources of variability in semi-adiabatic calorimetry, and an estimate of the confidence limits of the test is calculated. Then, twenty concrete mixtures are investigated using semi-adiabatic calorimetry. Activation energy values are calculated for each mixture using isothermal calorimetry. The adiabatic temperature rise is then calculated. The following mixture properties are investigated: cement type, cementitious content, water/cementitious material ratio, coarse aggregate type (siliceous river gravel and limestone), mixture placement temperature, and the effects of selected supplementary cementing materials. The following factors were the most important to reduce the adiabatic temperature rise: reduced cement content, use of a lower-heat cement, such as a Type V cement type, reduced aggregate specific heat, and substitution of cement with Class F fly ash.

6.1. INTRODUCTION

Accurate assessment of the in-place temperature of a concrete element is important for a variety of reasons. Time and temperature are among the most important factors that influence concrete mechanical properties, and can be combined and used as index to estimate the development of these properties¹. The tendency of a concrete

element to crack is highly dependent on the temperature development of the mixture². Accurate characterization of the temperature rise in very large concrete elements requires an estimate of the adiabatic temperature rise of a concrete mixture. Calorimetry testing is often used to estimate the adiabatic temperature rise, total heat evolution, rate of heat evolution, or temperature sensitivity of a mixture. Ideally, an adiabatic calorimeter would be used to characterize its heat of hydration development. However, adiabatic calorimetry is a rather complicated test to execute. Instead, semi-adiabatic calorimetry is commonly used to provide an estimate for the heat generation characteristics of a concrete mixture due to the relative simplicity of the test. The adiabatic temperature rise can be calculated from the results of the semi-adiabatic calorimetry test.

Even though the semi-adiabatic calorimetry method is a common test, there is no standard test method for semi-adiabatic calorimetry. The sensitivity of the test results to instrument bias, calibration procedure, within batch and batch-to-batch variation is unknown. Quantifying the reliability of the test method is necessary to accurately compare the effects of different mixture variables on the hydration of a concrete mixture. Additionally, several previous studies have examined the effects of different variables on the heat of hydration using semi-adiabatic calorimetry^{3,4}. These studies provide a good estimate of the effects of different mixture constituents on the hydration of a concrete mixture, but were limited to a small number of tests covering a large number of variables. Therefore, a more detailed study to confirm the effects of several variables is warranted.

This study has two goals. First, the variability of the semi-adiabatic calorimeter test will be investigated. Sources of error will be discussed, and confidence limits for the

test method will be presented. Second, selected results from a larger testing program of semi-adiabatic and isothermal calorimetry will be used to examine the effects of sample temperature, cementitious content, cement type, coarse aggregate type, and supplementary cementing material (SCM) type on hydration behavior of different mass concrete mixtures. Comparing the adiabatic temperature rise to the confidence limits of the test method will help to draw more robust conclusions about the effects of different variables.

6.1.1. BACKGROUND

Calorimeters can be classified into three types: adiabatic (no heat loss or gain through system), semi-adiabatic (known heat loss through system), and isothermal (constant temperature in system). Adiabatic calorimeters work by measuring the temperature of a concrete sample, and adjusting the temperature of the surrounding medium to match. In theory, no heat is allowed to escape from the concrete sample. In practice, a small amount of heat invariably escapes from the system. These systematic errors necessitate minor corrections to the experimental results. Most adiabatic calorimeters use a combination of water, air and/or oil circulation around the sample to maintain the temperature of the sample. A feedback loop is employed to regulate the temperature of the surrounding fluid. Large samples, usually concrete cubes, are used⁵, on the order of 0.027m³ to 0.216 m³ (1 ft³ to 8 ft³). The apparatus is heavily insulated. Fully adiabatic calorimeters naturally give the best estimate of the adiabatic temperature

rise of a concrete sample. However, high set-up costs and the large sample size make the testing apparatus less practical than a semi-adiabatic calorimeter.

Semi-adiabatic calorimeters differ from adiabatic calorimeters in that they allow a small amount of heat loss from the system. Insulation is used to slow down heat loss. The amount of heat loss is measured, and the measured temperature values of the concrete are corrected to account for this loss. Then, the results are corrected to back-calculate the temperature rise that would occur under fully adiabatic conditions. If the hydration characteristics of a sample in an adiabatic condition are the same as in a semi-adiabatic condition, corrections could be made based solely on the heat loss through the calorimeter. However, research has shown that hydration is a self-stoking process^{3,5}. Concrete samples exhibit different hydration characteristics depending on the time-temperature history of the mixture. In a semi-adiabatic condition, the concrete is retarded relative to the adiabatic condition because in the semi-adiabatic test, the concrete sample will be at a lower temperature for most of the duration of the test. RILEM suggests a calculation to produce an adiabatic curve from semi-adiabatic data⁵. A theoretical adiabatic hydration curve can be calculated based on the temperature sensitivity (activation energy), total heat of hydration, and calibrated heat loss of the semi-adiabatic calorimeter. This procedure will be explained next.

The calculation of the adiabatic temperature rise of a concrete mixture is an iterative procedure. To provide the proper background, the governing equations will be discussed briefly. The Arrhenius equation is commonly used to model hydration, since it accounts for the temperature sensitivity of a chemical reaction. This equation may be

modified to determine the equivalent age of a concrete mixture. The equivalent age (t_e) of concrete is a mathematical representation of its time temperature history, which allows one to determine the equivalent curing age compared to curing at a reference temperature⁶. The concept allows one to account for different temperature histories for a particular mix. Equation 6-1, proposed by Friesleben Hansen and Pederson⁶, is the most common expression used to compute equivalent age, and is used in the remainder of this chapter to model the effects of time and temperature on hydration:

$$t_e(T_r) = \sum_0^t e^{-\frac{E_a}{R}(\frac{1}{T_c} - \frac{1}{T_r})} \cdot \Delta t \quad \text{Equation 6-1}$$

where $t_e(T_r)$ = equivalent age at reference temperature (T_r), T_c = temperature of the concrete, E_a = activation energy (J/mol), Δt = time interval, and R = natural gas constant (8.314 J/mol/°K).

The progress of the hydration of portland cement may be quantified by the degree of hydration (α), which varies from 0 to 1, with a value of 1 indicating complete hydration. For this study, degree of hydration is taken as the ratio of heat evolved at time, t , to the total amount of heat available, as shown in Equation 6-2:^{3,4,7,8,9}

$$\alpha = \frac{H(t)}{H_u} \quad \text{Equation 6-2}$$

where α = degree of hydration at time t , $H(t)$ = heat evolved from time 0 to time t (J/gram), and H_u = total heat available for reaction (J/gram).

H_u is a function of cement composition and amount and type of supplementary cementing materials (SCMs) and may be calculated as follows⁴:

$$H_u = H_{cem} \cdot p_{cem} + 461 \cdot p_{slag} + 1800 \cdot p_{FA-CaO} \cdot p_{FA} \quad \text{Equation 6-3}$$

where p_{slag} = slag mass to total cementitious content ratio, p_{FA} = fly ash mass to total cementitious content ratio, p_{FA-CaO} = fly ash CaO mass to total fly ash content ratio, p_{cem} = cement mass to total cementitious content ratio, and H_{cem} = heat of hydration of the cement (J/gram). H_{cem} can be calculated as shown in Equation 2-4⁴:

$$H_{cem} = 500 \cdot p_{C_3S} + 260 \cdot p_{C_2S} + 866 \cdot p_{C_3A} + 420 \cdot p_{C_4AF} + 624 \cdot p_{SO_3} + 1186 \cdot p_{FreeCa} + 850 \cdot p_{MgO} \quad \text{Equation 6-4}$$

where H_{cem} = total heat of hydration of portland cement (J/gram) at $\alpha = 1.0$, and p_i = mass of i-th component to total cement content ratio.

The most commonly used relationship to characterize cement hydration is a three-parameter model based on degree of hydration data, as shown in Equation 6^{4,10}:

$$\alpha(t_e) = \alpha_u \cdot e^{-\left[\frac{\tau}{t_e}\right]^\beta} \quad \text{Equation 6-5}$$

where $\alpha(t_e)$ = degree of hydration at equivalent age t_e , τ = hydration time parameter (hours), β = hydration shape parameter, and α_u = ultimate degree of hydration. The rate of heat evolution of concrete can be calculated using Equation 6-6. Heat evolved at time t is as follows⁴:

$$Q_h(t) = H_u \cdot W_c \cdot \left(\frac{\tau}{t_e}\right)^\beta \cdot \left(\frac{\beta}{t_e}\right) \cdot \alpha(t_e) \cdot \exp\left(\frac{E}{R} \left(\frac{1}{273+T_r} - \frac{1}{273+T_c}\right)\right) \quad \text{Equation 6-6}$$

where Q_h = rate of heat generation (W/m^3), H_u = total heat available (J/kg), and W_c = cementitious materials content (kg/m^3).

The specific heat of concrete can be estimated using Equation 6-7. Specific heat is an input into Equation 6-6, and is assumed to vary with degree of hydration³. Specific heat of concrete can be calculated as follows:

$$C_p = \frac{1}{\rho} \cdot (W_c \alpha C_{ref} + W_c \cdot (1 - \alpha) \cdot C_c + W_a C_a + W_w C_w) \quad \text{Equation 6-7}$$

where C_p = specific heat of concrete mixture (J/kg), ρ = unit weight of concrete (kg/m^3); W_c , W_a , W_w = amount by weight of cement, aggregate, and water (kg/m^3); C_c , C_a , C_w = specific heat of cement, aggregate, and water ($\text{J/kg/}^\circ\text{C}$), and C_{ref} = specific heat of hydrated cement = $8.4 \times T_c + 339$ ($\text{J/kg/}^\circ\text{C}$).

6.1.2. VARIABILITY IN SEMI-ADIABATIC CALORIMETRY

The variability of the semi-adiabatic calorimetry test has not been well documented. There is no standard method to construct a semi-adiabatic calorimeter. Therefore, the between-instrument variation must be calculated in order to compare results between instruments. In addition, the batch-to-batch variation must also be calculated. Morabito⁵ reported on a round-robin study that was performed on a variety of adiabatic and semi-adiabatic calorimeters. The range of semi-adiabatic tests results for temperature rise after 72 hours was shown to be -4.4% to + 4.8%. Six different semi-adiabatic calorimeters were tested as part of the study. However, tests were run for only one concrete mixture. The variability of the test method will be assessed in the next section using a variety of different mixtures and five semi-adiabatic calorimeters.

In this chapter, the results from eight different concrete mixtures are analyzed. The results from four different calorimeters (A, B, C, and O) are presented as well. Three calorimeters (A, B, and C) were purchased from a third-party supplier, and one calorimeter (O) was constructed in the laboratory. Also, a fifth calorimeter (from the same supplier) was used for one of the mixtures. The following variables are investigated: measurement bias, calibration error, within-batch variation, and batch-to-batch variation. The sources of error in the test will be discussed, and a consistent method for analysis will be selected. Since it is difficult to quantify the variability of the calibration factors alone, they will be evaluated by comparing the results from the eight different concrete mixtures. The variability of the tests will be quantified by comparing the variation in the curve fit parameters (α , τ , and β) for the eight mixtures.

6.1.3. EXPERIMENTAL WORK

To determine the adiabatic temperature rise, each concrete mixture is batched and mixed as per ASTM C 192¹¹. The starting mixture temperature is shown in Table 6-3. One 150 x 300 mm (6 x 12 in.) cylinder is made, and its weight recorded. The cylinder is placed inside the semi-adiabatic calorimeter as soon as possible after mixing (generally around 30 minutes after water is added to the cement). The cylinder temperature and heat flux out of the calorimeter is recorded at 15 minute intervals. The test is run for approximately 150 hours.

To determine the activation energy (E_a) of each mixture, isothermal calorimetry was performed on various cementitious pastes at 5, 15, 23, 38, and 60 °C (41, 59, 73, 100, and 140 °F) using a TAM Air calorimeter. The calorimeter was kept in a

temperature-controlled room at 21 ± 3 °C (70 ± 5 °F). Cement pastes were proportioned using 250 g (0.55 lb) of cementitious material. Prior to mixing, materials were kept as close as possible to the test temperature. Pastes were mixed in a kitchen blender for approximately three minutes. Eight tests were run simultaneously in the isothermal calorimeter. Each test sample had a mass of approximately 20 grams (0.044 lb). Tests were conducted for 44 hours at 60 °C (140 °F) to over 100 hours at 5 °C (41 °F).

The following cements conforming to ASTM C150¹² were used: one low-alkali Type I cement (C1), one high-alkali Type I cement (C2), one low-alkali Type I/II cement (C6), one Type III cement (C8), and one Type V cement (C9). The following SCMs were used: two ASTM C 618 Class F¹³ fly ashes (FF1 and FF2), two ASTM C 618 Class C¹³ fly ashes (FC1 and FC2), and one Grade 120¹⁴ ground-granulated blast-furnace slag (S1). Chemical and physical properties of the materials are summarized in Table 1. Cement phases were calculated from x-ray fluorescence data using Bogue calculations¹². An ASTM Type F¹⁵ polycarboxylate-based high-range water reducing (HRWR) admixture and a Type A&D¹⁵ glucose-based water reducing admixture were used in some of the mixtures.

6.1.4. CALCULATION OF FULLY ADIABATIC TEMPERATURE RISE

The fully adiabatic temperature rise is calculated using Equation 6-1 through Equation 6-7. The steps required for this analysis are as follows:

1. Perform a calibration test on the specific semi-adiabatic calorimeter.

2. Run a semi-adiabatic calorimeter test. The concrete temperature, heat flux out of the calorimeter, and time are recorded at 15 minute intervals.
3. Determine the activation energy (E_a) of the mixture with an isothermal calorimeter¹⁶. E_a is used to determine the equivalent age (t_e) of the mixture at each time step.
4. Calculate t_e at each time step (every 15 minutes) using Equation 6-1.
5. Calculate the heat evolved at each time step with Equation 6-2 through Equation 6-6.
6. Determine the heat lost through the calorimeter, and add the heat back to the heat generated in the test.
7. Calculate curve fit parameters α_u , τ , and β as shown in Equation 6-5. These are determined iteratively by comparing a theoretical semi-adiabatic curve (calculated with the three-parameter model, and accounting for heat loss from the specimen) with the actual temperature results from the calorimeter.
8. Calculate the adiabatic temperature rise (“false” adiabatic temperature rise) based on the temperature and heat loss data from Step 1.
9. Calculate the adiabatic temperature rise (“true” adiabatic temperature rise) based on the model parameters developed in Step 7.

The “false” and “true” adiabatic curves are a result of the self-stoking nature of cement hydration. In a semi-adiabatic test, the heat lost from the test device does not contribute to the hydration of the mixture. As a result, the calculated adiabatic temperature rise will be artificially low (hence “false” adiabatic) when the heat lost from the device is added

back to the test results. “True” adiabatic temperature rise is a theoretical calculation that accounts for self-stoking^{3,4}, and is based on the curve fit parameters (α , τ , β , and E_a) determined from the test. Figure 6-1 compares the difference between “false” and “true” adiabatic temperature rise for a mixture of 100% Type I cement and a mixture with 60% Type V cement and 40% ground-granulated blast-furnace (GGBF) slag. The difference is 0.5 °F (0.3 °C) for the mixture with 100% cement, while the difference is 36.0 °F (20.0°C) for the mixture with GGBF slag. Adiabatic temperature rise in this study will refer to the ‘true’ adiabatic temperature rise.

6.1.5. CALIBRATION PROCEDURE

The heat loss from the semi-adiabatic calorimeter must be measured and corrected for. Accurate calculation of the adiabatic temperature rise requires proper calibration of the instrument. There are two calibration methods available. The first method, suggested in RILEM 119 TCE¹⁷, recommends calibration of the calorimeter by heating a sample in the calorimeter with a power source until a constant temperature is reached. Then, the heat is removed, and the sample is allowed to cool. This method measures the dissipation of heat to the environment, and allows direct calculation of the thermal capacity of the instrument. The second method¹⁸ uses heated water as the calibration medium, since the thermal properties are known. As long as the instruments have a fairly uniform specific heat, the procedure should work well. This second method will be used in this study due to its simplicity.

The water calibration procedure is as follows: First, de-ionized water is heated to a temperature of 45 to 50 °C (113 to 122 °F). Next, the water is placed in a 150 mm x

300 mm cylindrical mold (6"x12"), and weighed. Finally, the cylinder is placed inside the calorimeter. Time, temperature, and heat flux are recorded at 15 minute intervals. Typical results are shown in Figure 6-2. The calculation of the heat loss is a simple measure of conduction, as follows¹⁹:

$$\frac{dQ}{dt} = \frac{\kappa \cdot A \cdot (T_{Hot} - T_{Cold})}{d} \quad \text{Equation 6-8}$$

where κ = thermal conductivity of the instrument; A = area where heat transfer occurs; T_{hot} = temperature on the hot side of the barrier; T_{cold} = temperature on the cold side of the barrier; and d = thickness of the barrier. In this case, T_{hot} and T_{cold} are temperatures at inner and outer points in the insulation. The difference may also be expressed as the heat flux, with units of mV. Either temperature difference or heat flux may be used, since the units of the correction factor will adjust accordingly. The term $\kappa A/d$ determines the rate of heat loss.

6.2. RESULTS AND DISCUSSION

6.2.1. VARIATION FROM CONDUCTION MODEL

Figure 6-2 shows that the rate of heat loss is non-linear in the early portions of the test. Therefore, the correction factor should be non-linear as well. Several different heat loss equations were investigated. Equation 6-9 was selected to describe the heat transfer from the instrument.

$$\frac{dQ}{dt} = q_{flux} \cdot (C_{f1} \cdot \ln(t) + C_{f2}) \quad \text{Equation 6-9}$$

where q_{flux} = heat flux, t = time, and C_{f1} , C_{f2} = correction factors. Equation 6-9 uses time as the dependent variable, which may not be appropriate given that heat flux is not

governed by time. Temperature may be a more appropriate dependent variable because higher temperature differences will drive a greater amount of heat out of the drum. However, the results of the testing suggest that time is the better variable. When temperature is used as the dependent variable, significant difference in results was seen between the calorimeters. Calibrations using time (Equation 6-9) eliminate the bias between instruments. However, ambient temperature should be controlled accordingly to eliminate any effects from the environment.

6.2.2. VARIABILITY IN HEAT CAPACITY OF CALORIMETER

Figure 6-2 shows the results from a calibration test performed on all of the calorimeters at the same time with the same temperature water. Several details should be noted. First, the drop in temperature does not mirror the drop in heat flux in the first 5-7 hours, likely due to the absorption of heat by the drum and the time it takes for equilibrium to be reached between the warm specimen and the room temperature chamber. After this time, the loss of heat becomes more linear, which indicates that heat transfer out of the instrument is the dominant mechanism of heat loss. Note that the time at which the heat flux stabilizes is approximately the same for all of the calorimeters. The area under the curves is relatively similar as well, suggesting that the heat capacity of the instruments is somewhat uniform. However, calorimeter O loses less heat than the other calorimeters in the first hours of the test. Calorimeters B and C lose about the same amount of heat, and calorimeter A loses the most heat in the first few hours. These differences in the early heat loss of each calorimeter will affect the output of the semi-adiabatic test.

To quantify this effect, an estimate of the effects of early heat loss on the calibration of the drum was completed by truncating 0, 1, and 5 hours of data from the calibration. The truncation of data effectively eliminates the early variations in heat loss from the calibration of the drums. This procedure should be valid because semi-adiabatic calorimetry is usually performed on samples that begin at room temperature, and because heat is introduced into the drum more gradually with concrete at room temperature than with heated water. With zero hours of data truncated, the average coefficient of variation (C.V.) for the hydration parameters was 7.7%. For one hour of data truncated, the C.V. was 6.0%, and for five hours of data, the C.V. was 4.5%. The results from these tests indicate that variation is reduced by truncating the first five hours of temperature data from the calibration.

6.2.3. INSTRUMENT PRECISION

The semi-adiabatic tests in this study were run for approximately 150 hours. Typically, the temperature of the sample starts to mirror the ambient temperature around this time. However, a measurable amount of heat liberation is still apparent with mixtures containing reactive SCMs, such as GGBF slag or Class C fly ash. This portion of hydration is not captured in this testing program due to the precision of the instrumentation. The precision of the thermocouples used in the calorimeters is $\pm 0.3^{\circ}\text{C}$ (0.5°F). There was a small variation in results due to a bias between thermocouples. This bias resulted in a corresponding bias of approximately 4% in the hydration parameters. Therefore, the results from the thermocouples in any instrument should be

validated to ensure that they are accurate, either with an ice water bath or by comparing to another thermocouple.

6.2.4. CONFIDENCE LIMITS FOR SEMI-ADIABATIC CALORIMETRY

Based on the 31 duplicate tests presented in Table 6-2, the confidence intervals for the semi-adiabatic calorimeter test may be computed. The curve fit parameters (α_u , τ , and β) were calculated using the calibration factors derived from Equation 6-9. Five different calorimeters from two labs were used. The single batch, multiple instrument coefficient of variation was $\pm 2.6\%$ for α_u , $\pm 7.5\%$ for τ , and $\pm 5.3\%$ for β . The multiple batch, multiple instrument C.V. was $\pm 3.2\%$ for α_u , $\pm 7.5\%$ for τ , and $\pm 6.0\%$ for β . The 95% confidence limits were $\pm 10.9\%$ for α_u , $\pm 25.8\%$ for τ , and $\pm 20.8\%$ for β . The coefficient of variation values compare well with the values reported by Morabito⁵. Also, if the standard deviation measured here is assumed to be the same as the population, the differences between two results may be compared as follows. ASTM C 670²⁰ states that the maximum acceptable range for two results from the same population is $2.8 \times \sigma$. Therefore, for any two test results, a difference of 8.8% for α_u , 20.9% for τ , and 16.9% for β is considered statistically significant at a 95% confidence level.

6.3. TRENDS IN HYDRATION BEHAVIOR

Twenty (20) concrete mixtures were investigated using semi-adiabatic calorimetry. Activation energy values were calculated for each mixture using isothermal calorimetry. Table 6-3 summarizes the relevant mixture information, material properties,

and hydration parameters. The following mixture properties were investigated: cement type, cementitious content, water/cementitious material (w/cm) ratio, coarse aggregate type (siliceous river gravel (SRG) versus limestone (LS)), and concrete placement temperature. In addition, several mixtures were run with different SCMs.

The following sections compare the heat evolution and adiabatic temperature rise for the mixtures in Table 6-3. Prior to this study, the order of magnitude of the results has not been compared with confidence intervals of the semi-adiabatic test. Because most of the mixtures were tested only one time, an estimate of the significance of the difference between two test results will be as follows: for any two test results, a difference of 8.8% for α_u , 20.9% for τ , and 16.9% for β is considered statistically significant at a 95% confidence level.

6.3.1. EFFECTS OF WATER-TO-CEMENTITIOUS MATERIALS RATIO ON HYDRATION

The water-to-cementitious materials ratio (w/cm) has several effects on hydration that may be observed by calorimetry. First, low w/c has been linked to a decrease in the ultimate degree of hydration^{21,22}. These results are supported by the test results presented here. Figure 6-3 shows the effect of varying the w/cm from 0.32 to 0.42 on the adiabatic temperature rise of a Type I cement, C1. The calculated adiabatic temperature rise for a mixture with the w/cm of 0.32 was 6 °C (10.7 °F) lower than the same mixture with the w/cm of 0.42. The difference in temperature rise correlates with the difference in the degree of hydration parameter, α_u . For mixes with w/cm of 0.32 to 0.42, α_u was 0.636 to 0.740. Similarly, Mills²² reported that a decrease in w/cm from 0.45 to 0.35 gave a

decrease in α_u of 0.715 from 0.671. The reduced adiabatic temperature rise associated with w/cm is significant based on the confidence limits presented in this chapter. However, a higher w/cm has little effect on the other hydration parameters (τ and β) of a mixture.

6.3.2. EFFECTS OF CEMENT CONTENT ON HYDRATION

One of the easiest ways to reduce the adiabatic temperature rise is to reduce the cement content in a concrete mixture. To test the effects of different amounts of cementitious material in a mixture, mixtures 1, 2, and 3 were run at a w/cm of 0.42 with 396, 335, and 279 kg/m³ (658, 564, and 470 lb/yd³) of cement C1. The difference in adiabatic temperature rise associated with different cement contents (Mixtures 1, 2, and 3) is shown in Figure 6-4. By reducing the cement content from 396 kg/m³ to 279 kg/m³ (658 lb/yd³ to 470 lb/yd³), the adiabatic temperature rise is reduced by 9.6 °C (17.3 °F). This difference is significant based on the confidence limits presented in this chapter. Clearly, a reduction of cement content is a very effective way to reduce the heat evolution of a mixture. The time parameter τ increases as cement content is reduced, while α_u and β show little change.

6.3.3. EFFECTS OF AGGREGATE TYPE ON HYDRATION

The adiabatic temperature rise of a mixture with limestone coarse aggregate should be lower than a mixture with siliceous river gravel because limestone has a higher specific heat than river gravel². The effect of aggregate on the hydration parameters is within the confidence limits of the test method, but the corresponding temperature

difference is significant. Figure 6-5 shows the results from Mixtures 2, 5, and 9. Limestone coarse aggregate reduces the adiabatic temperature rise by approximately 4.7°C (8.4 °F). The reduction in temperature may be attributed to the difference in specific heat³, as modeled by Equation 6-7.

6.3.4. EFFECTS OF PLACEMENT TEMPERATURE ON HYDRATION

If the concept of equivalent age is valid, there should be no difference in the results obtained from mixtures that are mixed at different temperatures. The activation energy and heat transfer calculations should account for any variations. Figure 6-6 shows the effects of mixing temperature on the adiabatic temperature rise of a mixture of 100% cement C1 (Mixtures 4, 5, and 6) and mixture of 30% Class F fly ash (FF2) and 70% cement C1 (Mixtures 17, 18, and 19). Placement temperature has a small effect on the calorimeter results, but these differences are within the error of the test method. However, the result should not be construed to mean that lower placing temperatures in the field have a minimal effect on the temperature rise. Lowering the placement temperature is one of the best methods to control temperature rise in a concrete element²³. These results indicate that the equivalent age concept works well, and that the activation energy is successfully accounting for the variations in mixture temperature.

6.3.5. EFFECTS OF CEMENT TYPE ON HYDRATION

Cement chemistry and fineness are common methods by which the heat of hydration of a concrete mixture is estimated. ACI 207.2²⁴ provides an estimate of the difference in adiabatic temperature rise that may be expected from different cement

types. Type III cement is expected to have an adiabatic temperature rise of approximately 45 °C (80 °F)²⁴. The temperature rise of Type I cement is reported to be approximately 36 °C (65 °F)²⁴. However, the fineness of the cements reported in ACI 207.2²⁴ is much lower than the cements used in this study.

Figure 6-7 compares the temperature rise of Mixtures 9 through 13. Mixture 9, with 100% Type I cement (C1) and a superplasticizer, generates the most heat. The Type III cement, C8, generates heat at a greater rate than the remaining cements. The Type V cement, C9, generates heat at a lower rate than the other cements. Type I cement (C2) and Type I/II cement (C6) generate heat at approximately the same rate as one another. The time parameter (τ) is lower for the Type III cement, and is higher for the Type V cement, as expected. The calculated adiabatic temperature rise was approximately the same for the Type I, I/II, and III cements, and was approximately 6°C (10.8°F) lower for the Type V cement. The test results suggest that the differences between the specific Type I, I/II, and III cements are not as large as compared to the generic differences reported in ACI 207.2²⁴. These data illustrates that the specific cement used for a project could affect the in-place temperature rise of the member. Of all the cement compared in this chapter, the Type V cement showed the lowest adiabatic temperature rise. One should not expect a change in cement type to reduce the heat evolution of a mixture, unless a Type V cement is specified. The activation energy (E_a) for each of the cements was roughly the same.

Cements C1 and C2 have slight differences in C₃S, C₂S, loss on ignition (LOI), free lime (CaO), and fineness. However, based on their composition and fineness they

should have exhibited similar adiabatic temperature rise behavior. The difference between the two cements is 6.7 °C (12.0 °F), which is significant based on the confidence limits presented here. Also, the hydration peak of Cement C1 was delayed. Cement C1 was mixed with a slightly lower w/cm, and a HRWR admixture was used. HRWR admixtures alter the rate of hydration to some degree by either dispersion or increased solubility of the reaction products²⁵. Typically, a HRWR admixture will be used at a lower w/cm, so the lower degree of hydration will be offset by the increase in solubility caused by the admixture. A more detailed investigation than is presented here is necessary to confirm the exact nature of these effects.

6.3.6. EFFECTS OF SCMS ON HYDRATION

The effects of different types of SCMs on the three hydration parameters (α_h , τ and β) depend highly on the interaction between the SCM, cement, and the admixture in the concrete. SCMs are known to alter hydration in several ways. First, high-lime fly ashes and GGBF slag typically have much greater amounts of reactive crystalline phases than low lime fly ashes²⁵. Therefore, the more reactive SCMs should exhibit different hydration behavior than the less reactive SCMs. Also, SCMs typically retard the hydration of the mixture to some degree^{4,26}. In general, the induction period of mixtures with reactive SCMs, such as GGBF slag or Class C fly ash, tends to be longer compared to mixtures with less reactive SCMs, such as Class F fly ash. The accelerating portion of the hydration curve tends to be less steep^{4,26}. When this delay occurs, the slope parameter (β) is reduced and the time parameter (τ) is increased.

These trends are highlighted in the following results. Figure 6-8 compares the effects of a Class F fly ash (FF1), a Class C fly ash (FC2), and GGBF slag (S1) with two different cements (C2 and C9). Fly ash FF1 reduces the temperature rise of Cement C2 primarily by dilution. The addition of 30% by mass of fly ash FF1 lowers the adiabatic temperature rise of the mixture close to that of the Type V Cement (C9). The replacement of Cement C9 with FC2 and S1 increases the adiabatic temperature rise by 15°C (27°F).

6.4. CONCLUSIONS

The variability of the semi-adiabatic calorimeter test was quantified in this study. These results allow the comparison of results from different mixtures, instruments, and laboratories. Several conclusions may be drawn. First, the calibration method should use a conduction model based on time to reduce the variation between instruments. Second, the accuracy of the calorimeter instrumentation causes bias in the calculated adiabatic temperature rise. However, the precision and accuracy of the lab-made calorimeter was comparable to the calorimeter manufactured by a third party. Finally, for any two test results, a difference of 8.8% for α_u , 20.9% for τ , and 16.9% for β is considered statistically significant at a 95% confidence level.

The change in adiabatic temperature rise associated with w/cm, cement content, aggregate type, placement temperature, cement type, and SCMs was investigated. The following factors were the most important to reduce the adiabatic temperature rise: reduced cement content, use of a lower-heat cement, such as a Type V cement type, reduced aggregate specific heat, and substitution of cement with Class F fly ash.

Through the use of heat transfer calculations and a mixture-specific activation energy, the effect that placement temperature has on the rate of hydration can be accounted for to convert semi-adiabatic calorimeter test results into fully adiabatic test results.

6.5. REFERENCES

1. Chanvillard, G., and L. D'Aloia, "Concrete Strength Estimation at Early Ages: Modification of the Method of Equivalent Age," *ACI Materials Journal*, V. 94, No. 6, Nov.-Dec. 1997, pp. 520-530.
2. ACI Committee 207, "Guide to Mass Concrete", ACI 207.1R-05, American Concrete Institute, Farmington Hills, Michigan, 2005.
3. Van Breugel, K., "Prediction of Temperature Development in Hardening Concrete", *Prevention of Thermal Cracking in Concrete at Early Ages*, RILEM Report 15, E & FN Spon, London 1998.
4. Schindler, A.K., and K.J. Folliard, "Heat of Hydration Models for Cementitious Materials", *ACI Materials Journal*, V. 102, No. 1, Jan.-Feb., 2005, pp. 24-33.
5. Morabito, P., "Methods to Determine the Heat of Hydration of Concrete", *Prevention of Thermal Cracking in Concrete at Early Ages*, RILEM Report 15, E & FN Spon, London 1998.
6. Freiesleben Hansen, P., and E.J. Pedersen, "Maturity computer for controlling curing and hardening of concrete," *Nordisk Betong*, V. 1, No. 19, 1977, pp. 21-25.
7. D'Aloia, L., and G. Chanvillard, "Determining the "Apparent" Activation Energy of Concrete; E_a – Numerical Simulations of the Heat of Hydration of Cement," *Cement and Concrete Research*, V. 32, 2002, pp. 1277-1289.

8. Kada-Benameur, H., E. Wirquin, and B. Duthoit, "Determination of Apparent Activation Energy of Concrete by Isothermal Calorimetry," *Cement and Concrete Research*, V. 30, 2000, pp. 301-305.
9. Copeland, L.E., Kantro, D.L., Verbeck, G., "Part IV-3 Chemistry of Hydration of Portland Cement," 4th International Symposium of the Chemistry of Cement, Washington, D.C., 1960, pp. 429-465.
10. Pane, I., and W. Hansen, "Concrete Hydration and Mechanical Properties under Nonisothermal Conditions," *ACI Materials Journal*, V. 99, No. 6, Nov.-Dec, 2002, pp. 534-542.
11. ASTM C 192, "Standard for Making and Curing Concrete Test Specimens in the Laboratory," Annual Book of ASTM Standards, Vol 04.01., ASTM International, West Conshohoken, PA, 2006, 8 pp.
12. ASTM C 150, "Standard Specification for Portland Cement," Annual Book of ASTM Standards, Vol 04.01., ASTM International, West Conshohoken, PA, 2002, 8 pp.
13. ASTM C 618, "Standard Specification for Coal Ash and Raw or Calcined Natural Pozzolans for Use in Concrete," Annual Book of ASTM Standards, Vol 04.01., ASTM International, West Conshohoken, PA, 2003, 3 pp.
14. ASTM C 989, "Standard Specification for Ground Granulated Blast-Furnace Slag for Use in Concrete and Mortars," Annual Book of ASTM Standards, Vol 04.01., ASTM International, West Conshohoken, PA, 2005, 5 pp.

15. ASTM C 494, "Standard Specification for Chemical Admixtures for Concrete," Annual Book of ASTM Standards, Vol 04.01., ASTM International, West Conshohoken, PA., 2005, 10 pp.
16. Poole, J.L., "Methods of Activation Energy Calculation for Portland Cement," Master's Thesis, The University of Texas at Austin, 2004, 75 pp.
17. RILEM 119-TCE, "Adiabatic and Semi-Adiabatic Calorimetry to Determine the Temperature Increase in Concrete due to Hydration Heat of Cement," RILEM Report 15, R. Springenschmid, ed., E&FN Spon, London, 1999, pp. 315-330.
18. NT Build 480, "Cement: Heat of Hydration," NORDTEST, Espoo, Finland, 1997, 6 pp.
19. Nave, C.R., "HyperPhysics", Department of Physics and Astronomy, Georgia State University, Atlanta, GA, 2005, <<http://hyperphysics.phy-astr.gsu.edu>> (1 June 2006).
20. ASTM C 670, "Preparing Precision and Bias Statements for Test Methods for Construction Materials," Annual Book of ASTM Standards, Vol 04.01., ASTM International, West Conshohoken, PA, 2003, 9 pp.
21. Powers, T.C., and T.L. Brownyard. "Studies of the Physical Properties of Hardened Portland Cement Paste", Journal of the American Concrete Institute, Volume 18, no. 2-8, October 1946-April 1947
22. Mills, R H. "Factors Influencing Cessation of hydration in Water Cured Cement Pastes." Special Report 90: Symposium on Structure of Portland Cement Paste and Concrete. Washington, D.C.: Highway Research Board, 1966. 406-424.

23. Springenschmid, R. and Breitenbücher, R., “Influence of Constituents, Mix Proportions, and Temperature on Cracking Sensitivity of Concrete”, *Prevention of Thermal Cracking in Concrete at Early Ages*, RILEM Report 15, E & FN Spon, London 1998.
24. ACI Committee 207, “Effect of Restraint, Volume Change, and Reinforcement on Cracking of Mass Concrete”, ACI 207.2R-05, American Concrete Institute, Farmington Hills, Michigan, 2005.
25. Hewlett, P.C., Lea’s Chemistry of Cement and Concrete, 4th ed. Arnold Publishers, New York, 1998.
26. Sandberg, P. and Roberts, L., “Cement-Admixture Interactions Related to Aluminate Control”, *Journal of ASTM International*, V. 2, No. 6 June 2005, pp. 6-13.

Table 6-1: Chemical and physical properties of cement

	Ty I LA	Ty I	Ty I/II LA	Ty III	Ty V	SCMs				
Cement	C1	C2	C6	C8	C9	FF1	FF2	FC1	FC2	S1
SiO ₂ (%)	20.45	19.18	20.77	20.3	21.63	56.63	51.69	37.83	33.31	34.48
Al ₂ O ₃ (%)	5.43	5.34	3.88	4.85	4.04	30.68	24.81	19.83	18.39	11.35
Fe ₂ O ₃ (%)	2.01	2.3	3.73	3.56	5.29	4.94	4.22	6.17	5.40	0.67
CaO (%)	64.51	63.17	64.5	63.94	63.07	0.69	13.12	23.13	28.91	41.73
MgO (%)	1.15	1.09	1.01	0.82	0.77	0.73	2.29	4.62	5.25	7.32
Na ₂ O (%)	0.14	0.12	0.18	0.07	0.27	0.12	0.18	1.74	1.64	0.14
K ₂ O (%)	0.56	0.95	0.6	0.66	0.23	2.26	0.84	0.06	0.35	0.38
Na ₂ O Eq. (%)	0.51	0.75	0.575	0.504	0.42	1.607	0.733	1.778	1.870	0.390
SO ₃ (%)	3.35	3.2	2.38	3.44	2.74	0.00	0.46	1.50	2.27	1.88
LOI* (%)	1.80	4.1	2.67	1.71	1.55	2.10	0.23	0.67	0.34	0.83
Insoluble Residue (%)	-	0.63	0.25	-	1.43	-	-	-	-	-
Free CaO	1.66	4	2.8	1.89	3.8	-	-	-	-	-
C ₃ S (%)	58.29	63.11	66.54	58.54	49.85	-	-	-	-	-
C ₂ S (%)	14.65	7.38	9.35	14.04	24.41	-	-	-	-	-
C ₃ A (%)	10.99	10.26	3.97	6.83	1.76	-	-	-	-	-
C ₄ AF (%)	6.12	7.00	11.35	10.83	16.10	-	-	-	-	-
Gypsum	5.70	5.44	4.05	5.85	4.66	-	-	-	-	-
Blaine fineness (m ² /kg)	350.0	390.9	365.4	539.0	409.0	147.3	165.5	348.4	299.9	331.6

*LOI = Loss on Ignition

Table 6-2: Summary Statistics for Semi-Calorimetry Variation

Mix #	No. of Tests	Slope Parameter β			Time Parameter τ			Degree of Hydration α_t		
		Avg.	Std. Dev. (σ)	C.V.	Avg. (hrs)	Std. Dev. (σ)	C.V.	Avg.	Std. Dev. (σ)	C.V.
2*	4	1.126	0.011	1.0%	12.506	0.859	6.9%	0.743	0.030	4.0%
4**	4	1.130	0.061	5.4%	12.349	1.123	9.1%	0.739	0.016	2.2%
10*	5	0.755	0.062	8.3%	11.564	1.057	9.1%	0.635	0.029	4.6%
14*	2	0.745	0.025	3.4%	14.806	0.309	2.1%	0.814	0.005	0.6%
15*	7	0.905	0.070	7.7%	16.633	1.361	8.2%	0.787	0.028	3.5%
18**	3	0.908	0.042	4.7%	24.750	0.697	2.8%	0.798	0.008	1.0%
19**	3	0.461	0.009	1.9%	45.540	2.914	6.4%	0.884	0.027	3.1%
20**	3	0.429	0.005	1.1%	74.740	3.965	5.3%	1.014	0.025	2.5%

*Multiple Batch, Multiple Instrument; **Single Batch, Multiple Instrument

Table 6-3: Summary of Semi-Adiabatic Test Results

Mix #	Cement	SCM (% Replacement by Mass)			Total Cement. Content kg/m ³	Mix. Temp °C	w/cm	Chemical Admixture (ASTM)		Coarse Aggregate		H _u kJ/kg	α_u	τ hrs	β	E _a J/mol
		Type	%	CaO				Type	% by	Type	$\frac{FA^*}{FA + CA}$					
1	C1	-	-	-	279	18.7	0.42	A&D	0.23	SRG	0.40	513	0.733	13.386	1.084	30,810
2	C1	-	-	-	335	21.1	0.42	A&D	0.23	SRG	0.40	513	0.743	12.506	1.126	30,810
3	C1	-	-	-	396	19.0	0.42	A&D	0.23	SRG	0.40	513	0.673	11.332	1.279	30,810
4	C1	-	-	-	335	13.4	0.42	F	0.31	LS	0.40	513	0.739	12.349	1.130	40,650
5	C1	-	-	-	335	19.0	0.42	F	0.31	LS	0.40	513	0.719	12.426	1.052	40,650
6	C1	-	-	-	335	29.1	0.42	F	0.31	LS	0.40	513	0.759	12.243	0.927	40,650
7	C1	-	-	-	335	21.0	0.32	F	0.50	SRG	0.40	513	0.636	12.013	1.246	40,650
8	C1	-	-	-	335	23.2	0.40	F	0.16	SRG	0.40	513	0.683	12.727	1.063	40,650
9	C1	-	-	-	335	19.3	0.42	F	0.21	SRG	0.40	513	0.740	11.564	1.193	40,650
10	C2	-	-	-	335	22.5	0.44	-	-	SRG	0.44	530	0.635	12.608	0.755	38,725
11	C6	-	-	-	335	23.7	0.44	-	-	SRG	0.44	496	0.702	11.373	0.739	37,165
12	C8	-	-	-	335	23.3	0.44	-	-	SRG	0.44	493	0.697	9.342	0.895	37,344
13	C9	-	-	-	335	23.2	0.44	-	-	SRG	0.44	464	0.635	15.170	0.813	38,597
14	C2	FF1	30	0.7	335	23.9	0.44	-	-	SRG	0.44	374	0.814	14.806	0.745	38,787
15	C1	FF2	30	13.1	335	15.0	0.42	A&D	0.23	SRG	0.40	430	0.788	18.953	0.929	31,975
16	C1	FF2	30	13.1	335	20.7	0.42	A&D	0.23	SRG	0.40	430	0.751	17.631	0.910	31,975
17	C1	FF2	30	13.1	335	28.9	0.42	A&D	0.23	SRG	0.40	430	0.787	16.633	0.905	31,975
18	C1	FC1	30	23.1	335	22.0	0.42	A&D	0.23	SRG	0.40	484	0.798	24.750	0.908	32,864
19	C9	FC2	30	28.9	335	23.0	0.44	-	-	SRG	0.44	481	0.884	45.540	0.461	41,164
20	C9	S1	40	-	335	23.4	0.44	-	-	SRG	0.44	463	1.000	58.143	0.440	45,077

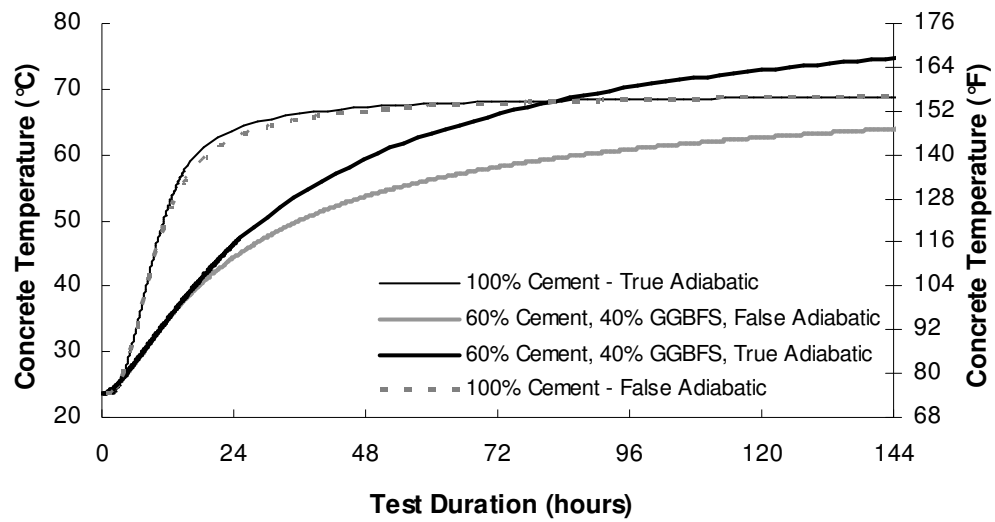


Figure 6-1: Comparison of Adiabatic Temperature Rise Calculations

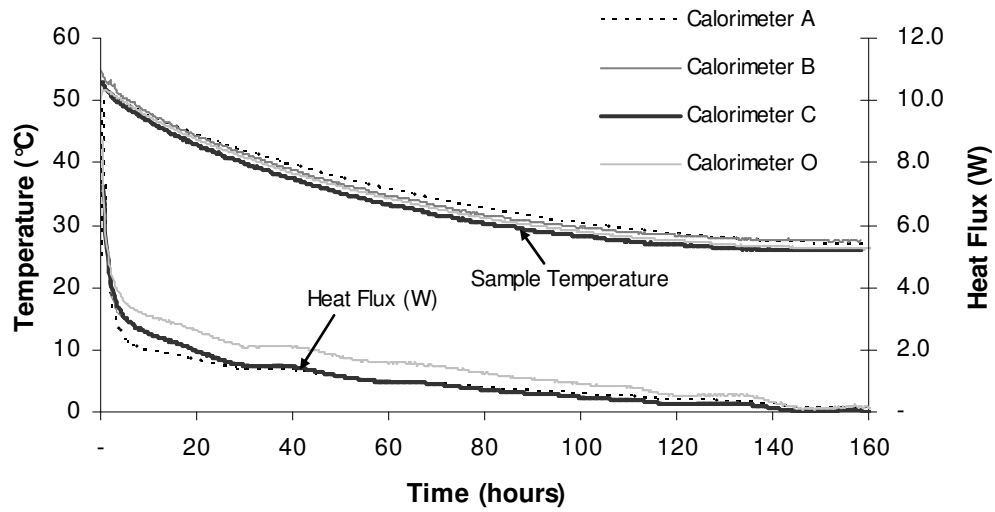


Figure 6-2: Water Calibration Results for Calorimeters Used in Study

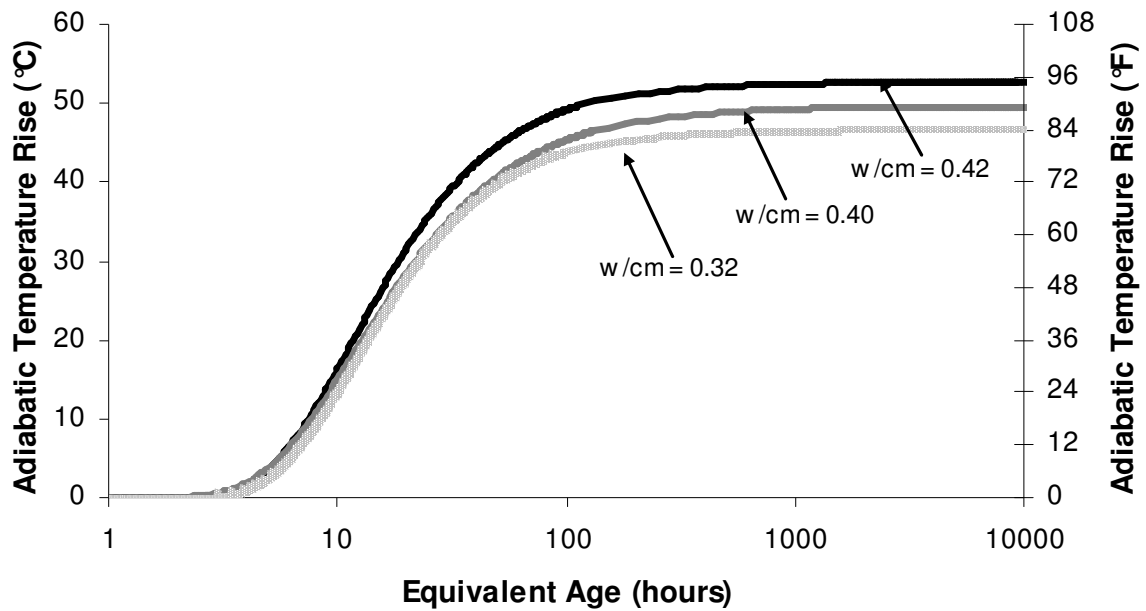


Figure 6-3: Effects of W/CM on Hydration Behavior

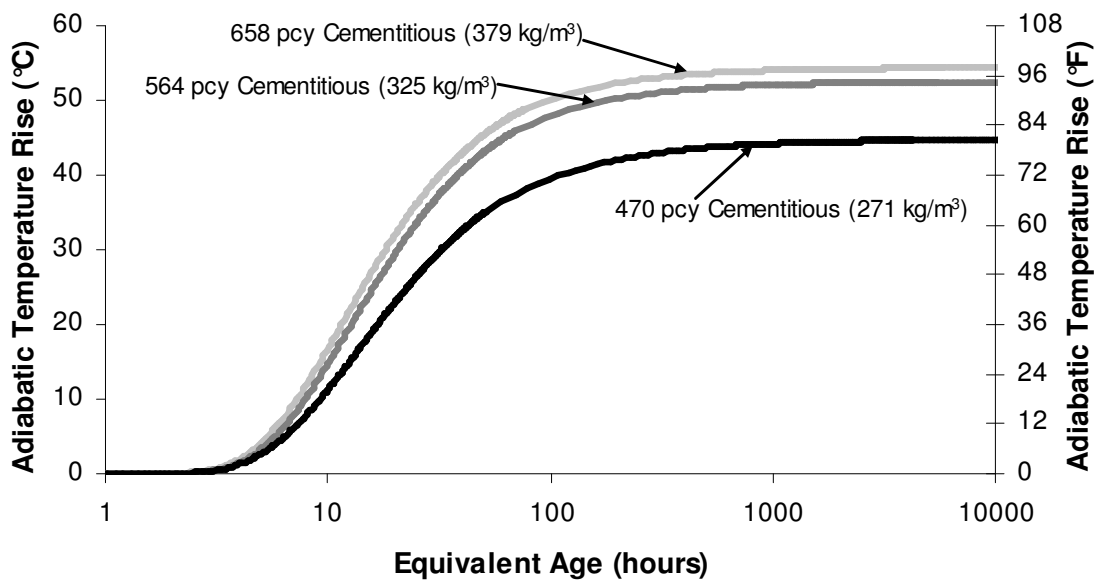


Figure 6-4: Effects of Cementitious Content on Hydration Behavior

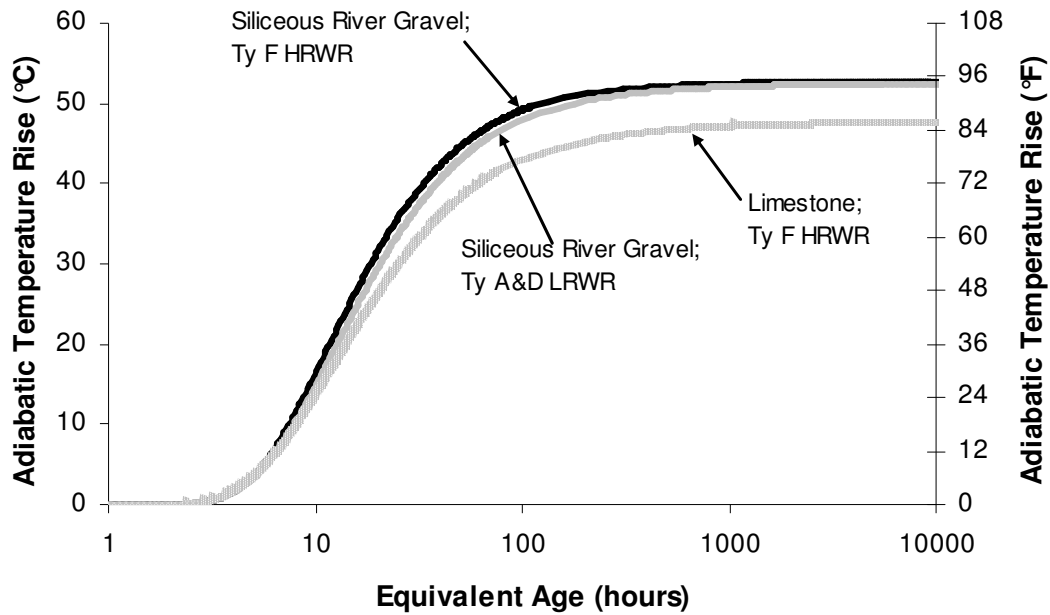


Figure 6-5: Effects of Aggregate Type and Admixture Type on Hydration Behavior

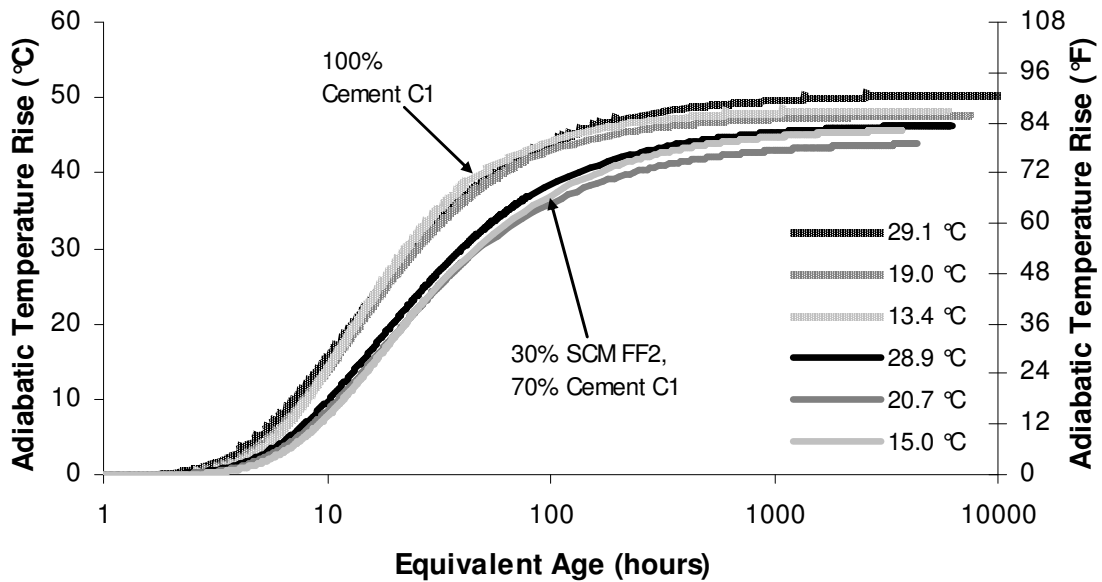


Figure 6-6: Effects of Placement Temperature on Calculated Adiabatic Temperature Rise for 100% Cement C1 (Mixtures 4, 5, and 6) and 30% FF2, 70% Cement C1 (Mixtures 15, 16, and 17)

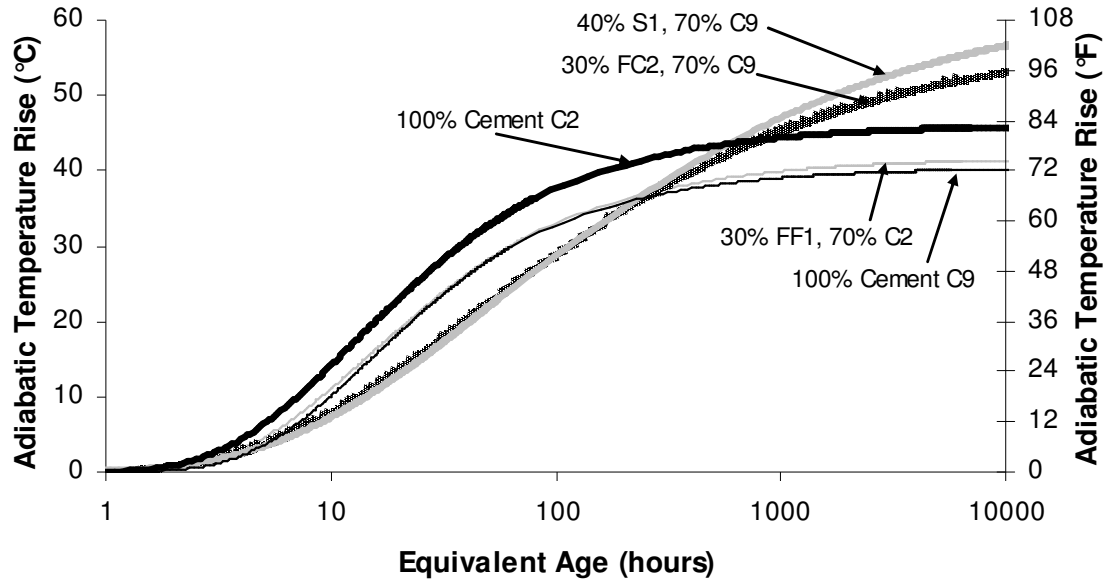


Figure 6-7: Effects of Cement Type on Adiabatic Temperature (Mixtures 9-13)

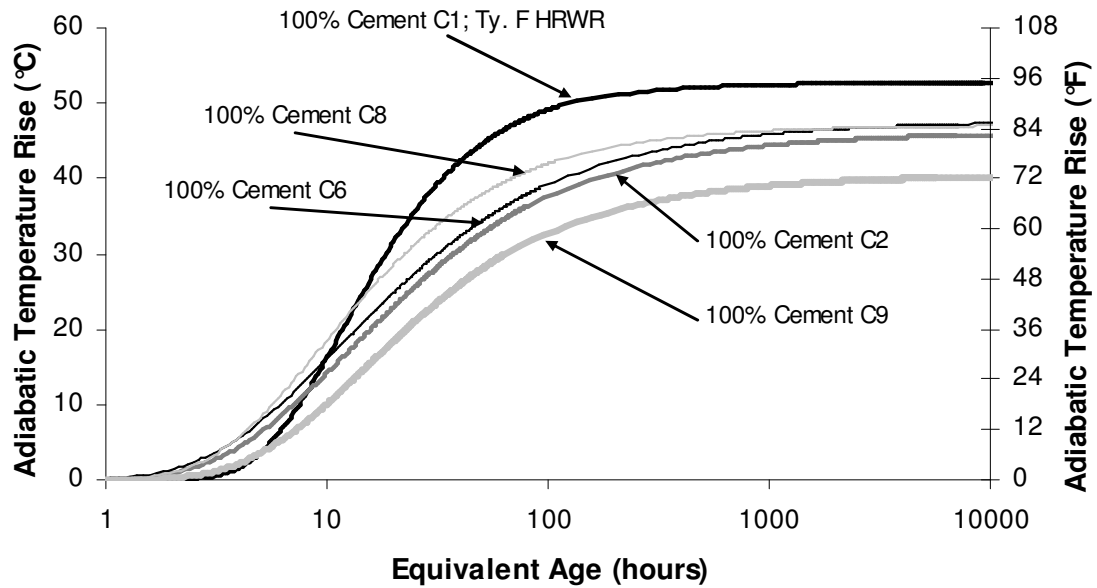


Figure 6-8: Effects of SCMs on Adiabatic Temperature Rise (Mixtures 10, 13, 14, 19 and 20)

CHAPTER 7. STUDY OF THE EFFECTS OF CHEMICAL ADMIXTURES ON HYDRATION

Mitigation of thermal cracking in concrete elements is important to ensuring the durability of the structure. Accurate estimation of the temperature development of concrete is crucial to determining the thermal cracking risk. The use of chemical admixtures in a concrete mixture can affect the timing and magnitude of the temperature development of the concrete mixture. A better estimate of the effects of chemical admixtures on hydration is needed. This chapter presents a comprehensive study of the effects of different chemical admixtures on the hydration of concrete using semi-adiabatic calorimetry. The results of the study provide a better estimate of the rate of heat evolution and adiabatic temperature rise of concrete with chemical admixtures.

7.1. INTRODUCTION

In large concrete elements, the magnitude and timing of the temperature rise should be controlled in order to prevent thermal cracking. Admixtures such as water reducers, retarders, accelerators, and air entraining admixtures may play a significant role in the rate of temperature rise of a particular mixture, although they are not expected to reduce the total adiabatic temperature rise. Accurate modeling of the progress of hydration requires an estimate of the effects of these chemical admixtures on the hydration of cementitious systems.

The mechanisms of most commonly used admixtures have been previously investigated. For example, Bhatt¹ provides an excellent literature review on the mechanisms of different accelerators, retarders, water reducers, and air entraining

admixtures, with a focus on x-ray diffraction (XRD), thermogravimetric analysis (TGA), and differential thermal analysis (DTA) to measure the progress of hydration. Chapter 3² examined the effects of chemical admixtures on the activation energy of cement pastes as determined from isothermal calorimetry on cement pastes. The mechanisms that govern the effects of admixtures on hydration are relatively well understood. However, only a limited amount of research has been done to effectively relate the behavior of admixtures in paste to the hydration of actual concrete. The behavior of admixtures varies considerably depending on the cement and supplementary cementing material (SCM) that is used in a concrete mixture. Also, the chemistry of admixtures of the same ASTM designation can vary considerably. Chapter 3² has shown that cement, SCM, and admixture interactions can play a large role in the hydration of cement pastes. Therefore, a comprehensive study of the hydration of concrete with a variety of cements, SCMs, and chemical admixture combinations is needed.

Semi-adiabatic calorimetry has been used to investigate the hydration behavior of mixtures with different cement types³, supplementary cementing materials (SCMs)³ in the absence of chemical admixtures, and a limited number of combinations of SCM and chemical admixture^{4,5}. The details of this technique, including calculation techniques, calibration, and variability have been discussed previously^{3,4,6}. However, previous work was limited in scope. This study will investigate the effects of a wider variety of different chemical admixtures on the hydration of cementitious systems using semi-adiabatic calorimetry. The results from semi-adiabatic calorimetry will be compared to existing literature to identify the trends in heat evolution and adiabatic temperature rise

associated with water reducing (low-range, mid-range, and high-range), retarding, accelerating, and air entraining admixtures.

7.2. RESEARCH SIGNIFICANCE

Accurate prediction of the rate and magnitude of temperature development in a concrete element is needed to guard against thermal cracking. An estimation of the effects of chemical admixtures on the development of temperature in a concrete element is needed, especially given that chemical admixtures are ubiquitous in modern concrete construction. Semi-adiabatic calorimetry is a useful test method to rapidly quantify the effects of different admixtures in concrete, and will be used in this chapter to examine the effects of water reducing, retarding, accelerating, and air entraining admixtures on the hydration and adiabatic temperature rise of concrete.

7.3. BACKGROUND

The following section is derived from previous literature³ to show the calculation of the adiabatic temperature rise of a concrete mixture, and to provide some background for presenting the test results. The hydration of cementitious systems may be divided into five stages⁷. The effects of admixtures on hydration will be discussed in relation to these five phases.

The first stage occurs immediately after water is added, and results in an initial period of rapid heat evolution and first deceleration, and is not studied extensively here. The second stage is referred to as the dormant, or induction period. This is the stage that permits the placing and handling of concrete since it is still in a plastic state. Initial set

generally occurs at the end of this stage, and the paste fraction of the concrete starts to stiffen considerably. When the calcium and silicon concentrations in solution reach a critical value, reactions of C_3S and C_3A proceed at a rapid rate and the acceleration stage is reached⁷. Final set is reached at some point just after the start of this stage, when strength and stiffness development start to occur. In the third stage, the C_3S hydration accelerates to a very high level of activity, and the maximum rate of heat evolution is reached during this stage. During this stage, acceleration of the C_3A reaction occurs, ettringite is formed and the heat of hydration of the C_3A compound adds to the total heat evolution. Two peaks representing the bulk of C_3S and C_3A hydration may appear in heat evolution curves. The exact stage at which monosulfoaluminate and ettringite develop will be determined by the amount of gypsum added during the cement manufacture and the amount and type of aluminate phases in the portland cement. The more gypsum in the system, the longer the ettringite will remain stable.

In the fourth stage, the rate of reaction slows down because the thick layer of hydration products formed on the cement grains inhibits further dissolution of ions. The formation of new hydration products will be controlled by the rate of diffusion of ions through this layer. The hydration of C_2S to CH and $C-S-H$ and C_4AF to monosulfoaluminoferrite generally begins during this period, since these reactions progress very slowly and little heat is developed. The final stage involves the slow reaction of the remaining portion of the material, and the concrete is approaching its long-term strength. When pozzolans are present, $Ca(OH)_2$ will be converted into $C-S-H$

through the pozzolanic reaction during this stage. Most often, complete hydration of all of the cementitious material does not occur⁸.

The fully adiabatic temperature rise is calculated using Equation 7-1 through Equation 7-7 using the procedure discussed in detail in previous chapters^{3,4}. The Arrhenius equation is commonly used to model hydration, since it accounts for the temperature sensitivity of this chemical reaction. The equivalent age (t_e) of concrete is a mathematical representation of its time-temperature history, which allows one to determine the equivalent curing age compared to curing at a reference temperature⁹. The concept allows one to model the hydration behavior when concrete is cured with different temperature histories. Equation 7-1, proposed by Friesleben Hansen and Pederson⁹, is the most common expression used to compute equivalent age, and is used in the remainder of this chapter to model the effects of time and temperature on hydration:

$$t_e(T_r) = \sum_0^t e^{-\frac{E_a}{R}(\frac{1}{T_c} - \frac{1}{T_r})} \cdot \Delta t \quad \text{Equation 7-1}$$

where $t_e(T_r)$ = equivalent age at reference temperature (T_r), T_c = temperature of the concrete (°K), E_a = activation energy (J/mol), Δt = time interval, and R = natural gas constant (8.314 J/mol/°K).

The progress of the hydration of portland cement may be quantified by the degree of hydration (α), which varies from 0 to 1, with a value of 1 indicating complete hydration. For this study, degree of hydration is taken as the ratio of heat evolved at time, t , to the total amount of heat available, as shown in Equation 7-2: ^{4,10,11,12,13,14}

$$\alpha = \frac{H(t)}{H_u} \quad \text{Equation 7-2}$$

where α = degree of hydration at time t , $H(t)$ = heat evolved from time 0 to time t (J/gram), and H_u = total heat available for reaction (J/gram).

H_u is a function of cement composition and amount and type of supplementary cementing materials (SCMs) and may be calculated as follows⁴:

$$H_u = H_{cem} \cdot p_{cem} + 461 \cdot p_{slag} + 1800 \cdot p_{FA-CaO} \cdot p_{FA} \quad \text{Equation 7-3}$$

where p_{slag} = slag mass to total cementitious content ratio, p_{FA} = fly ash mass to total cementitious content ratio, p_{FA-CaO} = fly ash CaO mass to total fly ash content ratio, p_{cem} = cement mass to total cementitious content ratio, and H_{cem} = heat of hydration of the cement (J/gram). H_{cem} can be calculated as shown in Equation 7-4⁴:

$$H_{cem} = 500 \cdot p_{C_3S} + 260 \cdot p_{C_2S} + 866 \cdot p_{C_3A} + 420 \cdot p_{C_4AF} + 624 \cdot p_{SO_3} + 1186 \cdot p_{FreeCa} + 850 \cdot p_{MgO} \quad \text{Equation 7-4}$$

where H_{cem} = total heat of hydration of portland cement (J/gram) at $\alpha = 1.0$, and p_i = mass of i-th component to total cement content ratio.

The most commonly used relationship to characterize cement hydration is a three-parameter model based on degree of hydration data, as shown in Equation 6^{4,15}:

$$\alpha(t_e) = \alpha_u \cdot e^{-\left[\frac{\tau}{t_e}\right]^\beta} \quad \text{Equation 7-5}$$

where $\alpha(t_e)$ = degree of hydration at equivalent age t_e , τ = hydration time parameter (hours), β = hydration shape parameter, and α_u = ultimate degree of hydration. This model will be referred to as the exponential model for the remainder of the chapter. The

rate of heat evolution of concrete can be calculated using Equation 7-6. Heat evolved at time t is as follows⁴:

$$Q_h(t) = H_u \cdot W_c \cdot \left(\frac{\tau}{t_e}\right)^\beta \cdot \left(\frac{\beta}{t_e}\right) \cdot \alpha(t_e) \cdot \exp\left(\frac{E}{R} \left(\frac{1}{273+T_r} - \frac{1}{273+T_c}\right)\right) \quad \text{Equation 7-6}$$

where Q_h = rate of heat generation (W/m³), H_u = total heat available (J/kg), and W_c = cementitious materials content (kg/m³).

The specific heat of concrete can be estimated using Equation 7-7. Specific heat is assumed to vary with degree of hydration¹⁶. Specific heat of concrete can be calculated as follows:

$$C_p = \frac{1}{\rho} \cdot (W_c \alpha C_{ref} + W_c \cdot (1 - \alpha) \cdot C_c + W_a C_a + W_w C_w) \quad \text{Equation 7-7}$$

where C_p = specific heat of concrete mixture (J/kg), ρ = unit weight of concrete (kg/m³); W_c , W_a , W_w = amount by weight of cement, aggregate, and water (kg/m³); C_c , C_a , C_w = specific heat of cement, aggregate, and water (J/kg/°C), and C_{ref} = specific heat of hydrated cement = $8.4 \times T_c + 339$ (J/kg/°C).

7.3.1. CALCULATION OF E_A

E_a was calculated from a multivariate regression model¹⁷ shown in Equation 7-8 as follows:

$$\begin{aligned} E_a = & 41,230 + 1,416,000 \cdot [(C_3 A + C_4 AF) \cdot p_{Cement} \cdot SO_3 \cdot p_{Cement}] \\ & - 347,000 \cdot Na_2O_{eq} - 19.8 \cdot Blaine \\ & + 29,600 \cdot p_{FlyAsh} \cdot p_{CaO-FlyAsh} + 16,200 \cdot p_{GGBFS} - 51,600 \cdot p_{SF} \\ & - 3,090,000 \cdot WRRET - 345,000 \cdot ACCL \end{aligned} \quad \text{Equation 7-8}$$

where p_{cement} = % cement in mixture; p_{FlyAsh} = % fly ash in mixture; $p_{CaO-FlyAsh}$ = % CaO in fly ash; p_{GGBFS} = % GGBFS in mixture; p_{SF} = % silica fume in mixture; $Blaine$ = Blaine fineness of cement; Na_2O_{eq} = % Na₂O_{eq} in cement ($0.658 \times \%K_2O + \%Na_2O$); C_3A = % C₃A in cement; C_4AF = % C₄AF in cement; SO_3 = % SO₃ in cement; $WRRET$ = ASTM Type A&D water reducer/retarder, % solids per gram of cementitious material; $ACCL$ = ASTM Type C calcium-nitrate based accelerator, % solids per gram of cementitious material.

7.4. EXPERIMENTAL PROGRAM

7.4.1. TEST METHODS

Semi-adiabatic calorimetry was performed to determine the rate of heat evolution and adiabatic temperature rise of different concrete mixtures. Each concrete mixture is batched and mixed as per ASTM C 192¹⁸. One 150 x 300 mm (6 x12 in.) cylinder is made, and its weight recorded. The cylinder is placed inside the semi-adiabatic calorimeter as soon as possible after mixing (generally around 30 minutes after water is added to the cement). The cylinder temperature and heat flux out of the calorimeter is recorded at 15 minute intervals. The test is run for approximately 150 hours. Detailed procedures for the calculation of the adiabatic temperature rise have been previously reported^{3,4,6}. Activation energy (E_a) for each of the mixtures was determined from a multivariate regression model based on isothermal calorimetry tests on cement pastes¹⁷.

7.4.2. MATERIALS

The following cements conforming to ASTM C 150¹⁹ were used: one low-alkali Type I cement (C1), one high-alkali Type I cement (C2), two low-alkali Type I/II

cements (C6 and C10), and one Type V cement (C9). The following SCMs were used: two ASTM C 618 Class F²⁰ fly ashes (FF1 and FF2), two ASTM C 618 Class C²⁰ fly ashes (FC1 and FC2), and one ASTM C 989 Grade 120²¹ ground-granulated blast-furnace slag (S1). Chemical and physical properties of the materials are summarized in Table 7-1. Mixture information is summarized in Table 7-2 and Table 7-3. Cement phases were calculated from x-ray fluorescence data using Bogue calculations¹⁵, and from Rietveld analysis²² using quantitative X-ray diffraction (QXRD). The following admixtures were used as part of this study: a Type A²³ glucose-based water-reducing admixture (LRWR), a Type B&D²³ lignosulfonate-based low-range water-reducing and retarding admixture (WRRET), a Type C²³ calcium-nitrate-based non-chloride accelerating admixture (ACCL), a Type F²³ naphthalene-sulfonate-based high-range water-reducing admixture (NHRWR), a Type F²³ polycarboxylate-based high-range water reducing admixture (PCHRWR), a mid-range water reducing admixture (MRWR), and an air entraining admixture (AEA).

All mixtures had a cementitious materials content of 325 kg/m³ (564 lbs/yd³). Siliceous river gravel (#57²⁴) and siliceous river sand were used for the coarse (CA) and fine aggregates (FA) in all of the mixtures. FA/ (FA+CA) was between 0.40 and 0.44. The amounts of CA and FA in the mixture had no effect on the hydration characteristics of the mixture, because both aggregates were roughly the same mineralogy and have approximately the same specific heat. Also, the w/cm was varied slightly in some cases to produce mixtures with the appropriate workability. Chemical admixture addition rates were chosen to sample the range of manufacturer's recommended dosage rates.

Type A LRWR was added at a dosage of 0.29%. Type B&D WRRET was added at a dosage from 0.18% to 0.54%. Type C ACCL was added at a dosage from 0.78% to 2.23%. Type F NHRWR was added at a dosage from 0.78% to 1.25%, and PCHRWR was added at 0.20% to 0.68%. MRWR was added at a dosage of 0.74%. AEA was added at a dosage of 0.04 to 0.08%. Each admixture was paired with different combinations of cement and SCM, which allowed potential interactions between the constituents to be evaluated.

7.4.3. COMPARISON BETWEEN ISOTHERMAL AND SEMI-ADIABATIC CALORIMETRY

There are several differences between the isothermal tests presented previously² and the semi-adiabatic calorimeter tests presented here. First, isothermal calorimeter test samples are generally small paste samples (approximately 20 to 30 grams). Semi-adiabatic calorimeter test samples are larger concrete samples that fill a 150 mm×300 mm (6×12 in.) cylinder. The aggregate in the concrete will absorb some of the heat from the cement hydration due to the aggregate's specific heat. This will lower the amount of heat measured from the test. Next, the heat of hydration for concrete mixtures measured using semi-adiabatic calorimetry is different from the heat of hydration for the equivalent pastes measured using isothermal calorimetry. The semi-adiabatic calorimeter measures temperature at several locations in the instrument to determine the amount of heat evolved from a mixture. The isothermal calorimeter measures the amount of power needed to maintain a constant temperature of the paste. Finally, the concrete temperature

in a semi-adiabatic test is free to rise and fall, whereas the paste temperature in isothermal calorimetry is held to a single temperature.

Water reducers and retarders composed of lignosulfonates and glucose have been shown² to significantly affect the magnitude and timing of the aluminate peak. Isothermal calorimeter tests on pastes² show a large increase in peak height with the addition of a Type B&D WRRET. Type A LRWR produces less of a pronounced peak. However, the peak is not as sharp when tested using semi-adiabatic calorimetry on concrete. The effect of these factors on the test results may be seen in Figure 7-1, which compares semi-adiabatic and isothermal test results of mixtures with Cement C1 with no admixture, 0.29% LRWR, and 0.35% WRRET. Two distinct peaks are seen in the isothermal data, while the same mixtures tested with semi-adiabatic calorimetry have a single peak. Finally, the rate of heat evolution in the semi-adiabatic tests is higher than the rate of heat evolution in the isothermal tests, because the sample temperature can be much higher than 23 °C (73 °F) in the semi-adiabatic test.

7.5. RESULTS AND DISCUSSION

In this chapter, the effects of chemical admixtures on hydration are investigated by calorimeter testing. The results are compared in the following sections by examining the differences in the rate of heat evolution, the changes in exponential model parameters, and the adiabatic temperature rise. The exponential model parameters (as shown in Equation 7-5) are summarized for mixtures with 100% portland cement in Table 7-2, and are summarized for mixtures with SCMs in Table 7-3. The rate of heat evolution gives an indication of the timing and magnitude of the silicate and aluminate phase hydration

peak. When the hydration of the mixture is retarded, the induction period is generally extended, and the slope of the accelerating portion of the hydration curve is reduced. These trends are reflected in the time parameter, τ , and the slope parameter, β . All of the exponential model parameters depend highly on the interactions between the SCM, cement, and the chemical admixture in the concrete. The total adiabatic temperature rise gives an overall indication of the combined effects of different cements, SCMs, and admixtures on hydration. The way that chemical admixtures affect the rate of heat evolution, the hydration parameters, and the adiabatic temperature rise will be discussed in the following sections.

7.5.1. EFFECTS OF LOW-RANGE WATER REDUCING/RETARDING ADMIXTURES ON MIXTURES WITH 100% CEMENT

The following sections evaluate the effects of ASTM Type A water reducing and Type B&D water reducing/retarding admixtures. Figure 7-2 shows the effects of different dosages of Type B&D WRRET and Type A LRWR on the hydration of Cement C1, C2, C6, and C9. The Type V cement, C9, shows the largest delay with the addition of WRRET and the least delay is seen with Cement C1. Also, increasing dosages of WRRET appear to systematically increase the amount of retardation. WRRET lowers the peak height, and increases the amount of time over which the majority of the heat is evolved. The retardation from LRWR is similar to the retardation of the WRRET for Cement C2 and C6, while C1 shows little retardation from the LRWR. There is some correlation between the amount of C_3A in the cements and the amount of delay caused by the retarding admixture.

The timing of the accelerating portion of the hydration curve is strongly affected by the type and dosage of water reducer and the type of cementitious material present in the mixture. The addition of a LRWR and WRRET to a mixture is not expected to affect the total adiabatic temperature rise of a mixture. However, these admixtures may alter the timing of the temperature rise significantly, as shown in Figure 7-3. A delay in the onset of hydration is directly correlated with a delay in temperature rise for all cements tested here. This delay may or may not be beneficial, because a lower temperature will proportionally retard the development of mechanical properties compared to a mixture with no admixtures.

7.5.2. EFFECTS OF LOW-RANGE WATER REDUCING/RETARDING ADMIXTURES ON MIXTURES WITH FLY ASH

Figure 7-4 shows the effects of the addition of WRRET and LRWR to a mixture of 70% Cement C1 and 30% FF2. The amount of retardation increases as the dosage of WRRET increases. The LRWR shifts the increasing portion of the hydration curve approximately 2 hours, while the WRRET shifts this part of the curve 5 to 20 hours, depending on dosage. Figure 7-5 and Figure 7-6 show the effects of the same dosages of admixture on a mixture of 70% Cement C1 and 30% FC1 and FC2, respectively. Without admixture, the dormant period is slightly delayed and the slope is reduced compared to a mixture of cement only. The addition of WRRET and LRWR to the mixtures with fly ash extends the dormant period in proportion to the potency and dosage of admixture.

The addition of low-range reducing/retarding admixtures to a mixture with fly ash produces retardation which, as in the plain cement mixes, is in proportion to the potency of the retarder. However, the type of fly ash also plays a role in the amount of retardation of the mixture. Figure 7-7, Figure 7-8, and Figure 7-9 show the changes in adiabatic temperature rise caused by LRWR and WRRET on mixtures with 30% FF2, FC1, and FC2. These mixtures are retarded more by the addition of the WRRET than by the LRWR, just as with the mixtures with 100% cement. However, the adiabatic temperature rise of the mixtures is not significantly affected by the chemical admixtures. The exceptions are the mixture with FF2 and 0.53% WRRET and the mixture with 0.35% WRRET and FC2; these are greatly retarded and show a reduction in the adiabatic temperature rise of approximately 8 °C (15 °F). It is unknown whether the reduction in temperature rise is an artifact of the semi-adiabatic calculation procedure, due to the duration of the test, the test procedure, and/or is related to any mechanism of the admixture itself. However, one limitation of the semi-adiabatic calorimetry test is that the test may sometimes be too short and this may result in misinterpretation of the data. For example, large dosages of WRRET with SCMs may delay the onset of hydration enough to alter the results of the semi-adiabatic test. The test is only run for 150 hours and it is possible that a significant percentage of the hydration in these cases may be delayed until after the test is complete. The problem is most pronounced with mixtures that already have a tendency to be retarded, such as those with high fly ash contents. The results from the tests presented here are not intended to show conclusively that these

admixtures reduce the ultimate adiabatic temperature rise. A longer, more accurate test is needed to draw any further conclusions.

7.5.3. EFFECTS OF MID-RANGE AND HIGH-RANGE WATER REDUCING ADMIXTURES ON HYDRATION AND TEMPERATURE RISE

This section will evaluate mixtures made with ASTM Type F naphthalene and polycarboxylate-based high-range water reducing admixtures. Figure 7-10 shows the changes in rate of heat evolution with the addition of NHRWR to mixtures with 100% Cement C2, C6, C10, and C12. NHRWR slightly delays the onset of the accelerating portion of the hydration curve, and slightly increases the maximum height of the hydration peak, possibly due to the improved dispersion of cementitious particles. Figure 7-11 shows that PCHRWR produces similar results for mixtures with 100% Cement C1, C2, C10, and C12. The rate of heat evolution of a mixture of 70% Cement C2 and 30% FC2 was not affected by the addition of a high-range water reducer. These results are included in Appendix E. The total adiabatic temperature rise of all mixtures was not affected by the addition of a high-range water reducer. Both NHRWR and PCHRWR produce very slight retardation compared to the WRRET.

Figure 7-12 shows the effects of a mid-range water reducing admixture (MRWR) on the heat of hydration of mixtures with 100% Cement C1, 100% Cement C2, and 70% Cement C6 with 30% FF2. The MRWR in this study causes more retardation than either of the high-range water reducers. This may be because the admixture has a percentage of lignosulfonate, which tends to act as a retarder. However, the retardation with MRWR is less than the retardation caused by the WRRET.

7.5.4. EFFECTS OF ACCELERATING AND AIR ENTRAINING ADMIXTURE ON HYDRATION AND TEMPERATURE RISE

An ASTM Type C²³ non-chloride based accelerating admixture (ACCL) was tested with cement C2. The rate of heat evolution for mixtures with 100% cement is shown in Figure 7-13 and the adiabatic temperature rise of these mixtures is shown in Figure 7-14. ACCL decreased the induction period, steepened the slope of the curve in the accelerating stage, and increased the maximum rate of heat evolution for the mixture with 100% Cement C2. The accelerator slightly increases the adiabatic temperature rise. The addition of the accelerator to a mixture of 70% Cement C2 and 30% FC1 had the same effect as for 100% Cement C2, but the increase in peak height was greater, as shown in Figure 7-15. The results of ACCL with other cement/SCM combinations are in Appendix E and confirm the results shown in Figure 7-13 and Figure 7-14. It should be noted that ACCL also increased the maximum rate of heat evolution for Cement C2 and C10. This trend was also seen in isothermal calorimetry testing with the same accelerating admixture²⁵ and is likely due to the additional reactive phases in the fly ash⁴.

An air entraining admixture (AEA) was tested with 100% Cement C2 and 80% Cement C6, 20% FF2. AEA did not significantly change the rate of heat evolution or the adiabatic temperature rise. These results are shown in Appendix E.

7.6. SUMMARY OF HYDRATION TRENDS

In general, the behavior of mixtures presented in the previous sections largely confirms what is already known about the effects of retarding, accelerating, and water reducing admixtures in concrete. However, the results allow quantification of the relative

magnitude of the effects of retarding, accelerating, and water reducing admixtures, as well as cementitious material type, which enables their use in hydration prediction models. The three parameters of exponential hydration model shown in Equation 7-5 are used in the following section to compare the effects of each admixture.

The amount of retardation of a mixture is represented by a combination of the time parameter (τ) and the slope parameter (β). The time parameter also has been shown to correlate with time of set²⁶. The total amount of heat evolved from the test is reflected in the degree of hydration parameter α_u . However, this parameter is only a measure of the heat evolved after a seven day test at elevated temperatures. The calorimeter tests are not run beyond one week because of the sensitivity of the semi-adiabatic calorimeter and the effects of the environment. Also, the total heat (H_u) is based on an independent, fractional model of the total heat available from all constituents (Equation 7-3 and Equation 7-4). Therefore, the results presented for α_u may not accurately represent the true “ultimate” degree of hydration. However, α_u provides a useful index of the amount of heat that will evolve in the early stages of hydration.

7.6.1. EFFECTS OF LOW-RANGE WATER REDUCING AND RETARDING ADMIXTURES ON HYDRATION PARAMETERS

Figure 7-16 shows the changes in τ , and Figure 7-17 shows the changes in β when a glucose based low-range water reducer (LRWR) is added to mixtures with and without fly ash. In general, the LRWR has a minimal effect on τ , and tends to increase β . However, the admixture caused an increase in τ when combined with a mixture of either

70% Cement C1 and 30% FC1, or 100% Cement C2. Interactions between Type A water reducing admixtures and certain cement-fly ash combinations have been reported to cause delays in set time in the field²⁷. This may be the explanation for the first mixture. This does not explain the delay with the mixture of 100% cement C2. However, the results were confirmed with a second mixture and time of set testing, which showed initial set occurring at 10 hours (vs. 6 hours for the same mixture with cement C1). This result suggests that C2 with FC1 will be retarded more than C1 with FC1 in the presence of a LRWR. LRWR did not significantly alter α_u , as shown in Table 7-2 and Table 7-3.

Figure 7-18 shows the changes in τ , and Figure 7-19 shows the changes in β with WRRET. Both parameters increase with increasing dosage of admixture for all concrete mixtures. Three different dosages were tested: 0.18%, 0.35%, and 0.53% by mass. As dosage increases, the induction period of hydration (measured by determining the first peak of the second derivative with time) appears to increase non-linearly. For example, the induction period of the mixture with 70% Cement C2 and 30% FF2 increases from 2.8 to 5.3, 11.0, and 28.8 hours as admixture dosage is increased from 0.00% to 0.18%, 0.35%, and 0.53% by mass, respectively. These results are shown in Appendix E. This indicates that a logarithmic or exponential model of τ may effectively represent the effects of admixture dosage on hydration. The trend for β is less clear. However, there is also a slight non-linearity to the results presented in Figure 7-19. Further analysis is needed to determine if a linear, logarithmic, or exponential model most appropriate. Finally, α_u drops with the addition of WRRET, as shown in Figure 7-20.

7.6.2. EFFECTS OF ACCELERATING AND AIR ENTRAINING ADMIXTURE ON HYDRATION PARAMETERS

Three different dosages of non-chloride calcium-nitrate-based accelerator (ACCL) were tested: 0.74%, 1.30%, and 2.23%. ACCL generally reduced τ , as shown in Figure 7-21. Additional data is shown in Appendix F. ACCL had no effect on β , as shown in Figure 7-22. The mixtures with Cement C2 and 20% FF1 and 50% S1 showed a slight increase in τ from 14.724 to 16.396 hours, and from 21.698 to 23.750 hours, respectively. However, this effect was with a dosage of 0.74%, which is the low range of the manufacturer's recommended dosage. The multiple batch, multiple instrument coefficient of variation for τ is 6.0%. Therefore, it is possible that the addition of ACCL to these two mixtures had no effect on hydration, because the decrease in τ is within the error of the test method. ACCL did not significantly alter α_u , as shown in Table 7-2 and Table 7-3.

7.6.3. EFFECTS OF MID-RANGE AND HIGH-RANGE WATER REDUCING ADMIXTURES ON HYDRATION PARAMETERS

Figure 7-23 and Figure 7-24 show the changes in τ and β with the addition of NHRWR, PCHRWR, and MRWR. Figure 7-10 and Figure 7-11 show that the hydration curve is not significantly delayed with the addition of NHRWR and PCHRWR, and the fact that τ was not significantly altered with the addition of either admixture agrees with this observation. τ did increase with the addition of MRWR because the admixture delayed hydration compared to the mixtures without admixture. β increased for all high-range water reducers tested, which agrees with the increase in hydration peak height seen

with these mixtures. Finally, the degree of hydration parameter (α_u) drops with the addition of NHRWR and PCHRWR as shown in Figure 7-25.

Another limitation is that a lack of knowledge about the constituents of chemical admixtures hampers the accurate characterization of the hydration behavior of admixtures. Manufacturer's data sheets generally do not specify the composition (type or amount) of active ingredients in a particular admixture, making it difficult, if not impossible, to predict behavior of a given admixture.

7.7. CONCLUSIONS

This is the first chapter to comprehensively investigate the effects of chemical admixtures on the hydration of concrete using semi-adiabatic calorimetry. The results presented in this chapter largely confirm what has been previously reported in literature, and may be used to better model the temperature rise in concrete structures.

The addition of a lignosulfonate-based water reducing and retarding admixture (WRRET) will extend the dormant period of hydration, and the addition of an accelerator will increase the slope and magnitude of the hydration curve. The adiabatic temperature rise is delayed with WRRET, and is accelerated with ACCL, but the temperature of the mixtures eventually rises to a level similar to a control mixture without retarder. A glucose-based low-range water reducing admixture (LRWR) will slightly extend the dormant period of hydration, except in certain cases where cement and fly ash may interact. The dispersing action of high-range water-reducing admixtures (NHRWR and PCHRWR) tends to increase the peak height of hydration curve as well. NHRWR and PCHRWR did not greatly retard the hydration, at least in the dosages evaluated in this

study. There was no appreciable difference in hydration with either type of HRWR. However, the mid-range water reducer (MRWR) did retard the mixtures with which it was paired. Finally, the addition of an air entraining admixture had little effect on hydration. NHRWR, PCHRWR, MRWR, and AEA had little effect on the adiabatic temperature rise of concrete.

7.8. REFERENCES

1. Bhatti, J.I., "A Review of the Application of Thermal Analysis to Cement-Admixture Systems", *Thermochemica Acta*, No.189, 1991, pp 313-350.
2. Poole, J.L., "The Effects of Chemical Admixtures on Activation Energy of Cementitious Materials," PhD Dissertation, Chapter 3, The University of Texas at Austin, Austin, TX, 2007, pp 38-68.
3. Poole, J.L., "Hydration Study of Cementitious Materials Using Semi-Adiabatic Calorimetry," PhD Dissertation, Chapter 6, The University of Texas at Austin, Austin, TX, 2007, pp 141-171.
4. Schindler, A.K., and K.J. Folliard, "Heat of Hydration Models for Cementitious Materials", *ACI Materials Journal*, V. 102, No. 1, Jan.-Feb., 2005, pp. 24-33.
5. Ge, Zhi, "Predicting Temperature and Strength Development of the Field Concrete", PhD Dissertation, Iowa State University, 2006.
6. RILEM 119-TCE, "Adiabatic and Semi-Adiabatic Calorimetry to Determine the Temperature Increase in Concrete due to Hydration Heat of Cement," RILEM Report 15, R. Springenschmid, ed., E&FN Spon, London, 1999, pp. 315-330.

7. Gartner, E.M., J.F. Young, D.A. Damidot, and I. Jawed, "Hydration of Portland Cement", *Structure and Performance of Cements*, 2nd ed., J. Bensted and P. Barnes, eds, 2002, pp 57-113
8. Mills, R H. "Factors Influencing Cessation of hydration in Water Cured Cement Pastes." Special Report 90: Symposium on Structure of Portland Cement Paste and Concrete. Washington, D.C.: Highway Research Board, 1966. 406-424.
9. Freiesleben Hansen, P., and E.J. Pedersen, "Maturity computer for controlling curing and hardening of concrete," *Nordisk Betong*, V. 1, No. 19, 1977, pp. 21-25.
10. D'Aloia, L., and G. Chanvillard, "Determining the "Apparent" Activation Energy of Concrete; E_a – Numerical Simulations of the Heat of Hydration of Cement," *Cement and Concrete Research*, V. 32, 2002, pp. 1277-1289.
11. Kada-Benameur, H., E. Wirquin, and B. Duthoit, "Determination of Apparent Activation Energy of Concrete by Isothermal Calorimetry," *Cement and Concrete Research*, V. 30, 2000, pp. 301-305.
12. Copeland, L.E., Kantro, D.L., Verbeck, G., "Part IV-3 Chemistry of Hydration of Portland Cement," 4th International Symposium of the Chemistry of Cement, Washington, D.C., 1960, pp. 429-465.
13. De Schutter, G., and Taerwe, L., "Degree of Hydration-Based Description of Mechanical Properties of Early-Age Concrete," *Materials and Structures*, Vol. 29, No. 7, 1996, pp. 335-344.

14. Verbeck, G., and Forster, C.W. "Long-Time Study of Cement Performance in Concrete. Chapter 6 – The Heats of Hydration of the Cement," Proceedings of the American Society for Testing Materials, Vol. 50, 1950, pp. 1235-1262.
15. Pane, I., and W. Hansen, "Concrete Hydration and Mechanical Properties under Nonisothermal Conditions," *ACI Materials Journal*, V. 99, No. 6, Nov.-Dec, 2002, pp. 534-542.
16. Van Breugel, K., "Prediction of Temperature Development in Hardening Concrete", *Prevention of Thermal Cracking in Concrete at Early Ages*, RILEM Report 15, E & FN Spon, London 1998.
17. Poole, J.L., "A Model for Estimating the Activation Energy of Cementitious Systems," PhD Dissertation, Chapter 5, The University of Texas at Austin, Austin, TX, 2007, pp 109-140.
18. ASTM C 192, "Standard Practice for Making and Curing Concrete Test Specimens in the Laboratory," Annual Book of ASTM Standards, V. 04.01., ASTM International, West Conshohocken, PA., 2006, 8 pp.
19. ASTM C 150, "Standard Specification for Portland Cement," Annual Book of ASTM Standards, Vol 04.01., ASTM International, West Conshohocken, PA., 2002, 8 pp.
20. ASTM C 618, "Standard Specification for Coal Ash and Raw or Calcined Natural Pozzolans for Use in Concrete," Annual Book of ASTM Standards, V. 04.01., ASTM International, West Conshohocken, PA., 2003, 3 pp.

21. ASTM C 989, “Standard Specification for Ground Granulated Blast-Furnace Slag for Use in Concrete and Mortars,” Annual Book of ASTM Standards, V. 04.01., ASTM International, West Conshohocken, PA., 2005, 5 pp.
22. Scrivener, K.L., T. Füllmann, E. Gallucci, G. Walenta, and E. Bermejo, “Quantitative Study of Portland Cement Hydration by X-Ray Diffraction/Rietveld Analysis and Independent Methods”, *Cement and Concrete Research*, V. 34, 2004, pp 1541-1547.
23. ASTM C 494, “Standard Specification for Chemical Admixtures for Concrete,” Annual Book of ASTM Standards, V. 04.01., ASTM International, West Conshohocken, PA., 2005, 10 pp.
24. ASTM C 33, “Standard Specification for Concrete Aggregates” Annual Book of ASTM Standards, V. 04.01., ASTM International, West Conshohocken, PA., 2003, 11 pp.
25. Poole, J.L., “The Effects of Supplementary Cementing Materials on Activation Energy of SCMs,” PhD Dissertation, Chapter 4, The University of Texas at Austin, Austin, TX, 2007, pp 69-108.
26. Schindler, A.K., “Prediction of Concrete Setting”, RILEM International Symposium on “Advances in Concrete Through Science and Engineering”, Evanston, Illinois, March 22-24, 2004.
27. Roberts, L.R. and P.C. Taylor, “Understanding Cement-SCM-Admixture Interaction Issues” *Concrete International*, V. 29, No. 1, 2007 pp 33-41.

Table 7-1: Chemical and Physical Properties of Cementitious Materials

	Cements						Fly Ashes				Other SCMs
	C1	C2	C6	C9	C10	C12	FF1	FF2	FC1	FC2	S1
SiO ₂ (%)	20.45	19.18	20.77	21.63	21.03	19.38	56.63	51.69	37.83	33.31	34.48
Al ₂ O ₃ (%)	5.43	5.34	3.88	4.04	4.13	4.79	30.68	24.81	19.83	18.39	11.35
Fe ₂ O ₃ (%)	2.01	2.3	3.73	5.29	3.78	3.17	4.94	4.22	6.17	5.40	0.67
CaO (%)	64.51	63.17	64.5	63.07	63.4	65.24	0.69	13.12	23.13	28.91	41.73
MgO (%)	1.15	1.09	1.01	0.77	1.32	1.44	0.73	2.29	4.62	5.25	7.32
Na ₂ O (%)	0.14	0.12	0.18	0.27	0.14	0.16	0.12	0.18	1.74	1.64	0.14
K ₂ O (%)	0.56	0.95	0.60	0.23	0.55	0.36	2.26	0.84	0.06	0.35	0.38
Na ₂ O Eq. (%)	0.51	0.75	0.575	0.42	0.502	0.397	1.607	0.733	1.778	1.870	0.390
SO ₃ (%)	3.35	3.20	2.38	2.74	3.02	2.43	0.00	0.46	1.50	2.27	1.88
LOI (%)	1.80	4.10	2.67	1.55	1.5	2.4	2.10	0.23	0.67	0.34	0.83
Insoluble Residue (%)	-	0.63	0.25	1.43	0.17	0.36	-	-	-	-	-
CaO (%)**	0.0	0.0	0.0	0.0	0.0	0.0					
C ₃ S (%)*	58.29	63.1	66.5	49.85	56.51	68.75	-	-	-	-	-
C ₃ S (%)**	61.20	61.0	55.7	49.00	64.00	67.60	-	-	-	-	-
C ₂ S (%)*	14.65	7.4	9.4	24.41	17.66	3.70	-	-	-	-	-
C ₂ S (%)**	16.00	15.6	21.1	26.40	15.30	7.30	-	-	-	-	-
C ₃ A (%)*	10.99	10.3	4.0	1.76	4.55	7.33	-	-	-	-	-
C ₃ A (%)**	13.10	9.6	4.0	4.40	5.10	5.40	-	-	-	-	-
C ₄ AF (%)*	6.12	7.0	11.4	16.10	11.50	9.56	-	-	-	-	-
C ₄ AF (%)**	3.50	6.0	10.7	12.10	11.00	10.10	-	-	-	-	-
C \hat{S} H ₂ (%)**	1.4	0.4	3.1	2.3	1.6	1.6	-	-	-	-	-
C \hat{S} H _{0.5} (%)**	1.5	1.2	1.3	2	0.6	2.2	-	-	-	-	-
C \hat{S} (%)**	0.6	0.7	0.6	0.4	0.6	0.4	-	-	-	-	-
K ₂ SO ₄ (%)**	1.5	1.0	0.7	0.9	0	0.3	-	-	-	-	-
CaCO ₃ (%)**	0.8	3.6	3.2	2.5	1.0	3.6					
Blaine fineness (m ² /kg)	350	391	365	409	349	393	147	166	348	300	332

Table 7-2: Summary of Three-Parameter Model Parameters for Mixtures with 100% Cement

Mix #	Cement	SCM (% Replacement by Mass)			w/cm	Chemical Admixture (ASTM)		H_u	α_u	τ	β	E_a
		Type	%	CaO		Type	%					
	ID							kJ/kg		hrs		J/mol
1	C1	-	-	-	0.44	-	-	481	0.793	13.80	0.847	40,650
2	C1	-	-	-	0.42	A	0.29	481	0.790	12.61	1.109	30,800
3	C1	-	-	-	0.44	B&D	0.35	481	0.761	15.65	1.386	29,850
4	C2	-	-	-	0.44	-	-	482	0.711	12.49	0.950	38,750
5	C2	-	-	-	0.44	B&D	0.35	482	0.674	19.30	1.592	27,900
6	C2	-	-	-	0.40	B&D	0.35	482	0.687	17.59	1.652	27,900
7	C2	-	-	-	0.40	B&D	0.52	482	0.652	25.21	2.404	25,000
8	C2	-	-	-	0.44	C	0.78	482	0.774	12.60	0.887	36,150
9	C2	-	-	-	0.44	C	1.30	482	0.785	12.14	0.929	34,250
10	C2	-	-	-	0.44	C	2.23	482	0.803	10.65	0.793	31,050
11	C2	-	-	-	0.42	MR	0.32	482	0.648	15.73	1.109	38,750
12	C2	-	-	-	0.44	F-PC	0.34	482	0.645	11.68	1.138	38,750
13	C2	-	-	-	0.44	F-N	1.25	482	0.690	13.47	1.165	38,750
14	C2	-	-	-	0.42	A	0.29	482	0.622	18.27	1.484	28,900
15	C6	-	-	-	0.44	-	-	496	0.753	11.40	0.737	37,150
16	C6	-	-	-	0.44	B&D	0.35	463	0.693	14.90	1.208	26,350
17	C6	-	-	-	0.44	B&D	0.52	463	0.691	23.34	1.680	25,000
18	C6	-	-	-	0.42	A	0.29	463	0.677	11.38	1.137	27,350
19	C6	-	-	-	0.42	A AEA	0.29 0.04	463	0.656	11.01	1.140	27,350
20	C6	-	-	-	0.44	F-N	0.78	463	0.684	10.15	0.929	37,150
21	C7	-	-	-	0.32	F-PC	0.68	485	0.614	11.19	1.387	39,050
22	C7	-	-	-	0.32	F-N B&D	1.25 0.32	485	0.657	13.39	1.543	29,200
23	C8	-	-	-	0.44	-	-	474	0.726	9.35	0.893	37,350
24	C8	-	-	-	0.32	F-PC	0.68	474	0.614	10.29	1.073	37,350
25	C9	-	-	-	0.44	-	-	419	0.714	14.86	0.807	38,600
26	C9	-	-	-	0.44	B&D	0.35	419	0.694	27.22	1.436	27,750
27	C9	-	-	-	0.44	MR	0.32	419	0.790	20.78	0.919	38,600
28	C10	-	-	-	0.44	-	-	446	0.793	12.78	0.709	39,450
29	C10	-	-	-	0.44	B&D	0.35	446	0.738	18.19	1.186	28,600
30	C10	-	-	-	0.44	B&D	0.24	446	0.678	15.01	1.191	32,050
31	C10	-	-	-	0.44	F-N	0.78	446	0.731	11.22	0.955	39,450
32	C10	-	-	-	0.44	F-PC	0.27	446	0.750	12.29	0.783	39,450
33	C10	-	-	-	0.44	C	1.30	446	0.875	11.97	0.638	34,950
34	C12	-	-	-	0.44	-	-	462	0.811	13.01	0.803	38,600
35	C12	-	-	-	0.44	B&D	0.24	462	0.843	14.86	0.987	31,200

Table 7-3: Summary of Mixtures with SCMs

Mix #	Cement	SCM (% Replacement by Mass)			w/cm	Chemical Admixture (ASTM)		H _u	α_u	τ	β	E _a
	ID	Type	%	CaO		Type	% by Mass	kJ/kg		Hrs		J/mol
36	C1	FF1	20	0.7	0.42	A	0.29	387	0.923	15.63	0.957	27,950
37	C1	FF1	30	0.7	0.42	A	0.29	340	0.970	16.30	0.876	26,750
38	C1	FF2	20	13.1	0.42	A	0.29	432	0.854	16.79	0.962	28,650
39	C1	FF2	30	13.1	0.44	-	-	408	0.832	18.08	0.710	37,700
40	C1	FF2	30	13.1	0.42	A	0.29	408	0.848	18.31	0.914	27,850
41	C1	FF2	30	13.1	0.42	B&D	0.18	408	0.726	17.50	1.321	21,450
42	C1	FF2	30	13.1	0.42	B&D	0.35	408	0.761	24.15	1.314	26,850
43	C1	FF2	30	13.1	0.42	B&D	0.54	408	0.698	39.12	2.251	32,250
44	C1	FC1	20	23.1	0.42	A	0.29	468	0.839	17.66	1.076	29,250
45	C1	FC1	30	23.1	0.44	-	-	462	0.747	16.78	0.904	38,550
46	C1	FC1	30	23.1	0.42	A	0.29	462	0.818	23.24	0.970	28,750
47	C1	FC1	30	23.1	0.42	B&D	0.35	462	0.770	29.58	1.121	27,750
48	C1	FC2	20	28.9	0.42	A	0.29	489	0.813	20.47	1.062	29,600
49	C1	FC2	30	28.9	0.44	-	-	492	0.787	22.71	0.753	39,100
50	C1	FC2	30	28.9	0.42	A	0.29	492	0.812	26.44	0.951	33,650
51	C1	FC2	30	28.9	0.42	B&D	0.18	492	0.740	21.42	1.028	28,250
52	C1	FC2	30	28.9	0.42	B&D	0.35	492	0.662	32.02	1.324	29,250
53	C1	S1	50	-	0.42	A	0.29	471	0.921	28.37	0.664	32,800
54	C1	S1	50	-	0.42	B&D	0.18	471	0.797	26.55	0.694	37,250
55	C1	S1	50	-	0.42	B&D	0.35	471	0.699	26.20	1.094	31,850
56	C2	FF2	20	13.1	0.44	-	-	433	0.766	14.72	0.835	36,700
57	C2	FF2	20	13.1	0.44	C	0.78	433	0.753	16.40	0.915	32,600
58	C2	FF2	20	13.1	0.44	AEA	0.08	433	0.713	14.90	0.883	36,700
59	C2	FC1	30	23.1	0.44	-	-	462	0.841	22.17	0.724	36,800
60	C2	FC1	30	23.1	0.40	B&D	0.35	462	0.696	28.09	1.560	25,950
61	C2	FC1	30	23.1	0.44	C	1.30	462	0.790	15.95	0.919	28,300
62	C2	FC2	30	28.9	0.44	-	-	494	0.721	18.65	0.917	37,300
63	C2	FC2	30	28.9	0.42	B&D	0.35	494	0.668	36.80	1.735	26,500
64	C2	FC2	30	28.9	0.44	F-N	0.78	494	0.655	17.81	0.941	37,300
65	C2	FC2	30	28.9	0.44	F-PC	0.27	494	0.699	19.03	0.913	37,300
66	C2	S1	50	-	0.44	-	-	472	0.735	21.70	0.757	40,950
67	C2	S1	50	-	0.44	C	0.78	472	0.737	23.75	0.780	38,400
68	C6	FF2	30	13.1	0.44	-	-	395	0.776	16.49	0.593	35,700
69	C6	FF2	30	13.1	0.42	B&D	0.35	395	0.622	24.28	1.388	25,000
70	C6	FF2	30	13.1	0.38	MR	0.74	395	0.692	23.18	0.839	35,700
71	C6	FC2	30	28.9	0.44	-	-	480	0.770	27.67	0.566	26,250
72	C6	FC2	30	28.9	0.42	B&D	0.35	480	0.739	34.27	1.103	26,250
73	C10	FC2	30	28.9	0.38	F-N	0.78	468	0.746	19.21	0.770	38,500
74	C12	FC1	30	23.1	0.44	-	-	448	0.973	29.77	0.697	37,150
75	C12	FC1	30	23.1	0.44	F-PC	0.20	448	1.000	29.31	0.691	37,150
76	C12	FF3	50	1.3	0.44	-	-	331	1.000	17.78	0.6768	35,250
77	C12	FF3	50	1.3	0.44	F-PC	0.27	331	1.000	17.13	0.7685	35,250

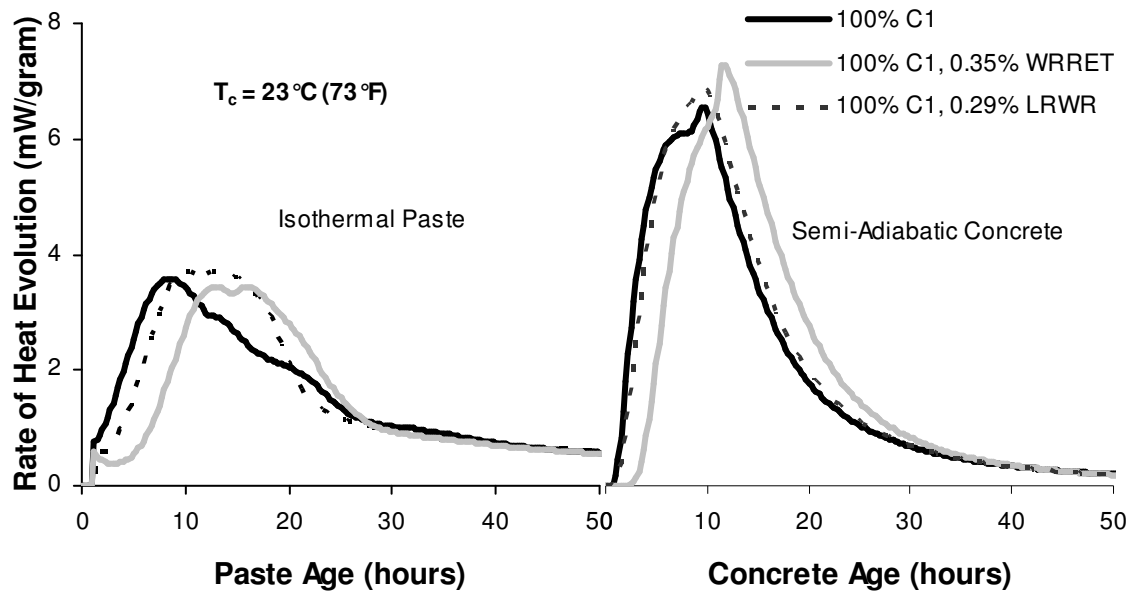


Figure 7-1: Comparison Between Isothermal Calorimetry Results and Semi-Adiabatic Calorimetry Results for Mixtures with Cement C1 and Different Water Reducing Admixtures

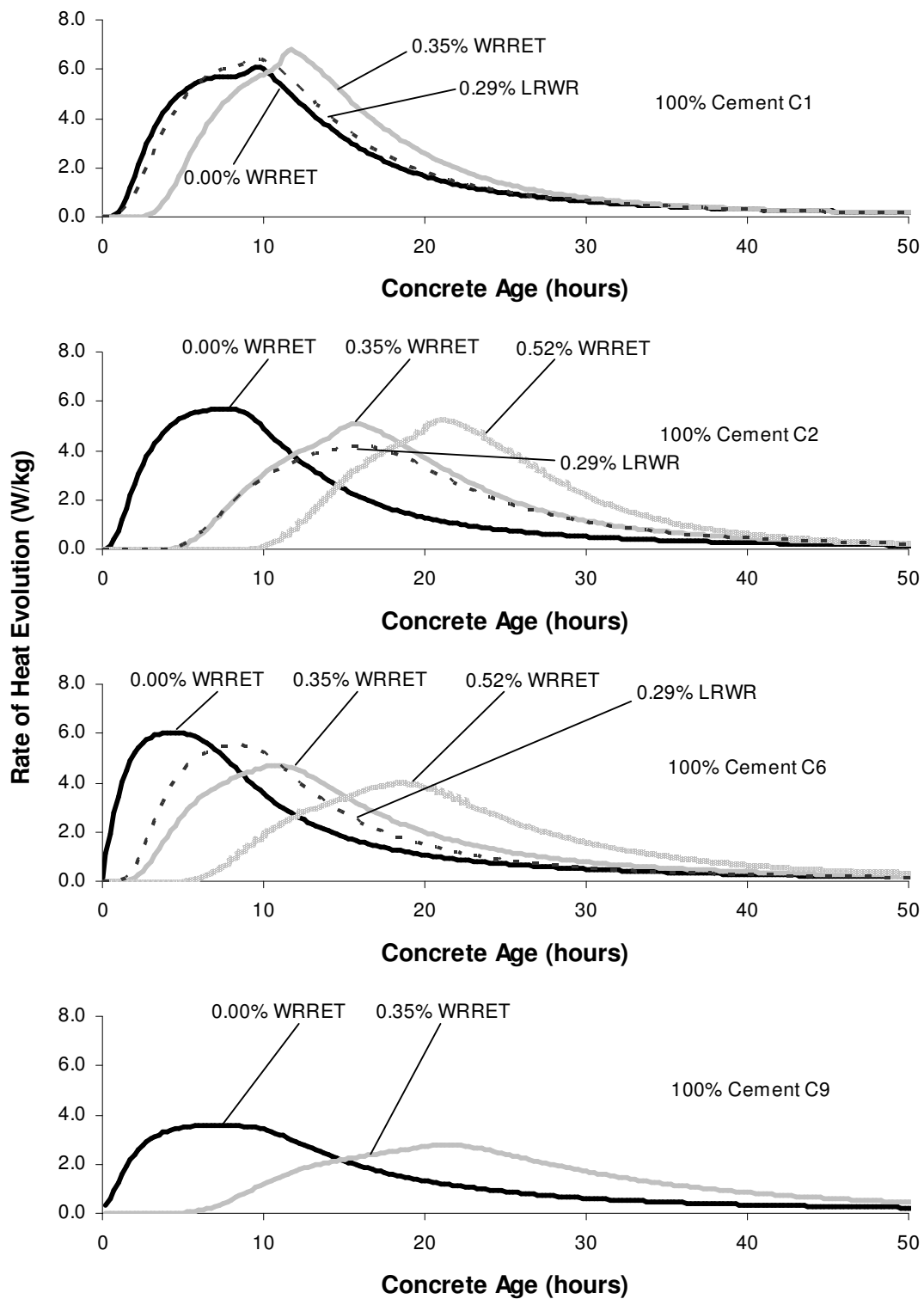


Figure 7-2: Effects of Type B&D WRRET on Rate of Heat Evolution of Cements C1, C2, C6, and C9

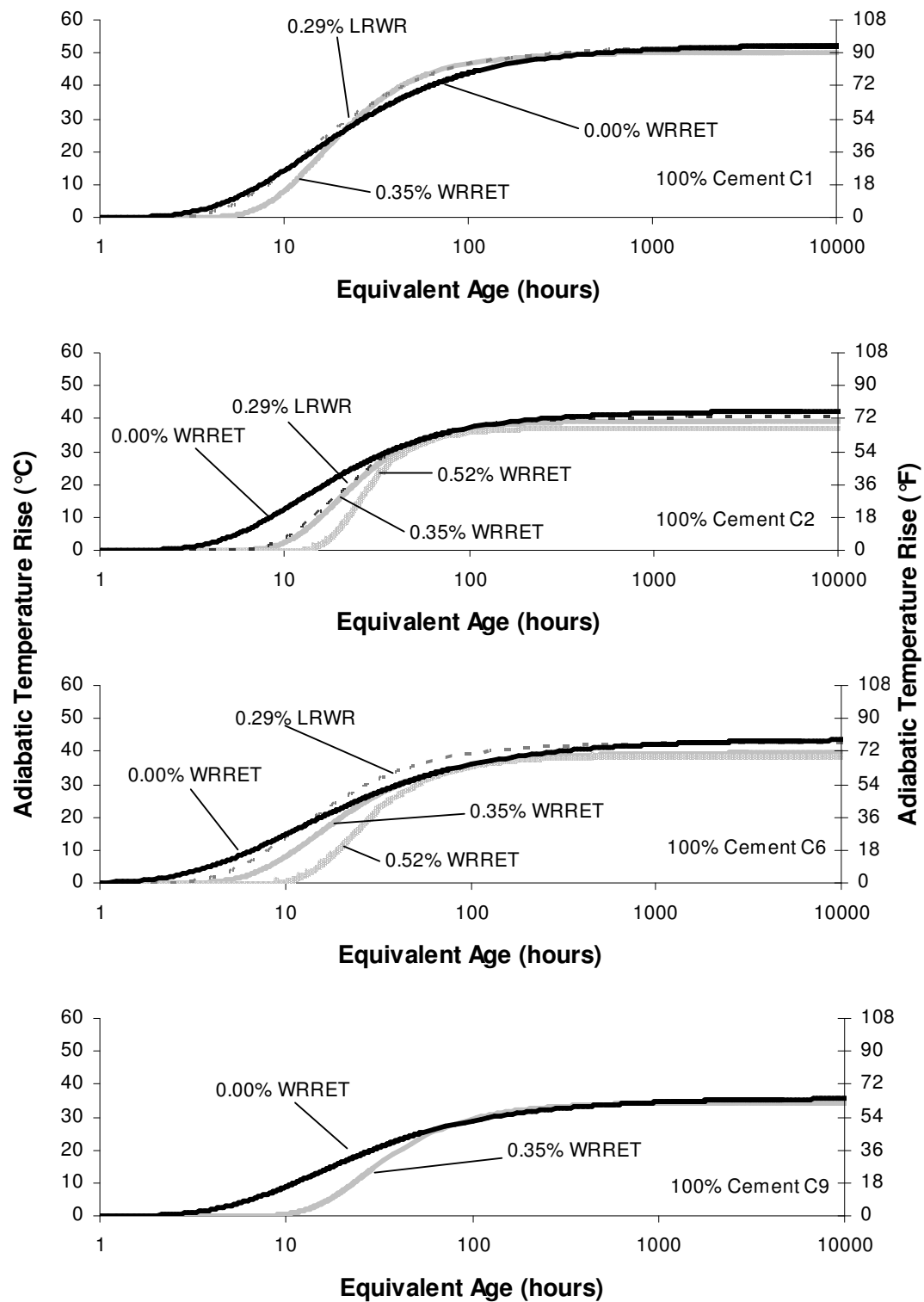


Figure 7-3: Effects of Type B&D WRRET on Adiabatic Temperature Rise of Cements C1, C2, C6, and C9

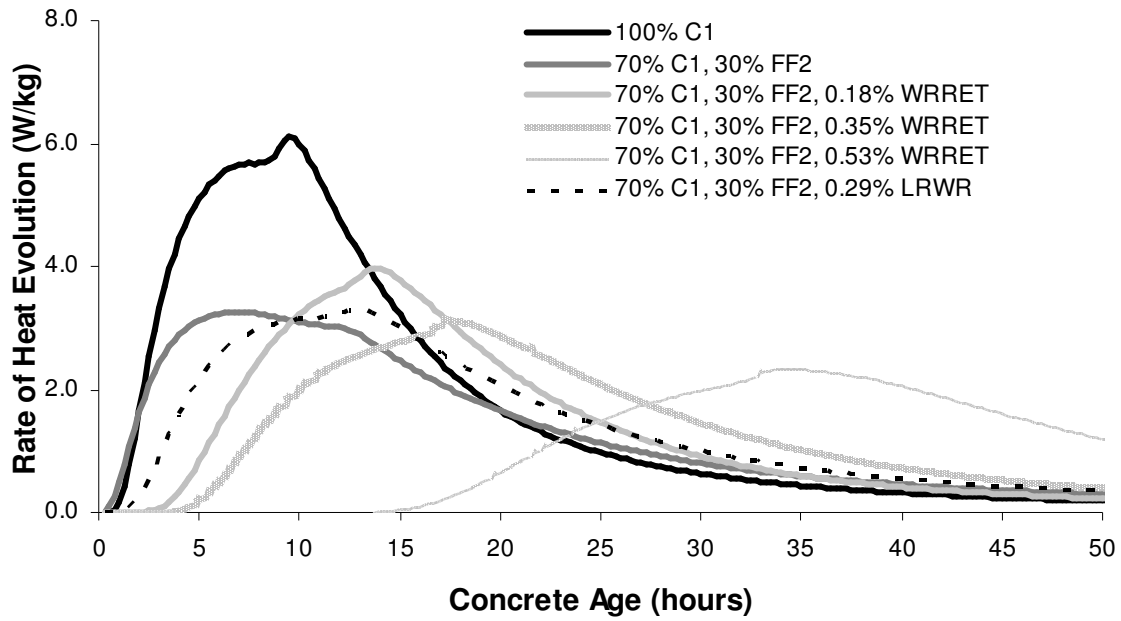


Figure 7-4: Effects of Type A LRWR and Type B&D WRRET on Hydration of a Mixture of 70% Cement C1 and 30% FF2

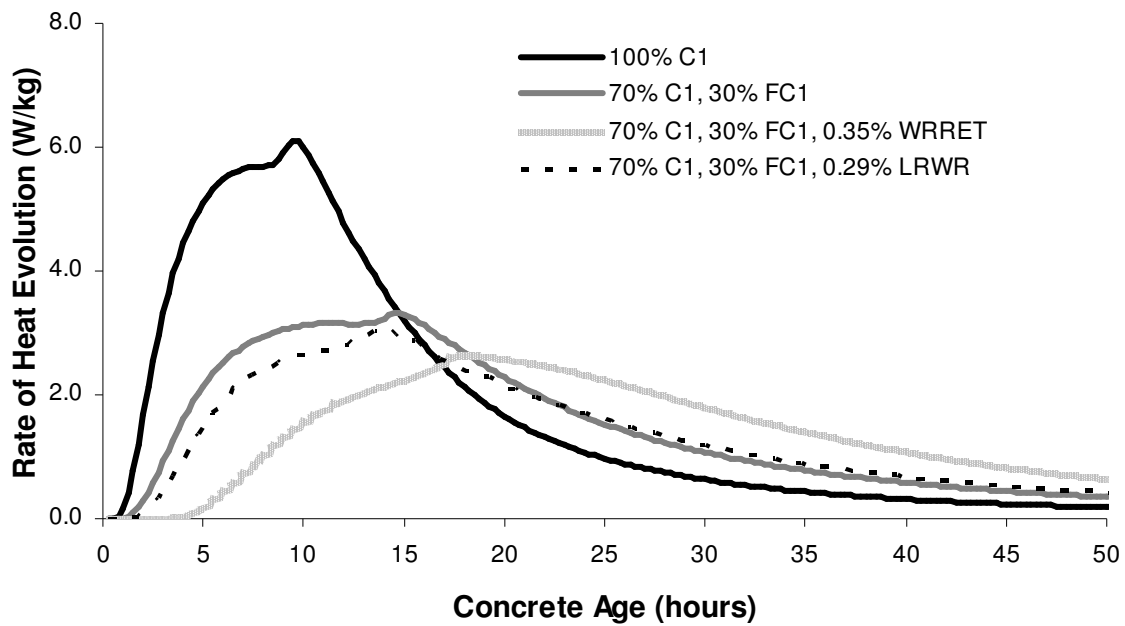


Figure 7-5: Effects of Type A LRWR and Type B&D WRRET on Hydration of a Mixture of 70% Cement C1 and 30% FC1

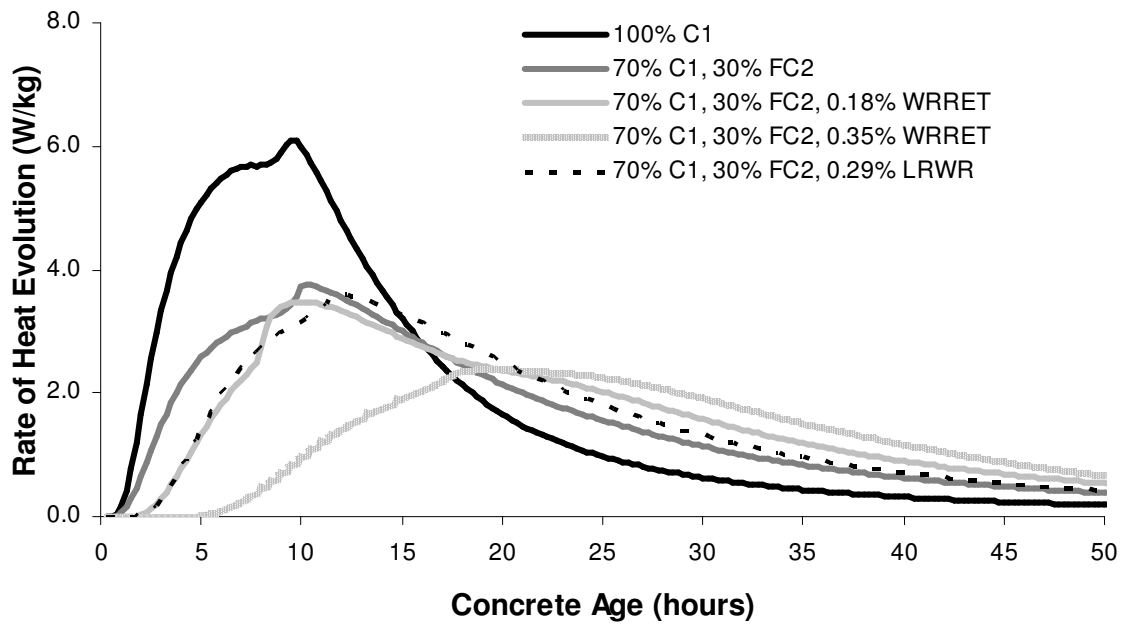


Figure 7-6: Effects of Type A LRWR and Type B&D WRRET on Hydration of a Mixture of 70% Cement C1 and 30% FC2

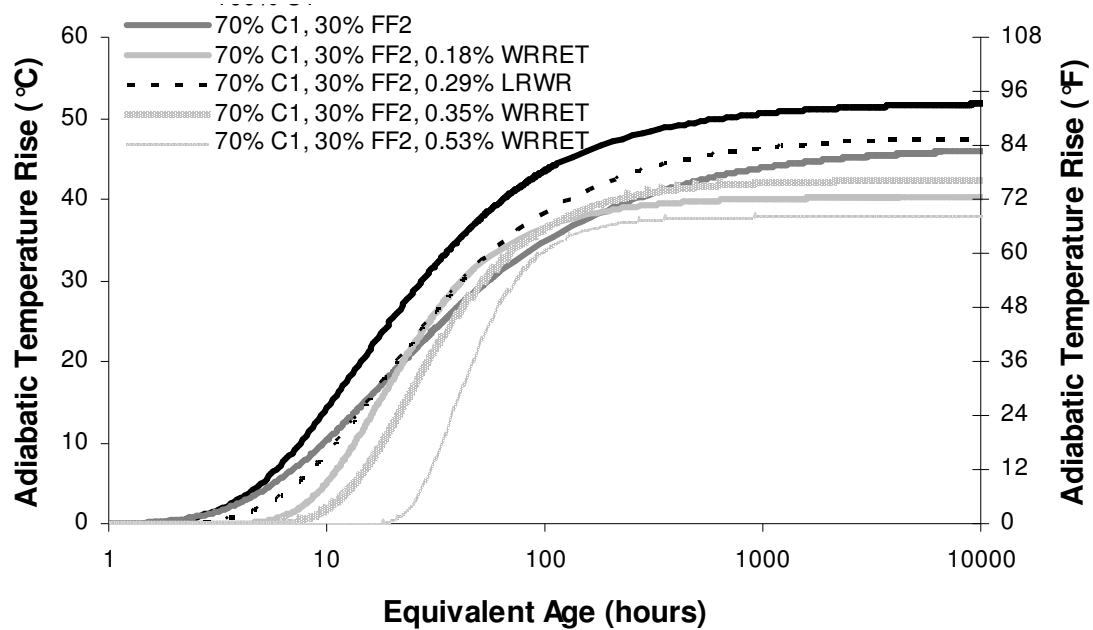


Figure 7-7: Effects of Type A LRWR and Type B&D WRRET on Adiabatic Temperature Rise of a Mixture of 70% Cement C1 and 30% FF2

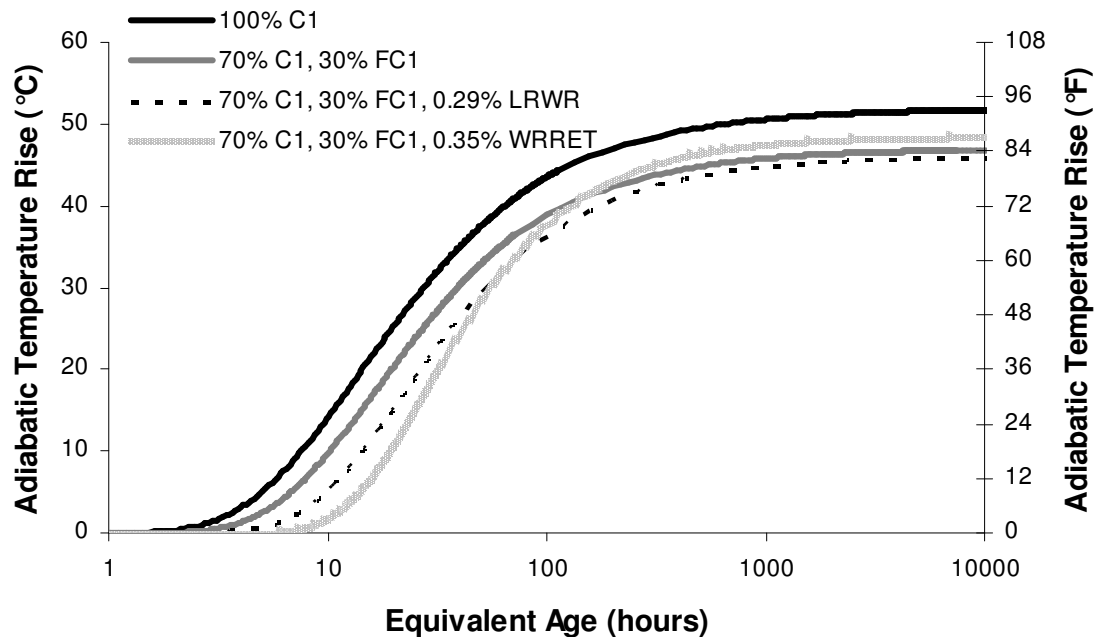


Figure 7-8: Effects of Type A LRWR and Type B&D WRRET on Rate of Heat Evolution of a Mixture of 70% Cement C1 and 30% FC1

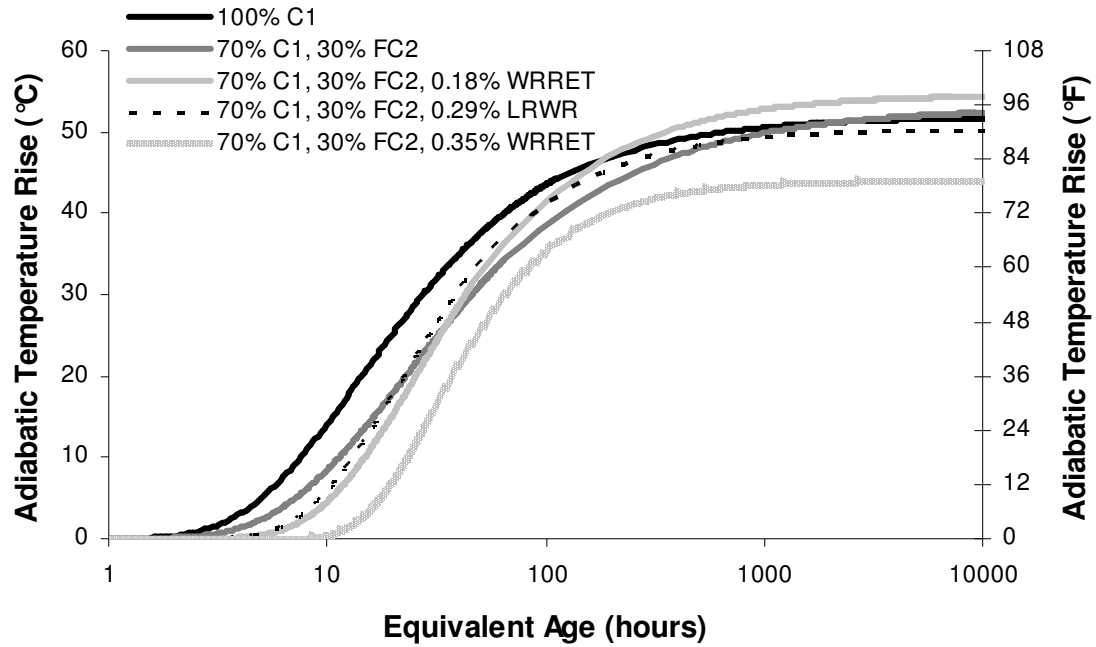


Figure 7-9: Effects of Type A LRWR and Type B&D WRRET on Adiabatic Temperature Rise of a Mixture of 70% Cement C1 and 30% FC2

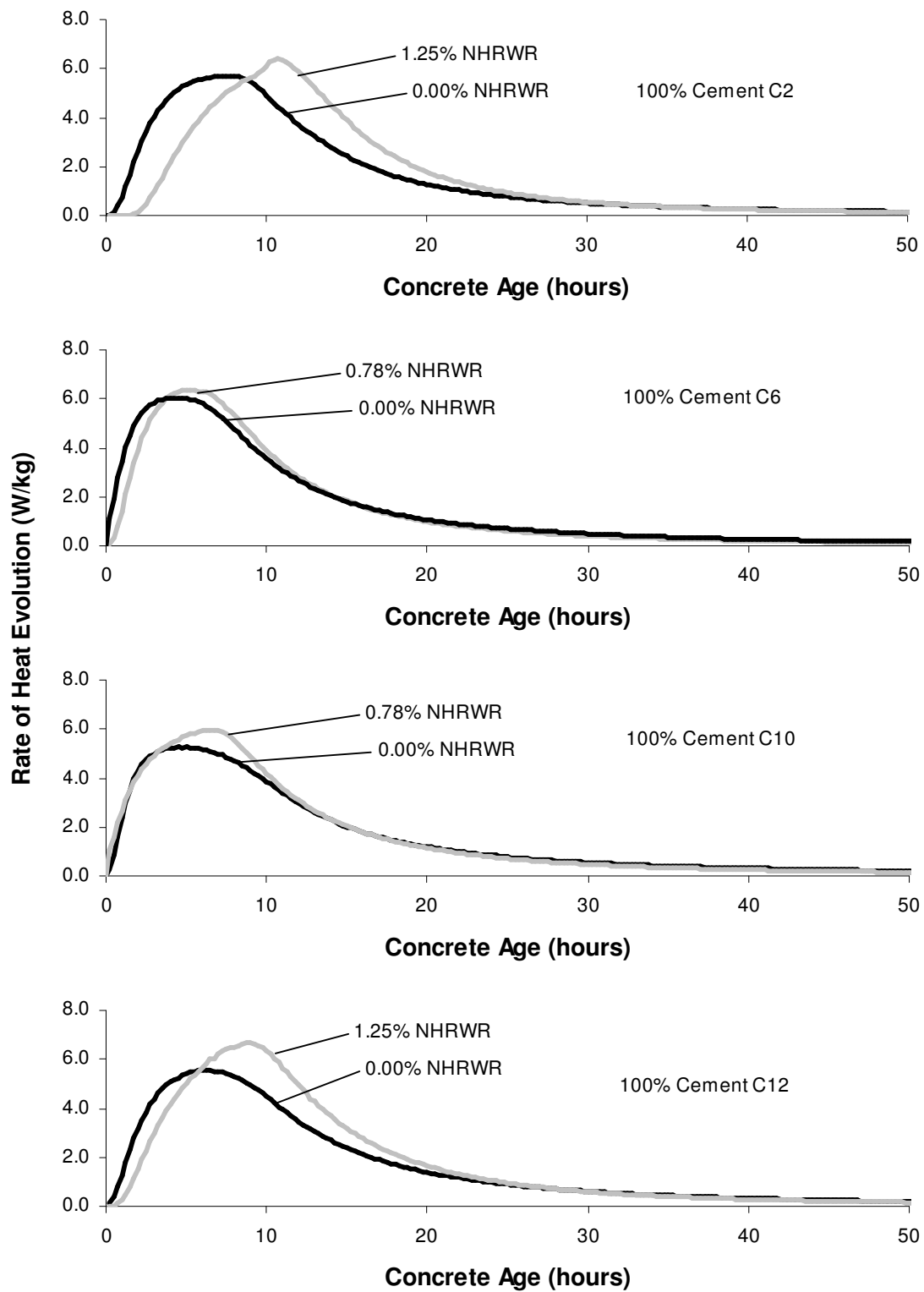


Figure 7-10: Effects of Naphthalene-Based HRWR on Rate of Heat Evolution of Cement C2, C6, C10, and C12

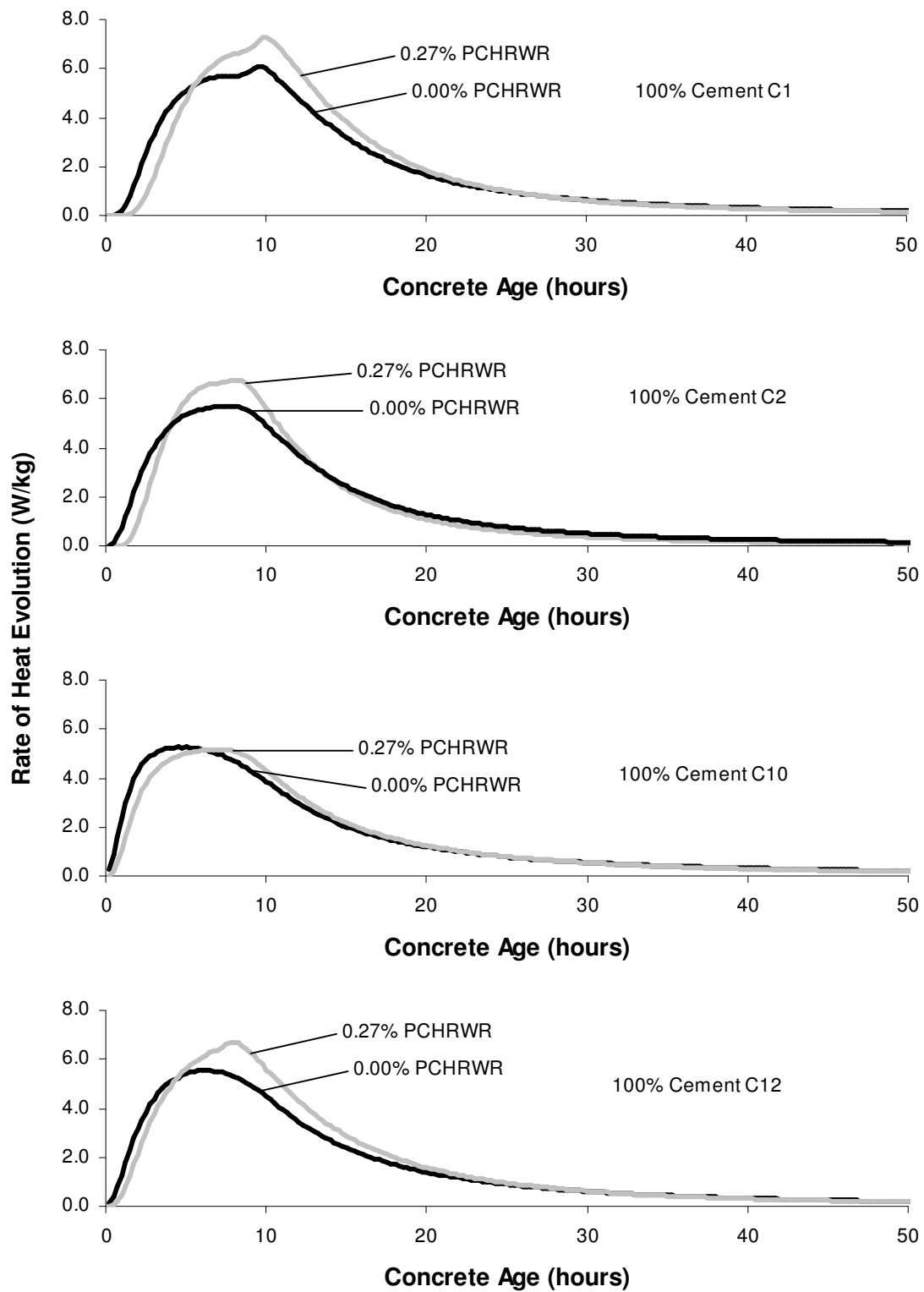


Figure 7-11: Effects of Polycarboxylate-Based HRWR on Rate of Heat Evolution of Cement C1, C2, C10, and C12

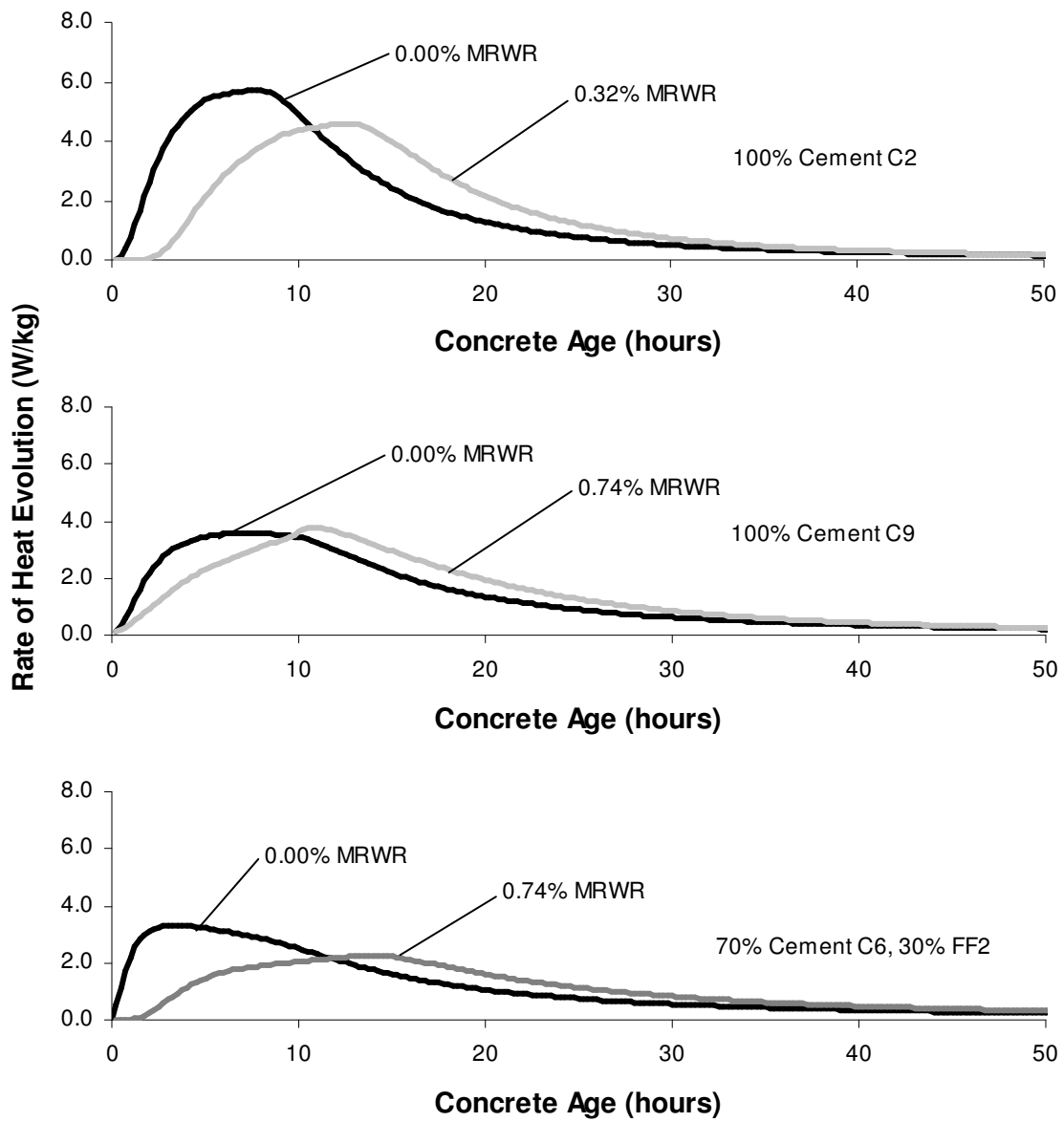


Figure 7-12: Effects of MRWR on Rate of Heat Evolution of Mixtures of 100% Cement C2, 100% C9, and 70% C6 with 30% FF2

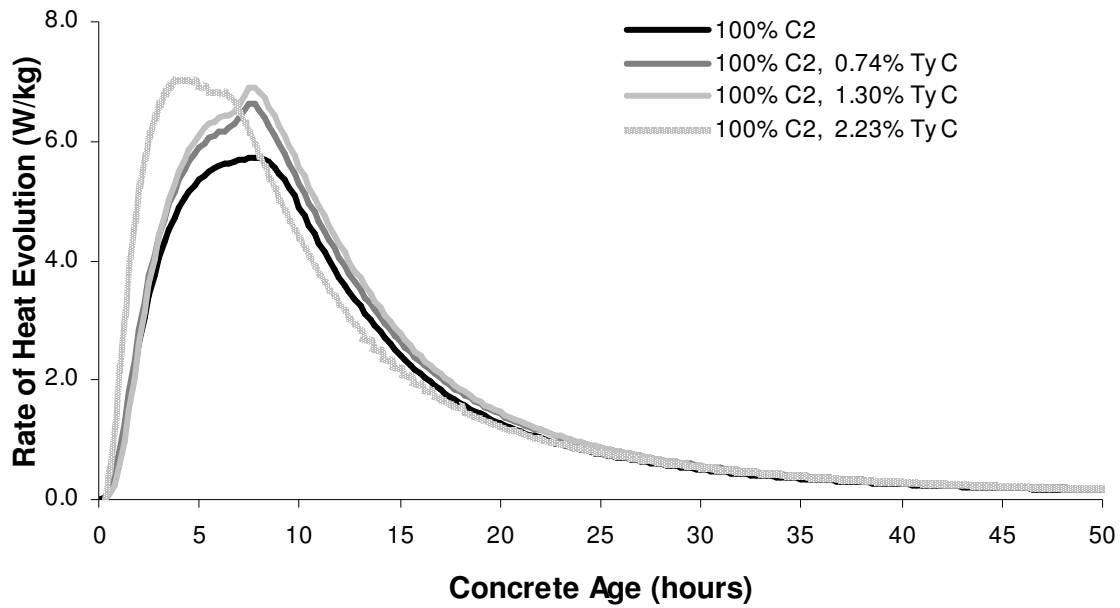


Figure 7-13: Effects of Type C Non-Chloride Accelerator on Hydration of a Mixture of 100% Cement C2

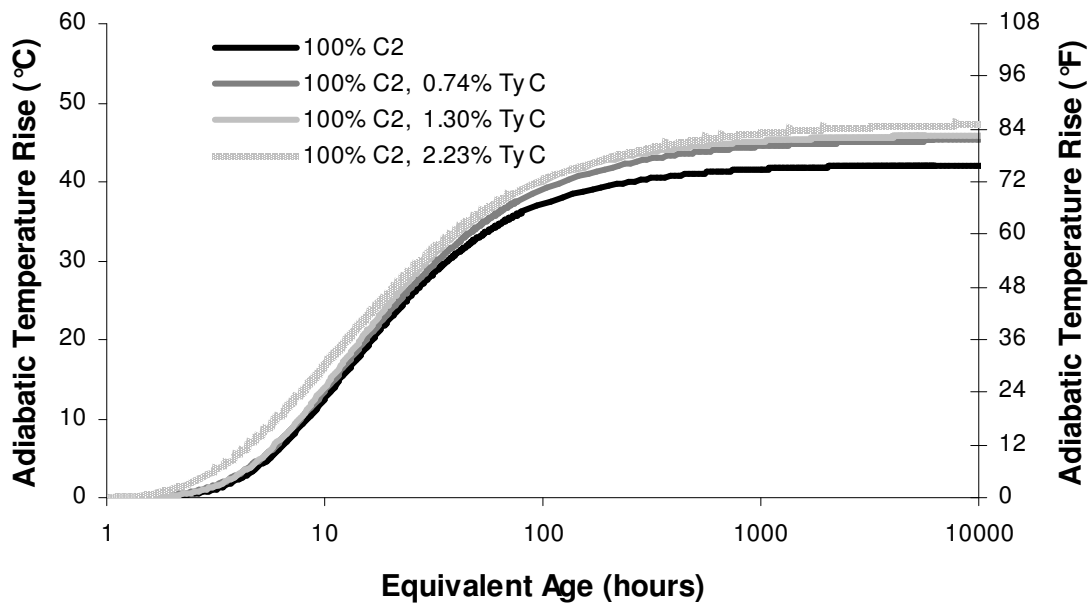


Figure 7-14: Effects of Type C Non-Chloride Accelerator on Hydration of a Mixture of 100% Cement C2

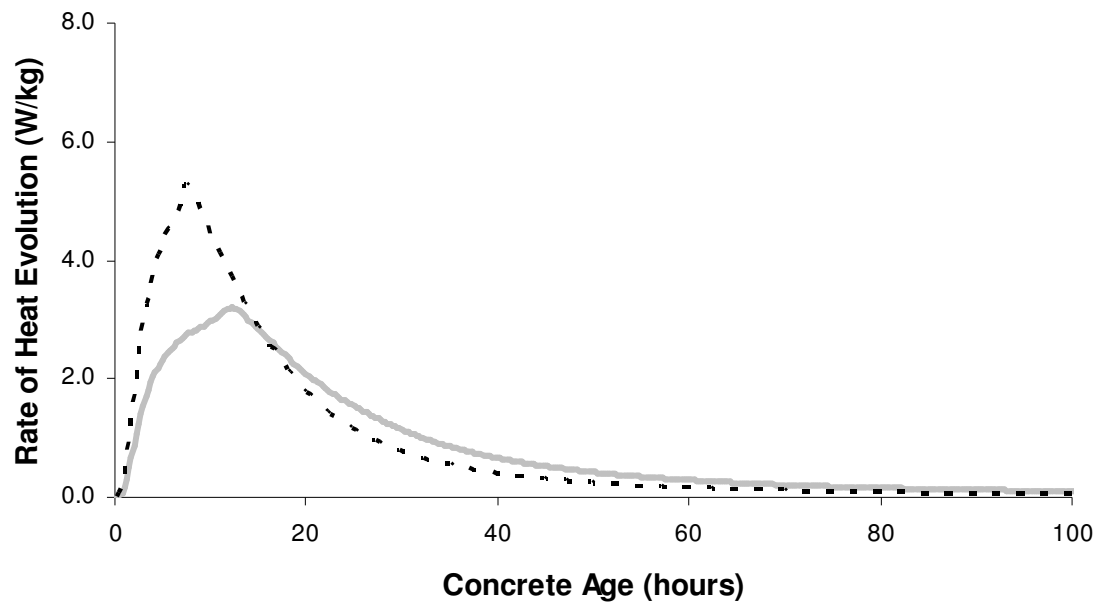


Figure 7-15: Effects of Type C ACCL and Type B&D WRRET on Rate of Heat Evolution of a Mixture of 70% Cement C2 and 30% FC1

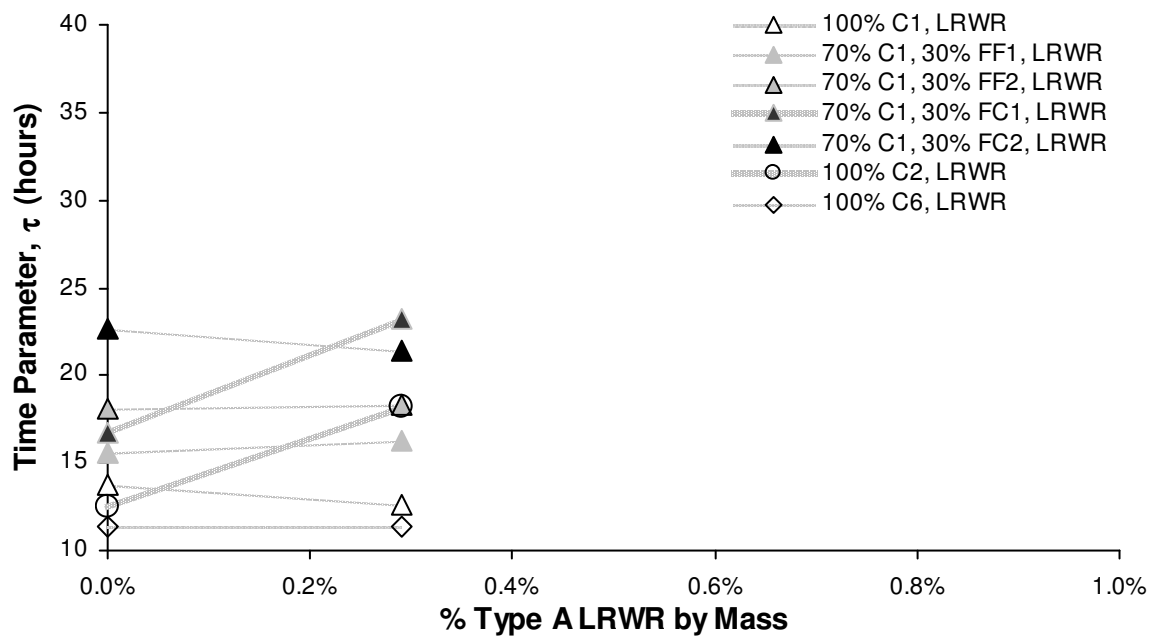


Figure 7-16: Effects of Type A LRWR on Time Parameter (τ)

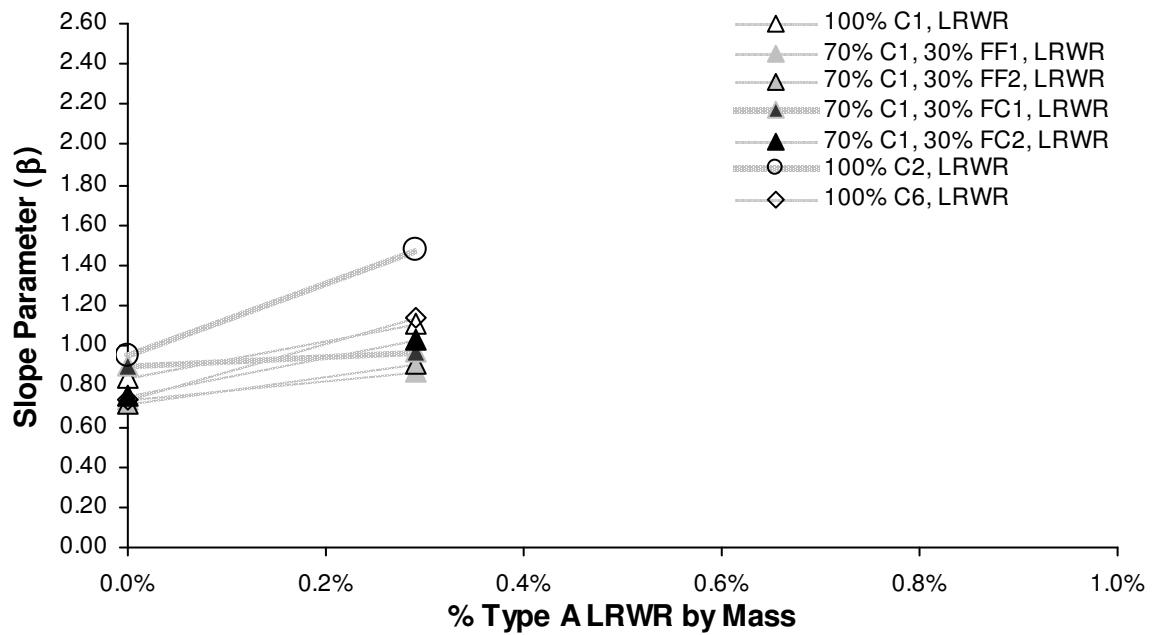


Figure 7-17: Effects of Type A LRWR on Slope Parameter (β)

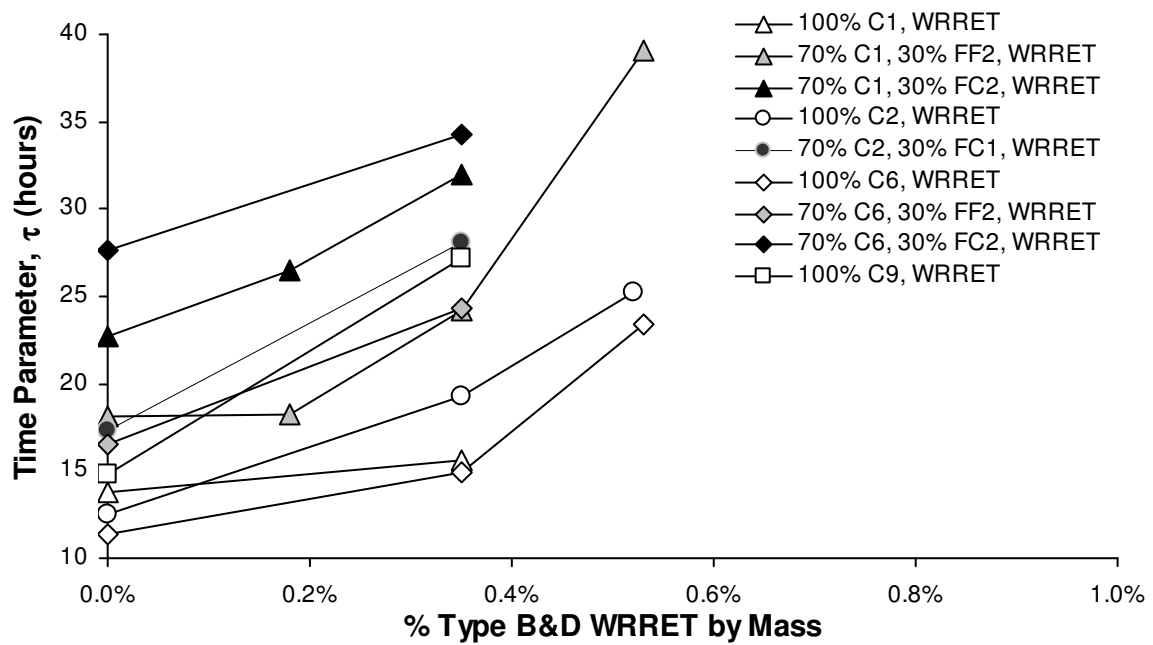


Figure 7-18: Effects of Type B&D WRRET on Time Parameter (τ)

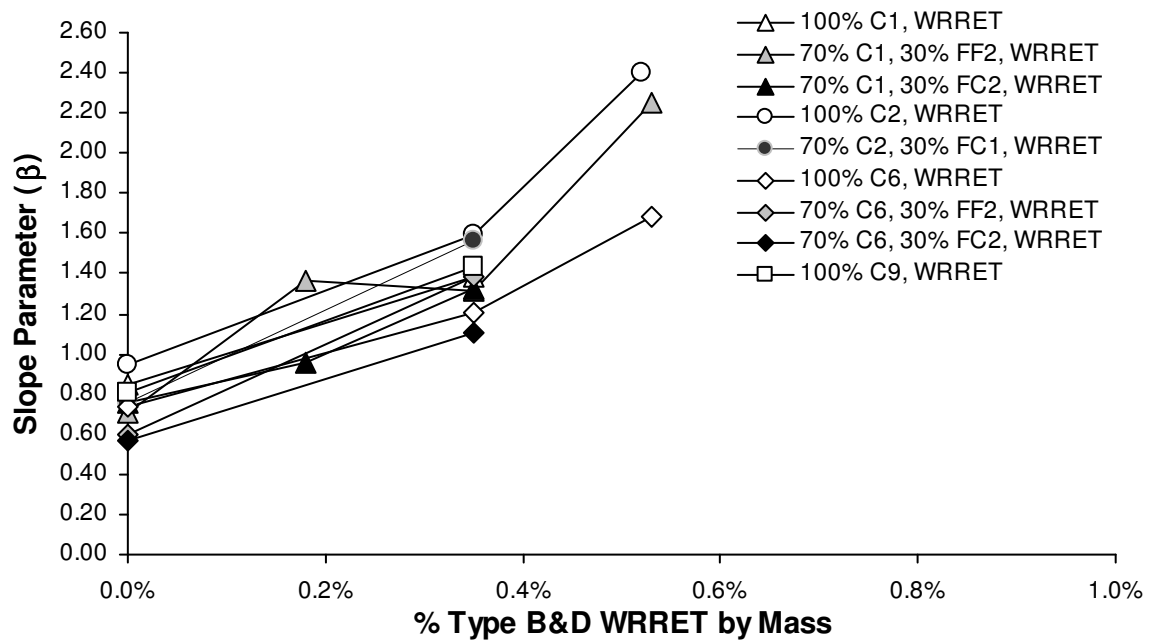


Figure 7-19: Effects of Type B&D WRRET on Slope Parameter (β)

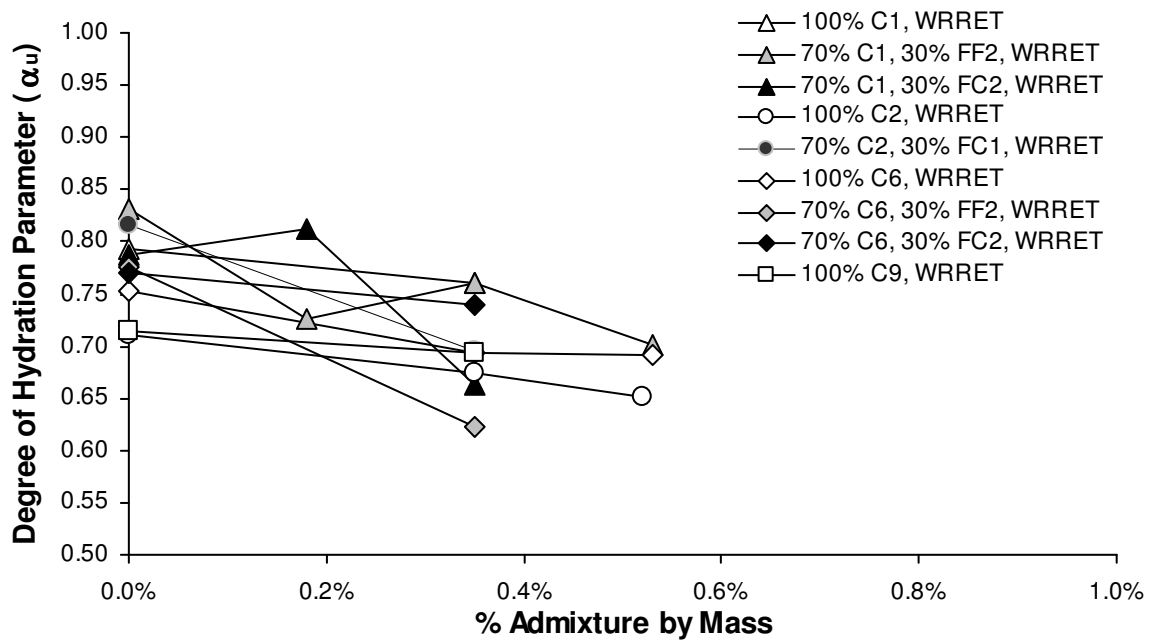


Figure 7-20: Effects of Type B&D WRRET on Degree of Hydration Parameter (α_u)

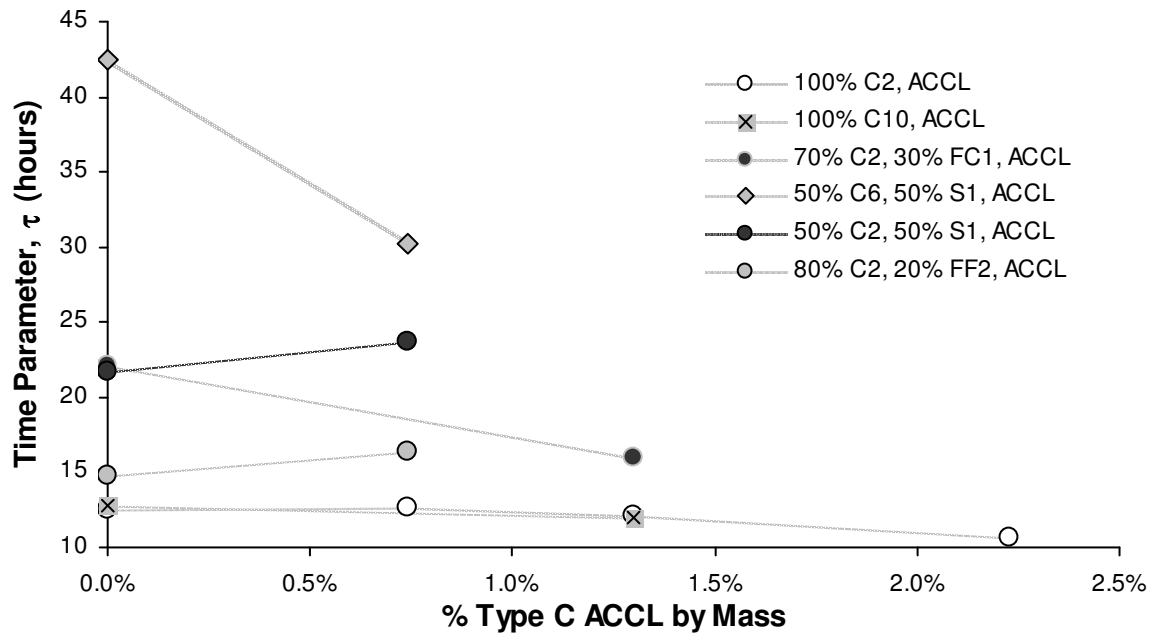


Figure 7-21: Effects of Type C ACCL on Time Parameter (τ)

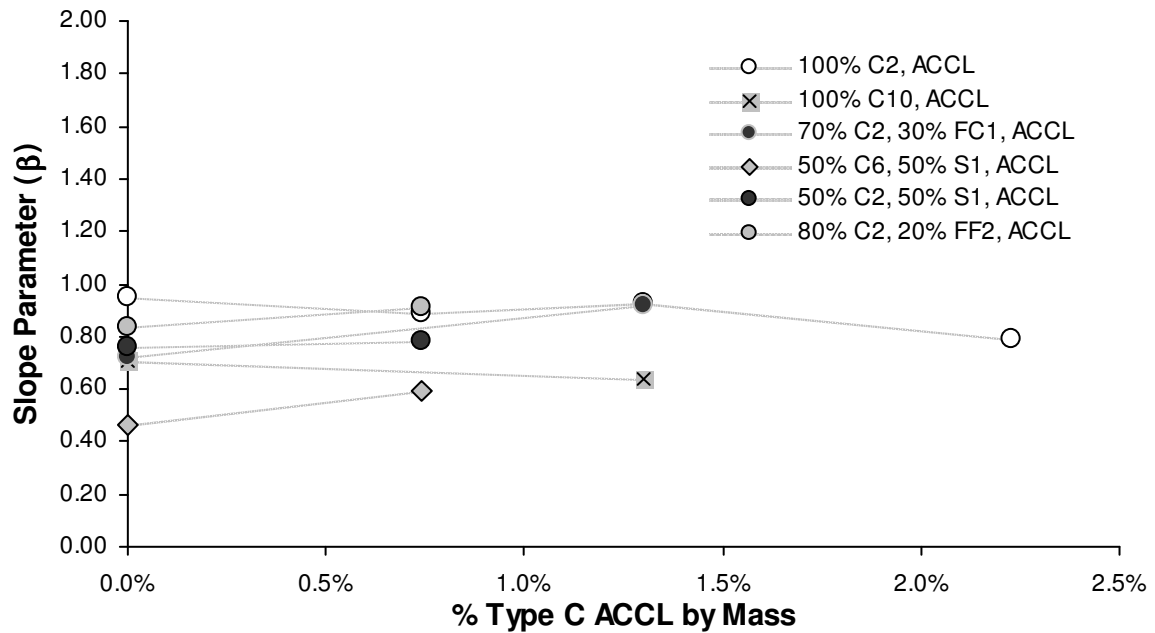


Figure 7-22: Effects of Type C ACCL on Slope Parameter (β)

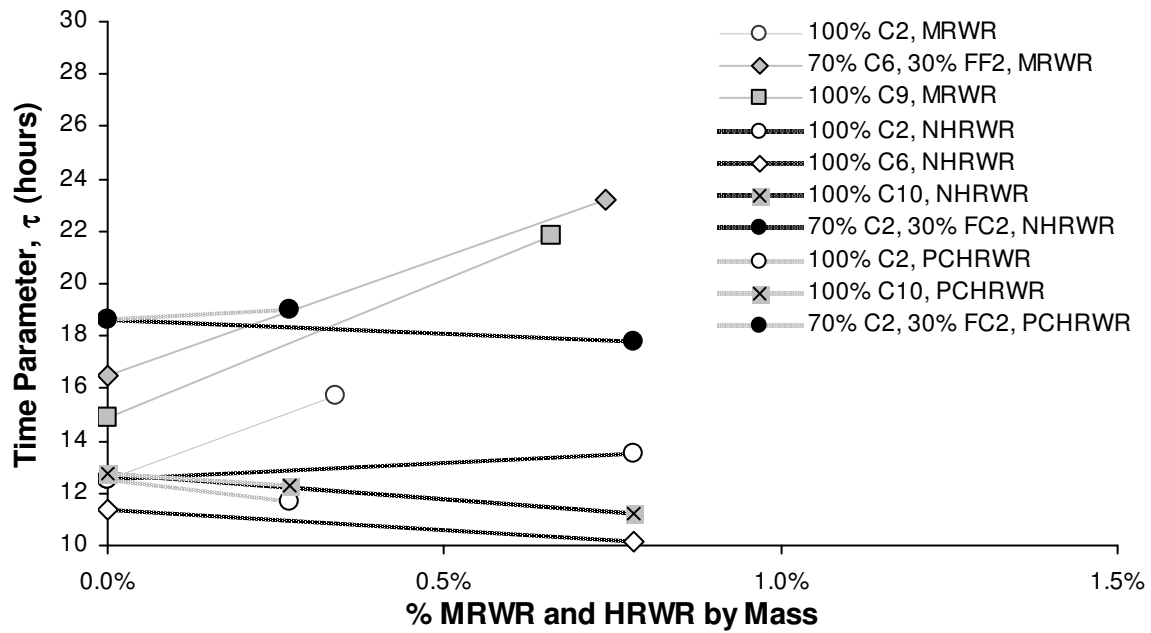


Figure 7-23: Effects of NHRWR, PCHRWR, and MRWR on Time Parameter (τ)

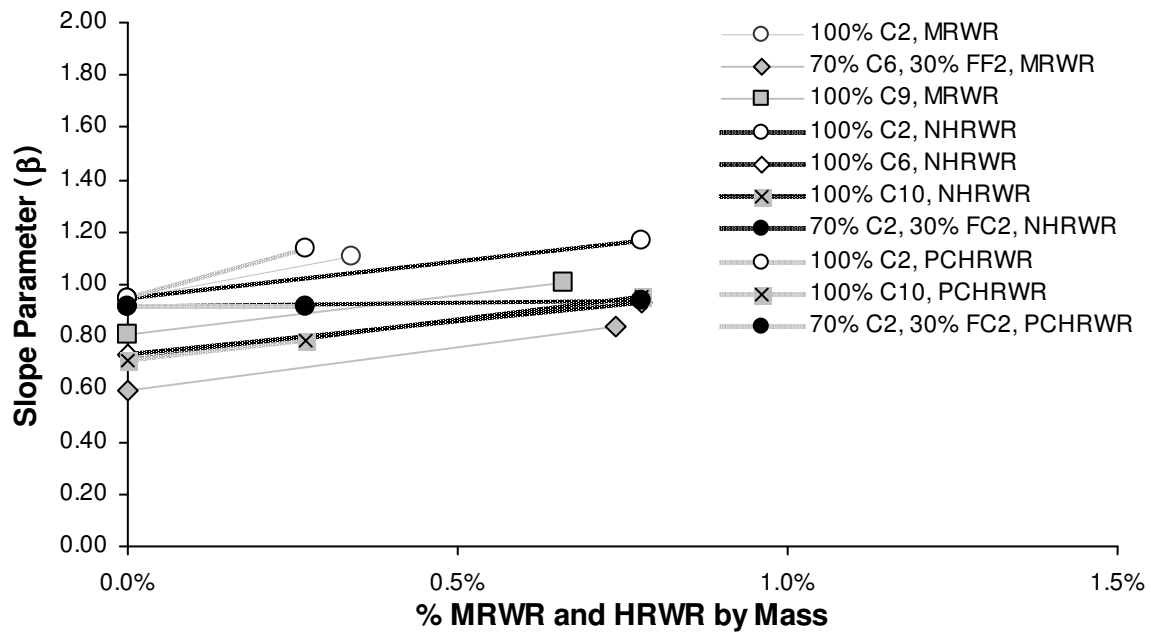


Figure 7-24: Effects of Type F HRWR (N-Naphthalene, PC-Polycarboxylate, M-Mid-Range) on Slope Parameter (β)

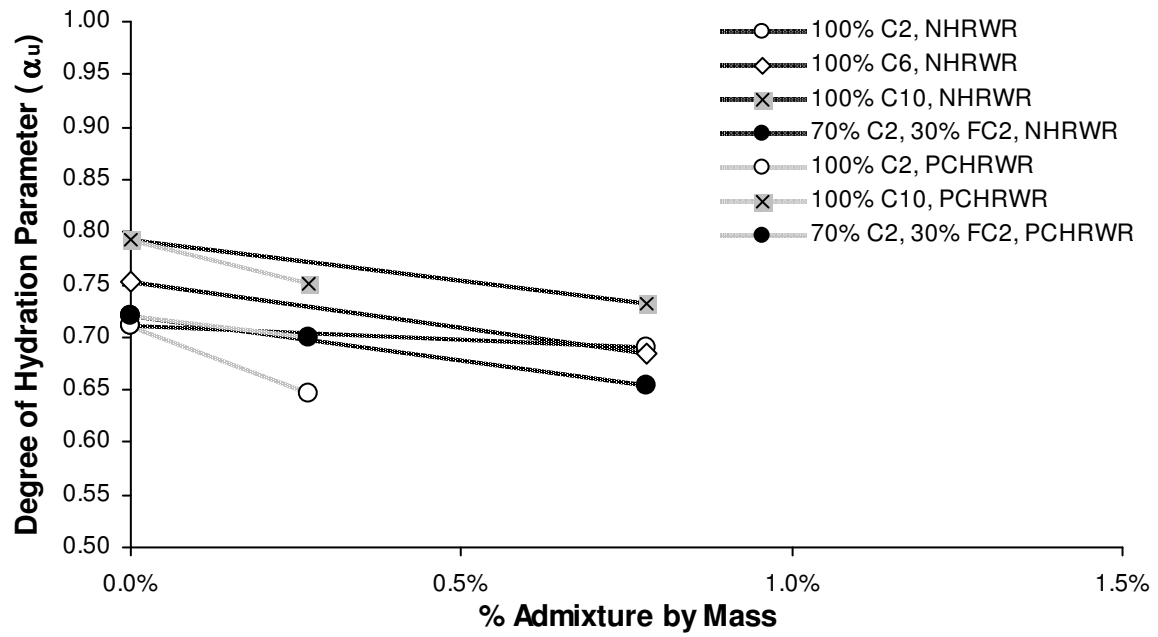


Figure 7-25: Effects of Type F HRWR (N-Naphthalene, PC-Polycarboxylate) on Degree of Hydration Parameter (α_u)

CHAPTER 8. STUDY OF THE HYDRATION OF SUPPLEMENTARY CEMENTING MATERIALS USING SEMI- ADIABATIC CALORIMETRY

This chapter compares the effects of different supplementary cementing materials (SCMs) and cements on the hydration behavior of typical concrete mixtures as determined by semi-adiabatic calorimetry. The study examines the effects of four different fly ashes, seven different cements, one ground-granulated blast-furnace slag, and one silica fume. The cements in the study were characterized with both Bogue calculations from x-ray fluorescence (XRF) data and Rietveld analysis, and the fly ashes were characterized with XRF. Interactions between cement and SCM are examined based on chemistry, SCM type, and SCM replacement percentage. The results permit the validation of hydration mechanisms in literature, and form the basis for a mechanistic-empirical model to describe hydration.

8.1. INTRODUCTION

The hydration of cement in concrete is exothermic. In large elements, the heat caused by hydration can dissipate at the surface, but is trapped in the interior, resulting in potentially large thermal gradients and thermal stresses. When the thermal stress exceeds the tensile strength of the material, thermal cracking will occur. One of the most effective ways to reduce the risk of thermal cracking is to control temperature differentials in a concrete element. Since the tendency of a concrete element to crack is highly dependent on the temperature development of the mixture¹, one of the best ways to control temperature differentials in an element is to reduce the rate of heat evolution of

the concrete mixture. Supplementary cementing materials (SCMs) such as fly ash, ground-granulated blast-furnace (GGBF) slag, and silica fume are often used in place of some of the cement in a mixture to reduce the heat evolution of a mixture¹.

In addition to lowering the heat evolution of the mixture, SCMs may improve the workability², increase strength^{2,3,4}, and improve resistance to alkali-silica reaction (ASR), sulfate attack, and delayed ettringite formation (DEF)^{2,3,4}. In addition, SCMs may be more economical than portland cement². However, the hydration characteristics of a SCM are difficult to determine purely from their chemical composition. The reactivity of a SCM is not easily determined from its bulk composition, since many of the mineralogical phases are amorphous or poorly crystalline². The reactivity is highly dependent on the cement and the types of chemical admixtures that are used.

ASTM C 618⁵ classifies fly ashes depending on the oxides present in the fly ash. Class F fly ashes are the by-products of the combustion of bituminous and anthracite coals², and are characterized by a CaO content nominally less than 20%. Class C fly ash is typically produced from subbituminous coal², and is characterized by a CaO content nominally greater than 20%⁵. However, CaO content is only marginally related to the hydration characteristics of the fly ash, because the behavior depends highly on the phases present, particle size distribution, alkalinity of the pore solution, and source of the fly ash². ASTM C 989⁶ classifies the reactivity of GGBF slag according to its 28-day compressive strength in relation to a control mixture of 100% cement. The reactivity of silica fume is also specified according to the compressive strength of mortar cubes in relation to a control. However, these properties have not been directly correlated with the

temperature rise of concrete mixtures with these SCMs. A better estimate of the effect of fly ash on heat of hydration is needed.

Previous research has used semi-adiabatic calorimetry to highlight the differences in SCMs⁷ and cements⁸. Semi-adiabatic calorimetry offers a rapid method to assess the early age hydration characteristics of a mixture. The techniques for measurement are well documented^{8,9}, and the test is quite repeatable. This chapter presents a subset of the results from a larger testing program to develop a comprehensive hydration model based on semi-adiabatic and isothermal calorimetry. This study examines the effects of four different fly ashes, one GGBF slag, and seven different cements on the heat of hydration and adiabatic temperature rise of typical concrete mixtures. The results presented here allow hydration mechanisms proposed in literature to be validated, and will be the basis for a future mechanistic-empirical model of hydration.

8.2. RESEARCH SIGNIFICANCE

Thermal cracking in large concrete elements is caused by excessive thermal gradients. SCMs are commonly used to reduce these thermal gradients by reducing the heat of hydration. However, the hydration characteristics of SCMs are difficult to ascertain from their chemical composition and are highly dependent on the cement and chemical admixtures that are used in the mixture. This chapter presents the hydration behavior, determined from semi-adiabatic calorimetry, of different combinations of fly ash, GGBF slag, silica fume, and cement. The results are used to validate reaction mechanisms suggested in literature, and may become the basis for a future mechanistic-empirical model of hydration.

8.3. BACKGROUND

The following section provides background on the calculation of the adiabatic temperature rise of concrete mixtures⁸ to provide the proper framework for the presentation of results. The hydration of cementitious systems may be divided into five stages¹⁰. The effects of SCMs on hydration will be discussed in relation to these five phases.

The first stage occurs immediately after water is added, and results in an initial period of rapid heat evolution and first deceleration, and is not studied extensively here. The second stage is referred to as the dormant, or induction period. This is the stage that permits the placing and handling of portland cement and concrete since it is still in a plastic state. Initial set generally occurs at the end of this phase, and the paste fraction of the concrete starts to stiffen considerably. When the calcium and silicon concentrations in solution reach a critical value, reactions of C_3S and C_3A proceed at a rapid rate and the acceleration stage is reached¹⁰. Final set is reached at some point just after the start of this stage, when strength and stiffness development start to occur. In the third stage, the C_3S hydration accelerates to a very high level of activity, and the maximum rate of heat evolution is reached during this stage. During this stage, acceleration of the C_3A reaction occurs, ettringite is formed and the heat of hydration of the C_3A compound adds to the total heat evolution. Two peaks representing the bulk of C_3S and C_3A hydration may appear in heat evolution curves. The exact stage at which monosulfoaluminate and ettringite develop will be determined by the amount of gypsum added during the cement manufacture. The more gypsum in the system, the longer the ettringite will remain stable.

In the fourth stage, the rate of reaction slows down because the thick layer of hydration products formed on the cement grains inhibits further dissolution of ions. The formation of new hydration products will be controlled by the rate of diffusion of ions through this layer. The hydration of C_2S to CH and $C-S-H$ and C_4AF to monosulfoaluminate generally begin during this period, since these reactions progress very slowly and little heat is developed. The final stage involves the slow reaction of the remaining portion of the material, and the concrete is approaching its long-term strength. When pozzolans are present, $Ca(OH)_2$ will be converted into $C-S-H$ through the pozzolanic reaction primarily during this stage. Generally, complete hydration of all of the cementitious material does not occur¹¹.

The fully adiabatic temperature rise is calculated using Equation 8-1 through Equation 8-8 using the procedure discussed in detail previously^{7,8}. The Arrhenius equation is commonly used to model hydration and accounts for the temperature sensitivity of this chemical reaction. The equivalent age (t_e) of concrete is a mathematical representation of its time temperature history, which allows one to determine the equivalent curing age compared to curing at a reference temperature¹². The concept allows one to model the hydration behavior when concrete is cured under different temperature histories. Equation 8-1, proposed by Friesleben Hansen and Pederson¹², is the most common expression used to compute equivalent age, and is used in the remainder of this chapter to model the effects of time and temperature on hydration:

$$t_e(T_r) = \sum_0^t e^{-\frac{E_a}{R}(\frac{1}{T_c} - \frac{1}{T_r})} \cdot \Delta t \quad \text{Equation 8-1}$$

where $t_e(T_r)$ = equivalent age at reference temperature (T_r), T_c = temperature of the concrete (°K), E_a = activation energy (J/mol), Δt = time interval, and R = natural gas constant (8.314 J/mol/°K).

The progress of the hydration of portland cement may be quantified by the degree of hydration (α), which varies from 0 to 1, with a value of 1 indicating complete hydration. For this study, degree of hydration is taken as the ratio of heat evolved at time, t , to the total amount of heat available, as shown in Equation 8-2:^{7,21,22,23,24,25,26}

$$\alpha = \frac{H(t)}{H_u} \quad \text{Equation 8-2}$$

where α = degree of hydration at time t , $H(t)$ = heat evolved from time 0 to time t (J/gram), and H_u = total heat available for reaction (J/gram).

H_u is a function of cement composition and amount and type of supplementary cementing materials (SCMs) and may be calculated as follows⁷:

$$H_u = H_{cem} \cdot p_{cem} + 461 \cdot p_{slag} + 1800 \cdot p_{FA-CaO} \cdot p_{FA} \quad \text{Equation 8-3}$$

where p_{slag} = slag mass to total cementitious content ratio, p_{FA} = fly ash mass to total cementitious content ratio, p_{FA-CaO} = fly ash CaO mass to total fly ash content ratio, p_{cem} = cement mass to total cementitious content ratio, and H_{cem} = heat of hydration of the cement (J/gram). H_{cem} can be calculated as shown in Equation 8-4⁷:

$$H_{cem} = 500 \cdot p_{C_3S} + 260 \cdot p_{C_2S} + 866 \cdot p_{C_3A} + 420 \cdot p_{C_4AF} + 624 \cdot p_{SO_3} + 1186 \cdot p_{FreeCa} + 850 \cdot p_{MgO} \quad \text{Equation 8-4}$$

where H_{cem} = total heat of hydration of portland cement (J/gram) at $\alpha = 1.0$, and p_i = mass of i-th component to total cement content ratio.

The most commonly used relationship to characterize cement hydration is a three-parameter model based on degree of hydration data, as shown in Equation 8-5^{7,18}:

$$\alpha(t_e) = \alpha_u \cdot \exp\left[-\left(\frac{\tau}{t_e}\right)^\beta\right] \quad \text{Equation 8-5}$$

where $\alpha(t_e)$ = degree of hydration at equivalent age t_e , τ = hydration time parameter (hours), β = hydration shape parameter, and α_u = ultimate degree of hydration. This model will be referred to as the exponential model for the remainder of the chapter. For continuity with previous research this model is selected. The rate of heat evolution of concrete can be calculated using Equation 8-6. Heat evolved at time t is as follows⁷:

$$Q_h(t) = H_u \cdot W_c \cdot \left(\frac{\tau}{t_e}\right)^\beta \cdot \left(\frac{\beta}{t_e}\right) \cdot \alpha(t_e) \cdot \exp\left(\frac{E_a}{R} \left(\frac{1}{T_r} - \frac{1}{T_c}\right)\right) \quad \text{Equation 8-6}$$

where Q_h = rate of heat generation (W/m³), H_u = total heat available (J/kg), and W_c = cementitious materials content (kg/m³), and all other parameters as defined previously.

The specific heat of concrete can be estimated using Equation 8-7. Specific heat is required to determine the adiabatic temperature rise and is assumed to vary with degree of hydration¹⁹. Specific heat of concrete can be calculated as follows¹⁹:

$$C_p = \frac{1}{\rho} \cdot (W_c \alpha C_{ref} + W_c \cdot (1 - \alpha) \cdot C_c + W_a C_a + W_w C_w) \quad \text{Equation 8-7}$$

where C_p = specific heat of concrete mixture (J/kg), ρ = unit weight of concrete (kg/m³); W_c , W_a , W_w = amount by weight of cement, aggregate, and water (kg/m³); C_c , C_a , C_w =

specific heat of cement, aggregate, and water (J/kg/°C), and C_{ref} = specific heat of hydrated cement = $8.4 \times T_c + 339$ (J/kg/°C).

If the total heat evolved (or the adiabatic temperature rise) is plotted versus equivalent age, the curve tends to be S-shaped. Each of the parameters of this exponential model changes the shape of this curve in different ways. For example, an increase in the time parameter, τ , models a delay in the hydration curve, and the S-curve will shift further out on the time axis. An increase in the slope parameter, β , represents an increase in the rate of heat evolution, and is accompanied by an increase in the slope of the S-curve. An increase in the degree of hydration parameter, α_u , represents an increase in the total amount heat evolved for a particular mixture, and results in an increase in the ultimate height of the S-curve.

8.3.1. CALCULATION OF E_A

E_a was calculated from a multivariate regression model²⁰ shown in Equation 8-8 as follows:

$$\begin{aligned} E_a = & 41,230 + 1,416,000 \cdot [(C_3A + C_4AF) \cdot p_{Cement} \cdot SO_3 \cdot p_{Cement}] \\ & - 347,000 \cdot Na_2O_{eq} - 19.8 \cdot Blaine \\ & + 29,600 \cdot p_{FlyAsh} \cdot p_{CaO-FlyAsh} + 16,200 \cdot p_{GGBFS} - 51,600 \cdot p_{SF} \\ & - 3,090,000 \cdot WRRET - 345,000 \cdot ACCL \end{aligned} \quad \text{Equation 8-8}$$

where p_{cement} = % cement in mixture; p_{FlyAsh} = % fly ash in mixture; $p_{CaO-FlyAsh}$ = % CaO in fly ash; p_{GGBFS} = % GGBF slag in mixture; p_{SF} = % silica fume in mixture; $Blaine$ = Blaine fineness of cement; Na_2O_{eq} = % Na_2O_{eq} in cement ($0.658 \times \%K_2O + \%Na_2O$); C_3A = % C_3A in cement; C_4AF = % C_4AF in cement; SO_3 = % SO_3 in cement; $WRRET$ = ASTM Type A&D water reducer/retarder, % solids per gram of cementitious material; $ACCL$ =

ASTM Type C calcium-nitrate based accelerator, % solids per gram of cementitious material.

8.4. EXPERIMENTAL PROGRAM

8.4.1. TEST METHODS

During this study, semi-adiabatic calorimetry was performed on a variety of different mixtures with different types of fly ash and chemical admixtures. To determine the adiabatic temperature rise, each concrete mixture is batched and mixed as per ASTM C 192²¹. One 150 x 300 mm (6 x 12 in.) cylinder is made, and its weight recorded. The cylinder is placed inside the semi-adiabatic calorimeter as soon as possible after mixing (generally around 30 minutes after water is added to the cement). The cylinder temperature and heat flux out of the calorimeter is recorded at 15 minute intervals. The test is run for approximately 150 hours.

8.4.2. MATERIALS

The cements were chosen to provide a range of different cement chemistries, alkali contents, and fineness. The following cements conforming to ASTM C150²² were used: one low-alkali Type I cement (C1), one high-alkali Type I cement (C2), two low-alkali Type I/II cement (C6 and C10), two Type III cements (C7 and C8), and one Type V cement (C9). SCMs were chosen to provide a range of CaO contents. The following SCMs were used: three ASTM C 618⁵ Class F fly ashes (FF1, FF2, and FF3), two ASTM C 618⁵ Class C fly ashes (FC1 and FC2), one ASTM C 989⁶ Grade 120 ground granulated blast-furnace slag (S1), and one ASTM C 1240²³ condensed silica fume. Chemical and physical properties of the materials are summarized in Table 8-1. Mixture

information is summarized in Table 8-2, Table 8-3, and Table 8-4. Cement phases were calculated from x-ray fluorescence data using Bogue calculations and Rietveld analysis²⁴ using quantitative X-ray diffraction (QXRD).

All mixtures had a cementitious materials content of 325 kg/m³ (564 lbs/yd³). Siliceous river gravel (#57²⁵) and siliceous river sand were used for the coarse (CA) and fine aggregates (FA) in all of the mixtures. FA/ (FA+CA) was between 0.40 and 0.44. The amounts of CA and FA in the mixture had no effect on the hydration characteristics of the mixture because both aggregates were roughly of the same mineralogy and have approximately the same specific heat. The w/cm was 0.44 for all mixtures. Replacement percentages (by mass) were as follows: 20%, 30%, and 40% fly ash; 30%, 40%, 50%, and 70% GGBF slag; 5% and 10% silica fume.

8.5. ANALYSIS OF RESULTS

The rate of heat evolution gives an indication of the timing and magnitude of the silicate and aluminate phase hydration. When the hydration of the mixture is retarded, the induction period is generally extended, and the slope of the accelerating portion of the hydration curve is reduced. These trends are reflected in the time parameter, τ , and the slope parameter, β . All of these parameters depend highly on the interaction between the SCM and cement in the concrete. The total adiabatic temperature rise gives an overall indication of the combined effects of different cements and SCMs on hydration.

The total amount of heat evolved from the test is reflected in the degree of hydration parameter α_u . However, this parameter is only a measure of the heat evolved after a seven day test at elevated temperatures. The calorimeter tests are not run beyond

one week because of the sensitivity of the semi-adiabatic calorimeter and the effects of the environment. Also, the total heat (H_u) is based on an independent, fractional model of the total heat available from all constituents (Equation 8-3 and Equation 8-4). Therefore, the results presented for α_u may not accurately represent the true “ultimate” degree of hydration. However, α_u provides a useful index of the amount of heat that will evolve in the early stages of hydration.

8.5.1. EFFECTS OF CLASS F FLY ASH ON RATE OF HEAT EVOLUTION

Figure 8-1 and Figure 8-2 show the effect of 20, 30, and 40 % replacement by mass of Cement C2 with FF1 and FF2, respectively, on the rate of heat evolution. The addition of a Class F fly ash to a mixture affects the heat of hydration in several ways. Figure 8-1 shows that the addition of FF1 (CaO = 0.7%) to a concrete mixture with Cement C2 reduces the rate of heat evolution in proportion to the dosage. Also, FF1 causes almost no change in the shape of the hydration curve. Figure 8-2 shows that the addition of FF2 (CaO=13.1%) to a concrete mixture with Cement C2 reduces the rate of heat evolution, and causes a slight decrease in the initial slope of the hydration curve. Also, after 24 hours, the rates of heat evolution start to converge in both cases. The relative differences in the hydration curves are also similar, which is reflected in the time and slope parameters (τ and β), as seen in the next section.

8.5.2. EFFECTS OF CLASS C FLY ASH ON RATE OF HEAT EVOLUTION

High-lime fly ashes typically have much greater amounts of reactive crystalline phases than low lime fly ashes²⁶, to the extent that some Class C fly ashes will produce heat in the absence of cement. Therefore, the more highly reactive SCMs should exhibit more discernable changes in hydration behavior than the less reactive SCMs. The addition of a Class C fly ash to a mixture will have a greater effect on hydration than a Class F fly ash. Table 8-3 shows the curve fit parameters for mixtures with Class C fly ash. Several trends are discussed in the next paragraph.

Figure 8-3 and Figure 8-4 show the effect of 20, 30, and 40 % replacement by mass of Cement C2 with FC1 and FC2, respectively⁸, on the rate of heat evolution. Figure 8-5 compares the rate of heat evolution for a mixture with 30% Class C fly ash (FC1) and Cement C2 and C6. The rate of heat evolution of the mixtures with 30% FC1 is significantly lower than the mixture with 100% Cement C2 or C6. However, the addition of FC1 causes the second hydration peak to be slightly more pronounced in relation to the first hydration peak, compared to the mixtures with 100% cement. This graph

Also, there are several differences between FC1 in Figure 8-3 and FC2 in Figure 8-4 as compared to Class F fly ash as shown in Figure 8-1 and Figure 8-2. First, there is an increase in the height of the second hydration peak with the addition of a high CaO fly ash, which may represent the hydration of the aluminates⁴. This increase is more noticeable in isothermal calorimetry than with semi-adiabatic calorimetry, for reasons discussed previously. Second, the initial slope of the hydration curve is lower with Class

C fly ash than it is with Class F fly ash. These differences may be due to the additional reactive phases from the Class C fly ash, the reduction in soluble sulfate available to properly retard the aluminate phases (associated with dilution of the cement), or a combination of these mechanisms.

8.5.3. EFFECTS OF GROUND GRANULATED BLAST-FURNACE SLAG ON RATE OF HEAT EVOLUTION

The behaviors reported for Class C fly ash from semi-adiabatic calorimetry may also be seen in the data for GGBF slag. The reactivity of GGBF slag is known to depend on the fineness, presence of alkalis, CaOH, and SO_4^{2-} in the pore solution, and the composition of the raw materials from which the slag is derived²⁷. The addition of GGBF slag to a mixture affects hydration in a similar way to Class C fly ash. Unlike Class C fly ash, the hydraulicity of GGBF slag comes primarily from the glassy phases, and depends on the alkalinity of the pore solution to dissolve the glassy phases. However, the semi-adiabatic calorimeter tests on GGBF slag are somewhat similar to the tests on Class C fly ash in this study.

Figure 8-6 shows the results of 30, 40, 50, and 70% replacement by mass of Grade 120 GGBF slag (S1) with cement C2. 30-50% S1 reduces the rate of heat evolution in the first 15 hours after mixing, but increases the rate of hydration substantially after 15 hours. The results for Cement C2 and 30% FC1, as shown in Figure 8-3, are comparable to the results for Cement C2 and 50% S1, as shown in Figure 8-6. The shape of the hydration curve for both of these mixtures is very similar.

8.5.4. EFFECTS OF SILICA FUME ON RATE OF HEAT EVOLUTION

Silica fume consists of very small, spherical particles of amorphous silica. Silica fume increases the strength and reduces permeability of concrete, primarily because the small particle size acts as a mineral filler in smaller pores in the concrete and provides preferential nucleation sites for the formation of C-S-H⁴. This small size also promotes dissolution of silica, which may allow the pozzolanic reaction to proceed more quickly⁴. The silica fume in this study has a Blaine fineness equal to approximately 20,000 m²/kg.

Figure 8-7 shows the rate of heat evolution of mixtures with 5% silica fume and 95% Cement C2, 20% FF1, and 30% FC2, as well as a mixture with 10% silica fume and 90% Cement C6. The rate of heat evolution is impacted only slightly for the mixtures with 5% silica fume, but was reduced more significantly for the mixture with 10% silica fume. The heat of hydration in the first 10-20 hours of the ternary blends was slightly reduced with silica fume.

8.5.5. EFFECTS OF SCMS AND CEMENT ON HYDRATION PARAMETERS

The three-parameter exponential model defined in Equation 8-5 provides a method to assess the interactions between the cement and the SCM in a system. The parameters of the model, τ , β and α_u , are used in the following section to compare the hydration characteristics of different mixtures.

First, the retardation of the onset of the accelerating portion of the hydration curve and the reduction in peak rate of heat evolution are reflected in the parameters τ and β . Figure 8-8, Figure 8-9, and Figure 8-10 show the effects of Cement C2, C6 and C9,

respectively with 30% FF1, 30% FF2, 30% FC1, 30% FC2, and 50% S1 on the time parameter τ . Cement C9 is also tested with 30% FF3. Figure 8-11, Figure 8-12, and Figure 8-13 show the effects of the same mixtures on the slope parameter, β .

Several trends may be seen. First, τ tends to rise and β tends to drop as the percentage replacement of SCM increases. Furthermore, these parameters rise as the CaO content of the fly ash increases. For example, the addition of a Class F fly ash will slightly increase τ , and will decrease β . The addition of a reactive SCM (e.g. FC1 and FC2) will increase τ (the amount of retardation), which has been reported previously^{7,8,28}. Figure 8-8 through Figure 8-10 confirm that the more reactive SCMs will have a greater τ , as will mixtures with cements with lower aluminate contents. S1 also has a large effect on τ and β , and the results are a similar magnitude to the effects of FC1 and FC2. Next, the reactivity of the cement affects how much τ increases. This trend is discussed further in section 8.5.6 Finally, data in Table 8-4 show that silica fume has a negligible effect on β and τ . These data are plotted in Appendix F.

The addition of SCMs to a mixture has a significant effect on the degree of hydration parameter, α_u . Figure 8-14, Figure 8-15, and Figure 8-16 show the effects of different SCMs on the α_u parameter for Cement C2, C6, and C9, respectively. With Cement C2, α_u increases with the addition of FF1, FC1, and S1, but does not increase with the addition of FF2 or FC2. With Cement C6 and C9, α_u increases for all SCMs except FF2. The increases may be due to an error in the estimated amount of heat that is contributed from the fly ash (as shown in Equation 8-3), or may be the result of

interactions with cements with different chemistries. The addition of silica fume to all of the mixtures tested caused the α_u parameter to slightly increase for all mixtures, as shown in Figure 8-17.

Note that α_u values approaching 1.0 are calculated for some of the mixtures with FF1 and S1. The following mixtures had a degree of hydration above 0.90: 60% C6, 40% FC1; 70% C9, 30% FC2; 60% C2, 40% S1; 50% C6, 50% S1; and C9 with 30, 40, and 50% S1. It is unknown whether this is due to the calculation procedure (and its inherent inaccuracies) or to the extent of hydration that occurs after the test is ended. However, many of these mixtures are either significantly retarded, or have a very low rate of heat evolution.

Some of the results for α_u may be the result of an underestimation of H_u . For example, FF1, FF3, and silica fume yielded a higher α_u . These SCMs are not expected to have a large amount of reactive, crystalline phases. There are several reasons for this. First, low-lime fly ashes are generally composed of quartz, mullite, ferrite spinel, and hematite², as well as various glassy phases. Ashes with CaO<20% generally have CaO present in a siliceous glass structure, whereas ashes with CaO>20% will often have CaO present as either C₃A or C₂S². The use of CaO as an independent variable to describe fly ash presumes that linear increases in CaO cause linear increases in these crystalline phases. In reality, low- and high-CaO fly ashes are two discrete types of SCMs and there is not a continuum in CaO content. In addition, the solubility of the crystalline and amorphous phases in real concrete is poorly understood. Also, it is likely that the presence of the fly ash or silica fume provides preferential nucleation sites for the C-S-

H²⁶, which is a difficult characteristic to isolate. However, no procedures are currently available to rapidly classify the reactivity of crystalline amorphous phases in cementitious materials. Until a procedure is developed, CaO content remains one of the few indices of fly ash reactivity.

8.5.6. RETARDATION WITH CEMENT AND REACTIVE SCMS

It is unknown exactly how the chemistry of the cement and SCM dictates the extent to which the hydration is delayed, though the trends in the previous section suggest that the amount of C₃A in the cement and the hydraulicity of the SCM are related. However, C₃A and gypsum content of the cement almost certainly play a role in the amount of retardation of the mixture. For example, Lerch²⁹ reported that cements with high aluminate contents and high alkali contents required more gypsum than cements with low aluminate contents. It was also reported that for cements with equal aluminate contents, higher alkali contents tended to consume gypsum more rapidly than those with low alkali contents. Lerch²⁹ showed that the addition of SO₄²⁻ (generally in the form of gypsum) to a mixture reduced the solubility of the aluminate phases, and had the effect of retarding the formation of ettringite.

It has also been reported³⁰ that the crystalline compounds in Class C fly ashes may play a role in the amount of gypsum consumed in the early stages of hydration. Because the SO₄²⁻ content of cement is generally determined in relation to the aluminates in the cement only, the addition of a Class C fly ash (which contains additional reactive aluminate phases) may alter this balance. As a result, the timing of the aluminate hydration will be affected, which will alter the overall rate of hydration of the mixture.

Previous research²⁰ has also shown that the activation energy of cement pastes was correlated with the amount of aluminate and gypsum in the cement.

Figure 8-18 shows that the change in τ with FC1, FC2, and S1 is correlated to the amount of C_3A , normalized by mass of cementitious material in the mixture. The fact that this correlation also works for S1 suggests that the mechanism of retardation may not entirely be associated with the reactive crystalline phases. Instead, pore solution alkalinity and availability of SO_4^{2-} to properly regulate C_3A may be the largest contributors to retardation of a mixture. Further study is needed to determine the details of this interaction with SCMs.

8.5.7. EFFECTS OF SCMS ON ADIABATIC TEMPERATURE RISE

Figure 8-19 and Figure 8-20 show the effects of 30% replacement by mass of FF1, FF2, FC1, FC2, and 50% replacement by mass of S1 on the adiabatic temperature rise of mixtures with cement C2 and C6, respectively. As shown in Figure 8-1 through Figure 8-4 and Figure 8-6, each of the SCMs tested here reduces the *rate* of heat evolution compared to plain portland cement mixtures. However, the adiabatic temperature rise is increased in some cases and decreased in others, depending greatly on the reactivity of the SCM in the mixture. The mixtures with 30% FF1 and FF2 reduced the adiabatic temperature rise by 4.5-6 °C (8-11 °F) for both cements tested. The mixtures with 30% FC2, 50% S1, and 30% FC1 cause the adiabatic temperature rise to increase by 2.5, 6.5, and 3.3 °C (4.4, 11.8, and 5.9 °F), respectively for cement C2. The same mixtures cause the adiabatic temperature rise to increase by 5.9, 12.1, and 5.9 °C

(10.6, 21.8, and 10.6 °F) for Cement C6. It is unknown why the adiabatic temperature rise is different with the two cements. Several explanations will be offered in Section 8.5.9.

8.5.8. COMPARISON BETWEEN ISOTHERMAL AND SEMI-ADIABATIC CALORIMETRY

Cement paste tested in an isothermal calorimeter will behave differently than concrete tested using semi-adiabatic calorimetry. These differences were presented previously³¹ for mixtures with chemical admixtures. This disparity is primarily due to the non-uniform temperature and the specific heat of the aggregate in semi-adiabatic calorimetry. The effect of these factors on the test results using SCMs may be seen in Figure 8-21, which compares semi-adiabatic and isothermal test results with one another. Two distinct peaks are seen in the isothermal data, while the same mixtures tested with semi-adiabatic calorimetry have a smoother hydration curve. Also, the sharp peak seen in isothermal results with 30% and 40% FC2 is shorter in the semi-adiabatic results. Like the results presented for chemical admixtures³¹, the rate of heat evolution in the semi-adiabatic tests is higher than the rate of heat evolution in the isothermal tests, because the sample temperature can be much higher than 23 °C (73 °F) for the semi-adiabatic results.

8.5.9. LIMITATIONS OF SEMI-ADIABATIC CALORIMETRY WITH SCMS

Rietveld analysis provides a useful method to accurately quantify the crystalline phases in cement. These results permit the effective validation of independent, fractional models such as those used in Equation 8-3 and Equation 8-4. However, the investigation of hydration mechanisms of SCMs is limited by the ability to quantify the amount and

reactivity of the glassy and crystalline phases in the material. Quantitative x-ray diffraction, scanning electron microscopy, and image analysis techniques for performing this task are not fully developed. CaO content is one of the few material properties widely available to characterize the heat evolution of a fly ash. The problem is the same for GGBF slag and silica fume. The information available on GGBF slag is even less than fly ash. In general, the glass content and the fineness of GGBF slag are some of the few measurable quantities that can be correlated with hydraulic activity³.

The semi-adiabatic calorimeter provides a useful measure of the heat evolution of a concrete mixture during the first week of hydration. The semi-adiabatic condition causes an increase in temperature, so hydration is effectively studied for an equivalent age of 200 to 300 hours. However, the test requires regression analysis to obtain the required hydration parameters. These results may lead to erroneous conclusions about the extent of hydration in some cases. In general for SCMs, an increase in α_u without a substantial increase in τ and decrease in β suggests that more heat is being evolved in the first week of hydration than is modeled by the independent, fraction model for H_u . This seems to be the case for FF1, silica fume, and many of the mixtures with S1. If an increase in α_u is accompanied by an increase in τ and a decrease in β , the mixture may be evolving heat over a longer period of time than is covered by the test. Mixtures that have very low rates of heat evolution, such as Cement C9 paired with S1, FC1, or FC2, tend to show this increase in α_u . The α_u determined from regression analysis may be unrealistic when results are projected to later ages, since the test method is extrapolating the long-term behavior of a mixture on the basis of 200 to 300 hours of equivalent age of testing.

α_u for GGBF slag determined from isothermal calorimetry²⁸ is highly dependent on the cement that is paired with the SCM. The original testing performed by Bogue involved heat of solution tests on pure phases hydrated for a long period of time. This type of testing has not been performed on these mixtures. Therefore, the results are still valid for characterizing hydration behavior up to approximately three hundred (300) hours of chronological time. However, it is recommended to cap the α_u term at 1.0, unless further analysis can substantiate a H_u greater than what is modeled in Equation 8-3 and Equation 8-4.

8.6. CONCLUSIONS

Semi-adiabatic calorimetry was performed on fifty-five (55) different concrete mixtures to test the effects of fly ash, slag, silica fume, and ternary blends on hydration. The effects of each SCM were tested by examining the rate of heat evolution, the adiabatic temperature rise, and the effects of these SCMs on the parameters of an exponential three-parameter model.

There are several trends that are apparent from the results in this study. First, the addition of a fly ash (Class F or C) or GGBF slag will reduce the rate of heat evolution by dilution of the cementitious system. This is generally in proportion to the SCM replacement percentage. However, this dilution is offset by the reactive aluminate phases in the fly ash, which will generate a substantial amount of heat in the first 24-48 hours after mixing. GGBF slag and silica fume will also generate a substantial amount of heat. The time parameter, τ , will generally increase and the slope parameter, β , will generally decrease with the addition of fly ash and GGBF slag.

Also, high-CaO fly ashes and GGBF slag tend to reduce the slope of the accelerating portion of the hydration curve. Next, the cement that is paired with the SCM plays a critical role in determining the amount of heat that will evolve from a mixture. The total amount of sulfates and reactive aluminates in the cementitious system will determine the amount of retardation a mixture experiences. However, a detailed, systematic study is needed to quantify the effects of different SCMs on pore solution chemistry, as well as the solubility of the different crystalline and amorphous constituents in the SCM.

8.7. REFERENCES

1. ACI Committee 207, “Mass Concrete”, ACI 207.1R-05, American Concrete Institute, Farmington Hills, Michigan, 2005.
2. ACI Committee 232, “Use of Fly Ash in Concrete”, ACI 232.2R-03, American Concrete Institute, Farmington Hills, Michigan, 2003.
3. ACI Committee 233, “Ground Granulated Blast-Furnace Slag as a Cementitious Constituent in Concrete”, ACI 233 R-00, American Concrete Institute, Farmington Hills, Michigan, 2000.
4. ACI Committee 234, “Guide for the Use of Silica Fume in Concrete”, ACI 234R-06, American Concrete Institute, Farmington Hills, Michigan, 2006.
5. ASTM C 618, “Standard Specification for Coal Ash and Raw or Calcined Natural Pozzolans for Use in Concrete,” Annual Book of ASTM Standards, V. 04.01., ASTM International, West Conshohocken, PA., 2003, 3 pp.

6. ASTM C 989, "Standard Specification for Ground Granulated Blast-Furnace Slag for Use in Concrete and Mortars," Annual Book of ASTM Standards, V. 04.01., ASTM International, West Conshohocken, PA., 2005, 5 pp.
7. Schindler, A.K., and K.J. Folliard, "Heat of Hydration Models for Cementitious Materials", *ACI Materials Journal*, V. 102, No. 1, Jan.-Feb., 2005, pp. 24-33.
8. Poole, J.L., "Hydration Study of Cementitious Materials Using Semi-Adiabatic Calorimetry," PhD Dissertation, Chapter 6, The University of Texas at Austin, Austin, TX, 2007, pp 141-171.
9. RILEM 119-TCE, "Adiabatic and Semi-Adiabatic Calorimetry to Determine the Temperature Increase in Concrete due to Hydration Heat of Cement," RILEM Report 15, R. Springenschmid, ed., E&FN Spon, London, 1999, pp. 315-330.
10. Gartner, E.M., J.F. Young, D.A. Damidot, and I. Jawed, "Hydration of Portland Cement", Structure and Performance of Cements, 2nd ed., J. Bensted and P. Barnes, eds, 2002, pp 57-113.
11. Mills, R H. "Factors Influencing Cessation of hydration in Water Cured Cement Pastes." Special Report 90: Symposium on Structure of Portland Cement Paste and Concrete. Washington, D.C.: Highway Research Board, 1966. 406-424.
12. Freiesleben Hansen, P., and E.J. Pedersen, "Maturity computer for controlling curing and hardening of concrete," *Nordisk Betong*, V. 1, No. 19, 1977, pp. 21-25.
13. D'Aloia, L., and G. Chanvillard, "Determining the "Apparent" Activation Energy of Concrete; E_a – Numerical Simulations of the Heat of Hydration of Cement," *Cement and Concrete Research*, V. 32, 2002, pp. 1277-1289.

14. Kada-Benameur, H., E. Wirquin, and B. Duthoit, "Determination of Apparent Activation Energy of Concrete by Isothermal Calorimetry," *Cement and Concrete Research*, V. 30, 2000, pp. 301-305.
15. Copeland, L.E., Kantro, D.L., Verbeck, G., "Part IV-3 Chemistry of Hydration of Portland Cement," 4th International Symposium of the Chemistry of Cement, Washington, D.C., 1960, pp. 429-465.
16. De Schutter, G., and Taerwe, L., "Degree of Hydration-Based Description of Mechanical Properties of Early-Age Concrete," *Materials and Structures*, Vol. 29, No. 7, 1996, pp. 335-344.
17. Verbeck, G., and Forster, C.W. "Long-Time Study of Cement Performance in Concrete. Chapter 6 – The Heats of Hydration of the Cement," Proceedings of the American Society for Testing Materials, Vol. 50, 1950, pp. 1235-1262.
18. Pane, I., and W. Hansen, "Concrete Hydration and Mechanical Properties under Nonisothermal Conditions," *ACI Materials Journal*, V. 99, No. 6, Nov.-Dec, 2002, pp. 534-542.
19. Van Breugel, K., "Prediction of Temperature Development in Hardening Concrete", *Prevention of Thermal Cracking in Concrete at Early Ages*, RILEM Report 15, E & FN Spon, London 1998.
20. Poole, J.L., "A Model for Estimating the Activation Energy of Cementitious Systems," PhD Dissertation, Chapter 5, The University of Texas at Austin, Austin, TX, 2007, pp 109-140.

21. ASTM C 192, “Standard Practice for Making and Curing Concrete Test Specimens in the Laboratory,” Annual Book of ASTM Standards, V. 04.01., ASTM International, West Conshohocken, PA., 2006, 8 pp.
22. ASTM C 150, “Standard Specification for Portland Cement,” Annual Book of ASTM Standards, Vol 04.01., ASTM International, West Conshohocken, PA., 2002, 8 pp.
23. ASTM C 1240, “Standard Specification for Silica Fume Used in Cementitious Mixtures” Annual Book of ASTM Standards, V. 04.01., ASTM International, West Conshohocken, PA., 2005, 7 pp.
24. Scrivener, K.L., T. Füllmann, E. Gallucci, G. Walenta, and E. Bermejo, “Quantitative Study of Portland Cement Hydration by X-Ray Diffraction/Rietveld Analysis and Independent Methods”, *Cement and Concrete Research*, V. 34, 2004, pp 1541-1547.
25. ASTM C 33, “Standard Specification for Concrete Aggregates” Annual Book of ASTM Standards, V. 04.01., ASTM International, West Conshohocken, PA., 2003, 11 pp.
26. Massazza, F., “Pozzolana and Pozzolanic Cements,” Lea’s Chemistry of Cement and Concrete, 4th ed., ed. P.C. Hewlett, Arnold Publishers, New York, 1998, p 471-631.
27. Lang, E. “Blast Furnace Cements”, Structure and Performance of Cements, 2nd ed. eds. J. Bensted and P. Barnes, Spon Press, New York, 2002, p 310-325.

28. Poole, J.L., "The Effects of Supplementary Cementing Materials on Activation Energy of SCMs," PhD Dissertation, Chapter 4, The University of Texas at Austin, Austin, TX, 2007, pp 69-108.
29. Lerch, W., "The Influence of Gypsum on the Hydration and Properties of Portland Cement Paste," Proceedings of the American Society for Testing Materials, V. 46, 1946.
30. Sandberg, P. and Roberts, L., "Cement-Admixture Interactions Related to Aluminate Control", *Journal of ASTM International*, V. 2, No. 6, June 2005, pp 6-13.
31. Poole, J.L., "Study of the Effects of Chemical Admixtures on Hydration," PhD Dissertation, Chapter 7, The University of Texas at Austin, Austin, TX, 2007, pp 172-215.

Table 8-1: Chemical and physical properties of cement

	Cements					Fly Ashes				Other SCMs	
	C1	C2	C6	C9	C10	FF1	FF2	FC1	FC2	S1	S.F.
SiO ₂ (%)	20.45	19.18	20.77	21.63	21.03	56.63	51.69	37.83	33.31	34.48	94.28
Al ₂ O ₃ (%)	5.43	5.34	3.88	4.04	4.13	30.68	24.81	19.83	18.39	11.35	0.04
Fe ₂ O ₃ (%)	2.01	2.3	3.73	5.29	3.78	4.94	4.22	6.17	5.40	0.67	0.06
CaO (%)	64.51	63.17	64.5	63.07	63.4	0.69	13.12	23.13	28.91	41.73	0.51
MgO (%)	1.15	1.09	1.01	0.77	1.32	0.73	2.29	4.62	5.25	7.32	0.57
Na ₂ O (%)	0.14	0.12	0.18	0.27	0.14	0.12	0.18	1.74	1.64	0.14	0.06
K ₂ O (%)	0.56	0.95	0.60	0.23	0.55	2.26	0.84	0.06	0.35	0.38	0.99
Na ₂ O Eq. (%)	0.51	0.75	0.575	0.42	0.502	1.607	0.733	1.778	1.870	0.390	0.71
SO ₃ (%)	3.35	3.20	2.38	2.74	3.02	0.00	0.46	1.50	2.27	1.88	0.16
LOI (%)	1.80	4.10	2.67	1.55	1.5	2.10	0.23	0.67	0.34	0.83	3.10
Insoluble Residue (%)	-	0.63	0.25	1.43	0.17	-	-	-	-	-	-
CaO (%)**	0.0	0.0	0.0	0.0	0.0	-	-	-	-	-	-
C ₃ S (%)*	58.29	63.1	66.5	49.85	56.51	-	-	-	-	-	-
C ₃ S (%)**	61.20	61.0	55.7	49.00	64.00	-	-	-	-	-	-
C ₂ S (%)*	14.65	7.4	9.4	24.41	17.66	-	-	-	-	-	-
C ₂ S (%)**	16.00	15.6	21.1	26.40	15.30	-	-	-	-	-	-
C ₃ A (%)*	10.99	10.3	4.0	1.76	4.55	-	-	-	-	-	-
C ₃ A (%)**	13.10	9.6	4.0	4.40	5.10	-	-	-	-	-	-
C ₄ AF (%)*	6.12	7.0	11.4	16.10	11.50	-	-	-	-	-	-
C ₄ AF (%)**	3.50	6.0	10.7	12.10	11.00	-	-	-	-	-	-
C \hat{S} H ₂ (%)**	1.4	0.4	3.1	2.3	1.6	-	-	-	-	-	-
C \hat{S} H _{0.5} (%)**	1.5	1.2	1.3	2	0.6	-	-	-	-	-	-
C \hat{S} (%)**	0.6	0.7	0.6	0.4	0.6	-	-	-	-	-	-
K ₂ SO ₄ (%)**	1.5	1.0	0.7	0.9	0						
CaCO ₃ (%)**	0.8	3.6	3.2	2.5	1.0						
Blaine fineness (m ² /kg)	350	391	365	409	349	147	166	348	300	332	20000

* = Bogue Calculations, ** = Rietveld Analysis

Table 8-2: Curve Fit Parameters for Mixtures with 100% Cement or Class F Fly Ash Replacement

Mix #	Cement	SCM (% Replacement by Mass)			w/cm	H_u	α_u	τ	β	E_a
		ID	Type	%	CaO					
						kJ/kg		hrs		J/mol
1	C1	-	-	-	0.44	481	0.793	13.80	0.847	40,650
2	C1	FF1	30	0.7	0.44	340	0.741	13.63	0.820	36,550
3	C1	FF2	30	13.1	0.44	408	0.832	18.07	0.710	37,700
4	C2	-	-	-	0.44	482	0.711	12.49	0.950	38,750
5	C2	FF1	20	0.7	0.44	388	0.803	13.14	0.815	35,950
6	C2	FF1	30	0.7	0.44	341	0.885	14.03	0.776	34,800
7	C2	FF1	40	0.7	0.44	294	0.896	14.24	0.741	33,800
8	C2	FF2	20	13.1	0.44	433	0.766	14.72	0.835	36,700
9	C2	FF2	30	13.1	0.44	408	0.710	13.85	0.872	35,900
10	C2	FF2	40	13.1	0.44	384	0.701	16.10	0.834	35,250
11	C6	-	-	-	0.44	463	0.753	11.40	0.737	37,150
12	C6	FF1	20	0.7	0.44	372	0.845	12.34	0.651	35,350
13	C6	FF1	30	0.7	0.44	327	0.836	11.92	0.655	34,600
14	C6	FF1	40	0.7	0.44	282	0.902	13.31	0.665	33,950
15	C6	FF2	20	13.1	0.44	417	0.725	12.67	0.699	36,100
16	C6	FF2	30	13.1	0.44	395	0.776	16.49	0.593	35,700
17	C6	FF2	40	13.1	0.44	372	0.709	15.39	0.670	35,400
18	C9	-	-	-	0.44	419	0.714	14.86	0.807	38,600
19	C9	FF1	30	0.7	0.44	297	0.832	16.71	0.678	35,150
20	C9	FF2	30	13.1	0.44	364	0.691	16.59	0.695	36,250
21	C10	-	-	-	0.44	446	0.793	12.78	0.709	39,450
22	C10	FF1	30	0.7	0.44	316	0.788	13.12	0.676	36,000
23	C10	FF2	30	13.1	0.44	386	0.682	15.02	0.707	37,100

Table 8-3: Curve Fit Parameters for Mixtures with Class C Fly Ash

Mix #	Cement	SCM (% Replacement by Mass)			w/cm	H_u	α_u	τ	β	E_a
		ID	Type	%	CaO					
						kJ/kg		hrs		J/mol
24	C1	FC1	30	23.1	0.44	462	0.747	16.78	0.904	38,550
25	C1	FC2	30	28.9	0.44	492	0.787	22.71	0.753	39,100
26	C2	FC1	20	23.1	0.44	469	0.817	17.36	0.760	37,300
27	C2	FC1	30	23.1	0.44	462	0.841	22.17	0.724	36,800
28	C2	FC1	40	23.1	0.44	456	0.742	22.94	0.765	36,450
29	C2	FC2	20	28.9	0.44	490	0.764	17.38	0.823	37,600
30	C2	FC2	30	28.9	0.44	494	0.721	18.65	0.917	37,300
31	C2	FC2	40	28.9	0.44	497	0.714	23.68	0.915	37,150
32	C6	FC1	20	23.1	0.44	453	0.670	19.16	0.605	36,650
33	C6	FC1	30	23.1	0.44	449	0.890	28.07	0.538	36,600
34	C6	FC1	40	23.1	0.44	444	1.000	43.45	0.495	36,600
35	C6	FC2	20	28.9	0.44	474	0.773	16.23	0.717	37,000
36	C6	FC2	30	28.9	0.44	480	0.739	34.27	1.103	26,250
37	C6	FC2	40	28.9	0.44	457	0.817	21.17	0.669	34,150
38	C9	FC1	30	23.1	0.44	418	0.804	24.66	0.574	37,100
39	C9	FC2	30	28.9	0.44	450	0.923	41.84	0.483	37,650
40	C10	FC1	30	23.1	0.44	437	0.839	23.94	0.561	38,000
41	C10	FC2	30	28.9	0.44	468	0.852	26.86	0.566	38,500

Table 8-4: Curve Fit Parameters for Silica Fume, GGBF Slag, and Ternary Blends

Mix #	Cement	SCM (% Replacement by Mass)			w/cm	H_u	α_u	τ	β	E_a
		ID	Type	%	CaO					
						kJ/kg		hrs		J/mol
42	C2	SF	5	-	0.44	458	0.739	11.77	1.024	35,400
43	C6	SF	10	-	0.44	416	0.944	14.81	0.643	31,000
44	C2	FF1	20	0.7	0.44	364	0.870	14.04	0.868	30,800
		SF	5	-						
45	C2	FC2	30	28.9	0.44	470	0.758	18.73	0.861	34,200
		SF	5	-						
46	C6	FC2	30	28.9	0.44	457	0.817	21.18	0.669	34,150
		SF	5	-						
47	C2	S1	30	-	0.44	476	0.889	21.29	0.638	39,600
48	C2	S1	40	-	0.44	474	0.918	26.06	0.592	40,200
49	C2	S1	50	-	0.44	472	0.735	21.70	0.757	40,950
50	C2	S1	70	-	0.44	467	0.560	26.49	0.708	42,950
51	C6	S1	50	-	0.44	462	0.961	42.53	0.461	41,400
52	C9	S1	30	-	0.44	432	1.000	38.99	0.497	39,900
53	C9	S1	40	-	0.44	436	1.000	49.67	0.474	40,650
54	C9	S1	50	-	0.44	440	1.000	81.59	0.439	41,500
55	C1	FF2	30	13.1	0.44	399	0.733	35.39	0.544	40,900
		S1	40	-						

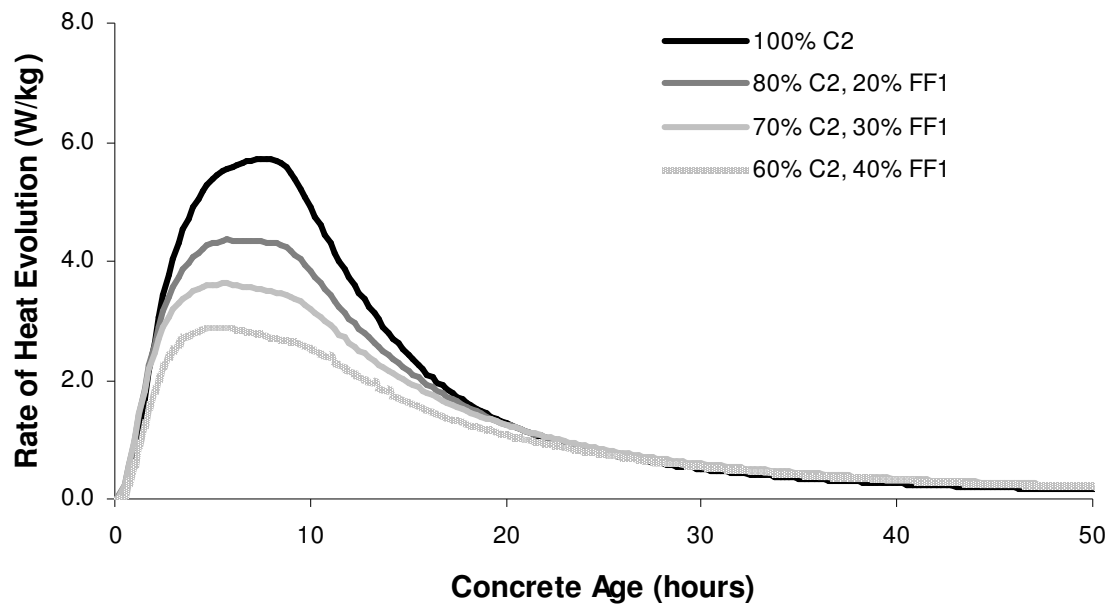


Figure 8-1: Rate of Heat Evolution per Kilogram of Cementitious Material for Concrete Mixtures with Different Dosages of FF1 (CaO = 0.7%)

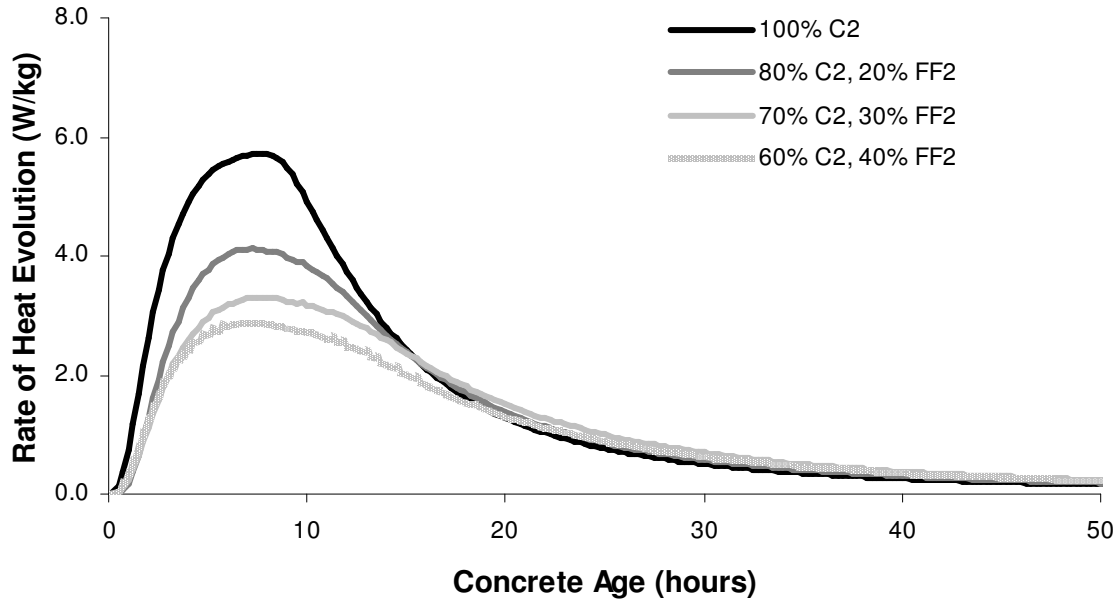


Figure 8-2: Rate of Heat Evolution per Kilogram of Cementitious Material for Concrete Mixtures with Different Dosages of FF2 (CaO = 13.1%)

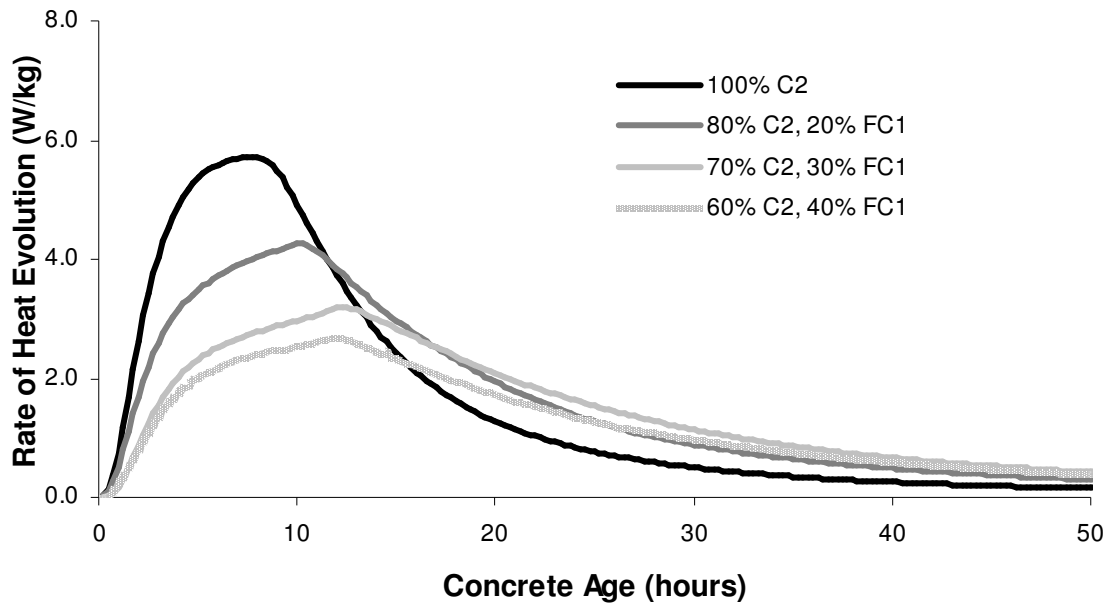


Figure 8-3: Rate of Heat Evolution per Kilogram of Cementitious Material for Concrete Mixtures with Different Dosages of FC1 (CaO = 23.1%)

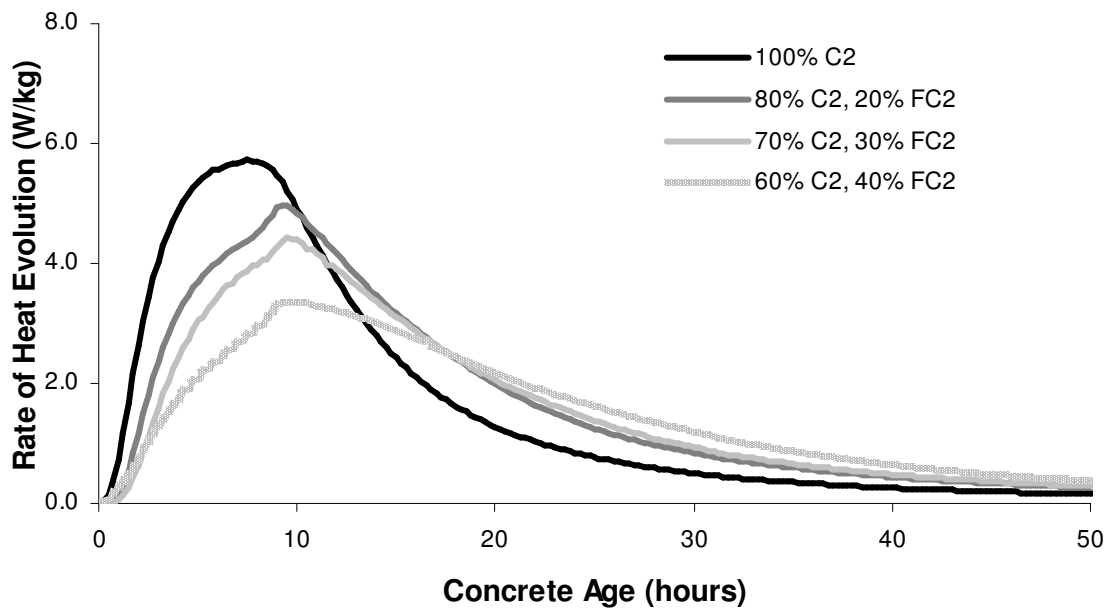


Figure 8-4: Rate of Heat Evolution per Kilogram of Cementitious Material for Concrete Mixtures with Different Dosages of SCM FC2 (CaO = 28.9%)

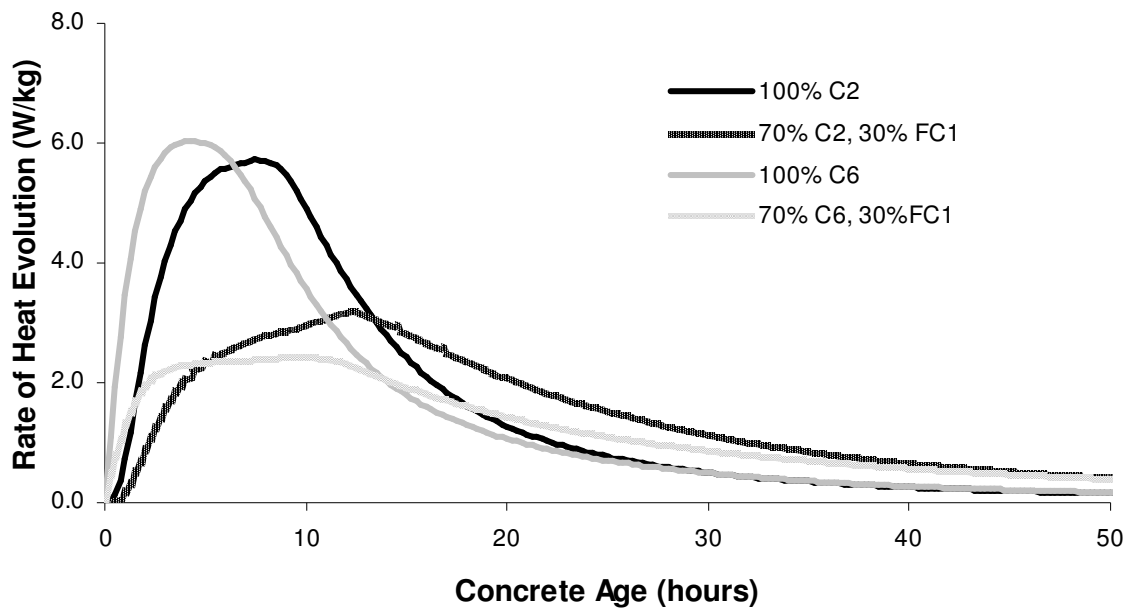


Figure 8-5: Rate of Heat Evolution per Kilogram of Cementitious Material for Mixtures with 30% SCM FC1 and Cement C2 or C6

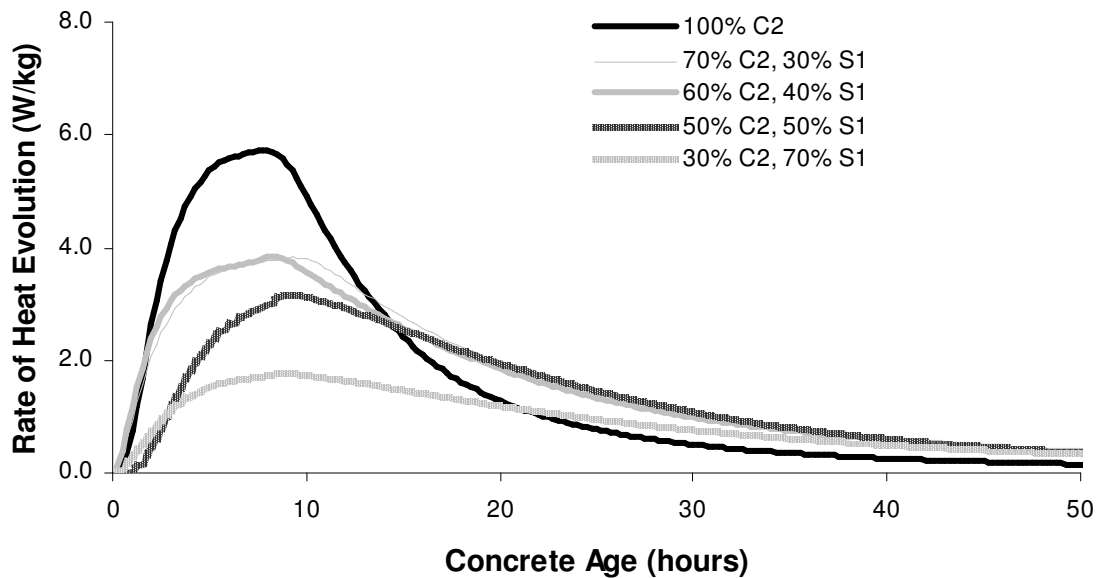


Figure 8-6: Rate of Heat Evolution per Kilogram of Cementitious Material for Mixtures with Cement C2 and Different Dosages of S1

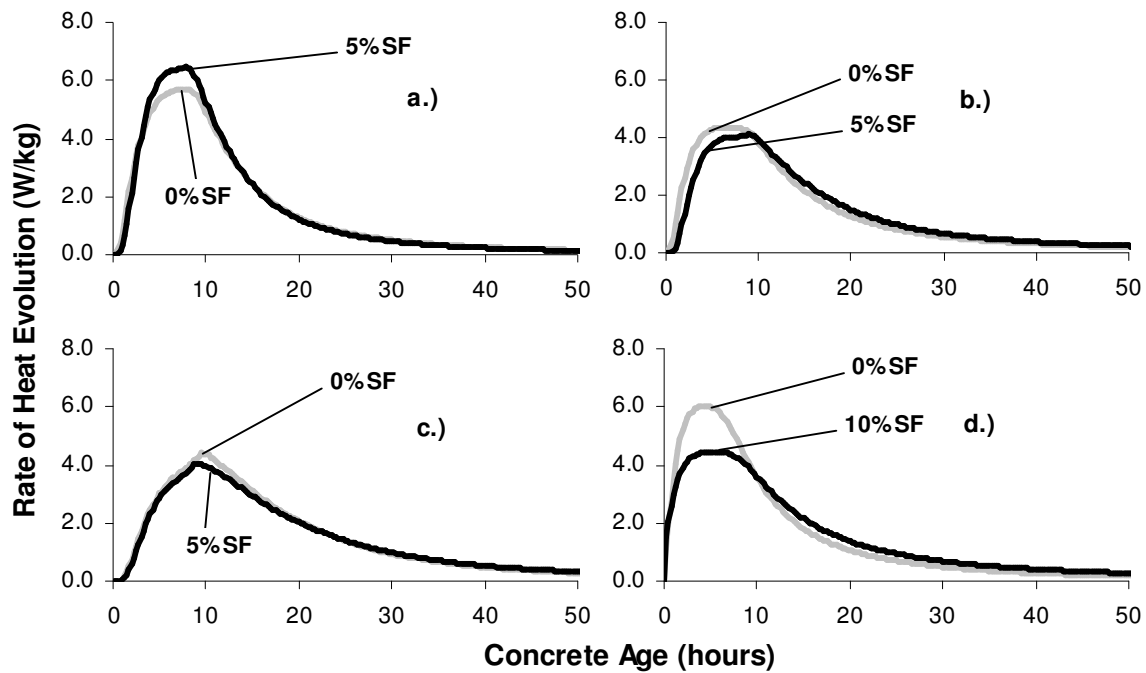


Figure 8-7: Rate of Heat Evolution per Kilogram of Cementitious Material for Mixtures with a.) Cement C2, b.) Cement C2, 20% FF1, c.) Cement C2, 30% FC2, and d.) Cement C6

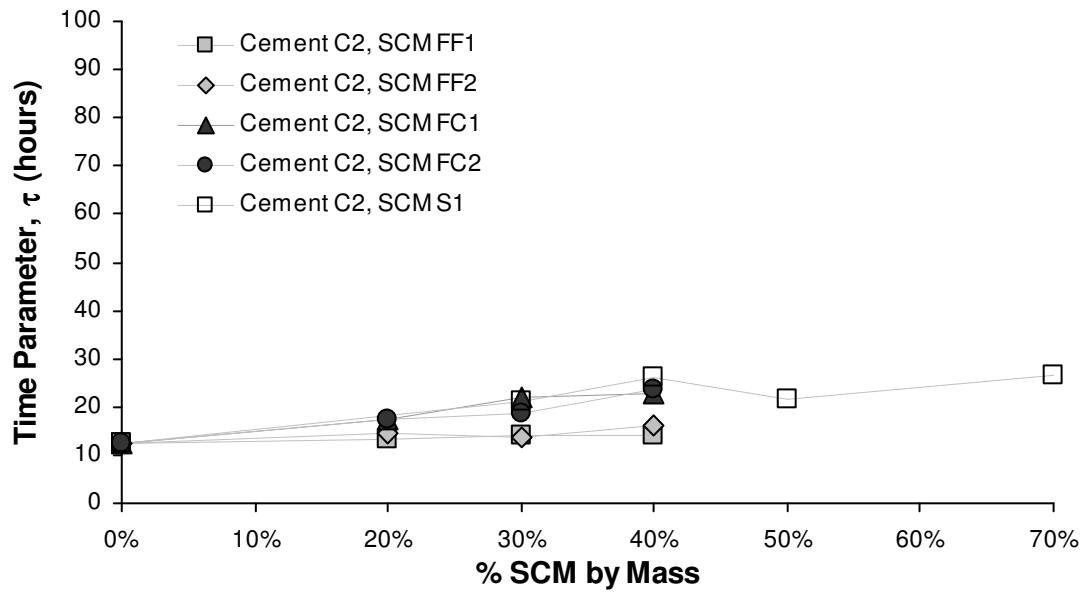


Figure 8-8: Effect of SCM Type and Dosage on τ - Cement C2

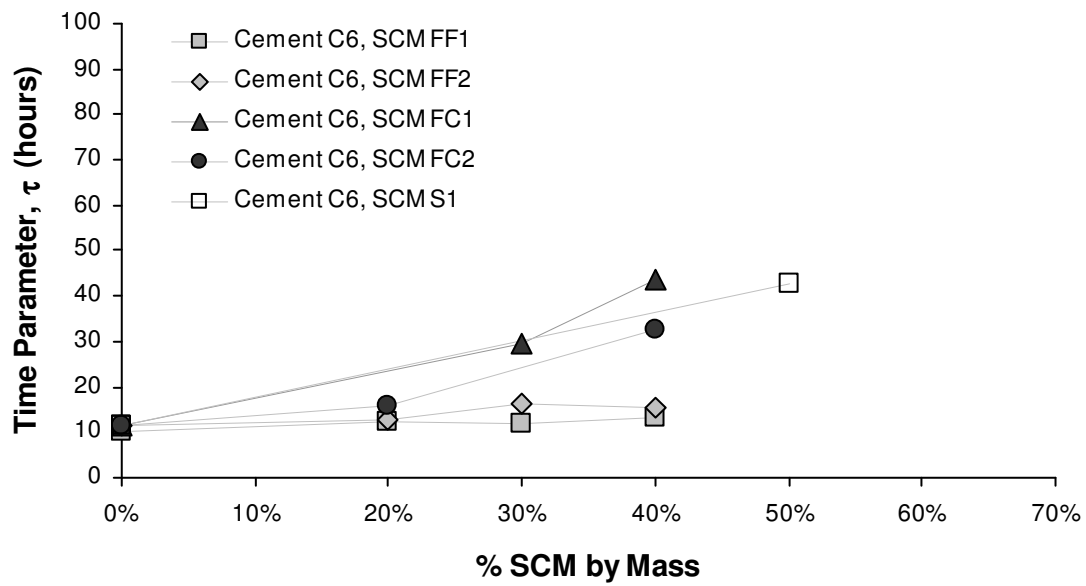


Figure 8-9: Effect of SCM Type and Dosage on τ - Cement C6

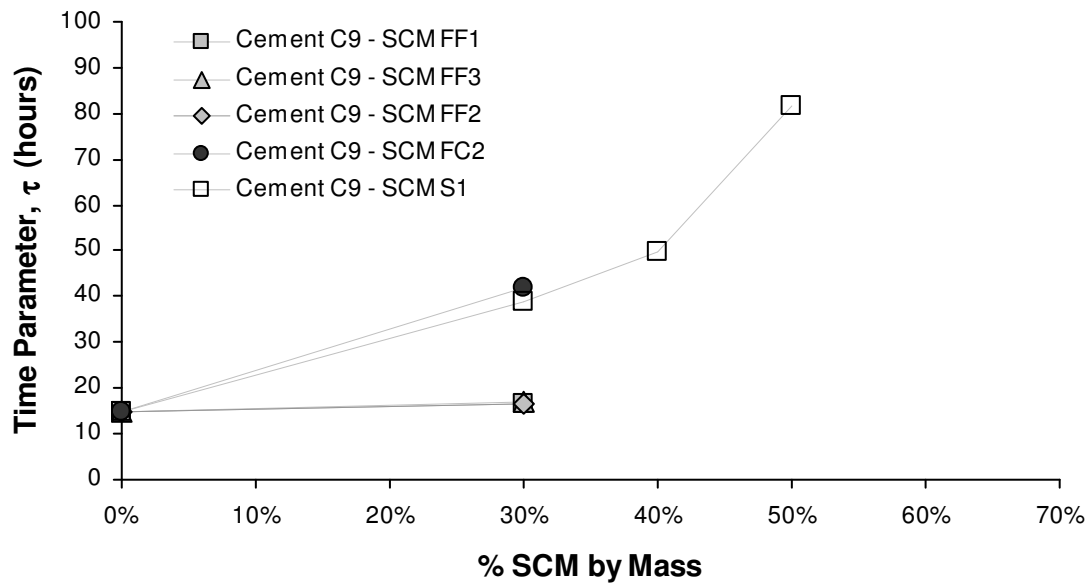


Figure 8-10: Effect of SCM Type and Dosage on τ - Cement C9

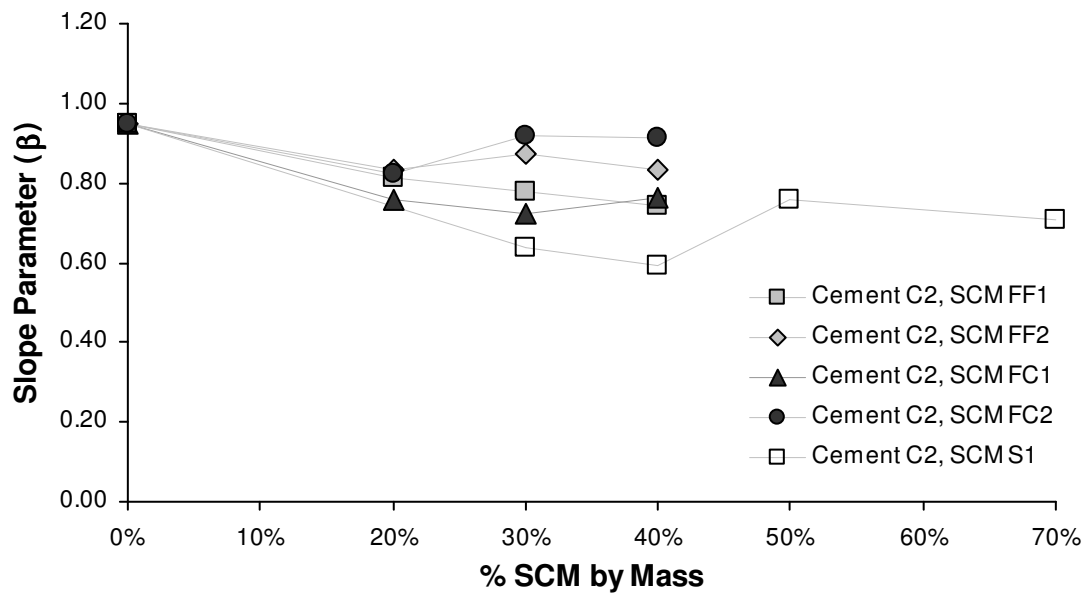


Figure 8-11: Effect of SCM Type and Dosage on β - Cement C2

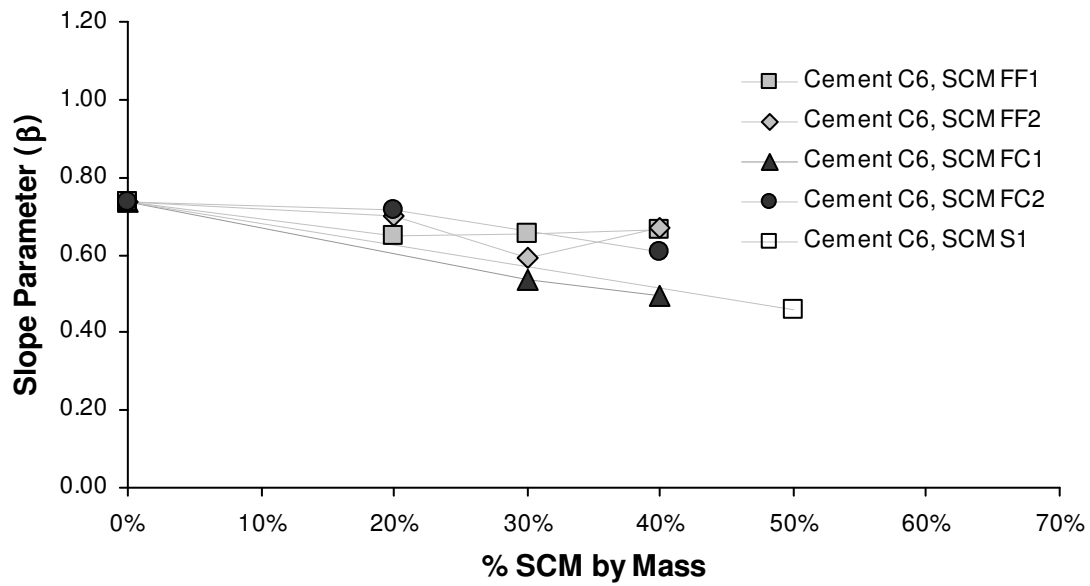


Figure 8-12: Effect of SCM Type and Dosage on β - Cement C6

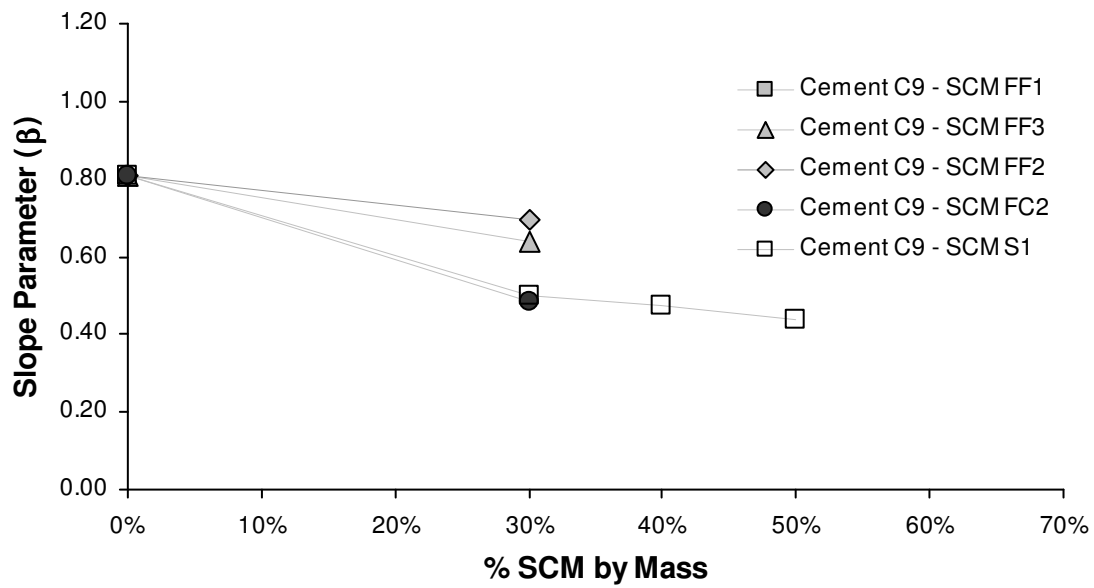


Figure 8-13: Effect of SCM Type and Dosage on β - Cement C9

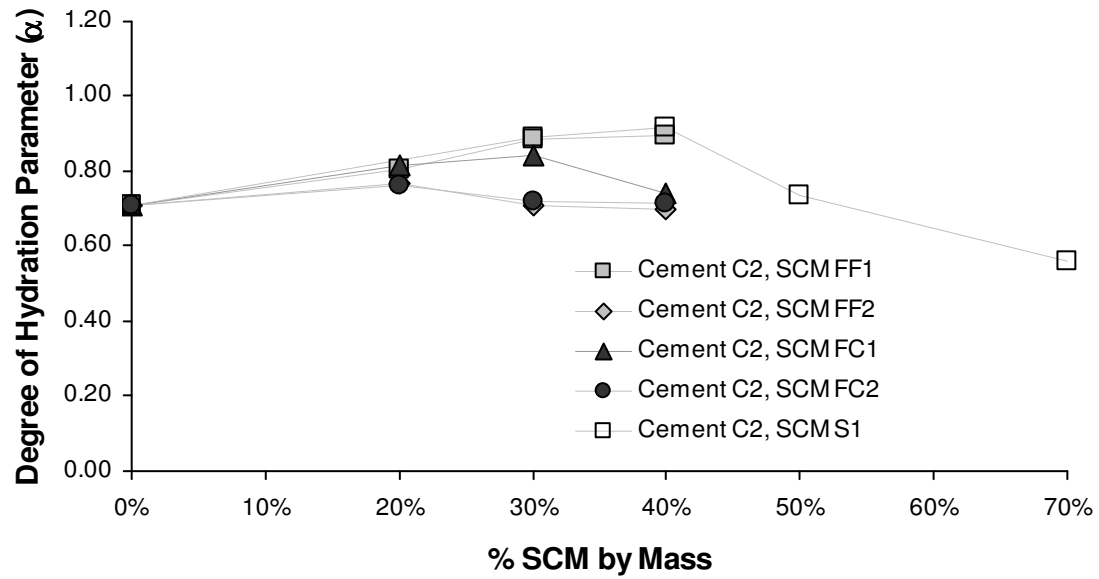


Figure 8-14: Effect of SCM Type and Dosage on α - Cement C2

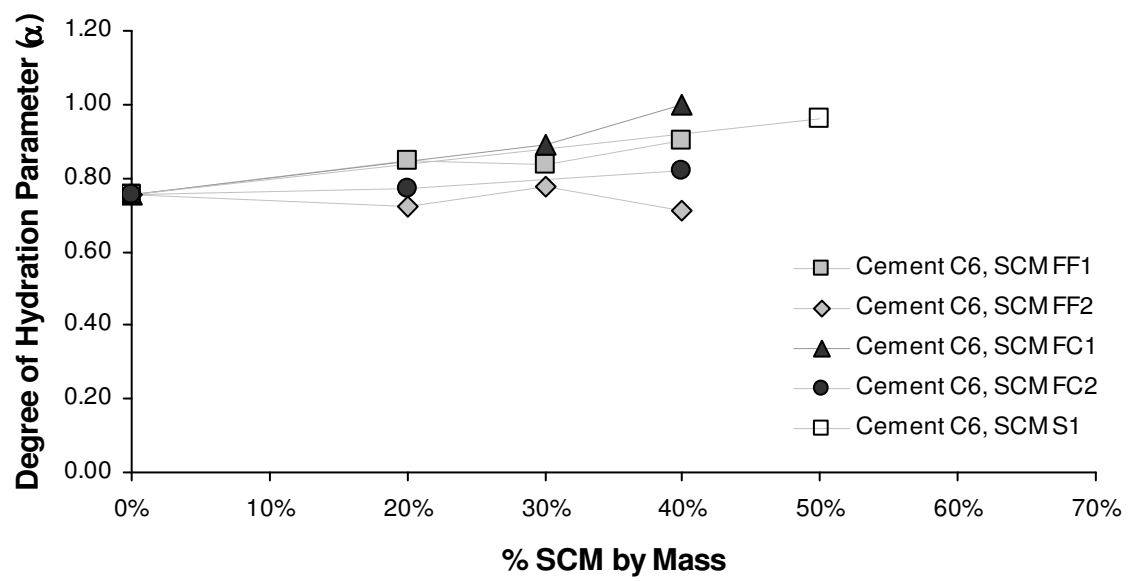


Figure 8-15: Effect of SCM Type and Dosage on α - Cement C6

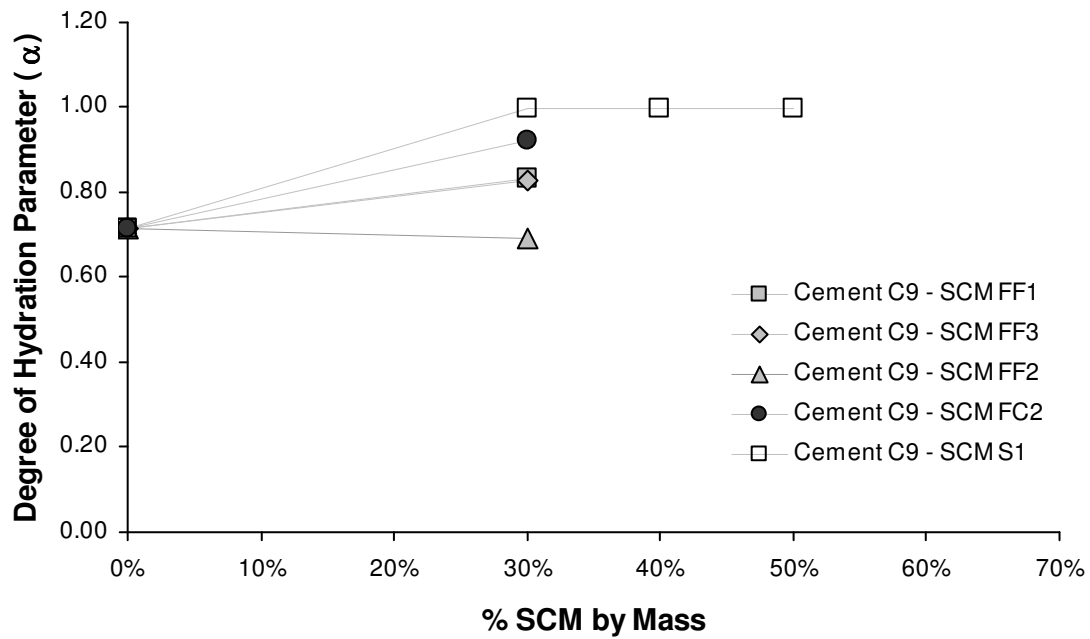


Figure 8-16: Effect of SCM Type and Dosage on α_t - Cement C9

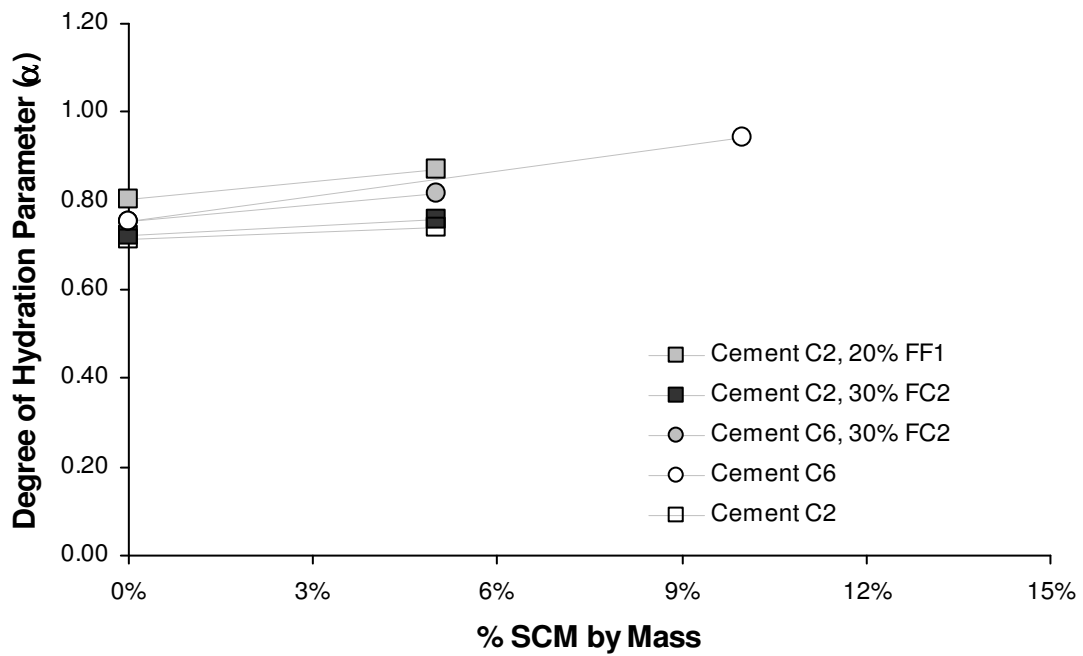


Figure 8-17: Effect of Silica Fume on α_t

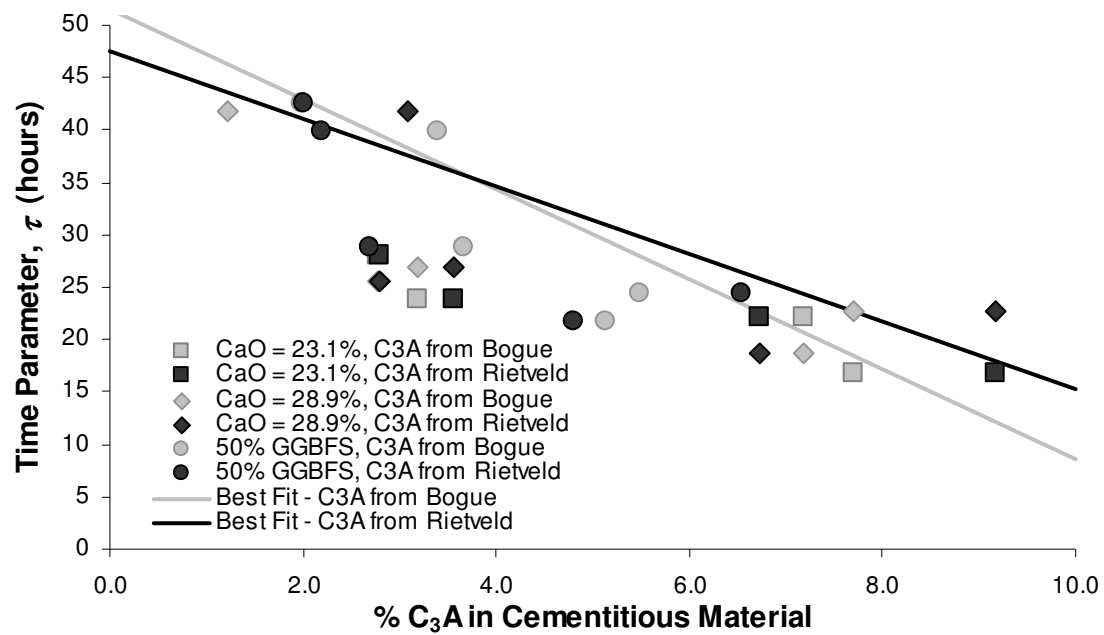


Figure 8-18: Effect of C_3A Content of Cementitious Material on τ with 30% Class C Fly Ash (FC1 and FC2) and 50% GGBF Slag (S1)

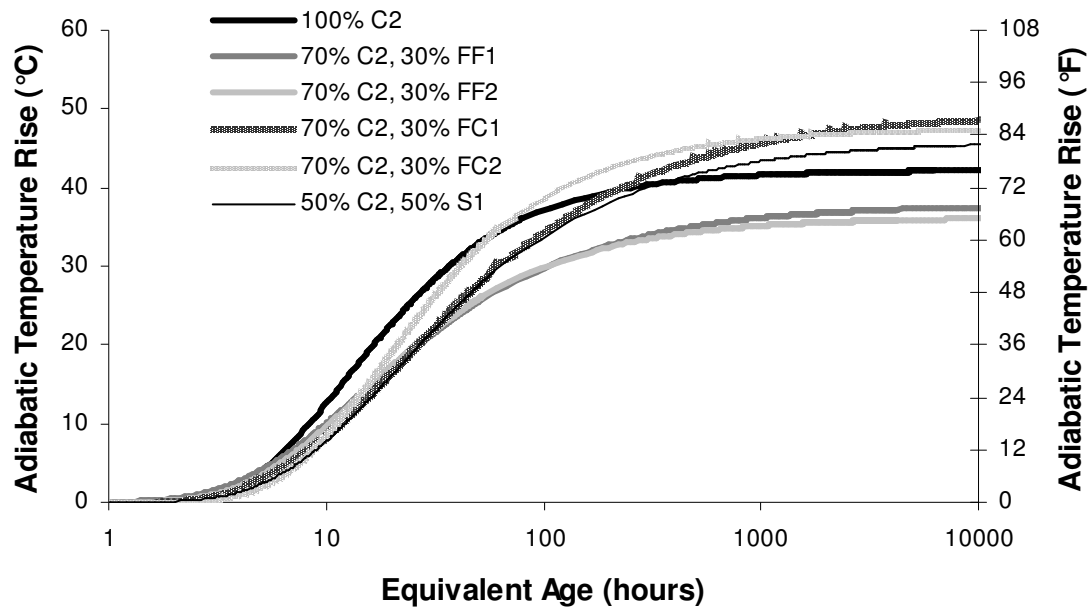


Figure 8-19: Adiabatic Temperature Rise of Mixtures with 100% Cement C2, 70% Cement C2 with 30% FF1, FF2, FC1, FC2, and 50% Cement C2 and 50% S1

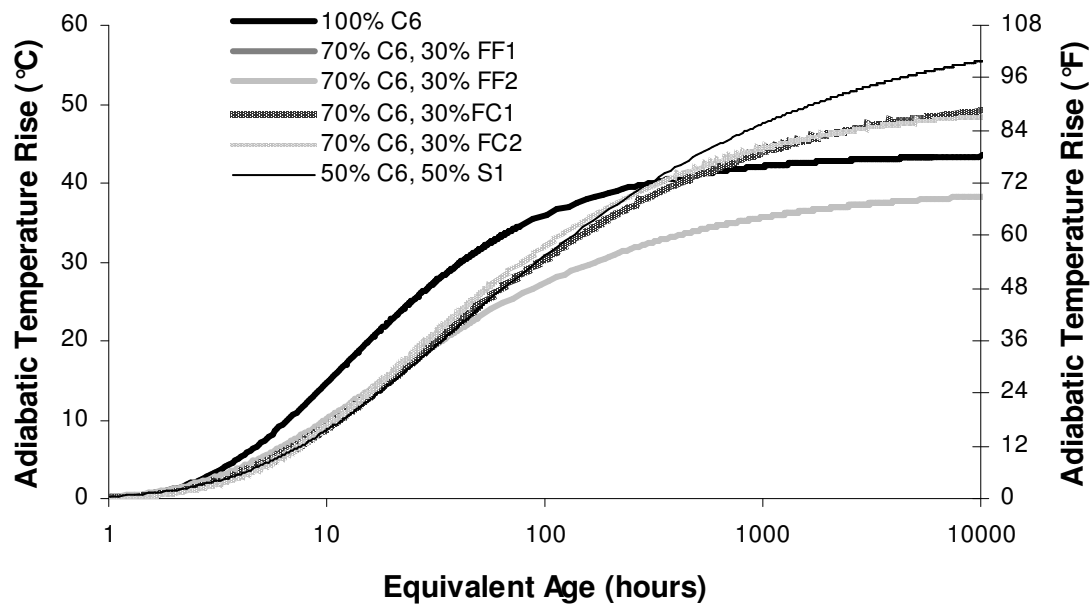


Figure 8-20: Adiabatic Temperature Rise of Mixtures with 100% Cement C6, 70% Cement C6 with 30% FF1, FF2, FC1, FC2, and 50% Cement C6 and 50% S1

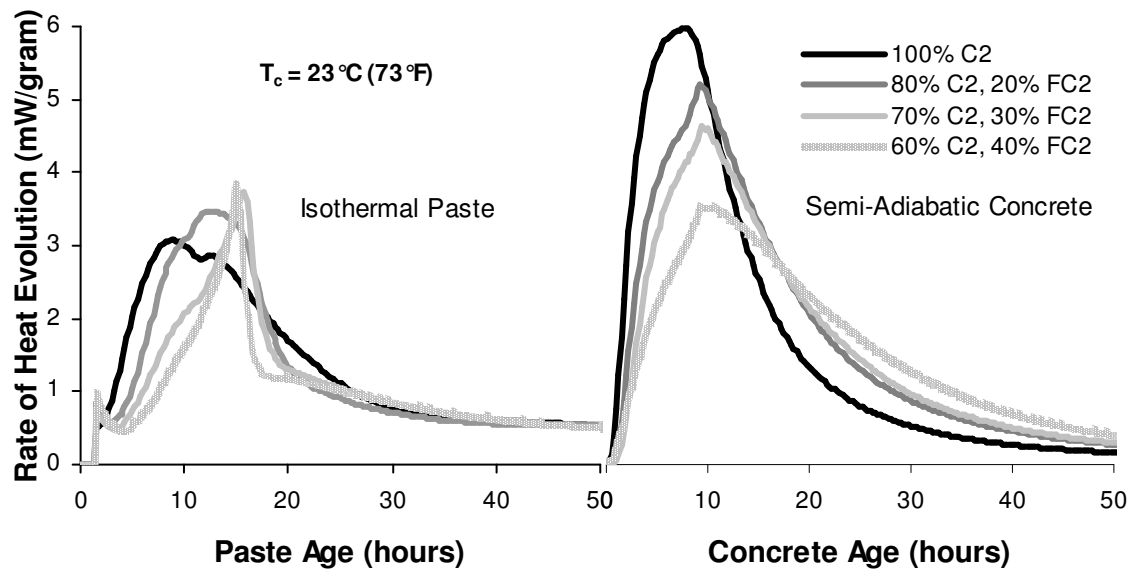


Figure 8-21: Comparison Between Isothermal Calorimetry Results and Semi-Adiabatic Calorimetry Results for Mixtures with Cement C2 and Different Replacement Percentages of FC2 (28.9% CaO)

CHAPTER 9. MODELING THE HYDRATION OF CEMENTITIOUS SYSTEMS

9.1. ABSTRACT

This chapter presents a multivariate regression model, developed from semi-adiabatic calorimetry testing that predicts the temperature development of concrete mixtures based on material properties (e.g., cement chemistry and fineness, SCM chemistry), mixture proportions, and chemical admixture types and dosages. The final model provides a useful tool to assess the temperature development of concrete mixtures, and thereby reduce the thermal cracking risk of concrete structures.

9.2. INTRODUCTION

Estimating the magnitude of early age thermal stresses in large concrete elements is challenging. The properties of a concrete mixture that determine the risk of thermal cracking include the hydration heat, mechanical properties, early age creep and relaxation, autogenous shrinkage, coefficient of thermal expansion, and specific heat. Of these variables, the rate and magnitude of heat evolution of a concrete mixture is one of the best predictors of thermal stress risk¹. Therefore, an accurate, predictive estimate of the heat evolution of a concrete mixture is needed as part of any model developed to predict thermal stresses.

Previous chapters have studied the effects of cement type^{2,3}, aggregate type², placement temperature^{2,3}, supplementary cementing materials (SCMs)^{2,3,4,5}, and chemical admixtures⁶ on the rate of heat evolution and the adiabatic temperature rise of concrete mixtures, as measured using semi-adiabatic calorimetry. The influence of these variables on the hydration of a concrete mixture was examined in this research using a three-

parameter exponential model based on degree of hydration data, as shown in Equation 9-1^{3,7}:

$$\alpha(t_e) = \alpha_u \cdot \exp \left[- \left(\frac{\tau}{t_e} \right)^\beta \right] \quad \text{Equation 9-1}$$

where $\alpha(t_e)$ = degree of hydration at equivalent age t_e , τ = hydration time parameter (hours), β = hydration slope parameter, and α_u = ultimate degree of hydration. Equivalent age is calculated as follows⁸:

$$t_e(T_r) = \sum_0^t e^{-\frac{E_a}{R} \left(\frac{1}{T_c} - \frac{1}{T_r} \right)} \cdot \Delta t \quad \text{Equation 9-2}$$

where $t_e(T_r)$ = equivalent age at reference temperature (T_r), T_c = temperature of the concrete(°K), E_a = activation energy (J/mol), and R = natural gas constant (8.314 J/mol/K). The progress of the hydration of portland cement may be quantified by the degree of hydration (α), which varies from 0 to 1, with a value of 1 indicating complete hydration^{3,9,10,11,12,13,14}.

$$\alpha = \frac{H(t)}{H_u} \quad \text{Equation 9-3}$$

where α = degree of hydration at time t , $H(t)$ = heat evolved from time 0 to time t (J/gram), and H_u = total heat available for reaction (J/gram). H_u is a function of cement composition and amount and type of supplementary cementing materials (SCMs) and may be calculated as follows³:

$$H_u = H_{cem} \cdot p_{cem} + 461 \cdot p_{slag} + 1800 \cdot p_{FA-CaO} \cdot p_{FA} \quad \text{Equation 9-4}$$

where p_{slag} = slag mass to total cementitious content ratio, p_{FA} = fly ash mass to total cementitious content ratio, p_{FA-CaO} = fly ash CaO mass to total fly ash content ratio, p_{cem} =

cement mass to total cementitious content ratio, and H_{cem} = heat of hydration of the cement (J/gram). H_{cem} can be calculated as shown in Equation 9-5³:

$$H_{cem} = 500 \cdot p_{C_3S} + 260 \cdot p_{C_2S} + 866 \cdot p_{C_3A} + 420 \cdot p_{C_4AF} + 624 \cdot p_{SO_3} + 1186 \cdot p_{FreeCa} + 850 \cdot p_{MgO} \quad \text{Equation 9-5}$$

where H_{cem} = total heat of hydration of portland cement (J/gram) at $\alpha = 1.0$, and p_i = mass of i-th component to total cement content ratio.

The parameters of the exponential model, α_u , τ , and β , relate to the shape of the hydration curve, and are used to capture the effects of different mixture constituents on the amount of acceleration, retardation, rate of hydration, and ultimate degree of hydration of a mixture. However, to determine the equivalent age, the activation energy (E_a) of a mixture is needed. Equation 9-6 (based on Bogue compounds) was developed previously¹⁵ from isothermal calorimetry and non-linear regression analysis, and is used to model E_a for each of the semi-adiabatic calorimeter tests presented here.

$$E_a = 41,230 + 1,416,000 \cdot [(C_3A + C_4AF) \cdot p_{Cement} \cdot SO_3 \cdot p_{Cement}] - 347,000 \cdot Na_2O_{eq} - 19.8 \cdot Blaine + 29,600 \cdot p_{FlyAsh} \cdot p_{CaO-FlyAsh} + 16,200 \cdot p_{GGBFS} - 51,600 \cdot p_{SF} - 3,090,000 \cdot WRRET - 345,000 \cdot ACCL \quad \text{Equation 9-6}$$

where p_{cement} = % cement in mixture; p_{FlyAsh} = % fly ash in mixture; $p_{CaO-FlyAsh}$ = % CaO in fly ash; p_{GGBF} = % GGBF slag in mixture; p_{SF} = % silica fume in mixture; $Blaine$ = Blaine fineness of cement; Na_2O_{eq} = % Na_2O_{eq} in cement ($0.658 \times \%K_2O + \%Na_2O$); C_3A = % C_3A in cement; C_4AF = % C_4AF in cement; SO_3 = % SO_3 in cement; $WRRET$ = ASTM Type A&D water reducer/retarder, % solids per gram of cementitious material; $ACCL$ = ASTM Type C calcium-nitrate based accelerator, % solids per gram of cementitious material.

Previous chapters reported on a large number of semi-adiabatic calorimeter tests to examine the effects of cement type, aggregates, water-cementitious materials ratio (w/cm)², SCMs⁴, and chemical admixtures⁶ on the hydration of concrete mixtures. Several trends in the parameters from Equation 9-1 are apparent in the data. First, SCM type and reactivity have a large effect on the degree of retardation of a mixture (expressed as the time parameter, τ)⁴. Also, retarders tend to increase τ , and accelerators tend to reduce τ . Next, β tends to increase when water reducers, retarders, and accelerators are added to a mixture⁶, while SCMs generally reduced β ⁴. α_u rises with the addition of Class C fly ash and ground granulated blast-furnace slag⁴, and generally drops with the addition of water reducers⁶. Cement type alone does not greatly affect the hydration parameters. However, interactions between cement type, SCM type and replacement percentage, and admixture type and dosage are apparent, but are more complex than can be characterized by simple, two-variable linear regression analysis.

9.2.1. CHALLENGES WITH REGRESSION ANALYSIS AND MATERIAL CHARACTERIZATION

Various multivariate statistical models have been developed^{3,5} to assess the effects of different mixture constituents on α_u , τ , and β . However, this previous research^{3,5} only examined a limited number of cements, SCMs, and chemical admixture combinations. A larger dataset is needed to fully incorporate the variety of mixtures that are possible. This methodology will not elucidate subtle hydration mechanisms and interactions, but it is useful for providing an estimate of the relative magnitude of the effects of variables known to have an effect on hydration.

Multivariate regression analysis requires accurate information about the raw material composition. A model that is to be easily implemented must use independent variables that are easily available to the end user. This presents challenges to the development of a model because information that is available to a researcher may not be available to end user of a model, i.e. engineers and contractors. For example, previous models have relied heavily on phase analysis of cement compounds using Bogue calculations. However, Rietveld analysis¹⁶ has been shown to provide a more accurate estimation of crystalline phases in cement. The results of this analysis are not readily available for most cements. Also, the characteristics of SCMs that affect hydration are poorly defined. In the case of fly ash, the reactivity is generally classified according to the CaO content. However, such a simple measure of reactivity fails to account for the phase in which the CaO is located, the solubility of the phase, and other factors such as the degree of crystallinity or size of the phase. Finally, information available about commercial chemical admixture components is incomplete at best. In this study, information about the specific chemicals that make up the chemical admixtures was provided by the manufacturers, but precise information about component percentages was not available. However, chemical admixtures are generally only defined by their ASTM designation, not their composition. This classification system fails to account for the wide variety of differences within each ASTM classifications. All of these uncertainties impact the choice of independent variables that may be used in a model.

This chapter uses the data from the previous three chapters in this series^{2,4,6} to develop a mechanistic-empirical model for the progress of hydration as represented by heat evolution. The current research incorporates a dataset of over 300 tests that will be

used to develop an expanded, robust hydration model. A multivariate regression analysis procedure developed previously^{3,5,15} will be used to identify the variables that have the greatest effects on the exponential model parameters in Equation 9-1. This chapter will develop two models: one based on information available from mill certifications, such as Bogue compounds, and CaO content; and a second model based on Rietveld analysis of the cement phases and crystalline phases of the fly ash determined by quantitative x-ray diffraction (QXRD). The multivariate regression models will be developed from test results presented in Chapters 6 through 8. The predictive ability of the regression models developed here will be assessed by comparing results of additional tests from this program and previous research^{3,5} to the regression model output.

9.3. RESEARCH SIGNIFICANCE

A model that describes the effects of different concrete mixture constituents on hydration is needed to properly address the effects of temperature development on thermal cracking risk of concrete elements. This chapter presents two models that describe the progress of hydration of concrete as characterized by the heat evolved. The first model uses commonly available information about the cementitious materials in the concrete mixture through oxide analysis. The second model is based on more precise information about the cementitious materials available from quantitative x-ray diffraction methods. Both models account for the effects of cement chemistry, aggregate type, w/cm, SCMs, chemical admixture type and dosage, and temperature on hydration.

9.4. SUMMARY OF HYDRATION TRENDS

As part of the development of a hydration model of concrete, over 300 semi-adiabatic tests were performed on a variety of different concrete mixtures. A number of

these results were presented in previous chapters^{2,4,6} to examine the effects of cement type, SCM type and replacement percentage, and admixture type and dosage. Other mixtures were used to assess the variability of the test method². These mixtures are used to develop a multivariate statistical model of hydration of concrete. A number of additional tests were run in the lab, at field sites, and were taken from literature^{3,5}. These additional results are used as a dataset to validate the predictive ability of the proposed model. These additional results were not used in the multivariate regression analysis to calibrate the hydration model.

9.4.1. EFFECTS OF SCMS ON HYDRATION

Several trends were seen in the previous chapters^{2,4,6} on hydration behavior of different mixtures. The relative magnitude of these trends and the range of tests are summarized in Table 9-1. First, the composition of cement plays a role in the hydration parameters, but changes in SCM type, replacement percentage, and the use of chemical admixtures generally alter the degree of hydration more than the cement. For example, the value of τ for all cements ranged from 9.3 hours for Type III cement to 15.0 hours for Type V cement, with an average value of approximately 12.0 hours. The slope parameter, β , had a range from 0.68 to 0.92 for all cement types. For comparison, the addition of GGBF slag raised τ from 25 to 45 hours, and lowered β from 0.45 to 0.75. The addition of SCMs and chemical admixtures had a greater effect on the behavior of the mixture, and tended to magnify the differences between cements.

Next, the chemistry and type of fly ash greatly affect the hydration of a mixture. Previous studies^{2,3,4,5} showed that fly ash tends to retard set time, depending on the amount of reactive phases in the fly ash. Fly ash is currently classified in these modeling

efforts only by the CaO content, which does not capture the subtleties of the variations between fly ash hydration characteristics. However, CaO content does provide an index of the hydraulicity of the material and may be used as a rough comparison between ashes. Previous research⁴ showed that low-CaO fly ashes tend to reduce the heat of hydration of the mixture primarily through dilution of the portland cement. They reduce the slope of the accelerating portion of the hydration curve as well. Higher CaO fly ashes also reduce the heat of hydration, but show some hydraulic properties beyond pure dilution of the portland cement. They reduce the slope of the accelerating portion of the hydration curve and they increase the duration of the induction period of the mixture.

Several other SCMs were tested as part of this study. Only one grade of GGBF slag (Grade 120) was incorporated in the dataset for the model, which does not provide enough information to draw conclusions about the mechanisms caused by different GGBF slag chemistries and finenesses. However, the results provide enough information to comment on the general trends seen with GGBF slag. GGBF slag reduced the rate of heat evolution of a mixture, reduced the slope of the accelerating portion of the hydration curve, and increased the induction period, just like the high-CaO fly ash. It should be noted that two different types of Grade 120 slag were tested, and four additional slags were included in the validation dataset. Also, ultra-fine fly ash and silica fume were tested as binary systems, and in ternary blends. The addition of silica fume slightly increased the peak rate of heat of hydration peak. Ultra-fine fly ash affected hydration like the parent fly ash from which it was derived¹⁷.

9.4.2. EFFECTS OF CHEMICAL ADMIXTURES ON HYDRATION

A variety of chemical admixtures were tested. An ASTM Type A low-range water reducer (LRWR) had a generally mild effect on the hydration parameters, while a Type B&D low-range water reducer/retarder (WRRET) increased both τ and β substantially. An ASTM Type C accelerator (ACCL) decreased τ . Also, most of the admixtures tested tended to increase β and decrease α_u . However, LRWR, WRRET, and ACCL tended to show some interaction with SCMs, which makes modeling of the various hydration parameters difficult.

9.5. SUGGESTED MODIFICATIONS TO HEAT OF HYDRATION VALUES OF CEMENTITIOUS MATERIALS

Previous chapters^{4,17} showed that α_u may increase with the addition of certain types and replacement percentages of SCM. Some of this behavior is likely due to an error in the estimate of the total amount of heat that may be evolved from mixtures with these SCMs. The heat of hydration values for SCMs in Equation 8-3 are based on a limited number of tests from the literature^{3,18}. However, given the number of tests presented here, it is possible to experimentally determine the heat contribution of each of the SCMs. Figure 9-1 compares the rate of heat evolution of determined from semi-adiabatic calorimetry for a mixture of 100% Cement C2 and a mixture of 40% GGBF slag and 60% Cement C2, with the rate of heat evolution normalized by the cement content in the mixture. In theory, the amount of heat evolved per gram of cement should not change if the SCM is inert. Since more heat is produced in the mixture with SCM, the additional heat must be attributed to the SCM. The difference between the heat

produced by the SCM mixture and the control approximates the contribution of the SCM to the total heat evolved.

9.5.1. ANALYSIS OF HEAT OF HYDRATION DATA

There are several steps to this analysis. First, the amount of heat evolved for each mixture after 150 hours of testing was measured as part of the calculation procedure^{2,3,15,21} for the hydration parameters. The results are an upper and lower bound estimate of heat evolution of the mixture. The lower bound is based only on the amount of heat measured to have come out of the mixture. The upper bound is the theoretical amount of heat evolved from the mixture based on a back-calculated adiabatic condition. This calculation is necessary to accurately estimate how a mixture would behave in a truly adiabatic test. The results generally correspond with the degree of hydration parameter (α_u) multiplied by H_u . Next, linear regression analysis and ANOVA (as will be done with the hydration parameters) was performed to identify the primary variables that affected the heat evolved.

9.5.2. RESULTS

An R^2 of 0.79 for the lower bound and 0.85 for the upper bound was obtained with only three variables: $p_{FA-CaO} \times p_{FA}$, p_{GGBF} , and $p_{S.F.}$. These results indicate that the effect of SCMs on the rate of heat evolution is significant. Based on these results, the contribution to heat of hydration from the CaO in the fly ash ($p_{FA-CaO} \times p_{FA}$) was between $1530 \times (p_{FA-CaO} \times p_{FA})$ J/gram and $2030 \times (p_{FA-CaO} \times p_{FA})$ J/gram. This agrees well with the value suggested in Equation 8-3 of $1800 \times (p_{FA-CaO} \times p_{FA})$ J/gram.

Next, the contribution to heat of hydration from the slag (p_{GGBF}) was between 500 and 800 J/gram. The value of 461 J/gram in Equation 8-3 is slightly lower, but was based

on the assumption that the GGBF slag contributed approximately as much heat as portland cement¹⁸. However, the reactivity of slag in the previous research¹⁸ is unknown. Grade 120 slag, which was used in the present research, should have a slag activity index of at least 95% of portland cement at 7 days, and 115% at 28 days when cured at 73°F (23°C)²². Based on the results presented here, the heat contribution of Grade 120 GGBF slag is suggested to be approximately 550 J/gram of slag, which is approximately 1.2 times the value for slag suggested previously^{3,18}.

Finally, the contribution to heat of hydration from the silica fume was between 290 and 370 J/gram. A uniform increase in α_u was seen with the addition of silica fume⁴. A value of 330 J/gram is thus recommended for the contribution of silica fume to the heat evolution of a mixture.

Based on the results of this study, Equation 9-4 should be modified as shown in Equation 9-7:

$$H_u = H_{cem} \cdot p_{cem} + 461 \cdot p_{GGBF-100} + 550 \cdot p_{GGBF-120} + 1800 \cdot p_{FA-CaO} \cdot p_{FA} + 330 \cdot p_{S.F.} \quad \text{Equation 9-7}$$

where $p_{GGBF-100}$ = % Grade 100 blast furnace slag (GGBF slag) in mixture; $p_{GGBF-120}$ = % Grade 120 blast furnace slag (GGBF slag) in mixture; and $p_{S.F.}$ = % silica fume in mixture, and all other variables are as previously defined in Equation 9-4.

9.5.3. CHALLENGES WITH DEGREE OF HYDRATION (α_U) MODELING

Care should be taken with interpretation of the results for the degree of hydration parameter, α_u , because this parameter represents a projected degree of hydration based on approximately 200 to 300 hours of equivalent age. It is the result of a best-fit of the semi-adiabatic data, and may not represent the true “ultimate” degree of hydration.

Variations in this parameter from results presented in literature are quite possible, especially if the heat of hydration of a material differs from Equation 9-4. However, the parameter is useful for estimating the early-age effects of different mixture parameters, and it can highlight heat of hydration differences between materials. Therefore, it will be referred to as the degree of hydration parameter, rather than the ultimate degree of hydration, for the remainder of the chapter.

Long-term heat of solution testing is likely necessary to obtain more accurate heat of hydration values for SCMs. This testing may also require companion calorimetry so that early age and later age results may be correlated. The results here only give an approximate indication of the amount of heat contributed by the SCMs. The large number and diversity of tests presented here confer a sense of confidence that interactions between the cement and the SCM are somewhat captured.

9.6. ANALYTICAL METHODS FOR HYDRATION MODEL

9.6.1. MODEL SELECTION

For this study, a linear or non-linear model for the exponential parameters may be appropriate. Figure 9-2⁶ and Figure 9-3⁶ compare the effects of different dosages of WRRET on τ and β of a variety of different mixtures. Linear increases in WRRET cause a non-linear increase in the hydration parameters, which suggests that a non-linear model may fit the data better. The linear form of a model is shown in Equation 9-8, and two non-linear forms of a model are shown in Equation 9-9³ and Equation 9-10.

$$y = c_0 + c_1 x_1 + c_2 x_2 + \dots \quad \text{Equation 9-8}$$

$$y = e^{c_0} \cdot x_1^{c_1} \cdot x_2^{c_2} \cdot \dots \quad \text{Equation 9-9}$$

$$y = \exp(c_0 + c_1 \cdot x_1 + c_2 \cdot x_2 + \dots)$$

Equation 9-10

where y = dependent variable, x_i = independent variable, and c_i = coefficient. Any of these forms of the model may be appropriate. Equation 9-8 is a linear model that is appropriate if the effect of each of the dependent variables (x_i) on the independent variable (y) is linear. However, if the effect of each x_i is non-linear, then the model should reflect this (as shown in Equation 9-9 and Equation 9-10). In addition, some combination of linear and non-linear models could be appropriate. Schindler and Folliard³ used a combined non-linear model of the forms shown in Equation 9-9 and Equation 9-10 to determine the best fit parameters of the exponential model. Both linear and non-linear models are included in the analysis.

The models shown in Equation 9-8 through Equation 9-10 were tested to see which model gave the best fit of the data. Equation 9-8 produce the poorest fit and Equation 9-9 provided the best fit. However Equation 9-9 required modification to account for values of x_i of 0, which made the model more complicated. All three models had an R^2 greater than 0.99. Therefore, Equation 9-10 was chosen for its simplicity, and because it modeled the nonlinear effects of WRRET and reactive SCMs better than a linear model.

9.6.2. VARIABLE SELECTION PROCEDURE

The first step to determine a model for hydration is to identify the trends in the hydration parameters that are visible without multivariate regression analysis. Table 9-1 summarizes the independent variables that were shown^{2,4,6} to have an effect on the parameters α_u , τ , and β (in Equation 9-1). From univariate analysis, several independent variables seemed to have a relatively large effect on the hydration parameters. The

independent variables that have the greatest effect on α_u , were % GGBF slag, % fly ash and % CaO in fly ash, % silica fume (SF), and dosages of WRRET, HRWR, and PCHRWR. The independent variables that have the greatest effect on τ were % GGBF slag, % fly ash and % CaO in fly ash, and dosages of WRRET and MRWR. The dependent variables that have the greatest effect on β were % fly ash and % CaO in fly ash, dosages of WRRET, HRWR, and PCHRWR, and w/c. These variables are potential candidates for inclusion in a multivariate model of the parameters in Equation 9-1.

The multivariate regression analysis has several steps. First, α_u , τ , β , and the independent variables from the semi-adiabatic test results are summarized in a database. Next, a specified number of combinations of the independent variables are analyzed and ranked according to their coefficient of determination (R^2). Additionally, the correlation coefficient, $Corr(x_1, x_2)$, between each of the variables (x_1 and x_2) is calculated to ensure that the variables are truly independent. For the purposes of this study, $Corr(x_1, x_2) < 0.65$ was chosen as a sufficiently weak correlation between two variables to allow both to be included in the model for α_u , τ , and β . The combination of variables that has the highest R^2 and a correlation coefficient for any two variables less than 0.65 is considered a candidate for the model. Next, an analysis of variance (ANOVA) for Type I and Type III errors is performed on each potential variable combination. A Type I error measures the probability that the model shows a relationship between an independent variable and the dependent variable (in this case, E_a) when there is really no relationship¹⁹. A Type III evaluates the probability that the choice of independent variables shows a statistical correlation, but that wrong direction or variable has been chosen¹⁹. Variables with a probability greater than 5% of Type I or III errors are not included in the model. These

errors are substantially reduced by selecting variables that have been clearly shown to affect hydration, such as those presented in Table 9-1. Finally, the analysis produces a linear multivariate model of the hydration parameters (α_u , τ , and β). The coefficients of the independent variables may be used as seed values for the non-linear analysis that is presented next. Both Bogue calculations and Rietveld analysis were used to determine the crystalline phases of the cement, so two sets of variables were selected using linear regression analysis. Computational details, code, and output from the linear regression analysis are included in Appendix G.

9.6.3. NON-LINEAR REGRESSION ANALYSIS

Previous research^{3,14} showed that the degree of hydration of a mixture is a rational function (a ratio of two polynomials) that depends on w/cm. The effects of other variables, such as GGBF slag, SF, or chemical admixtures can be modeled with linear, log-linear, or exponential relationships. Non-linear regression analysis allows these different relationships to be modeled together. To use least squares regression analysis, it is necessary to break the data into discrete points. This requires several steps. First, Equation 9-2 is solved for different time steps, which gives discrete points that quantify the equivalent age at each point of hydration. Then, the degree of hydration is calculated at each time using Equation 9-1. Equation 9-1 uses curve fit parameters (α_u , β , and τ) generated experimentally from the semi-adiabatic calorimeter tests. The result of the calculations is a discrete estimate of the degree of hydration at different equivalent ages. The experimental results may then be compared to the modeled results from non-linear regression analysis. The regression analysis minimizes the difference between the

measured degree of hydration and the predicted degree of hydration for each of the data points.

Figure 9-4 shows the output of the modeling procedure for a mixture of 70% Type I cement and 30% Class F fly ash. The regression analysis repeats this procedure for each of the 204 semi-adiabatic tests used as part of the calibration dataset. Next, a validation dataset, which has 58 semi-adiabatic tests, is used to assess the predictive ability of the model. In addition, 63 tests were repeated to determine the variability of the test method¹. The degree of hydration was calculated for each test at 18 different times. This combination of data gives a total of 3,672 data points to determine the parameters for the exponential hydration model, and 1,044 data points to validate the model. Computational details, code, and output from the non-linear regression analysis are included in Appendix G.

9.7. REGRESSION ANALYSIS RESULTS

Non-linear regression analysis was performed on the calibration dataset for two cases. The first case used cement crystalline phases as calculated by Rietveld analysis¹⁶. The results based on Rietveld data for α_u , τ , and β are shown in Equation 9-11 through Equation 9-13, respectively.

$$\alpha_u = \frac{1.031 \cdot w/cm}{0.194 + w/cm} + \exp \left(\begin{array}{l} -0.297 - 9.73 \cdot p_{\text{Ferrite}} \cdot p_{\text{cem}} \\ -325 \cdot p_{\text{Na}_2\text{O}+0.658 \cdot \text{K}_2\text{O}} \cdot p_{\text{cem}} \\ -8.90 \cdot p_{\text{FA}} \cdot p_{\text{FA-CaO}} \\ -331 \cdot \text{WRRET} - 93.8 \cdot \text{PCHRWR} \end{array} \right) \quad \text{Equation 9-11}$$

$$\tau = \exp \left(\begin{array}{l} 2.95 - 0.972 \cdot p_{\text{Alite}} \cdot p_{\text{cem}} + 152 \cdot p_{\text{Na}_2\text{O}} \cdot p_{\text{cem}} + 1.75 \cdot p_{\text{GGBF}} \\ + 4.00 \cdot p_{\text{FA}} \cdot p_{\text{FA-CaO}} - 11.8 \cdot \text{ACCL} + 95.1 \cdot \text{WRRET} \end{array} \right) \quad \text{Equation 9-12}$$

$$\beta = \exp \left(\begin{array}{l} -0.418 + 2.66 \cdot p_{Aluminate} \cdot p_{cem} - 0.864 \cdot p_{GGBF} \\ + 108 \cdot WRRET + 32.0 \cdot LRWR + 13.3 \cdot MRWR \\ + 42.5 \cdot PCHRWR + 11.0 \cdot NHRWR \end{array} \right) \quad \text{Equation 9-13}$$

where p_{Alite} = % C₃S in cement, as determined by Rietveld analysis, $p_{Aluminate}$ = % C₃A in cement, as determined by Rietveld analysis, $p_{Ferrite}$ = % C₄AF in cement, as determined by Rietveld analysis, p_{Na_2O} = % Na₂O in cement, $p_{Na_2O+0.658 \cdot K_2O}$ = % Alkalis as Na₂O, p_{cem} = % cement in mixture, p_{GGBF} = % blast furnace slag (GGBF slag) in mixture, p_{FA} = % fly ash in mixture, p_{FA-CaO} = % CaO in fly ash, $p_{S.F.}$ = % silica fume in mixture, $ACCL$ = accelerator, $WRRET$ = ASTM Type B&D water-reducer/retarder, $LRWR$ = ASTM Type A water reducer, $MRWR$ = mid-range water reducer, $NHRWR$ = ASTM Type F naphthalene or melamine-based high-range water reducer, and $PCHRWR$ = ASTM Type F polycarboxylate-based high-range water reducer. All SCM dosages are percent replacement by mass of cementitious material. All admixture dosages are percent solids (by mass) per mass of cementitious material.

The second case used cement crystalline phases determined from oxide analysis and Bogue calculations, and the results for α_u , τ , and β are shown in Equation 9-14 through Equation 9-16.

$$\alpha_u = \frac{1.031 \cdot w/cm}{0.194 + w/cm} + \exp \left(\begin{array}{l} -0.0885 - 13.7 \cdot p_{C_4AF} \cdot p_{cem} \\ - 283 \cdot p_{Na_2O+0.658 \cdot K_2O} \cdot p_{cem} \\ - 9.90 \cdot p_{FA} \cdot p_{FA-CaO} \\ - 339 \cdot WRRET - 95.4 \cdot PCHRWR \end{array} \right) \quad \text{Equation 9-14}$$

$$\tau = \exp \left(\begin{array}{l} 2.92 - 0.757 \cdot p_{C_3S} \cdot p_{cem} + 98.8 \cdot p_{Na_2O} \cdot p_{cem} + 1.44 \cdot p_{GGBF} \\ + 4.12 \cdot p_{FA} \cdot p_{FA-CaO} - 11.4 \cdot ACCL + 98.1 \cdot WRRET \end{array} \right) \quad \text{Equation 9-15}$$

$$\beta = \exp \left(\begin{array}{l} -0.464 + 3.41 \cdot p_{C_3A} \cdot p_{cem} - 0.846 \cdot p_{GGBF} \\ + 107 \cdot WRRET + 33.8 \cdot LRWR + 15.7 \cdot MRWR \\ + 38.3 \cdot PCHRWR + 8.97 \cdot NHRWR \end{array} \right) \quad \text{Equation 9-16}$$

where p_{C_3S} = % C₃S in cement, as determined by Bogue calculations, p_{C_3A} = % C₃A in cement, as determined by Bogue calculations, p_{C_4AF} = %C₄AF in cement, as determined by Bogue calculations, p_{Na_2O} = %Na₂O in cement, $p_{Na_2O+0.658 \cdot K_2O}$ = % Alkalis as Na₂O, p_{cem} = % cement in mixture, p_{GGBF} = % blast furnace slag (GGBF slag) in mixture, p_{FA} =%fly ash in mixture, p_{FA-CaO} = %CaO in fly ash, $p_{S.F.}$ = % silica fume in mixture, $ACCL$ = accelerator, $WRRET$ = ASTM Type B&D water-reducer/retarder, $LRWR$ = ASTM Type A water reducer, $MRWR$ = mid-range water reducer, $NHRWR$ = ASTM Type F naphthalene or melamine-based high-range water All SCM dosages are percent replacement by mass of cementitious material. All admixture dosages are percent solids (by weight) per weight of cementitious material. Variables for each model were chosen so that only the method of cement analysis changed.

The accuracy of the proposed model is evaluated from Figure 9-5, which plots the predicted degree of hydration versus the measured degree of hydration for all of the mixtures in the calibration dataset. The two solid gray lines represent the 95% confidence limits of semi-adiabatic calorimetry². 95% of the error is within a degree of hydration of ± 0.078 , which suggest that the model is a statistically significant predictor of hydration behavior. The error is randomly distributed for each of the independent variables. This is observed by plotting the residuals versus the independent variable. These results are shown in Appendix G. The choice of Rietveld analysis or Bogue calculations made very little difference in the accuracy of the regression model (R^2 for both models is 0.994), and the outliers were the same for both models. Also, the

coefficients in Equation 9-11 through Equation 9-13 were approximately the same as the coefficients in Equation 9-14 through Equation 9-16. Therefore, Bogue compounds may be used to model the hydration of a mixture, unless Rietveld calculations are available.

9.8. SENSITIVITY ANALYSIS OF HYDRATION MODEL

The following section discusses how one of the hydration models (Equation 9-14 through Equation 9-16) reacts to different variables by comparing the effects of changing independent variables on the estimated degree of hydration of a mixture. The model based on Bogue compounds was selected for the sensitivity analysis because the inputs are more readily available. However, the results for the two models are very similar. To evaluate the sensitivity of the model to each variable, a control mixture is selected, individual variables are changed, and the response of the model is assessed.

9.8.1. MODELED RESPONSE OF THE BEHAVIOR OF SUPPLEMENTARY CEMENTING MATERIALS

SCMs affect the hydration model in several ways. The percentage of fly ash and its % CaO affects the degree of hydration (α_u) and the time parameter (τ). τ increases as both the % CaO and % fly ash in the mixture increases, as shown in Figure 9-6. Increases in the % CaO of the fly ash delays hydration, and reduces α_u , which is reflected in Figure 9-7.

Increases in the % GGBF slag of a mixture raise τ , and lower β , as shown in Figure 9-8. The figure also shows very little difference between Rietveld analysis (Equation 9-11 through Equation 9-13) and Bogue calculations (Equation 9-14 through Equation 9-16). The increase in τ is reflected in the delay in the onset of hydration in Figure 9-9. These trends largely agree with the results shown in Table 9-1, and with the

results in previous research^{3,5}. Finally, silica fume has a very large effect on the amount of heat that a mixture will evolve. The new heat of hydration model (Equation 9-7) accounts for the contribution of silica fume to the heat of hydration of a mixture. Silica fume has little effect on the other hydration parameters.

9.8.2. MODELED RESPONSE OF THE BEHAVIOR OF WATER-CEMENTITIOUS MATERIALS RATIO (W/CM)

The w/cm was modeled with an equation first proposed by Mills¹⁴. This model has been effectively incorporated into a degree of hydration model³ and was used in the present research because it modeled the effects of w/cm on degree of hydration better than an exponential relationship. Increases in the w/cm will raise α_u and will increase $\alpha(t_e)$, as shown Figure 9-10.

9.8.3. MODELED RESPONSE OF THE BEHAVIOR OF CHEMICAL ADMIXTURES

The type and dosage of chemical admixtures in a concrete mixture will determine how the progress of hydration is altered. Admixtures that accelerate or retard the mixture will have the most notable effect on hydration. For example, the addition of increasing dosages of WRRET will cause τ and β to increase, as shown in Figure 9-11. The admixture will delay the accelerating portion of hydration, as shown in Figure 9-12. Increasing ACCL dosage will reduce τ , and will cause an accelerating shift in the degree of hydration curve, as shown in Figure 9-13. Other water-reducing admixtures have less of an effect on hydration. The slope parameter (β) increases with the addition of NHRWR, PCHRWR, MRWR, and LRWR, as shown in Figure 9-14. LRWR slightly retards hydration at high dosages, as shown in Figure 9-15. The remaining admixtures have a similarly mild effect on the degree of hydration.

9.8.4. MODELED RESPONSE OF THE BEHAVIOR OF CEMENT CHEMISTRY

The cement characteristics that are modeled by Equation 9-11 through Equation 9-16 are limited to C_4AF and $\%Na_2O_{eq}$ ($Na_2O + 0.658 \times K_2O$) for α_u , C_3S and Na_2O for τ , and C_3A for β . Additional variables were not justified by the ANOVA. Several trends were apparent.

In general, the amount of C_3A in a mixture will decrease as the amount of C_4AF increases. Though not perfectly related, it is useful to examine the effects of both compounds on the degree of hydration together. Figure 9-16 shows that α_u and β increase as C_3A increases (and C_4AF decreases). The increase in α_u is likely an artifact of the calculation procedure necessary for semi-adiabatic calorimetry, rather than an error in the measurement of the heat of hydration of the crystalline compounds in the cement. Figure 9-17 shows that the slope of the hydration curve increases as C_3A content increases, and shows that the amount of heat liberated by mixtures with high C_3A contents is, as expected, higher than mixtures with low C_3A during the first weeks of the model.

The amount of alkalis in the cement had a large effect on the degree of hydration. α_u decreases and τ increases as $\%Na_2O_{eq}$ and $\%Na_2O$ increases, respectively, as shown in Figure 9-18. An increase in $\%Na_2O_{eq}$ is accompanied by an increase in the $\%Na_2O$, and may be approximately modeled by assuming a ratio of Na_2O_{eq}/Na_2O equal to three. The coupled effects of the two variables are modeled in Figure 9-19. This figure shows that increasing the alkalis in the cement will generally retard the hydration of the mixture.

9.9. VALIDATION OF MODEL USING CALIBRATION DATASET

Two datasets of forty-four (44) semi-adiabatic calorimeter results have been previously published^{3,5}. Also, eighteen (18) tests, primarily from field sites, were withheld from the model calibration dataset. These results were used to examine the predictive ability of the model in Equation 9-14 through Equation 9-16. R^2 of the measured versus predicted $\alpha(t_e)$ for the prediction dataset was 0.98, which is similar to the accuracy reported previously⁵. Figure 9-20 shows most of the data are within the confidence limits of the test method. Tests that deviate from the model were generally mixtures with high volumes of SCM (>50%), high dosages of retarder, or field tests where ambient conditions around the calorimeter may have varied more than in the lab. These results strongly suggest that the model presented in this chapter successfully predicts the degree of hydration for mixtures with a wide variety of cement chemistries, SCMs, and chemical admixtures.

Ultimately, this type of modeling is limited by several factors. First, limited information is available about the cement, SCM, and admixture chemistries. Rietveld analysis is certainly more accurate than Bogue calculations, but in many instances, Bogue calculations are the only available information about cement. Also, CaO content is often the only information available about a fly ash, and it is perhaps not the best predictor of the hydraulicity of this material. The same is true for chemical admixtures, which are composed of combinations of different chemicals that may alter hydration. The user generally is only aware of the ASTM designation of the admixture, unless specific information is available about the composition and chemistry of these ingredients. The

lack of information available for the materials used in a mixture is perhaps the biggest limitation to accurately model hydration.

Next, the accuracy of semi-adiabatic calorimetry limits the accuracy of the model. For example, the 95% confidence limit for α_u is $\pm 8.8\%$. Most of the results in this study are within this range. Adiabatic calorimetry should be run if greater accuracy is expected. Finally, regression models of calorimetry data are limited to quantifying the effects of different treatments whose effects on a concrete mixture are relatively easily observed from test data. It is difficult to propose new mechanisms of hydration with this type of work. A better model requires much more detailed study of the pore solution chemistry, fly ash, slag, and silica fume solubility, and interactions with gypsum, aluminates, and chemical admixtures.

9.10. CONCLUSIONS

This chapter presents the results of a mechanistic-empirical model of concrete hydration based on over 300 semi-adiabatic calorimeter results. Activation energies were calculated for each of the mixtures using a previously developed model that has been calibrated based on 116 isothermal calorimeter results. The effects of cement chemistry, SCMs, and chemical admixtures were modeled using multivariate nonlinear regression analysis. The results show several trends. First, the reactivity of an SCM determines the magnitude of its effect on hydration. More reactive SCMs, such as high CaO fly ash and GGBF slag alter the hydration significantly, while less reactive SCMs, like low-CaO fly ash, act primarily by dilution. This result is supported by literature. However, the precise interactions between SCMs, cement, and admixtures have not been explicitly modeled. This is primarily due to the test method used. In addition, complementary

information about the pore solution chemistry, crystalline phases of both the SCM and cement, and admixtures would be necessary to divulge the true mechanistic models of hydration.

Second, admixtures that contain retarders and accelerators have the greatest impact on the accelerating portion of the hydration curve. Many admixtures, such as water reducers or viscosity modifying admixtures may contain these ingredients. It is therefore important to fully understand what is actually in a particular chemical admixture.

Third, w/cm greatly impacts the degree of hydration. This has been shown previously^{3,14} and is again confirmed by the model presented here. Finally, the effects of cement chemistry are modeled using only five variables: C_3S , C_3A , C_4AF , % Na_2O , and % K_2O . The C_3A , C_4AF , and alkalis appear to interact in a manner consistent with known mechanisms. However the models presented here suggest that hydration depends on less variables than previously thought^{3,5}. The final model, based on Bogue compounds, is as defined in Equation 9-14, Equation 9-15, and Equation 9-16.

The model presented here accounts for only the major variables, and more subtle differences between cement types are not detected. The accuracy of the model is ultimately limited by the accuracy of the underlying test methods and the lack of information available on the SCMs composition (beyond CaO) and admixture composition. Nevertheless, the model successfully predicts the hydration behavior for a large variety of mixtures. The results of the model can become inaccurate if high volumes of SCMs are used (>50%), or if large amounts of retarder are used, such as in

the case of an overdose. To successfully estimate these trends, more testing would be needed at higher dosages of admixture or SCM.

9.11. REFERENCES

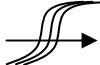





















1. ACI Committee 207, “Mass Concrete”, ACI 207.1R-05, American Concrete Institute, Farmington Hills, Michigan, 2005.
2. Poole, J.L., “Hydration Study of Cementitious Materials Using Semi-Adiabatic Calorimetry,” PhD Dissertation, Chapter 6, The University of Texas at Austin, Austin, TX, 2007, pp 141-171.
3. Schindler, A.K., and K.J. Folliard, “Heat of Hydration Models for Cementitious Materials”, *ACI Materials Journal*, V. 102, No. 1, Jan.-Feb., 2005, pp. 24-33.
4. Poole, J.L., “Hydration Study of Supplementary Cementing Materials Using Semi-Adiabatic Calorimetry,” PhD Dissertation, Chapter 8, The University of Texas at Austin, Austin, TX, 2007, pp 216-257.
5. Ge, Zhi, “Predicting Temperature and Strength Development of the Field Concrete”, PhD Dissertation, Iowa State University, 2006.
6. Poole, J. L., “Study of the Effects of Chemical Admixtures on Hydration,” PhD Dissertation, Chapter 7, The University of Texas at Austin, Austin, TX, 2007, pp 172-215.
7. Pane, I., and W. Hansen, “Concrete Hydration and Mechanical Properties under Nonisothermal Conditions,” *ACI Materials Journal*, V. 99, No. 6, Nov.-Dec, 2002, pp. 534-542.

8. Freiesleben Hansen, P. and Pederson, E. J., "Curing of Concrete Structures," Draft DEB-Guide to Durable Concrete Structures, Appendix 1, Comité Euro-International Du Béton, Switzerland, 1985.
9. D'Aloia, L., and G. Chanvillard, "Determining the "Apparent" Activation Energy of Concrete; E_a – Numerical Simulations of the Heat of Hydration of Cement," *Cement and Concrete Research*, V. 32, 2002, pp. 1277-1289.
10. Kada-Benameur, H., E. Wirquin, and B. Duthoit, "Determination of Apparent Activation Energy of Concrete by Isothermal Calorimetry," *Cement and Concrete Research*, V. 30, 2000, pp. 301-305.
11. Copeland, L.E., Kantro, D.L., Verbeck, G., "Part IV-3 Chemistry of Hydration of Portland Cement," 4th International Symposium of the Chemistry of Cement, Washington, D.C., 1960, pp. 429-465.
12. De Schutter, G., and Taerwe, L., "Degree of Hydration-Based Description of Mechanical Properties of Early-Age Concrete," *Materials and Structures*, Vol. 29, No. 7, 1996, pp. 335-344.
13. Verbeck, G., and Forster, C.W. "Long-Time Study of Cement Performance in Concrete. Chapter 6 – The Heats of Hydration of the Cement," *Proceedings of the American Society for Testing Materials*, Vol. 50, 1950, pp. 1235-1262.
14. Mills, R H. "Factors Influencing Cessation of hydration in Water Cured Cement Pastes." Special Report 90: Symposium on Structure of Portland Cement Paste and Concrete. Washington, D.C.: Highway Research Board, 1966. 406-424.

15. Poole, J.L., “A Model for Estimating the Activation Energy of Cementitious Systems,” PhD Dissertation, Chapter 5, The University of Texas at Austin, Austin, TX, 2007, pp 109-140.
16. Scrivener, K.L., T. Füllmann, E. Gallucci, G. Walenta, and E. Bermejo, “Quantitative Study of Portland Cement Hydration by X-Ray Diffraction/Rietveld Analysis and Independent Methods”, *Cement and Concrete Research*, V. 34, 2004, pp 1541-1547.
17. Poole, J.L., “The Effects of Supplementary Cementing Materials on Activation Energy of SCMs,” PhD Dissertation, Chapter 4, The University of Texas at Austin, Austin, TX, 2007, pp 69-108.
18. Maekawa, K., R. Chaube, and T. Kishi, *Modelling of Concrete Performance: Hydration, Microstructure Formation, and Mass Transport*, E&FN Spon, London, 1999.
19. Devore, Jay L., *Probability and Statistics for Engineering and the Sciences*, 4th ed. Duxbury Press, New York, 743 p, 1995.
20. Schindler, A.K., “Concrete Hydration, Temperature Development, and Setting at Early-Ages,” Ph.D. Dissertation, University of Texas at Austin, Austin, TX, 2002, 531 pp.
21. RILEM 119-TCE, “Adiabatic and Semi-Adiabatic Calorimetry to Determine the Temperature Increase in Concrete due to Hydration Heat of Cement,” RILEM Report 15, R. Springenschmid, ed., E&FN Spon, London, 1999, pp. 315-330.

22. ASTM C 989, “Standard Specification for Ground Granulated Blast-Furnace Slag for Use in Concrete and Mortars,” Annual Book of ASTM Standards, V. 04.01., ASTM International, West Conshohocken, PA., 2005, 5 pp.

Table 9-1: Effect of Different Mixture Characteristics on Exponential Model Hydration Parameters^{2,4,6}

Variable	Range of Tests	Effect on τ	Effect on β	Effect on α_u
Fly Ash (%Replacement)	15-55%			
Fly Ash (CaO%)	0.7-28.9% CaO			Varies
GGBF slag	30-70%	Large 	Small 	Varies
Silica Fume	5-10%	None	None	Small 
LRWR	0.22-0.29%	Varies	Small 	Varies
WRRET	0.18-0.53%	Large 	Large 	Large 
MRWR	0.34-0.74%	Large 	Small 	Varies
HRWR	0.78-1.25%	None	Small 	Small 
PCHRWR	0.27-0.68%	None	Small 	Small 
ACCL	0.74-2.23%	Small 	None	Varies
AEA	0.04-0.09%	None	None	None
Increasing w/c	0.32-0.68	None	None	Large 
Placement Temp	15-38 °C (50-100 °F)	None	None	None
Increase Cement Fineness	350-540 m ² /kg	Small 	Small 	Varies

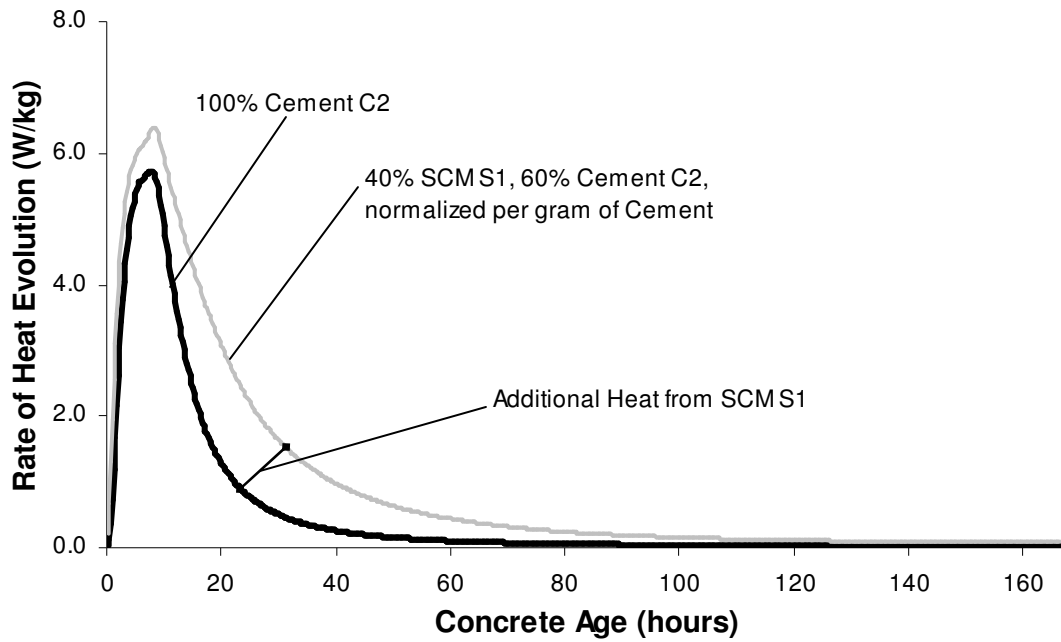


Figure 9-1: Rate of Heat Evolution (per gram of Cement) for a Control Mixture, and a Mixture with 40% GGBF Slag

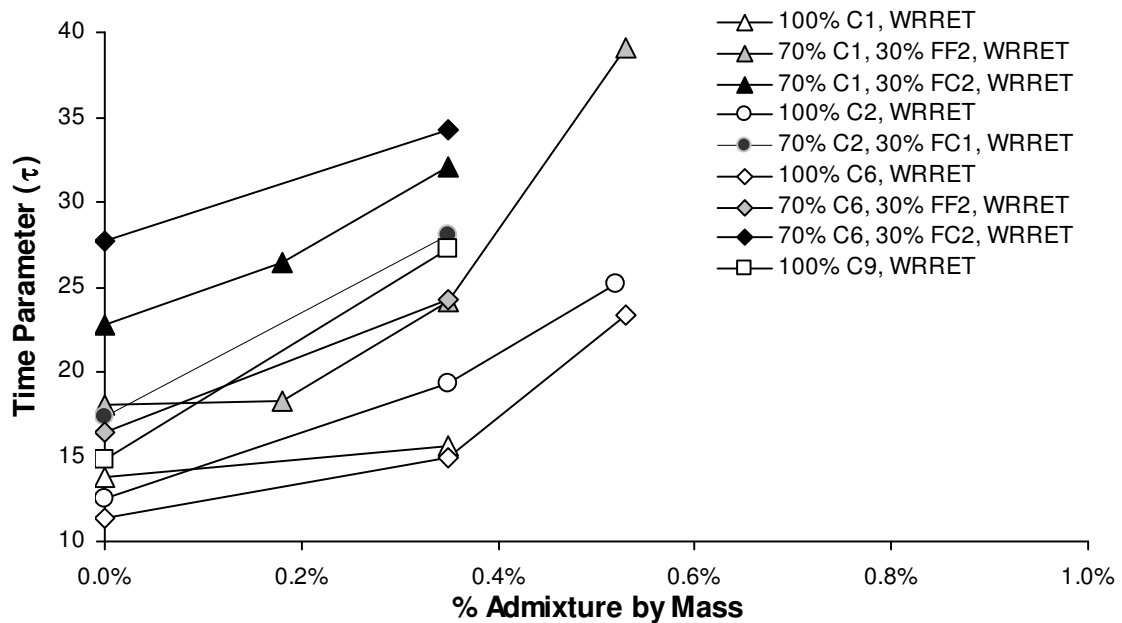


Figure 9-2: Effects of Type B&D WRRET on Time Parameter (τ)

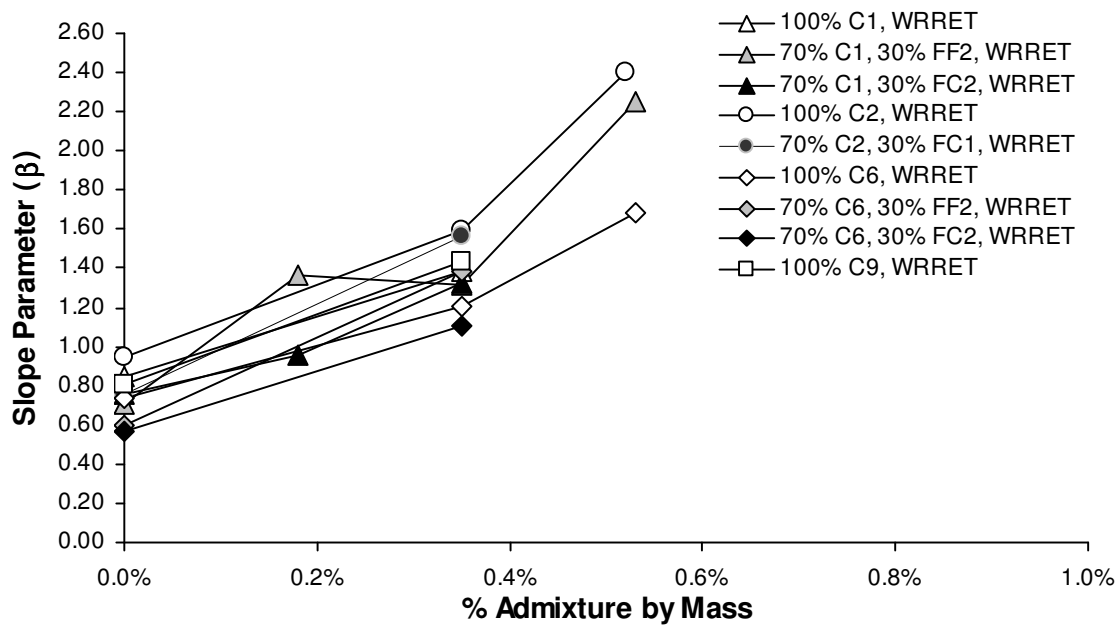


Figure 9-3: Effects of Type B&D WRRET on Slope Parameter (β)

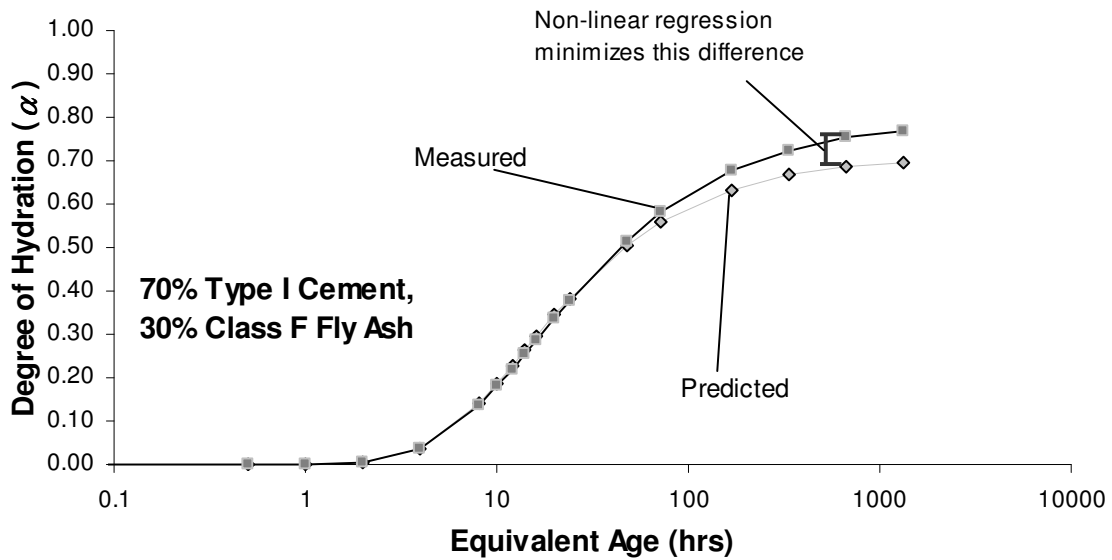


Figure 9-4: Regression Analysis Results for a Mixture of 70% Type I Cement and 30% Class F Fly Ash

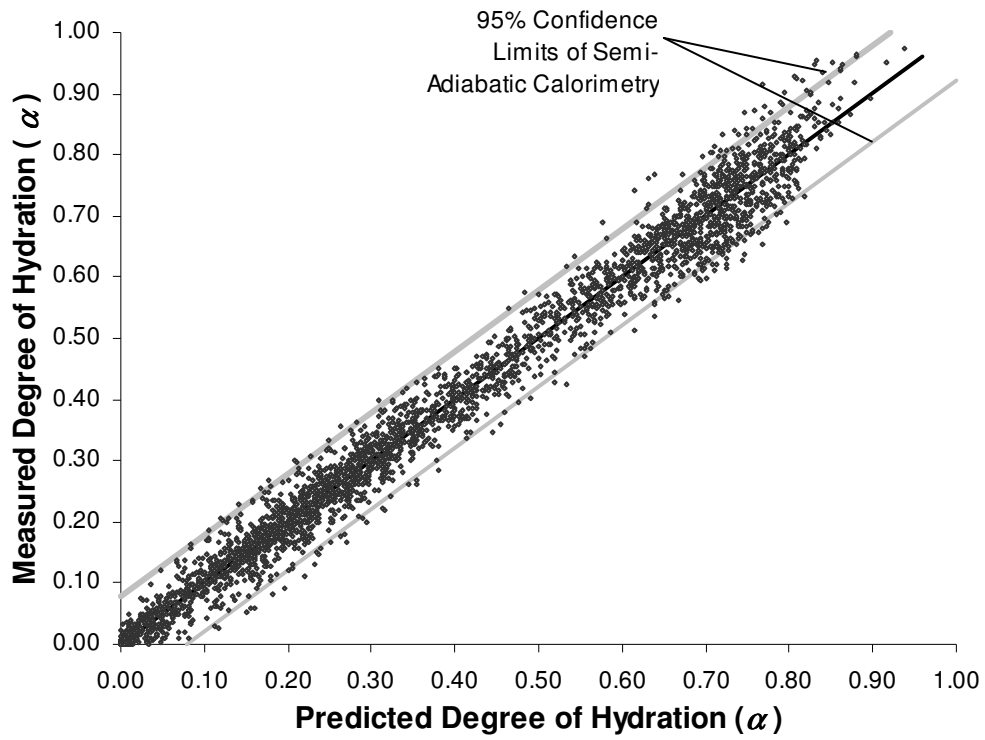


Figure 9-5: Predicted Versus Measured Degree of Hydration for Bogue Model

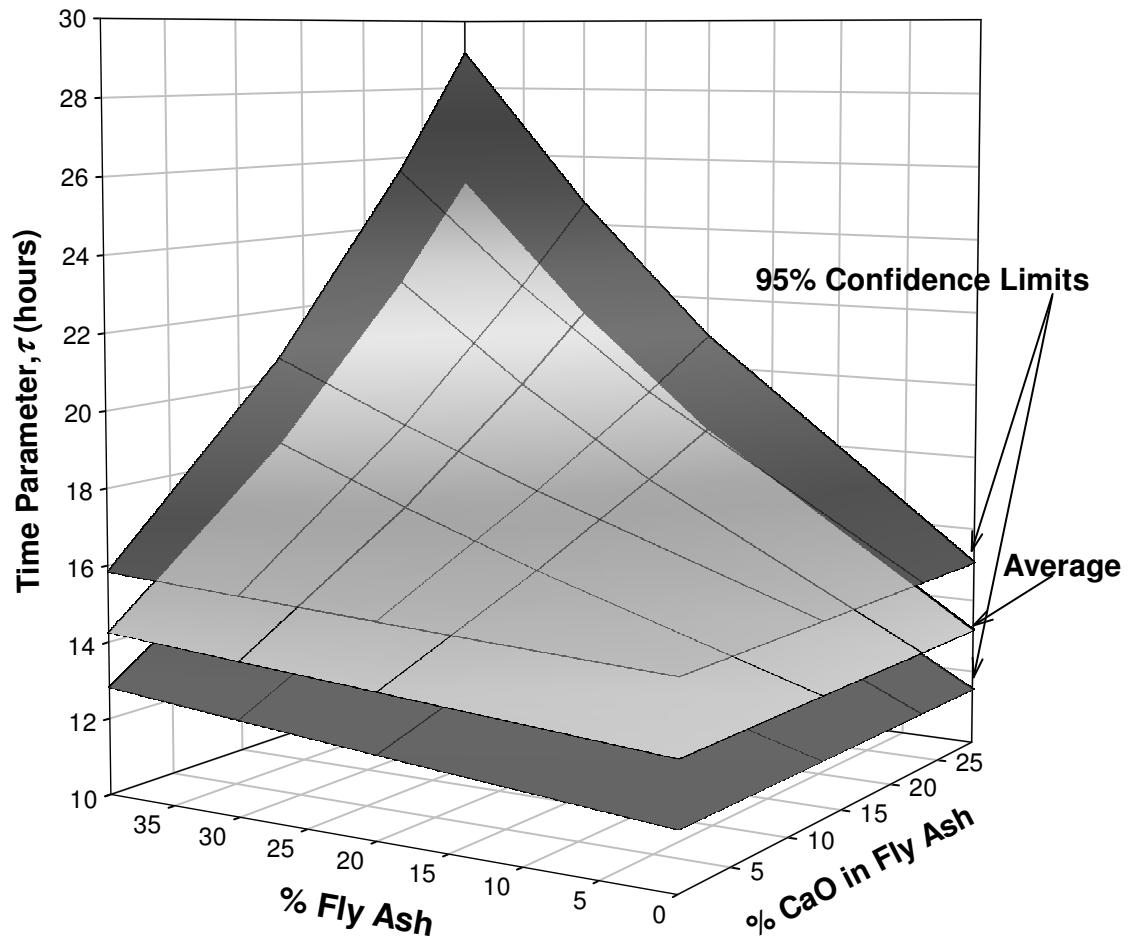


Figure 9-6: Effect of % Fly Ash and % CaO in Fly Ash on Time Parameter, τ

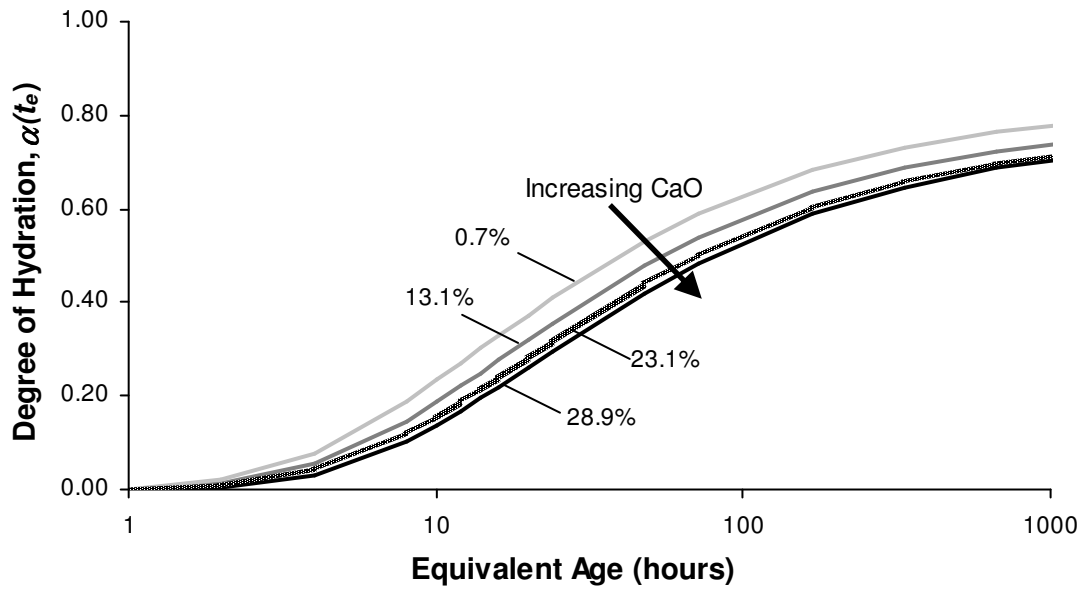


Figure 9-7: Effect of Fly Ash % CaO on Degree of Hydration

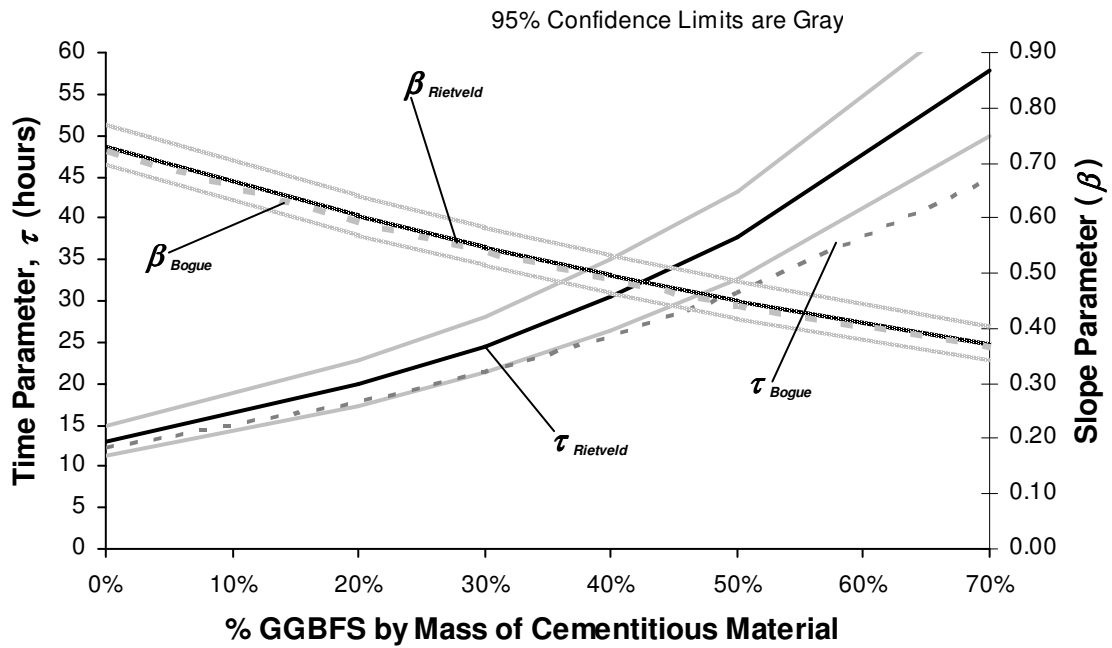


Figure 9-8: Effect of % GGBF Slag on τ and β

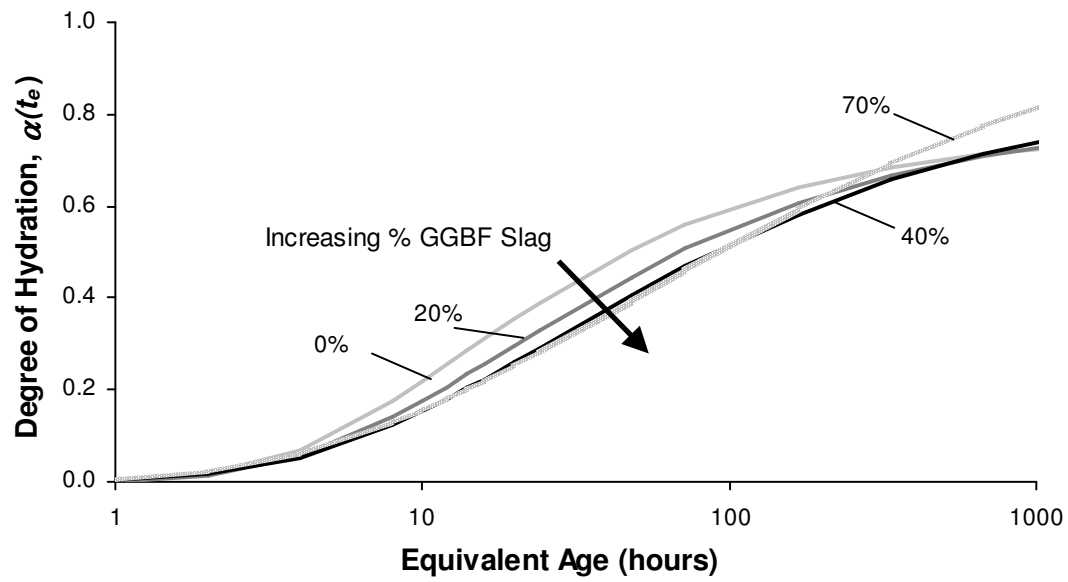


Figure 9-9: Effect of % GGBF Slag on Degree of Hydration

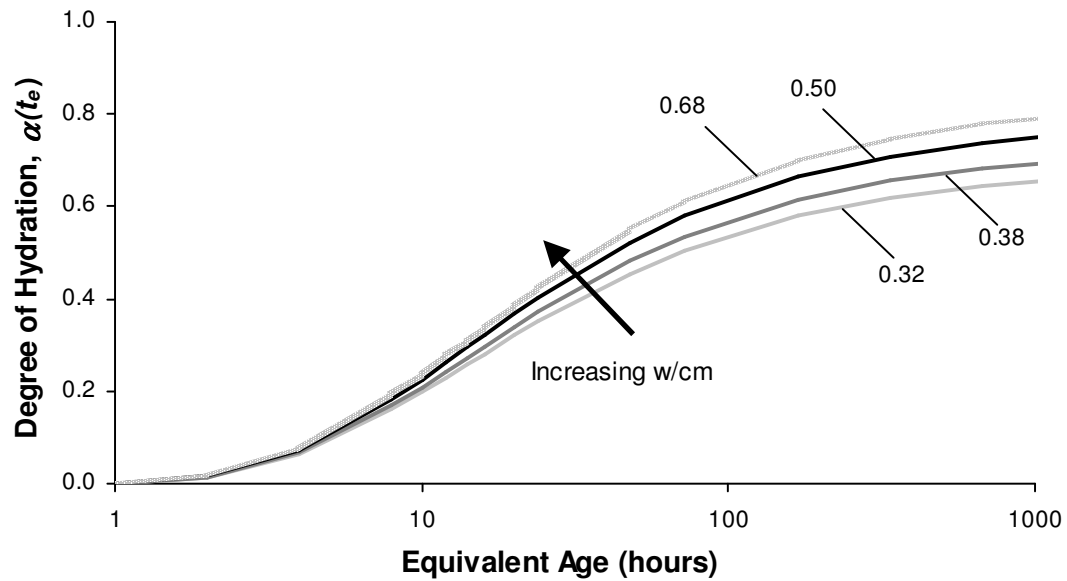


Figure 9-10: Effect of w/cm on Degree of Hydration

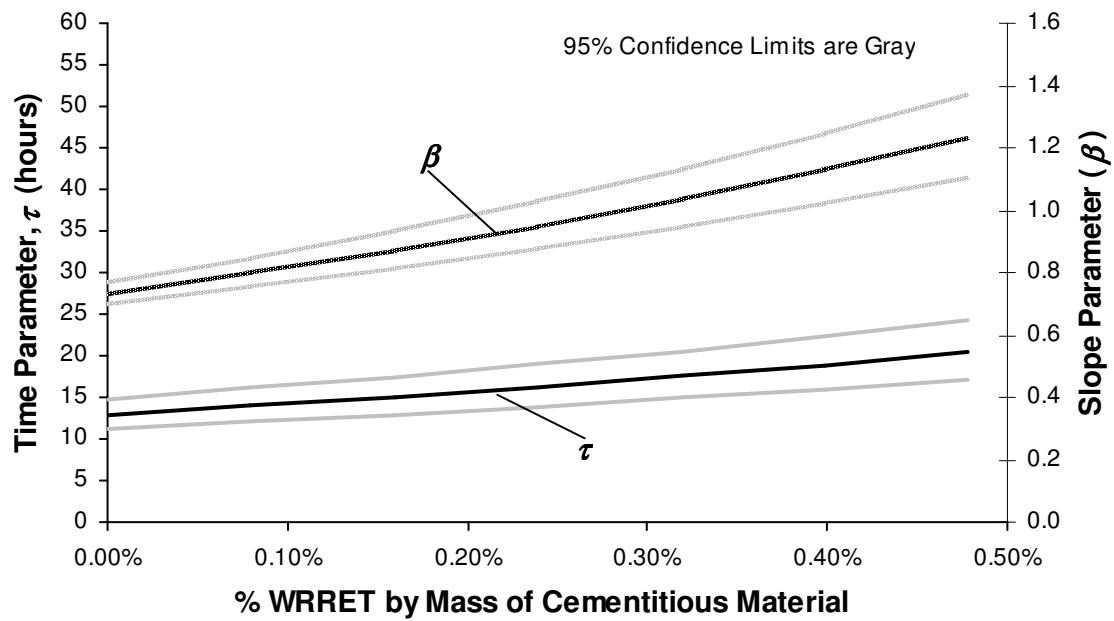


Figure 9-11: Effect of Type B&D WRRET on Time (τ) and Slope Parameter (β)

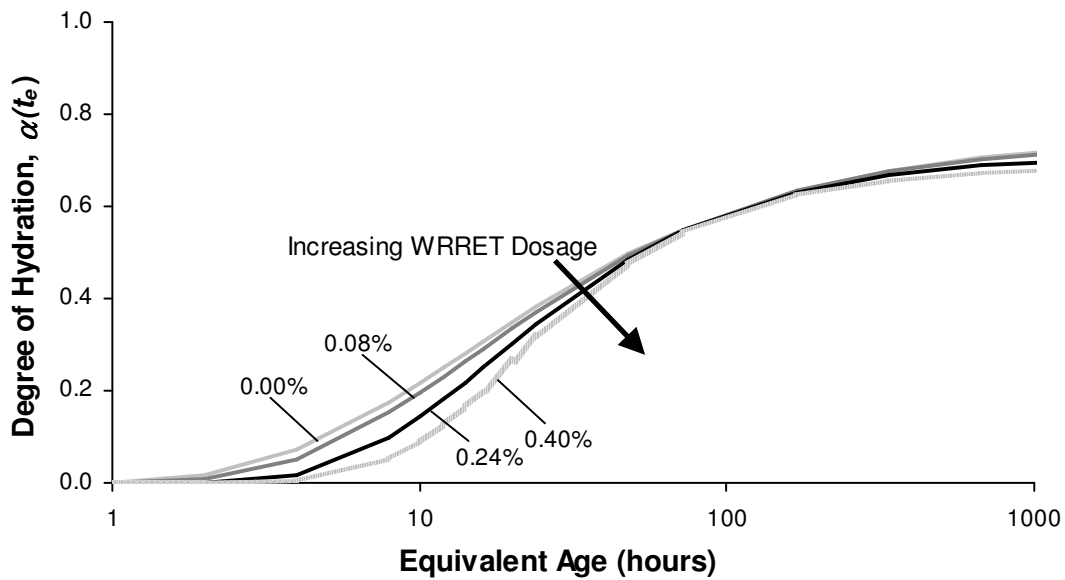


Figure 9-12: Effect of Type B&D WRRET Dosage on Degree of Hydration

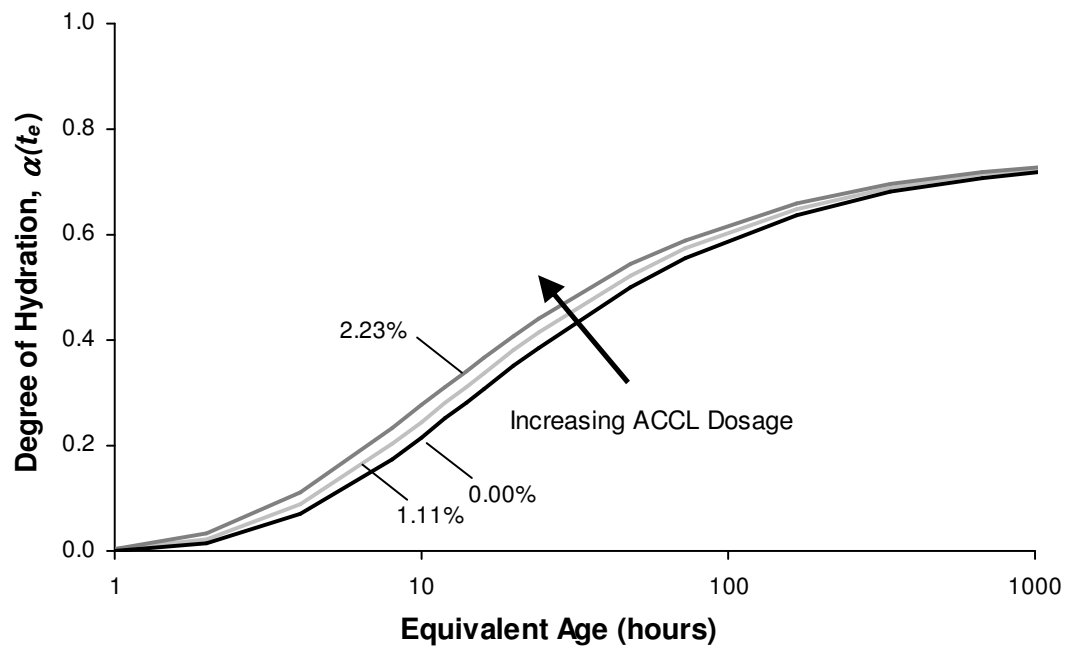


Figure 9-13: Effect of Type C ACCL Dosage on Degree of Hydration

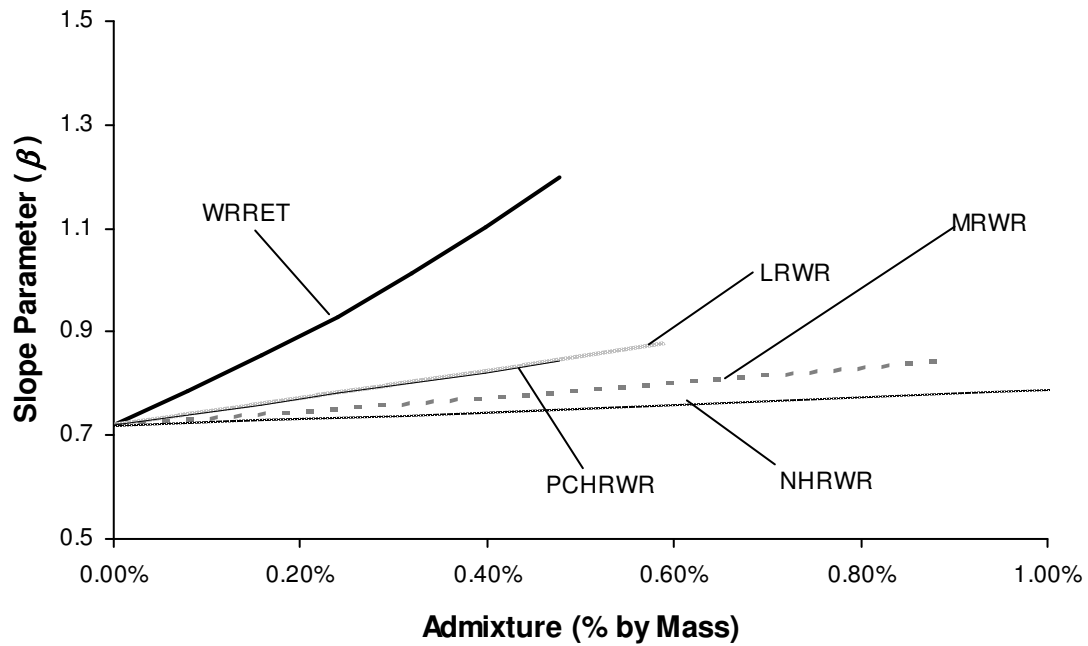


Figure 9-14: Effect of Various Water Reducers on the Slope Parameter, β

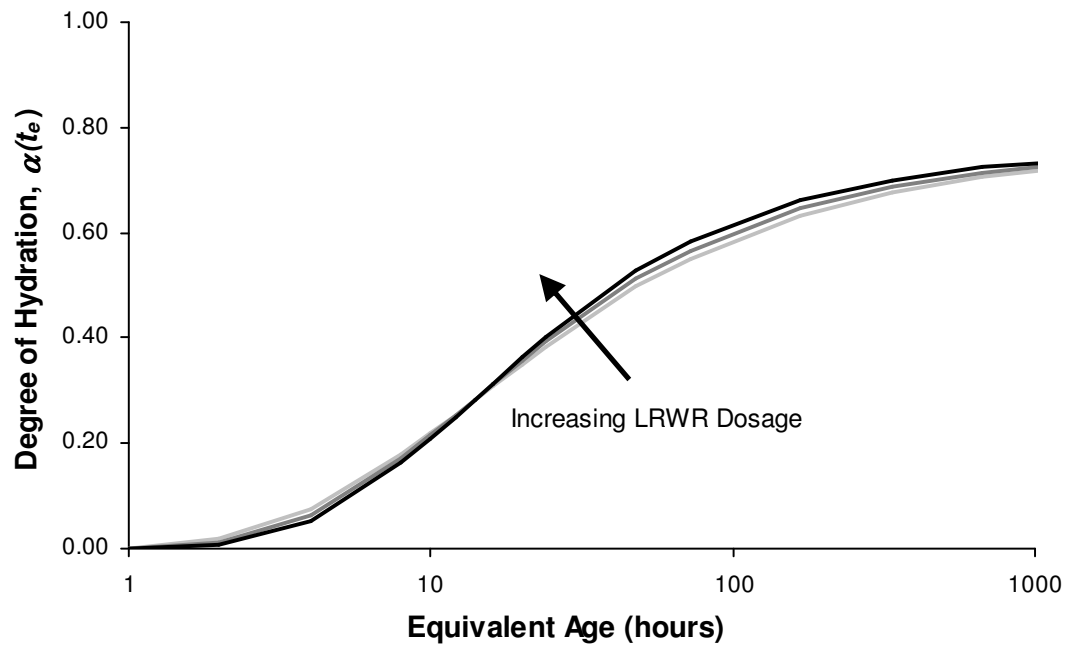


Figure 9-15: Effect of ASTM Type A LRWR on Degree of Hydration

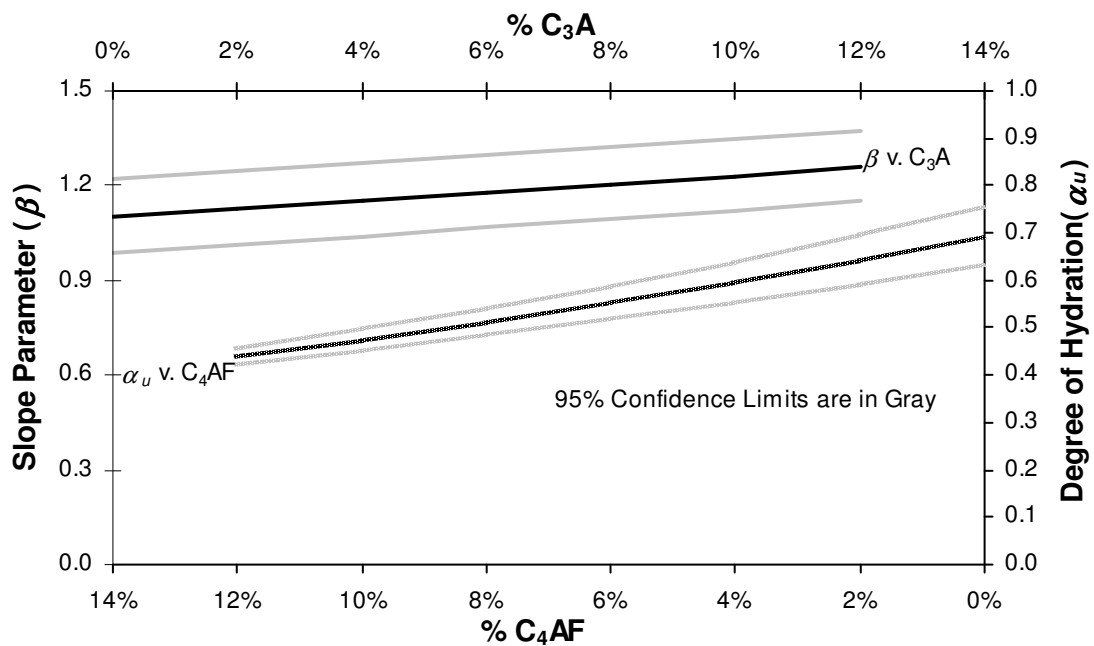


Figure 9-16: Effect of C_3A on Degree of Hydration Parameter (α_u) and C_4AF on Slope Parameter (β)

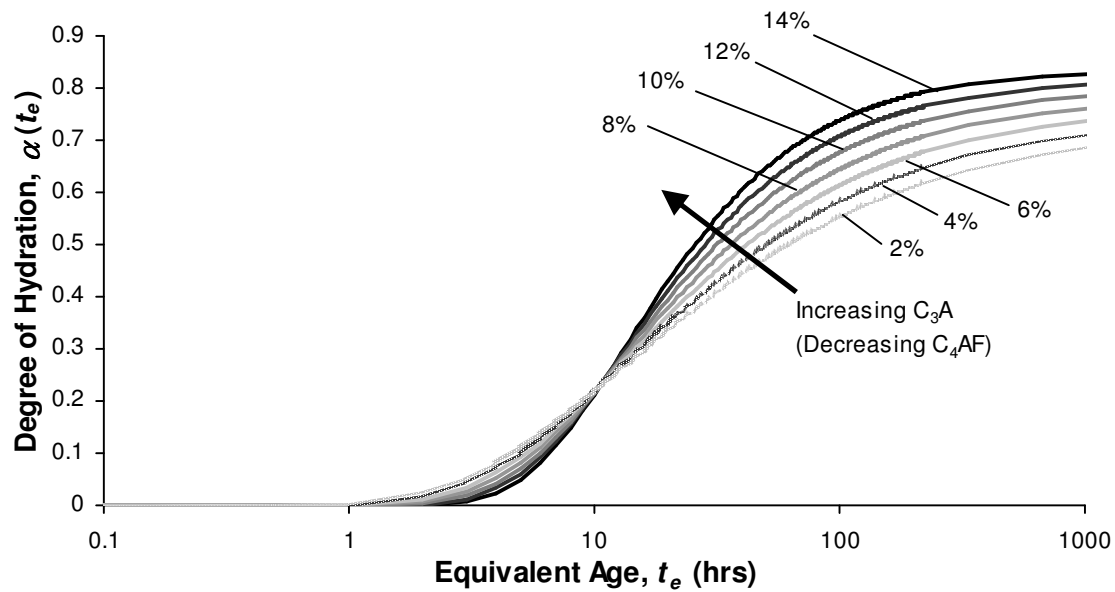


Figure 9-17: Effect of C_3A/C_4AF on Degree of Hydration

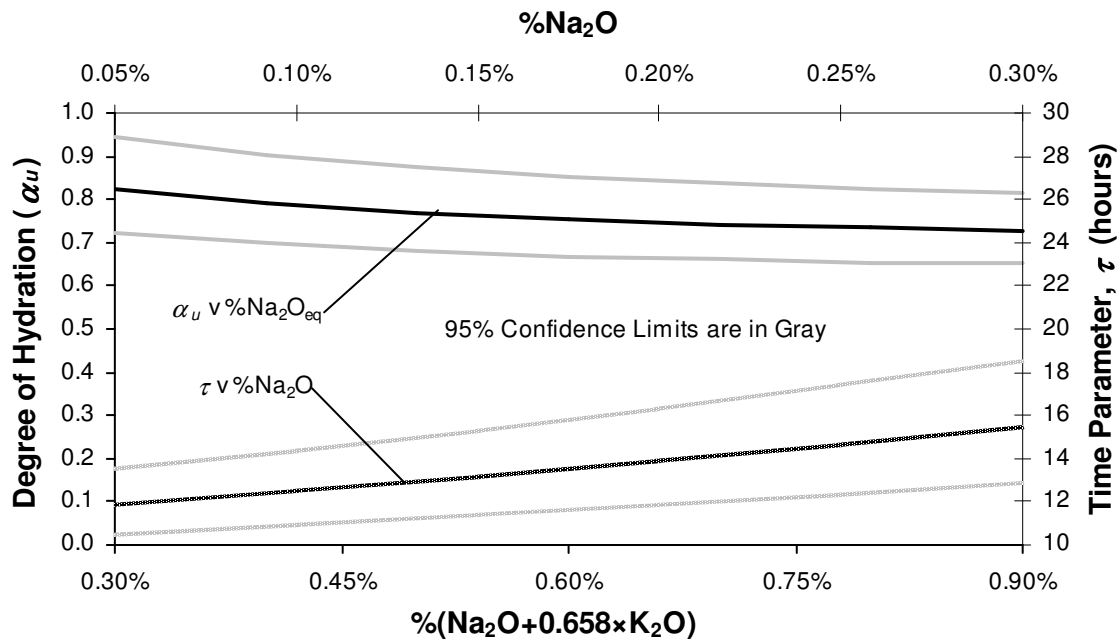


Figure 9-18: Effect of $\%Na_2O_{eq}$ on Degree of Hydration Parameter (α_u) and $\%Na_2O$ on Time Parameter (τ)

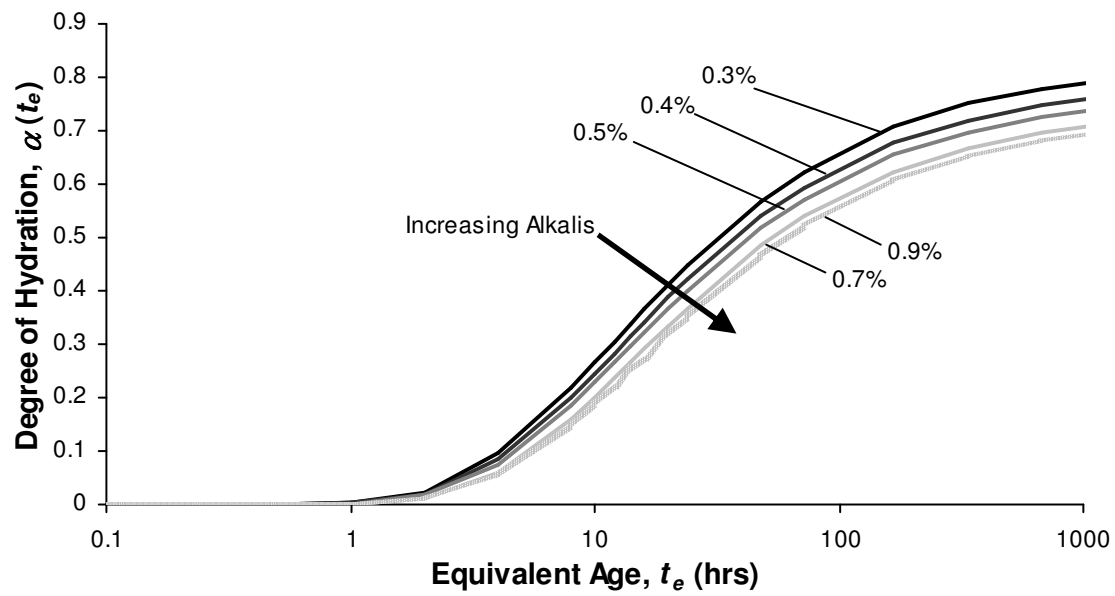


Figure 9-19: Effect of %Na₂O_{eq} on Degree of Hydration

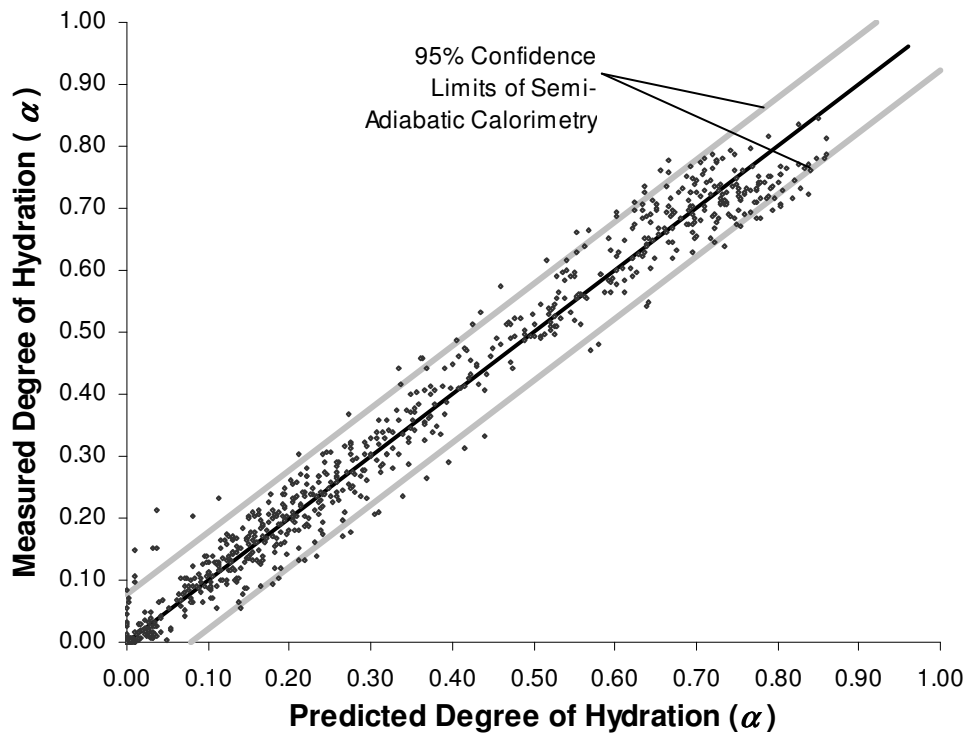


Figure 9-20: Predicted Versus Measured Degree of Hydration for Validation Dataset – Bogue Model

APPENDICES

APPENDIX A. ADDITIONAL ISOTHERMAL RESULTS FOR CHAPTER 2

A.1. EFFECTS OF W/CM ON RATE OF HEAT EVOLUTION OF 100% CEMENT PASTES

The following figures provide background for the effects of w/cm on hydration presented in Chapter 2. Results at each of the isothermal test temperatures are shown. Figure A.1 through Figure A.5 show the effects of w/cm on a mixture of 100% cement C2, and Figure A.6 through Figure A.10 show the same trends on a mixture of 100% cement C6.

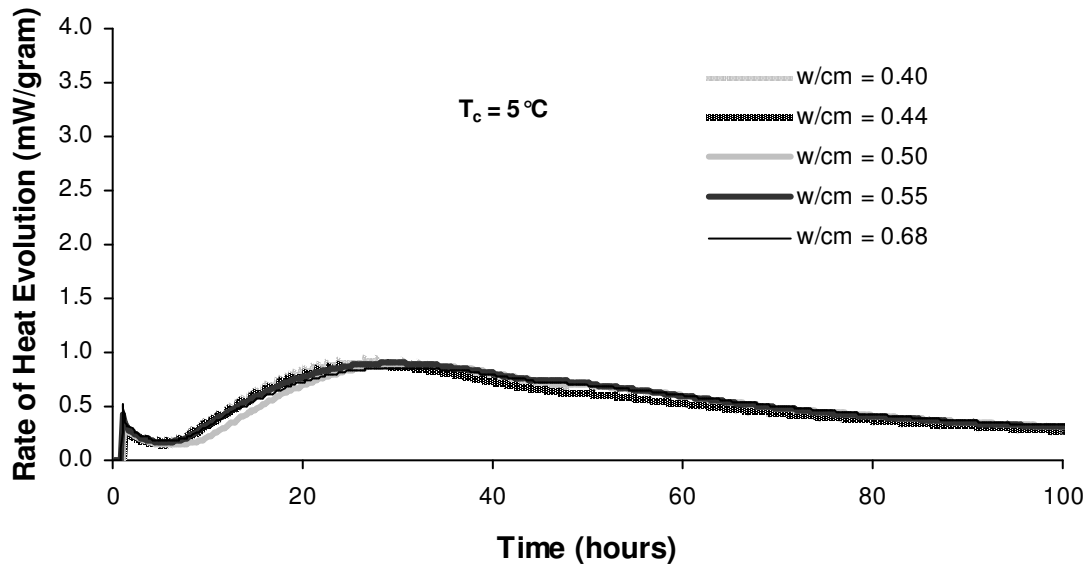


Figure A.1: Effects of w/cm on Rate of Heat Evolution of a Mixture of 100% Cement C2 (Paste) at 5 °C (41 °F)

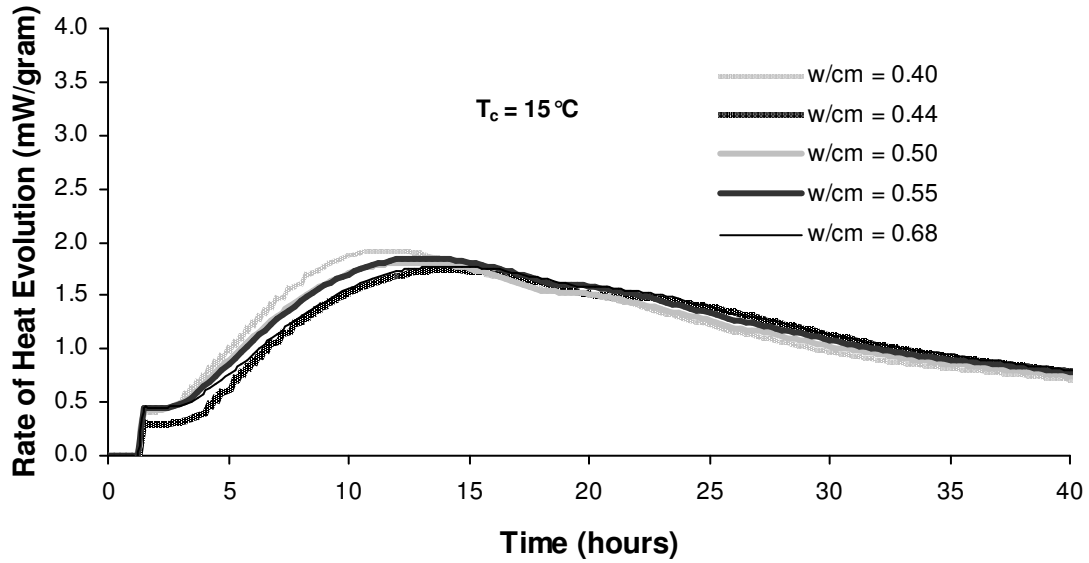


Figure A.2: Effects of w/cm on Rate of Heat Evolution of a Mixture of 100% Cement C2 (Paste) at 15 °C (59 °F)

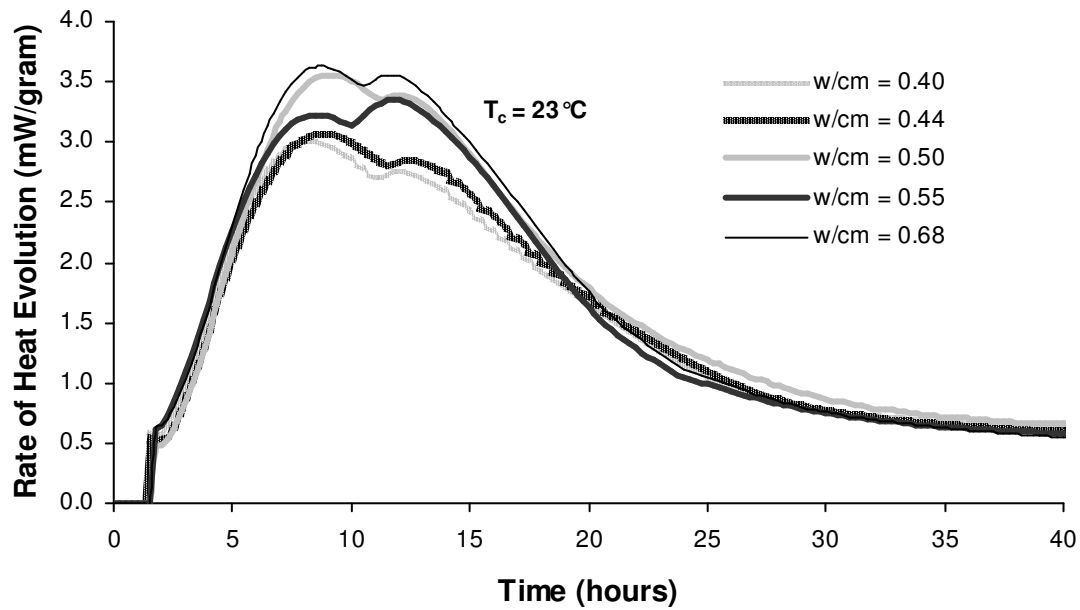


Figure A.3: Effects of w/cm on Rate of Heat Evolution of a Mixture of 100% Cement C2 (Paste) at 23 °C (73 °F)

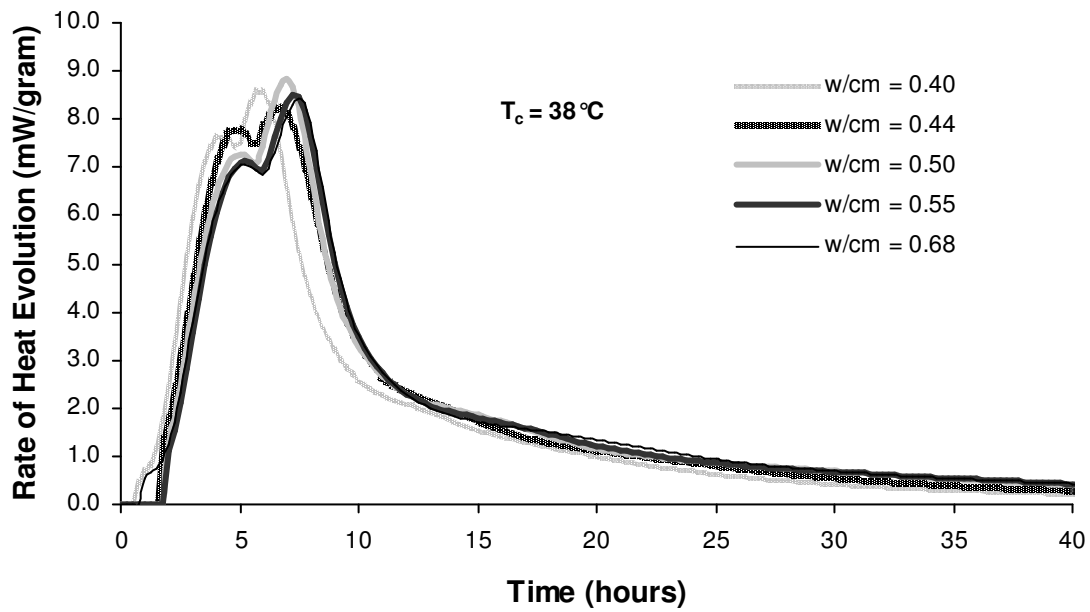


Figure A.4: Effects of w/cm on Rate of Heat Evolution of a Mixture of 100% Cement C2 (Paste) at 38°C (100°F)

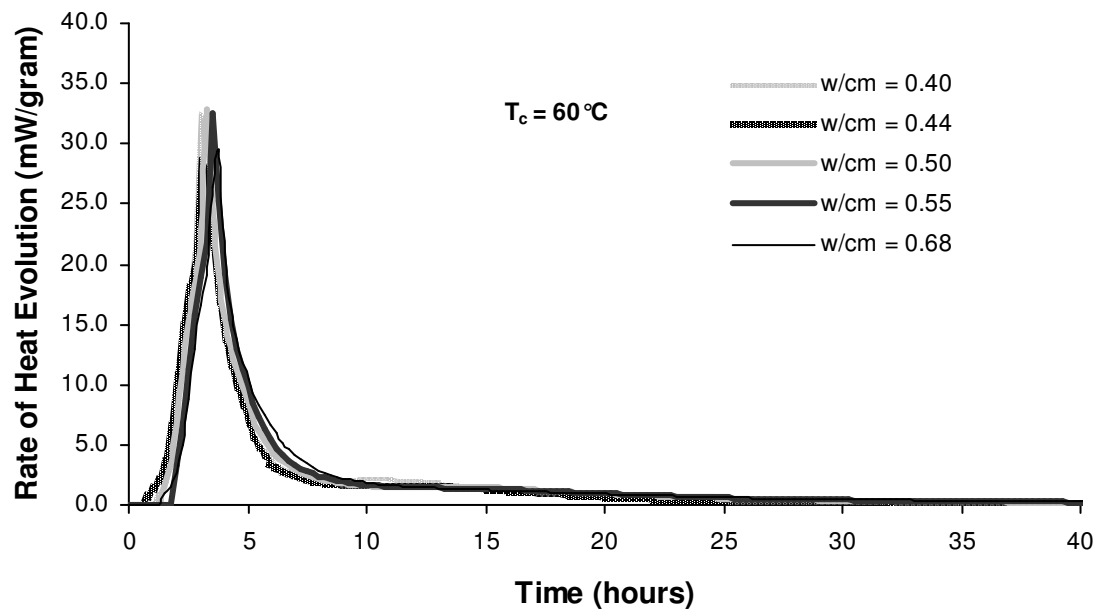


Figure A.5: Effects of w/cm on Rate of Heat Evolution of a Mixture of 100% Cement C2 (Paste) at 60°C (140°F)

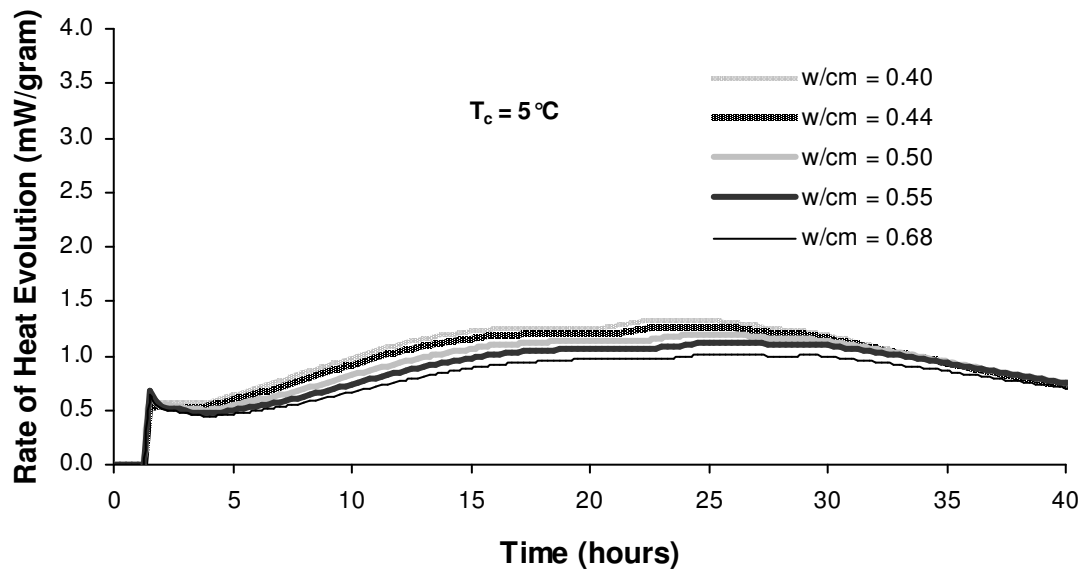


Figure A.6: Effects of w/cm on Rate of Heat Evolution of a Mixture of 100% Cement C6 (Paste) at 5 °C (41 °F)

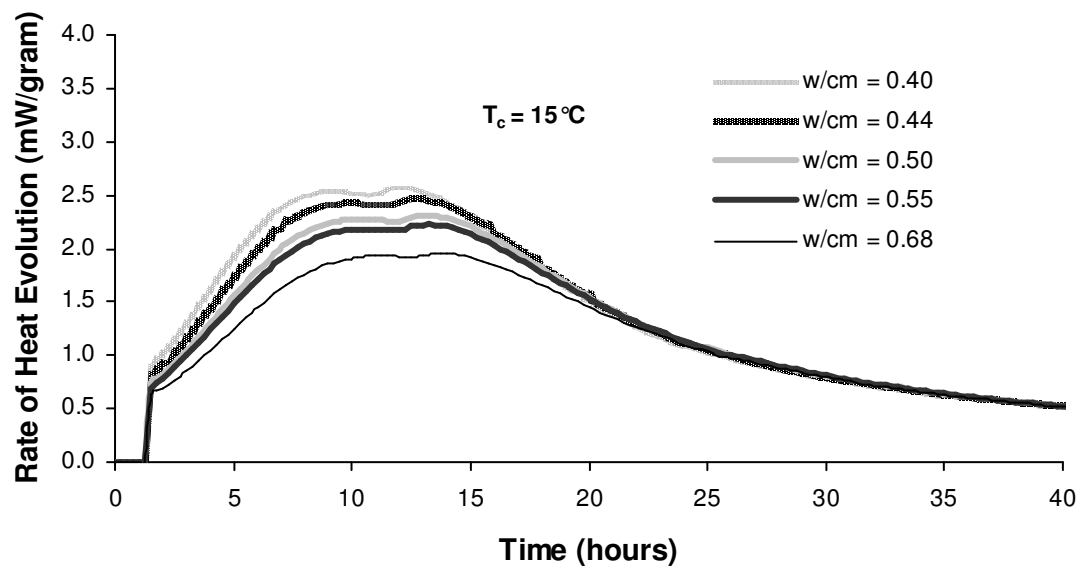


Figure A.7: Effects of w/cm on Rate of Heat Evolution of a Mixture of 100% Cement C6 (Paste) at 15 °C (59 °F)

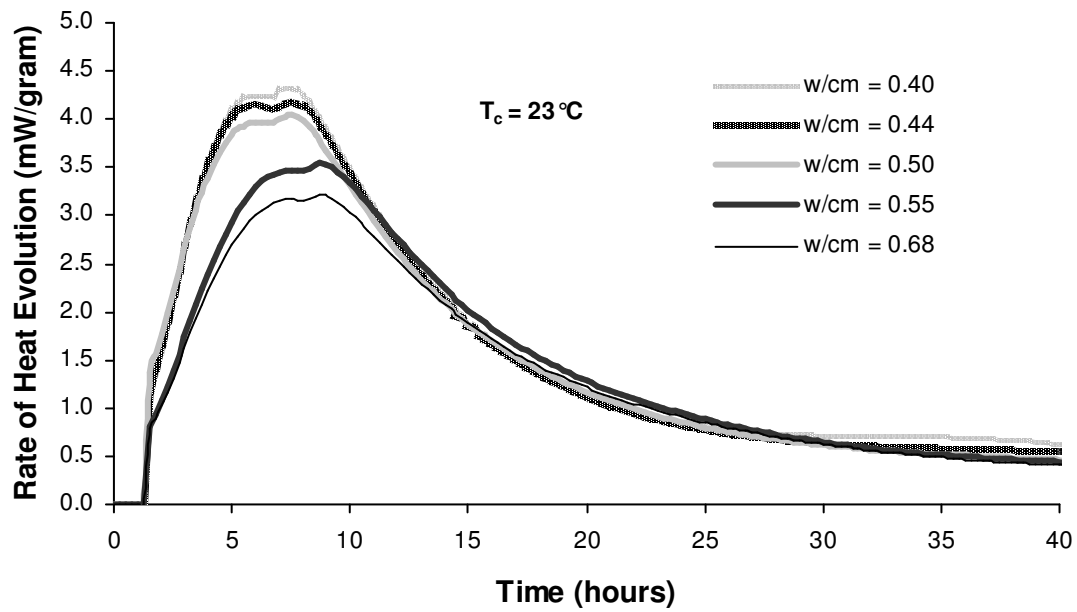


Figure A.8: Effects of w/cm on Rate of Heat Evolution of a Mixture of 100% Cement C6 (Paste) at 23 °C (73 °F)

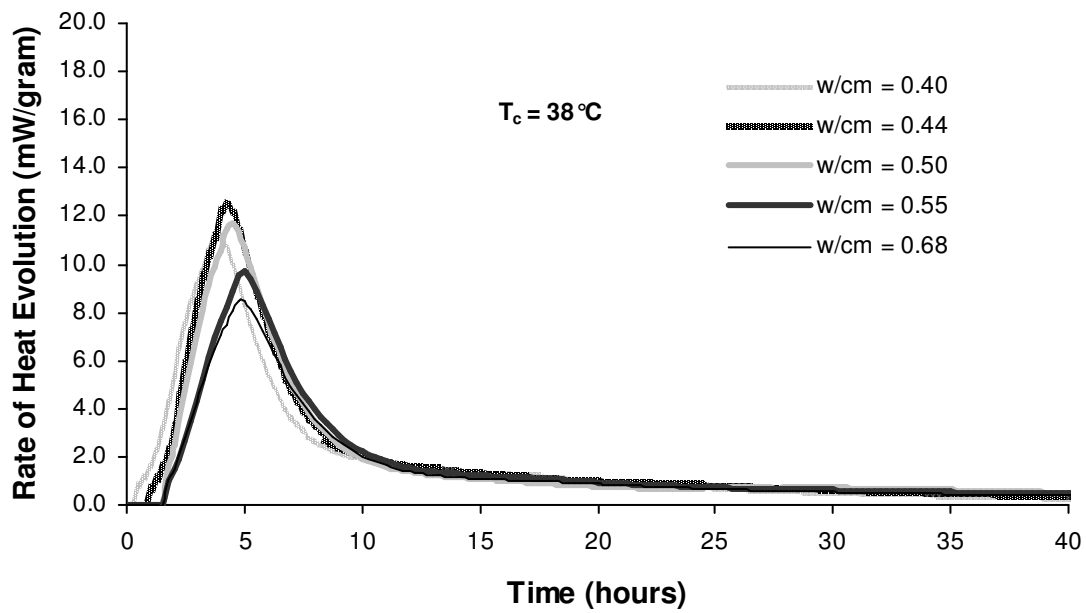


Figure A.9: Effects of w/cm on Rate of Heat Evolution of a Mixture of 100% Cement C6 (Paste) at 38 °C (100 °F)

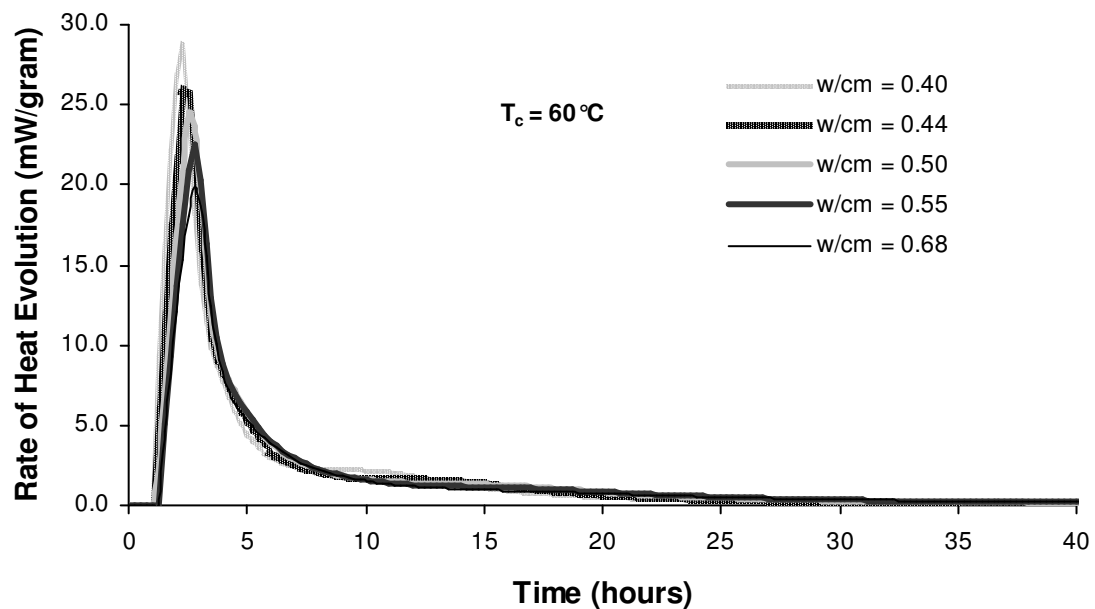


Figure A.10: Effects of w/cm on Rate of Heat Evolution of a Mixture of 100% Cement C6 (Paste) at 60 °C (140 °F)

A.2. EFFECTS OF ALKALI ADDITION ON RATE OF HEAT EVOLUTION

NaOH was added to several mixtures of 100% cement to investigate the effects of alkalis on the activation energy. Figure A.11 through Figure A.25 give additional background for the effects of NaOH addition on the rate of heat evolution at different temperatures.

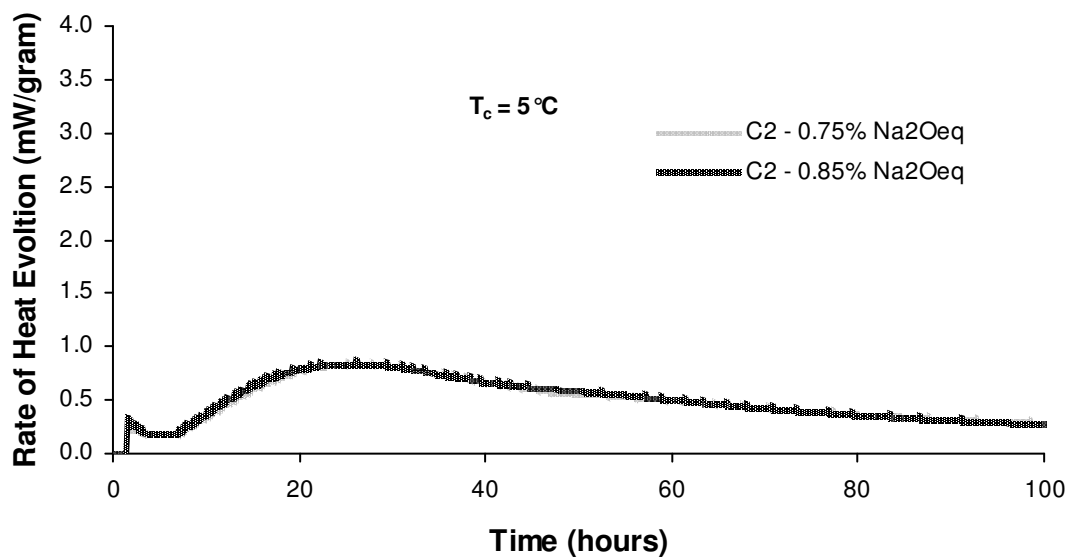


Figure A.11: Effects of Additional Alkalis as NaOH on Rate of Heat Evolution at 5 °C (41 °F) for a Mixture of 100% Cement C2

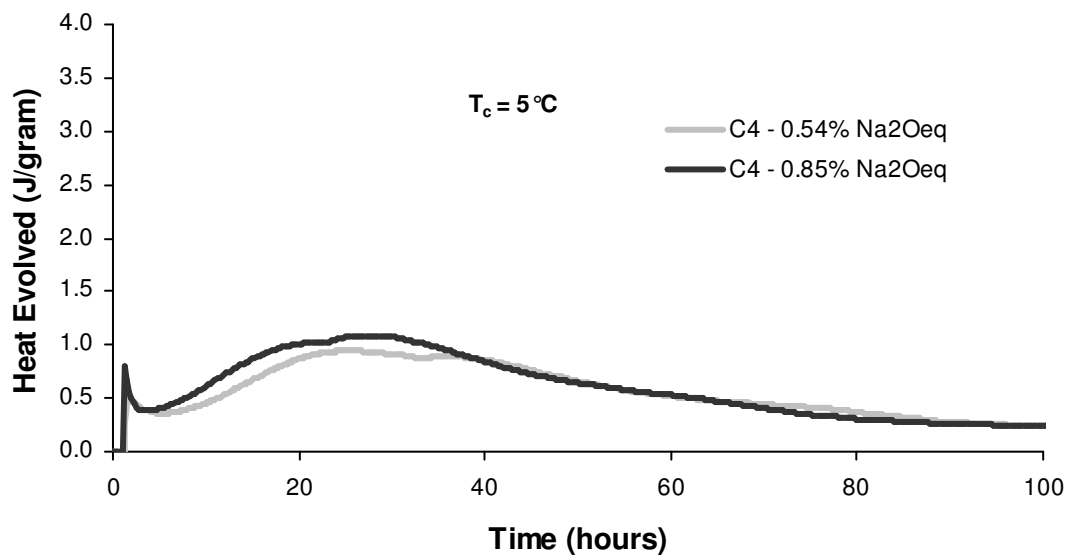


Figure A.12: Effects of Additional Alkalis as NaOH on Rate of Heat Evolution at 5 °C (41 °F) for a Mixture of 100% Cement C4

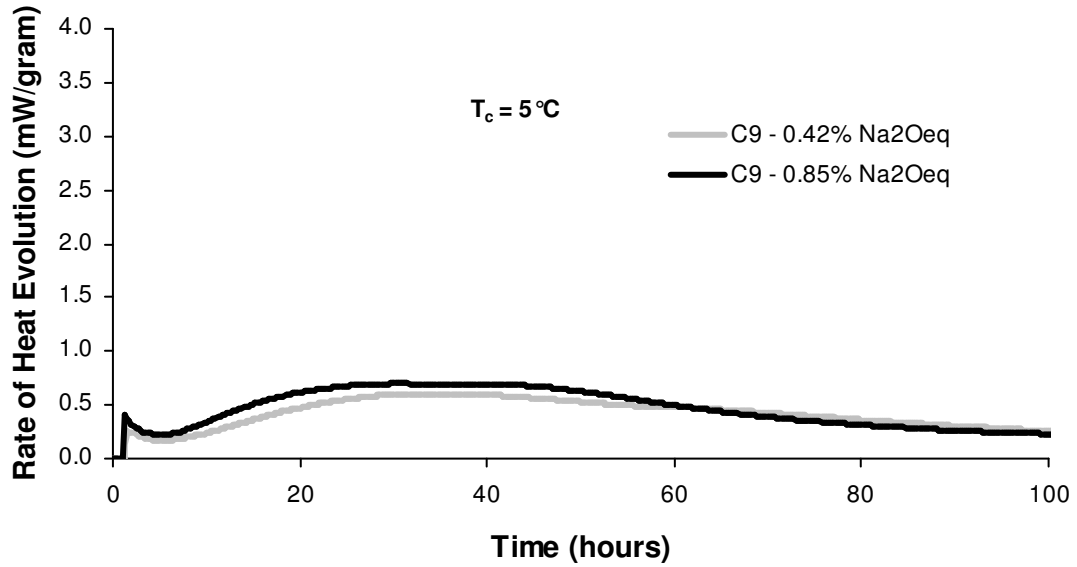


Figure A.13: Effects of Additional Alkalis as NaOH on Rate of Heat Evolution at 5 °C (41 °F) for a Mixture of 100% Cement C9

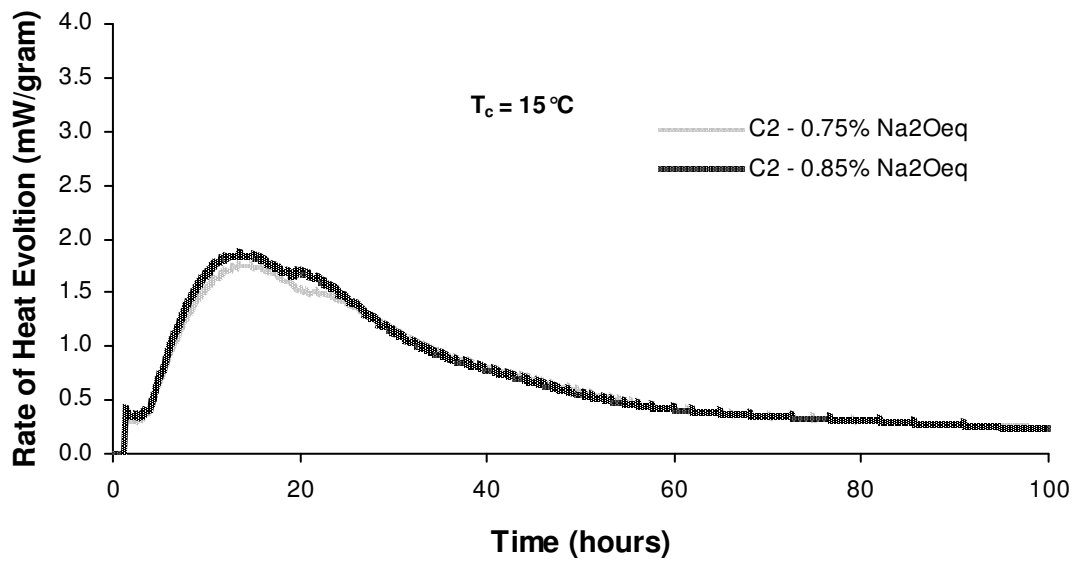


Figure A.14: Effects of Additional Alkalis as NaOH on Rate of Heat Evolution at 15 °C (59 °F) for a Mixture of 100% Cement C2

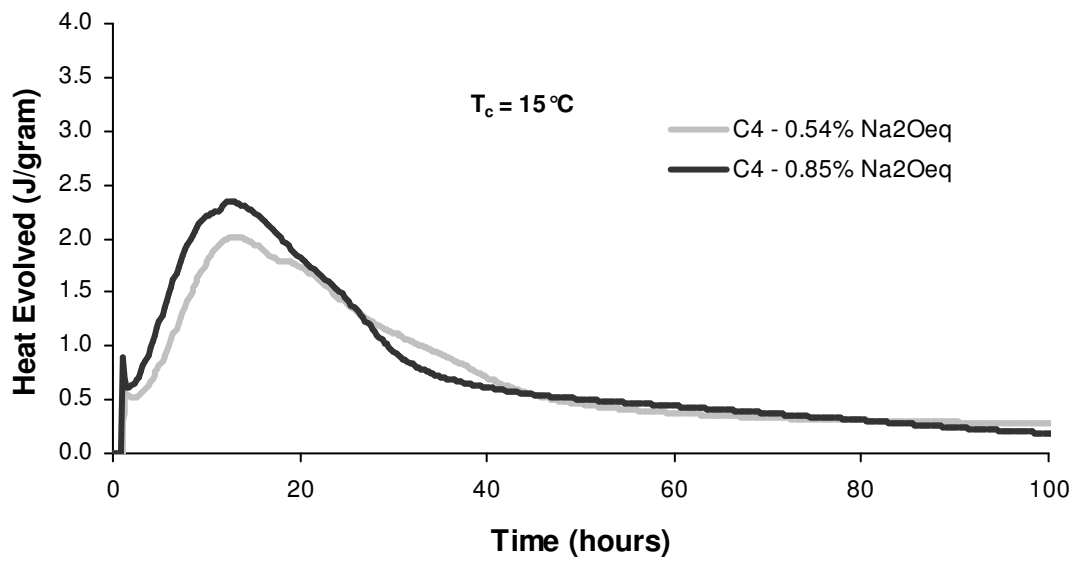


Figure A.15: Effects of Additional Alkalis as NaOH on Rate of Heat Evolution at 15 °C (59 °F) for a Mixture of 100% Cement C4

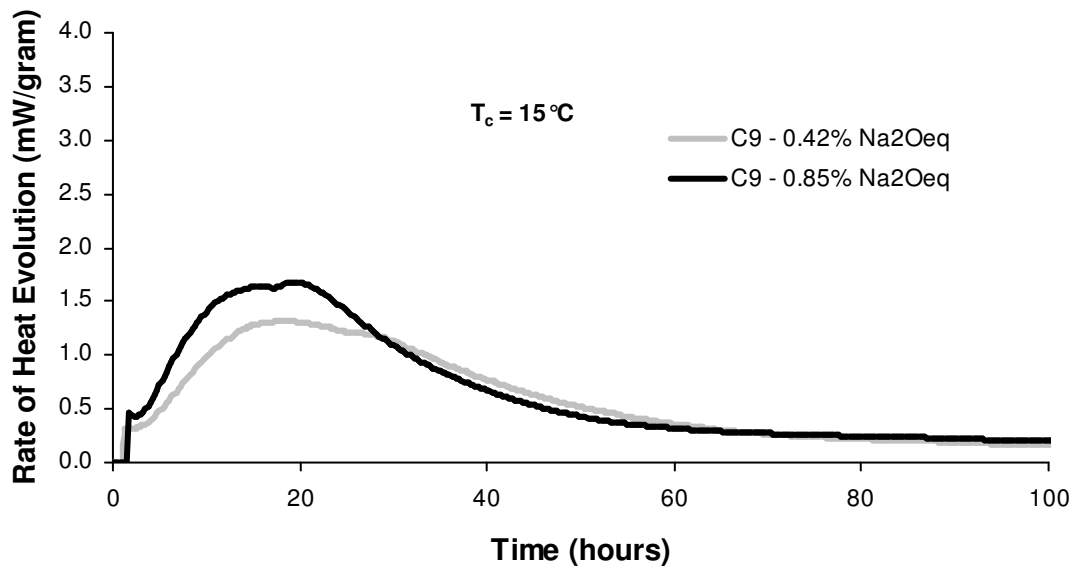


Figure A.16: Effects of Additional Alkalis as NaOH on Rate of Heat Evolution at 15 °C (59 °F) for a Mixture of 100% Cement C9

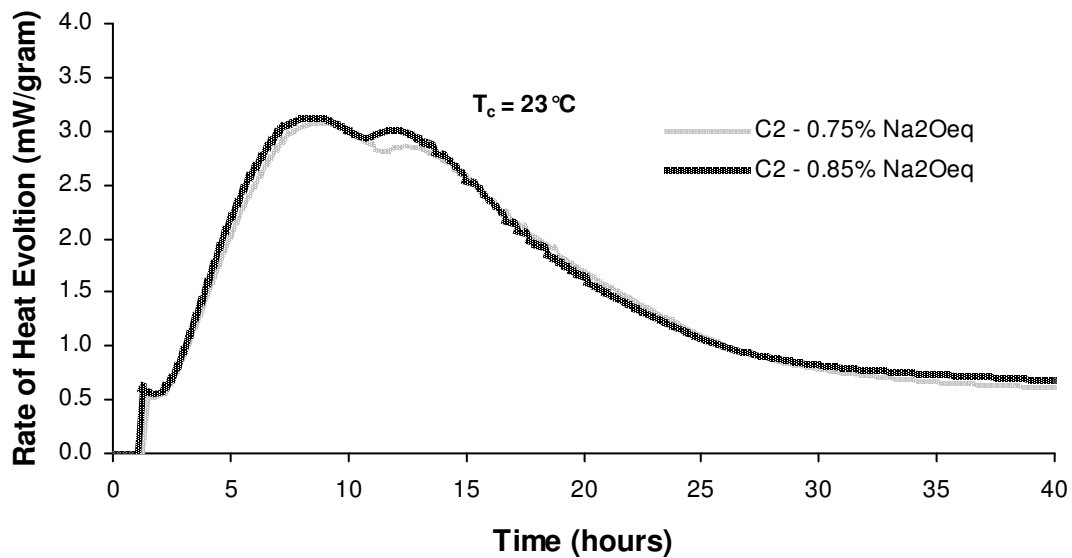


Figure A.17: Effects of Additional Alkalies as NaOH on Rate of Heat Evolution at 23 °C (73 °F) for a Mixture of 100% Cement C2

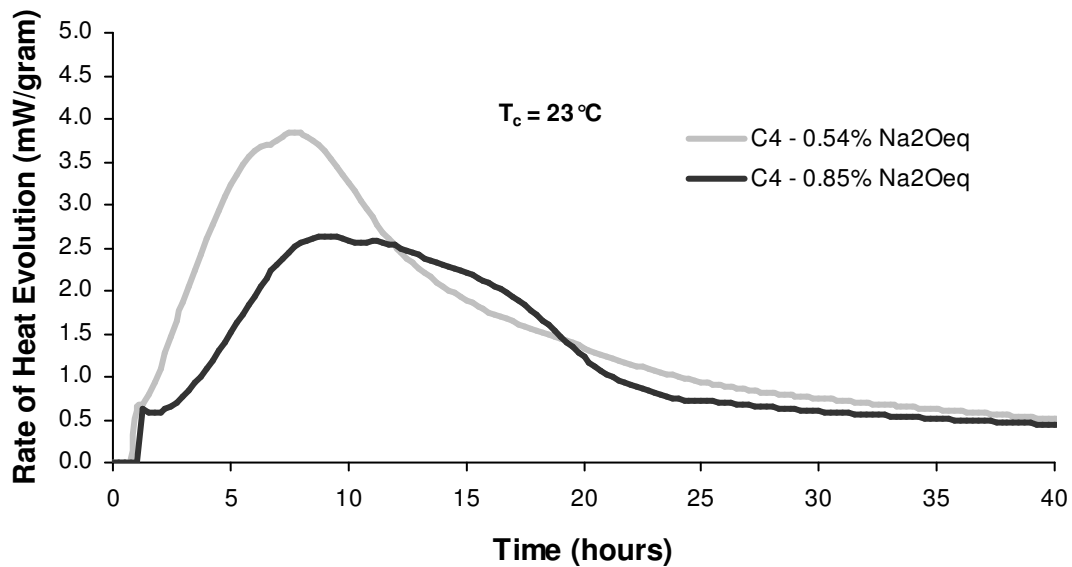


Figure A.18: Effects of Additional Alkalies as NaOH on Rate of Heat Evolution at 23 °C (73 °F) for a Mixture of 100% Cement C4

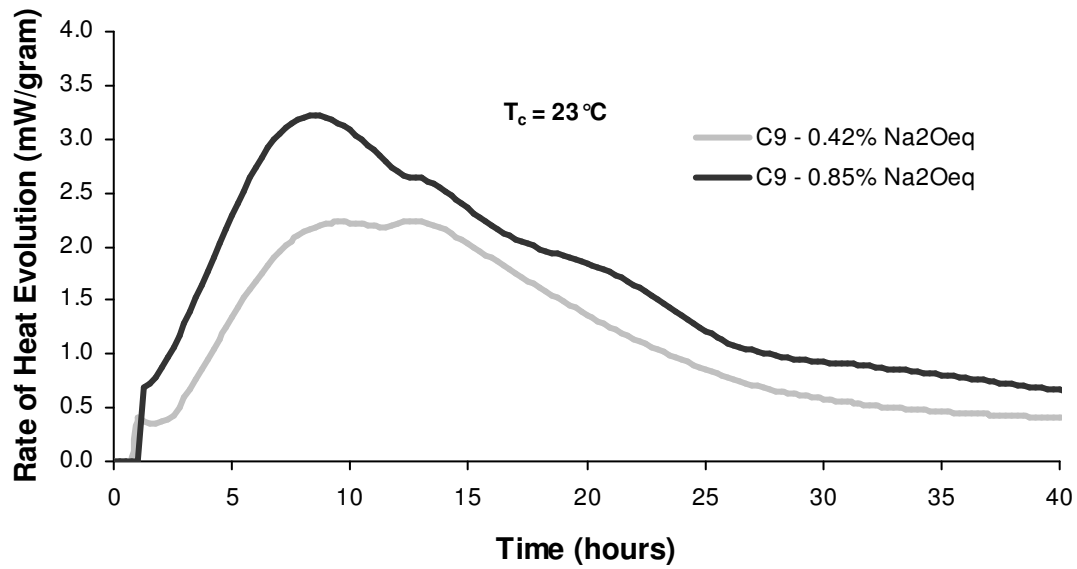


Figure A.19: Effects of Additional Alkalis as NaOH on Rate of Heat Evolution at 23 °C (73 °F) for a Mixture of 100% Cement C9

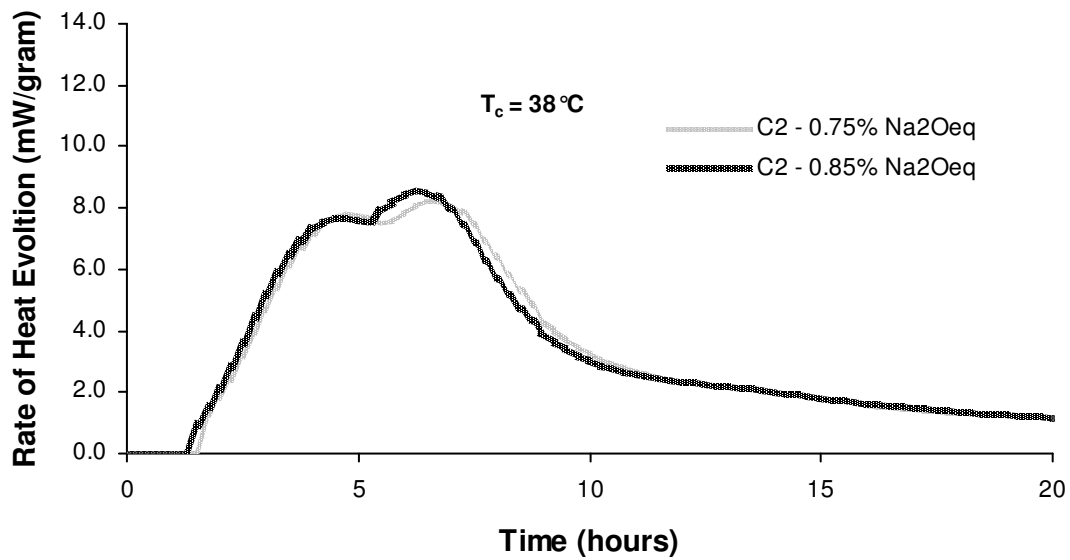


Figure A.20: Effects of Additional Alkalis as NaOH on Rate of Heat Evolution at 38 °C (100 °F) for a Mixture of 100% Cement C2

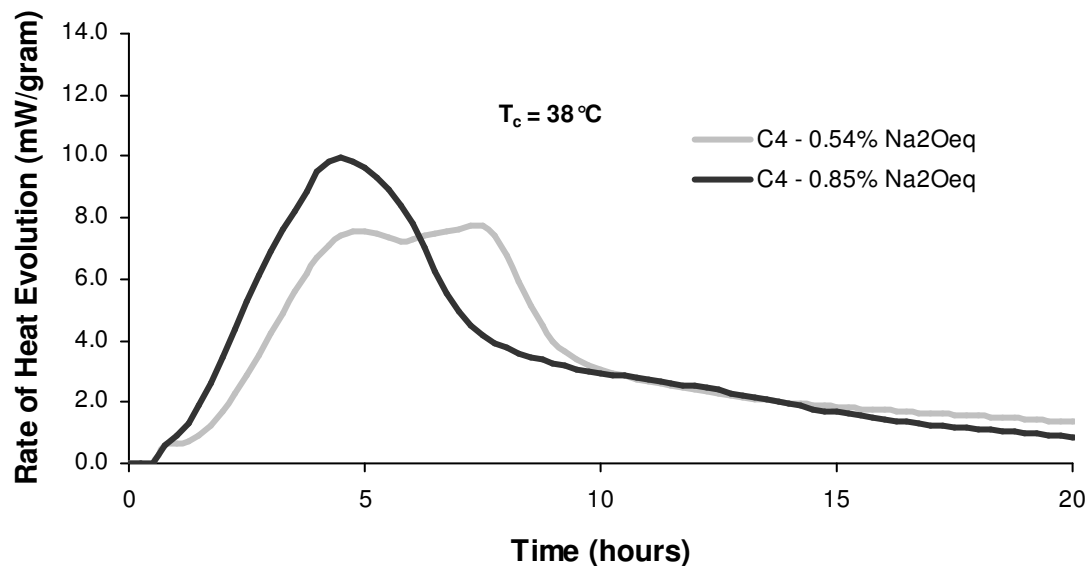


Figure A.21: Effects of Additional Alkalies as NaOH on Rate of Heat Evolution at 38 °C (100 °F) for a Mixture of 100% Cement C4

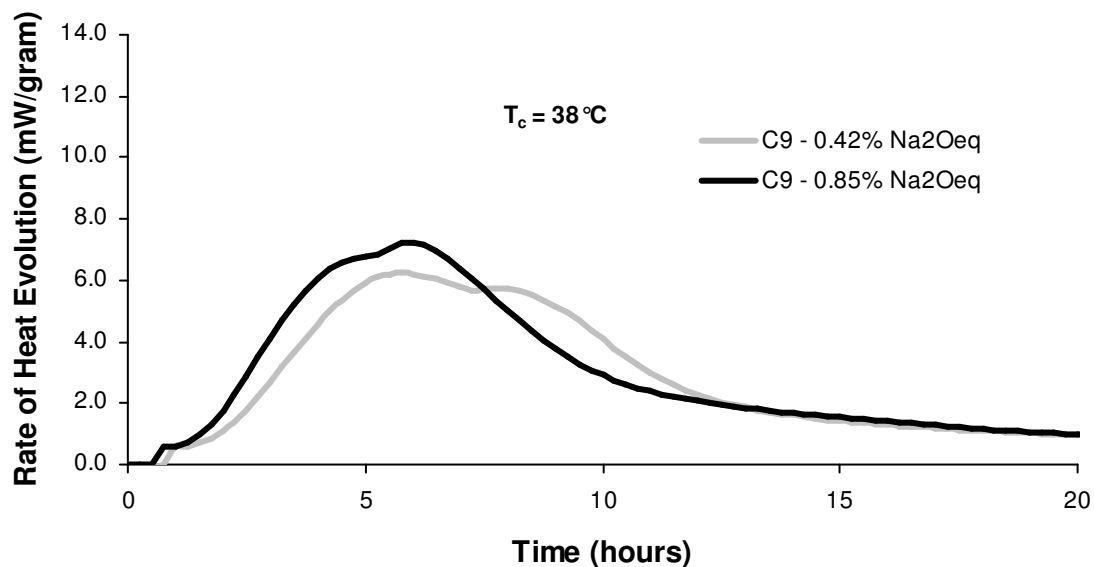


Figure A.22: Effects of Additional Alkalies as NaOH on Rate of Heat Evolution at 38 °C (100 °F) for a Mixture of 100% Cement C9

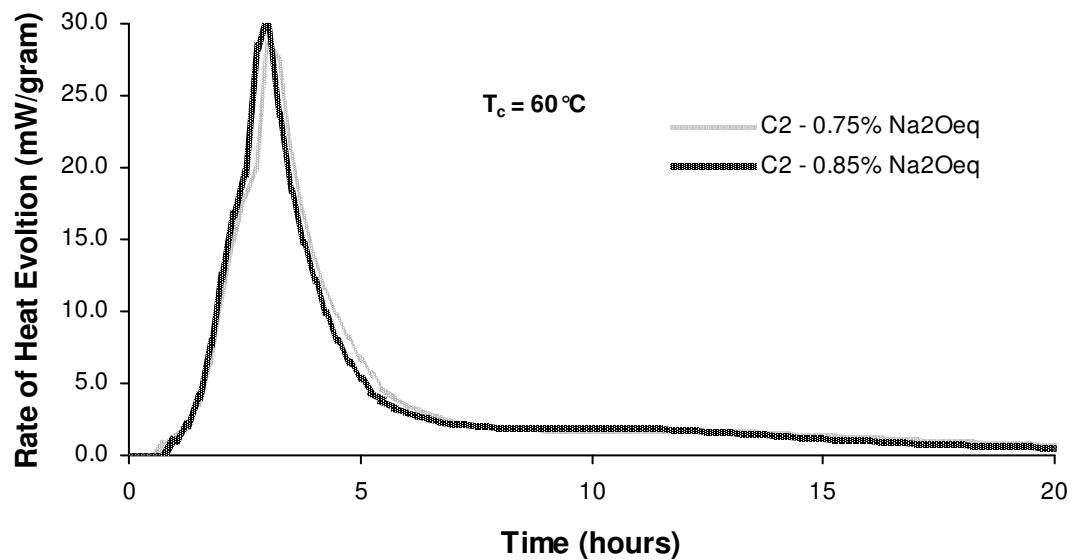


Figure A.23: Effects of Additional Alkalis as NaOH on Rate of Heat Evolution at 60 °C (140 °F) for a Mixture of 100% Cement C2

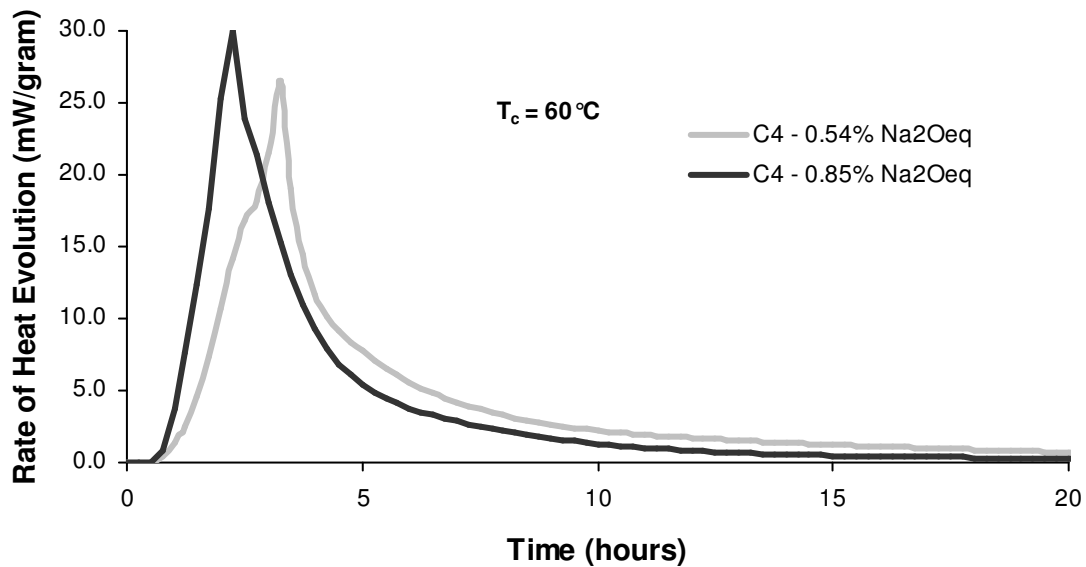


Figure A.24: Effects of Additional Alkalis as NaOH on Rate of Heat Evolution at 60 °C (140 °F) for a Mixture of 100% Cement C4

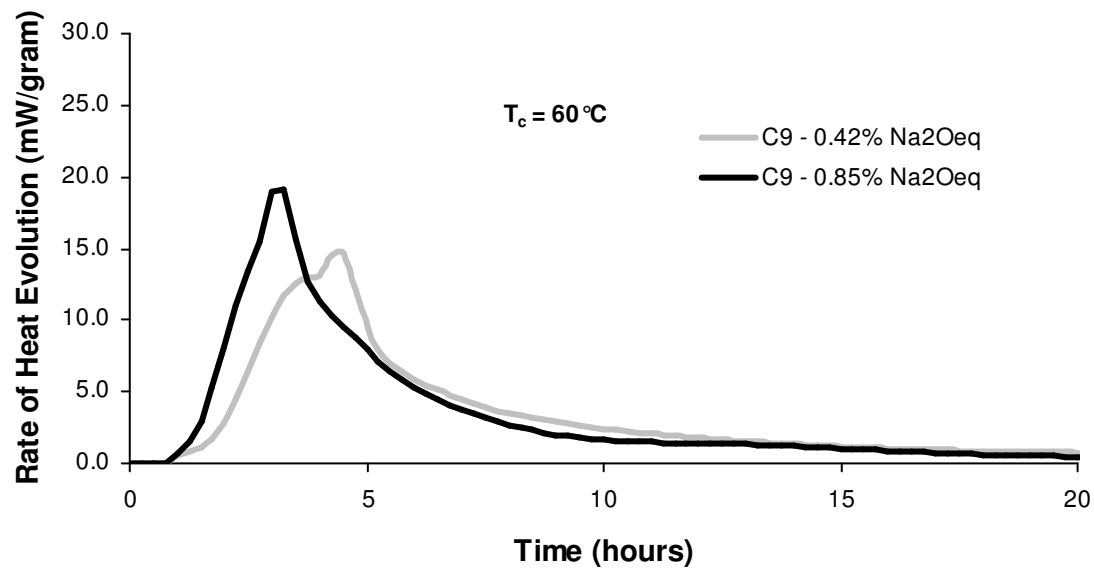


Figure A.25: Effects of Additional Alkalis as NaOH on Rate of Heat Evolution at 60 °C (140 °F) for a Mixture of 100% Cement C9

APPENDIX B. ADDITIONAL ISOTHERMAL RESULTS FOR CHAPTER 3

B.1. EFFECTS OF CHEMICAL ADMIXTURES ON RATE OF HEAT EVOLUTION OF 100% CEMENT PASTES

The following figures provide background for the effects of low-range water reducing and retarding admixtures (LRWR and WRRET) on hydration presented in Chapter 3. Results at each of the isothermal test temperatures are shown.

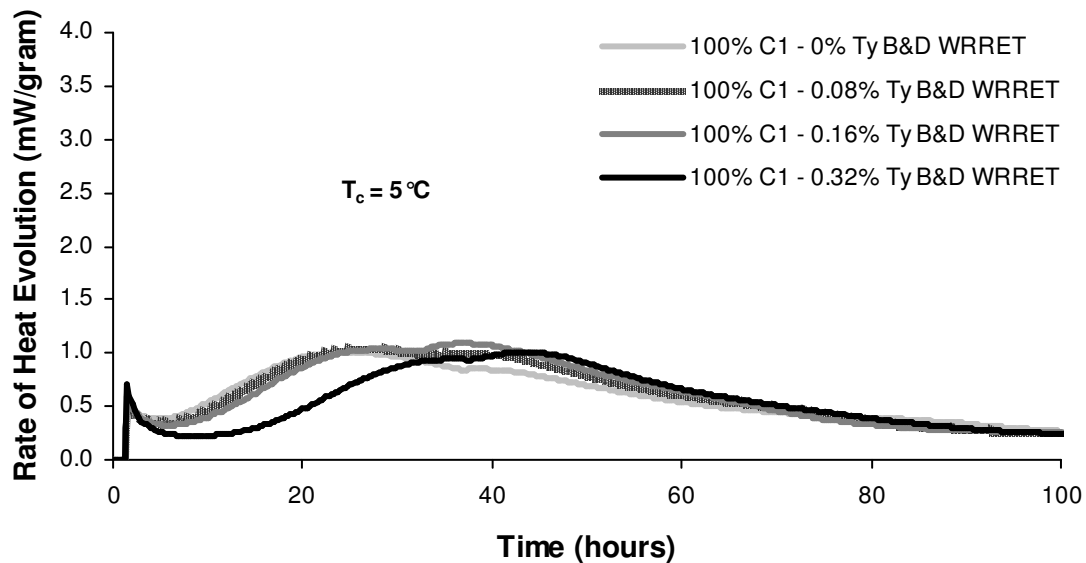


Figure B.1: Rate of Heat Evolution (Per Gram of Cementitious Material) for 100% Cement C1 (Paste) with Different Dosages of Lignosulfonate-Based Low Range Water Reducer/Retarder at 5 °C (41 °F)

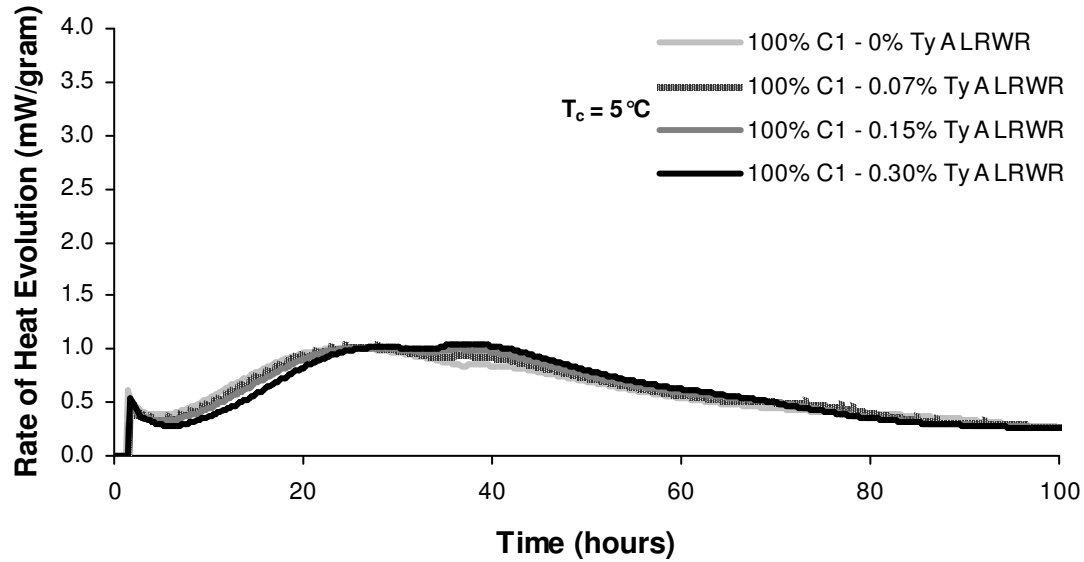


Figure B.2: Rate of Heat Evolution (Per Gram of Cementitious Material) for 100% Cement C1 (Paste) with Different Dosages of Glucose-Based Low Range Water Reducer at 5 °C (41 °F)

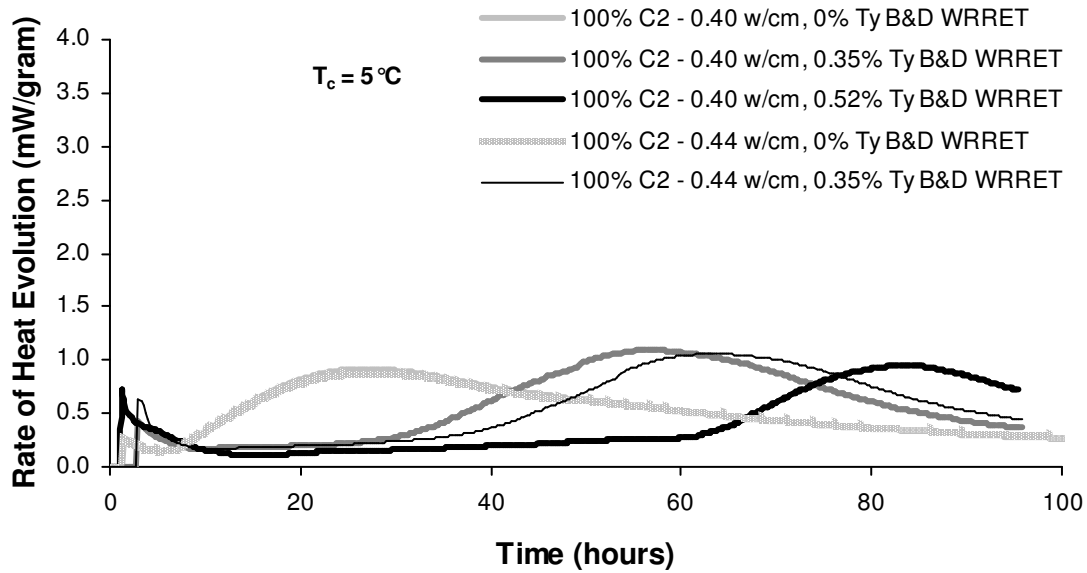


Figure B.3: Rate of Heat Evolution (Per Gram of Cementitious Material) for 100% Cement C2 (Paste) with Different Dosages of Lignosulfonate-Based Low Range Water Reducer/Retarder at 5 °C (41 °F)

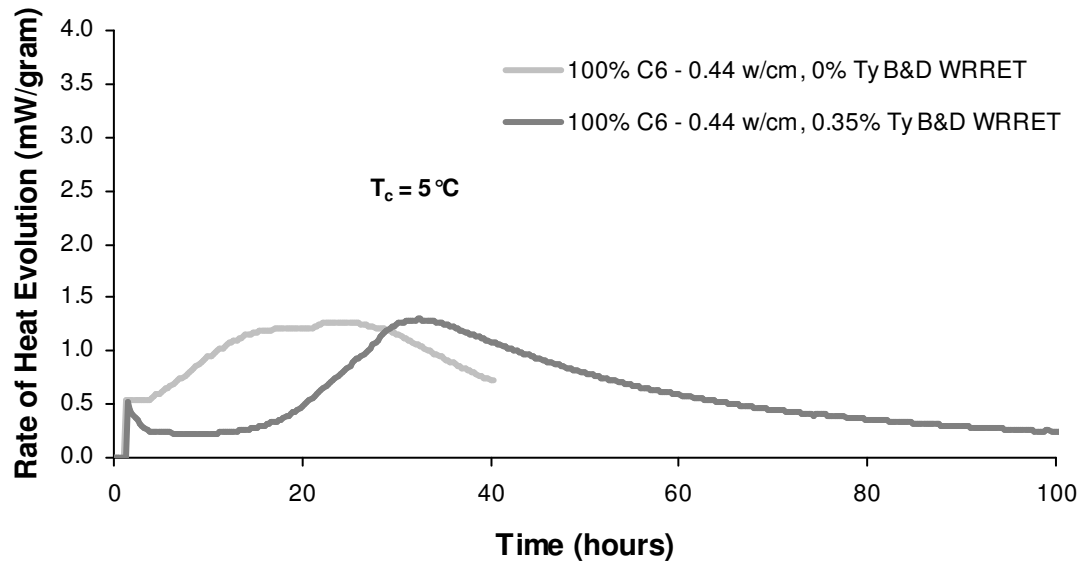


Figure B.4: Rate of Heat Evolution (Per Gram of Cementitious Material) for 100% Cement C6 (Paste) with and Without Lignosulfonate-Based Low Range Water Reducer/Retarder at 5 °C (41 °F)

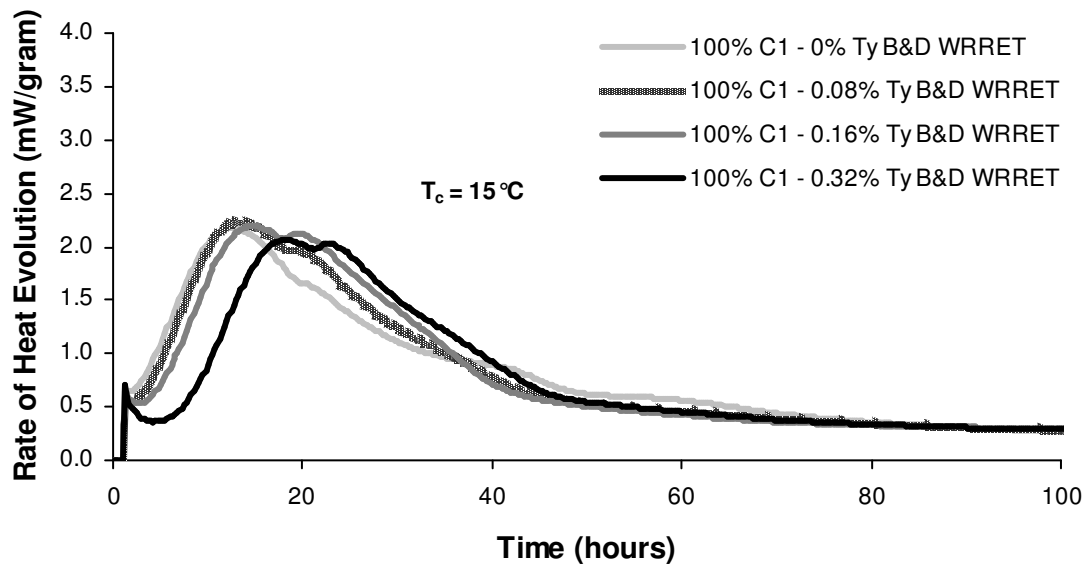


Figure B.5: Rate of Heat Evolution (Per Gram of Cementitious Material) for 100% Cement C1 (Paste) with Different Dosages of Lignosulfonate-Based Low Range Water Reducer/Retarder at 15 °C (59 °F)

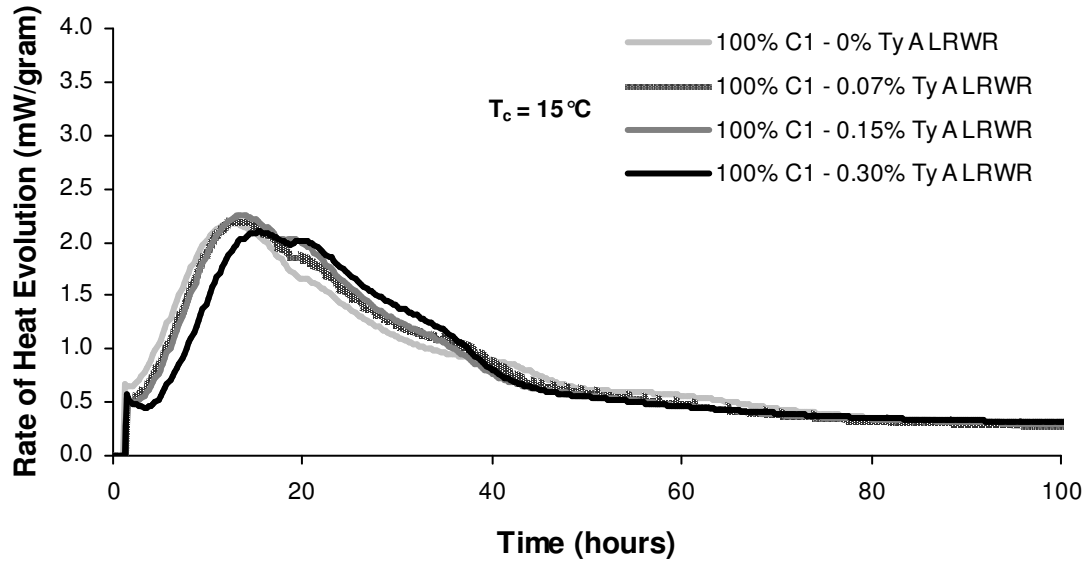


Figure B.6: Rate of Heat Evolution (Per Gram of Cementitious Material) for 100% Cement C1 (Paste) with Different Dosages of Glucose-Based Low Range Water Reducer at 15 °C (59 °F)

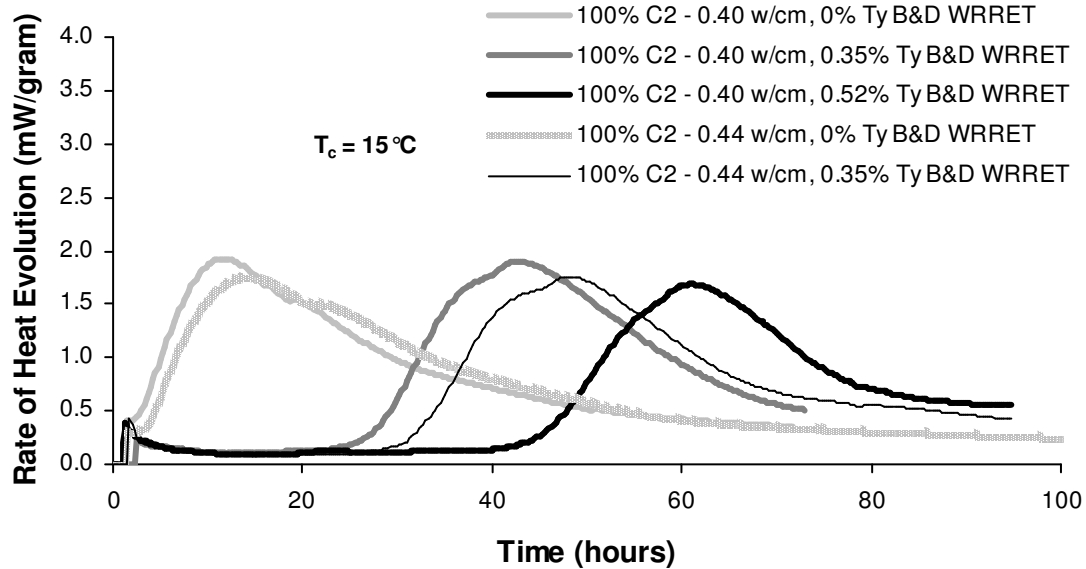


Figure B.7: Rate of Heat Evolution (Per Gram of Cementitious Material) for 100% Cement C2 (Paste) with Different Dosages of Lignosulfonate-Based Low Range Water Reducer/Retarder at 15 °C (59 °F)

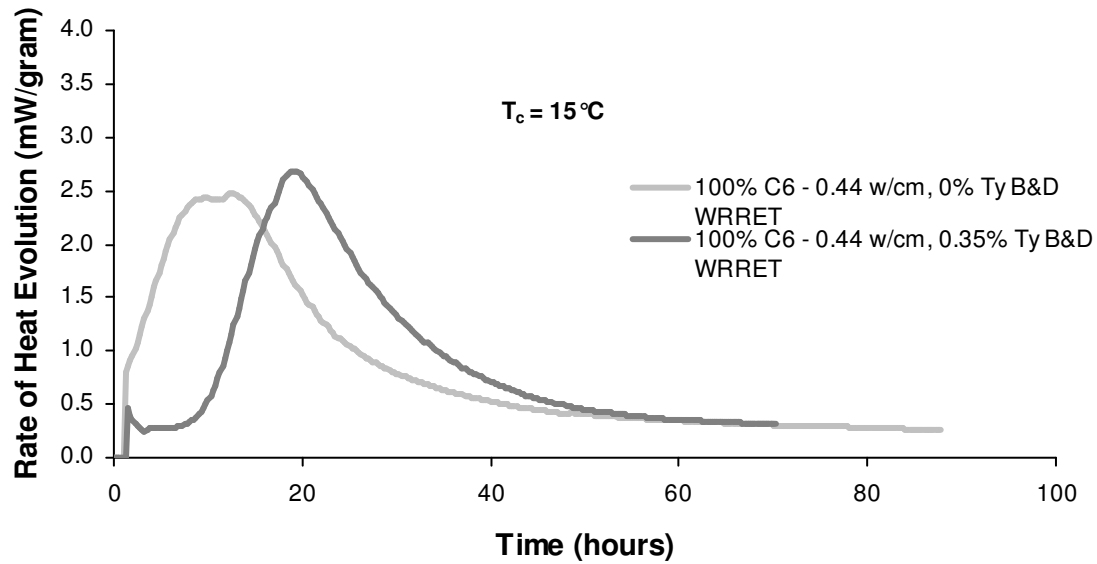


Figure B.8: Rate of Heat Evolution (Per Gram of Cementitious Material) for 100% Cement C6 (Paste) with and Without Lignosulfonate-Based Low Range Water Reducer/Retarder at 15 °C (59 °F)

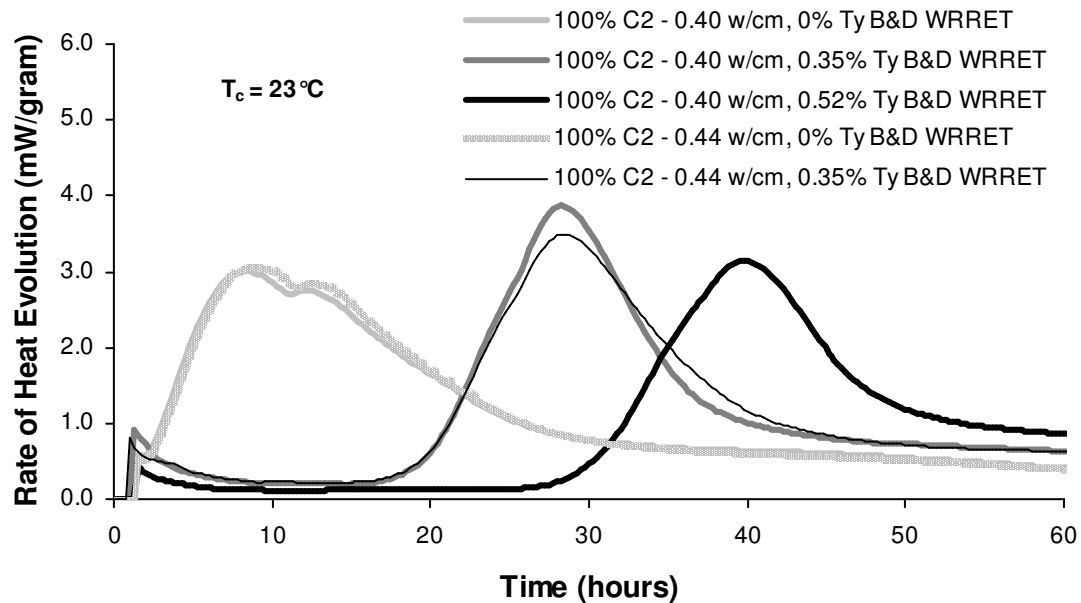


Figure B.9: Rate of Heat Evolution (Per Gram of Cementitious Material) for 100% Cement C2 (Paste) with Different Dosages of Lignosulfonate-Based Low Range Water Reducer/Retarder at 23 °C (73 °F)

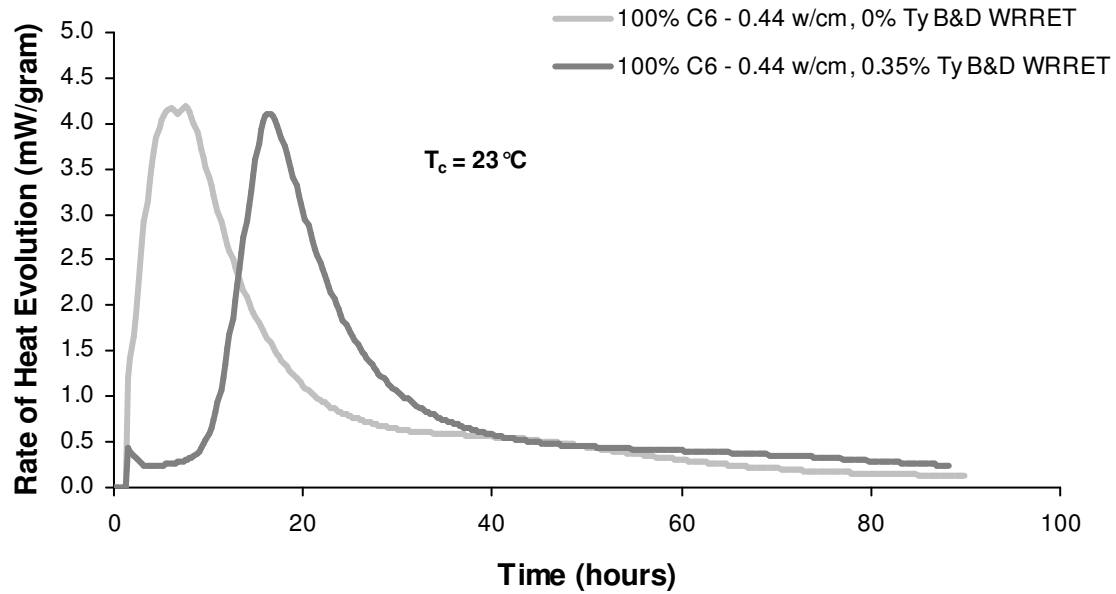


Figure B.10: Rate of Heat Evolution (Per Gram of Cementitious Material) for 100% Cement C6 (Paste) with and Without Lignosulfonate-Based Low Range Water Reducer/Retarder at 23 °C (73 °F)

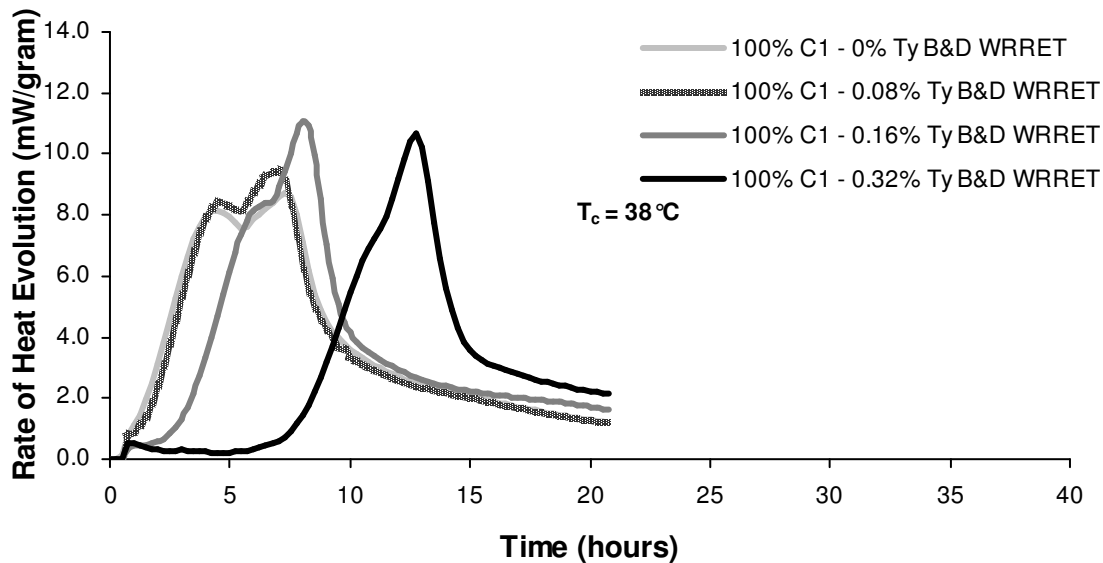


Figure B.11: Rate of Heat Evolution (Per Gram of Cementitious Material) for 100% Cement C1 (Paste) with Different Dosages of Lignosulfonate-Based Low Range Water Reducer/Retarder at 38 °C (100 °F)

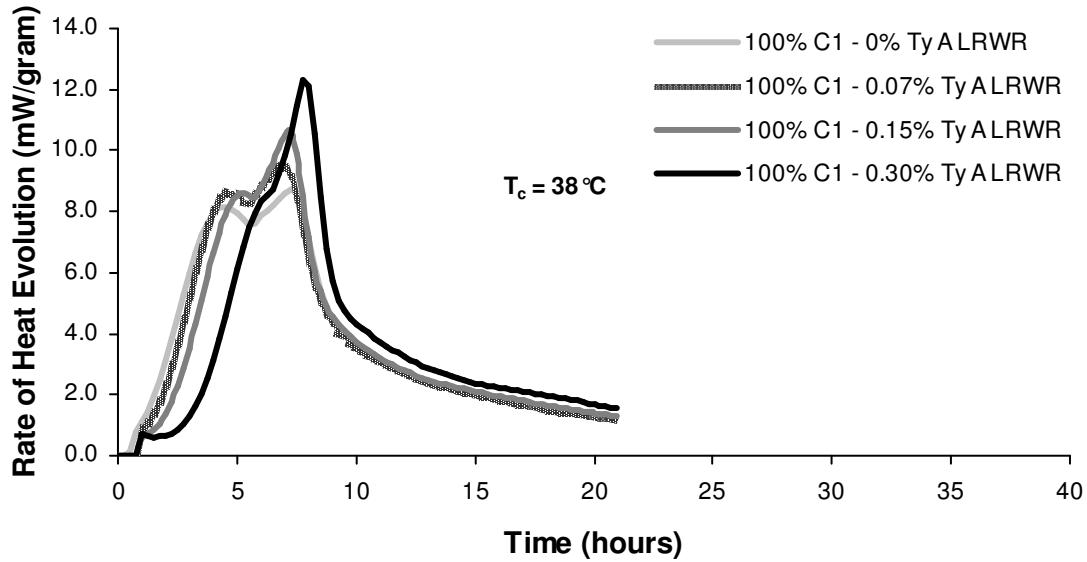


Figure B.12: Rate of Heat Evolution (Per Gram of Cementitious Material) for 100% Cement C1 (Paste) with Different Dosages of Glucose-Based Low Range Water Reducer at 38 °C (100 °F)

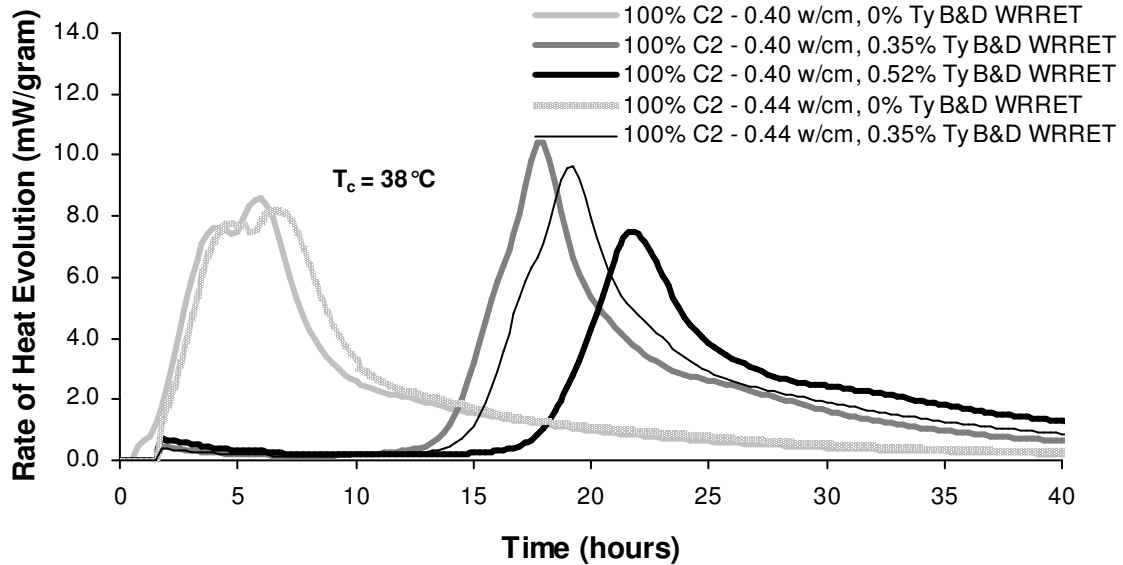


Figure B.13: Rate of Heat Evolution (Per Gram of Cementitious Material) for 100% Cement C2 (Paste) with Different Dosages of Lignosulfonate-Based Low Range Water Reducer/Retarder at 38 °C (100 °F)

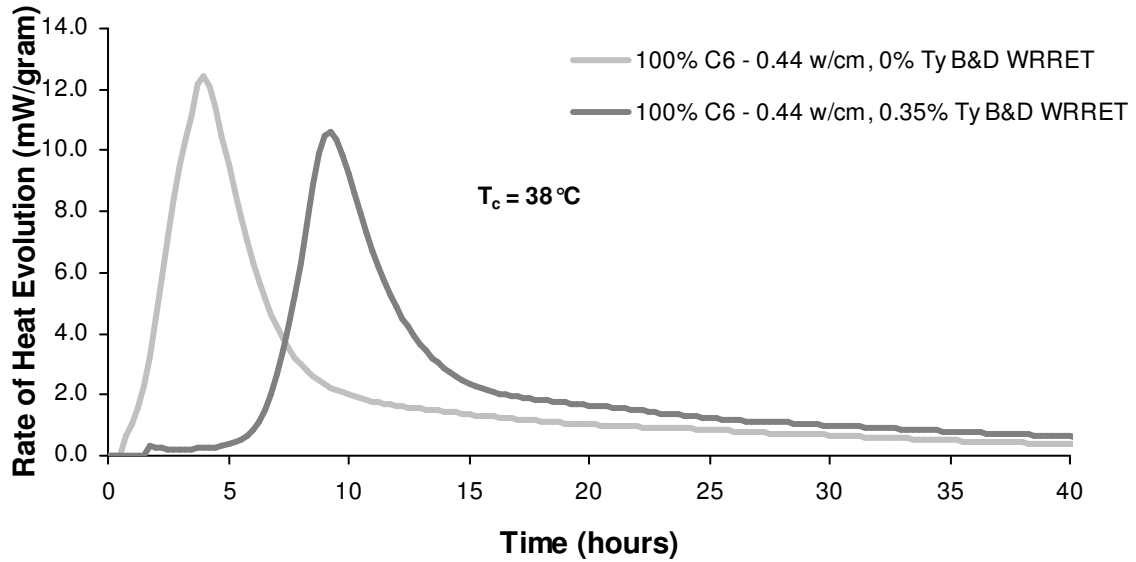


Figure B.14: Rate of Heat Evolution (Per Gram of Cementitious Material) for 100% Cement C6 (Paste) with and Without Lignosulfonate-Based Low Range Water Reducer/Retarder at 38 °C (100 °F)

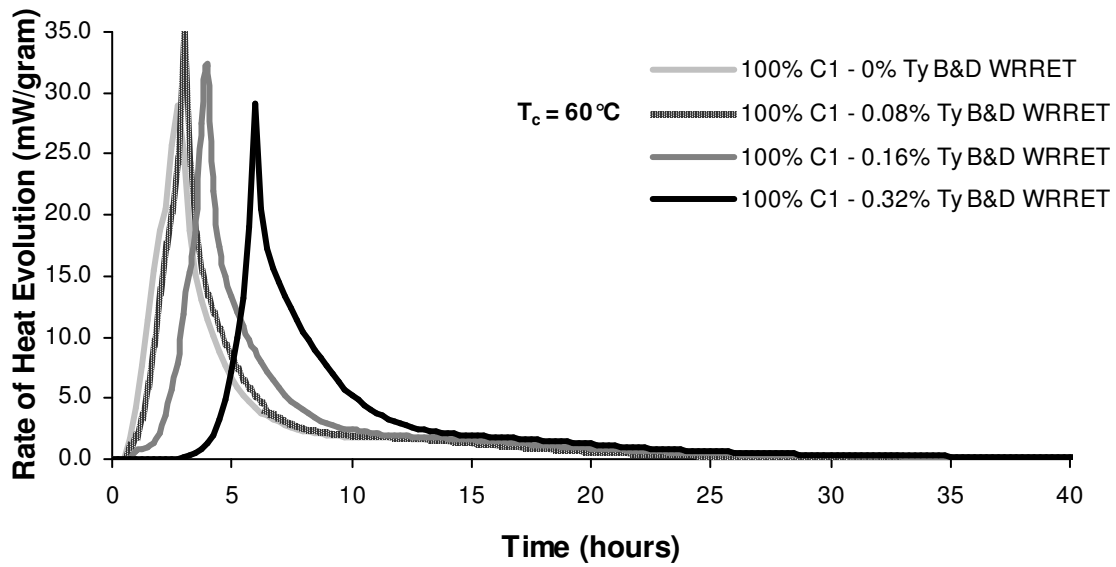


Figure B.15: Rate of Heat Evolution (Per Gram of Cementitious Material) for 100% Cement C1 (Paste) with Different Dosages of Lignosulfonate-Based Low Range Water Reducer/Retarder at 60 °C (140 °F)

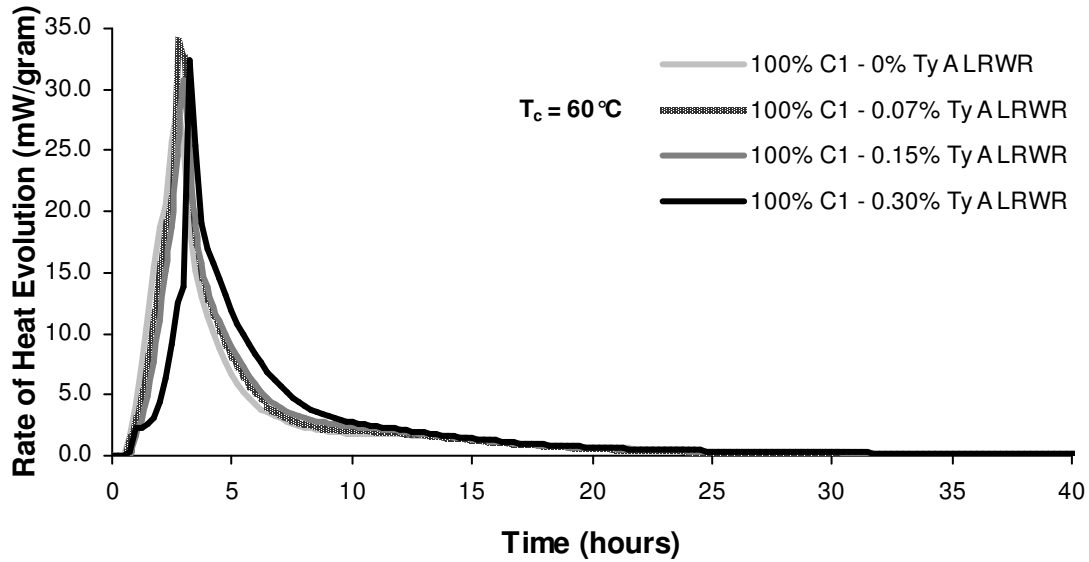


Figure B.16: Rate of Heat Evolution (Per Gram of Cementitious Material) for 100% Cement C1 (Paste) with Different Dosages of Glucose-Based Low Range Water Reducer at 60 °C (140 °F)

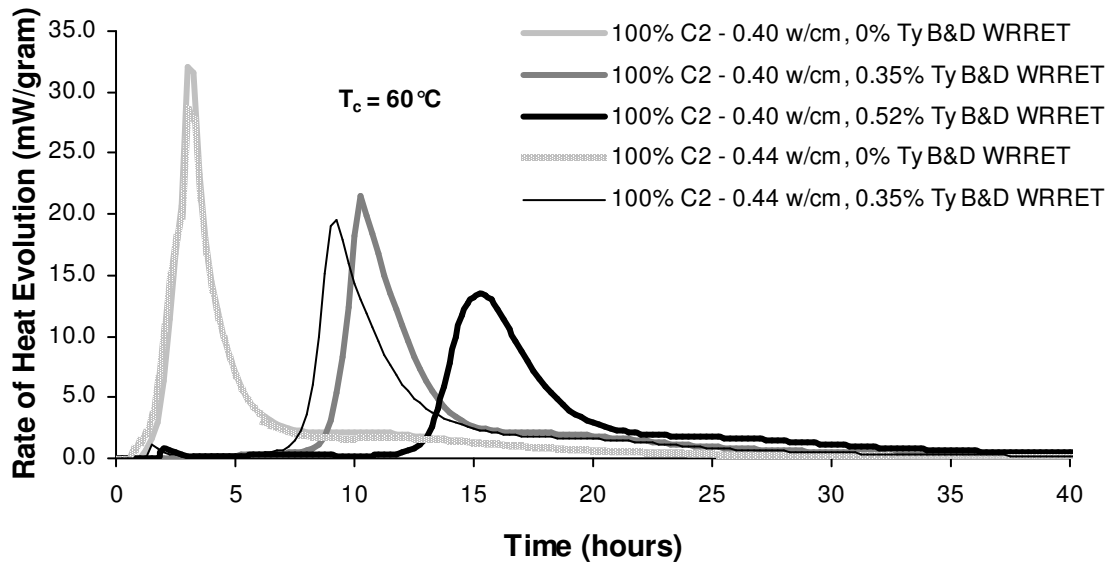


Figure B.17: Rate of Heat Evolution (Per Gram of Cementitious Material) for 100% Cement C2 (Paste) with Different Dosages of Lignosulfonate-Based Low Range Water Reducer/Retarder at 60 °C (140 °F)

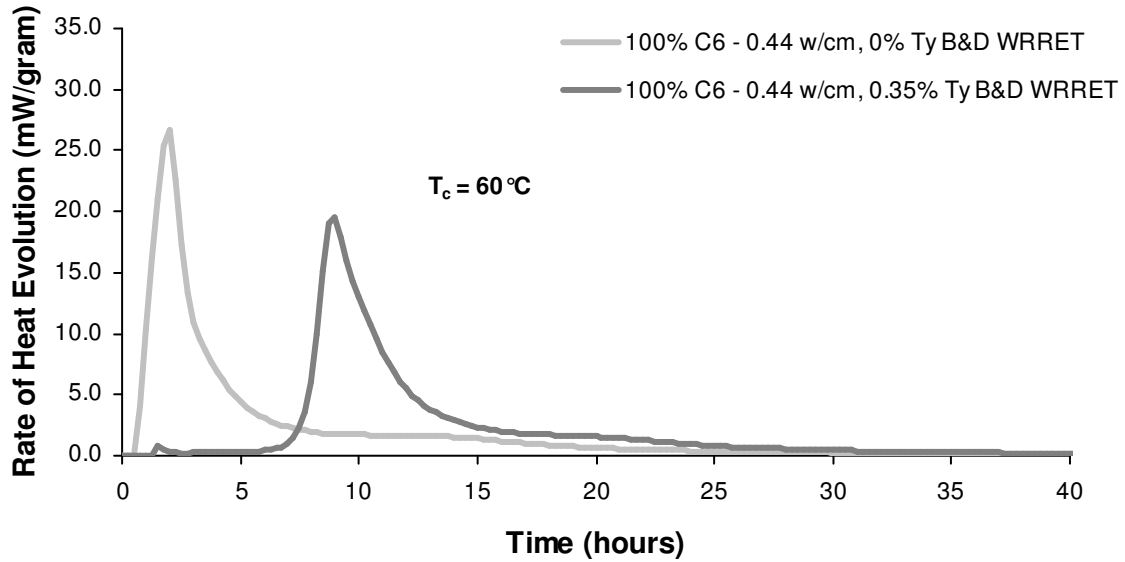


Figure B.18: Rate of Heat Evolution (Per Gram of Cementitious Material) for 100% Cement C6 (Paste) with and Without Lignosulfonate-Based Low Range Water Reducer/Retarder at 60 °C (140 °F)

B.2. EFFECTS OF ACCELERATORS AND AEA ON PASTES WITH 100% CEMENT

The following figures provide background for the effects of accelerating (ACCL) and air-entraining (AEA) admixtures on hydration presented in Chapter 3. Results at each of the isothermal test temperatures are shown.

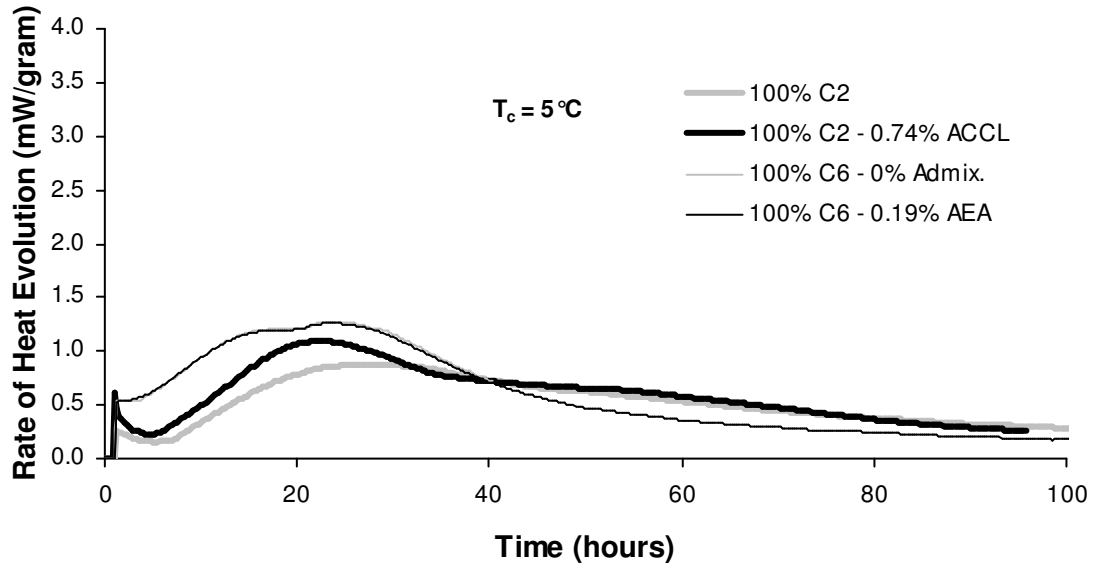


Figure B.19: Rate of Heat Evolution (Per Gram of Cementitious Material) for 100% Cement C2 With and Without ACCL, and 100% Cement C6 with and Without AEA at 5 °C (41 °F)

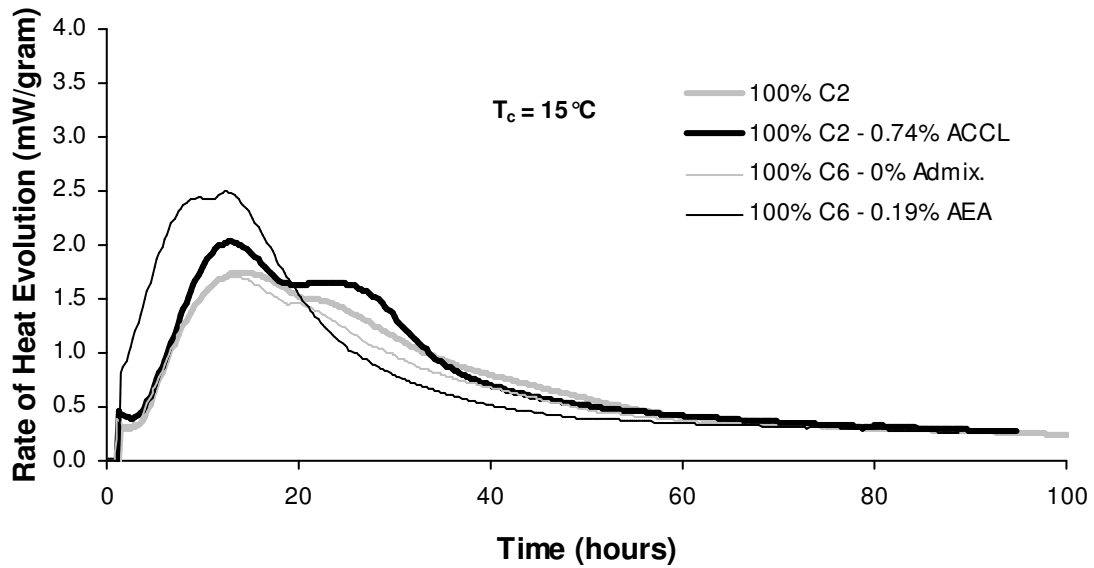


Figure B.20: Rate of Heat Evolution (Per Gram of Cementitious Material) for 100% Cement C2 With and Without ACCL, and 100% Cement C6 with and Without AEA at 15 °C (59 °F)

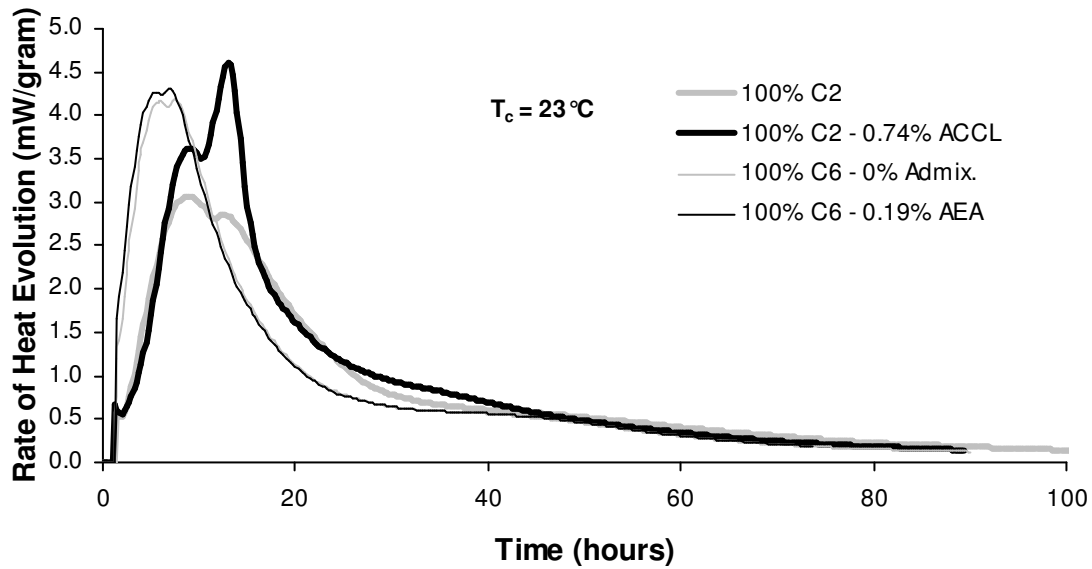


Figure B.21: Rate of Heat Evolution (Per Gram of Cementitious Material) for 100% Cement C2 With and Without ACCL, and 100% Cement C6 with and Without AEA at 23 °C (73 °F)

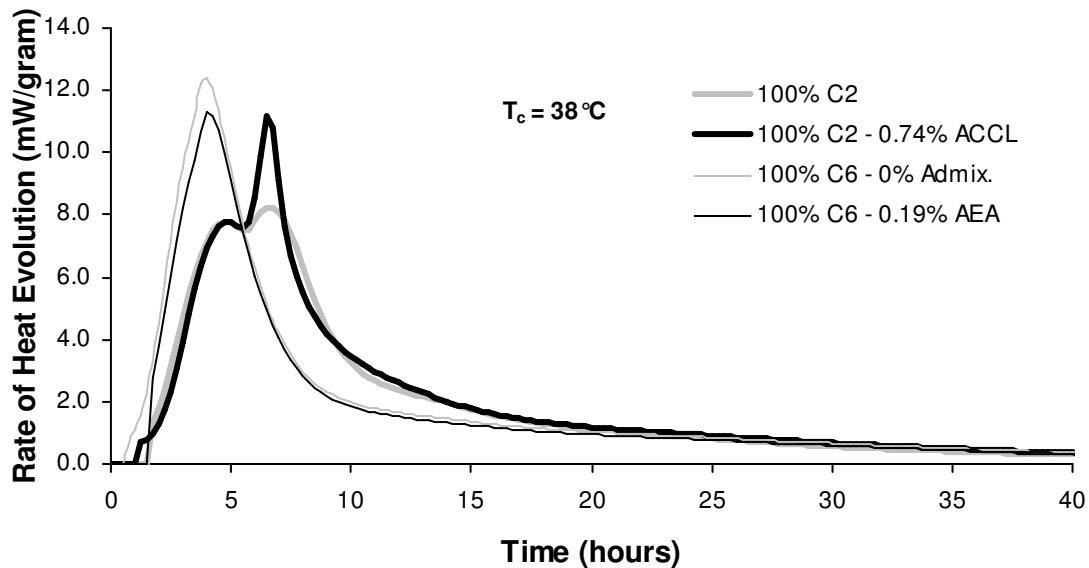


Figure B.22: Rate of Heat Evolution (Per Gram of Cementitious Material) for 100% Cement C2 With and Without ACCL, and 100% Cement C6 with and Without AEA at 38 °C (100 °F)

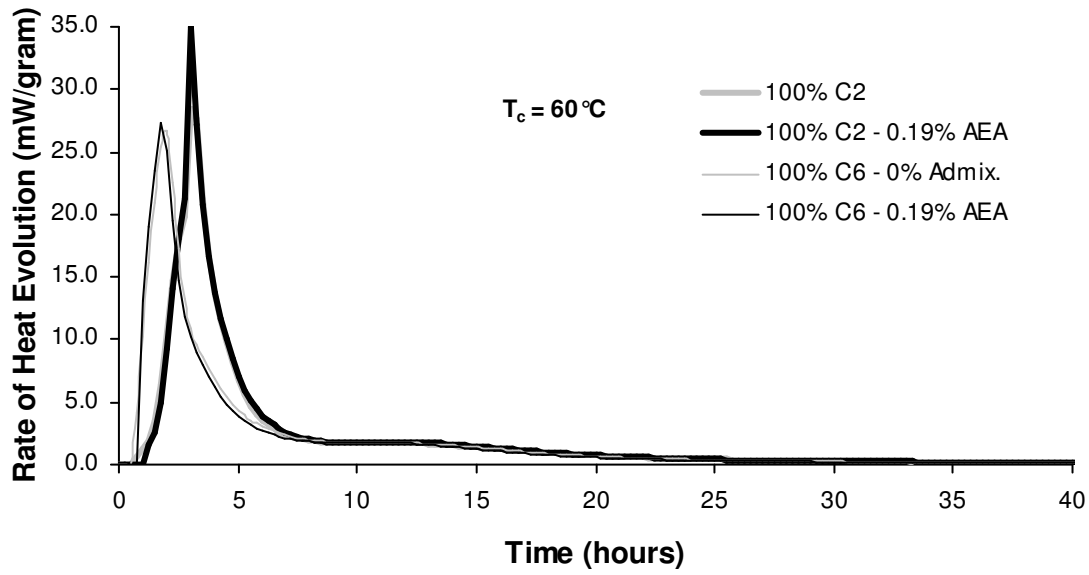


Figure B.23: Rate of Heat Evolution (Per Gram of Cementitious Material) for 100% Cement C2 With and Without ACCL, and 100% Cement C6 with and Without AEA at 60 °C (140 °F)

B.3. EFFECTS OF HRWR ON MIXTURES WITH 100% CEMENT

The following figures provide background for the effects of naphthalene- and polycarboxylate-based high range water reducing admixtures (NHRWR and PCHRWR) on hydration presented in Chapter 3. Results at each of the isothermal test temperatures are shown.

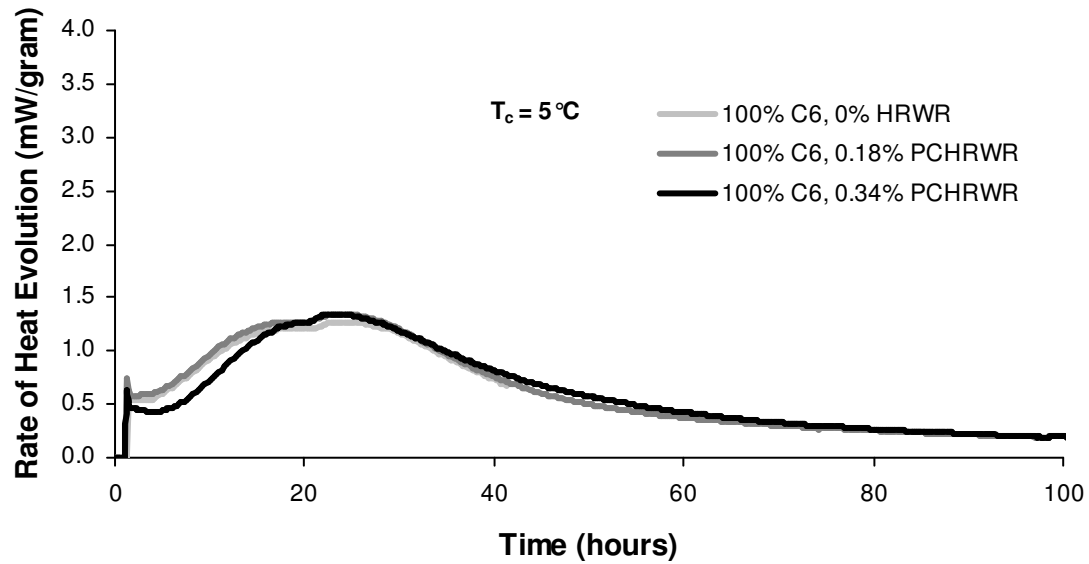


Figure B.24: Rate of Heat Evolution (Per Gram of Cementitious Material) for Paste Mixtures of 100% Cement C6 with PCHRWR at 5 °C (41 °F)

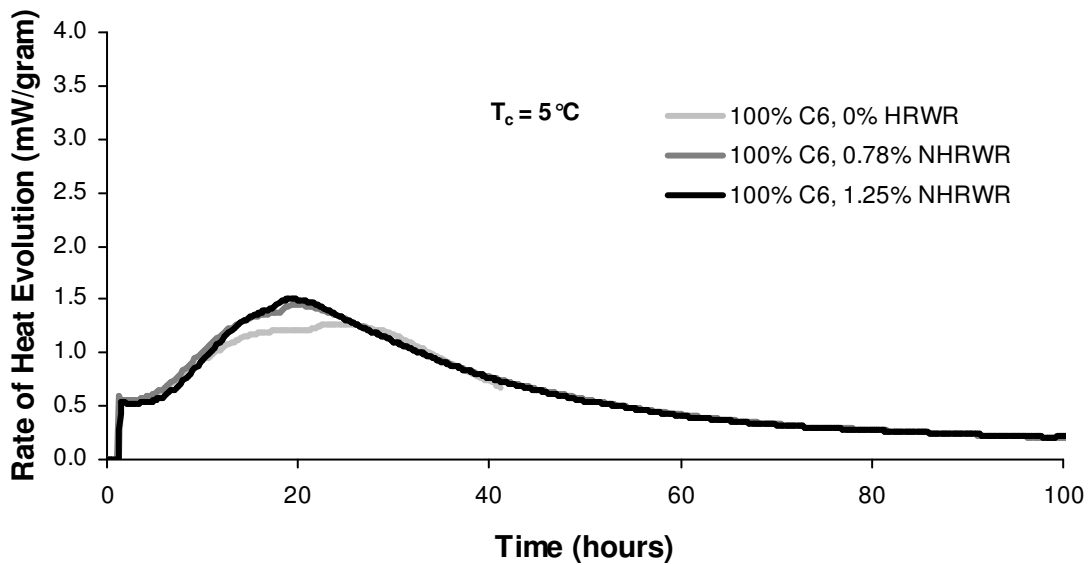


Figure B.25: Rate of Heat Evolution (Per Gram of Cementitious Material) for Paste Mixtures of 100% Cement C6 with NHRWR at 5 °C (41 °F)

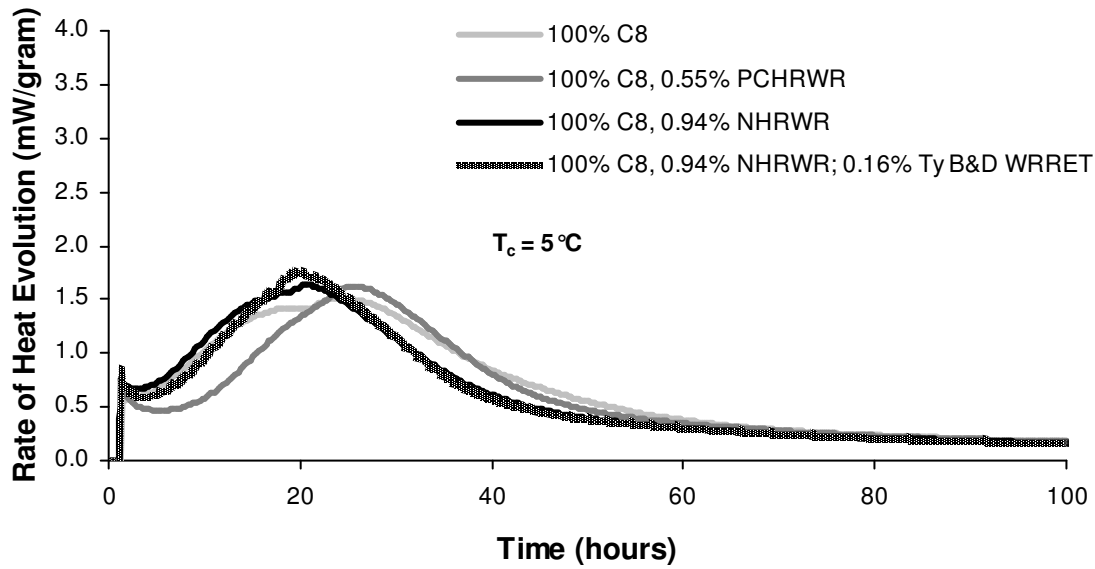


Figure B.26: Rate of Heat Evolution (Per Gram of Cementitious Material) for Paste Mixtures of 100% Cement C8 with NHRWR and PCHRWR at 5 °C (41 °F)

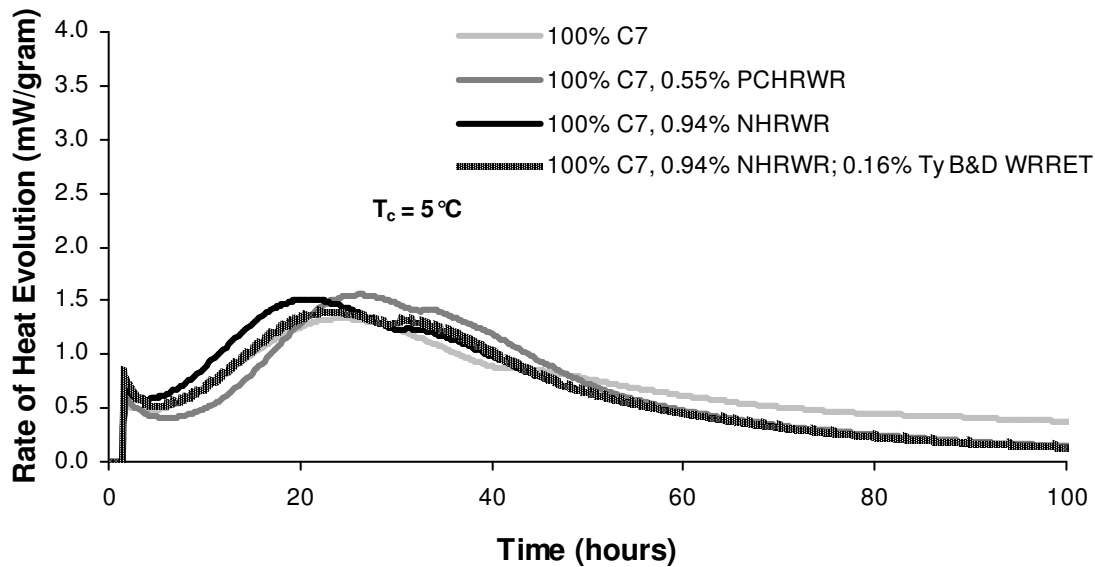


Figure B.27: Rate of Heat Evolution (Per Gram of Cementitious Material) for Paste Mixtures of 100% Cement C8 with NHRWR and PCHRWR at 5 °C (41 °F)

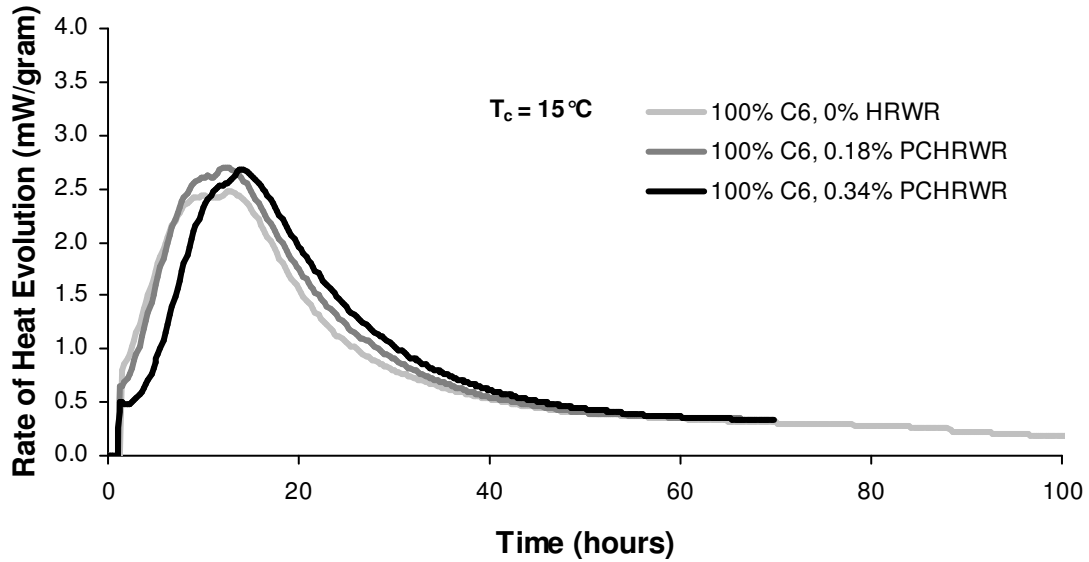


Figure B.28: Rate of Heat Evolution (Per Gram of Cementitious Material) for Paste Mixtures of 100% Cement C6 with PCHRWR at 15 °C (59 °F)

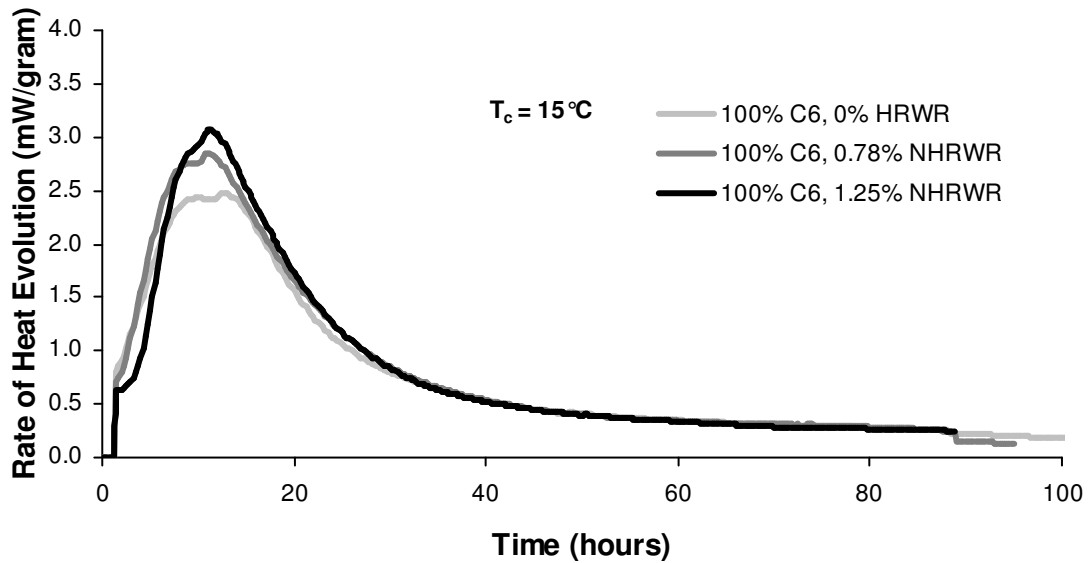


Figure B.29: Rate of Heat Evolution (Per Gram of Cementitious Material) for Paste Mixtures of 100% Cement C6 with NHRWR at 15 °C (59 °F)

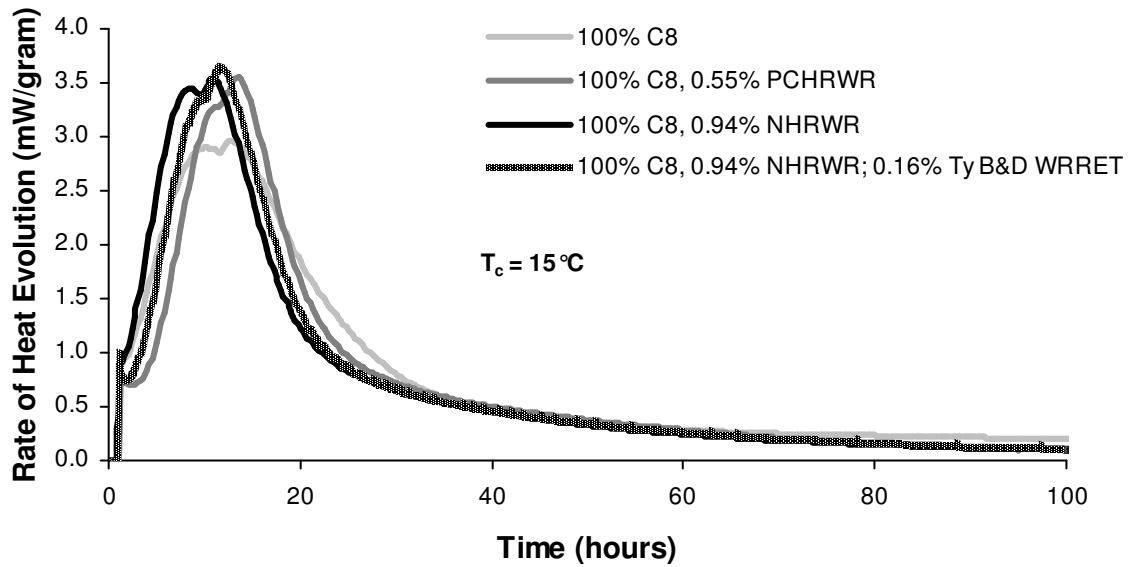


Figure B.30: Rate of Heat Evolution (Per Gram of Cementitious Material) for Paste Mixtures of 100% Cement C8 with NHRWR and PCHRWR at 15 °C (59 °F)

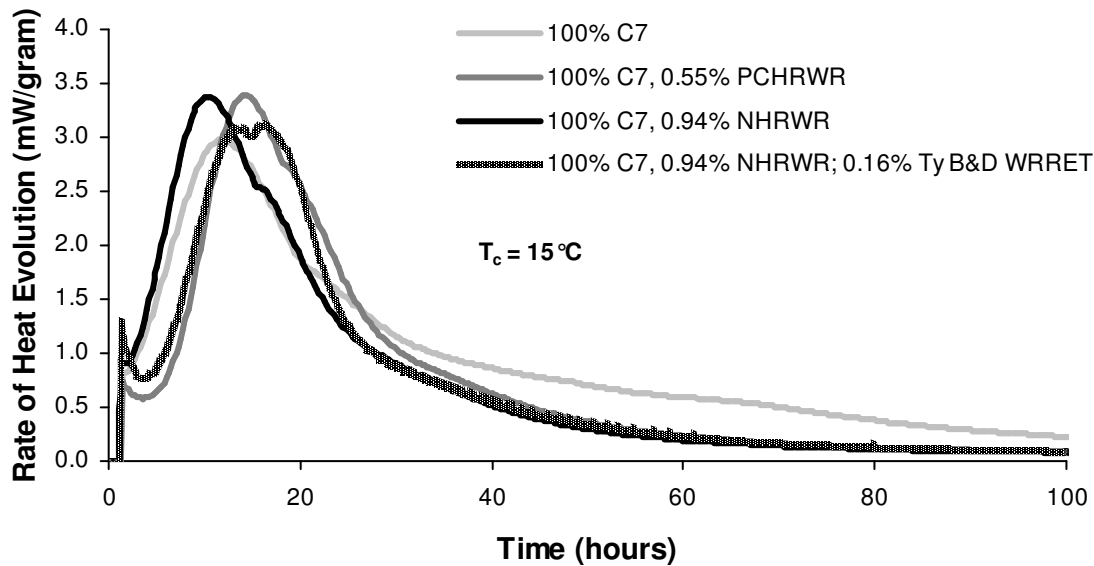


Figure B.31: Rate of Heat Evolution (Per Gram of Cementitious Material) for Paste Mixtures of 100% Cement C7 with NHRWR and PCHRWR at 15 °C (59 °F)

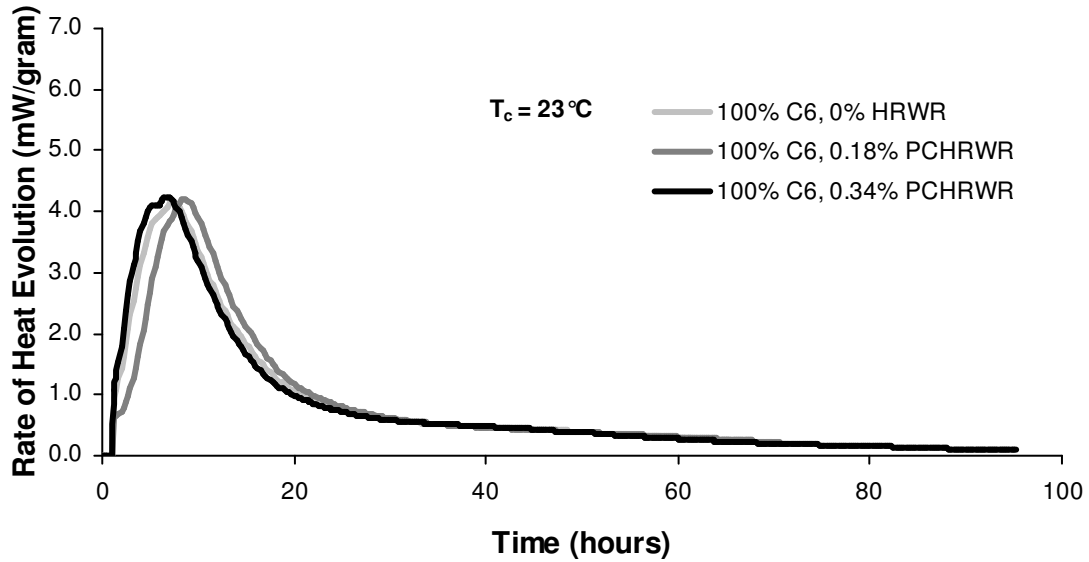


Figure B.32: Rate of Heat Evolution (Per Gram of Cementitious Material) for Paste Mixtures of 100% Cement C6 with PCHRWR at 23 °C (73 °F)

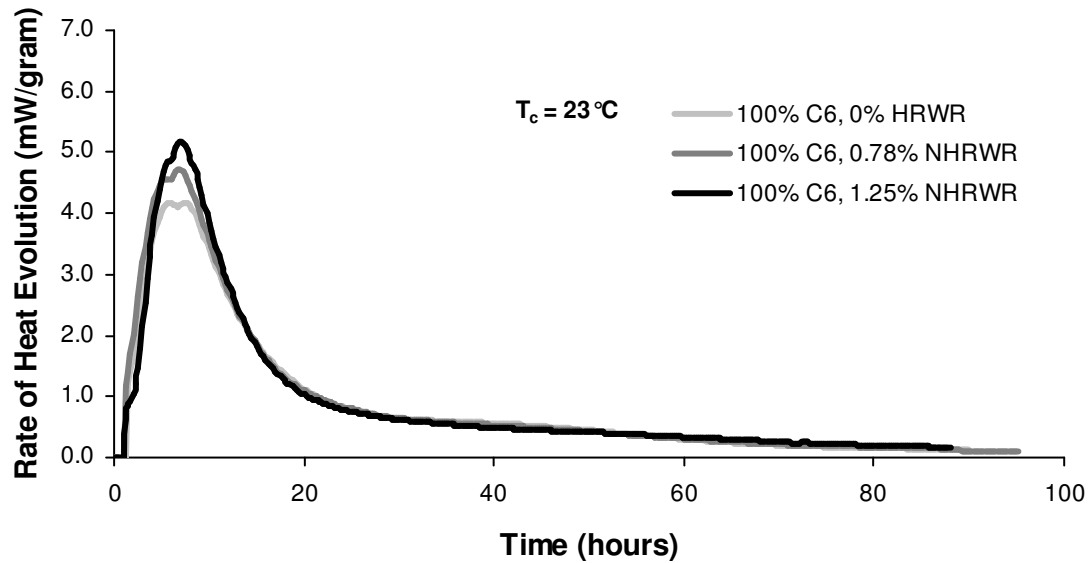


Figure B.33: Rate of Heat Evolution (Per Gram of Cementitious Material) for Paste Mixtures of 100% Cement C6 with NHRWR at 23 °C (73 °F)

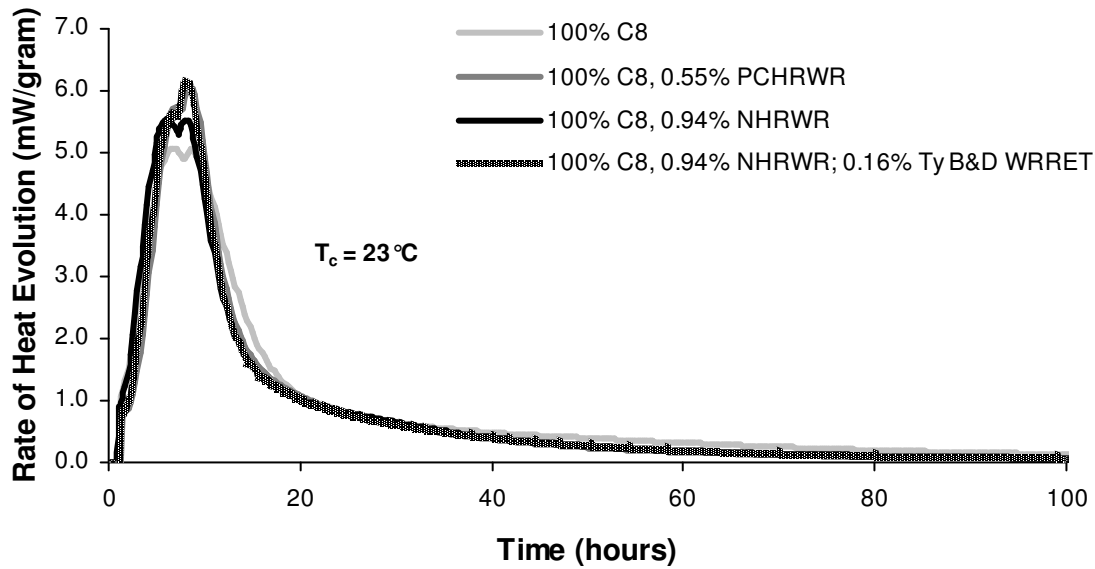


Figure B.34: Rate of Heat Evolution (Per Gram of Cementitious Material) for Paste Mixtures of 100% Cement C8 with NHRWR and PCHRWR at 23 °C (73 °F)

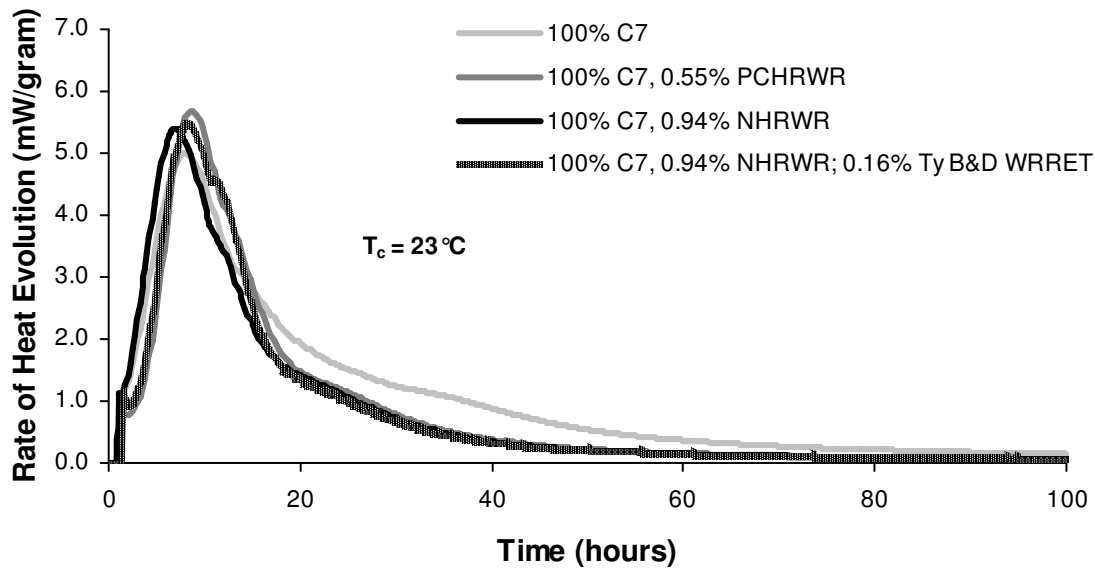


Figure B.35: Rate of Heat Evolution (Per Gram of Cementitious Material) for Paste Mixtures of 100% Cement C7 with NHRWR and PCHRWR at 23 °C (73 °F)

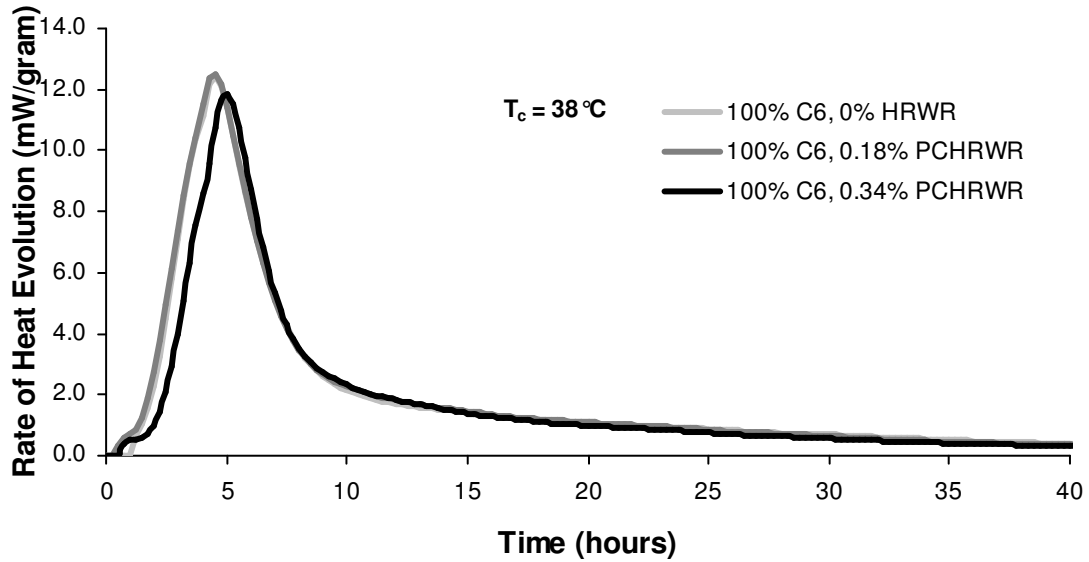


Figure B.36: Rate of Heat Evolution (Per Gram of Cementitious Material) for Paste Mixtures of 100% Cement C6 with PCHRWR at 38 °C (100 °F)

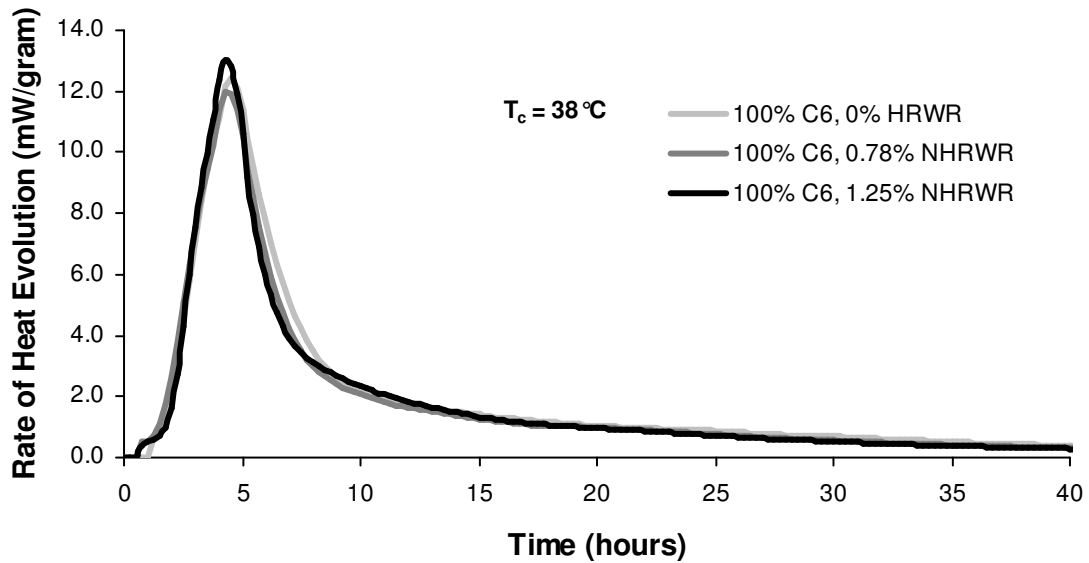


Figure B.37: Rate of Heat Evolution (Per Gram of Cementitious Material) for Paste Mixtures of 100% Cement C6 with NHRWR at 38 °C (100 °F)

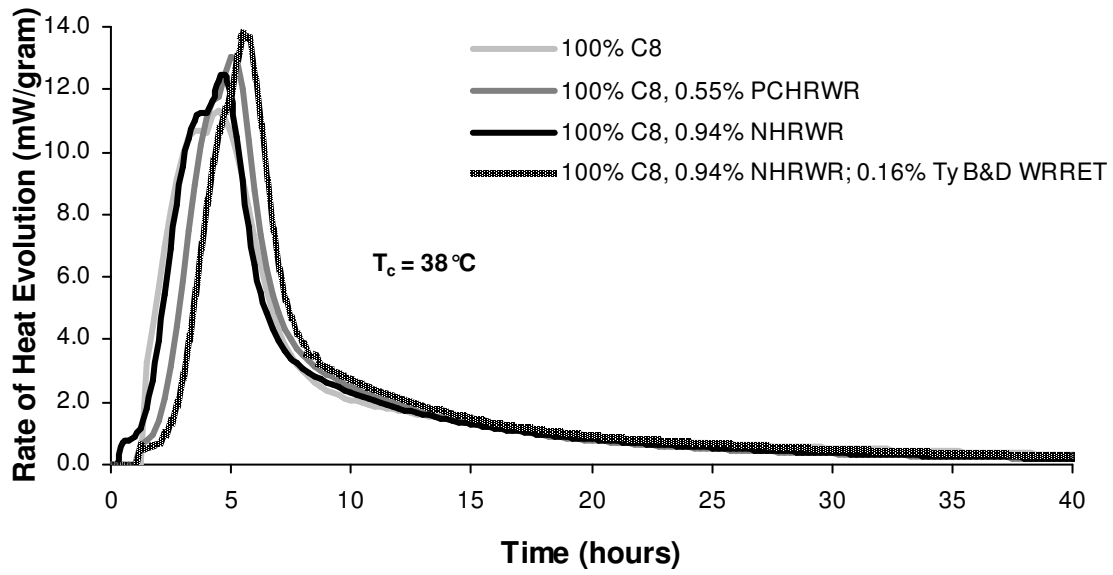


Figure B.38: Rate of Heat Evolution (Per Gram of Cementitious Material) for Paste Mixtures of 100% Cement C8 with NHRWR and PCHRWR at 38 °C (100 °F)

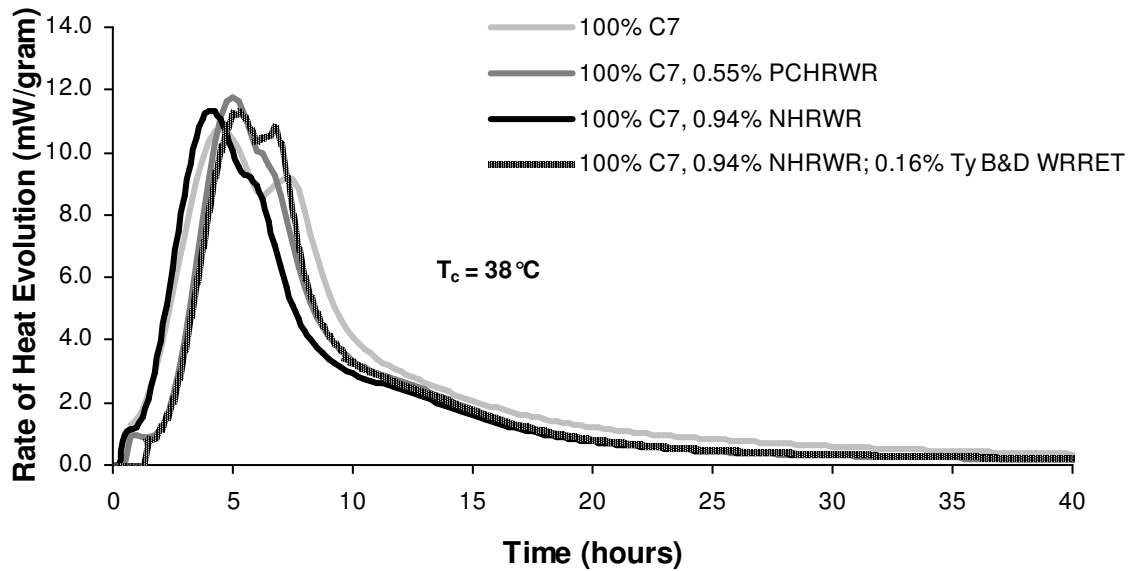


Figure B.39: Rate of Heat Evolution (Per Gram of Cementitious Material) for Paste Mixtures of 100% Cement C8 with NHRWR and PCHRWR at 38 °C (100 °F)

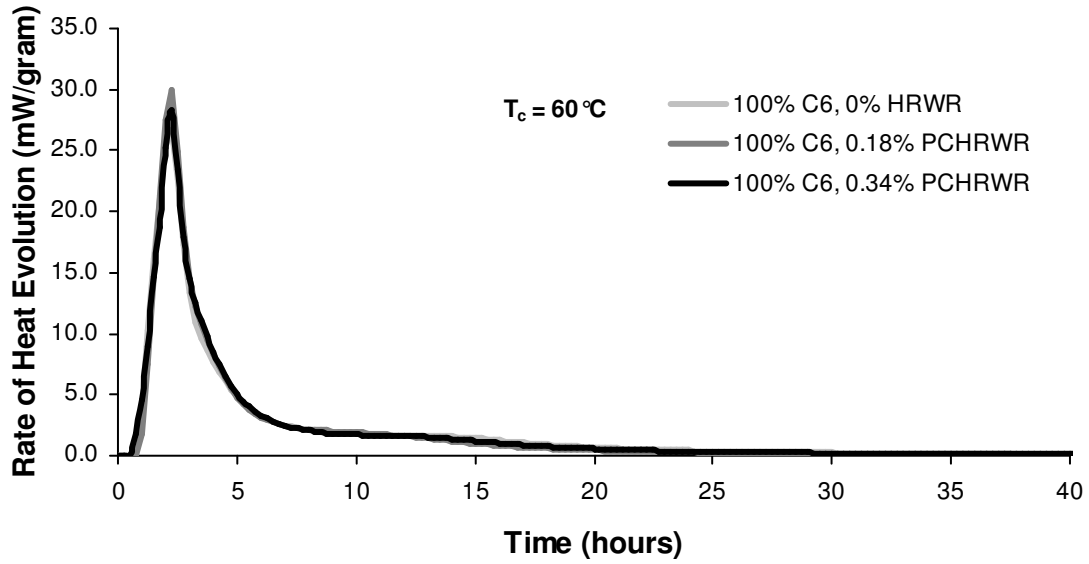


Figure B.40: Rate of Heat Evolution (Per Gram of Cementitious Material) for Paste Mixtures of 100% Cement C6 with PCHRWR at 60 °C (140 °F)

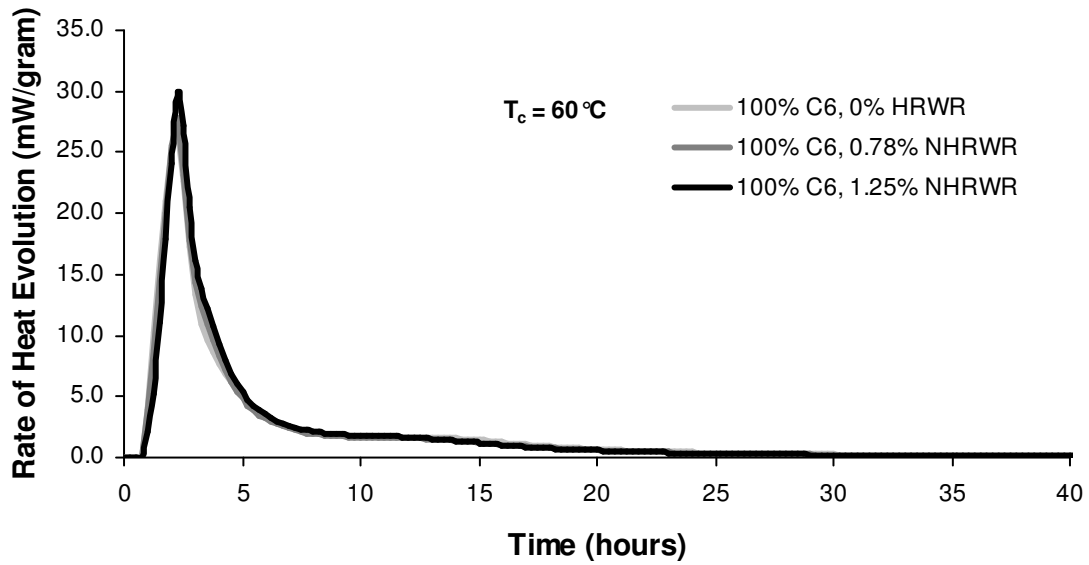


Figure B.41: Rate of Heat Evolution (Per Gram of Cementitious Material) for Paste Mixtures of 100% Cement C6 with NHRWR at 60 °C (140 °F)

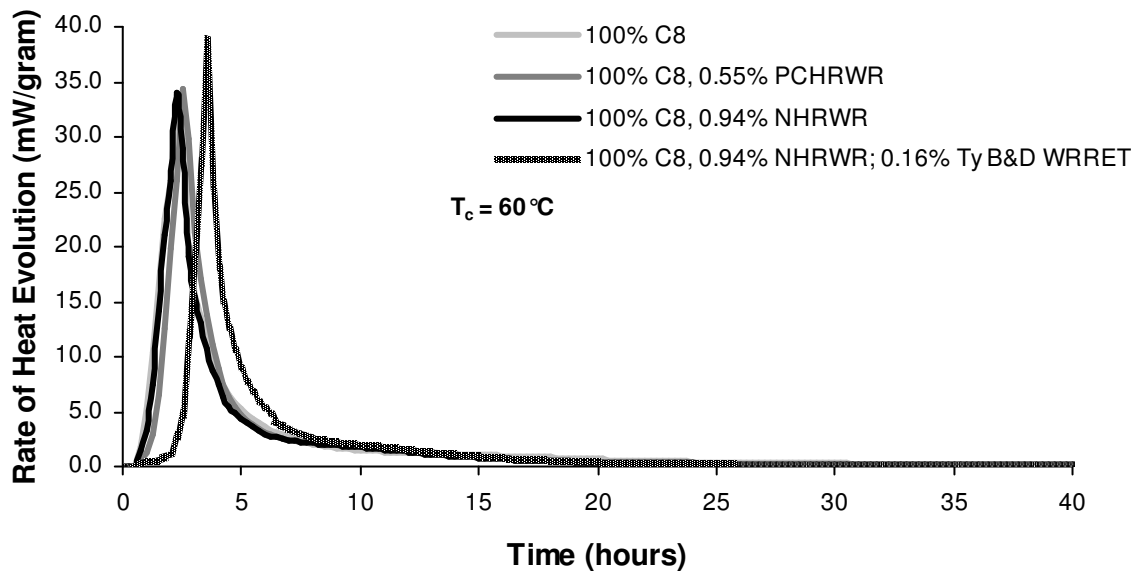


Figure B.42: Rate of Heat Evolution (Per Gram of Cementitious Material) for Paste Mixtures of 100% Cement C8 with NHRWR and PCHRWR at 60 °C (140 °F)

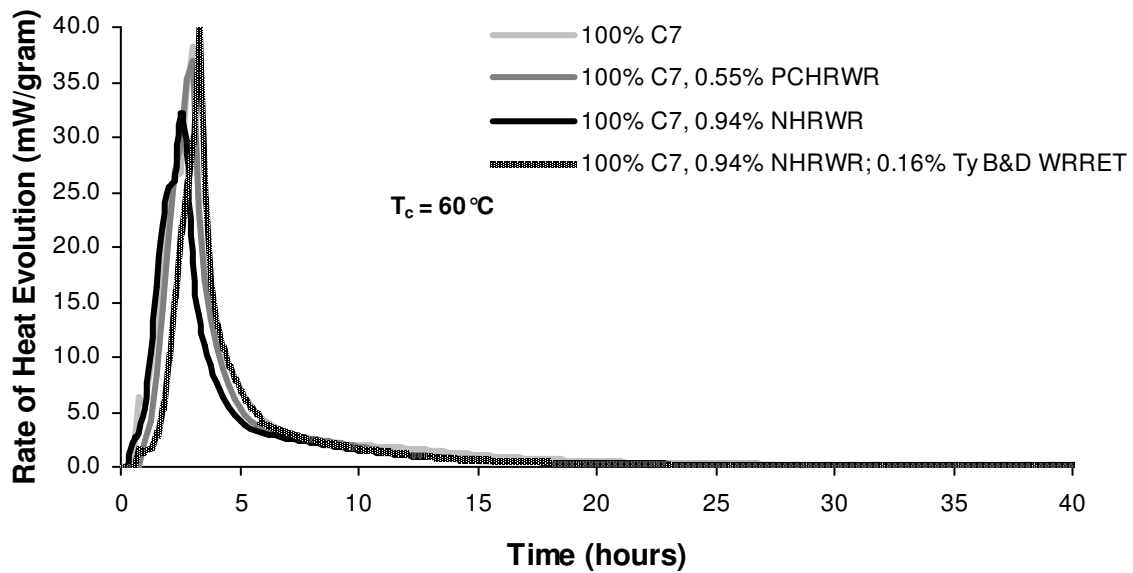


Figure B.43: Rate of Heat Evolution (Per Gram of Cementitious Material) for Paste Mixtures of 100% Cement C8 with NHRWR and PCHRWR at 60 °C (140 °F)

B.4. EFFECTS OF WRRET AND ACCL ON MIXTURES WITH SCMS

The following figures provide background for the effects of low-range water reducing and retarding (LRWR and WRRET) and calcium-nitrate based accelerating admixtures on hydration presented in Chapter 3. Results at each of the isothermal test temperatures are shown.

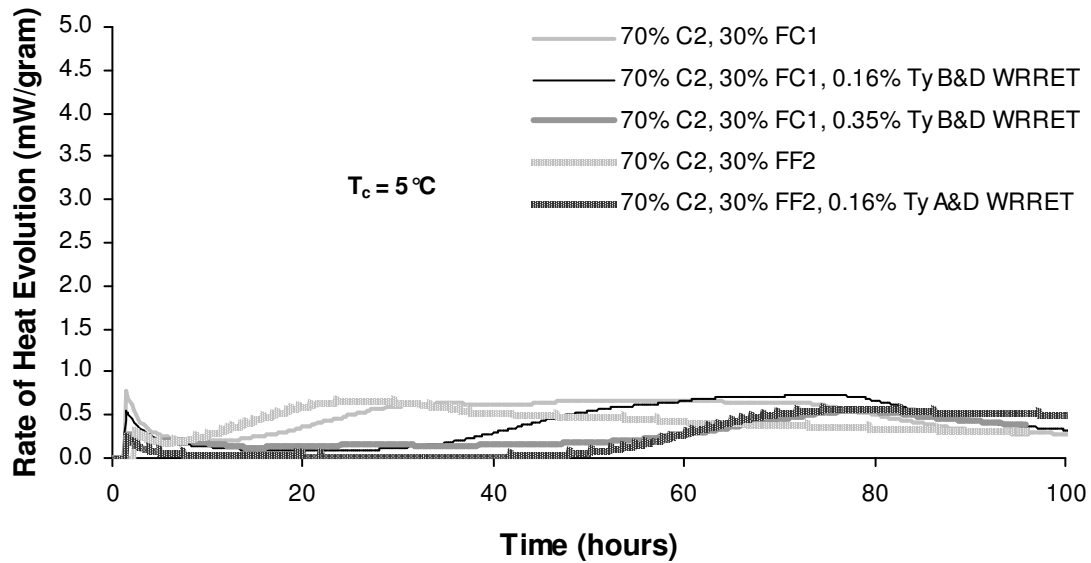


Figure B.44: Rate of Heat Evolution (Per Gram of Cementitious Material) for Paste Mixtures with 70% Cement C2, 30% FC1, and FF2 with WRRET at 5 °C (41 °F)

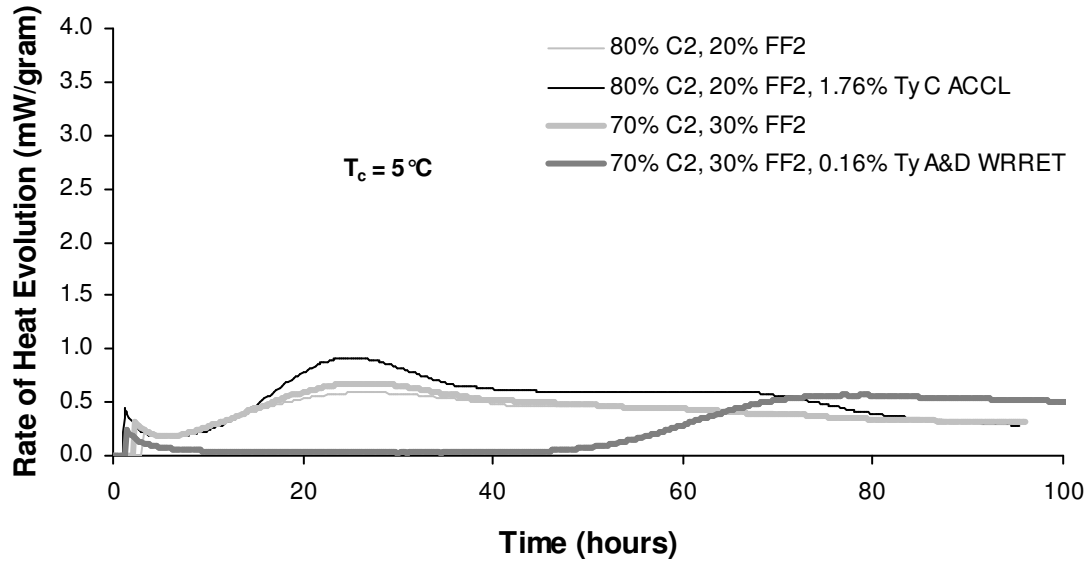


Figure B.45: Rate of Heat Evolution (Per Gram of Cementitious Material) for Paste Mixtures of 80% Cement C2, 20% FF2 with ACCL and 70% Cement C2, 30% FF2 with WRRET at 5 °C (41 °F)

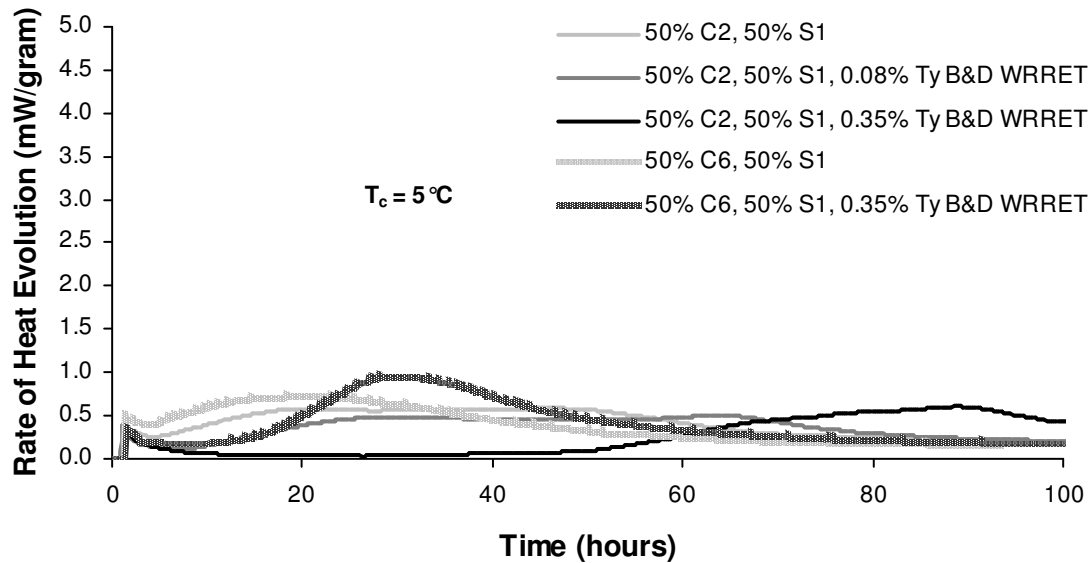


Figure B.46: Rate of Heat Evolution (Per Gram of Cementitious Material) for Paste Mixtures of 50% Cements C2 and C6 with 50% GGBFS with WRRET at 5 °C (41 °F)

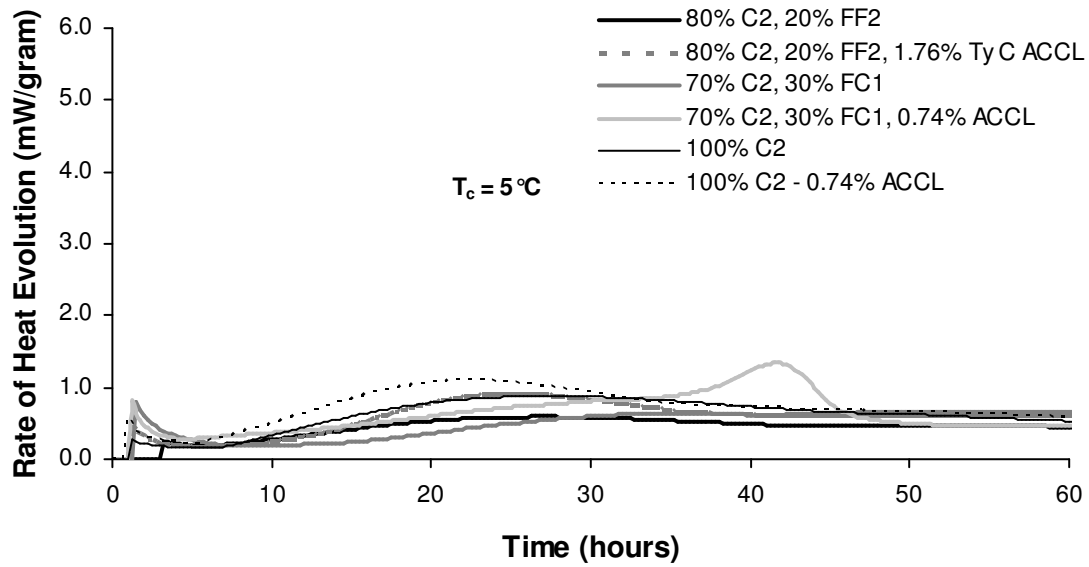


Figure B.47: Rate of Heat Evolution (Per Gram of Cementitious Material) for Paste Mixtures of 80% Cement C2, 20% FF2 with ACCL and 70% Cement C2, 30% FC2 with ACCL at 5 °C (41 °F)

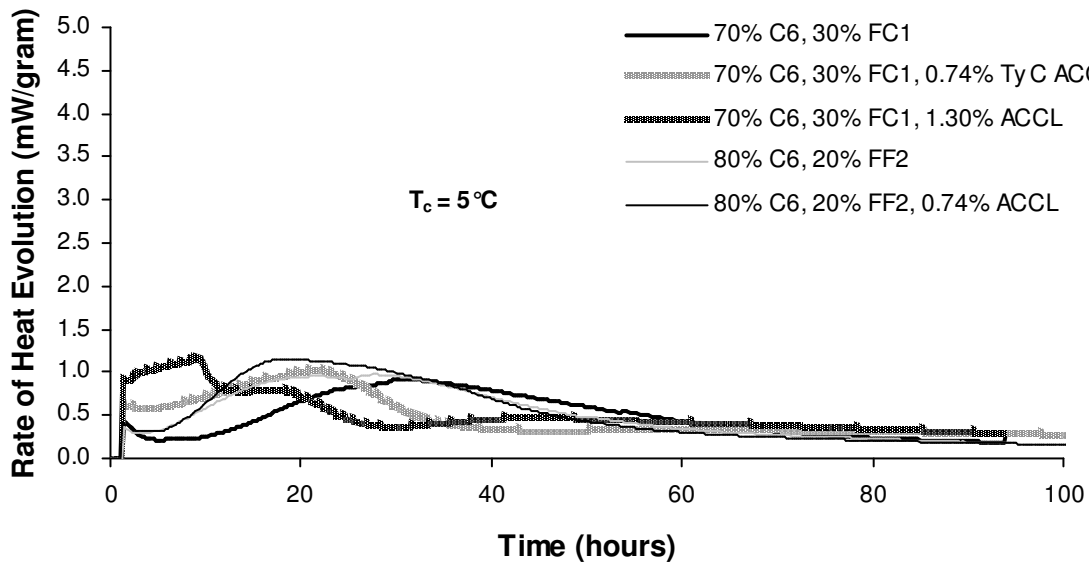


Figure B.48: Rate of Heat Evolution (Per Gram of Cementitious Material) for Paste Mixtures of 80% Cement C6, 20% FF2 with ACCL and 70% Cement C6, 30% FC1 with ACCL at 5 °C (41 °F)

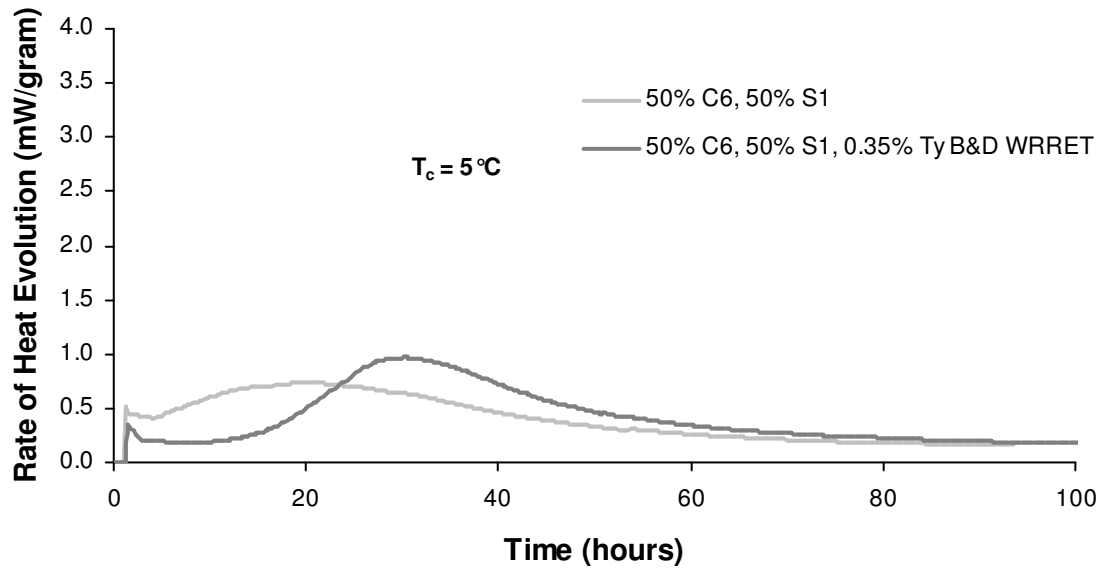


Figure B.49: Rate of Heat Evolution (Per Gram of Cementitious Material) for Paste Mixtures of 50% Cement C6, 50% S1 with WRRET at 5 °C (41 °F)

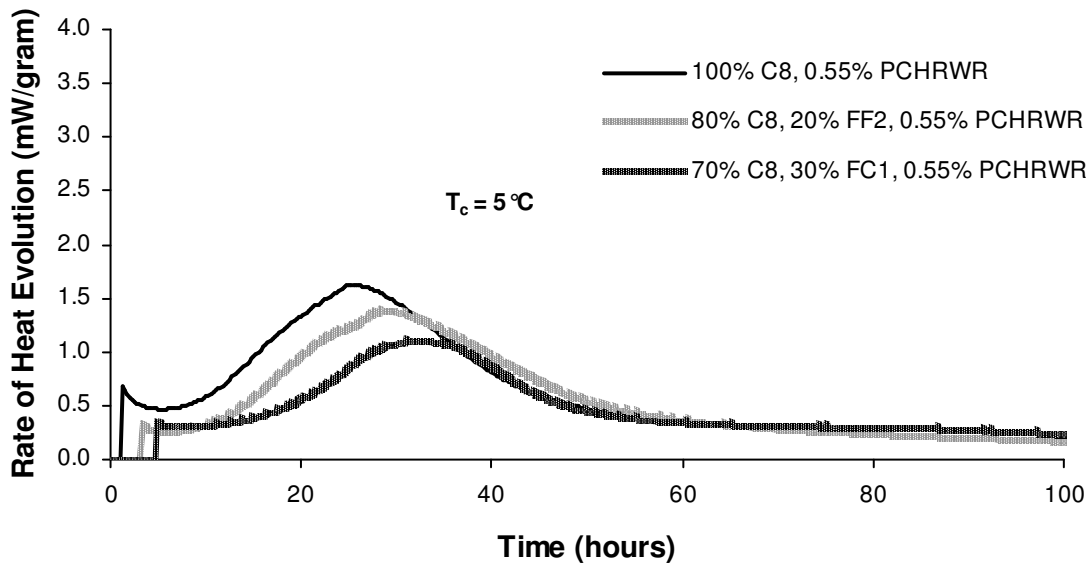


Figure B.50: Rate of Heat Evolution (Per Gram of Cementitious Material) for Paste Mixtures of 80% Cement C6, 20% FF2 with ACCL and 70% Cement C8, 30% FC1 with PCHRWR at 5 °C (41 °F)

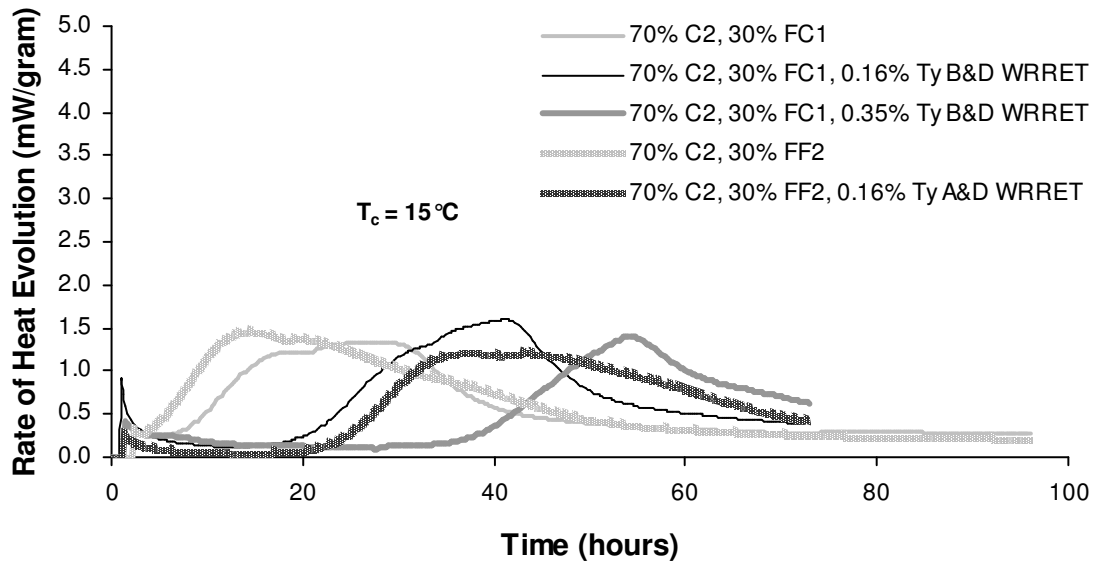


Figure B.51: Rate of Heat Evolution (Per Gram of Cementitious Material) for Paste Mixtures with 70% Cement C2, 30% FC1, and FF2 with WRRET at 15 °C (59 °F)

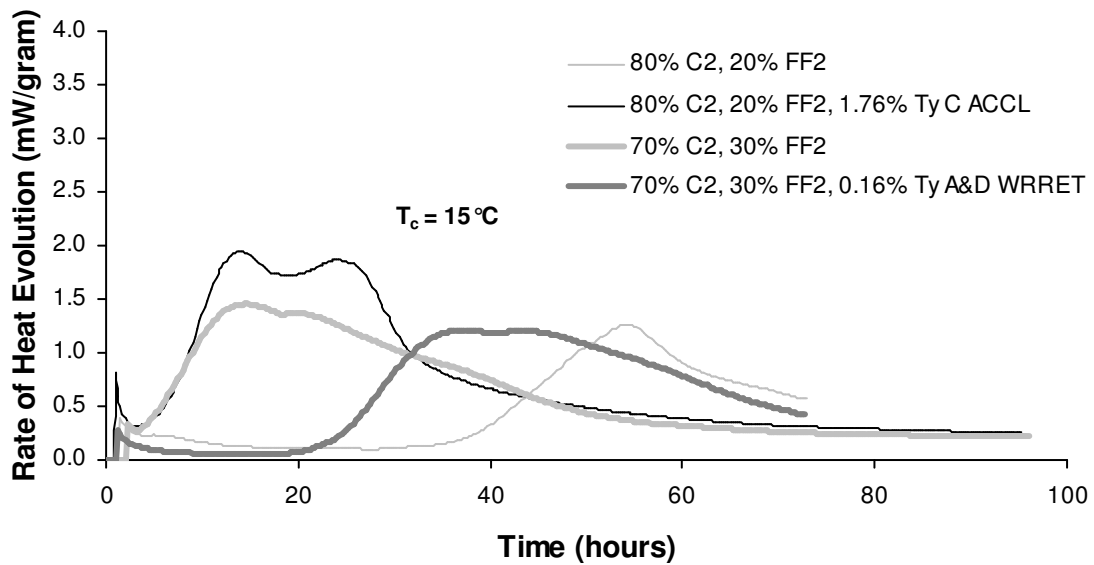


Figure B.52: Rate of Heat Evolution (Per Gram of Cementitious Material) for Paste Mixtures of 80% Cement C2, 20% FF2 with ACCL and 70% Cement C2, 30% FF2 with WRRET at 15 °C (59 °F)

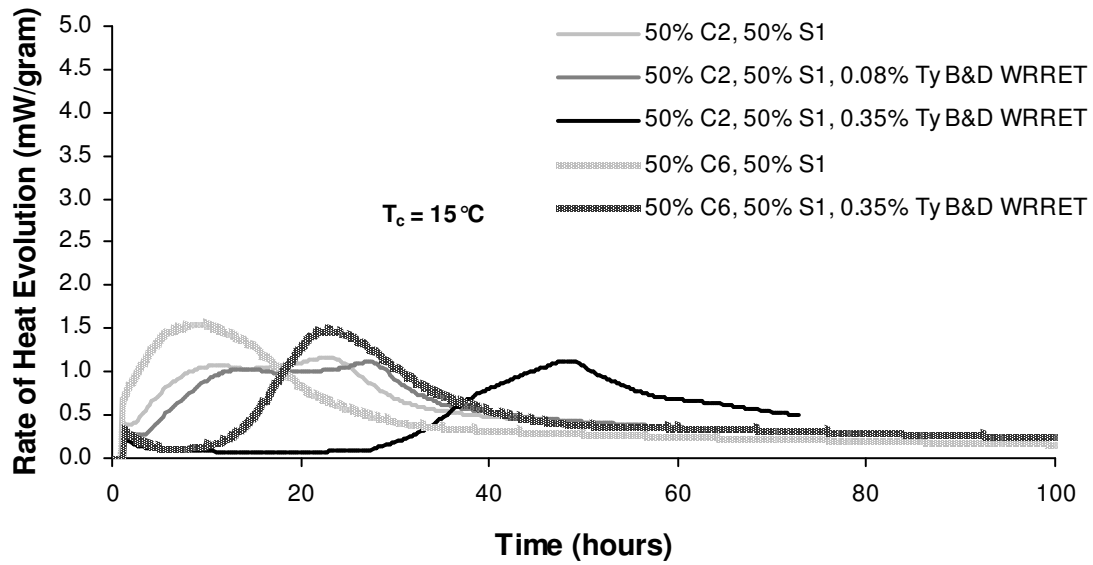


Figure B.53: Rate of Heat Evolution (Per Gram of Cementitious Material) for Paste Mixtures of 50% Cements C2 and C6 with 50% GGBFS with WRRET at 15 °C (59 °F)

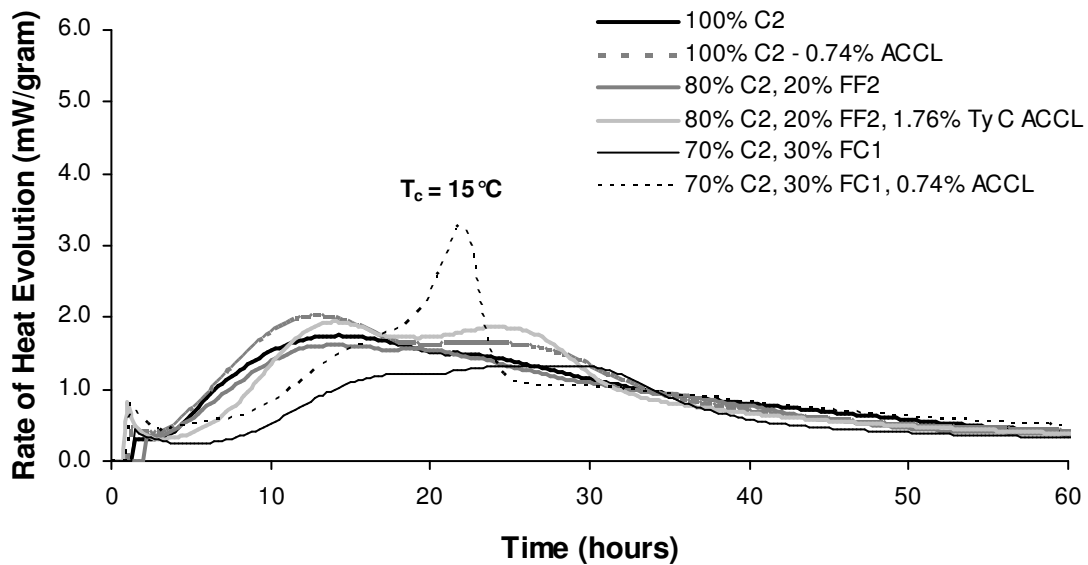


Figure B.54: Rate of Heat Evolution (Per Gram of Cementitious Material) for Paste Mixtures of 80% Cement C2, 20% FF2 with ACCL and 70% Cement C2, 30% FC2 with ACCL at 15 °C (59 °F)

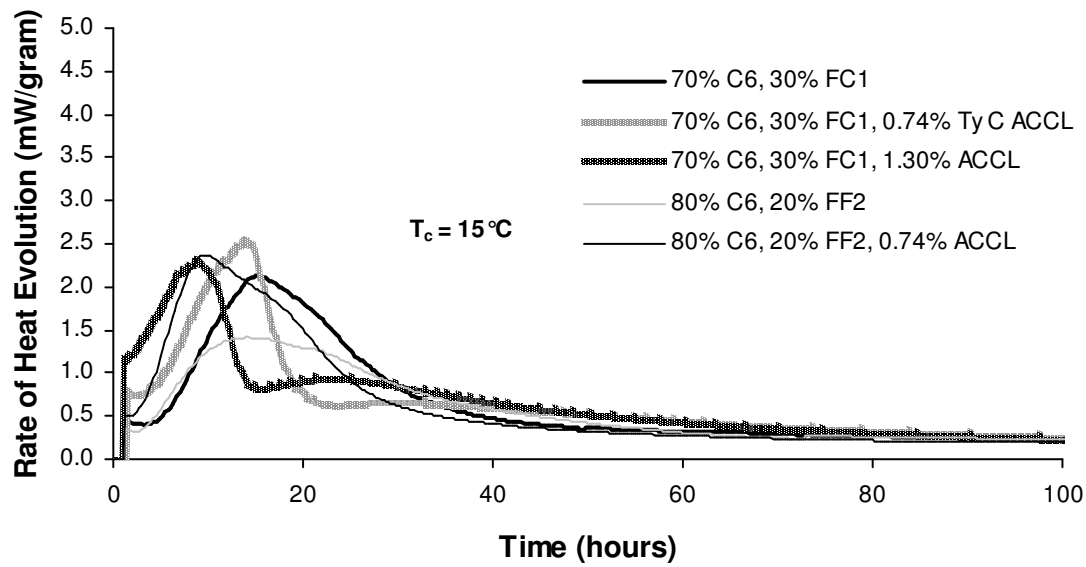


Figure B.55: Rate of Heat Evolution (Per Gram of Cementitious Material) for Paste Mixtures of 80% Cement C6, 20% FF2 with ACCL and 70% Cement C6, 30% FC1 with ACCL at 15 °C (59 °F)

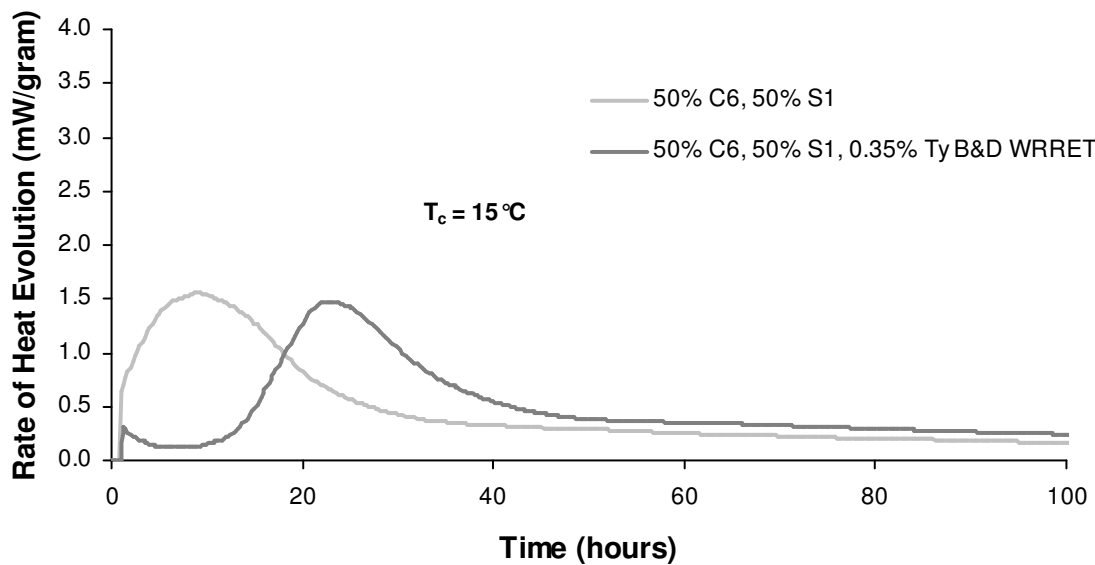


Figure B.56: Rate of Heat Evolution (Per Gram of Cementitious Material) for Paste Mixtures of 50% Cement C6, 50% S1 with WRRET at 15 °C (59 °F)

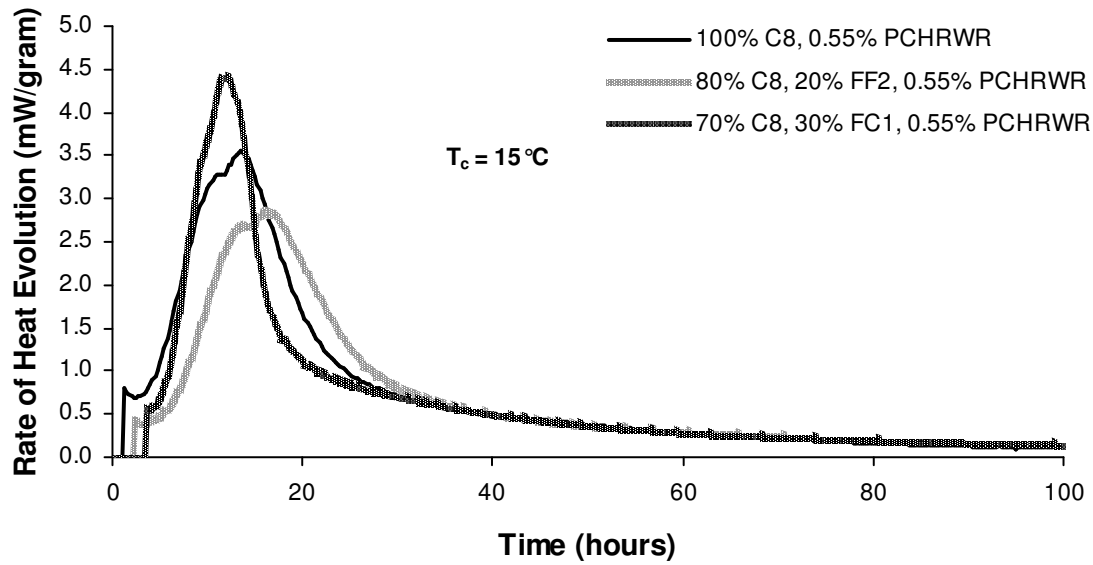


Figure B.57: Rate of Heat Evolution (Per Gram of Cementitious Material) for Paste Mixtures of 80% Cement C6, 20% FF2 with ACCL and 70% Cement C8, 30% FC1 with PCHRWR at 15 °C (59 °F)

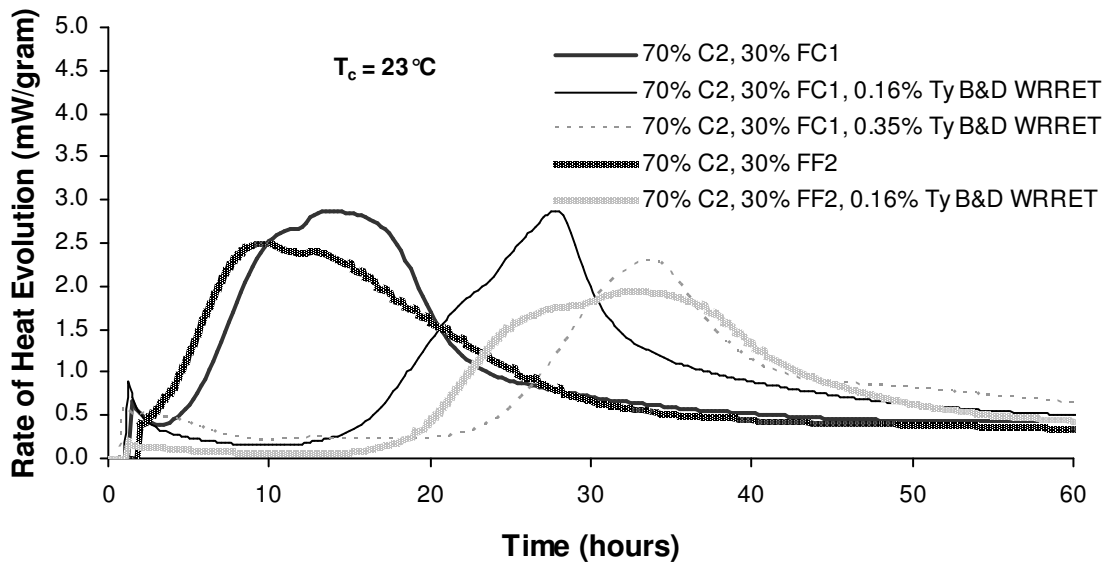


Figure B.58: Rate of Heat Evolution (Per Gram of Cementitious Material) for Paste Mixtures with 70% Cement C2, 30% FC1, and FF2 with WRRET at 23 °C (73 °F)

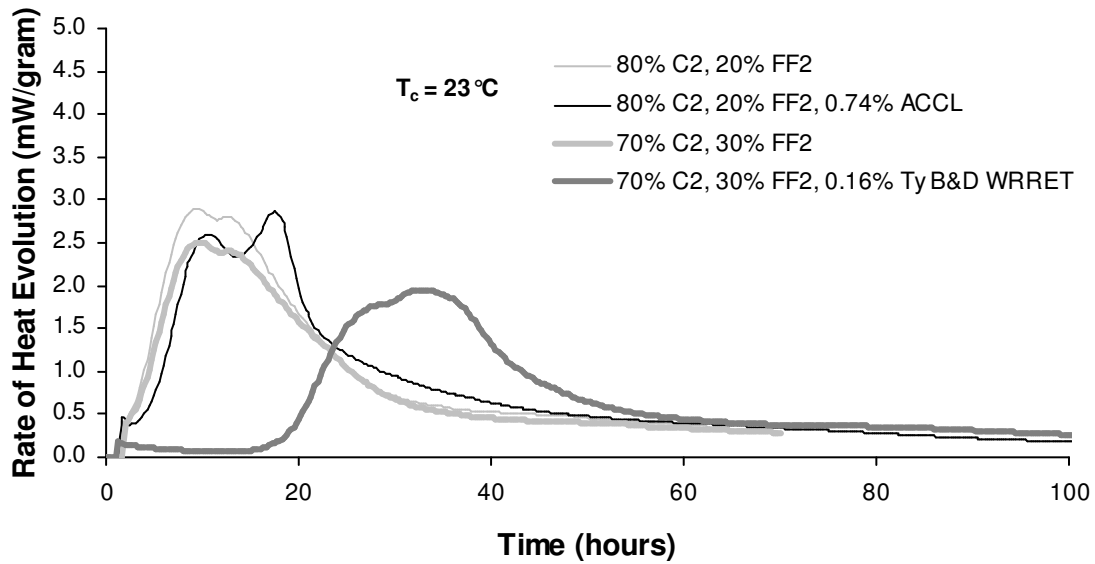


Figure B.59: Rate of Heat Evolution (Per Gram of Cementitious Material) for Paste Mixtures of 80% Cement C2 with 20% FF2 with ACCL and 70% Cement C2 with 30% FF2 with WRRET at 23 °C (73 °F)

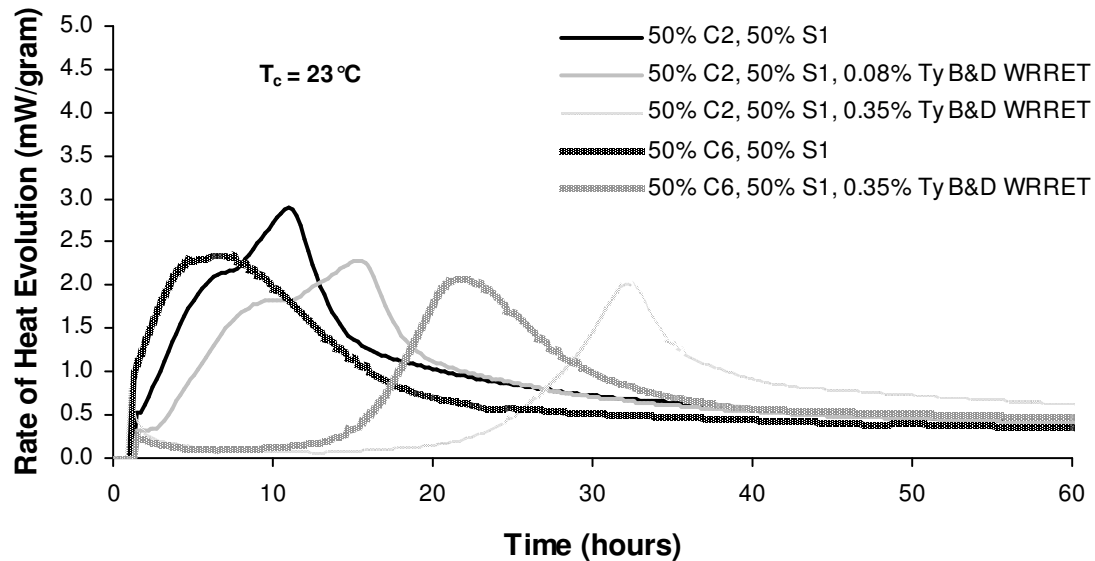


Figure B.60: Rate of Heat Evolution (Per Gram of Cementitious Material) for Paste Mixtures of 50% Cements C2 and C6 with 50% GGBFS with WRRET at 23 °C (73 °F)

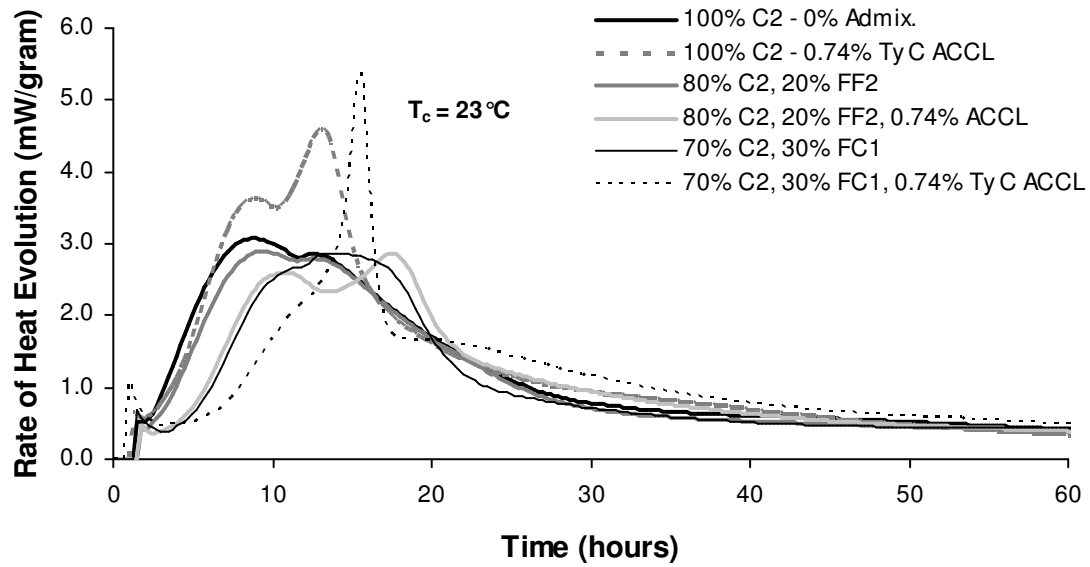


Figure B.61: Rate of Heat Evolution (Per Gram of Cementitious Material) for Paste Mixtures of 100% Cement C2, 80% Cement C2, 20% FF2, and 70% Cement C2, 30% FC2 with ACCL at 23 °C (41 °F)

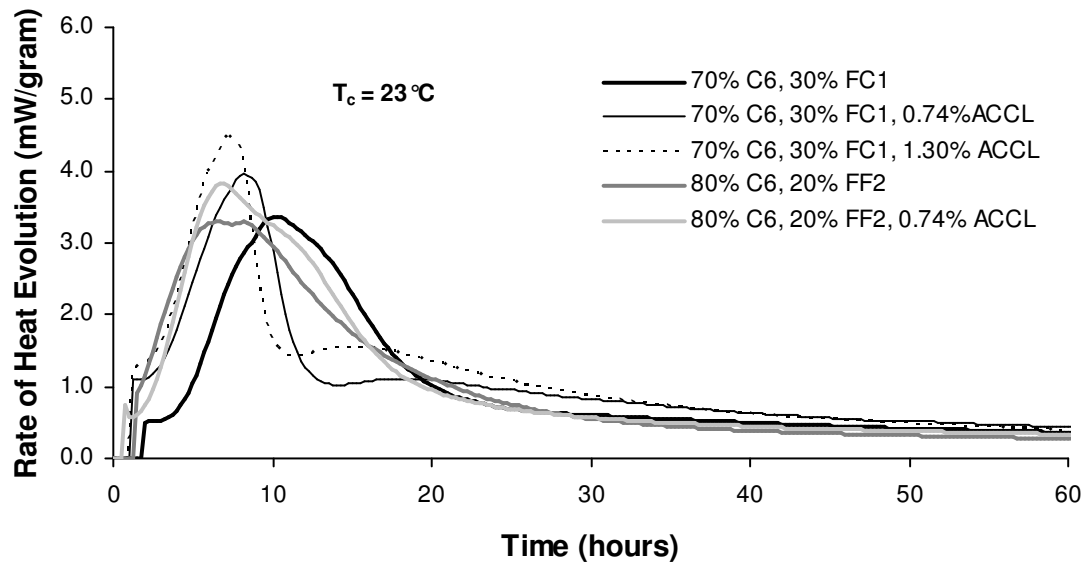


Figure B.62: Rate of Heat Evolution (Per Gram of Cementitious Material) for Paste Mixtures of 80% Cement C6, 20% FF2 with ACCL and 70% Cement C6, 30% FC1 with ACCL at 23 °C (73 °F)

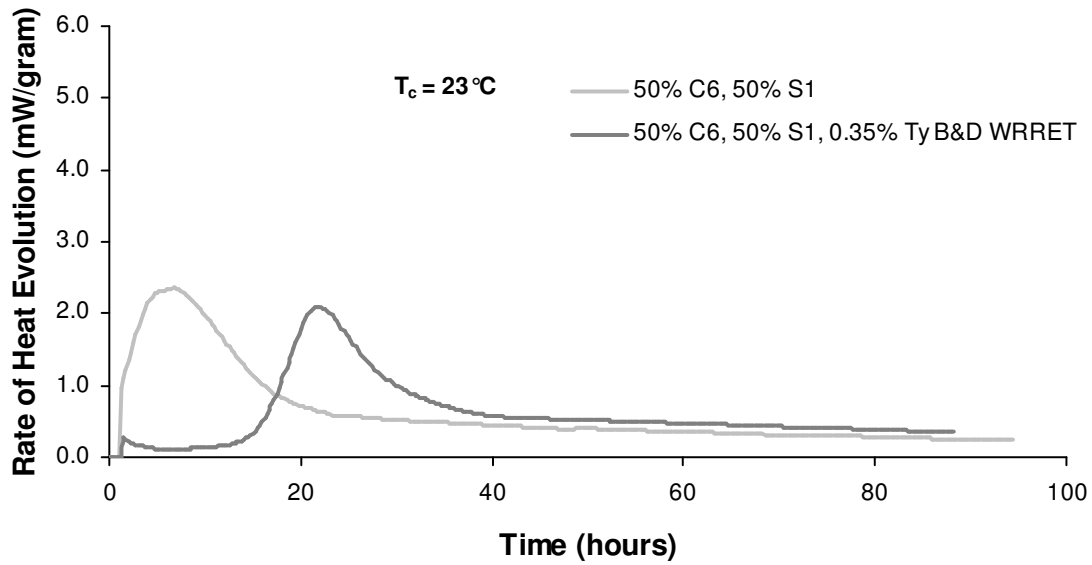


Figure B.63: Rate of Heat Evolution (Per Gram of Cementitious Material) for Paste Mixtures of 50% Cement C6, 50% S1 with WRRET at 23 °C (73 °F)

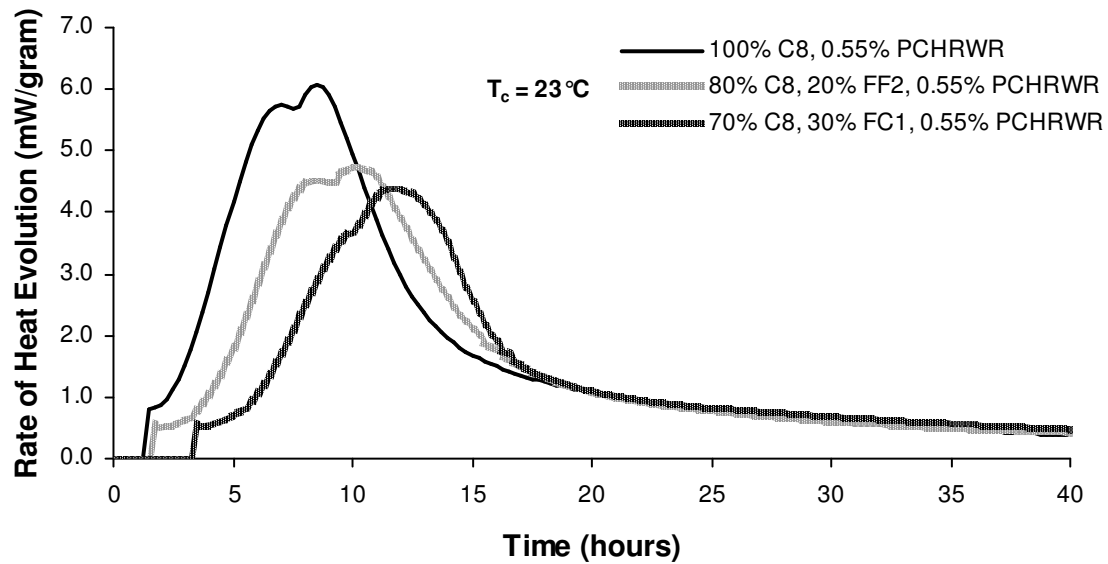


Figure B.64: Rate of Heat Evolution (Per Gram of Cementitious Material) for Paste Mixtures of 80% Cement C6, 20% FF2 with ACCL and 70% Cement C8, 30% FC1 with PCHRWR at 23 °C (73 °F)

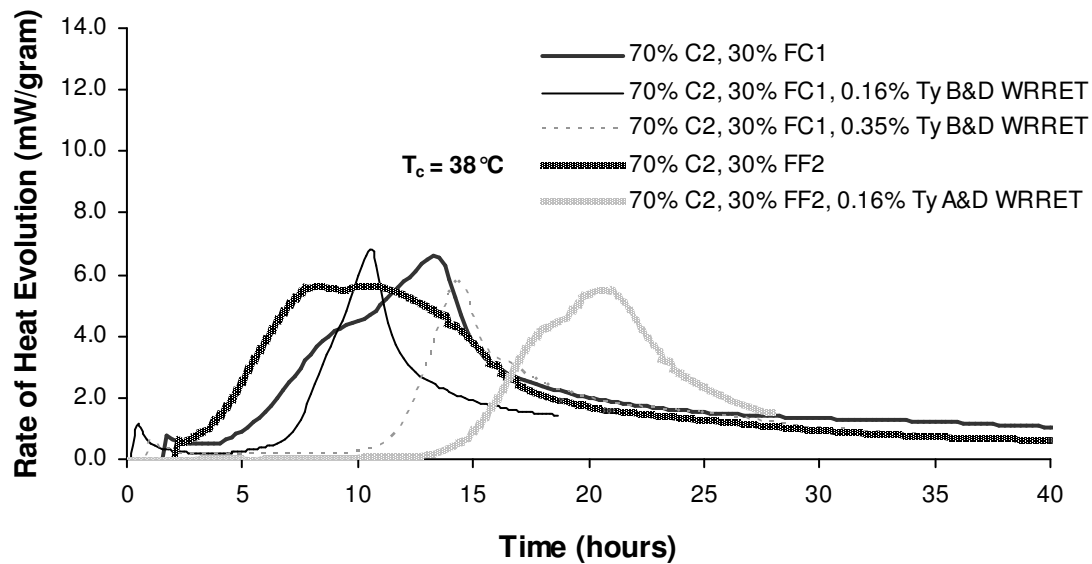


Figure B.65: Rate of Heat Evolution (Per Gram of Cementitious Material) for Paste Mixtures with 70% Cement C2, 30% FC1, and FF2 with WRRET at 38 °C (100 °F)

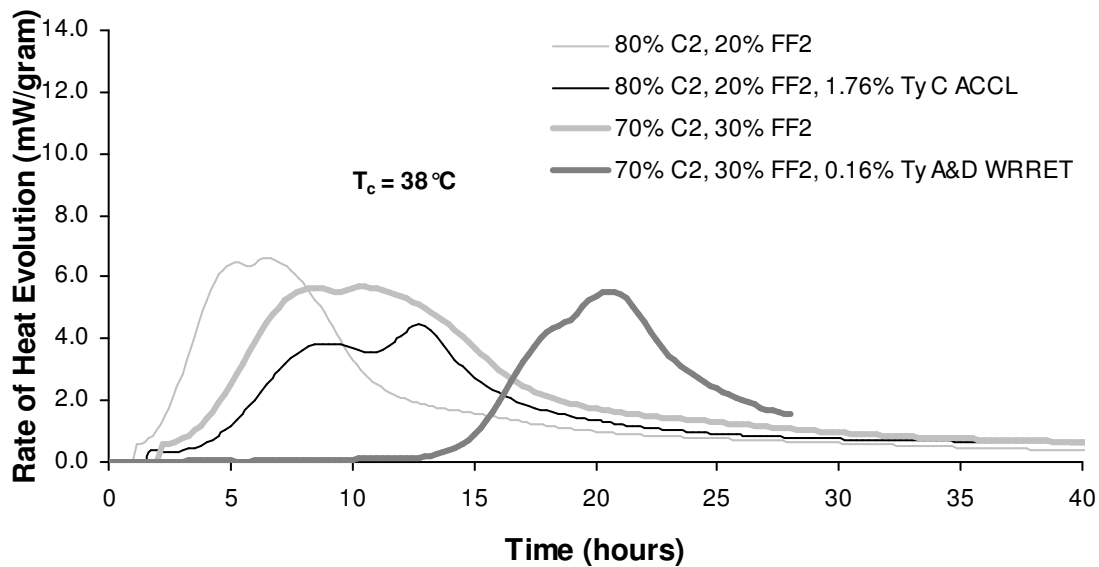


Figure B.66: Rate of Heat Evolution (Per Gram of Cementitious Material) for Paste Mixtures of 80% Cement C2, 20% FF2 with ACCL and 70% Cement C2, 30% FF2 with WRRET at 38 °C (100 °F)

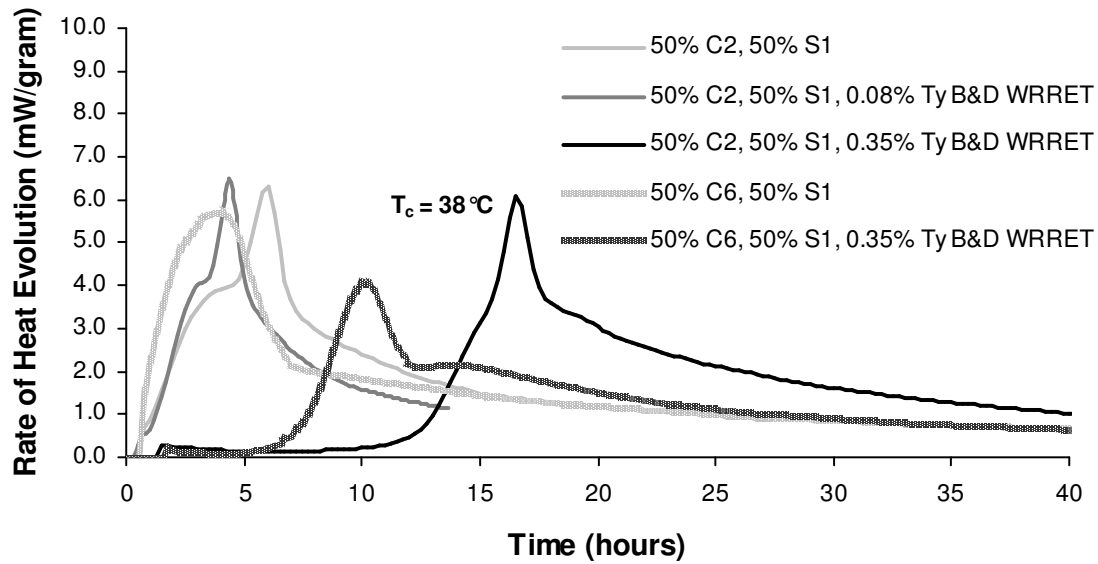


Figure B.67: Rate of Heat Evolution (Per Gram of Cementitious Material) for Paste Mixtures of 50% Cements C2 and C6 with 50% GGBFS with WRRET at 38 °C (100 °F)

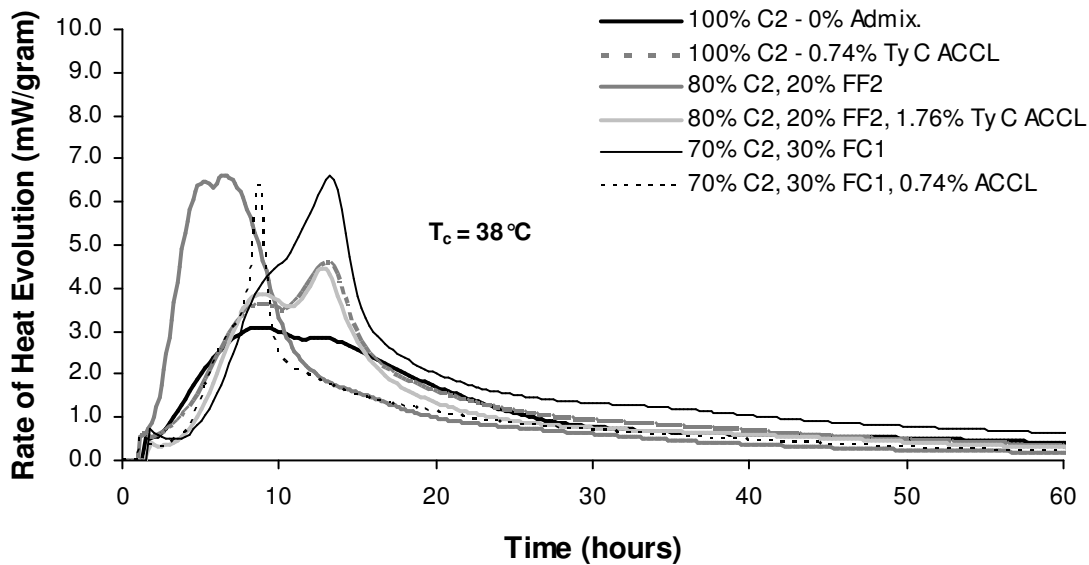


Figure B.68: Rate of Heat Evolution (Per Gram of Cementitious Material) for Paste Mixtures of 80% Cement C2, 20% FF2 with ACCL and 70% Cement C2, 30% FC2 with ACCL at 38 °C (100 °F)

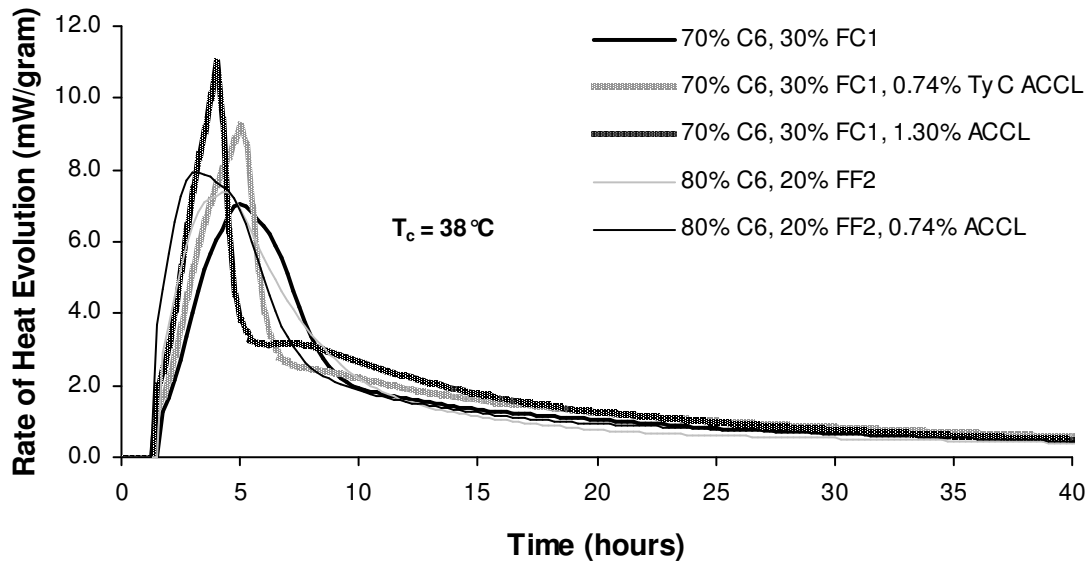


Figure B.69: Rate of Heat Evolution (Per Gram of Cementitious Material) for Paste Mixtures of 80% Cement C6, 20% FF2 with ACCL and 70% Cement C6, 30% FC1 with ACCL at 38 °C (100 °F)

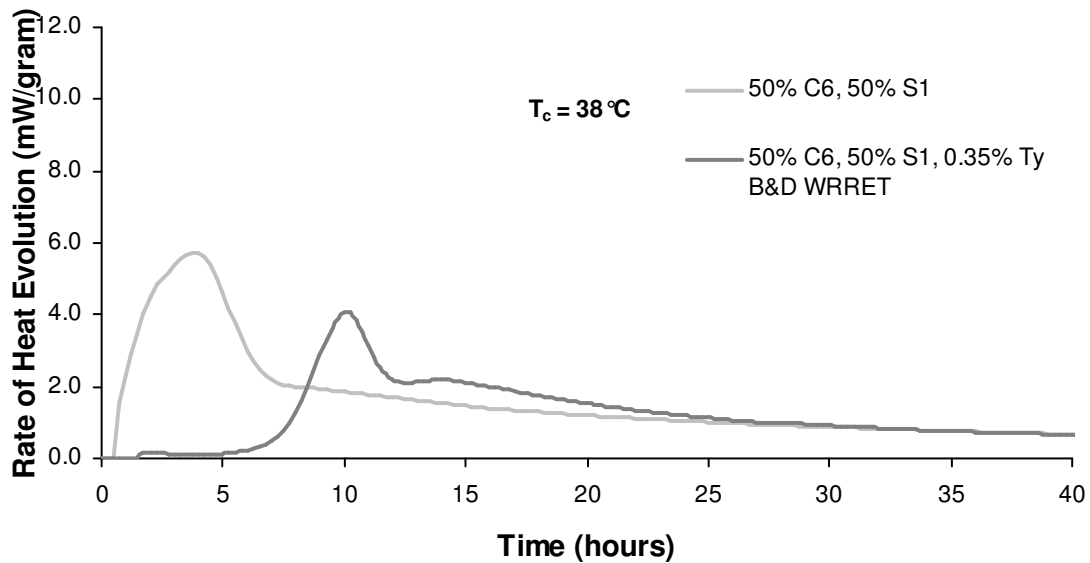


Figure B.70: Rate of Heat Evolution (Per Gram of Cementitious Material) for Paste Mixtures of 50% Cement C6, 50% S1 with WRRET at 38 °C (100 °F)

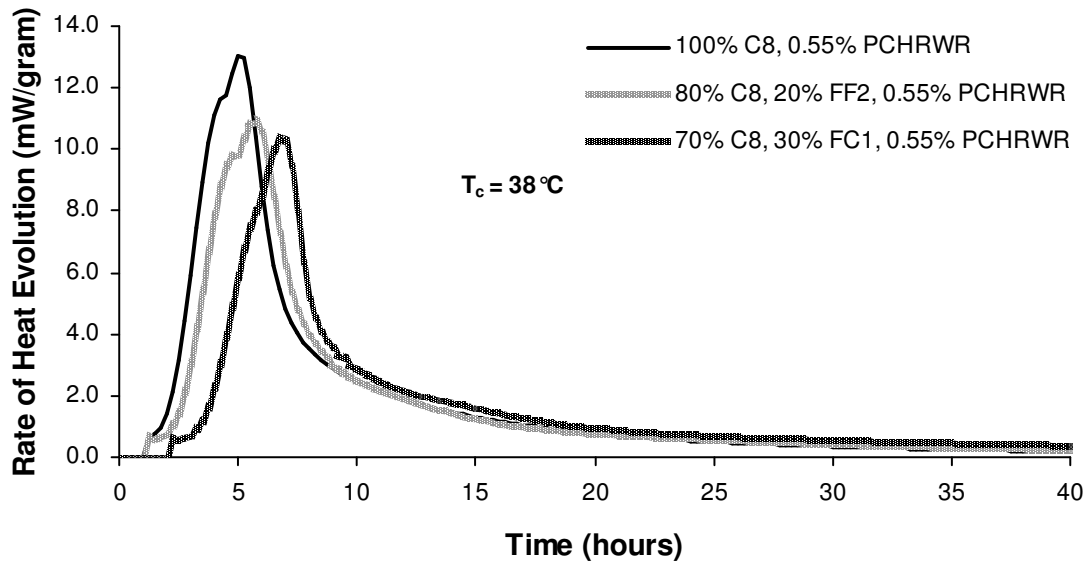


Figure B.71: Rate of Heat Evolution (Per Gram of Cementitious Material) for Paste Mixtures of 80% Cement C6, 20% FF2 with ACCL and 70% Cement C8, 30% FC1 with PCHRWR at 38 °C (100 °F)

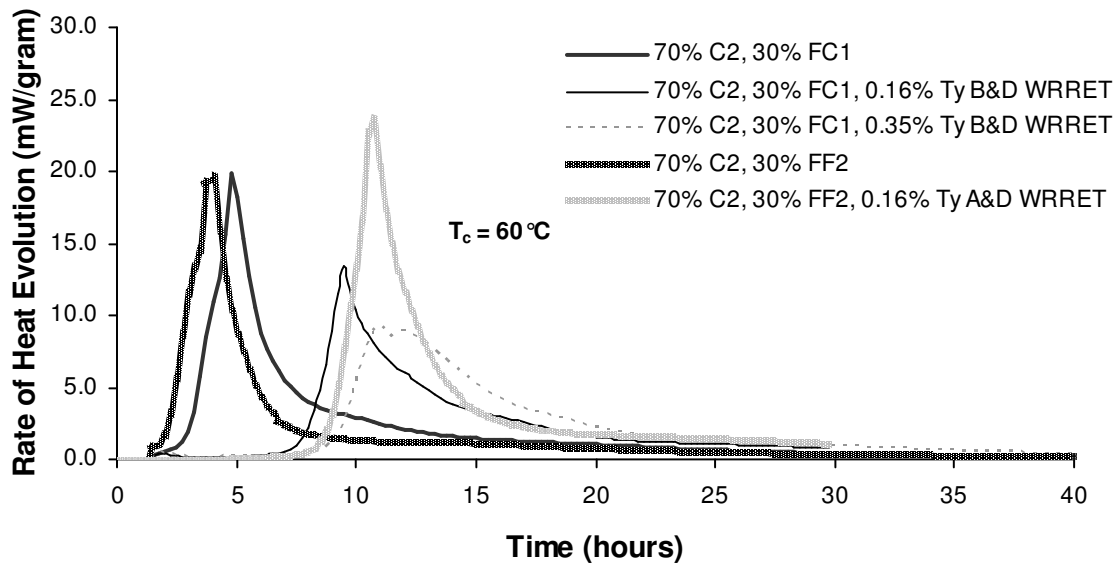


Figure B.72: Rate of Heat Evolution (Per Gram of Cementitious Material) for Paste Mixtures with 70% Cement C2, 30% FC1, and 30% FF2 with WRRET at 60 °C (140 °F)

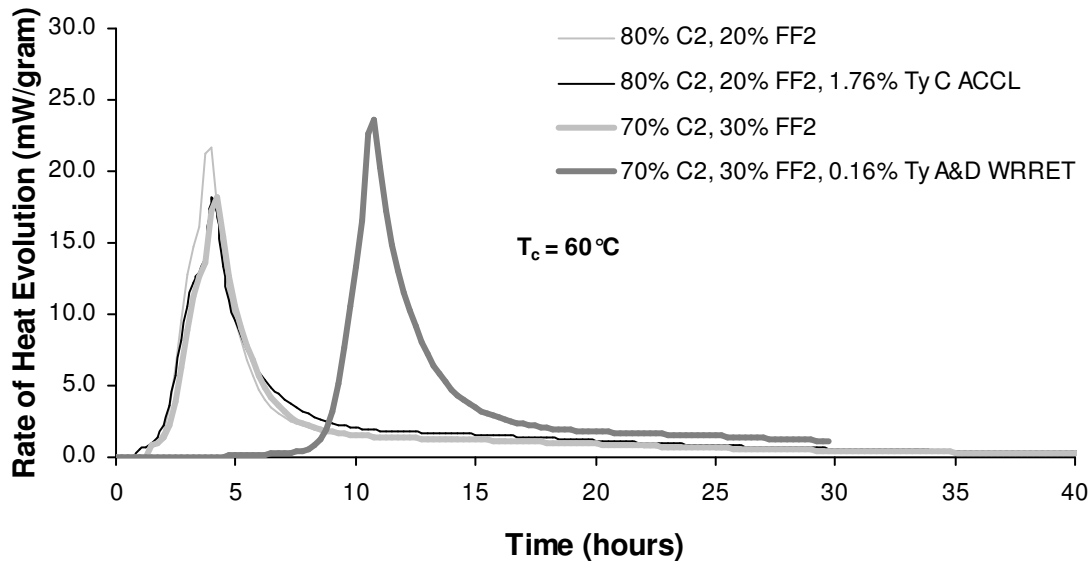


Figure B.73: Rate of Heat Evolution (Per Gram of Cementitious Material) for Paste Mixtures of 80% Cement C2, 20% FF2 with ACCL and 70% Cement C2, 30% FF2 with WRRET at 60 °C (140 °F)

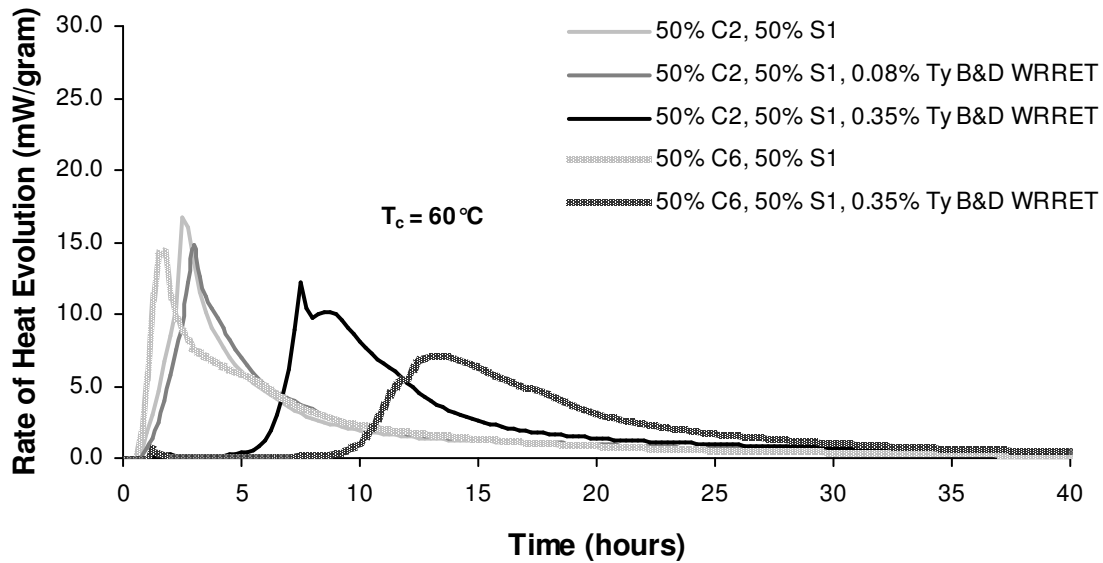


Figure B.74: Rate of Heat Evolution (Per Gram of Cementitious Material) for Paste Mixtures of 50% Cements C2 and C6 with 50% GGBFS with WRRET at 60 °C (140 °F)

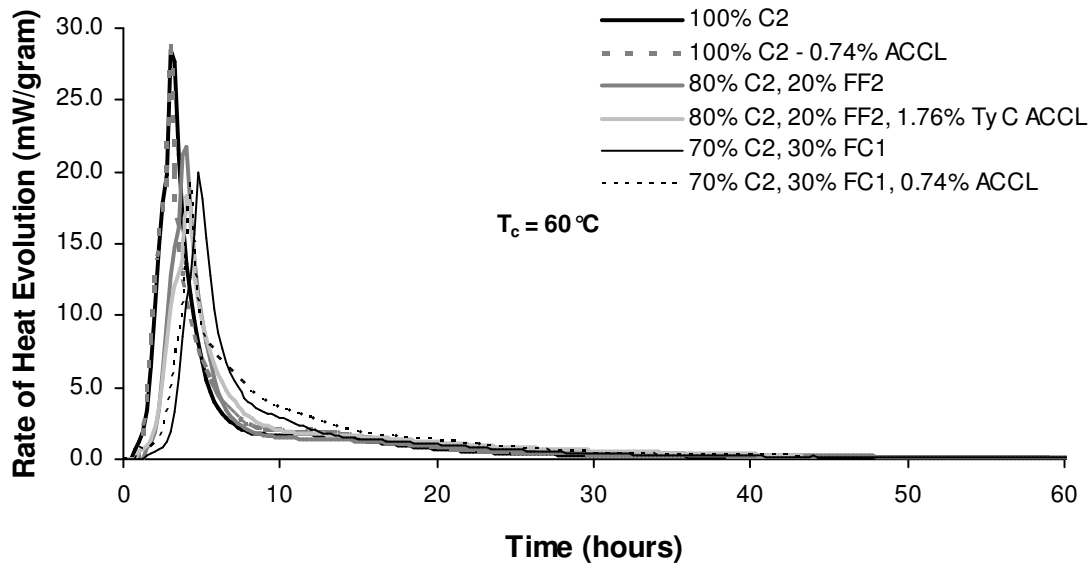


Figure B.75: Rate of Heat Evolution (Per Gram of Cementitious Material) for Paste Mixtures of 80% Cement C2, 20% FF2 with ACCL and 70% Cement C2, 30% FC2 with ACCL at 60 °C (140 °F)

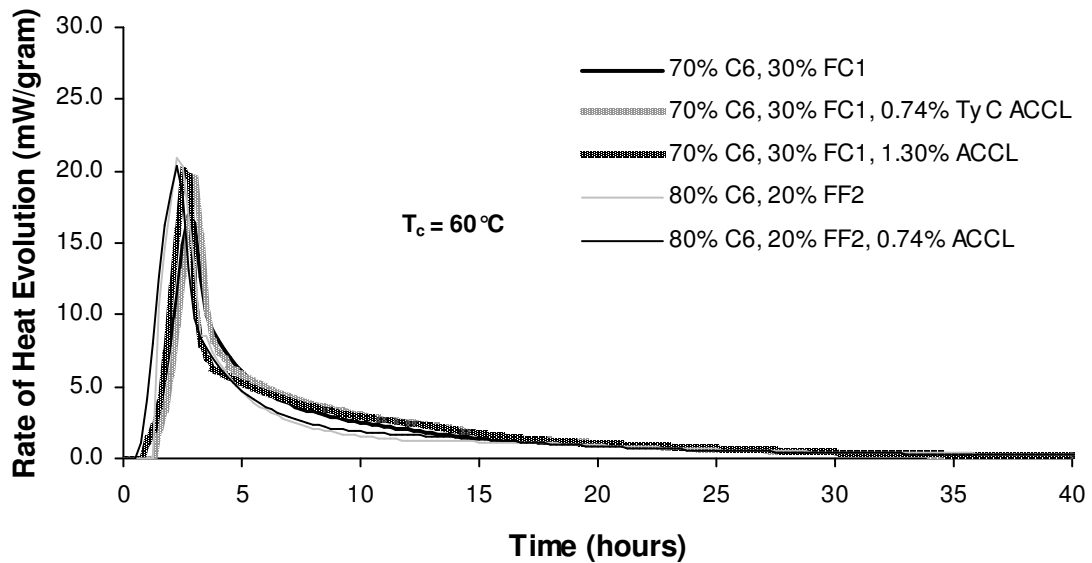


Figure B.76: Rate of Heat Evolution (Per Gram of Cementitious Material) for Paste Mixtures of 80% Cement C6, 20% FF2 with ACCL and 70% Cement C6, 30% FC1 with ACCL at 60 °C (140 °F)

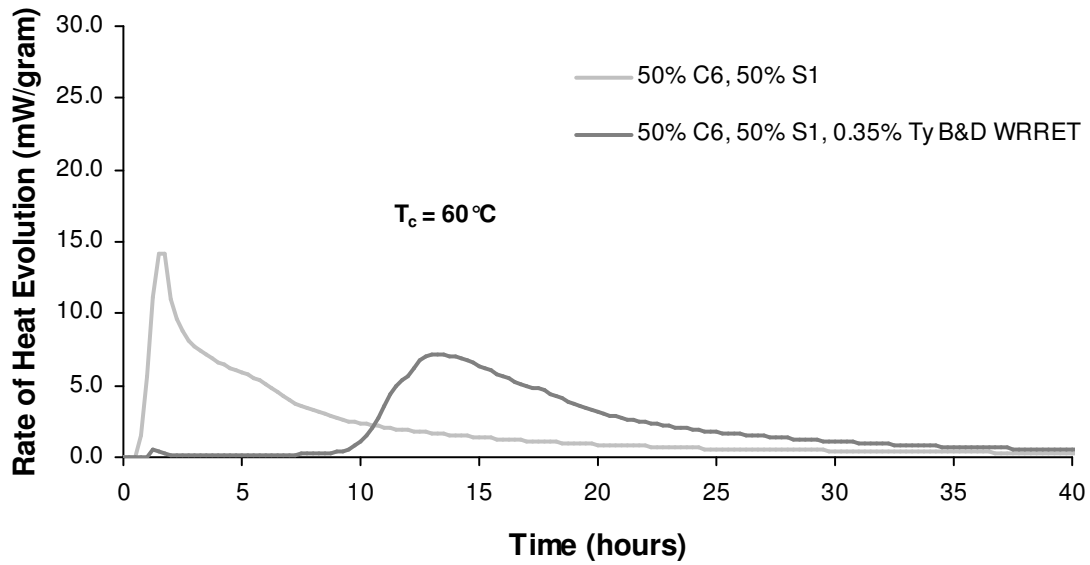


Figure B.77: Rate of Heat Evolution (Per Gram of Cementitious Material) for Paste Mixtures of 50% Cement C6, 50% S1 with WRRET at 60 °C (140 °F)

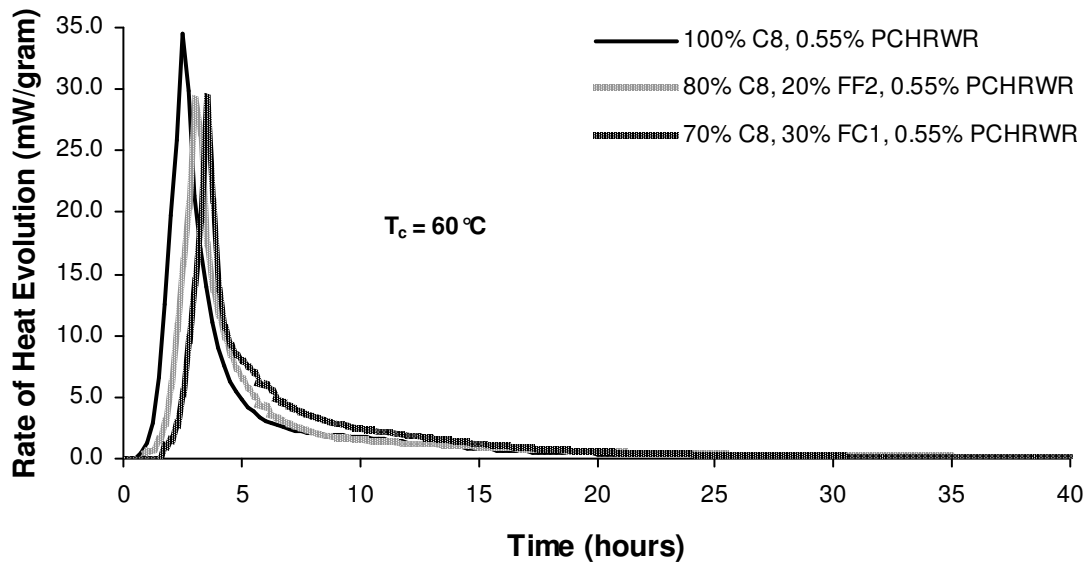


Figure B.78: Rate of Heat Evolution (Per Gram of Cementitious Material) for Paste Mixtures of 80% Cement C6, 20% FF2 with ACCL and 70% Cement C8, 30% FC1 with PCHRWR at 60 °C (140 °F)

APPENDIX C. ADDITIONAL ISOTHERMAL CALORIMETRY RESULTS FOR CHAPTER 4

C.1. EFFECTS OF FLY ASH FF1 ON RATE OF HEAT EVOLUTION OF PASTES

The following figures provide background for the effects of fly ash FF1 on rate of heat evolution of cementitious pastes presented in Chapter 4. Results at each of the isothermal test temperatures are shown.

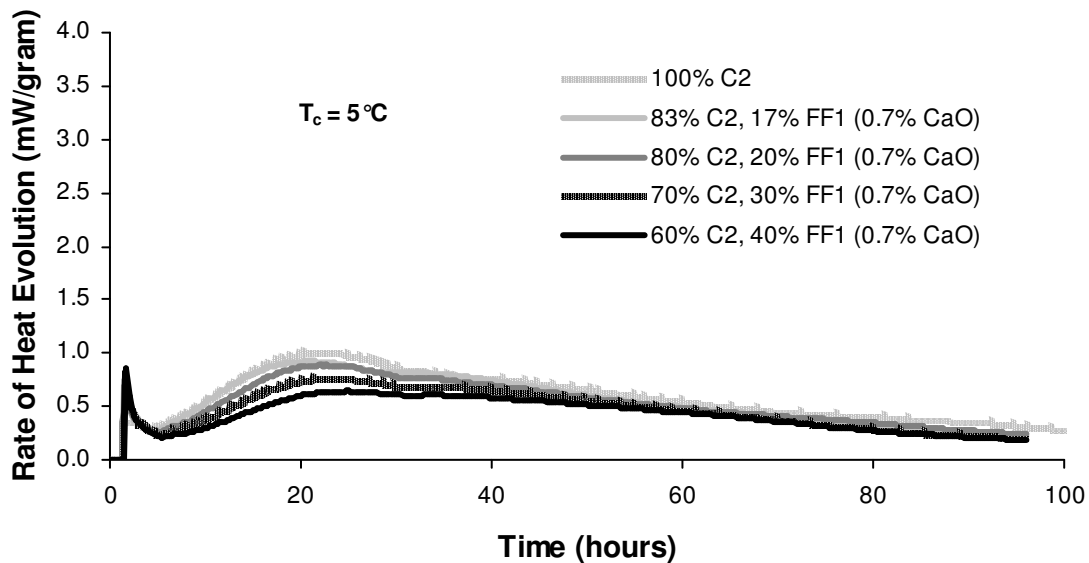


Figure C.1: Rate of Heat Evolution (Per Gram of Cementitious Material) for Paste Mixtures of Cement C2 with Different Replacements of FF1 (0.7% CaO) at 5 °C (41 °F)

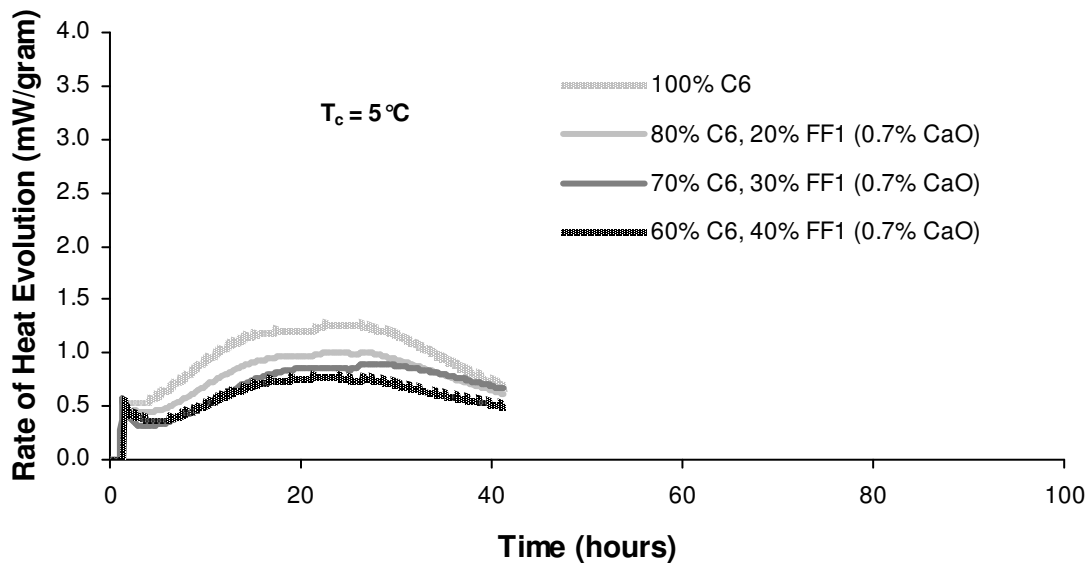


Figure C.2: Rate of Heat Evolution (Per Gram of Cementitious Material) for Paste Mixtures of Cement C6 with Different Replacements of FF1 (0.7% CaO) at 5 °C (41 °F)

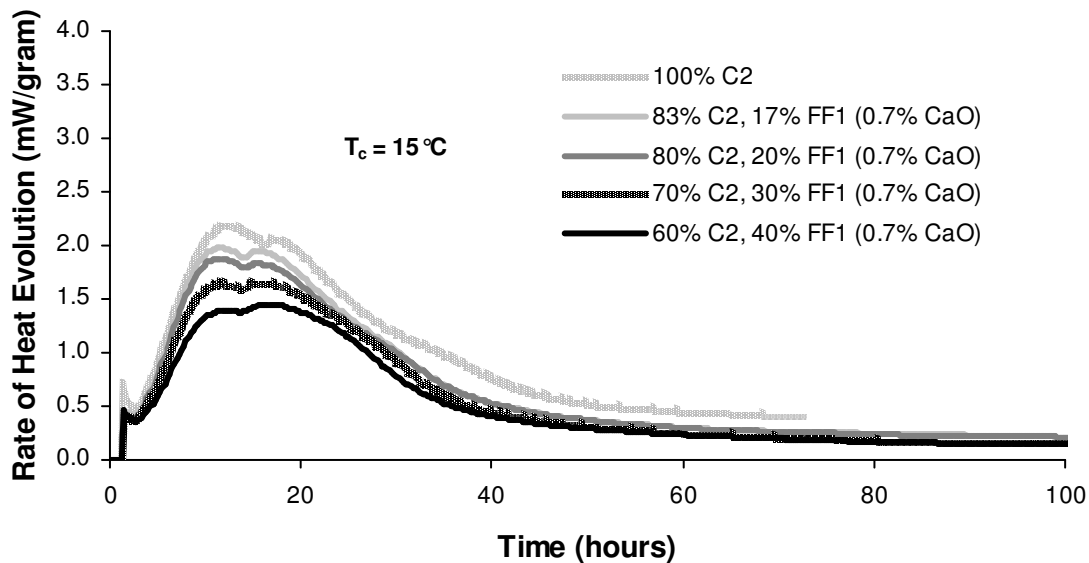


Figure C.3: Rate of Heat Evolution (Per Gram of Cementitious Material) for Paste Mixtures of Cement C2 with Different Replacements of FF1 (0.7% CaO) at 15 °C (59 °F)

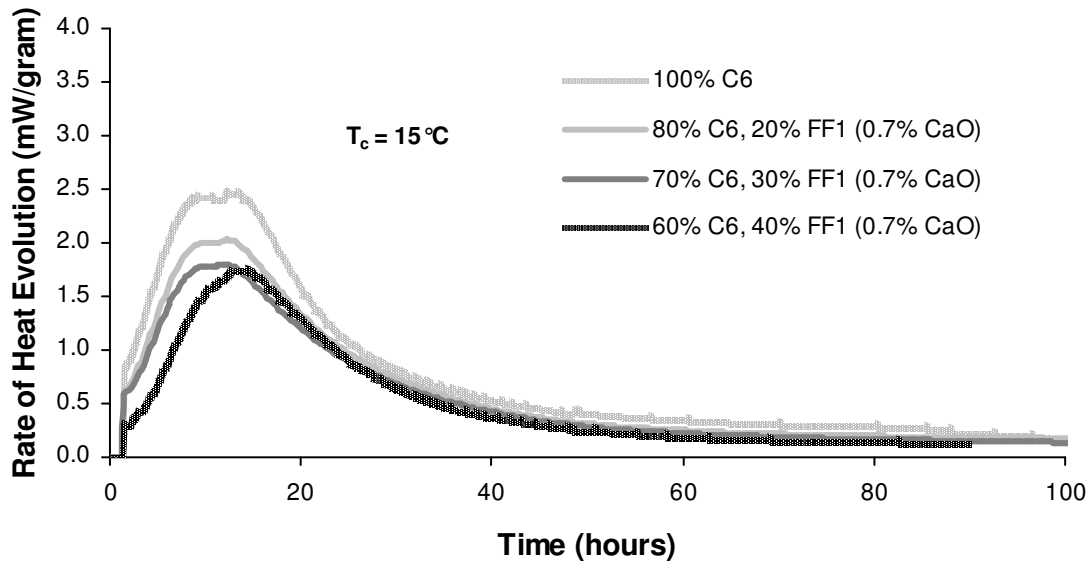


Figure C.4: Rate of Heat Evolution (Per Gram of Cementitious Material) for Paste Mixtures of Cement C6 with Different Replacements of FF1 (0.7% CaO) at 15 °C (59 °F)

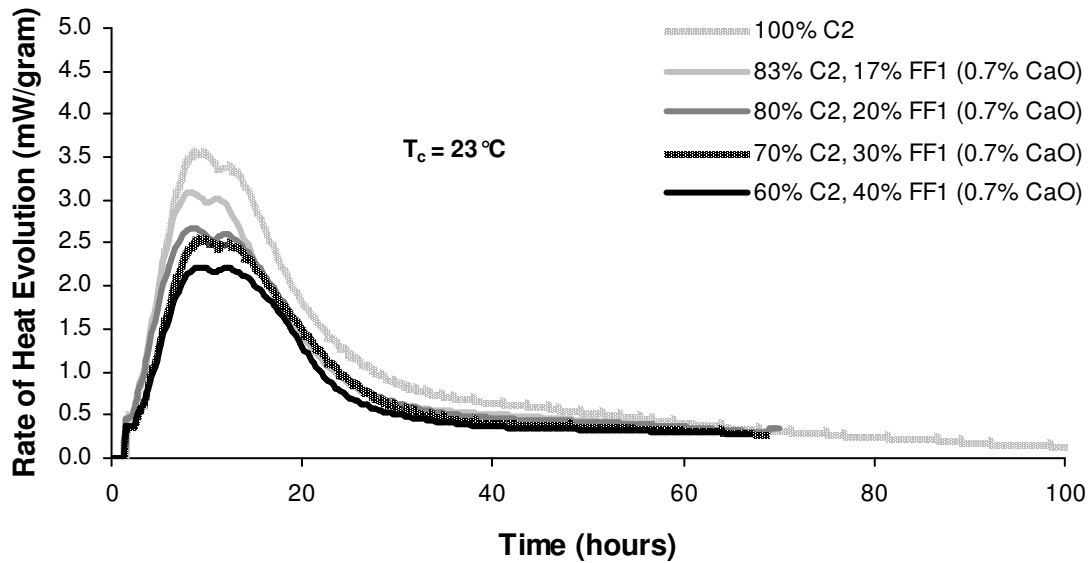


Figure C.5: Rate of Heat Evolution (Per Gram of Cementitious Material) for Paste Mixtures of Cement C2 with Different Replacements of FF1 (0.7% CaO) at 23 °C (73 °F)

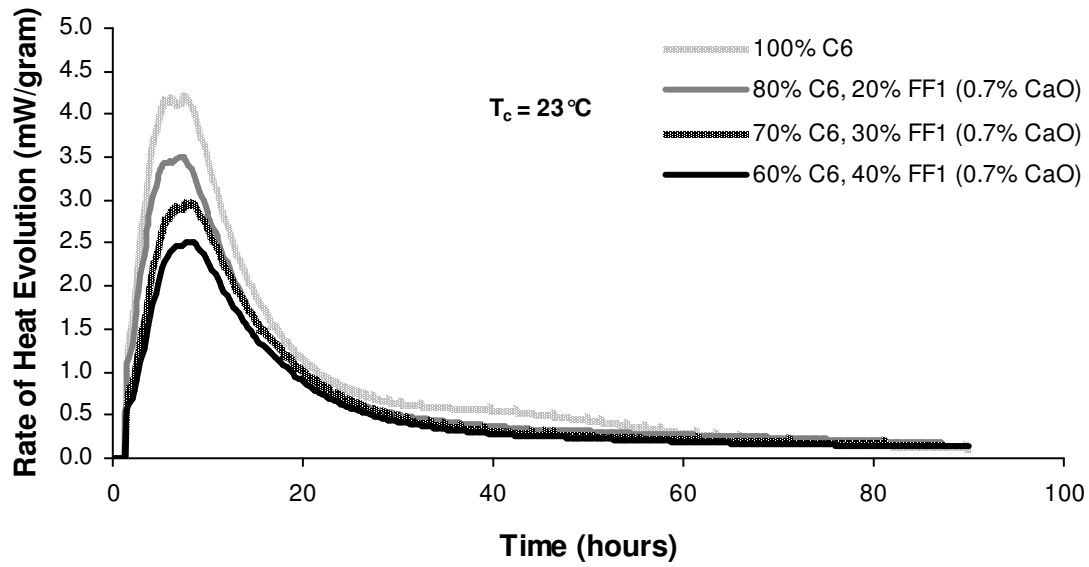


Figure C.6: Rate of Heat Evolution (Per Gram of Cementitious Material) for Paste Mixtures of Cement C6 with Different Replacements of FF1 (0.7% CaO) at 23 °C (73 °F)

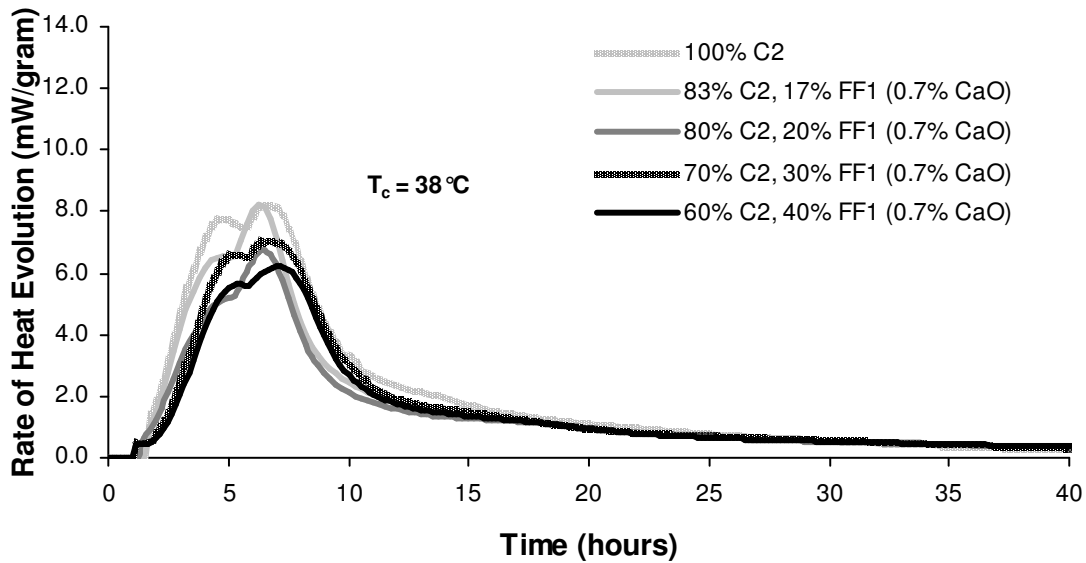


Figure C.7: Rate of Heat Evolution (Per Gram of Cementitious Material) for Paste Mixtures of Cement C2 with Different Replacements of FF1 (0.7% CaO) at 38 °C (100 °F)

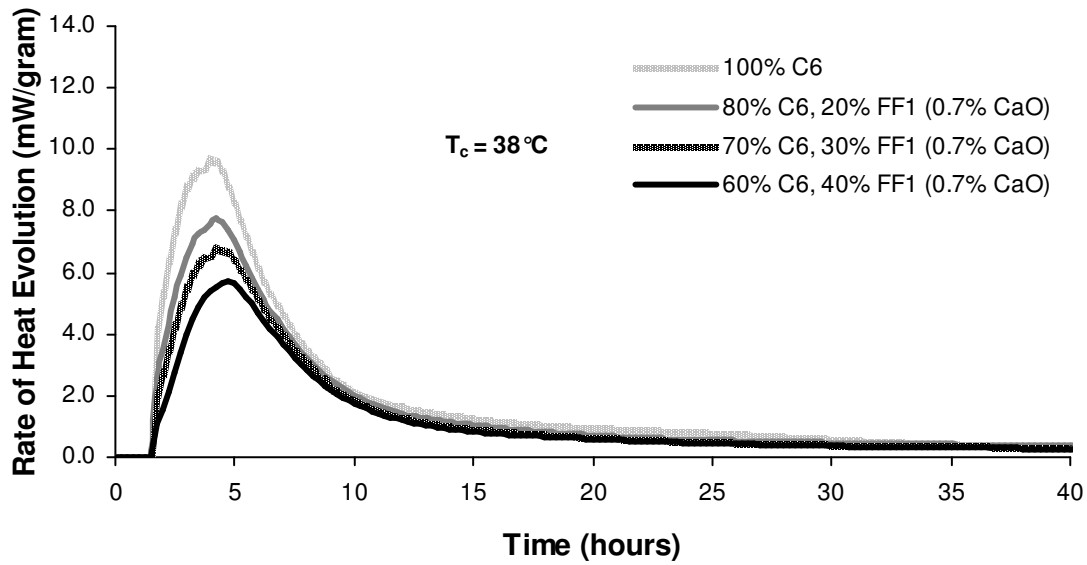


Figure C.8: Rate of Heat Evolution (Per Gram of Cementitious Material) for Paste Mixtures of Cement C6 with Different Replacements of FF1 (0.7% CaO) at 38 °C (100 °F)

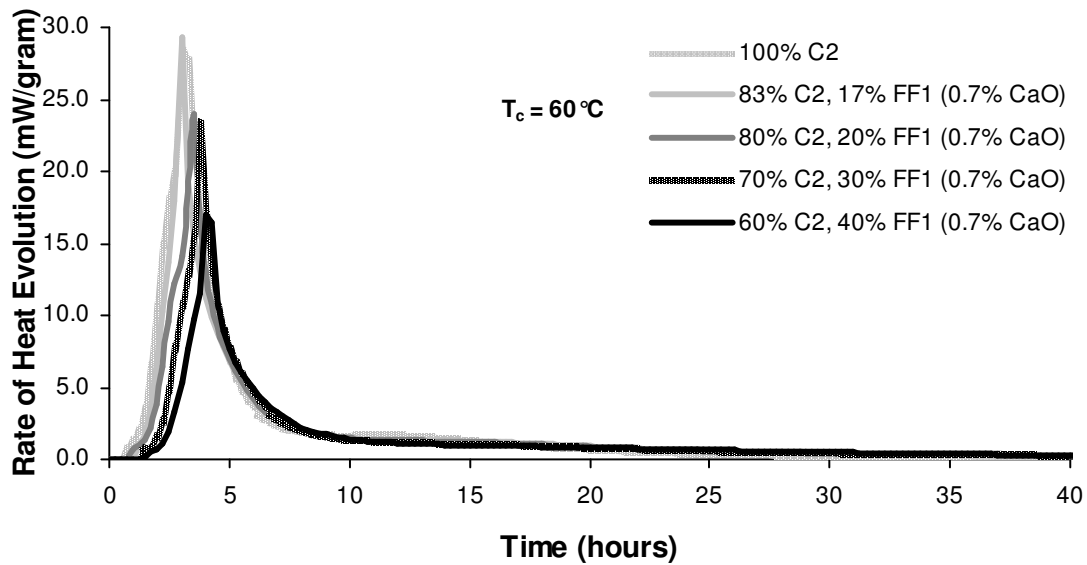


Figure C.9: Rate of Heat Evolution (Per Gram of Cementitious Material) for Paste Mixtures of Cement C2 with Different Replacements of FF1 (0.7% CaO) at 60 °C (140 °F)

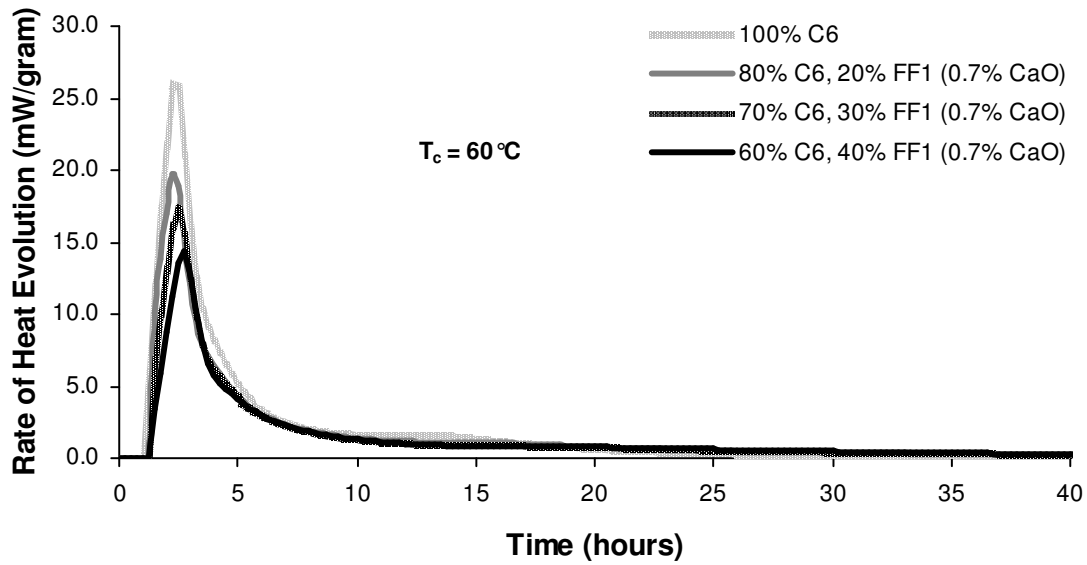


Figure C.10: Rate of Heat Evolution (Per Gram of Cementitious Material) for Paste Mixtures of Cement C6 with Different Replacements of FF1 (0.7% CaO) at 60 °C (140 °F)

C.2. EFFECTS OF FLY ASH FF2 ON RATE OF HEAT EVOLUTION OF PASTES

The following figures provide background for the effects of fly ash FF2 on rate of heat evolution of cementitious pastes presented in Chapter 4. Results at each of the isothermal test temperatures are shown.

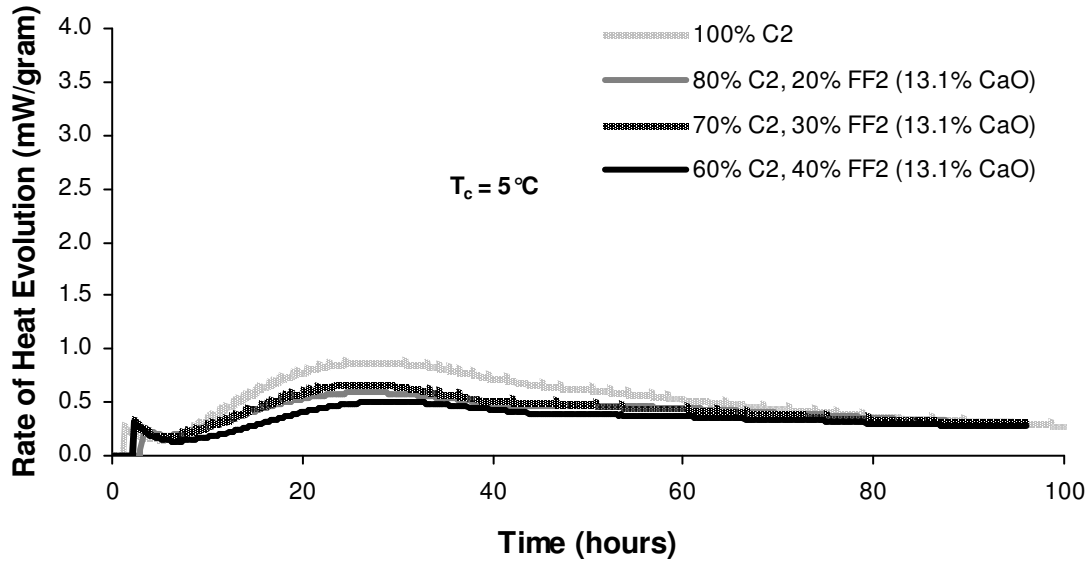


Figure C.11: Rate of Heat Evolution (Per Gram of Cementitious Material) for Paste Mixtures of Cement C2 with Different Replacements of FF2 (0.7% CaO) at 5 °C (41 °F)

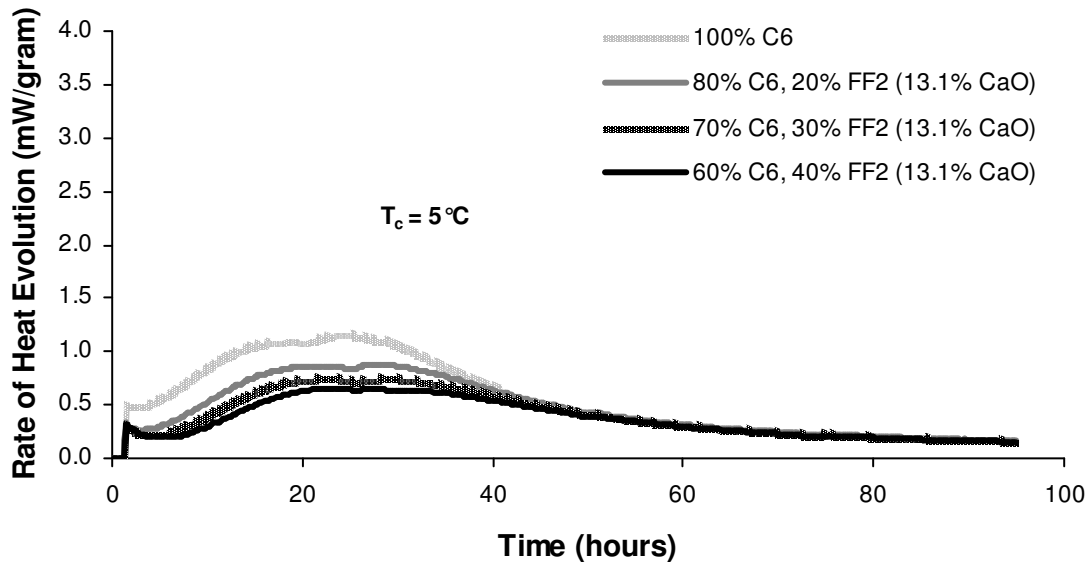


Figure C.12: Rate of Heat Evolution (Per Gram of Cementitious Material) for Paste Mixtures of Cement C6 with Different Replacements of FF2 (0.7% CaO) at 5 °C (41 °F)

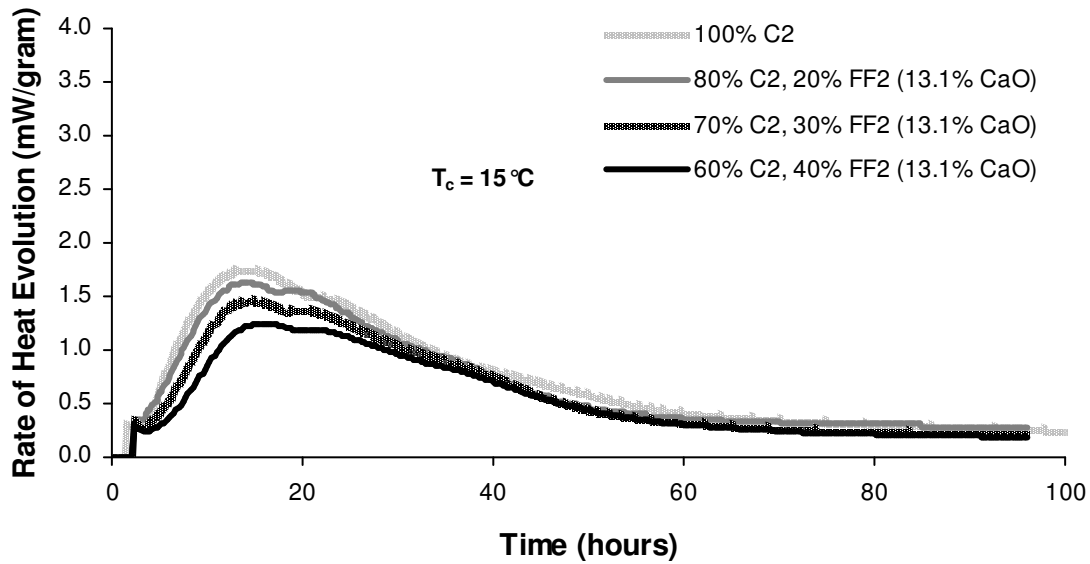


Figure C.13: Rate of Heat Evolution (Per Gram of Cementitious Material) for Paste Mixtures of Cement C2 with Different Replacements of FF2 (0.7% CaO) at 15 °C (59 °F)

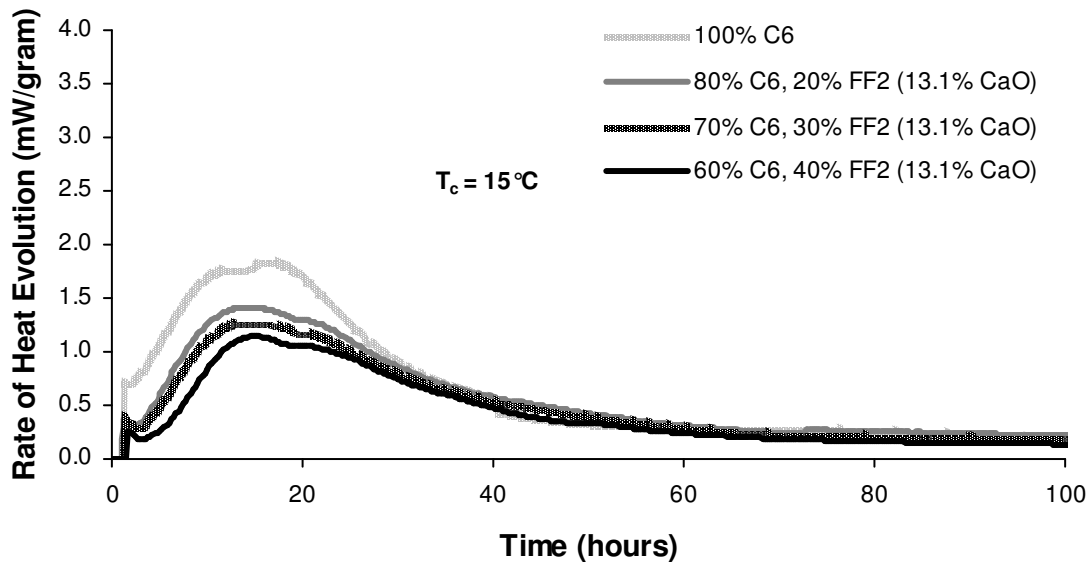


Figure C.14: Rate of Heat Evolution (Per Gram of Cementitious Material) for Paste Mixtures of Cement C6 with Different Replacements of FF2 (0.7% CaO) at 15 °C (59 °F)

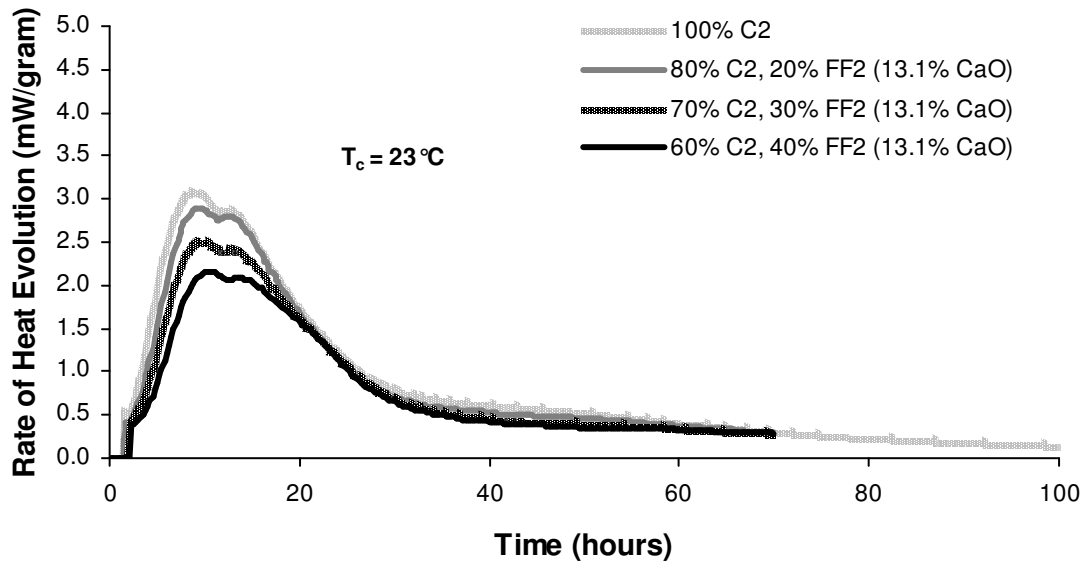


Figure C.15: Rate of Heat Evolution (Per Gram of Cementitious Material) for Paste Mixtures of Cement C2 with Different Replacements of FF2 (0.7% CaO) at 23 °C (73 °F)

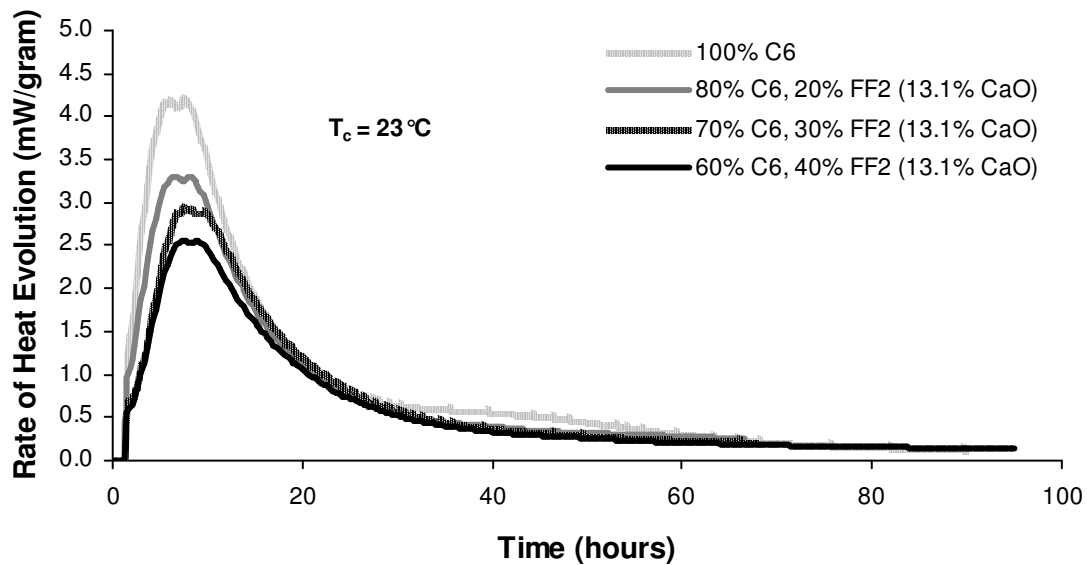


Figure C.16: Rate of Heat Evolution (Per Gram of Cementitious Material) for Paste Mixtures of Cement C6 with Different Replacements of FF2 (0.7% CaO) at 23 °C (73 °F)

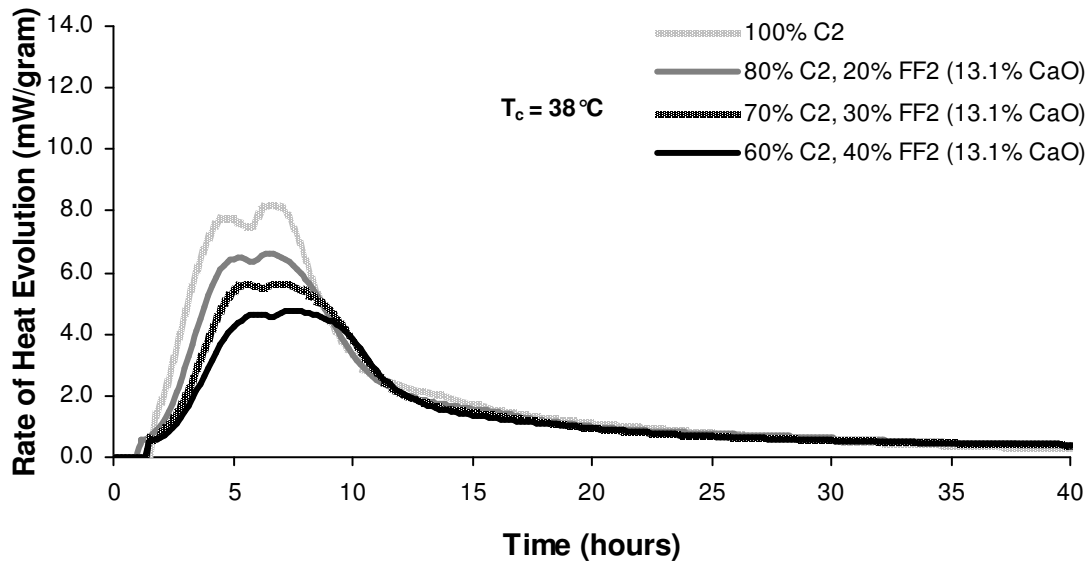


Figure C.17: Rate of Heat Evolution (Per Gram of Cementitious Material) for Paste Mixtures of Cement C2 with Different Replacements of FF2 (0.7% CaO) at 38 °C (100 °F)

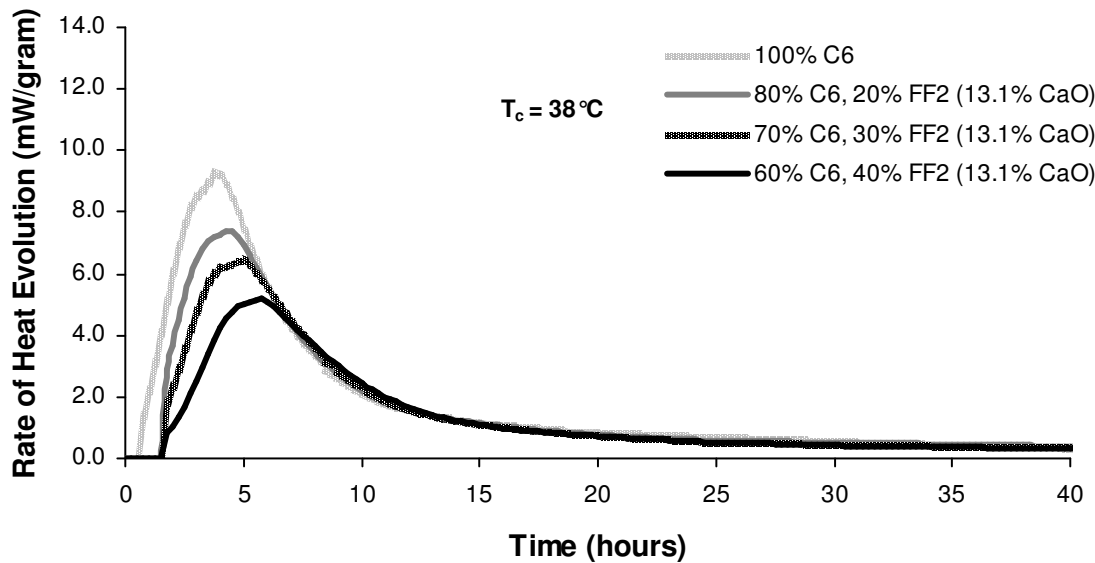


Figure C.18: Rate of Heat Evolution (Per Gram of Cementitious Material) for Paste Mixtures of Cement C6 with Different Replacements of FF2 (0.7% CaO) at 38 °C (100 °F)

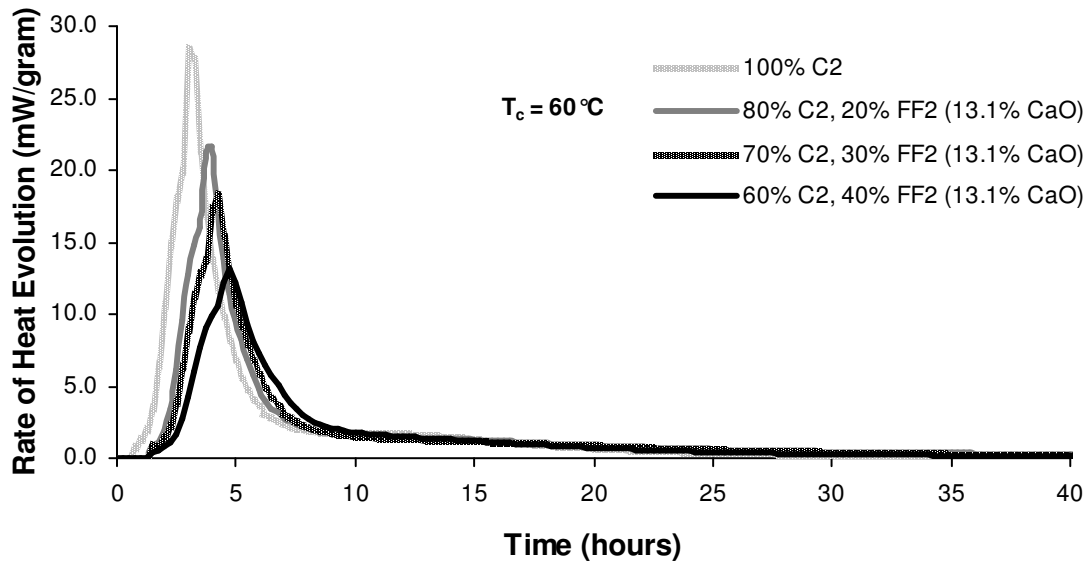


Figure C.19: Rate of Heat Evolution (Per Gram of Cementitious Material) for Paste Mixtures of Cement C2 with Different Replacements of FF2 (0.7% CaO) at 60 °C (140 °F)

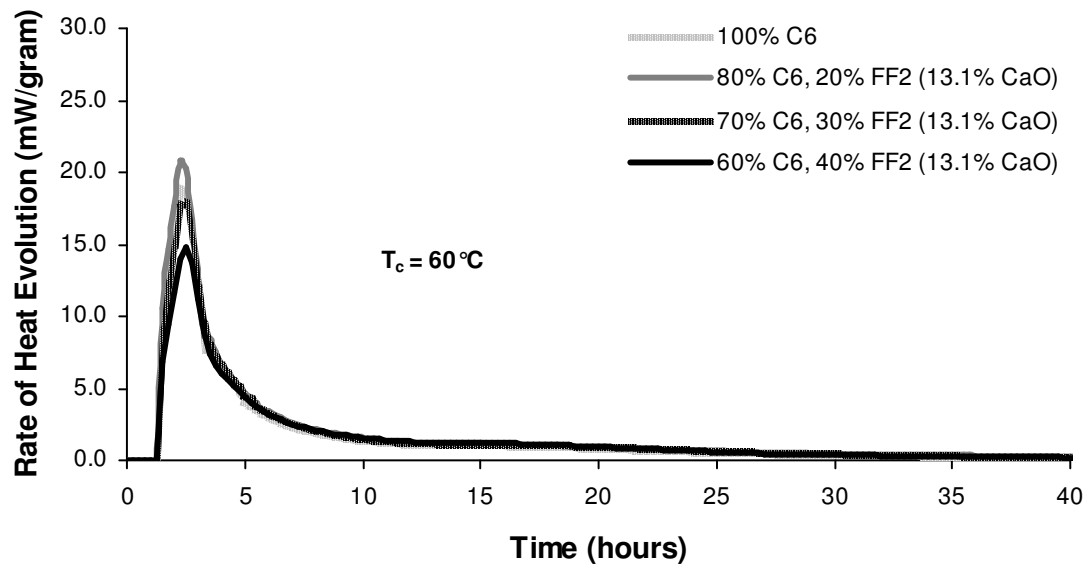


Figure C.20: Rate of Heat Evolution (Per Gram of Cementitious Material) for Paste Mixtures of Cement C6 with Different Replacements of FF2 (0.7% CaO) at 60 °C (140 °F)

C.3. EFFECTS OF FLY ASH FC1 ON RATE OF HEAT EVOLUTION OF PASTES

The following figures provide background for the effects of fly ash FC1 on rate of heat evolution of cementitious pastes presented in Chapter 4. Results at each of the isothermal test temperatures are shown.

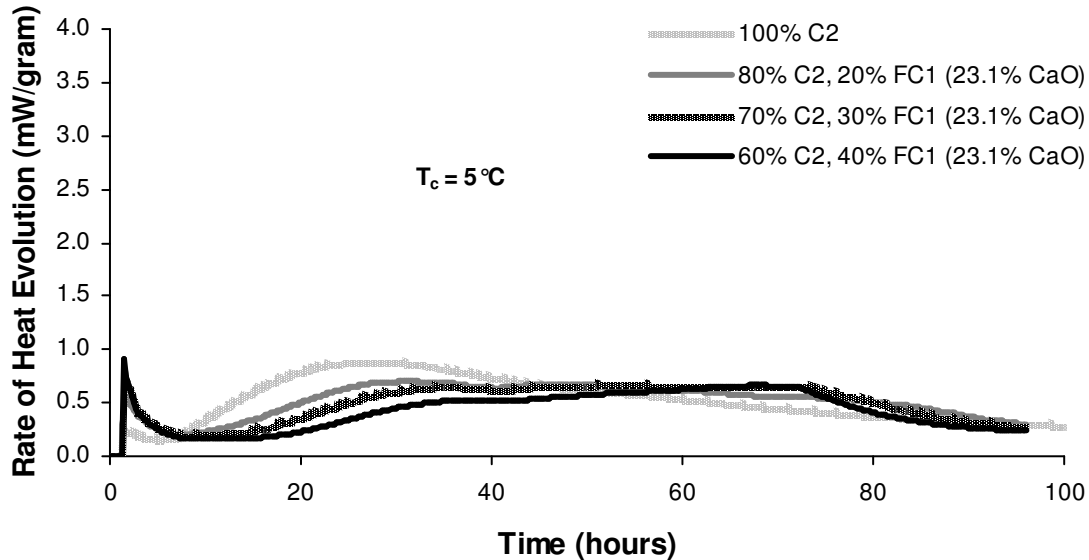


Figure C.21: Rate of Heat Evolution (Per Gram of Cementitious Material) for Paste Mixtures of Cement C2 with Different Replacements of FC1 (0.7% CaO) at 5 °C (41 °F)

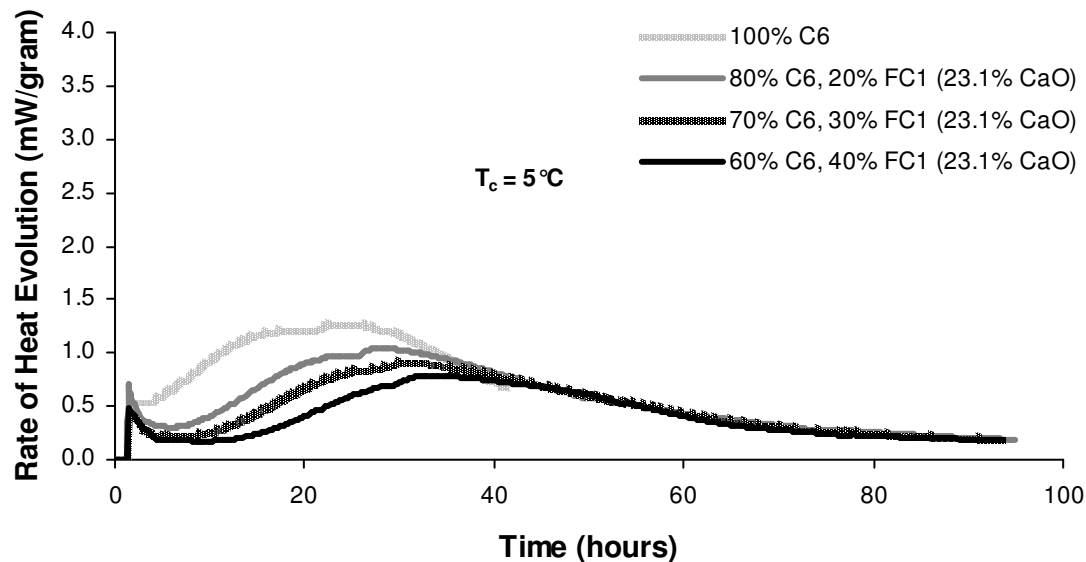


Figure C.22: Rate of Heat Evolution (Per Gram of Cementitious Material) for Paste Mixtures of Cement C6 with Different Replacements of FC1 (0.7% CaO) at 5 °C (41 °F)

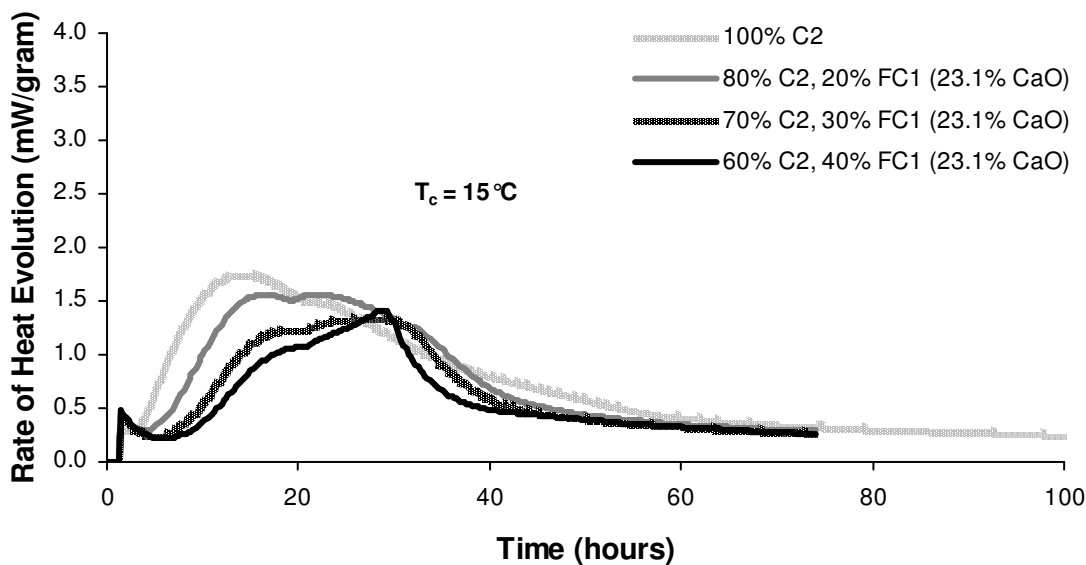


Figure C.23: Rate of Heat Evolution (Per Gram of Cementitious Material) for Paste Mixtures of Cement C2 with Different Replacements of FC1 (0.7% CaO) at 15 °C (59 °F)

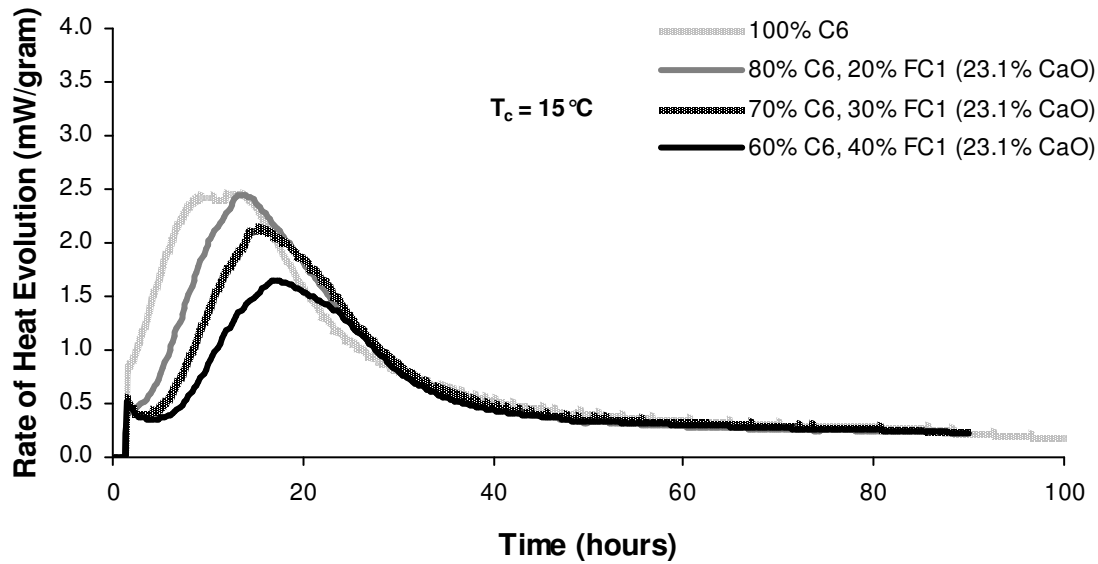


Figure C.24: Rate of Heat Evolution (Per Gram of Cementitious Material) for Paste Mixtures of Cement C6 with Different Replacements of FC1 (0.7% CaO) at 15 °C (59 °F)

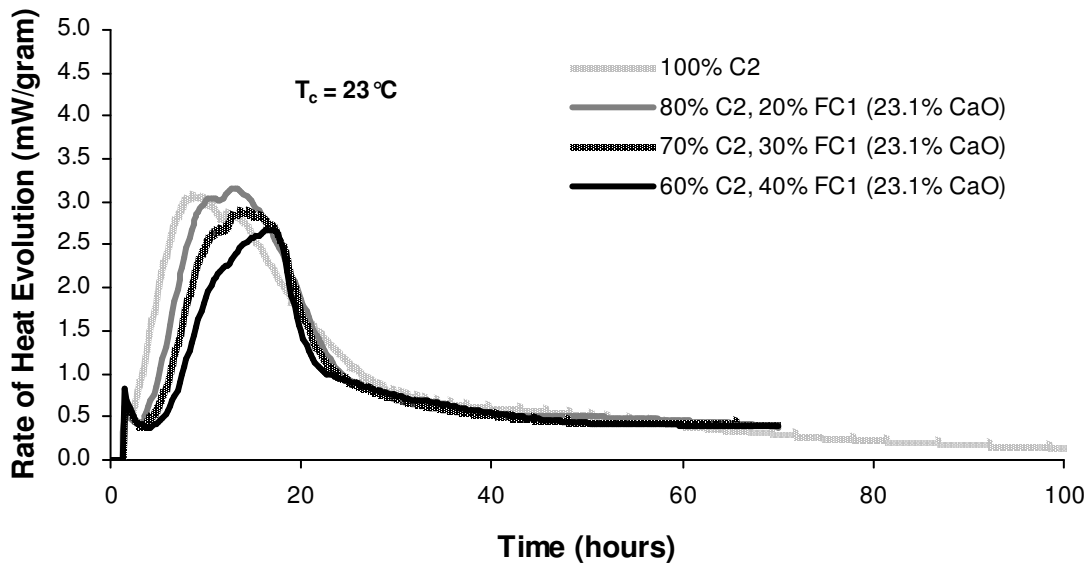


Figure C.25: Rate of Heat Evolution (Per Gram of Cementitious Material) for Paste Mixtures of Cement C2 with Different Replacements of FC1 (0.7% CaO) at 23 °C (73 °F)

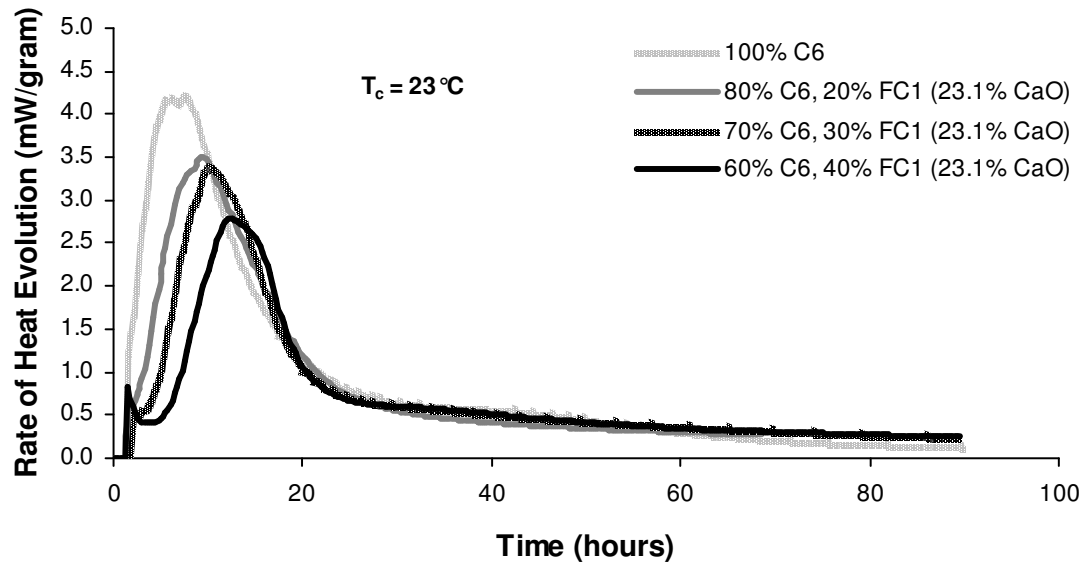


Figure C.26: Rate of Heat Evolution (Per Gram of Cementitious Material) for Paste Mixtures of Cement C6 with Different Replacements of FC1 (0.7% CaO) at 23 °C (73 °F)

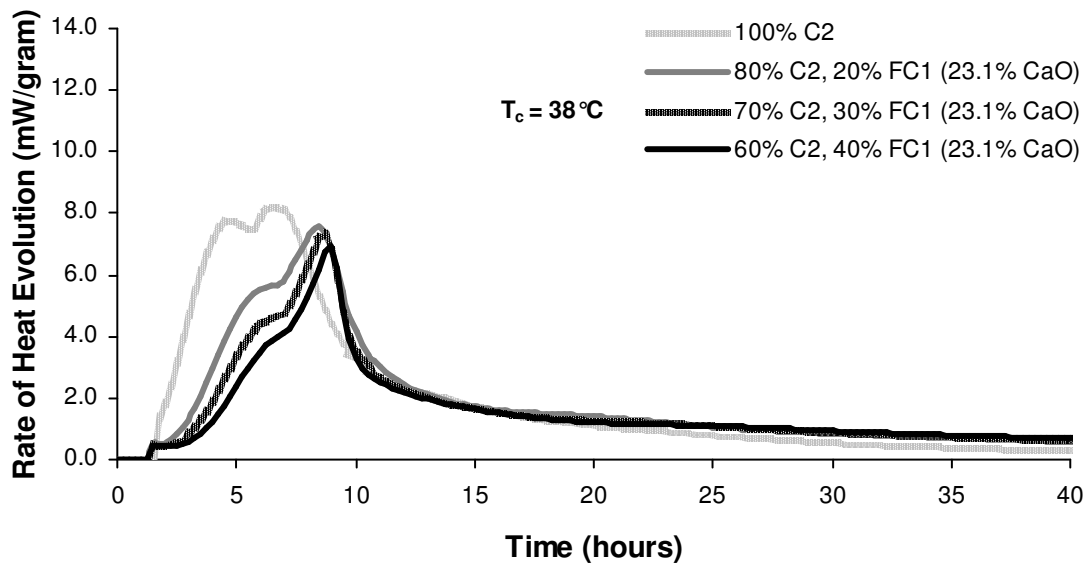


Figure C.27: Rate of Heat Evolution (Per Gram of Cementitious Material) for Paste Mixtures of Cement C2 with Different Replacements of FC1 (0.7% CaO) at 38 °C (100 °F)

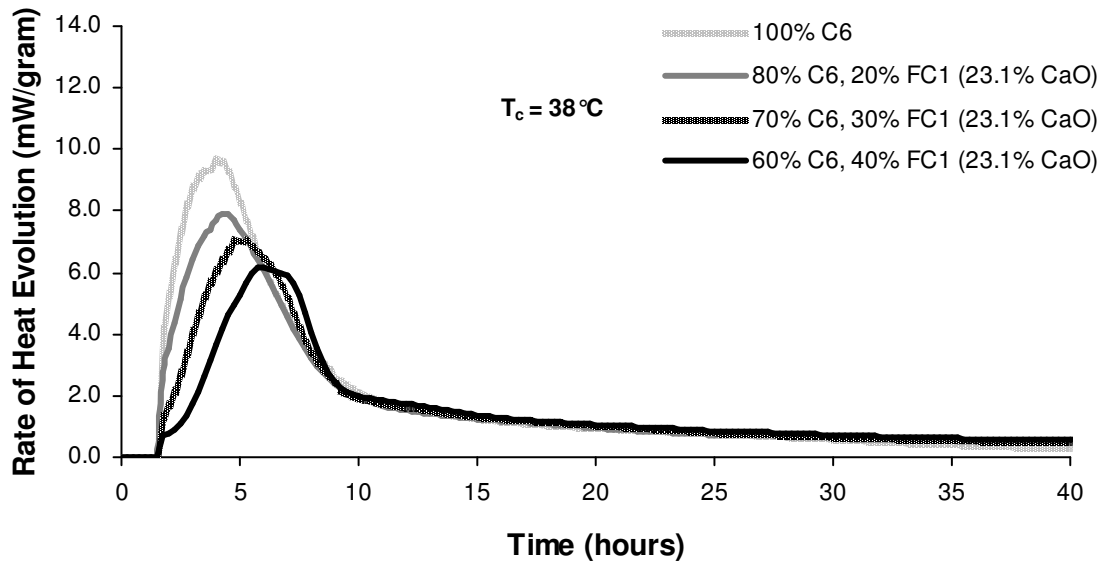


Figure C.28: Rate of Heat Evolution (Per Gram of Cementitious Material) for Paste Mixtures of Cement C6 with Different Replacements of FC1 (0.7% CaO) at 38 °C (100 °F)

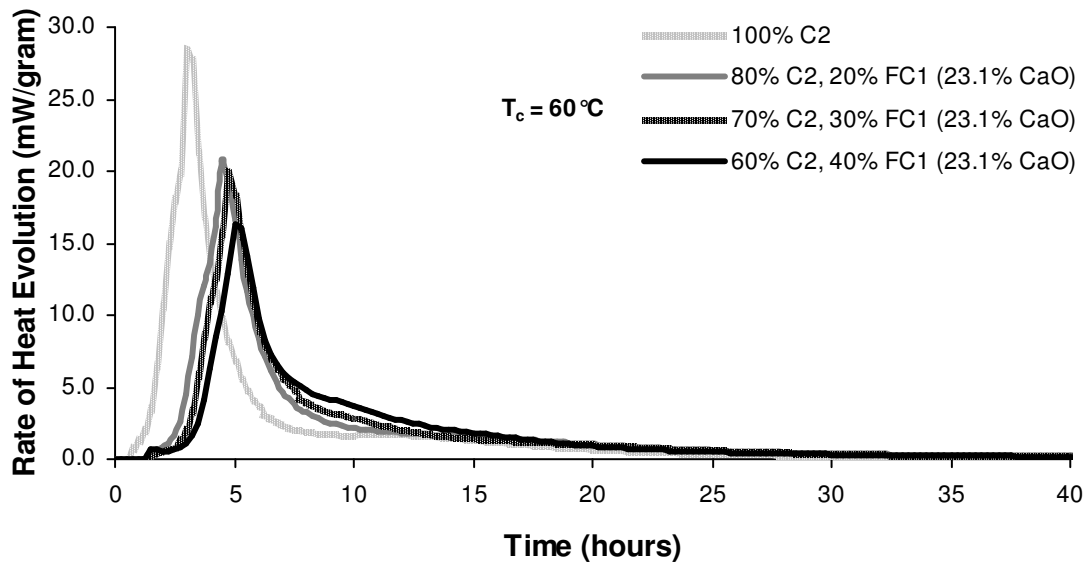


Figure C.29: Rate of Heat Evolution (Per Gram of Cementitious Material) for Paste Mixtures of Cement C2 with Different Replacements of FC1 (0.7% CaO) at 60 °C (140 °F)

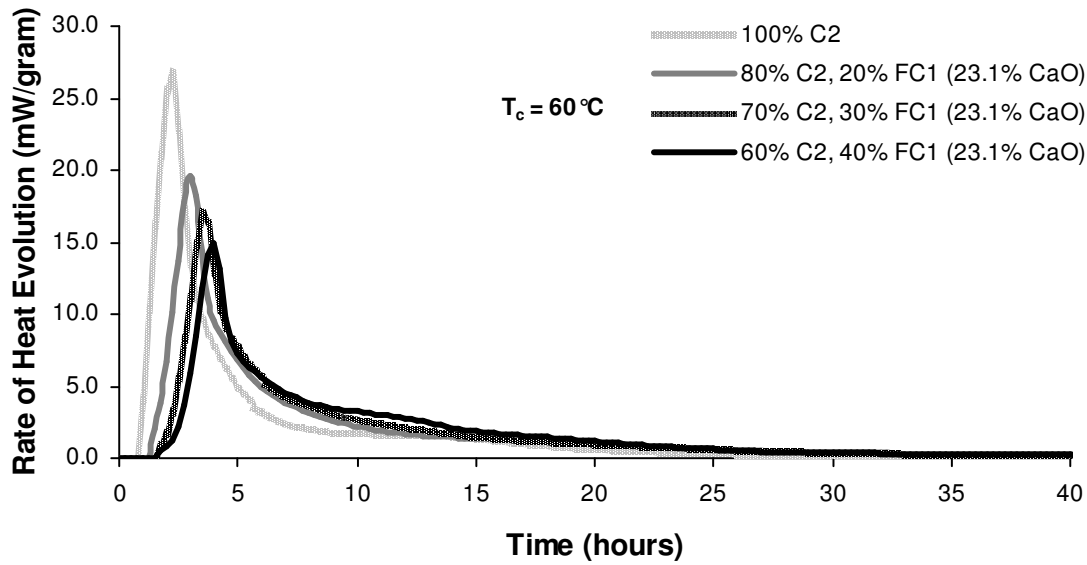


Figure C.30: Rate of Heat Evolution (Per Gram of Cementitious Material) for Paste Mixtures of Cement C6 with Different Replacements of FC1 (0.7% CaO) at 60 °C (140 °F)

C.4. EFFECTS OF FLY ASH FC2 ON RATE OF HEAT EVOLUTION OF PASTES

The following figures provide background for the effects of fly ash FC2 on rate of heat evolution of cementitious pastes presented in Chapter 4. Results at each of the isothermal test temperatures are shown.

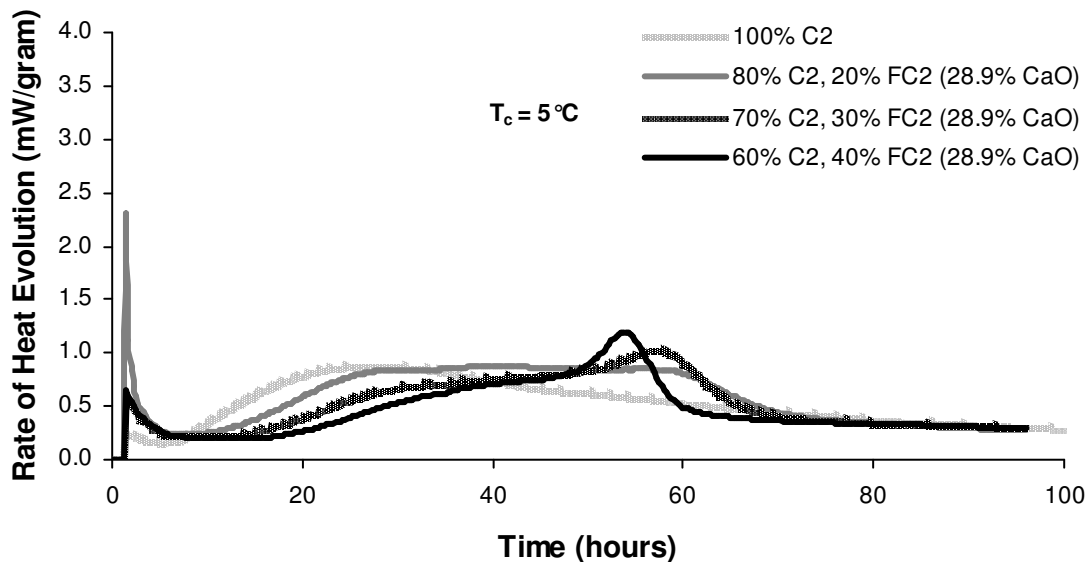


Figure C.31: Rate of Heat Evolution (Per Gram of Cementitious Material) for Paste Mixtures of Cement C2 with Different Replacements of FC2 (0.7% CaO) at 60 °C (140 °F)

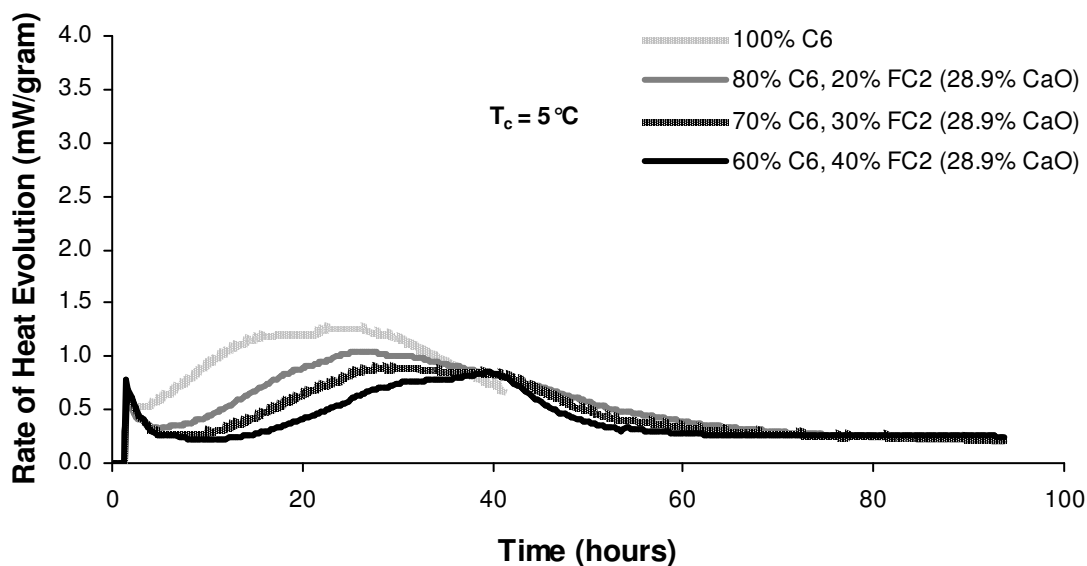


Figure C.32: Rate of Heat Evolution (Per Gram of Cementitious Material) for Paste Mixtures of Cement C2 with Different Replacements of FC2 (0.7% CaO) at 60 °C (140 °F)

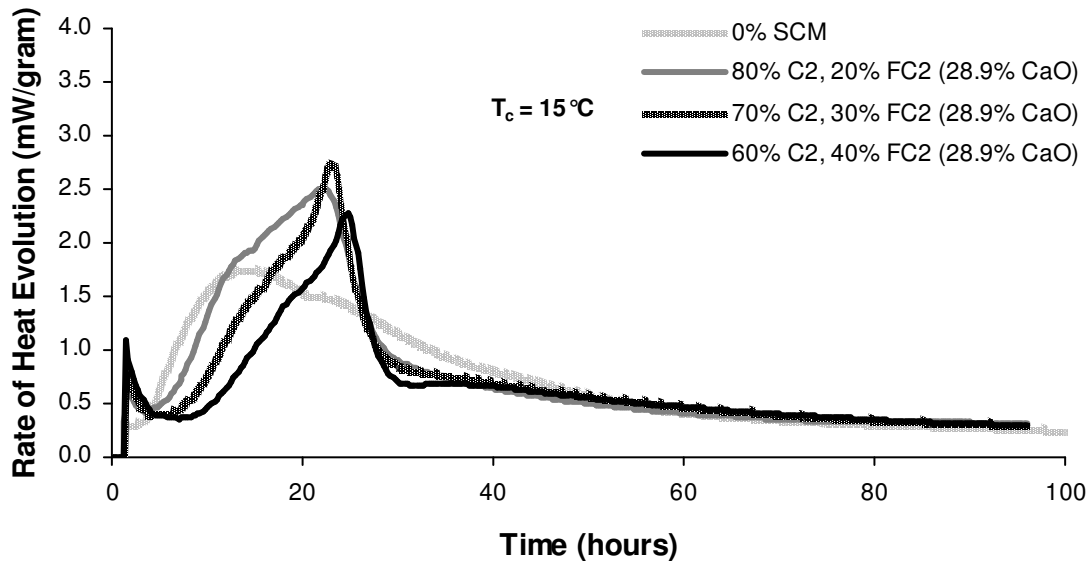


Figure C.33: Rate of Heat Evolution (Per Gram of Cementitious Material) for Paste Mixtures of Cement C2 with Different Replacements of FC2 (0.7% CaO) at 15 °C (41 °F)

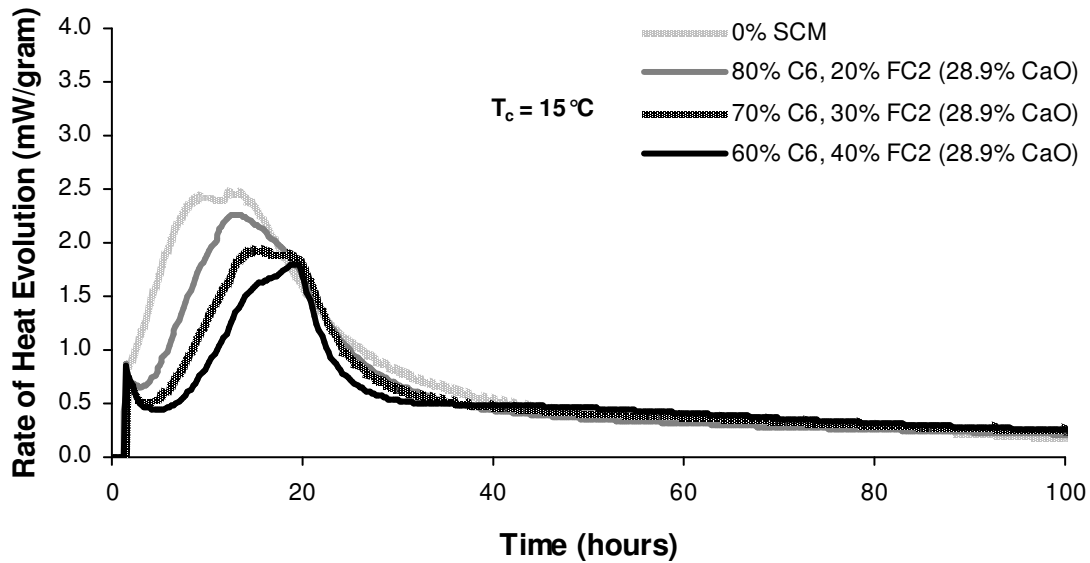


Figure C.34: Rate of Heat Evolution (Per Gram of Cementitious Material) for Paste Mixtures of Cement C6 with Different Replacements of FC2 (0.7% CaO) at 15 °C (59 °F)

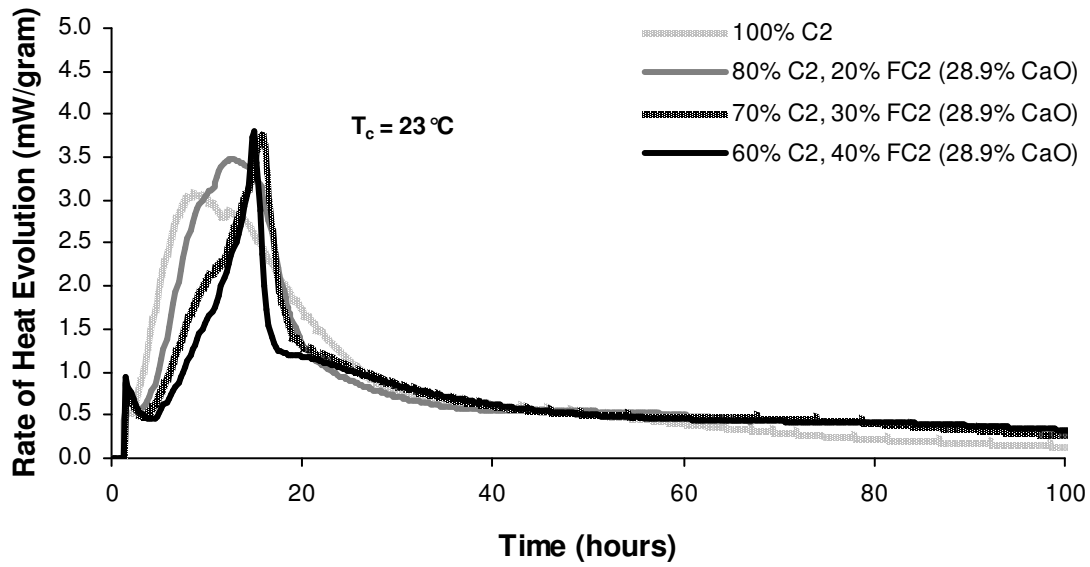


Figure C.35: Rate of Heat Evolution (Per Gram of Cementitious Material) for Paste Mixtures of Cement C2 with Different Replacements of FC2 (0.7% CaO) at 23°C (73°F)

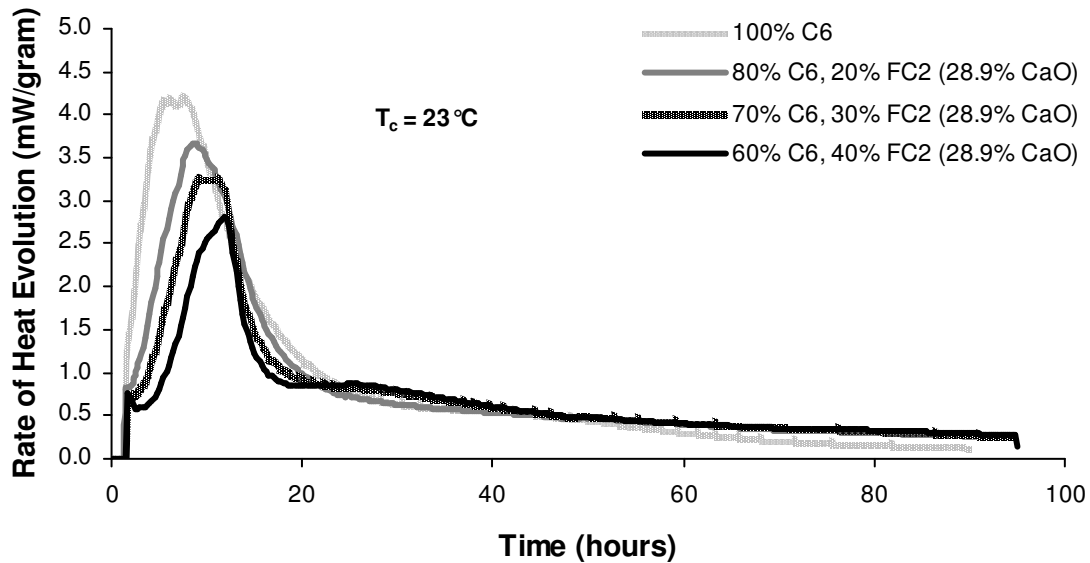


Figure C.36: Rate of Heat Evolution (Per Gram of Cementitious Material) for Paste Mixtures of Cement C6 with Different Replacements of FC2 (0.7% CaO) at 23°C (73°F)

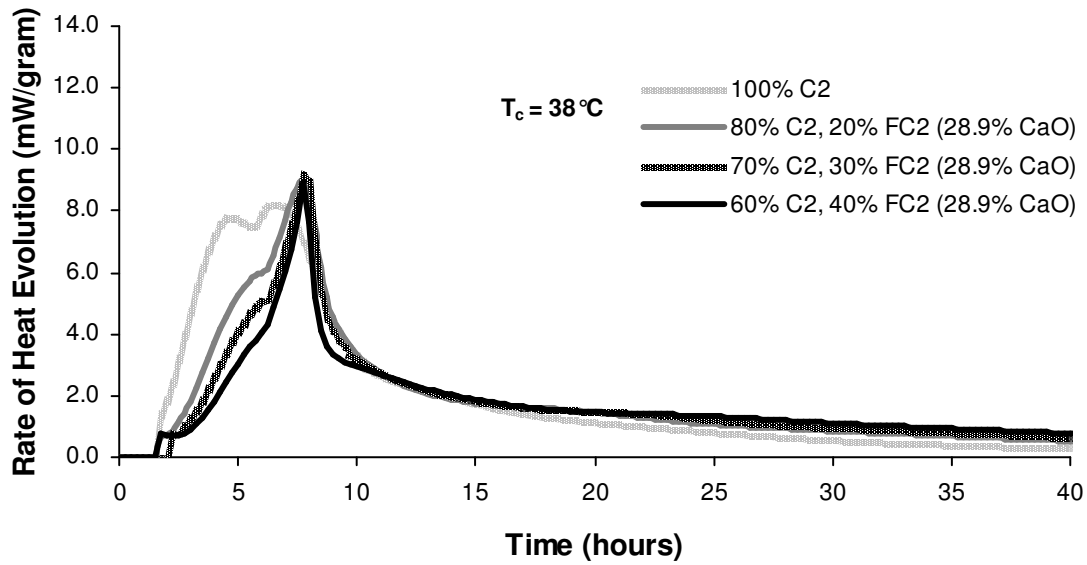


Figure C.37: Rate of Heat Evolution (Per Gram of Cementitious Material) for Paste Mixtures of Cement C2 with Different Replacements of FC2 (0.7% CaO) at 38 °C (100 °F)

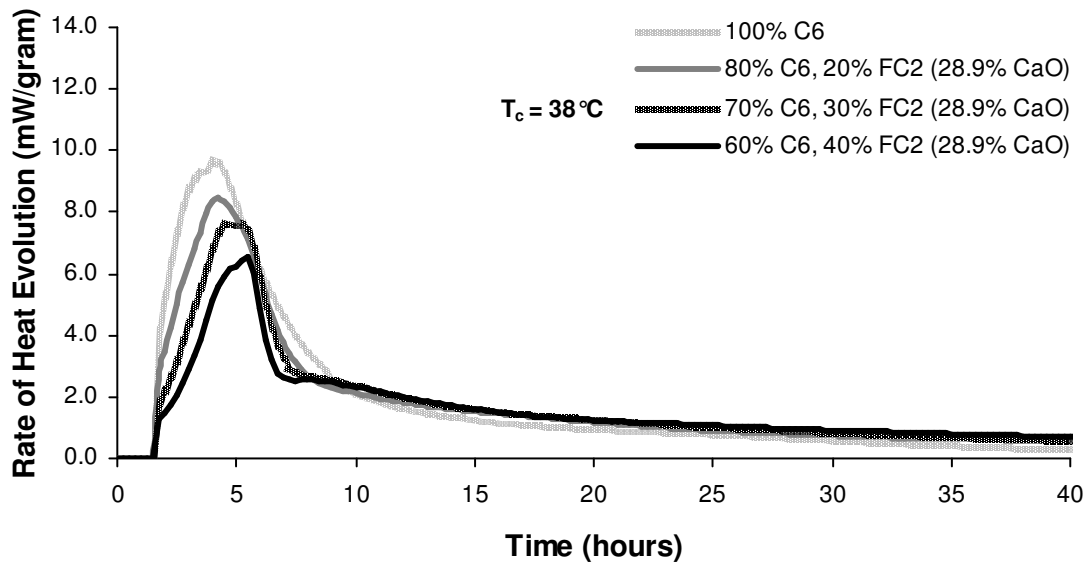


Figure C.38: Rate of Heat Evolution (Per Gram of Cementitious Material) for Paste Mixtures of Cement C6 with Different Replacements of FC2 (0.7% CaO) at 38 °C (100 °F)

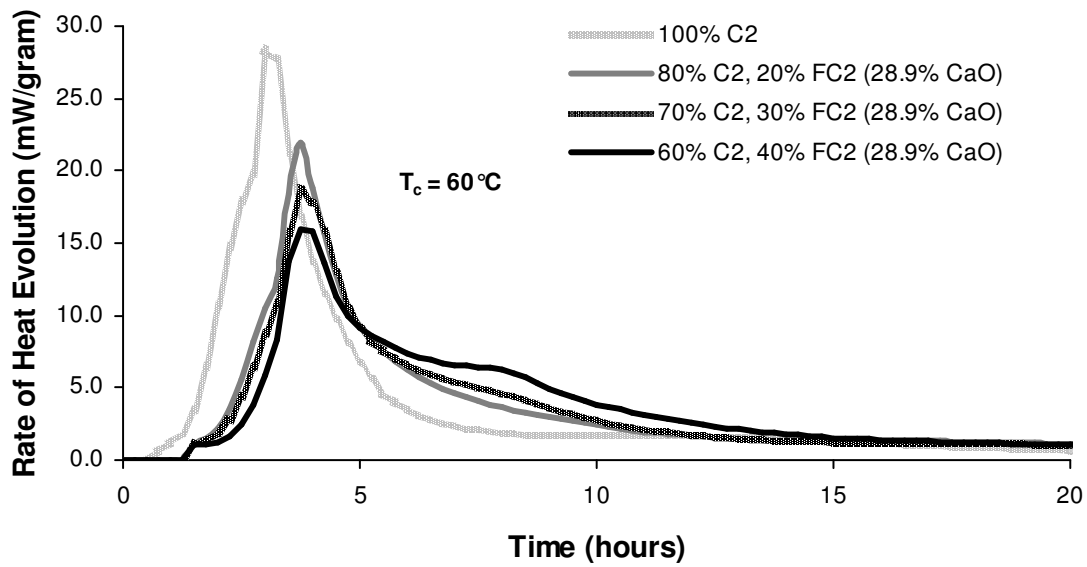


Figure C.39: Rate of Heat Evolution (Per Gram of Cementitious Material) for Paste Mixtures of Cement C2 with Different Replacements of FC2 (0.7% CaO) at 60 °C (140 °F)

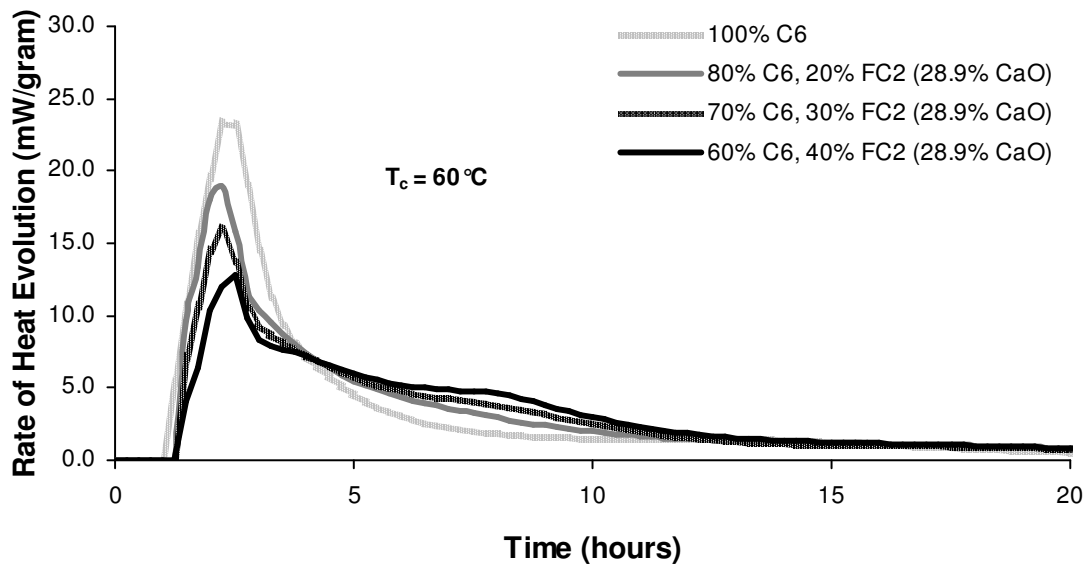


Figure C.40: Rate of Heat Evolution (Per Gram of Cementitious Material) for Paste Mixtures of Cement C6 with Different Replacements of FC2 (0.7% CaO) at 60 °C (140 °F)

C.5. EFFECTS OF GGBF SLAG ON RATE OF HEAT EVOLUTION OF PASTES

The following figures provide background for the effects of GGBF Slag on rate of heat evolution of cementitious pastes presented in Chapter 4. Results at each of the isothermal test temperatures are shown.

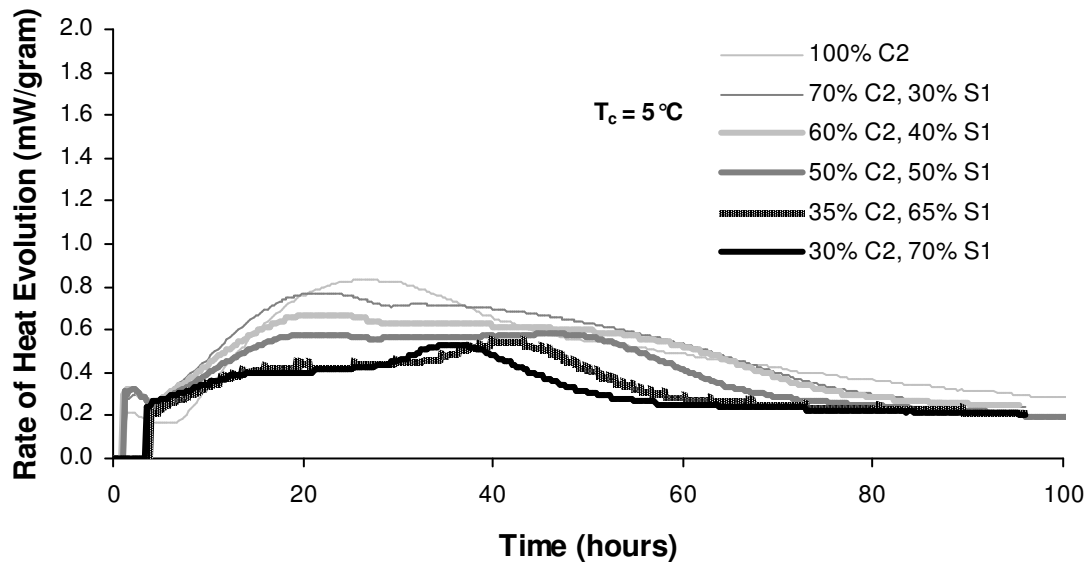


Figure C.41: Rate of Heat Evolution (Per Gram of Cementitious Material) for Paste Mixtures of Cement C2 with Different Replacements of GGBF Slag at 5 °C (41 °F)

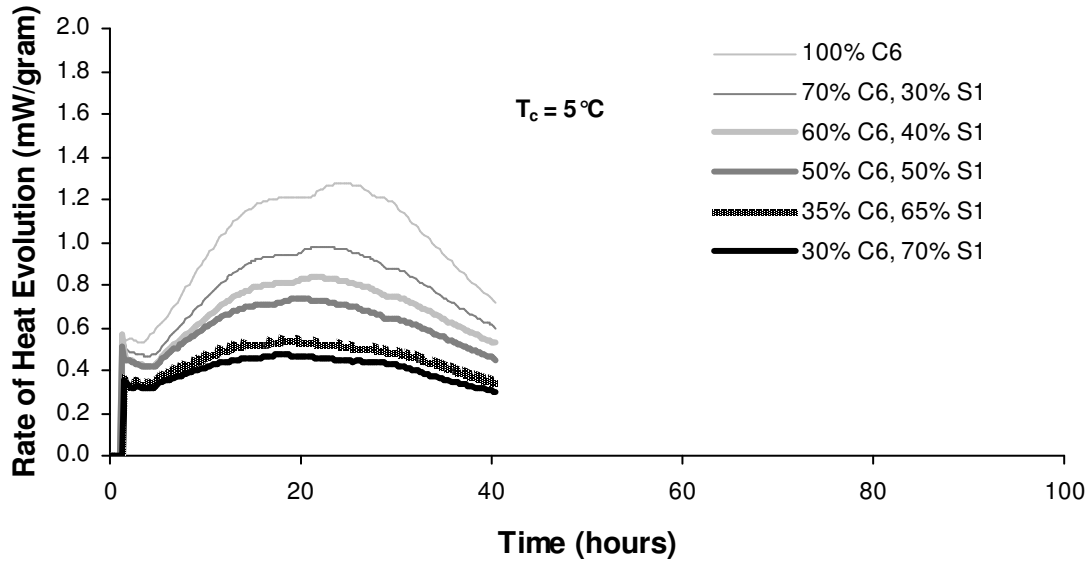


Figure C.42: Rate of Heat Evolution (Per Gram of Cementitious Material) for Paste Mixtures of Cement C6 with Different Replacements of GGBF Slag at 5 °C (41 °F)

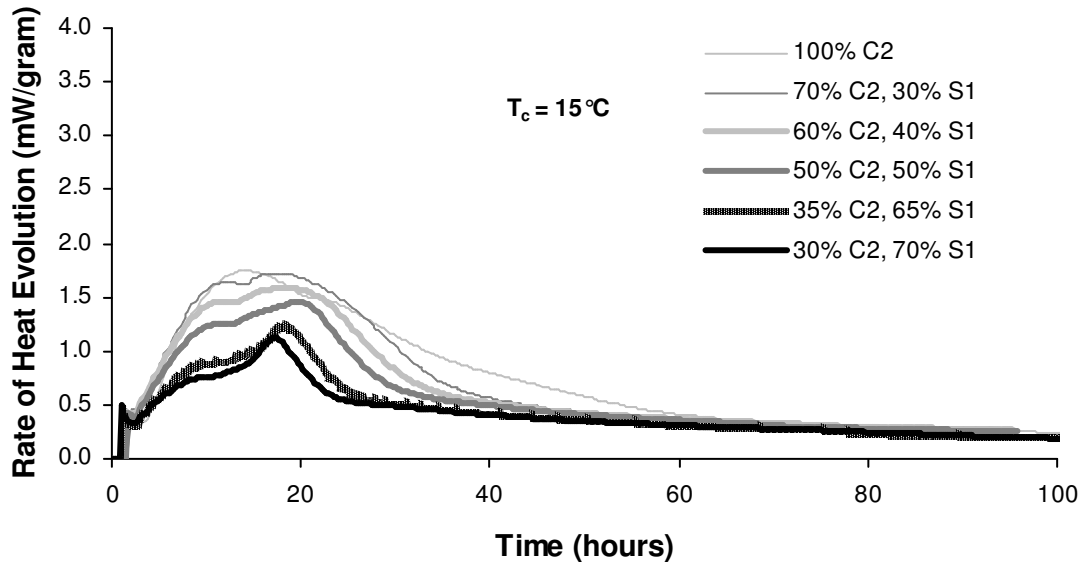


Figure C.43: Rate of Heat Evolution (Per Gram of Cementitious Material) for Paste Mixtures of Cement C2 with Different Replacements of GGBF Slag at 15 °C (59 °F)

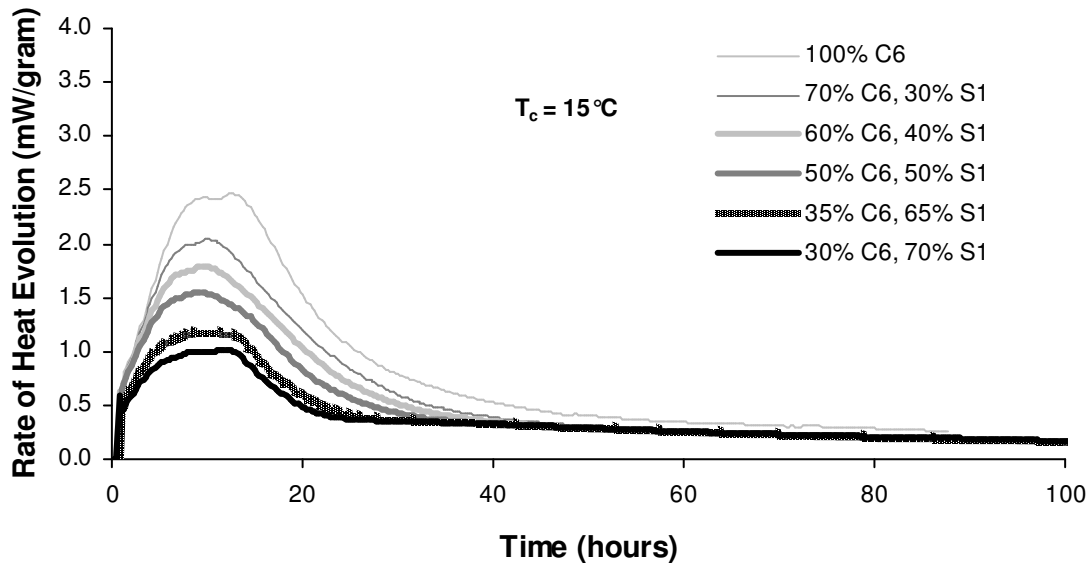


Figure C.44: Rate of Heat Evolution (Per Gram of Cementitious Material) for Paste Mixtures of Cement C6 with Different Replacements of GGBF Slag at 15 °C (59 °F)

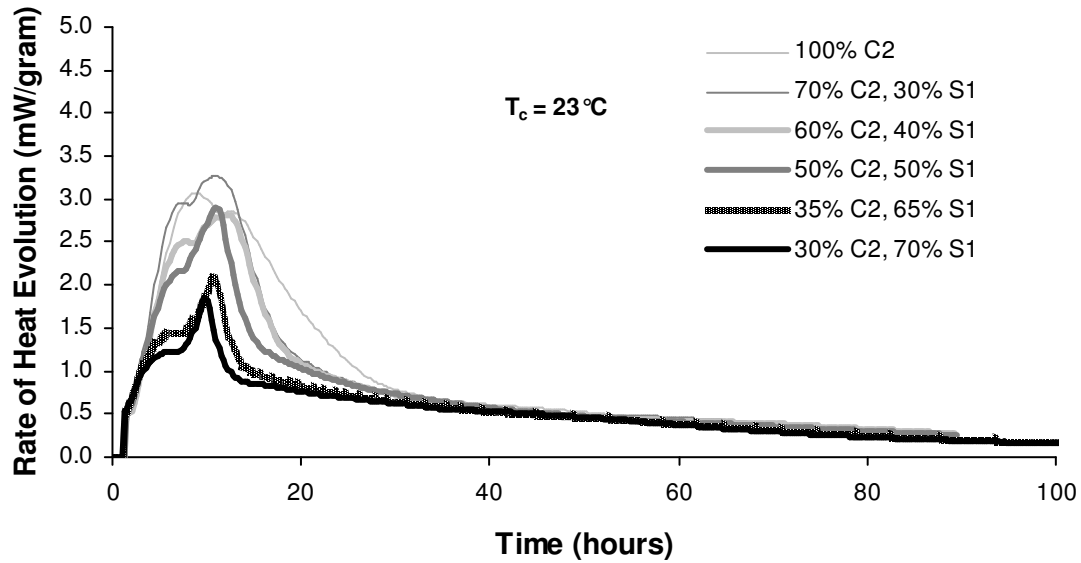


Figure C.45: Rate of Heat Evolution (Per Gram of Cementitious Material) for Paste Mixtures of Cement C2 with Different Replacements of GGBF Slag at 23 °C (73 °F)

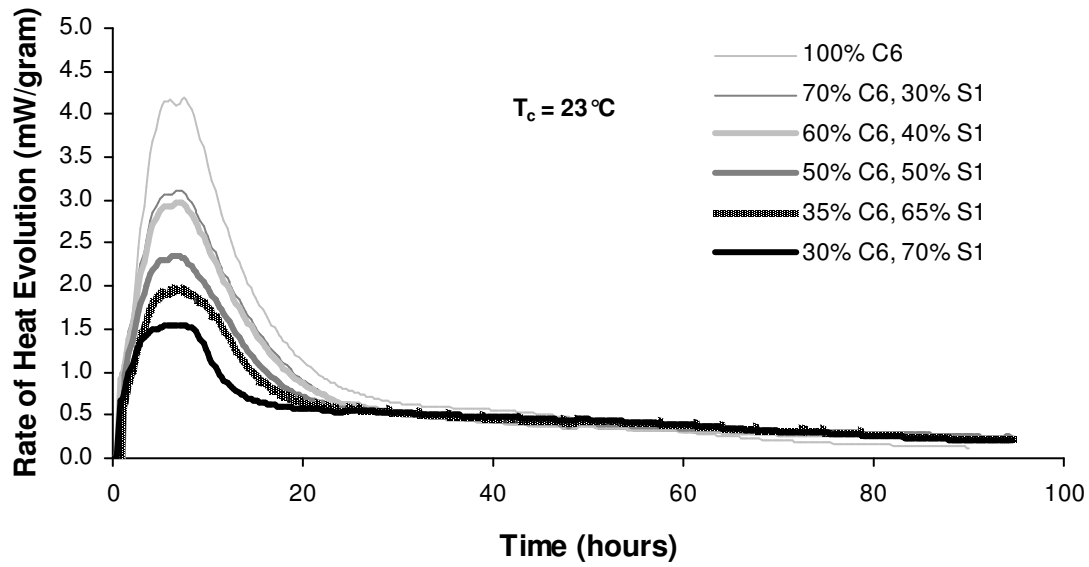


Figure C.46: Rate of Heat Evolution (Per Gram of Cementitious Material) for Paste Mixtures of Cement C6 with Different Replacements of GGBF Slag (S1) at 23 °C (73 °F)

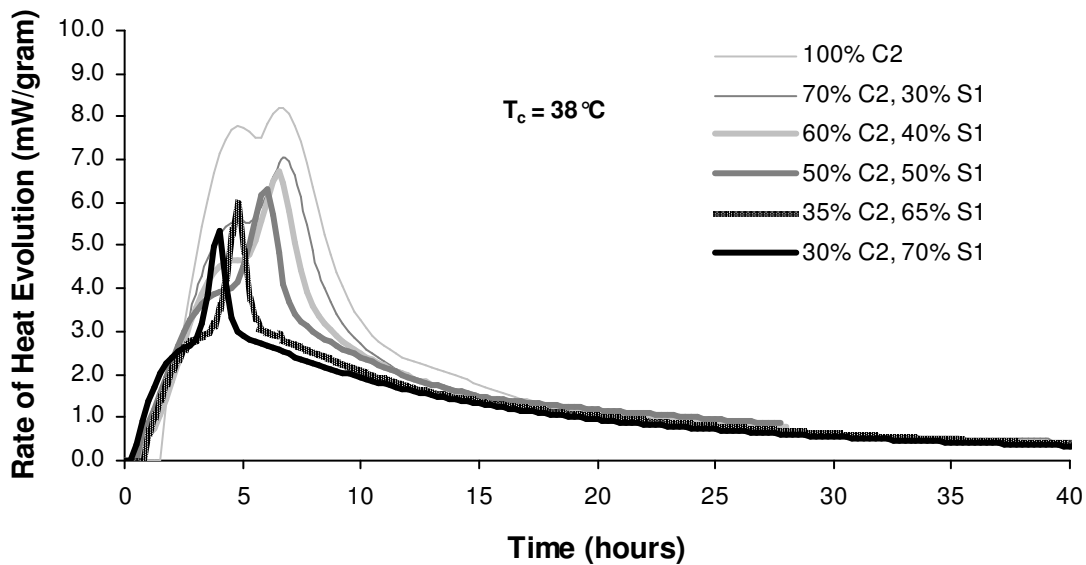


Figure C.47: Rate of Heat Evolution (Per Gram of Cementitious Material) for Paste Mixtures of Cement C2 with Different Replacements of GGBF Slag (S1) at 38 °C (100 °F)

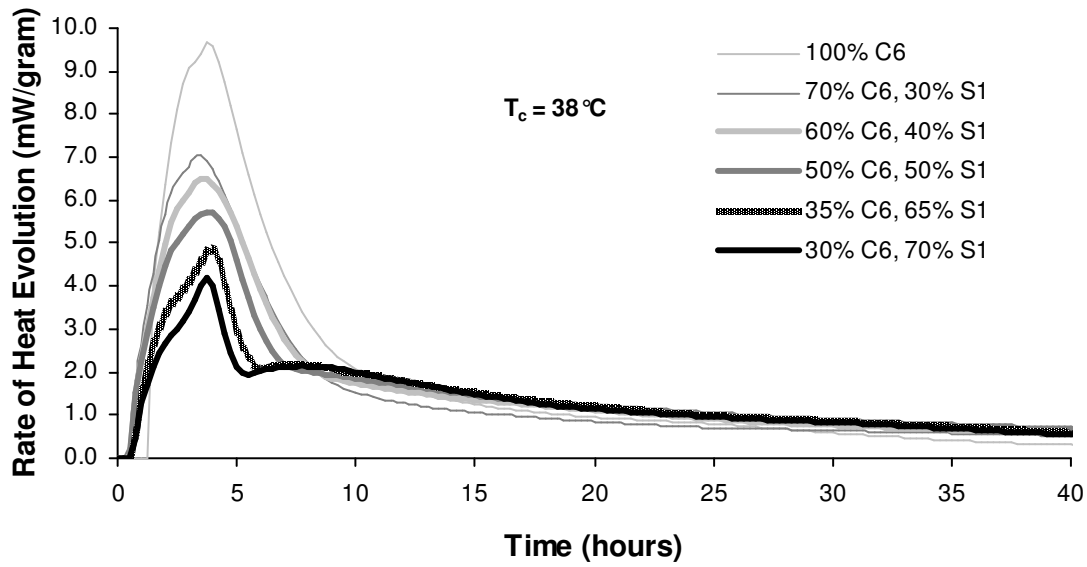


Figure C.48: Rate of Heat Evolution (Per Gram of Cementitious Material) for Paste Mixtures of Cement C6 with Different Replacements of GGBF Slag (S1) at 38 °C (100 °F)

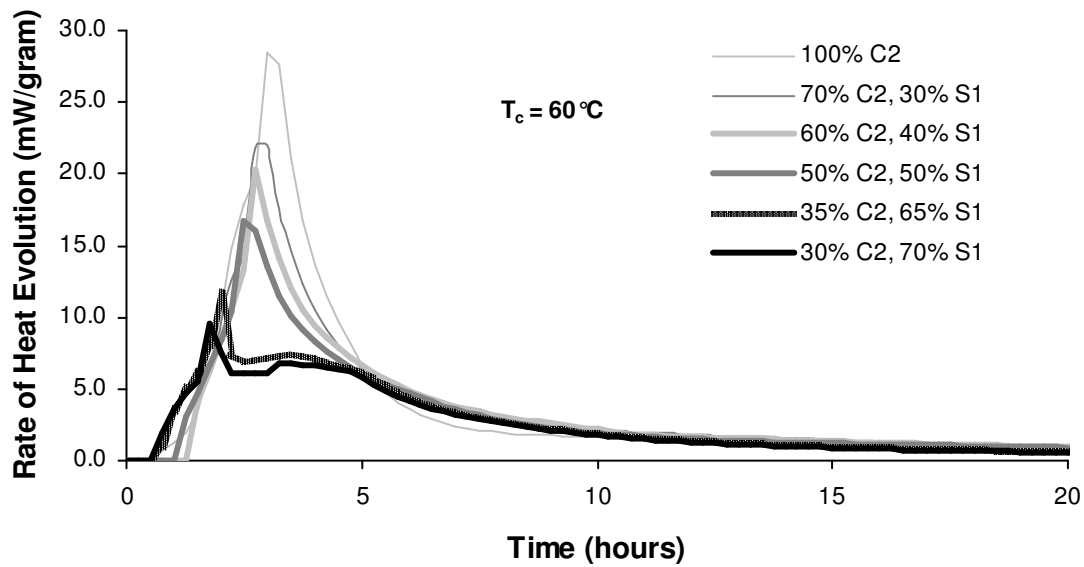


Figure C.49: Rate of Heat Evolution (Per Gram of Cementitious Material) for Paste Mixtures of Cement C2 with Different Replacements of GGBF Slag (S1) at 60 °C (140 °F)

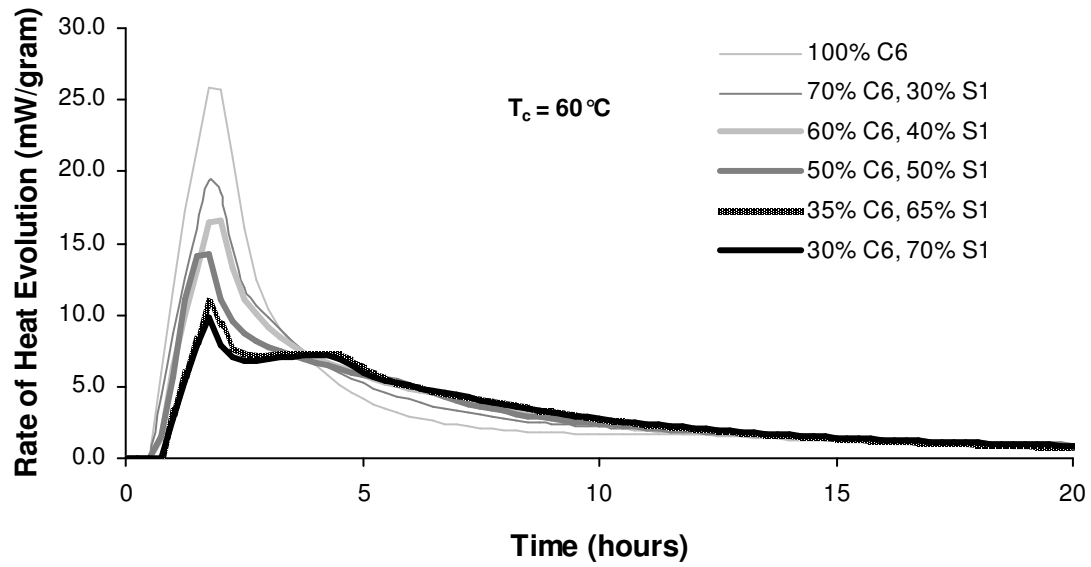


Figure C.50: Rate of Heat Evolution (Per Gram of Cementitious Material) for Paste Mixtures of Cement C6 with Different Replacements of GGBF Slag (S1) at 60 °C (140 °F)

C.6. EFFECTS OF SILICA FUME ON RATE OF HEAT EVOLUTION OF PASTES

The following figures provide background for the effects of silica fume and ternary blends of silica fume and fly ash on rate of heat evolution of cementitious pastes presented in Chapter 4. Results at each of the isothermal test temperatures are shown.

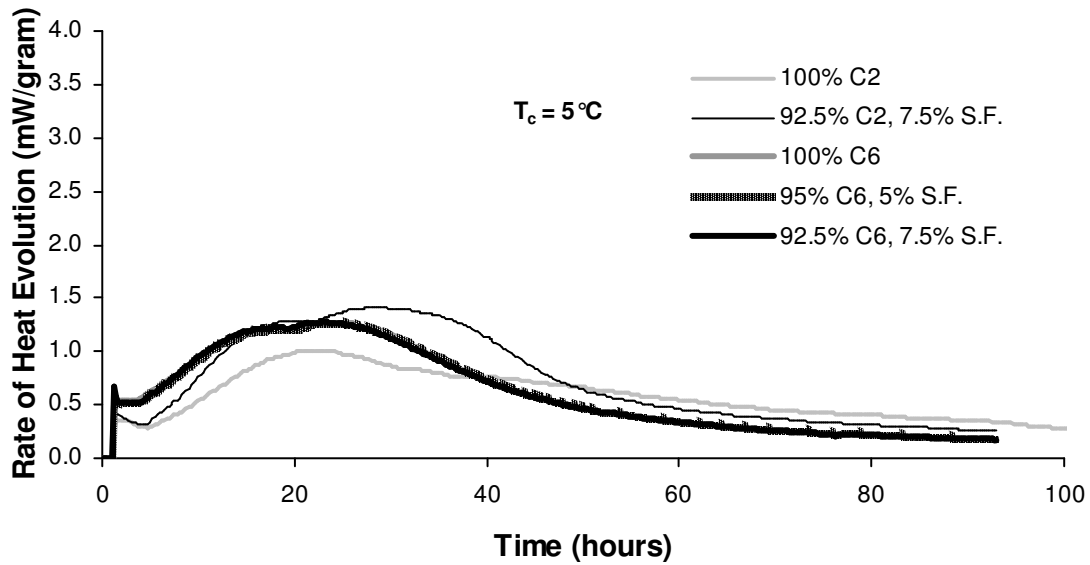


Figure C.51: Rate of Heat Evolution (Per Gram of Cementitious Material) for Paste Mixtures of Cement C2 with 7.5 % Silica Fume and Cement C6 with 5% and 7.5% Silica Fume at 5 °C (41 °F)

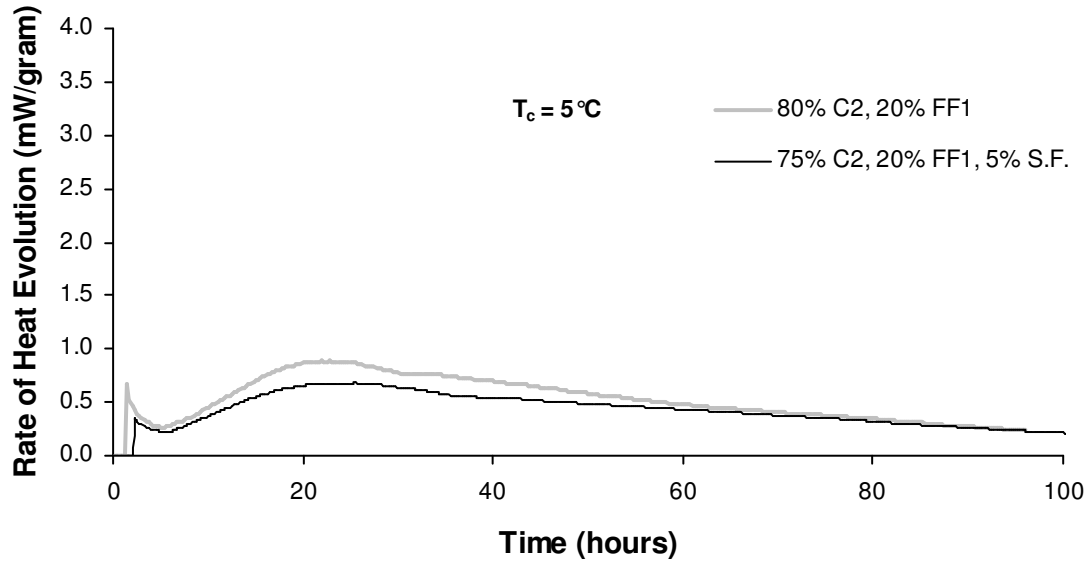


Figure C.52: Rate of Heat Evolution (Per Gram of Cementitious Material) for Paste Mixtures of Cement C2, 20% FF1 With and Without 5% Silica Fume at 5 °C (41 °F)

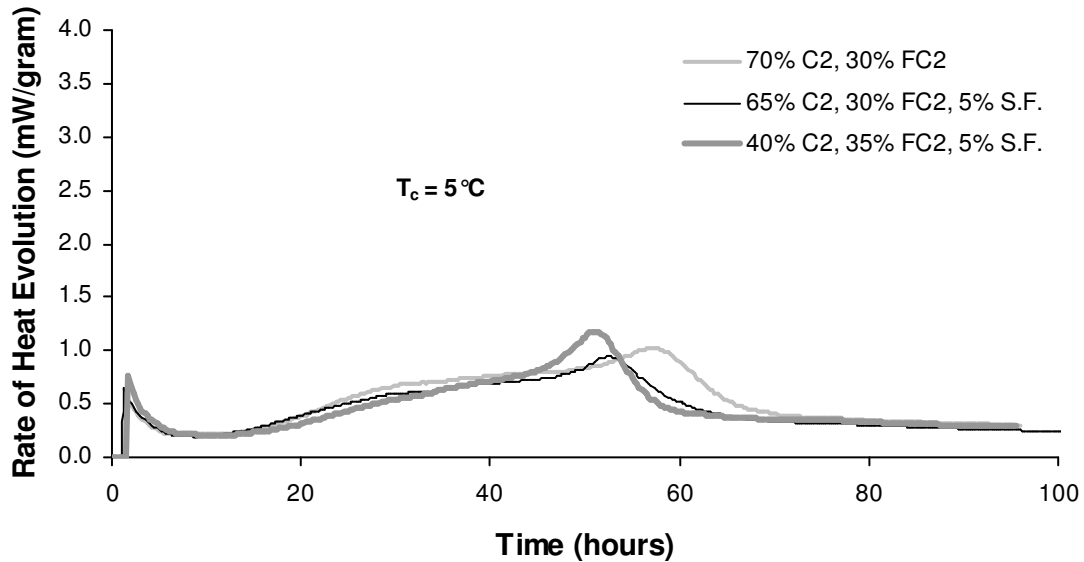


Figure C.53: Rate of Heat Evolution (Per Gram of Cementitious Material) for Paste Mixtures of Cement C2, 30-35% FC2 With and Without 5% Silica Fume at 5 °C (41 °F)

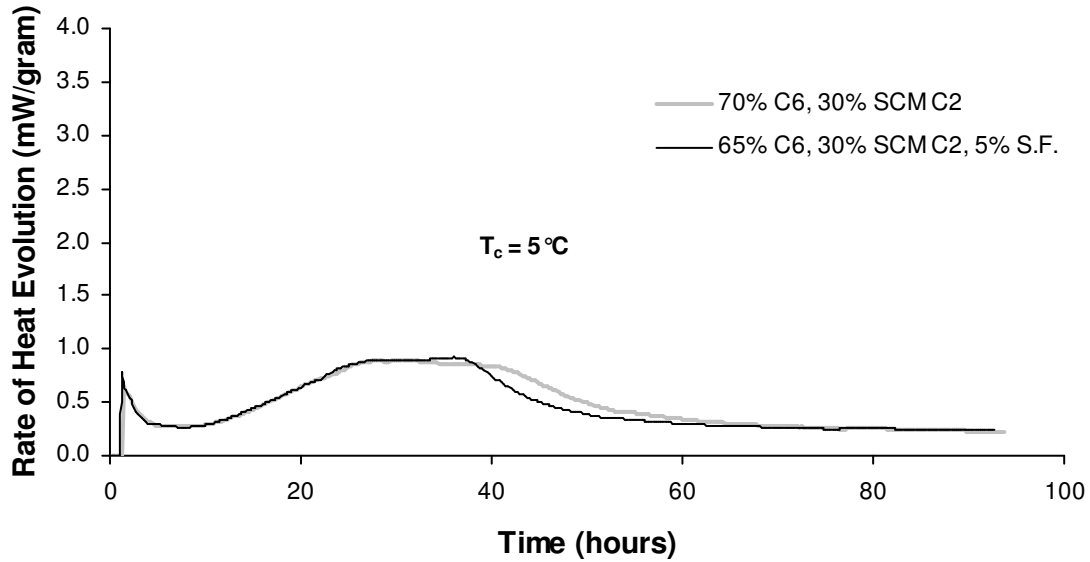


Figure C.54: Rate of Heat Evolution (Per Gram of Cementitious Material) for Paste Mixtures of Cement C6, 30% FC2 With and Without 5% Silica Fume at 5 °C (41 °F)

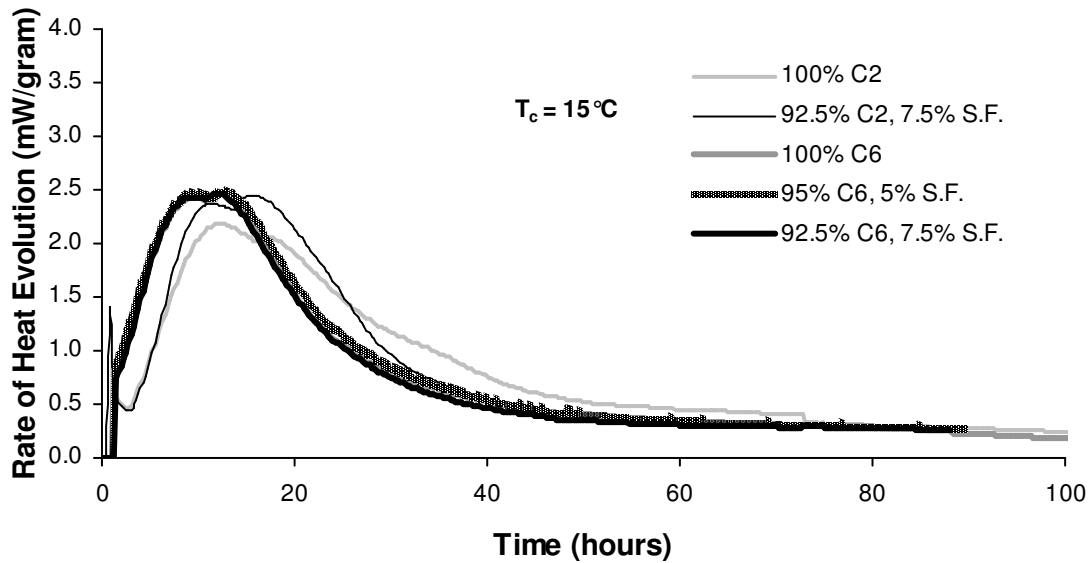


Figure C.55: Rate of Heat Evolution (Per Gram of Cementitious Material) for Paste Mixtures of Cement C2 with 7.5 % Silica Fume and Cement C6 with 5% and 7.5% Silica Fume at 15 °C (59 °F)

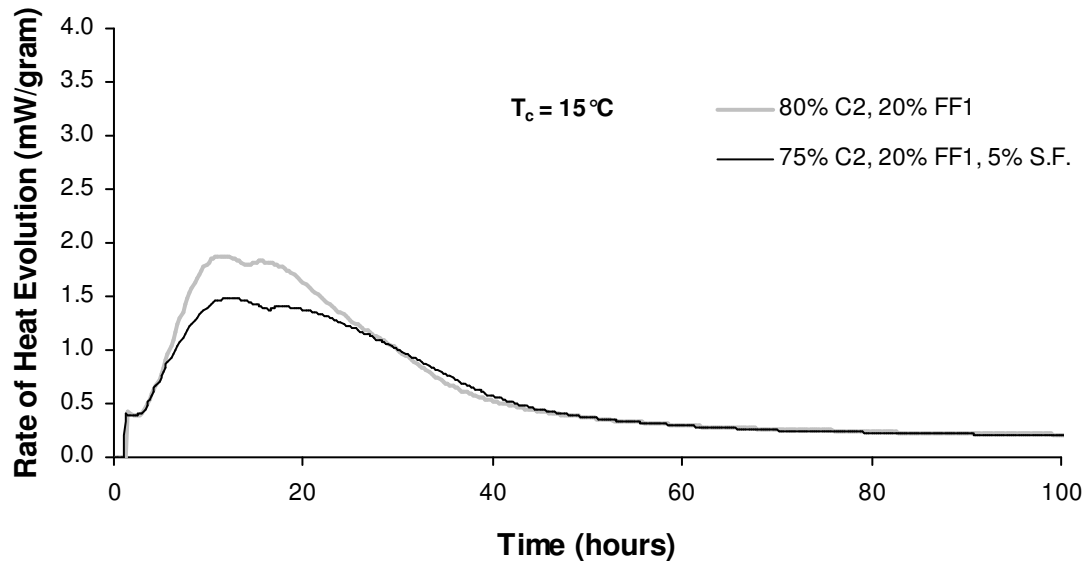


Figure C.56: Rate of Heat Evolution (Per Gram of Cementitious Material) for Paste Mixtures of Cement C2, 20% FF1 With and Without 5% Silica Fume at 15 °C (59 °F)

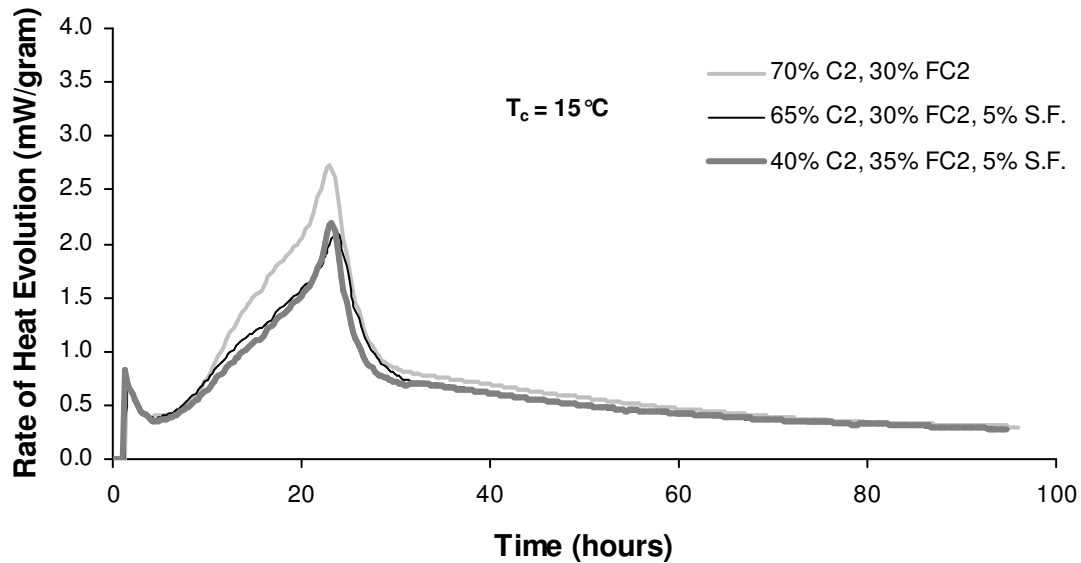


Figure C.57: Rate of Heat Evolution (Per Gram of Cementitious Material) for Paste Mixtures of Cement C2, 30-35% FC2 With and Without 5% Silica Fume at 15 °C (59 °F)

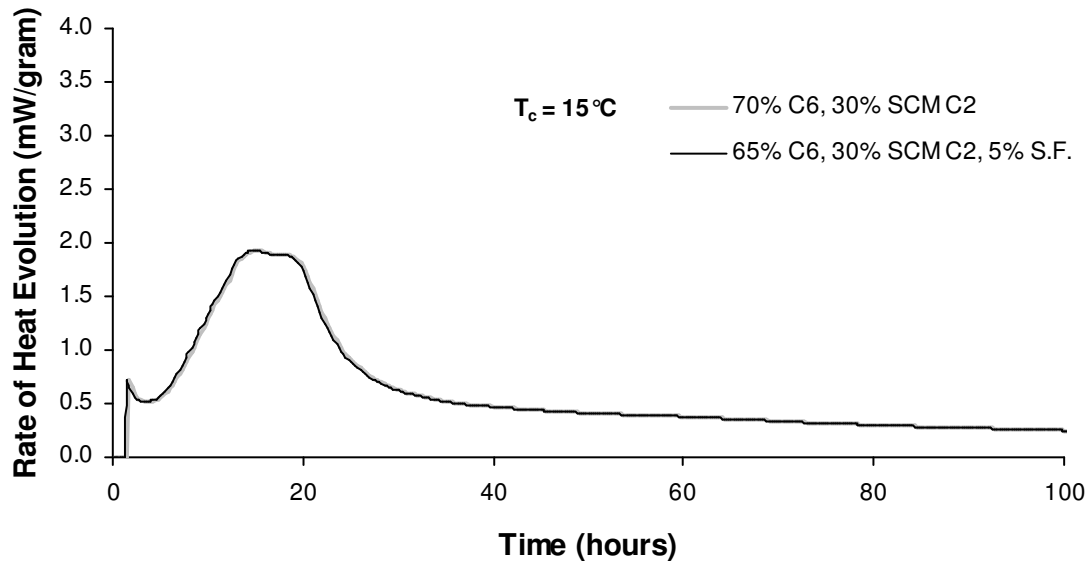


Figure C.58: Rate of Heat Evolution (Per Gram of Cementitious Material) for Paste Mixtures of Cement C6, 30% FC2 With and Without 5% Silica Fume at 15 °C (59 °F)

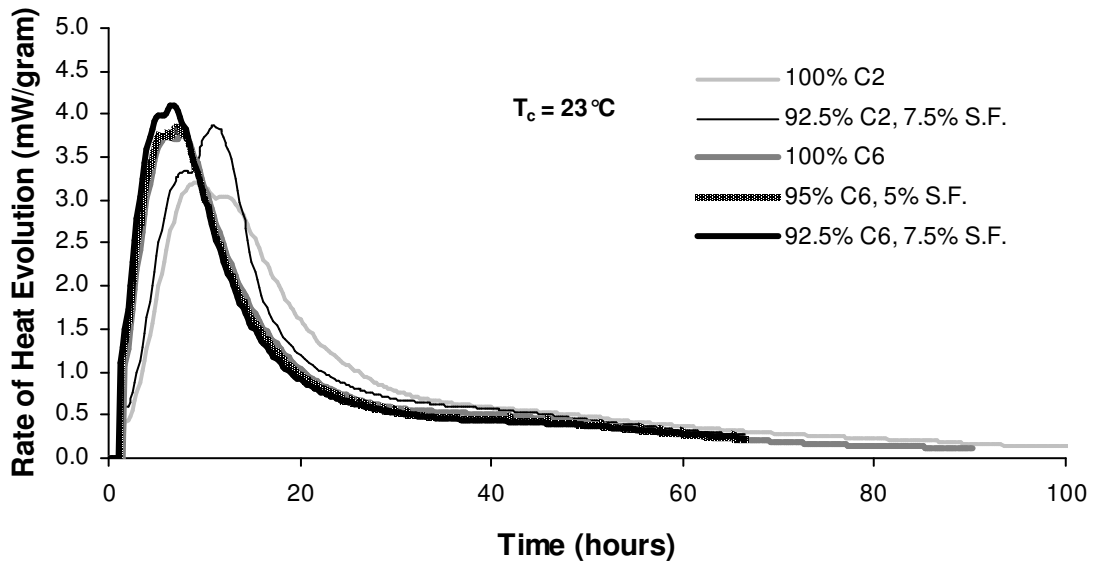


Figure C.59: Rate of Heat Evolution (Per Gram of Cementitious Material) for Paste Mixtures of Cement C2 with 7.5 % Silica Fume and Cement C6 with 5% and 7.5% Silica Fume at 23 °C (73 °F)

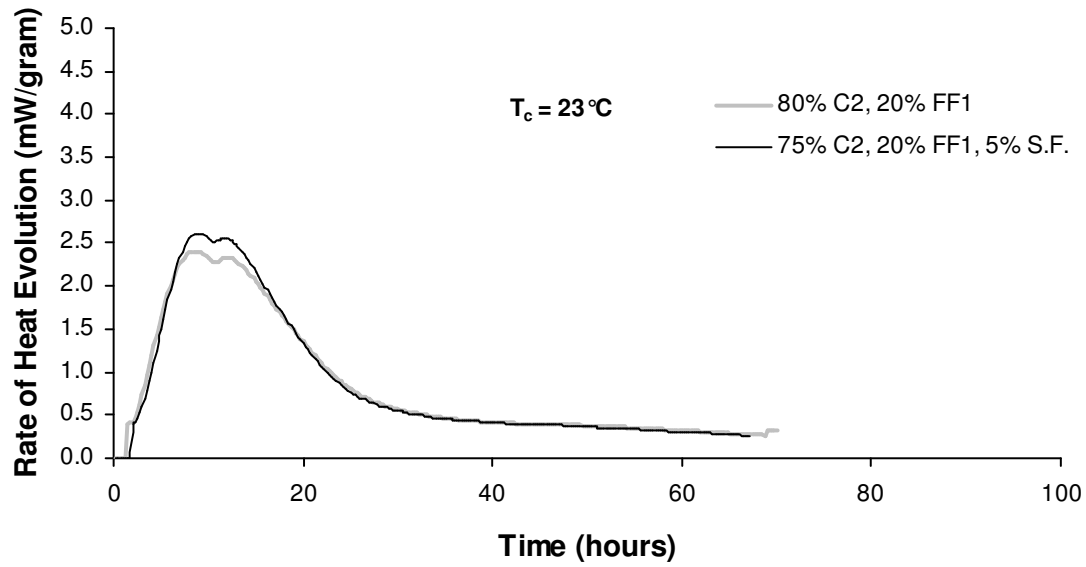


Figure C.60: Rate of Heat Evolution (Per Gram of Cementitious Material) for Paste Mixtures of Cement C2, 20% FF1 With and Without 5% Silica Fume at 23 °C (73 °F)

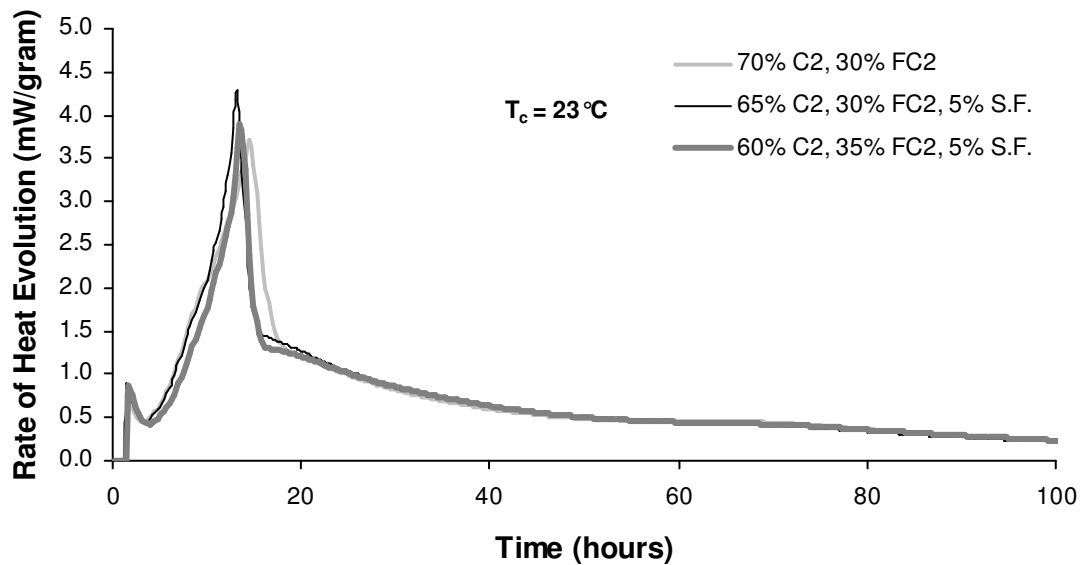


Figure C.61: Rate of Heat Evolution (Per Gram of Cementitious Material) for Paste Mixtures of Cement C2, 30-35% FC2 With and Without 5% Silica Fume at 23 °C (73 °F)

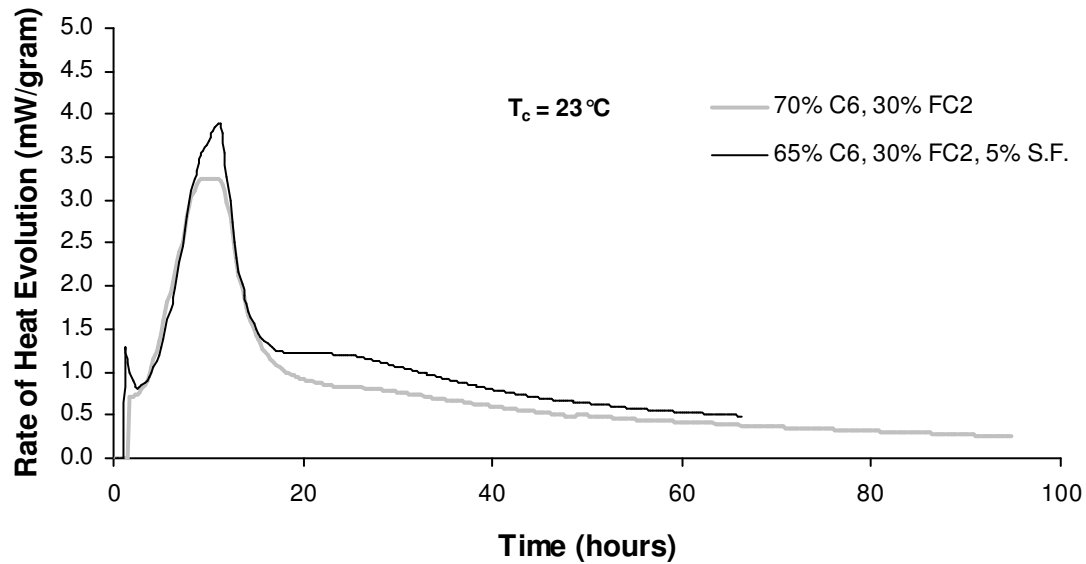


Figure C.62: Rate of Heat Evolution (Per Gram of Cementitious Material) for Paste Mixtures of Cement C6, 30% FC2 With and Without 5% Silica Fume at 23 °C (73 °F)

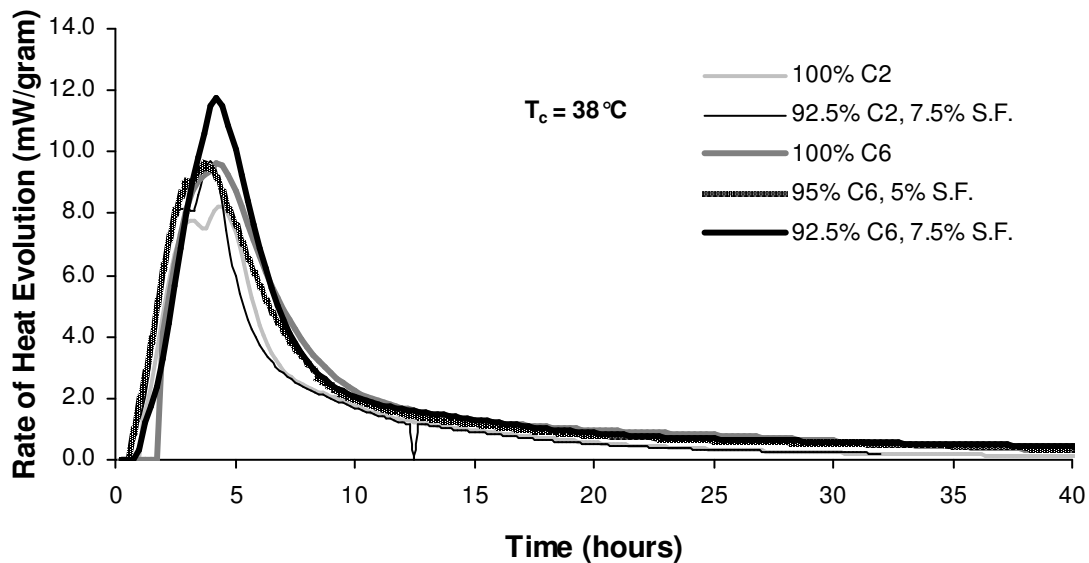


Figure C.63: Rate of Heat Evolution (Per Gram of Cementitious Material) for Paste Mixtures of Cement C2 with 7.5 % Silica Fume and Cement C6 with 5% and 7.5% Silica Fume at 38 °C (100 °F)

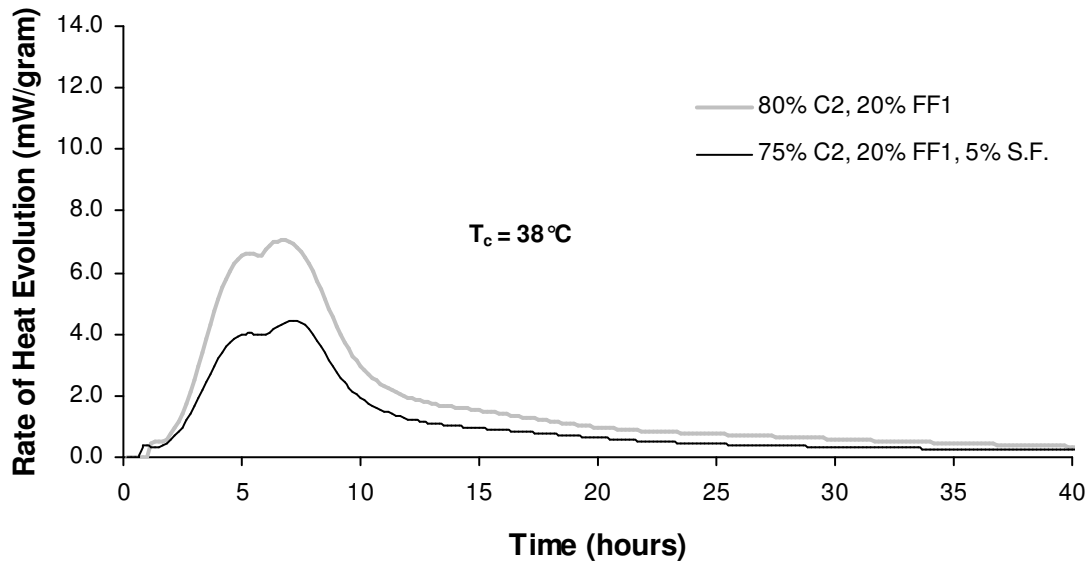


Figure C.64: Rate of Heat Evolution (Per Gram of Cementitious Material) for Paste Mixtures of Cement C2, 20% FF1 With and Without 5% Silica Fume at 38 °C (100 °F)

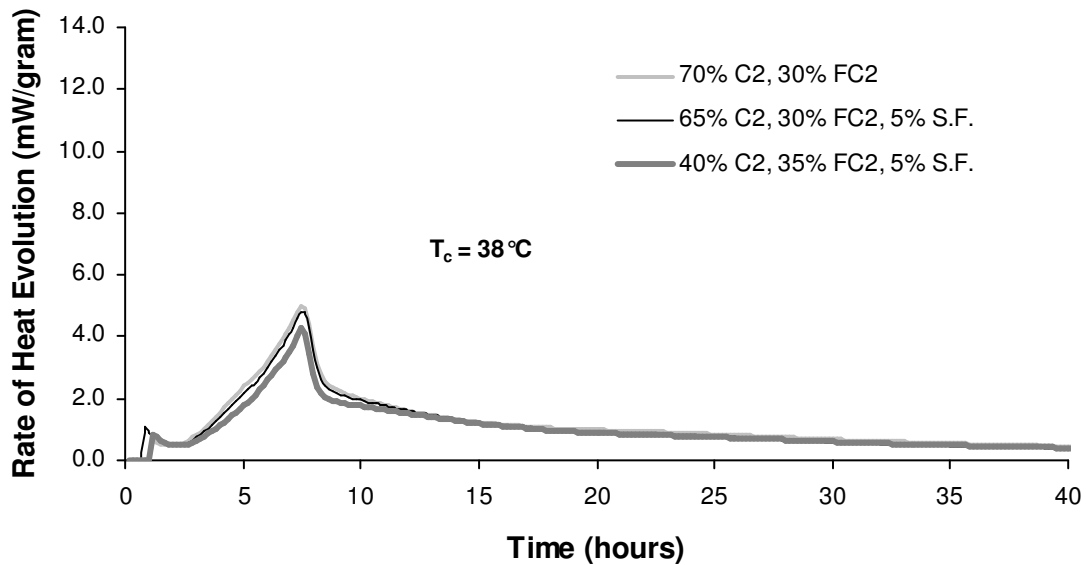


Figure C.65: Rate of Heat Evolution (Per Gram of Cementitious Material) for Paste Mixtures of Cement C2, 30-35% FC2 With and Without 5% Silica Fume at 38 °C (100 °F)

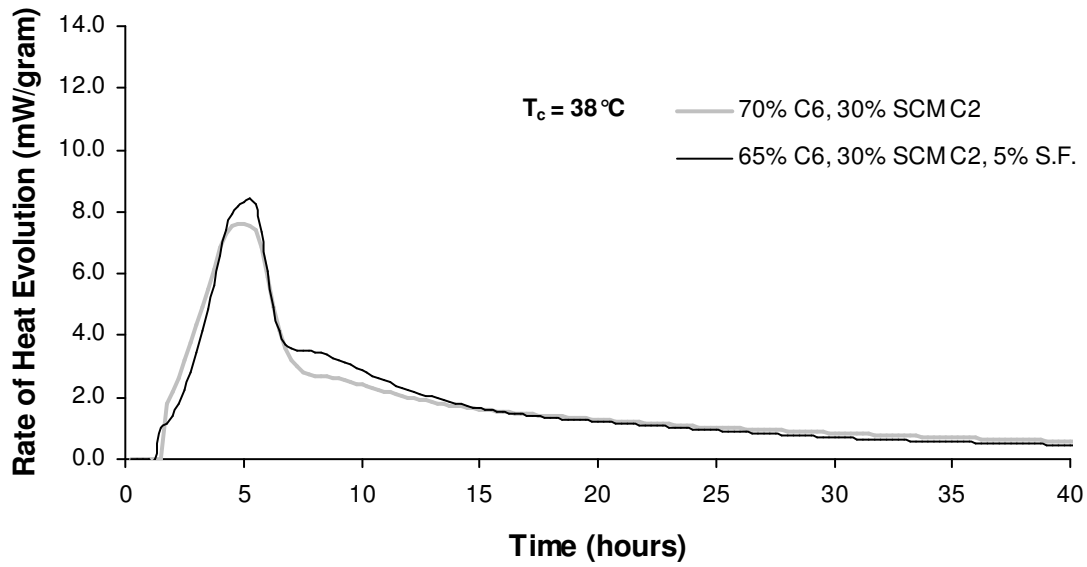


Figure C.66: Rate of Heat Evolution (Per Gram of Cementitious Material) for Paste Mixtures of Cement C6, 30% FC2 With and Without 5% Silica Fume at 38 °C (100 °F)

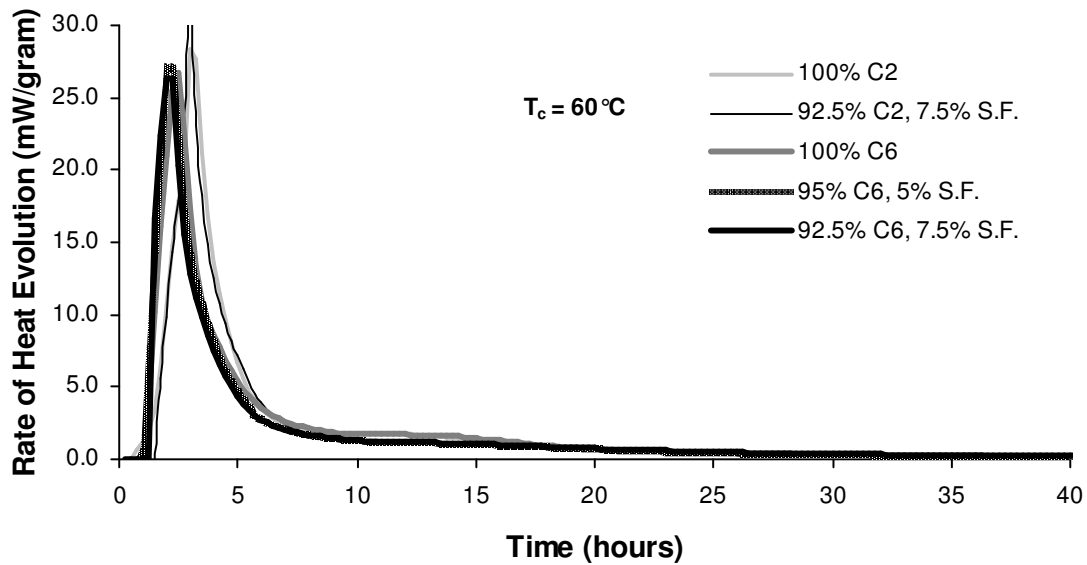


Figure C.67: Rate of Heat Evolution (Per Gram of Cementitious Material) for Paste Mixtures of Cement C2 with 7.5 % Silica Fume and Cement C6 with 5% and 7.5% Silica Fume at 60 °C (140 °F)

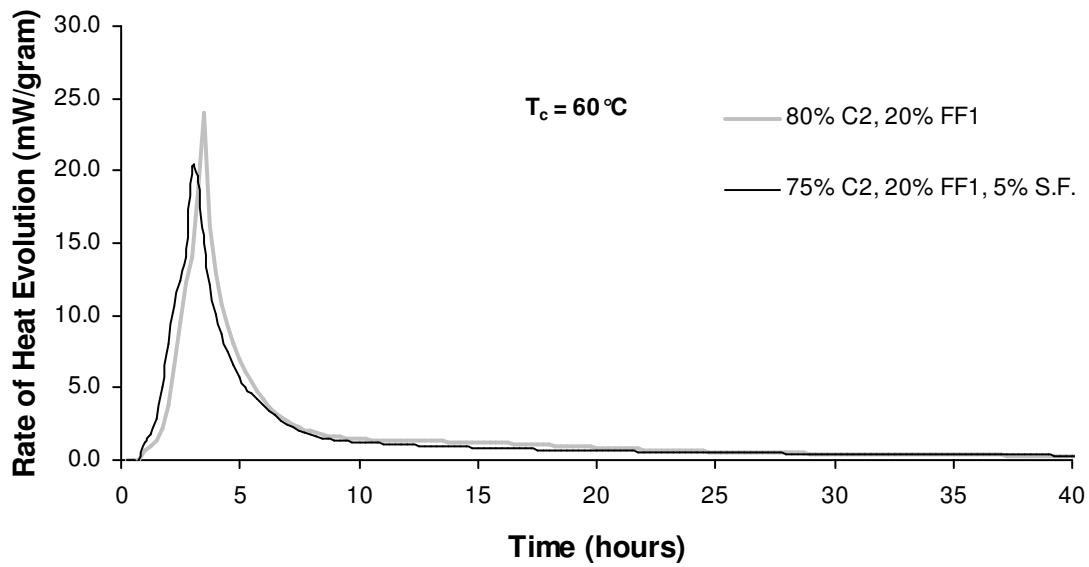


Figure C.68: Rate of Heat Evolution (Per Gram of Cementitious Material) for Paste Mixtures of Cement C2, 20% FF1 With and Without 5% Silica Fume at 60 °C (140 °F)

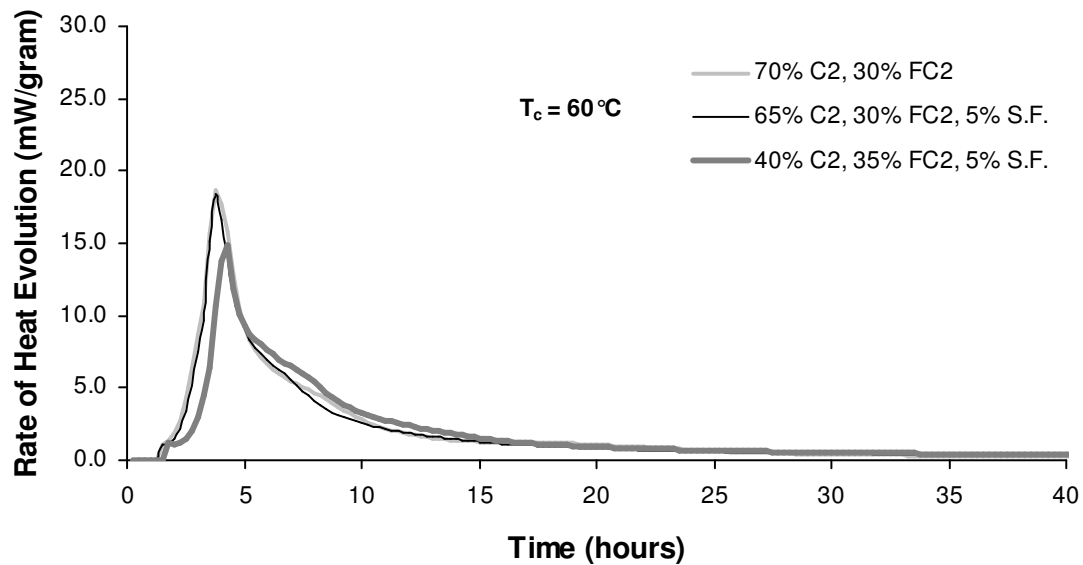


Figure C.69: Rate of Heat Evolution (Per Gram of Cementitious Material) for Paste Mixtures of Cement C2, 30-35% FC2 With and Without 5% Silica Fume at 60 °C (140 °F)

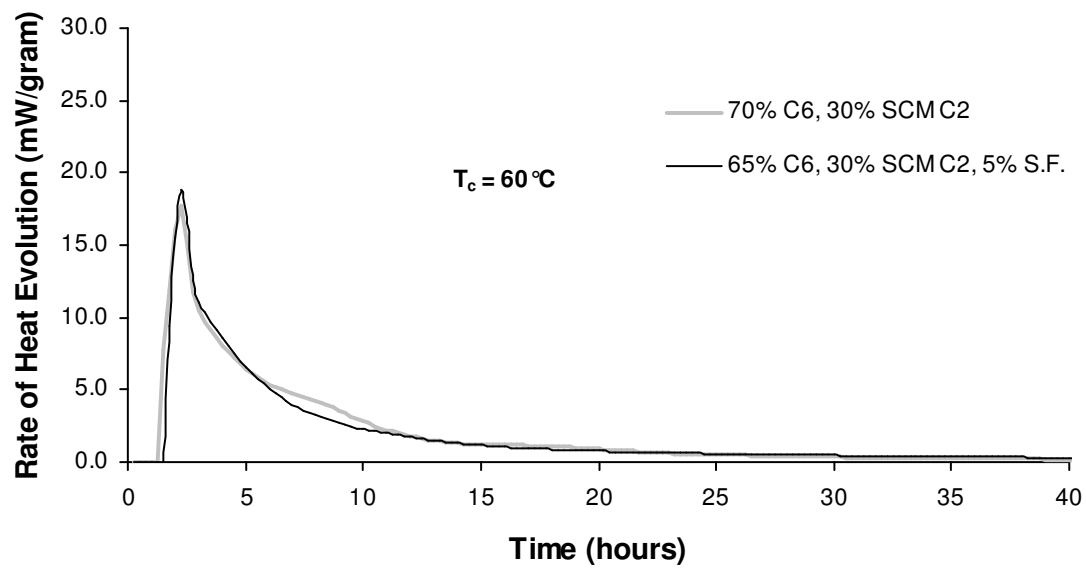


Figure C.70: Rate of Heat Evolution (Per Gram of Cementitious Material) for Paste Mixtures of Cement C6, 30% FC2 With and Without 5% Silica Fume at 60 °C (140 °F)

C.7. EFFECTS OF ALKALIS INCREASES ON RATE OF HEAT EVOLUTION OF PASTES WITH FLY ASH FF1 AND FC2

The following figures provide background for the effects of fly ash FF2 on rate of heat evolution of cementitious pastes presented in Chapter 4. Results at each of the isothermal test temperatures are shown.

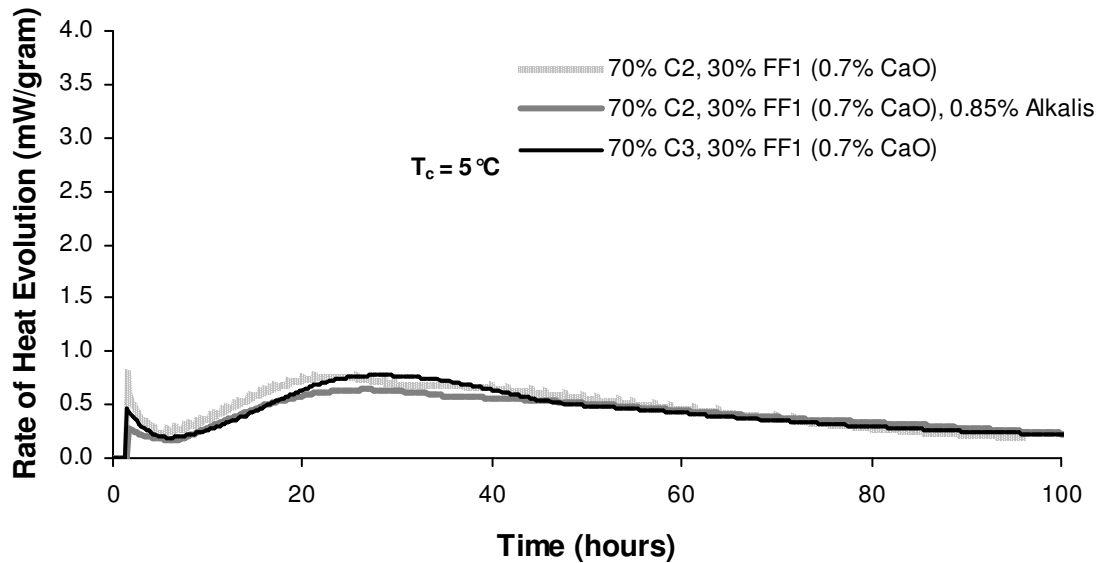


Figure C.71: Rate of Heat Evolution (Per Gram of Cementitious Material) for Paste Mixtures of 70% Cement C2, 30% FF1 With and Without 0.85% ($\text{Na}_2\text{O}+0.658\text{K}_2\text{O}$), and Cement C3, 30% FF1 at 5°C (41°F)

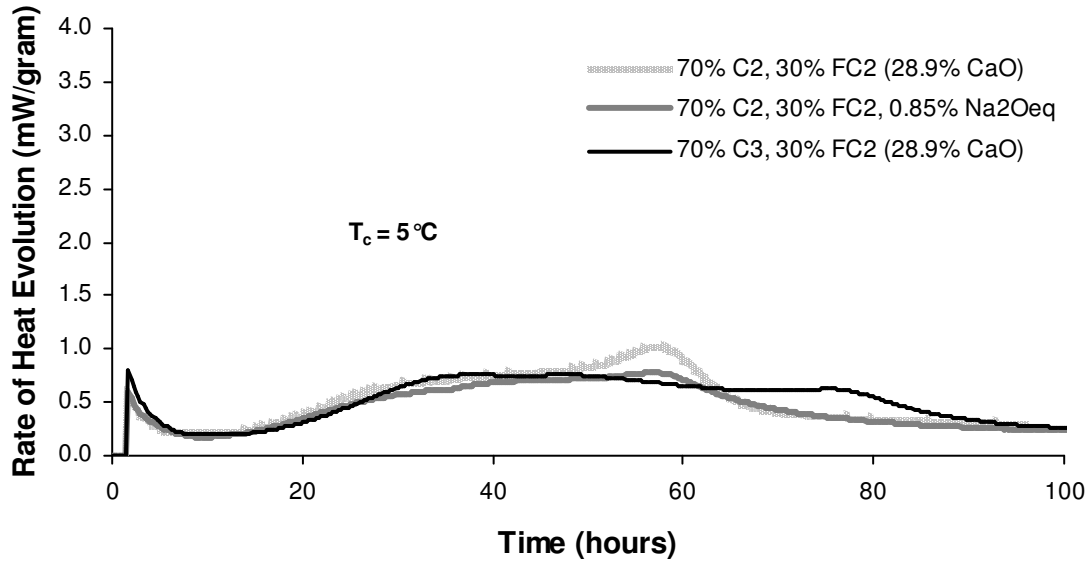


Figure C.72: Rate of Heat Evolution (Per Gram of Cementitious Material) for Paste Mixtures of 70% Cement C2, 30% FC2 With and Without 0.85% (Na₂O+0.658K₂O), and Cement C3, 30% FC2 at 5 °C (41 °F)

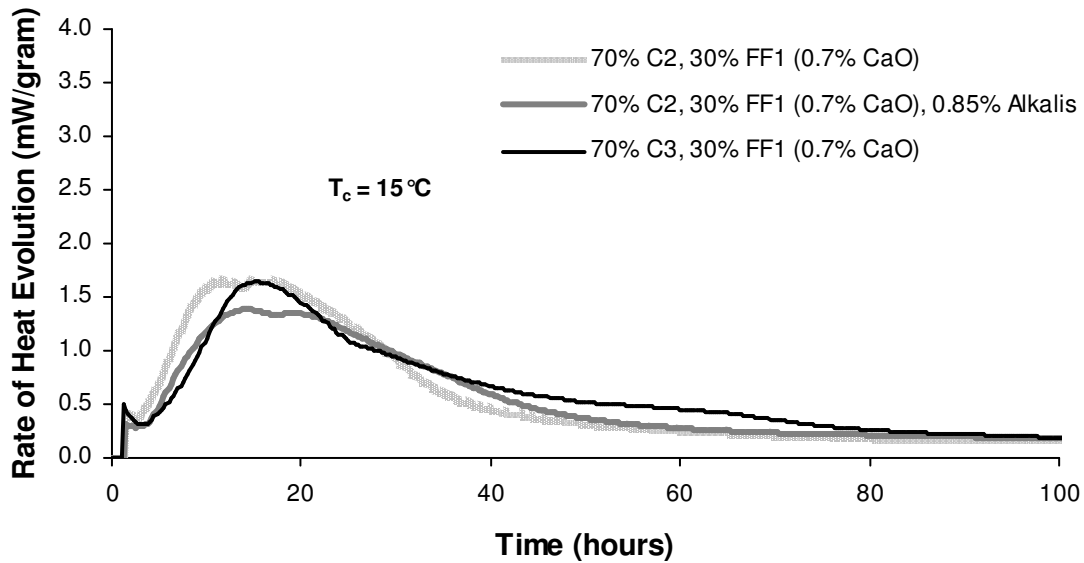


Figure C.73: Rate of Heat Evolution (Per Gram of Cementitious Material) for Paste Mixtures of 70% Cement C2, 30% FF1 With and Without 0.85% (Na₂O+0.658K₂O), and Cement C3, 30% FF1 at 5 °C (41 °F)

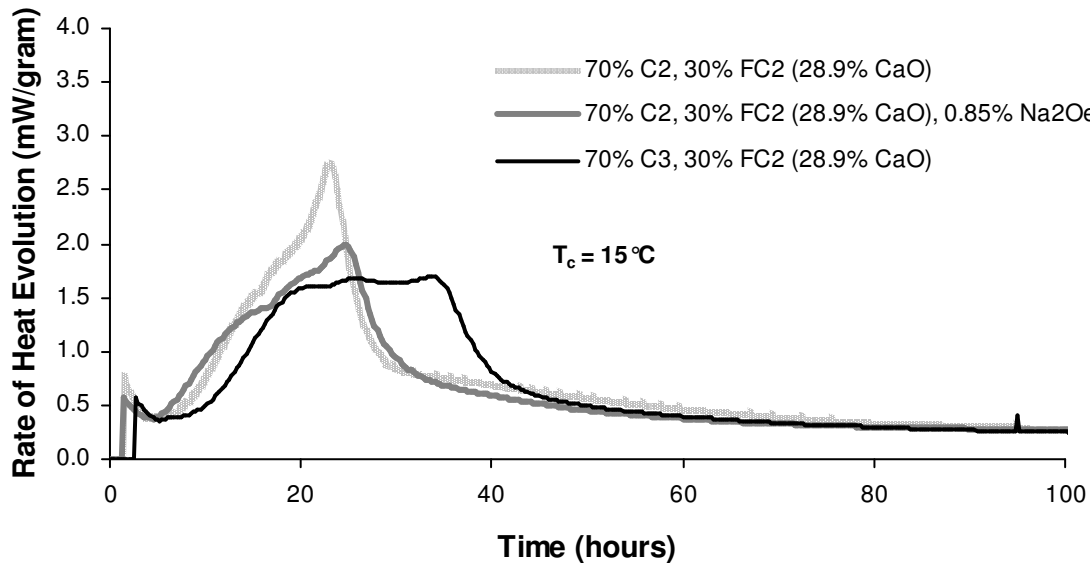


Figure C.74: Rate of Heat Evolution (Per Gram of Cementitious Material) for Paste Mixtures of 70% Cement C2, 30% FC2 With and Without 0.85% ($\text{Na}_2\text{O}+0.658\text{K}_2\text{O}$), and Cement C3, 30% FC2 at 15°C (59°F)

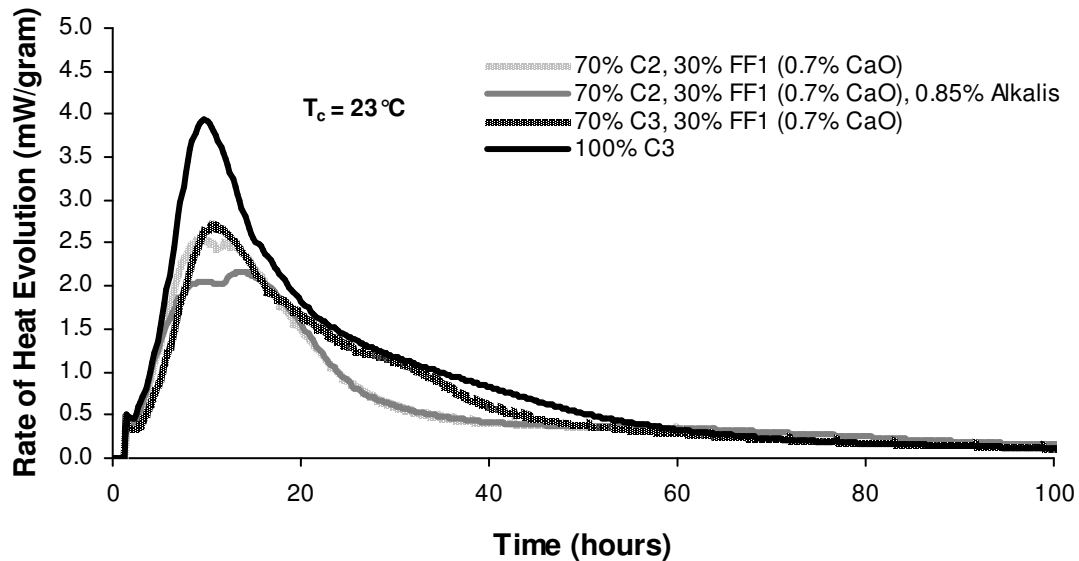


Figure C.75: Rate of Heat Evolution (Per Gram of Cementitious Material) for Paste Mixtures of 70% Cement C2, 30% FF1 With and Without 0.85% ($\text{Na}_2\text{O}+0.658\text{K}_2\text{O}$), and Cement C3, 30% FF1 at 5°C (41°F)

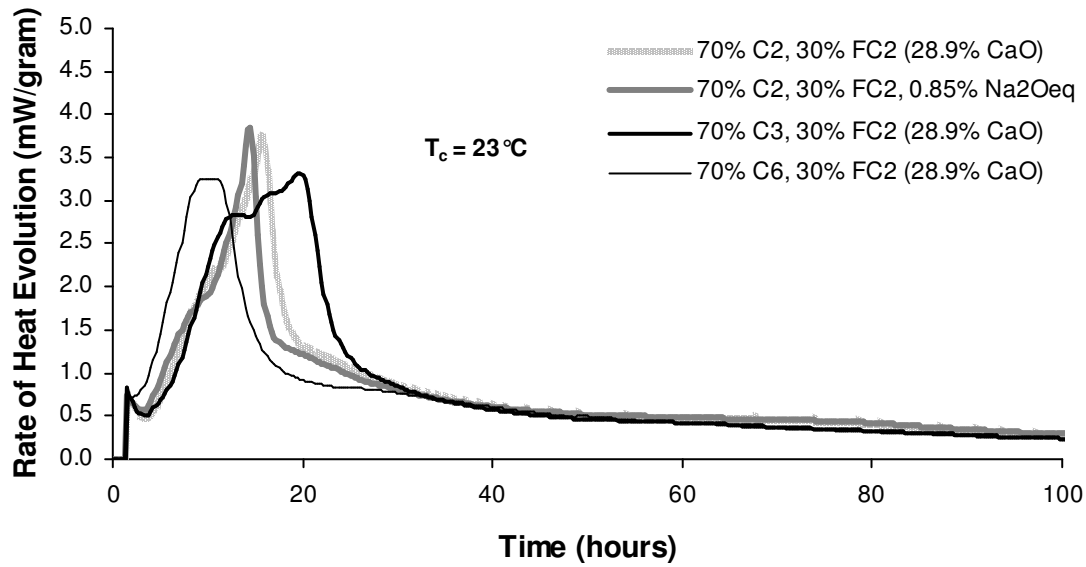


Figure C.76: Rate of Heat Evolution (Per Gram of Cementitious Material) for Paste Mixtures of 70% Cement C2, 30% FC2 With and Without 0.85% (Na₂O+0.658K₂O), and Cement C3, 30% FC2 at 23 °C (73 °F)

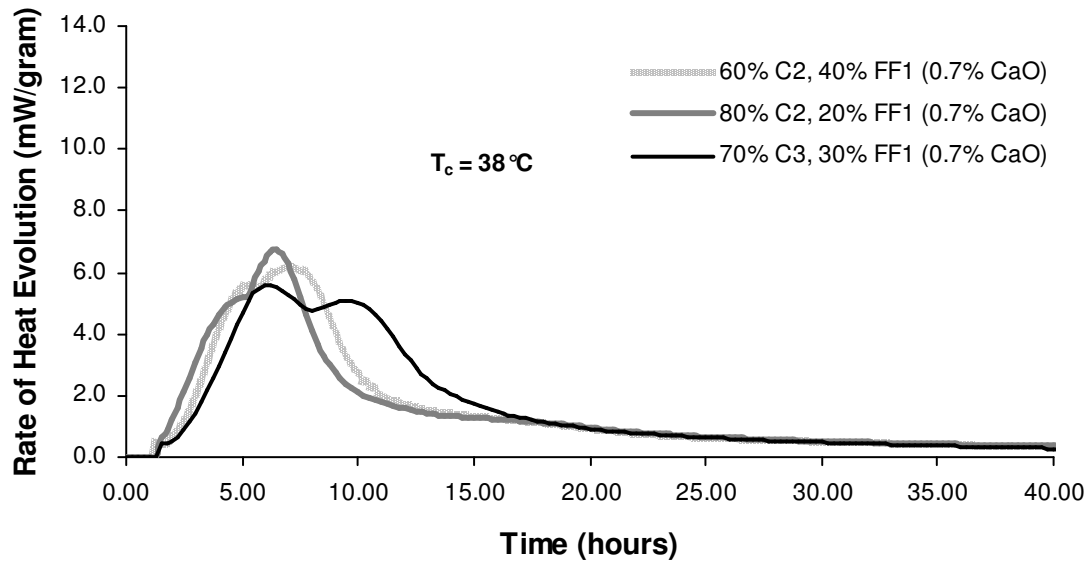


Figure C.77: Rate of Heat Evolution (Per Gram of Cementitious Material) for Paste Mixtures of 70% Cement C2, 30% FF1 With and Without 0.85% (Na₂O+0.658K₂O), and Cement C3, 30% FF1 at 38 °C (100 °F)

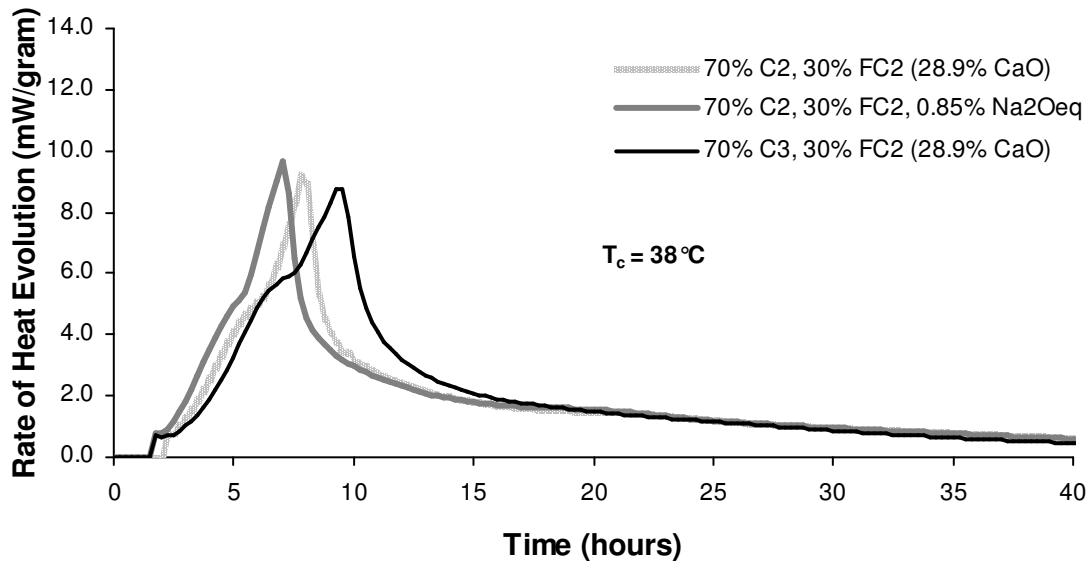


Figure C.78: Rate of Heat Evolution (Per Gram of Cementitious Material) for Paste Mixtures of 70% Cement C2, 30% FC2 With and Without 0.85% ($\text{Na}_2\text{O}+0.658\text{K}_2\text{O}$), and Cement C3, 30% FC2 at 38°C (100°F)

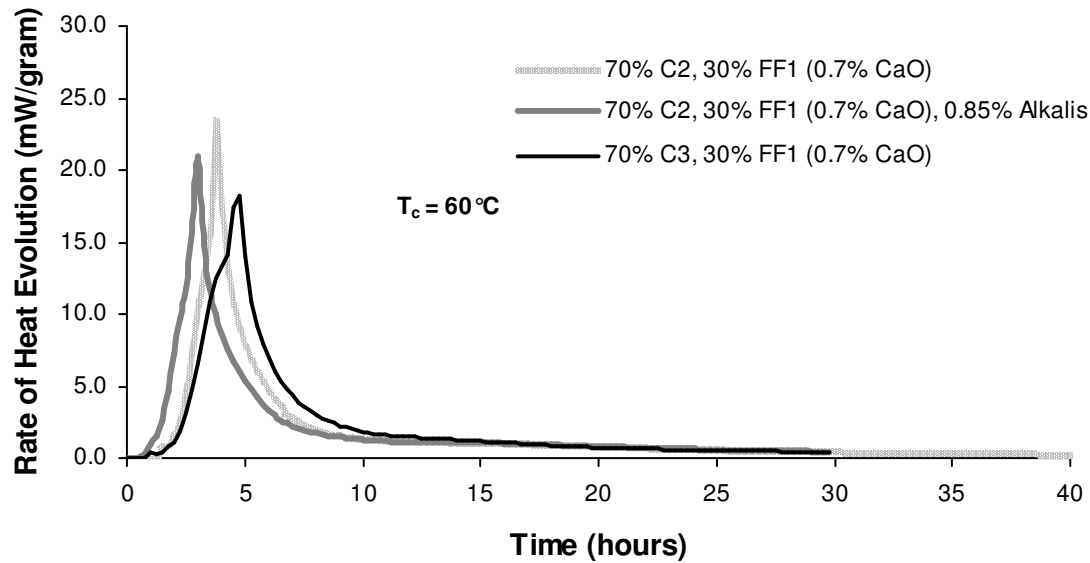


Figure C.79: Rate of Heat Evolution (Per Gram of Cementitious Material) for Paste Mixtures of 70% Cement C2, 30% FF1 With and Without 0.85% ($\text{Na}_2\text{O}+0.658\text{K}_2\text{O}$), and Cement C3, 30% FF1 at 60°C (140°F)

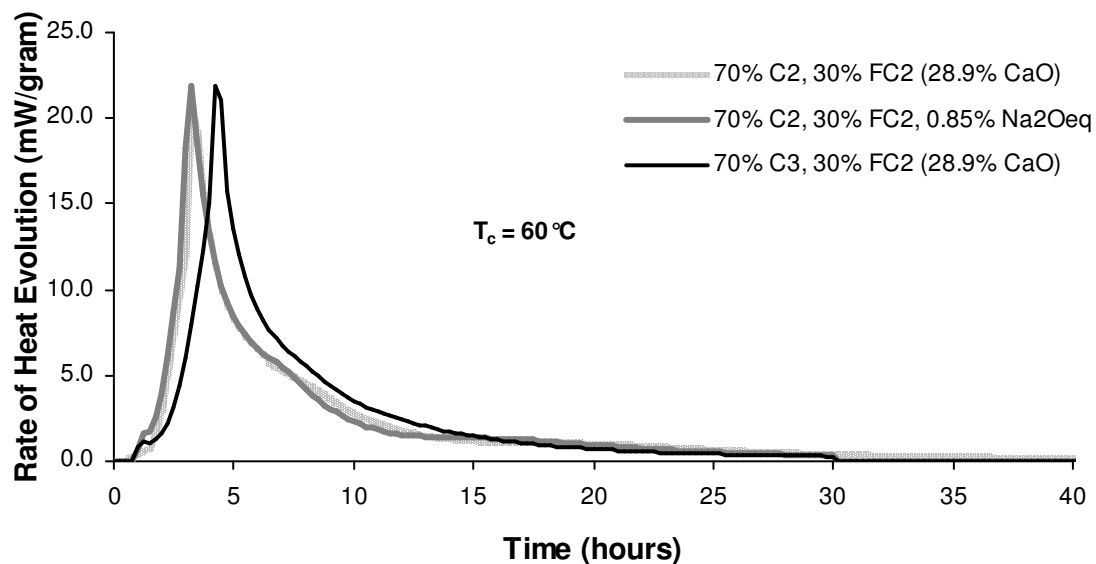


Figure C.80: Rate of Heat Evolution (Per Gram of Cementitious Material) for Paste Mixtures of 70% Cement C2, 30% FC2 With and Without 0.85% ($\text{Na}_2\text{O}+0.658\text{K}_2\text{O}$), and Cement C3, 30% FC2 at 60 °C (140 °F)

APPENDIX D. ADDITIONAL DISCUSSION OF MULTIVARIATE REGRESSION MODELING OF E_a FOR CHAPTER 5

Chapter 5 provides a summary of the independent variables that have the greatest effect on activation energy (E_a). The chapter presents two multivariate regression models that describe E_a based on cement chemistry, SCM type and replacement percentage, and chemical admixtures. The following sections will provide background information on the variable selection and regression analysis procedures that were used to develop the E_a models.

D.1. MULTIVARIATE REGRESSION ANALYSIS

There are several steps to develop a comprehensive model for E_a . The sequence of procedures used here to analyze the results is based on previous research¹⁴ and was presented briefly in Chapter 5. This appendix will discuss the procedures for regression analysis in greater detail.

Analyses of the isothermal calorimeter data requires several steps. First, the curve fit parameters (E_a , α_u , τ and β at 5, 15, 23, 38, and 60 °C) and independent variables from the isothermal testing are summarized in a database. These results are used to calculate the degree of hydration of the test at discrete points. This allows least-squares regression analysis to be performed on the results. Next, the independent variables that have the greatest effect on E_a are determined. In Chapters 2-4, the independent variables that had the greatest effect on E_a were selected visually. However, a more systematic analysis is needed to isolate the all of variables that may potentially effect on E_a , and to assure that these variables correlate well with visual observation. This process is detailed in the next

section on the PROC RSQUARE and GLM procedures. Once the independent variables are chosen, an estimate of their statistical significance is needed. An analysis of variance (ANOVA) is performed on the selected variables. Finally, a model is developed that estimates the contribution of each variable to E_a . The multivariate regression analysis was performed using SAS v.9.1.3. The following sections detail the statistical procedures that were followed to analyze the results.

D.2. INDEPENDENT VARIABLE SELECTION PROCEDURE USING PROC RSQUARE

PROC RSQUARE was used to isolate the independent variables (regressors or predictor variables) that could have an effect on the dependent variable (or response variable) E_a . The procedure analyzes a specified number of combinations of the independent variables and ranks them according to the coefficient of determination (R^2). The procedure also provides a matrix of the correlation coefficients of each variable combination. Figure D.1 through Figure D.6 summarizes the results from the RSQUARE procedure. The correlation matrix for the independent variables is summarized in Figure D.8 and Figure D.10. The correlation matrix gives the correlation coefficient between each of the independent variables.

The correlation coefficient is a measure of the degree of linear relationship between two variables²⁸. The correlation coefficient ($Corr(X,Y)$) is defined as follows:

$$Corr(x_1, x_2) = \frac{Cov(x_1, x_2)}{\sigma_{x1} \cdot \sigma_{x2}} \quad \textbf{Equation D-1}$$

Where $Cov(x_1, x_2)$ = covariance of variable x_1 and x_2

σ_{x1} or σ_{x2} = standard deviation of variable x_1 and x_2

R^2 and $Corr(x_1, x_2)$ provide measures to select variables that have a high correlation with changes in E_a , but that do not correlate with each other. To properly select independent variables to describe E_a , the correlations between these variables must be measured. Assessing the correlations between variables is somewhat subjective. The following guidelines have been suggested for use in clinical studies². Correlation coefficients of 0 to 0.25 indicate little or no relationship, 0.25 to 0.50 indicates a fair relationship, 0.50 to 0.75 indicate a moderate to good relationship, and 0.75 to 1.00 indicates an excellent relationship between the two variables. Guidelines related to engineering studies²⁸ suggest that correlations coefficients from 0 to 0.50 indicate a weak relationship, 0.50 to 0.80 indicate a moderate relationship, and 0.80 to 1.00 indicate a strong relationship. For the purposes of this study, $Corr(x_1, x_2) < 0.65$ was chosen as a sufficiently weak correlation between two variables to allow both to be included in the model for E_a . Variables with a covariance greater than 0.65 are generally composed of a combination of independent variables.

D.3. INDEPENDENT VARIABLES IN STUDY

Due to the computation speed necessary to investigate all of the variables at once, several iterations of the RSQUARE procedure were run to eliminate unlikely independent variables. Based on several iterations of the RSQUARE procedure, the following variables were chosen to be investigated more thoroughly:

wc = water-cementitious materials ratio;

$PerFash$ = % Class F fly ash in mixture;

$PerCash$ = % Class C fly ash in mixture;

$PerSF$ = % silica fume in mixture;

perC3S = weighted % C₃S in cementitious system (accounts for dilution by SCM's) by ASTM C150 Bogue calculations;

lperC3S = ln (*perC3S*);

perAlite = weighted % C₃S and associated polymorphs (as determined by Rietveld analysis) in cementitious system (accounts for dilution by SCM's);

perC2S = weighted % C₂S in cementitious system (accounts for dilution by SCM's) by ASTM C150 Bogue calculations;

lperC2S = ln (*perC2S*);

perBelite = weighted % C₂S and associated polymorphs (as determined by Rietveld analysis) in cementitious system (accounts for dilution by SCM's);

perC3A = weighted % C₃A in cementitious system (accounts for dilution by SCM's) by ASTM C150 Bogue calculations;

lperC3A = ln (*perC3A*);

perAluminate = weighted % C₃A and associated polymorphs (as determined by Rietveld analysis) in cementitious system (accounts for dilution by SCM's);

perC4AF = weighted % C₄AF in cementitious system (accounts for dilution by SCM's) by ASTM C150 Bogue calculations;

lperC4AF = ln (*perC4AF*);

perFerrite = weighted % C₄AF and associated polymorphs (as determined by Rietveld analysis) in cementitious system (accounts for dilution by SCM's);

perGypsum = weighted % gypsum in cementitious system (accounts for dilution by SCM's) by ASTM C150 Bogue calculations;

lperGypsum = ln (*perGypsum*);

perGypsumR = weighted % $\text{CaSO}_4 - \text{H}_2\text{O}$ (gypsum) (as determined by Rietveld analysis)

in cementitious system (accounts for dilution by SCM's);

perHemihydrate = weighted % $\text{CaSO}_4 - \frac{1}{2} \text{H}_2\text{O}$ (Hemihydrate) (as determined by

Rietveld analysis) in cementitious system (accounts for dilution by SCM's);

perAnhydrite = weighted % CaSO_4 (as determined by Rietveld analysis) in cementitious system (accounts for dilution by SCM's);

perK2SO4 = weighted % K_2SO_4 (arcanite) (as determined by Rietveld analysis) in cementitious system (accounts for dilution by SCM's);

FreeCaO = Free lime content in cement, as determined by Rietveld analysis;

CemBlaine = Blaine fineness of cement;

lCemBlaine = $\ln(\text{CemBlaine})$;

FABlaine = Blaine fineness of fly ash;

SlagBlaine = Blaine fineness of ground granulated blast furnace slag (GGBFS);

SFBlaine = Blaine fineness of silica fume;

perSlag = % ground granulated blast furnace slag (GGBFS) in mixture;

CemNa2Oeq = % $\text{Na}_2\text{O}_{\text{eq}}$ in cement ($0.658 \times \% \text{K}_2\text{O} + \% \text{Na}_2\text{O}$);

lCemNa2Oeq = $\ln(\text{CemNa2Oeq})$;

TotalNa2Oeq = % $\text{Na}_2\text{O}_{\text{eq}}$ in all cementitious material in mixture ($0.658 \times \% \text{K}_2\text{O} + \% \text{Na}_2\text{O}$);

lTotalNa2Oeq = $\ln(\text{TotalNa2Oeq})$;

CemNa2O = % Na_2O in cement

CemK2O = % K_2O in cement

WRRET = ASTM Ty A&D water reducer/retarder, OZ/100 lbs of cementitious material;

$$lWRRET = \ln (WRRET);$$

HRWR = ASTM Ty F naphthalene or melamine-based high range water reducer, OZ/100

lbs of cementitious material;

$$lHRWR = \ln (HRWR);$$

PCHRWR = ASTM F polycarboxylate-based high range water reducer, OZ/100 lbs of cementitious material;

$$lPCHRWR = \ln (PCHRWR);$$

ACCL = ASTM Ty C calcium-nitrate based accelerator, OZ/100 lbs of cementitious material;

$$lACCL = \ln (ACCL);$$

$$i5 = C3A \times \text{TotalNa2Oeq} \times \text{perCash};$$

$$i6 = C3A \times \text{CemNa2Oeq} \times \text{perCash};$$

$$i7 = \text{perCash} \times \text{perC3A};$$

$$i8 = \text{perCash} \times \text{perC3A} \times \text{perGypsum};$$

$$i9 = (\text{perC3A} + \text{perC4AF}) \times \text{perGypsum};$$

$$i9R = (\text{perAluminate}) \times (\text{perGypsum} + \text{perHemihydrate} + \text{perAnhydrite} + \text{perK2SO4});$$

$$i10 = \text{perC3A} \times (\text{perCash} + \text{perSlag});$$

$$i11 = (\text{perCash} + \text{perSlag}) \times \text{perC3A} \times \text{perGypsum};$$

$$i13 = C3A * \text{TotalNa2Oeq} \times (\text{perCash} + \text{perSlag});$$

$$i14 = C3A * \text{CemNa2Oeq} \times (\text{perCash} + \text{perSlag});$$

$$i15 = HRWR + PCHRWR;$$

$$i16 = (\text{perCash} + \text{perSlag}) \times \text{TotalFACaO} \times \text{perGypsum};$$

$$i17 = (\text{PerFA} + \text{PerUFFA}) \times \text{TotalFACaO};$$

Based on prior studies on activation energy, several possible variables were considered highly likely to have an effect on E_a . These variables were wc , $WRRET$, $HRWR$ and $PCHRWR$, $perSlag$, $perGypsum$, $perC3A$, $perC4AF$, or $perC3S$, $perCash \times FACaO$, $perFash$, $perSF$, $ACCL$, and $CemBlaine$. In addition, $perAluminate$, $perFerrite$, $perAlite$, $perGypsumR$, $perAnhydrite$, $perHemihydrate$, $perK2SO4$, $perPericlase$, and $perFreeCaO$ were considered. Possible interactions that were considered highly likely to have an effect on E_a were:

1. $WRRET$ and $C3A$
2. $WRRET$ and $perSlag$
3. $WRRET$ and $perCash$
4. $perCash$, $perC3A$, and $gypsum$
5. $perCash$, $perC3A$, and $TotalNa2Oeq$ or $CemNa2Oeq$
6. $ACCL$ and $perC3A$

From these variables, the strongest correlations with E_a were found with $WRRET$ ($R^2=0.36$) and $perSlag$ ($R^2=0.13$). The combination of $WRRET$ and $perSlag$ gave an $R^2=0.51$, as shown in Figure D.1. This trend suggests that only a few variables are needed to model E_a , because a large percentage (51%) of the variability can be explained by two variables. R^2 was not improved by taking the natural log of the variables.

D.4. NUMBER OF VARIABLES

A model for E_a should describe as much of the variability as possible with as few dependent variables as possible because incremental gains in accuracy may be offset by poor predictive ability of the model. A comparison of R^2 versus number of variables will provide an indication of the appropriate number of dependent variables to model. The

relationship between the coefficient of determination (R^2) and the number of independent variables is shown in Figure D.11. The data points in the figure represent the combination of variables with the highest R^2 value, and that had no pairs of variables with correlation coefficients greater than 0.65. Combinations greater than ten variables were not included because the variables showed excessive correlation. A comparison between the R^2 for the data with phases determined from Rietveld analysis and the data with phases from Bogue calculations indicates that the results are relatively similar. Rietveld analysis gives a slightly better R^2 than Bogue calculations, but the difference is not significant enough to preclude the use of Bogue calculations in a model.

The improvement in R^2 decreases as the number of variables increases. The number of variables chosen should reflect the breadth of the testing while remaining as uncomplicated as possible. Also, the number of independent variables is limited by the correlation coefficients. For the set of variables investigated here, the number of combinations with correlation coefficients above 0.65 becomes large. Therefore, eight to nine variables will be the maximum number of variables that should be used.

Based on the results from the RSQUARE procedure, the following variables were chosen for further investigation: *perFA*, *perFACaO*, *PerSF*, *perC3S*, *perC4AF*, *TotalNa2Oeq*, *WRRET*, *ACCL*, *i9*, and *i17*. In addition, the variables *wc*, *CemBlaine*, and *i15* (*HRWR+PCHRWR*) will be investigated since E_a showed some dependence on these variables in previous sections.

D.5. ANALYSIS OF VARIANCE (ANOVA) USING PROC GLM

Once the variables that will make up the model for E_a have been chosen, they must be evaluated to ensure that they provide an explanation for E_a that is statistically

significant. PROC GLM is procedure that relates one or more continuous dependent variables to one or more discrete or continuous independent variables⁶. For this study, all of the independent variables are continuous. Proc GLM stands for “Generalized Linear Models”, and uses the method of least squares fitting to fit a general linear model to the data. The output of the procedure is a linear, multivariate model of the dependent variable (E_a). The GLM procedure assumes that the observed values of each dependent variable may be written as a fixed component ($c_i x_i$) plus a random error component⁶. Also, the procedure assumes that errors from different observations are uncorrelated. In addition, the procedure assumes that the errors have a Gaussian (normal) distribution for the maximum likelihood estimates and confidence limits to be valid. However, the results will still be approximately accurate for distributions of error that are not exactly normal⁶.

D.6. GLM RESULTS

PROC GLM was run on a variety of different independent variable combinations. The final combination chosen for the dataset with Bogue compounds has eight variables: *PerSlag*, *PerSF*, *CemNa2Oeq*, *WRRET*, *ACCL*, *i9*, *CemBlaine*, and *i17*. The ANOVA results are shown in Figure D.14 and Figure D.15. For the combination of eight independent variables, R^2 was 0.683 for a linear model, and 0.688 for a non-linear model. The final combination chosen for the dataset with phases determined from Rietveld analysis has seven variables: *PerSlag*, *PerSF*, *WRRET*, *ACCL*, *i9R*, *CemBlaine*, and *i17*. R^2 was 0.685 for a linear model.

Depending on the variable combination, it was possible to get an R^2 as high as 0.730 for a linear model with as many as ten variables. However, R^2 is not the only

criteria for selecting a model. The complexity of the model should not be excessively complex given the scope of testing. Also, each variable chosen should be statistically significant. ANOVA gives the overall F test of significance for all of the variables investigated. Variables with the probability of a Type I and Type III error higher than 5.0% were rejected as potential variables in the E_a model. Based on these results, the combination with eight independent variables (for Bogue) and seven independent variables (for Rietveld) will be investigated using NLIN in the next section. A linear expression for E_a will be used, since the R^2 for a linear model was higher than the non-linear model.

A plot of the predicted E_a value versus the measured E_a value is shown in Figure D.12. The plot of the residuals for the same analysis is shown in Figure 5-2. The residual plot appears random, which indicates that the linear model of E_a captures the behavior fairly well. The residual plot also shows which tests were outliers. The outliers were generally tests that had fairly high dosages of low-range water-reducer/retarder, and that had large replacement percentages of GGBFS or class C fly ash.

The GLM procedure produces coefficients for each of the dependent variables. These coefficients may be used to reproduce the best-fit of the E_a data, and may also be used as a starting point for evaluating the results in a non-linear model using the NLIN procedure. The next section will discuss the development and validation of the E_a using a non-linear curve fitting procedure.

D.7. PROC NLIN

The NLIN procedure performs univariate non-linear regression analysis using the least squares method. This procedure is useful when the model that describes a process is

nonlinear⁶. The analysis in the previous sections using the GLM procedure suggested that a linear model provides the best fit to the experimental data. The NLIN procedure is appropriate to evaluate the model for E_a because the equations that will be used to evaluate E_a are nonlinear. Also, the procedure gives the flexibility to choose a non-linear model for E_a . If a linear model is chosen for E_a , then the results from the NLIN procedure should be relatively similar to the results from the GLM procedure. The relationship between E_a and most of the independent variables appears to be linear. However, there is some experimental evidence that the relationship between $WRRET$ and E_a is exponential or rational, as discussed in Chapter 5.

D.8. APPLICATION OF ARRHENIUS THEORY TO E_A REGRESSION ANALYSIS

Equation 2-2 and Equation 2-5 have been shown previously^{5,7,8,9,10}, and will be used to evaluate the accuracy of an E_a model.

$$t_e(T_r) = \sum_0^t e^{-\frac{E_a}{R} \left(\frac{1}{T_c} - \frac{1}{T_r} \right)} \cdot \Delta t \quad \text{Equation D-2}$$

where $t_e(T_r)$ = equivalent age at reference temperature (T_r), T_c = temperature of the concrete, and E_a , and R are as defined previously.

$$\alpha(t_e) = \alpha_u \cdot e^{-\left[\frac{\tau}{t_e} \right]^\beta} \quad \text{Equation D-3}$$

where $\alpha(t_e)$ = degree of hydration at equivalent age t_e , t_e = equivalent age determined from Equation 2-2 (hours), τ = hydration time parameter (hours), β = hydration shape parameter, and α_u = ultimate degree of hydration.

To use least squares regression analysis, it is necessary to break the data into discrete points. This requires several steps. First, Equation 2-2 is solved for different

time steps at 5, 15, 23, 38, and 60 °C (41, 59, 73, 100, and 140 °F). This step gives discrete points that quantify the equivalent age at each time and temperature. Then, the degree of hydration is calculated at each time and temperature using Equation 2-5. Equation 2-5 uses curve-fit parameters (α_u , β , and τ) generated experimentally from the isothermal tests used to generate the E_a results. The result of the calculations is a discrete estimate of the degree of hydration at different equivalent ages. The experimental results may then be compared to model from non-linear regression analysis. This procedure is shown graphically in Figure D.16.

One hundred and sixteen (116) E_a values were calculated using isothermal results from five (5) different isothermal temperatures. The degree of hydration was calculated for each test at eighteen (18) different times. This combination of data gives a total of 10,440 data points to validate the E_a model.

D.9. NLIN RESULTS

A linear model for E_a was evaluated using NLIN. A comparison of the predicted degree of hydration versus the measured degree of hydration from the isothermal calorimetry is shown in Chapter 5, and a plot of the residuals is shown in Figure D.17. The residual plot helps to identify the outliers from the analysis. As with the GLM results, the outliers were mixtures with either high dosages of *WRRET* or mixtures with high replacement percentages of Class C fly ash or GGBFS and high dosages of *WRRET*. A graphical comparison of the predicted and measured degree of hydration gives some insight into the magnitude of the errors.

Figure D.19 shows a mixture of 50% Cement C2 and 50% GGBFS with 0.35% addition by weight of an ASTM Type A & D low range water reducer/retarder. Two

other outliers are shown in Chapter 5. The largest difference between the predicted and measured degree of hydration (α) is for the test results at 60 °C (140 °F). Most of the other predicted values for α compare well with the measured values for α .

D.10. E_A MODEL BASED ON BOGUE CALCULATIONS

Based on the non-linear regression analysis presented above, a linear model was developed. The coefficients, standard error, and confidence limits are shown in Table D-1.

Table D-1: Coefficients for E_a Model

Independent Variable, X_i	Variable Name	C_i	Std. Error	95% Confidence Limits	
<i>Coefficient</i>	-	41229.6	306.3	40629.1	41830
<i>perSlag</i>	p_{GGBFS}	162	2.3634	157.4	166.7
<i>PerSF</i>	p_{SF}	-516	19.6834	-554.6	-477.4
<i>CemBlaine</i>	Blaine	-19.8257	0.7079	-21.2133	-18.438
<i>CemNa2Oeq</i>	Na_2O_{eq}	-3468.5	231.4	-3922.1	-3014.9
<i>WRRET</i>	WRRET	-2461.9	15.4328	-2492.2	-2431.7
<i>ACCL</i>	ACCL	-127.9	3.88	-135.5	-120.3
<i>i9</i>	$(p_{C3A} + p_{C4AF}) \times p_{Gypsum}$	83.2789	1.6007	80.1412	86.4167
<i>i17</i>	$p_{FlyA} \times FACaO$	2.9634	0.1196	2.7289	3.1979

The final form of the model is shown in Equation 5-5 as follows:

$$\begin{aligned}
 E_a = & 41,230 + 8,330 \cdot [(C_3A + C_4AF) \cdot p_{Cement} \cdot Gypsum \cdot p_{Cement}] \\
 & - 3,470 \cdot Na_2O_{eq} - 19.8 \cdot Blaine \\
 & + 2.96 \cdot p_{FlyAsh} \cdot p_{CaO-FlyAsh} + 162 \cdot p_{GGBFS} - 516 \cdot p_{SF} \\
 & - 30,900 \cdot WRRET - 1,450 \cdot ACCL
 \end{aligned}
 \tag{Equation D-4}$$

where p_{FlyAsh} = % fly ash in mixture; $p_{CaO-FlyAsh}$ = % CaO in fly ash; p_{GGBFS} = % GGBFS in mixture; p_{SF} = % silica fume in mixture; *Blaine* = Blaine fineness of cement; Na_2O_{eq} = % Na_2O_{eq} in cement ($0.658 \times \%K_2O + \%Na_2O$); C_3A = % C_3A in cement; C_4AF = % C_4AF in cement; *Gypsum* = % gypsum in cement; *WRRET* = ASTM Type A&D water reducer/retarder, % solids per gram of cementitious material; *ACCL* = ASTM Type C calcium-nitrate based accelerator, % solids per gram of cementitious material.

D.11. E_A MODEL BASED ON RIETVELD ANALYSIS OF CEMENT PHASES

Based on the non-linear regression analysis presented above, a linear model was developed. The coefficients, standard error, and confidence limits are shown in Table D-2.

Table D-2: Coefficients for E_a Model Using Rietveld Analysis

Independent Variable, X_i	Variable Name	C_i	Std. Error	95% Confidence Limits	
<i>Coefficient</i>	-	39138.3	250.8	38646.6	39629.9
<i>perSlag</i>	pGGBFS	120.4	1.7961	116.9	123.9
<i>PerSF</i>	pSF	-532.8	18.8414	-569.7	-495.8
<i>CemBlaine</i>	Blaine	-12.2365	0.6489	-13.5085	-10.964
<i>WRRET</i>	WRRET	-2405	14.8502	-2434.1	-2375.9
<i>ACCL</i>	ACCL	-127.4	3.8134	-134.9	-120
<i>i9</i>	(pAluminate)×(pC ₃ S _H +K ₂ SO ₄)	106.9	1.9334	103.1	110.7
<i>i17</i>	pFlyA×FACaO	1.2429	0.097	1.0528	1.4331

The final form of the second model, based on phase analysis of the cement using Rietveld analysis, is shown in Equation 5-6 as follows:

$$\begin{aligned}
 E_a = & 39,200 + 107 \cdot [(C_3A) \cdot p_{Cement} \cdot (CaSO_4 \cdot xH_2O + K_2SO_4) \cdot p_{Cement}] \\
 & - 12.2 \cdot Blaine + 1.24 \cdot p_{FlyAsh} \cdot p_{CaO-FlyAsh} + 120 \cdot p_{GGBFS} - 533 \cdot p_{SF} \\
 & - 30,100 \cdot WRRET - 1,440 \cdot ACCL
 \end{aligned}
 \quad \text{Equation D-5}$$

Where $CaSO_4 \cdot xH_2O$ = Sum of % by mass of gypsum, hemihydrate, and anhydrite, K_2SO_4 = % by mass of arcanite, and C_3A = % C_3A in cement, and all other variables the same as for Equation 5-5. Each of the variables should be randomly distributed about the mean of the model. To check this requirement, a plot of the residuals is prepared as shown in Figure D.27 through Figure D.34. All of the variables chosen for the E_a model appear to have a random distribution of error.

D.12. SENSITIVITY ANALYSIS

The sensitivity analysis for the model based on Bogue calculations is shown in Chapter 5. This section shows the sensitivity analysis of the proposed E_a model based on Rietveld analysis. The effect of each of the independent variables on E_a is shown in Figure D.20 through Figure D.26. These figures show the sensitivity of both models to

changes in each independent variable. The important trends are discussed further in Chapter 5.

D.13. RESIDUALS

Figure D.27 through Figure D.34 show plots of the residuals of the different independent variables included in the E_a model. The residual are random, which indicates that each of the variables is randomly distributed about the mean of the model. Figure D.35 shows a plot of the cumulative error distribution as a function of degree of hydration. This shows that the errors reported in the model are relatively small.

D.14. REFERENCES

1. Schindler, A. K., "Concrete Hydration, Temperature Development, and Setting at Early-Ages," Ph.D. Dissertation, University of Texas at Austin, Austin, TX, 531 pp.
2. Dawson, Beth, and Robert G. Trapp, Basic and Clinical Biostatistics, 4th ed. Lange Medical Books/McGraw Hill, New York, 438 p, 2004.
3. Devore, Jay L., Probability and Statistics for Engineering and the Sciences, 4th ed. Duxbury Press, New York, 743 p, 1995.
4. Hsu, J.C. Multiple Comparisons, Theory and Methods, 1st ed. Chapman & Hall/CRC, Boca Raton, FL, 1996
5. Schindler, A.K., and K.J. Folliard, "Heat of Hydration Models for Cementitious Materials", *ACI Materials Journal*, V. 102, No. 1, Jan.-Feb., 2005, pp. 24-33.
6. SAS/STAT User Guide, SAS 9.1.3 Online Manual, Ed. V. Clark, The SAS Institute, Cary, N.C. 2006

7. Pane, I., and W. Hansen, "Concrete Hydration and Mechanical Properties under Nonisothermal Conditions," *ACI Materials Journal*, V. 99, No. 6, Nov.-Dec, 2002, pp. 534-542.
8. Poole, J. L. "The Effects of Cement Chemistry and Water-Cement Ratio on Activation Energy," PhD Dissertation, Chapter 2, The University of Texas at Austin, Austin, TX, 2007, pp 6-38.
9. Poole, J. L. "The Effects of Chemical Admixtures on Activation Energy of Cementitious Materials," PhD Dissertation, Chapter 3, The University of Texas at Austin, Austin, TX, 2007, pp 39-69.
10. Poole, J. L. "The Effects of Supplementary Cementing Materials on Activation Energy of SCMs," PhD Dissertation, Chapter 4, The University of Texas at Austin, Austin, TX, 2007, pp 70-110.

Bogue		Rietveld	
R ²	Variables	R ²	Variables
	1		1
0.364	WRRET	0.363	WRRET
0.135	PerSlag	0.139	PerSlag
0.087	TotalNa2Oeq	0.058	perAnhydrite
0.041	perC3S	0.037	perAlite
0.029	PerSF	0.029	PerSF
0.023	PerFash	0.021	PerFash
0.022	perC3A	0.018	i17
0.021	FreeCaO	0.018	CemK2O
0.019	i17	0.015	CemNa2O
0.016	i20	0.013	ACCL
0.013	ACCL	0.012	wc
0.012	i16	0.011	PerCash
0.012	wc	0.010	perAluminate
0.011	perGypsum	0.008	perFerrite
0.011	PerCash	0.008	FreeCaO

Bogue			Rietveld		
R ²	Variables		R ²	Variables	
	1	2		1	2
0.506	PerSlag	WRRET	0.509	PerSlag	WRRET
0.493	TotalNa2Oeq	WRRET	0.414	PerSF	WRRET
0.415	PerSF	WRRET	0.398	PerFash	WRRET
0.401	PerFash	WRRET	0.397	WRRET	i17
0.400	WRRET	i17	0.396	WRRET	ACCL
0.397	WRRET	ACCL	0.394	perAnhydrite	WRRET
0.394	WRRET	i16	0.393	perFerrite	WRRET
0.391	PerCash	WRRET	0.390	PerCash	WRRET
0.390	FreeCaO	WRRET	0.384	WRRET	i9
0.388	perC3S	WRRET	0.383	CemK2O	WRRET
0.387	WRRET	i21	0.374	perAlite	WRRET
0.378	perC4AF	WRRET	0.373	perBelite	WRRET
0.374	CemNa2Oeq	WRRET	0.372	perGypsumR	WRRET
0.374	WRRET	i20	0.368	FreeCaO	WRRET
0.371	perC2S	WRRET	0.367	erHemihydrat	WRRET

Figure D.1: Results from PROC RSQUARE

Bogue Calculations								
R ²	Variables			R ²	Variables			
	1	2	3		1	2	3	4
0.568	PerSlag	WRRET	i9	0.596	PerSF	PerSlag	WRRET	i9
0.562	PerSlag	TotalNa2Oeq	WRRET	0.595	PerSlag	WRRET	ACCL	i9
0.560	perC2S	PerSlag	WRRET	0.590	PerSlag	TotalNa2Oeq	WRRET	ACCL
0.557	perC3S	TotalNa2Oeq	WRRET	0.589	FreeCaO	PerSlag	WRRET	i9
0.556	perC4AF	TotalNa2Oeq	WRRET	0.589	PerSlag	WRRET	i9	i22
0.554	perGypsum	PerSlag	WRRET	0.589	PerSlag	CemNa2Oeq	WRRET	i9
0.549	FreeCaO	PerSlag	WRRET	0.589	perC2S	PerSlag	WRRET	ACCL
0.545	PerSlag	WRRET	ACCL	0.587	PerSF	PerSlag	WRRET	ACCL
0.541	PerSF	PerSlag	WRRET	0.586	PerSF	perC2S	PerSlag	WRRET
0.531	PerSlag	CemNa2Oeq	WRRET	0.585	PerSF	PerSlag	TotalNa2Oeq	WRRET
0.527	perC3A	PerSlag	WRRET	0.585	perC2S	PerSlag	WRRET	i9
0.522	perC3S	PerSlag	WRRET	0.584	perGypsum	PerSlag	WRRET	i9
0.521	PerFash	PerSlag	WRRET	0.583	perC3S	TotalNa2Oeq	WRRET	ACCL
0.520	PerSF	TotalNa2Oeq	WRRET	0.583	perGypsum	PerSlag	WRRET	ACCL
0.517	PerSlag	WRRET	i16	0.582	PerSF	perGypsum	PerSlag	WRRET

Rietveld Analysis								
R ²	Variables			R ²	Variables			
	1	2	3		1	2	3	4
0.605	PerSlag	WRRET	i9	0.632	PerSlag	WRRET	ACCL	i9
0.569	perK2SO4	PerSlag	WRRET	0.629	PerSF	PerSlag	WRRET	i9
0.554	perAluminate	PerSlag	WRRET	0.622	PerSlag	CemK2O	WRRET	i9
0.548	PerSlag	WRRET	ACCL	0.620	perK2SO4	PerSlag	CemK2O	WRRET
0.548	perAlite	PerSlag	WRRET	0.617	PerSlag	CemNa2O	WRRET	i9
0.544	PerSF	PerSlag	WRRET	0.616	CemBlaine	PerSlag	WRRET	i9
0.537	PerSlag	CemK2O	WRRET	0.614	perAluminate	PerSlag	CemK2O	WRRET
0.533	perGypsumR	PerSlag	WRRET	0.614	perBelite	PerSlag	WRRET	i9
0.522	perBelite	PerSlag	WRRET	0.612	perAluminate	PerSlag	WRRET	i9
0.522	PerFash	PerSlag	WRRET	0.611	wc	PerSlag	WRRET	i9
0.518	PerCash	PerSlag	WRRET	0.609	perFerrite	PerSlag	WRRET	i9
0.518	PerSlag	WRRET	i17	0.608	PerSlag	WRRET	HRWR	i9
0.514	erHemihydrat	PerSlag	WRRET	0.607	PerSlag	WRRET	i9	i17
0.514	perAnhydrite	PerSlag	WRRET	0.606	FreeCaO	PerSlag	WRRET	i9
0.513	PerSlag	CemNa2O	WRRET	0.606	erHemihydrat	PerSlag	WRRET	i9

Figure D.2: Results from PROC RSQUARE

Bogue Calculations					
R^2	Variables				
	1	2	3	4	5
0.628	PerSF	PerSlag	WRRET	ACCL	i9
0.627	CemBlaine	PerSlag	WRRET	i9	i22
0.620	PerSF	perC2S	PerSlag	WRRET	ACCL
0.619	PerSF	PerSlag	TotalNa2Oeq	WRRET	ACCL
0.618	PerSF	perGypsum	PerSlag	WRRET	ACCL
0.614	PerSlag	WRRET	ACCL	i9	i22
0.613	PerFash	perC3S	TotalNa2Oeq	WRRET	ACCL
0.613	PerSlag	CemNa2Oeq	WRRET	ACCL	i9
0.613	FreeCaO	PerSlag	WRRET	ACCL	i9
0.612	PerFash	PerSF	PerSlag	WRRET	ACCL

Rietveld Analysis					
R^2	Variables				
	1	2	3	4	5
0.661	PerSF	PerSlag	WRRET	ACCL	i9
0.647	PerSlag	CemK2O	WRRET	ACCL	i9
0.645	perK2SO4	PerSlag	CemK2O	WRRET	ACCL
0.644	CemBlaine	PerSlag	WRRET	ACCL	i9
0.643	PerSF	PerSlag	CemK2O	WRRET	i9
0.643	PerSlag	CemNa2O	WRRET	ACCL	i9
0.642	perAluminate	PerSlag	CemK2O	WRRET	ACCL
0.642	PerSF	CemBlaine	PerSlag	WRRET	i9
0.641	perFerrite	perK2SO4	PerSlag	CemK2O	WRRET
0.641	PerSF	perK2SO4	PerSlag	CemK2O	WRRET

Figure D.3: Results from PROC RSQUARE– Variables in Gray Indicate Unacceptable Covariance of One or More of the Variables

Bogue Calculations						
R ²	Variables					
	1	2	3	4	5	6
0.652	CemBlaine	PerSlag	WRRET	ACCL	i9	i22
0.646	PerFash	PerSF	perC3S	TotalNa2Oeq	WRRET	ACCL
0.642	PerSF	CemBlaine	PerSlag	WRRET	ACCL	i9
0.641	PerSF	perGypsum	PerSlag	WRRET	ACCL	i9
0.641	PerSF	CemBlaine	PerSlag	WRRET	i9	i22
0.640	PerSF	FreeCaO	PerSlag	WRRET	ACCL	i9
0.640	PerFash	PerSF	perC3S	WRRET	ACCL	i16
0.639	PerSF	PerSlag	WRRET	ACCL	i9	i15
0.638	PerSF	PerSlag	WRRET	ACCL	i9	i17
0.638	PerSF	perC2S	PerSlag	WRRET	ACCL	i9

Rietveld Analysis						
R ²	Variables					
	1	2	3	4	5	6
0.676	PerSF	CemBlaine	PerSlag	WRRET	ACCL	i9
0.672	PerSF	PerSlag	CemK2O	WRRET	ACCL	i9
0.670	PerSF	perK2SO4	PerSlag	CemK2O	WRRET	ACCL
0.670	PerSF	perAluminate	PerSlag	CemK2O	WRRET	ACCL
0.670	PerSF	PerSlag	CemNa2O	WRRET	ACCL	i9
0.668	PerSF	PerSlag	WRRET	ACCL	i9	i17
0.668	PerSF	PerSlag	WRRET	HRWR	ACCL	i9
0.668	perFerrite	perK2SO4	PerSlag	CemK2O	WRRET	ACCL
0.667	wc	PerSF	PerSlag	WRRET	ACCL	i9
0.666	PerSF	perBelite	PerSlag	WRRET	ACCL	i9

Figure D.4: Results from PROC RSQUARE– Variables in Gray Indicate Unacceptable Covariance of One or More of the Variables

Bogue Calculations							
R ²	Variables						
	1	2	3	4	5	6	7
0.670	PerSF	CemBlaine	PerSlag	WRRET	ACCL	i9	i22
0.666	CemBlaine	PerSlag	WRRET	ACCL	i9	i17	i22
0.664	PerSF	perGypsum	PerSlag	WRRET	ACCL	i9	i17
0.663	CemBlaine	PerSlag	TotalNa2Oeq	WRRET	ACCL	i9	i17
0.663	PerFash	CemBlaine	PerSlag	TotalNa2Oeq	WRRET	i9	i21
0.662	PerSF	PerSlag	WRRET	ACCL	i9	i16	i21
0.662	PerSF	CemBlaine	PerSlag	WRRET	ACCL	i9	i17
0.661	CemBlaine	PerSlag	CemNa2Oeq	WRRET	ACCL	i9	i17
0.660	PerSF	FreeCaO	CemBlaine	PerSlag	WRRET	ACCL	i9
0.660	PerSF	PerSlag	TotalNa2Oeq	WRRET	ACCL	i9	i17

Rietveld Analysis							
R ²	Variables						
	1	2	3	4	5	6	7
0.693	PerSF	perFerrite	perK2SO4	PerSlag	CemK2O	WRRET	ACCL
0.692	PerSF	perBelite	PerSlag	WRRET	ACCL	i9	i17
0.688	PerSF	perGypsumR	PerSlag	CemNa2O	WRRET	ACCL	i9
0.686	PerSF	CemBlaine	PerSlag	CemK2O	WRRET	ACCL	i9
0.685	PerSF	Periclase	PerSlag	CemNa2O	WRRET	ACCL	i9
0.685*	PerSF	CemBlaine	PerSlag	WRRET	ACCL	i9	i17
0.685	PerSF	perAluminate	perK2SO4	PerSlag	CemK2O	WRRET	ACCL
0.684	PerSF	erHemihydrat	perK2SO4	PerSlag	CemK2O	WRRET	ACCL
0.683	PerSF	FreeCaO	PerSlag	CemNa2O	WRRET	ACCL	i9
0.683	PerSF	perBelite	perFerrite	PerSlag	CemK2O	WRRET	ACCL

*Final Model

Figure D.5: Results from PROC RSQUARE– Variables in Gray Indicate Unacceptable Covariance of One or More of the Variables

Bogue Calculations								
R ²	Variables							
	1	2	3	4	5	6	7	8
0.690	PerFash	CemBlaine	PerSlag	TotalNa2Oeq	WRRET	ACCL	i9	i21
0.690	PerSF	CemBlaine	PerSlag	TotalNa2Oeq	WRRET	ACCL	i9	i17
0.689	PerFash	PerCash	CemBlaine	PerSlag	TotalNa2Oeq	WRRET	ACCL	i9
0.686	PerSF	CemBlaine	PerSlag	WRRET	ACCL	i9	i17	i22
0.683*	PerSF	CemBlaine	PerSlag	CemNa2Oeq	WRRET	ACCL	i9	i17
0.682	PerSF	FreeCaO	CemBlaine	PerSlag	WRRET	ACCL	i9	i17
0.682	PerSF	perC3A	perC4AF	perGypsum	TotalNa2Oeq	WRRET	ACCL	i9
0.681	PerSF	perGypsum	CemBlaine	PerSlag	TotalNa2Oeq	WRRET	ACCL	i17
0.681	PerSF	CemBlaine	PerSlag	WRRET	ACCL	i9	i21	i22
0.680	PerFash	perGypsum	CemBlaine	PerSlag	TotalNa2Oeq	WRRET	i9	i21

*Final Model

Rietveld Analysis								
R ²	Variables							
	1	2	3	4	5	6	7	8
0.711	PerSF	perBelite	CemBlaine	PerSlag	WRRET	ACCL	i9	i17
0.709	PerSF	perGypsumR	PerSlag	CemNa2O	WRRET	ACCL	i9	i17
0.703	PerFash	perBelite	CemBlaine	PerSlag	WRRET	ACCL	i9	i17
0.703	PerSF	perAluminate	perK2SO4	PerSlag	CemK2O	WRRET	ACCL	i17
0.702	PerSF	perHemihydrat	CemBlaine	PerSlag	WRRET	ACCL	i9	i17
0.700	wc	PerSF	perBelite	PerSlag	WRRET	ACCL	i9	i17
0.700	PerSF	perBelite	PerSlag	WRRET	HRWR	ACCL	i9	i17
0.700	wc	PerSF	perFerrite	perK2SO4	PerSlag	CemK2O	WRRET	ACCL
0.700	PerFash	PerSF	perBelite	PerSlag	WRRET	ACCL	i9	i17
0.700	PerSF	Periclase	PerSlag	CemNa2O	WRRET	ACCL	i9	i17

Figure D.6: Results from PROC RSQUARE– Variables in Gray Indicate Unacceptable Covariance of One or More of the Variables

Variable	wc	PerFash	PerCash	PerSF	perC3S	perC2S	perC3A	perC4AF	perGypsum	FreeCaO	CemBlaine	PerSlag	CemNa2Oeq
wc	1.00	-0.03	-0.01	0.02	0.04	-0.03	-0.05	0.01	-0.20	0.32	-0.57	0.01	0.25
PerFash	-0.03	1.00	-0.25	-0.09	-0.25	-0.17	-0.19	-0.13	-0.26	0.06	-0.10	-0.20	0.00
PerCash	-0.01	-0.25	1.00	0.10	-0.29	-0.24	-0.15	-0.23	-0.25	0.15	-0.05	-0.19	0.15
PerSF	0.02	-0.09	0.10	1.00	0.05	-0.09	0.00	0.00	-0.03	0.13	-0.07	-0.10	0.22
perC3S	0.04	-0.25	-0.29	0.05	1.00	0.35	0.46	0.63	0.70	-0.14	0.18	-0.66	-0.24
perC2S	-0.03	-0.17	-0.24	-0.09	0.35	1.00	0.21	0.55	0.52	-0.60	0.08	-0.35	-0.40
perC3A	-0.05	-0.19	-0.15	0.00	0.46	0.21	1.00	-0.27	0.81	0.06	0.26	-0.37	0.23
perC4AF	0.01	-0.13	-0.23	0.00	0.63	0.55	-0.27	1.00	0.23	-0.35	0.08	-0.43	-0.48
perGypsum	-0.20	-0.26	-0.25	-0.03	0.70	0.52	0.81	0.23	1.00	-0.29	0.52	-0.54	-0.09
FreeCaO	0.32	0.06	0.15	0.13	-0.14	-0.60	0.06	-0.35	-0.29	1.00	-0.31	0.12	0.59
CemBlaine	-0.57	-0.10	-0.05	-0.07	0.18	0.08	0.26	0.08	0.52	-0.31	1.00	-0.13	-0.22
PerSlag	0.01	-0.20	-0.19	-0.10	-0.66	-0.35	-0.37	-0.43	-0.54	0.12	-0.13	1.00	0.15
CemNa2Oeq	0.25	0.00	0.15	0.22	-0.24	-0.40	0.23	-0.48	-0.09	0.59	-0.22	0.15	1.00
TotalNa2Oeq	0.09	0.27	0.69	0.19	-0.26	-0.32	0.02	-0.32	-0.20	0.36	-0.18	-0.37	0.49
WRRET	-0.14	-0.07	-0.10	-0.09	0.08	0.06	0.23	-0.10	0.13	-0.03	-0.05	0.01	-0.07
HRWR	-0.29	-0.15	-0.14	-0.08	0.32	0.06	0.13	0.21	0.31	-0.15	0.34	-0.11	-0.15
PCHRWR	-0.27	-0.09	-0.06	-0.07	0.23	0.01	0.04	0.19	0.18	-0.14	0.31	-0.10	-0.14
ACCL	0.02	-0.05	0.22	-0.07	-0.11	-0.15	-0.08	-0.09	-0.14	0.12	-0.08	0.04	0.08
i9	-0.15	-0.31	-0.32	-0.04	0.76	0.57	0.78	0.32	0.98	-0.29	0.47	-0.52	-0.14
i15	-0.34	-0.15	-0.13	-0.09	0.34	0.05	0.11	0.24	0.31	-0.17	0.39	-0.13	-0.17
i16	-0.02	-0.25	0.97	0.10	-0.30	-0.21	-0.09	-0.25	-0.20	0.15	-0.03	-0.19	0.21
i17	-0.04	0.07	0.90	0.08	-0.37	-0.28	-0.21	-0.25	-0.33	0.15	-0.08	-0.24	0.10
i20	-0.07	0.73	-0.18	-0.10	-0.18	-0.11	-0.15	-0.07	-0.21	0.01	-0.05	-0.14	-0.14
i21	-0.01	-0.25	0.99	0.13	-0.30	-0.23	-0.14	-0.23	-0.25	0.15	-0.06	-0.19	0.16
IEaMeas	0.12	-0.14	-0.09	-0.15	-0.17	0.06	-0.13	-0.04	-0.08	-0.15	0.02	0.32	-0.05
EaMeas	0.11	-0.15	-0.10	-0.17	-0.20	0.05	-0.15	-0.06	-0.11	-0.15	0.01	0.37	-0.06

Figure D.7: Correlation Matrix from PROC RSQUARE – Bogue Compounds– Variables in Gray Have a Covariance >0.65

Variable	TotalNa2Oeq	WRRET	HRWR	PCHRWR	ACCL	i9	i15	i16	i17	i20	i21	IEaMeas	EaMeas
wc	0.09	-0.14	-0.29	-0.27	0.02	-0.15	-0.34	-0.02	-0.04	-0.07	-0.01	0.12	0.11
PerFash	0.27	-0.07	-0.15	-0.09	-0.05	-0.31	-0.15	-0.25	0.07	0.73	-0.25	-0.14	-0.15
PerCash	0.69	-0.10	-0.14	-0.06	0.22	-0.32	-0.13	0.97	0.90	-0.18	0.99	-0.09	-0.10
PerSF	0.19	-0.09	-0.08	-0.07	-0.07	-0.04	-0.09	0.10	0.08	-0.10	0.13	-0.15	-0.17
perC3S	-0.26	0.08	0.32	0.23	-0.11	0.76	0.34	-0.30	-0.37	-0.18	-0.30	-0.17	-0.20
perC2S	-0.32	0.06	0.06	0.01	-0.15	0.57	0.05	-0.21	-0.28	-0.11	-0.23	0.06	0.05
perC3A	0.02	0.23	0.13	0.04	-0.08	0.78	0.11	-0.09	-0.21	-0.15	-0.14	-0.13	-0.15
perC4AF	-0.32	-0.10	0.21	0.19	-0.09	0.32	0.24	-0.25	-0.25	-0.07	-0.23	-0.04	-0.06
perGypsum	-0.20	0.13	0.31	0.18	-0.14	0.98	0.31	-0.20	-0.33	-0.21	-0.25	-0.08	-0.11
FreeCaO	0.36	-0.03	-0.15	-0.14	0.12	-0.29	-0.17	0.15	0.15	0.01	0.15	-0.15	-0.15
CemBlaine	-0.18	-0.05	0.34	0.31	-0.08	0.47	0.39	-0.03	-0.08	-0.05	-0.06	0.02	0.01
PerSlag	-0.37	0.01	-0.11	-0.10	0.04	-0.52	-0.13	-0.19	-0.24	-0.14	-0.19	0.32	0.37
CemNa2Oeq	0.49	-0.07	-0.15	-0.14	0.08	-0.14	-0.17	0.21	0.10	-0.14	0.16	-0.05	-0.06
TotalNa2Oeq	1.00	-0.10	-0.20	-0.13	0.12	-0.28	-0.20	0.70	0.72	0.08	0.69	-0.28	-0.30
WRRET	-0.10	1.00	-0.03	-0.11	-0.11	0.14	-0.07	-0.10	-0.09	0.05	-0.11	-0.64	-0.60
HRWR	-0.20	-0.03	1.00	0.37	-0.08	0.32	0.89	-0.14	-0.18	-0.11	-0.14	0.00	-0.02
PCHRWR	-0.13	-0.11	0.37	1.00	-0.08	0.18	0.76	-0.05	-0.08	-0.04	-0.06	0.04	0.03
ACCL	0.12	-0.11	-0.08	-0.08	1.00	-0.16	-0.09	0.17	0.18	0.00	0.18	-0.11	-0.11
i9	-0.28	0.14	0.32	0.18	-0.16	1.00	0.32	-0.28	-0.41	-0.23	-0.31	-0.06	-0.07
i15	-0.20	-0.07	0.89	0.76	-0.09	0.32	1.00	-0.12	-0.17	-0.10	-0.13	0.02	0.00
i16	0.70	-0.10	-0.14	-0.05	0.17	-0.28	-0.12	1.00	0.89	-0.18	0.98	-0.10	-0.11
i17	0.72	-0.09	-0.18	-0.08	0.18	-0.41	-0.17	0.89	1.00	0.25	0.91	-0.13	-0.14
i20	0.08	0.05	-0.11	-0.04	0.00	-0.23	-0.10	-0.18	0.25	1.00	-0.18	-0.14	-0.13
i21	0.69	-0.11	-0.14	-0.06	0.18	-0.31	-0.13	0.98	0.91	-0.18	1.00	-0.07	-0.08
IEaMeas	-0.28	-0.64	0.00	0.04	-0.11	-0.06	0.02	-0.10	-0.13	-0.14	-0.07	1.00	0.99
EaMeas	-0.30	-0.60	-0.02	0.03	-0.11	-0.07	0.00	-0.11	-0.14	-0.13	-0.08	0.99	1.00

Figure D.8: Correlation Matrix from PROC RSQUARE – Bogue Compounds– Variables in Gray Have a Covariance >0.65

Variable	wc	PerFash	PerCash	PerSF	perAlite	perBelite	perAluminate	perFerrite	Periclase	perGypsumF	Hemihydrate	perAnhydrite
wc	1.00	-0.03	-0.01	0.02	0.01	0.05	-0.06	0.03	-0.04	-0.11	-0.28	0.13
PerFash	-0.03	1.00	-0.25	-0.09	-0.27	-0.23	-0.22	-0.06	0.17	-0.05	-0.14	-0.22
PerCash	-0.01	-0.25	1.00	0.10	-0.31	-0.25	-0.18	-0.18	-0.04	-0.10	-0.20	-0.27
PerSF	0.02	-0.09	0.10	1.00	0.02	0.01	-0.01	0.01	-0.08	-0.10	-0.03	0.06
perAlite	0.01	-0.27	-0.31	0.02	1.00	0.62	0.73	0.29	0.01	0.28	0.40	0.87
perBelite	0.05	-0.23	-0.25	0.01	0.62	1.00	0.04	0.84	-0.09	0.00	0.77	0.67
perAluminate	-0.06	-0.22	-0.18	-0.01	0.73	0.04	1.00	-0.41	-0.10	0.30	-0.09	0.49
perFerrite	0.03	-0.06	-0.18	0.01	0.29	0.84	-0.41	1.00	0.18	-0.01	0.73	0.43
Periclase	-0.04	0.17	-0.04	-0.08	0.01	-0.09	-0.10	0.18	1.00	0.73	-0.16	-0.13
perGypsumR	-0.11	-0.05	-0.10	-0.10	0.28	0.00	0.30	-0.01	0.73	1.00	-0.14	-0.12
perHemihydrate	-0.28	-0.14	-0.20	-0.03	0.40	0.77	-0.09	0.73	-0.16	-0.14	1.00	0.47
perAnhydrite	0.13	-0.22	-0.27	0.06	0.87	0.67	0.49	0.43	-0.13	-0.12	0.47	1.00
perK2SO4	-0.07	-0.28	-0.17	-0.03	0.71	0.44	0.71	0.02	0.03	0.39	0.23	0.45
FreeCaO	-0.05	0.22	0.01	-0.06	-0.06	-0.19	-0.12	0.08	0.84	0.67	-0.19	-0.30
CemBlaine	-0.57	-0.10	-0.05	-0.07	0.23	0.09	0.24	0.04	0.00	0.19	0.46	0.07
PerSlag	0.01	-0.20	-0.19	-0.10	-0.66	-0.52	-0.36	-0.37	-0.11	-0.16	-0.36	-0.61
CemNa2O	0.23	0.07	-0.06	-0.04	-0.10	0.25	-0.43	0.47	0.56	0.49	0.03	-0.15
CemK2O	0.15	0.00	0.19	0.10	-0.06	-0.45	0.24	-0.54	-0.17	-0.17	-0.58	-0.06
WRRET	-0.14	-0.07	-0.10	-0.09	0.14	-0.04	0.25	-0.13	0.04	0.04	-0.05	0.11
HRWR	-0.29	-0.15	-0.14	-0.08	0.29	0.23	0.14	0.18	-0.08	0.02	0.36	0.26
PCHRWR	-0.27	-0.09	-0.06	-0.07	0.17	0.21	0.03	0.19	-0.08	-0.06	0.32	0.17
ACCL	0.02	-0.05	0.22	-0.07	-0.13	-0.10	-0.09	-0.07	-0.08	-0.11	-0.09	-0.09
i9	-0.20	-0.26	-0.26	-0.08	0.76	0.22	0.87	-0.16	0.09	0.55	0.21	0.43
i17	-0.04	0.07	0.90	0.08	-0.38	-0.33	-0.24	-0.18	0.08	-0.11	-0.23	-0.33

Figure D.9: Correlation Matrix from PROC RSQUARE – Rietveld Analysis - Variables in Gray Have a Covariance >0.65

Variable	perK2SO4	FreeCaO	CemBlaine	PerSlag	CemNa2O	CemK2O	WRRET	HRWR	PCHRWR	ACCL	i9	i17
wc	-0.07	-0.05	-0.57	0.01	0.23	0.15	-0.14	-0.29	-0.27	0.02	-0.20	-0.04
PerFash	-0.28	0.22	-0.10	-0.20	0.07	0.00	-0.07	-0.15	-0.09	-0.05	-0.26	0.07
PerCash	-0.17	0.01	-0.05	-0.19	-0.06	0.19	-0.10	-0.14	-0.06	0.22	-0.26	0.90
PerSF	-0.03	-0.06	-0.07	-0.10	-0.04	0.10	-0.09	-0.08	-0.07	-0.07	-0.08	0.08
perAlite	0.71	-0.06	0.23	-0.66	-0.10	-0.06	0.14	0.29	0.17	-0.13	0.76	-0.38
perBelite	0.44	-0.19	0.09	-0.52	0.25	-0.45	-0.04	0.23	0.21	-0.10	0.22	-0.33
perAluminate	0.71	-0.12	0.24	-0.36	-0.43	0.24	0.25	0.14	0.03	-0.09	0.87	-0.24
perFerrite	0.02	0.08	0.04	-0.37	0.47	-0.54	-0.13	0.18	0.19	-0.07	-0.16	-0.18
Periclase	0.03	0.84	0.00	-0.11	0.56	-0.17	0.04	-0.08	-0.08	-0.08	0.09	0.08
perGypsumR	0.39	0.67	0.19	-0.16	0.49	-0.17	0.04	0.02	-0.06	-0.11	0.55	-0.11
perHemihydrate	0.23	-0.19	0.46	-0.36	0.03	-0.58	-0.05	0.36	0.32	-0.09	0.21	-0.23
perAnhydrite	0.45	-0.30	0.07	-0.61	-0.15	-0.06	0.11	0.26	0.17	-0.09	0.43	-0.33
perK2SO4	1.00	0.04	0.25	-0.44	-0.22	0.15	0.14	0.16	0.13	-0.11	0.75	-0.30
FreeCaO	0.04	1.00	-0.03	-0.08	0.43	-0.02	0.03	-0.06	-0.06	-0.06	0.04	0.14
CemBlaine	0.25	-0.03	1.00	-0.13	-0.40	-0.03	-0.05	0.34	0.31	-0.08	0.40	-0.08
PerSlag	-0.44	-0.08	-0.13	1.00	-0.02	0.07	0.01	-0.11	-0.10	0.04	-0.36	-0.24
CemNa2O	-0.22	0.43	-0.40	-0.02	1.00	-0.59	-0.10	-0.14	-0.16	-0.02	-0.14	-0.02
CemK2O	0.15	-0.02	-0.03	0.07	-0.59	1.00	-0.02	-0.07	-0.05	0.08	-0.14	0.13
WRRET	0.14	0.03	-0.05	0.01	-0.10	-0.02	1.00	-0.03	-0.11	-0.11	0.21	-0.09
HRWR	0.16	-0.06	0.34	-0.11	-0.14	-0.07	-0.03	1.00	0.37	-0.08	0.23	-0.18
PCHRWR	0.13	-0.06	0.31	-0.10	-0.16	-0.05	-0.11	0.37	1.00	-0.08	0.09	-0.08
ACCL	-0.11	-0.06	-0.08	0.04	-0.02	0.08	-0.11	-0.08	-0.08	1.00	-0.14	0.18
i9	0.75	0.04	0.40	-0.36	-0.14	-0.14	0.21	0.23	0.09	-0.14	1.00	-0.33
i17	-0.30	0.14	-0.08	-0.24	-0.02	0.13	-0.09	-0.18	-0.08	0.18	-0.33	1.00

Figure D.10: Correlation Matrix from PROC RSQUARE – Rietveld Analysis - Variables in Gray Have a Covariance >0.65

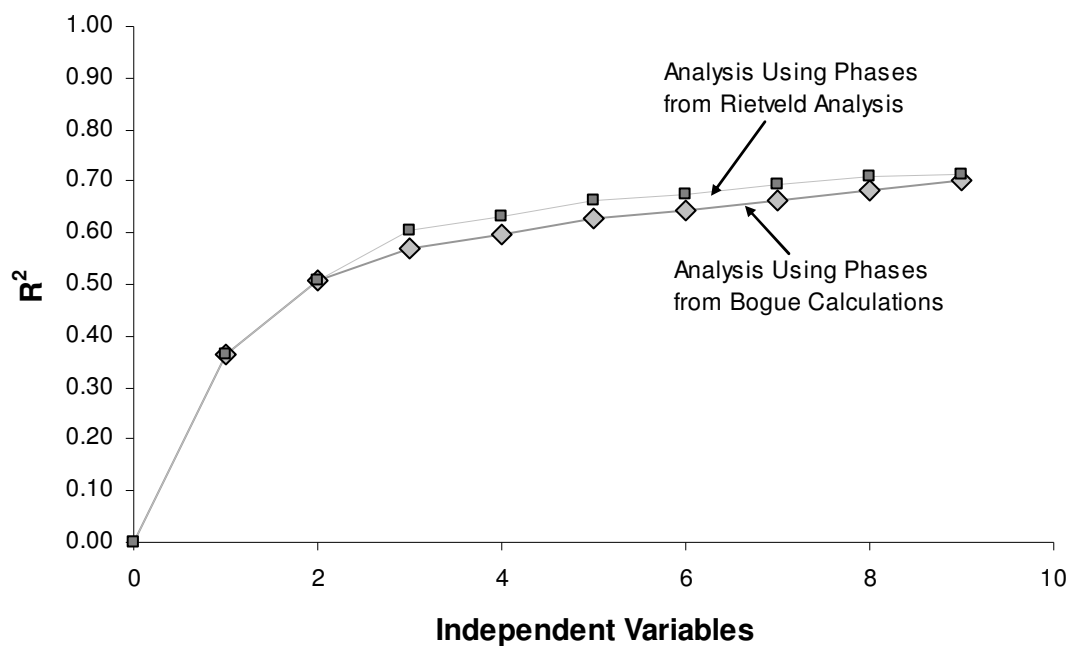


Figure D.11: Coefficient of Determination v. Number of Independent Variables

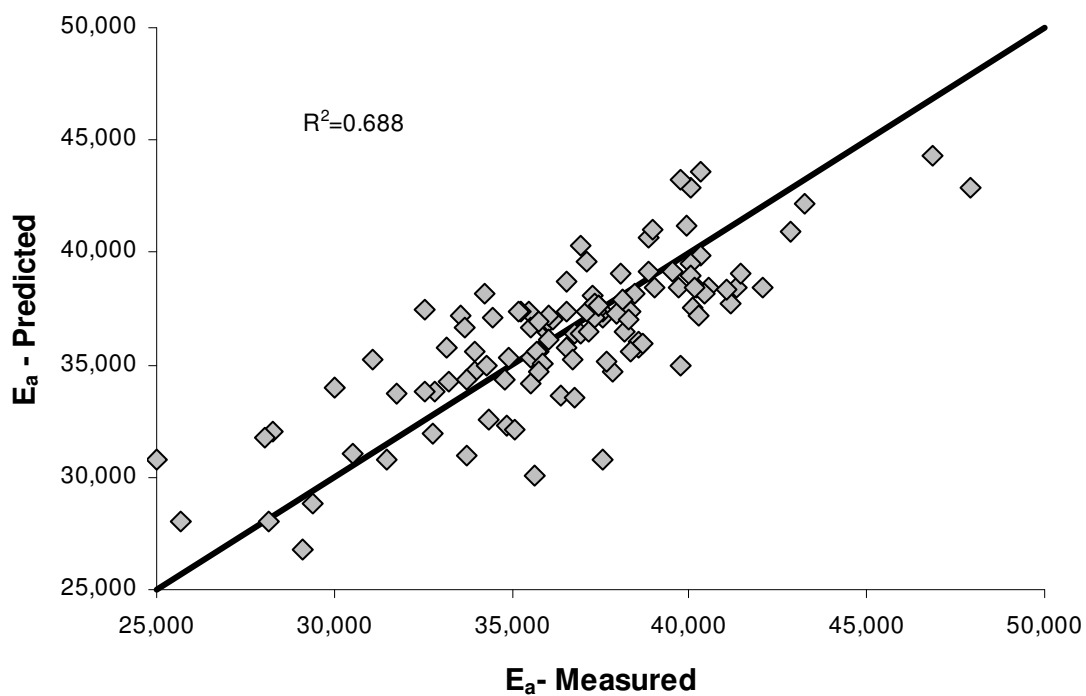


Figure D.12: Predicted E_a v. Measured E_a from GLM for Eight (8) variables

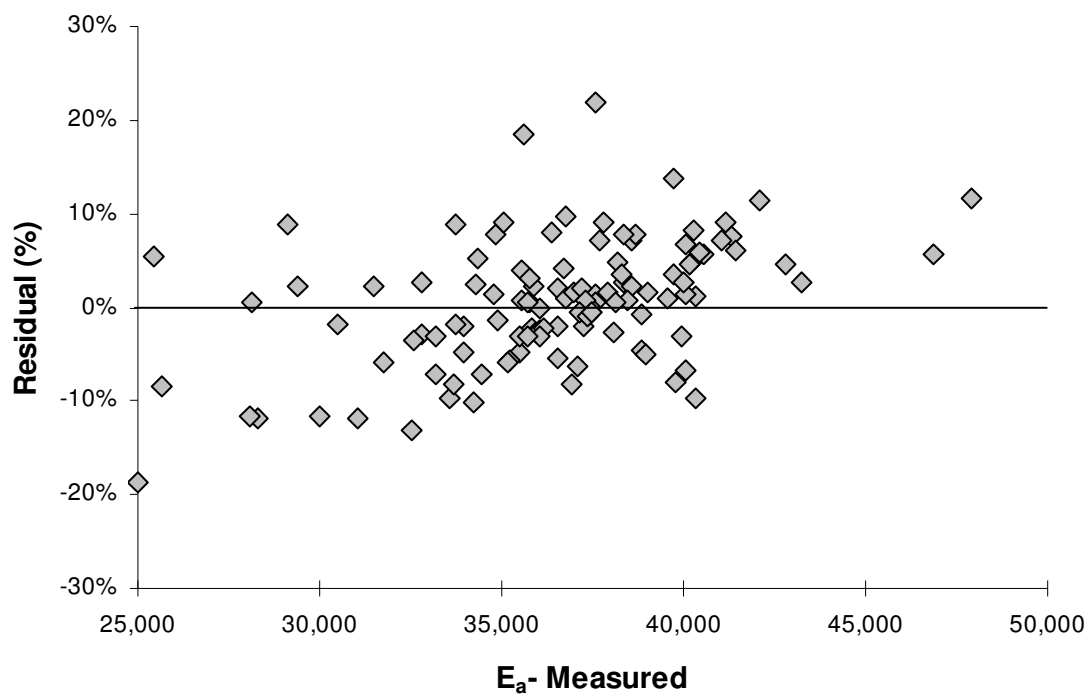


Figure D.13: Residual Plot for Linear E_a Model from GLM - Eight (8) Variables

PROC GLM - Final Run
The SAS System
Dependent Variable: EaMeas

Source	DF	Σ Squares	Mean Square	F Value	Pr>F
Model	8	1.283E+11	1.604E+10	2814.69	<.0001
Error	10431	5.944E+10	5.699E+06		
Corrected Total	10439	1.878E+11			

R ²	C.V.	Root MSE	EaMeas Mean
0.683	6.595	2387.15	36197.90

Type I F Test

Source	DF	Type I SS Mean	Mean Square	F Value	Pr>F
PerSlag	1	2.540E+10	2.540E+10	4456.56	<.0001
PerSF	1	3.265E+09	3.265E+09	572.93	<.0001
CemBlaine	1	3.626E+08	3.626E+08	63.63	<.0001
CemNa2Oeq	1	1.102E+09	1.102E+09	193.35	<.0001
WRRET	1	7.410E+10	7.410E+10	13003.2	<.0001
ACCL	1	7.983E+09	7.983E+09	1400.94	<.0001
i9	1	1.100E+10	1.100E+10	1929.59	<.0001
i17	1	5.113E+09	5.113E+09	897.33	<.0001

Type III F Test

Source	DF	Type III SS Mean	Mean Square	F Value	Pr>F
PerSlag	1	3.734E+10	3.734E+10	6553.42	<.0001
PerSF	1	4.228E+09	4.228E+09	742.01	<.0001
CemBlaine	1	6.449E+09	6.449E+09	1131.79	<.0001
CemNa2Oeq	1	4.073E+09	4.073E+09	714.82	<.0001
WRRET	1	9.174E+10	9.174E+10	16099.6	<.0001
ACCL	1	6.981E+09	6.981E+09	1225.08	<.0001
i9	1	1.577E+10	1.577E+10	2767.96	<.0001
i17	1	5.113E+09	5.113E+09	897.33	<.0001

t Test and Parameter Estimate

Parameter	Estimate	Standard Error	t Value	Pr> t
Intercept	43233.05	264.43	163.50	<.0001
PerSlag	166.06	2.05	80.95	<.0001
PerSF	-459.68	16.88	-27.24	<.0001
CemBlaine	-20.14	0.60	-33.64	<.0001
CemNa2Oeq	-5703.32	213.32	-26.74	<.0001
WRRET	-2289.80	18.05	-126.88	<.0001
ACCL	-130.55	3.73	-35.00	<.0001
i9	75.12	1.43	52.61	<.0001
i17	3.12	0.10	29.96	<.0001

Figure D.14: Results for PROC GLM for Eight (8) Variables

PROC GLM - Rietveld - Simple

The SAS System

Dependent Variable: EaMeas

Source	DF	Σ Squares	Mean Square	F Value	Pr>F
Model	7	1.2961E+11	1.8515E+10	3242.05	<.0001
Error	10432	5.9577E+10	5711013.98		
Corrected Total	10439	1.8919E+11			

R ²	C.V.	Root MSE	EaMeas Mean
0.685	6.600	2389.77	36210.28

Type I F Test

Source	DF	Type I SS Mean	Mean Square	F Value	Pr>F
PerSlag	1	2.630E+10	2.630E+10	4605.13	<.0001
PerSF	1	3.270E+09	3.270E+09	572.53	<.0001
CemBlaine	1	3.655E+08	3.655E+08	64	<.0001
WRRET	1	7.296E+10	7.296E+10	12775.6	<.0001
ACCL	1	8.702E+09	8.702E+09	1523.77	<.0001
i9	1	1.631E+10	1.631E+10	2855.01	<.0001
i17	1	1703639055	1703639055	298.31	<.0001

Type III F Test

Source	DF	Type III SS Mean	Mean Square	F Value	Pr>F
PerSlag	1	3.713E+10	3.713E+10	6500.92	<.0001
PerSF	1	6.187E+09	6.187E+09	1083.4	<.0001
CemBlaine	1	3.212E+09	3.212E+09	562.48	<.0001
WRRET	1	9.266E+10	9.266E+10	16224.30	<.0001
ACCL	1	7.454E+09	7.454E+09	1305.13	<.0001
i9	1	1.762E+10	1.762E+10	3085.71	<.0001
i17	1	1703639055	1703639055	298.31	<.0001

t Test and Parameter Estimate

Parameter	Estimate	Standard Error	t Value	Pr> t
Intercept	39600.94	203.52	194.58	<.0001
PerSlag	125.44	1.56	80.63	<.0001
PerSF	-541.23	16.44	-32.92	<.0001
CemBlaine	-12.65	0.53	-23.72	<.0001
WRRET	-2308.16	18.12	-127.37	<.0001
ACCL	-134.71	3.73	-36.13	<.0001
i9	96.71	1.74	55.55	<.0001
i17	1.47	0.09	17.27	<.0001

Figure D.15: Results for PROC GLM for Seven (7) Variables - Rietveld Analysis

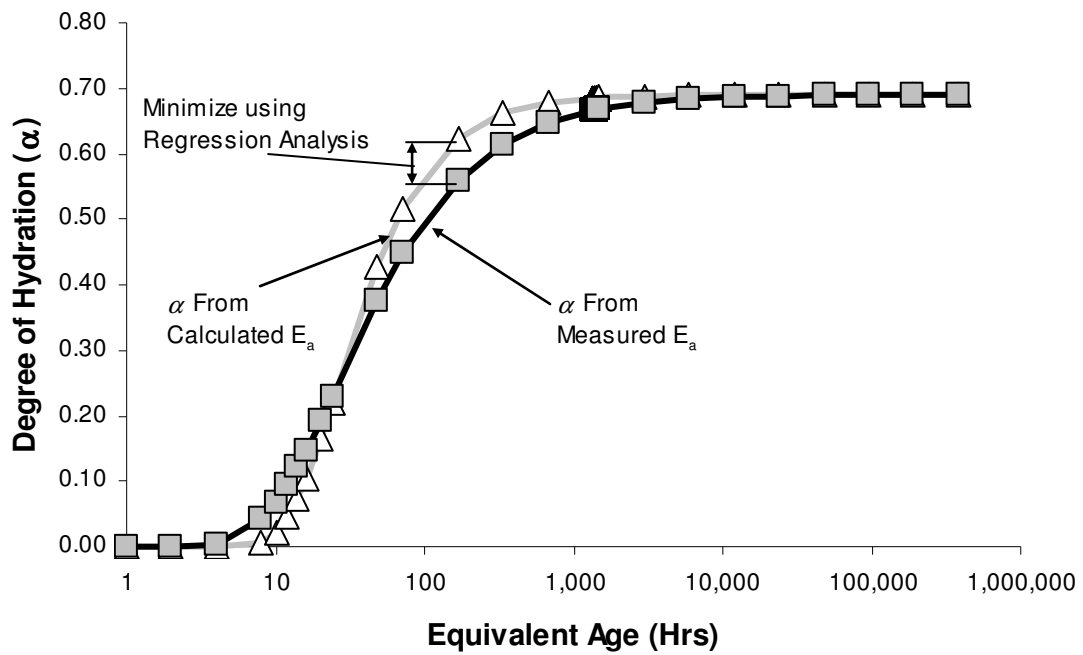


Figure D.16: Degree of Hydration (α) Model with Discrete Points

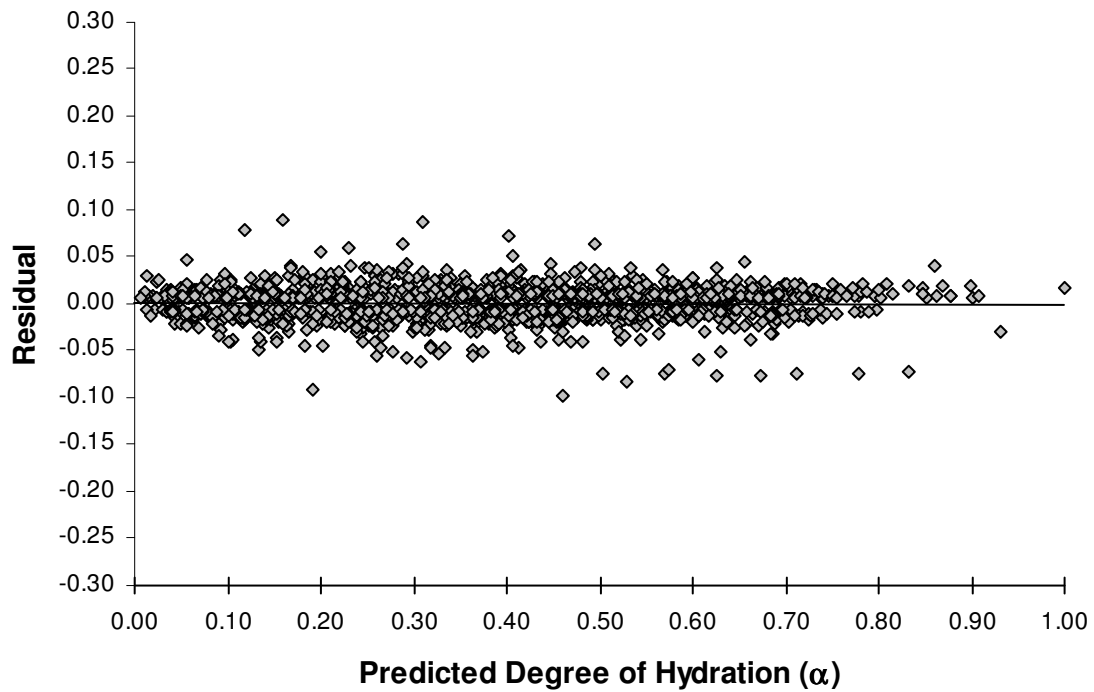


Figure D.17: Residual Plot from PROC NLIN Results for Predicted Degree of Hydration

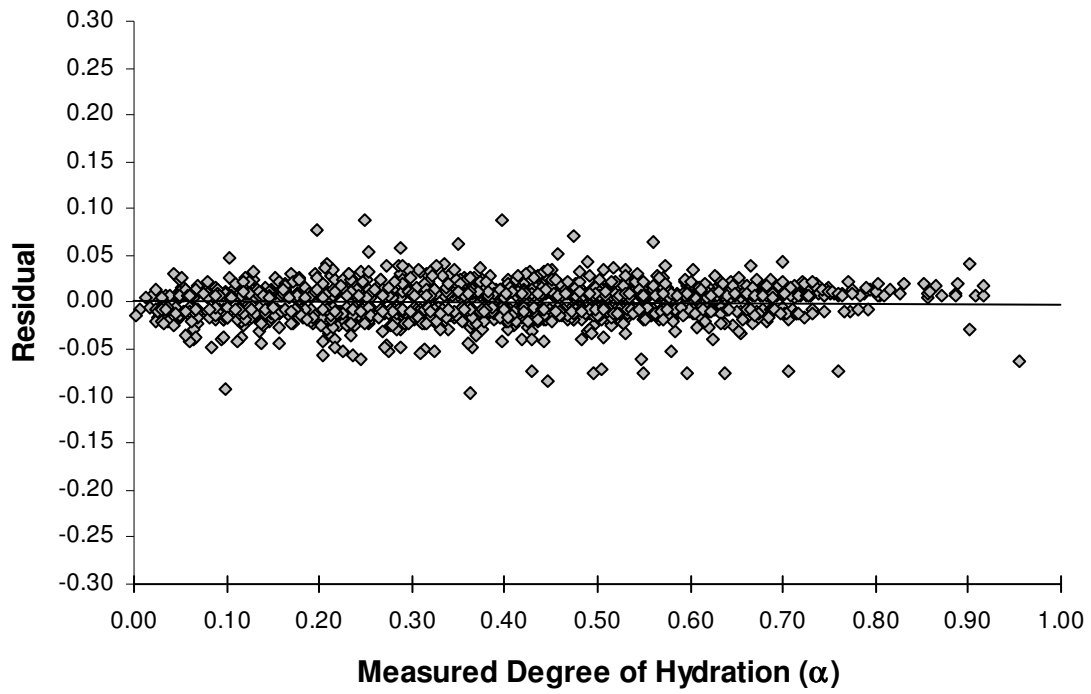


Figure D.18: Residual Plot from PROC NLIN Results for Measured Degree of Hydration

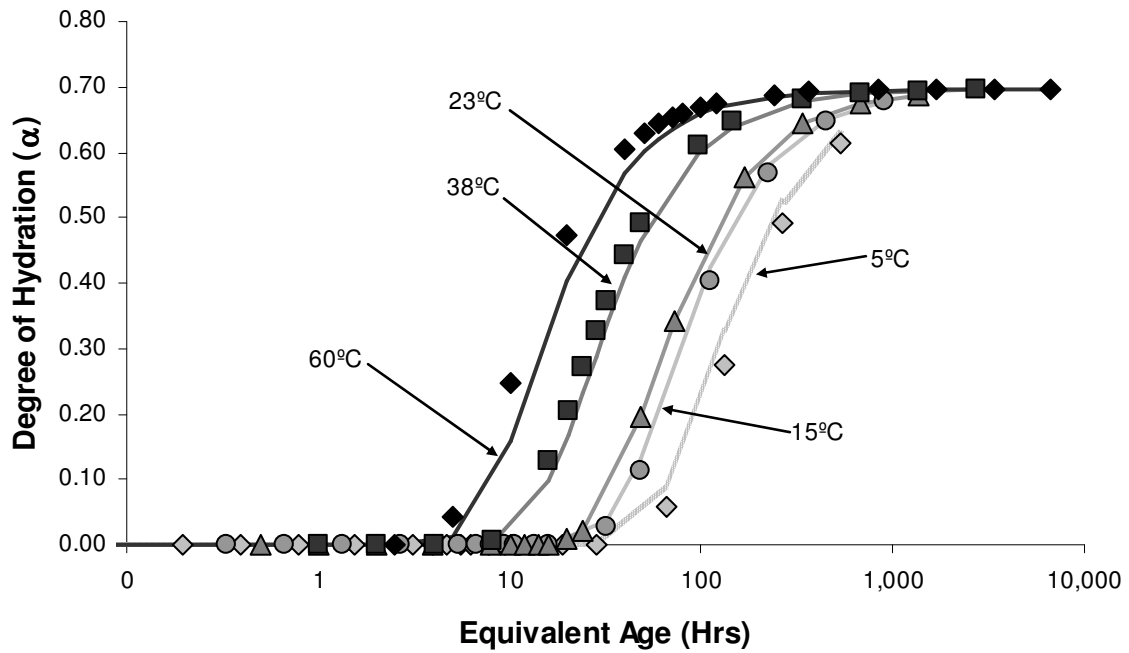


Figure D.19: 50% Cement C2, 50% GGBFS, 0.35% WRRET (Mix 315); Lines are predicted values; discrete points are measured values.

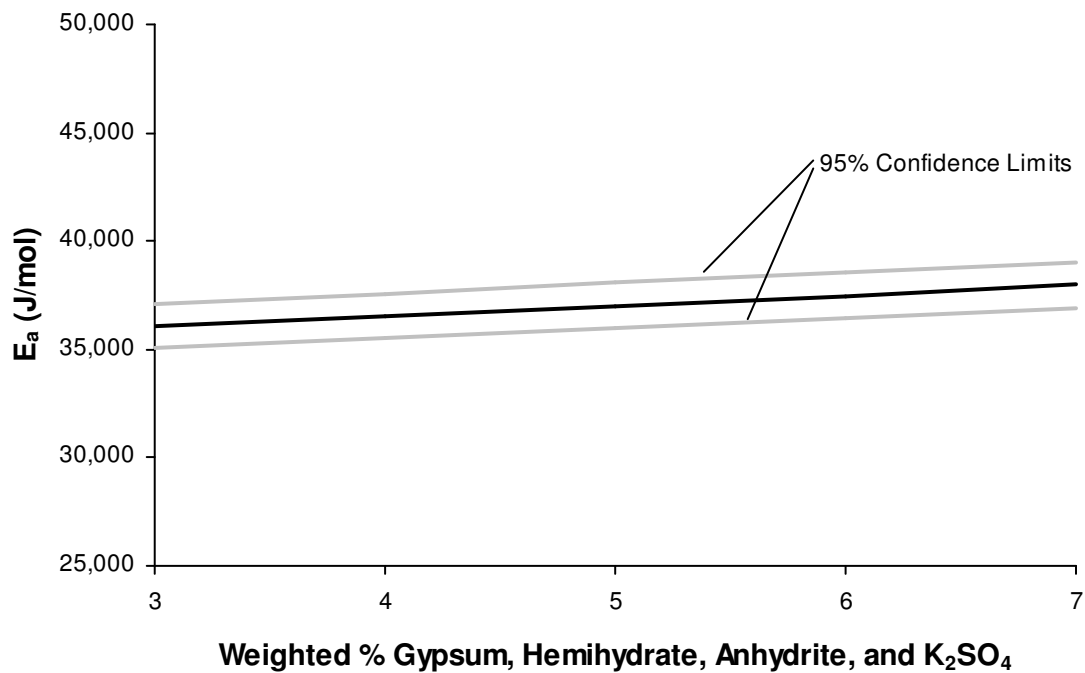


Figure D.20: Sensitivity of Proposed E_a Model to Gypsum ($C\hat{S}H_2$), Hemihydrate ($C\hat{S}H$), Anhydrite ($C\hat{S}$), and K_2SO_4 Percentage in Cementitious System

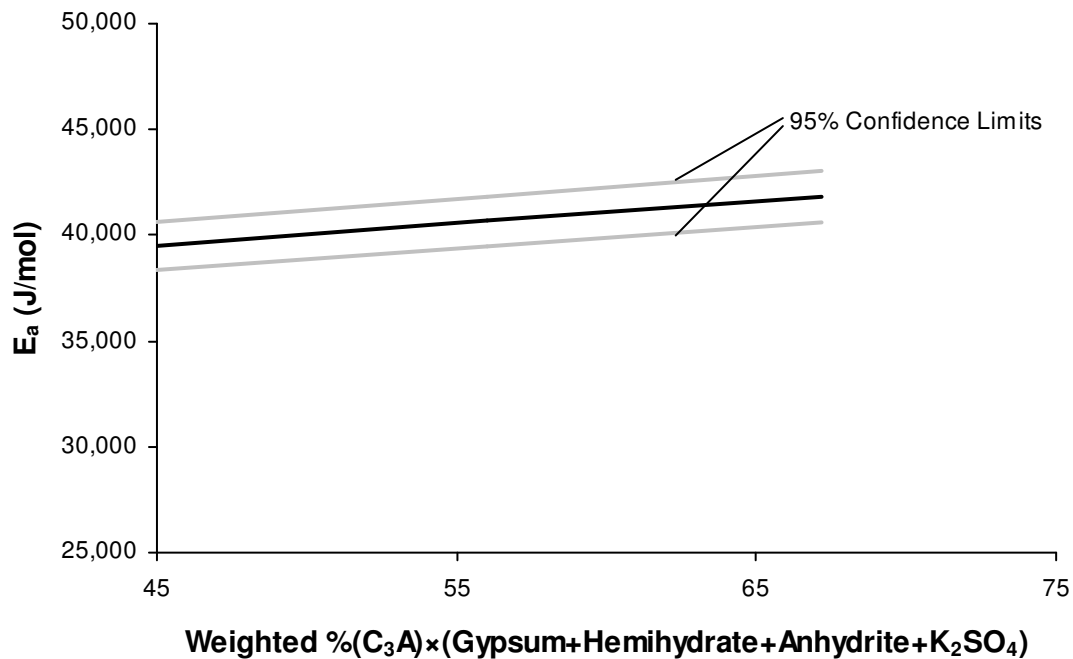


Figure D.21: Sensitivity of Proposed E_a Model to $(C_3A)\times$ (Gypsum+Hemihydrate+Anhydrite+ K_2SO_4) in Cementitious System

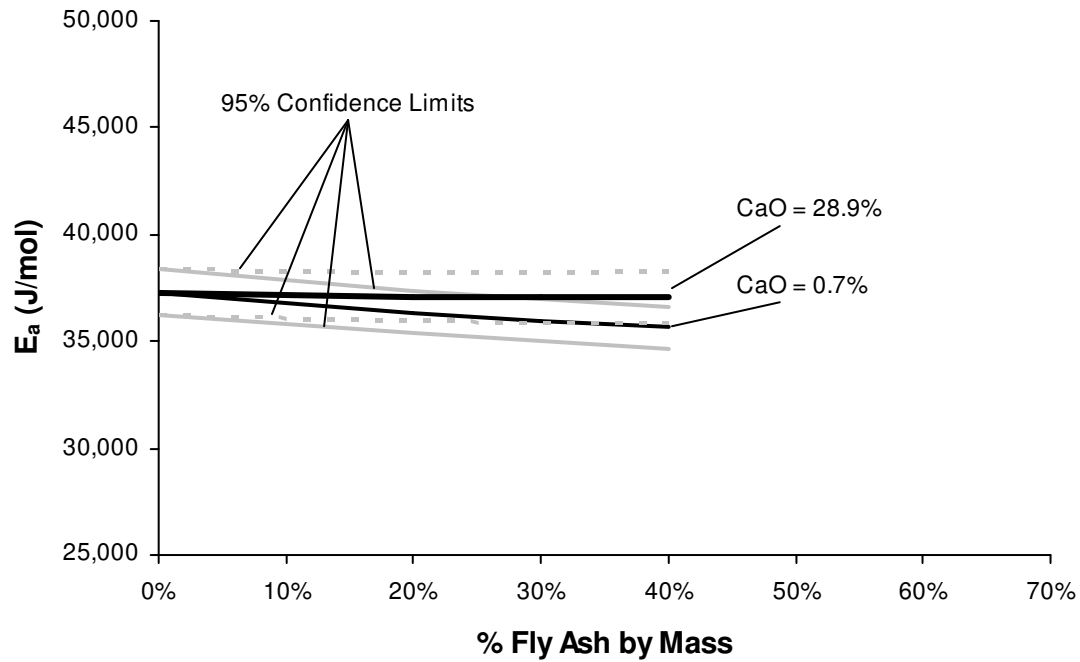


Figure D.22: Sensitivity of Proposed E_a Model (based on Rietveld Analysis) to Fly Ash CaO and Replacement Percentage

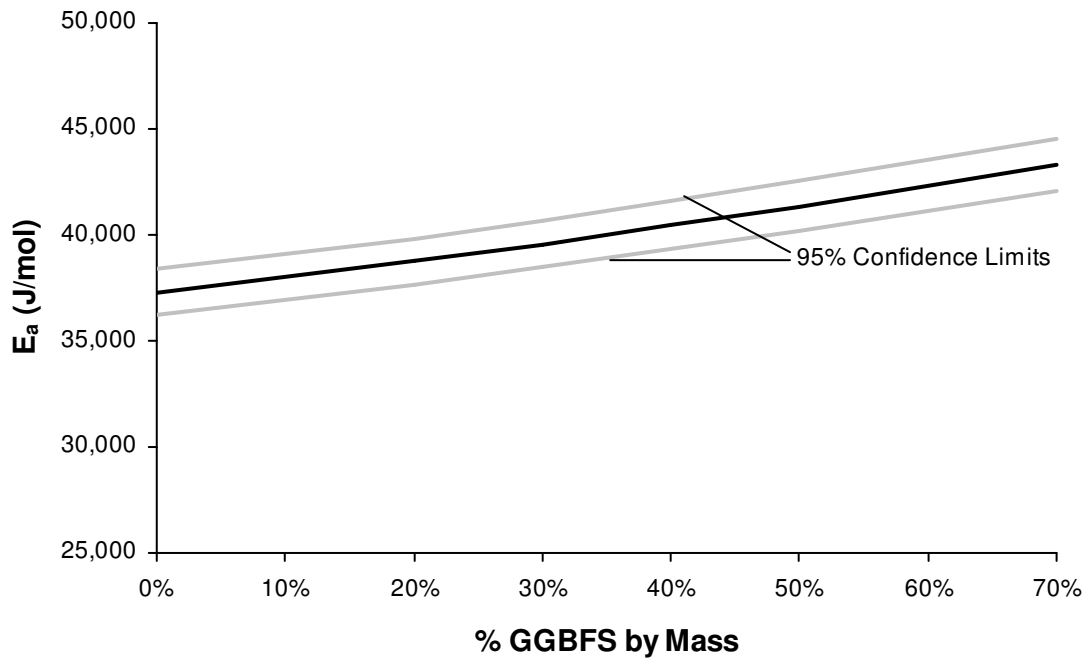


Figure D.23: Sensitivity of Proposed E_a Model (based on Rietveld Analysis) to GGBFS Replacement Percentage

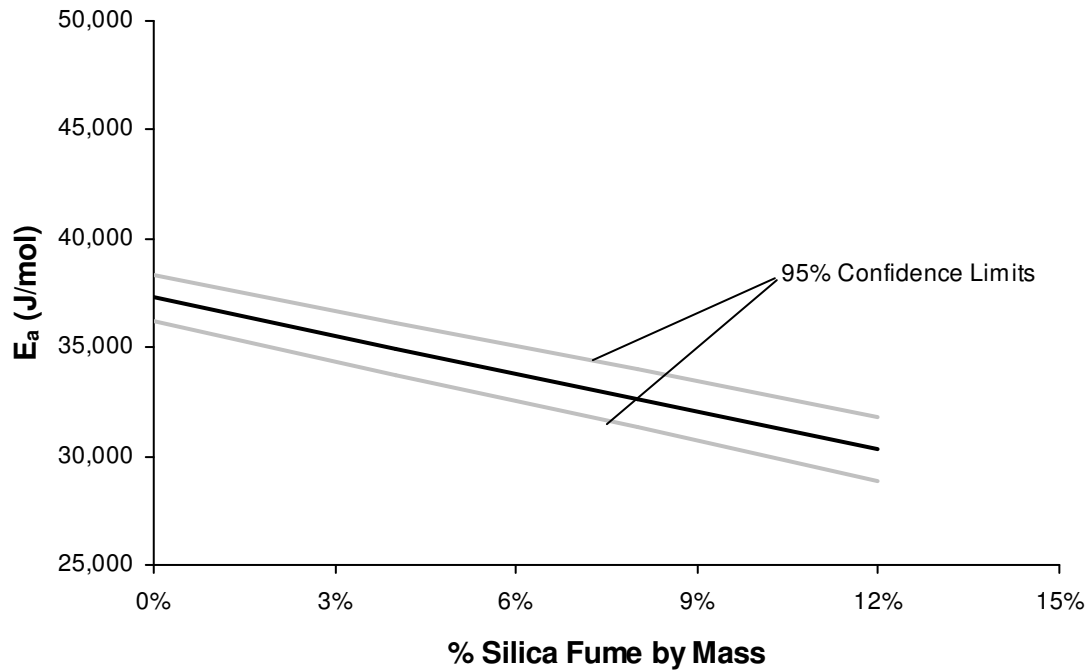


Figure D.24: Sensitivity of Proposed E_a Model (based on Rietveld Analysis) to Silica Fume Replacement Percentage

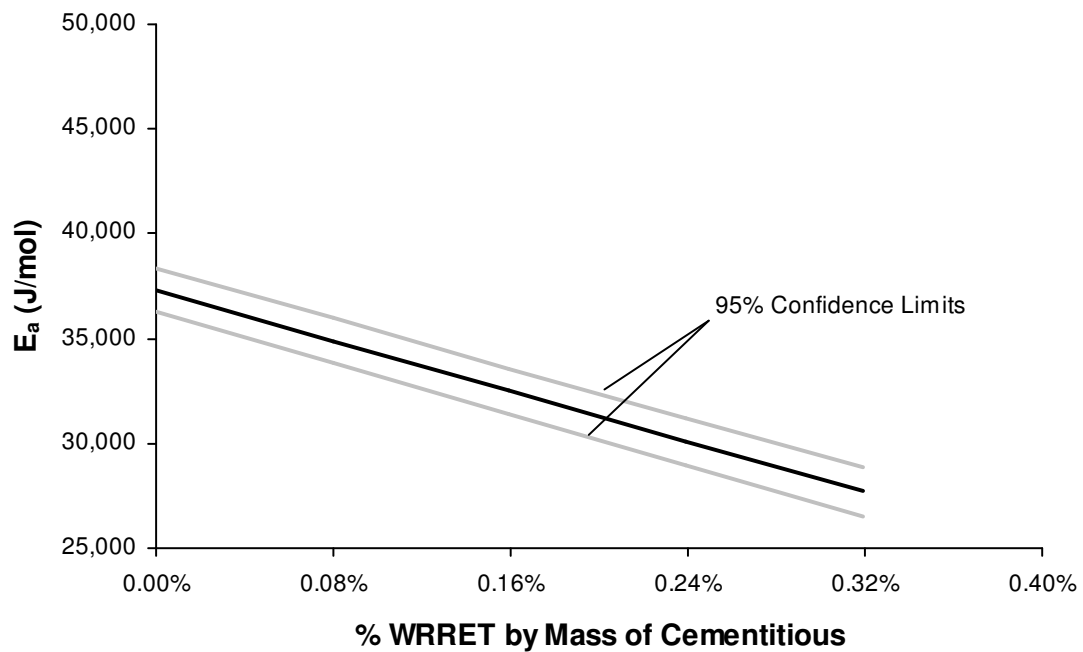


Figure D.25: Sensitivity of Proposed E_a Model (based on Rietveld Analysis) to WRRET Dosage

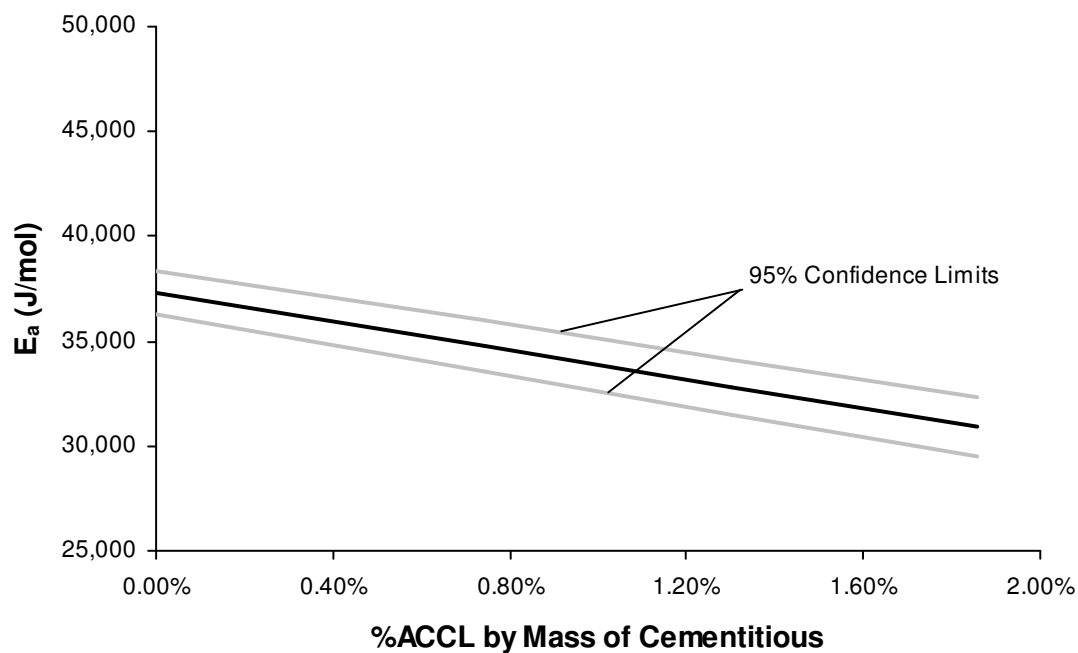


Figure D.26: Sensitivity of Proposed E_a Model (based on Rietveld Analysis) to ACCL Dosage

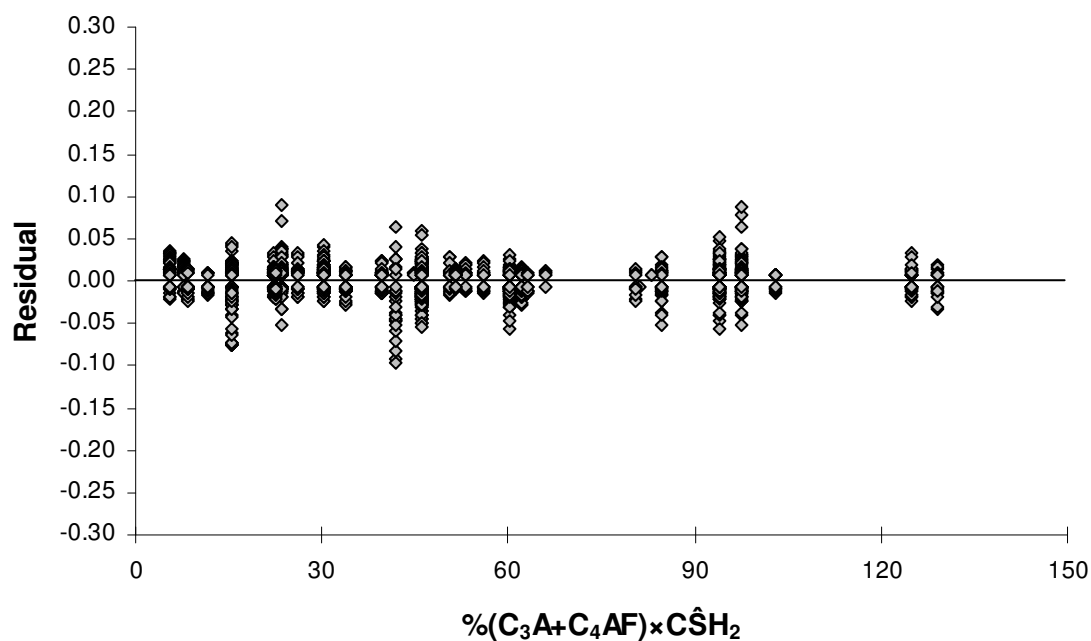


Figure D.27: Residuals v. Weighted % $(C_3A + C_4AF) \times$ Gypsum in Mixture

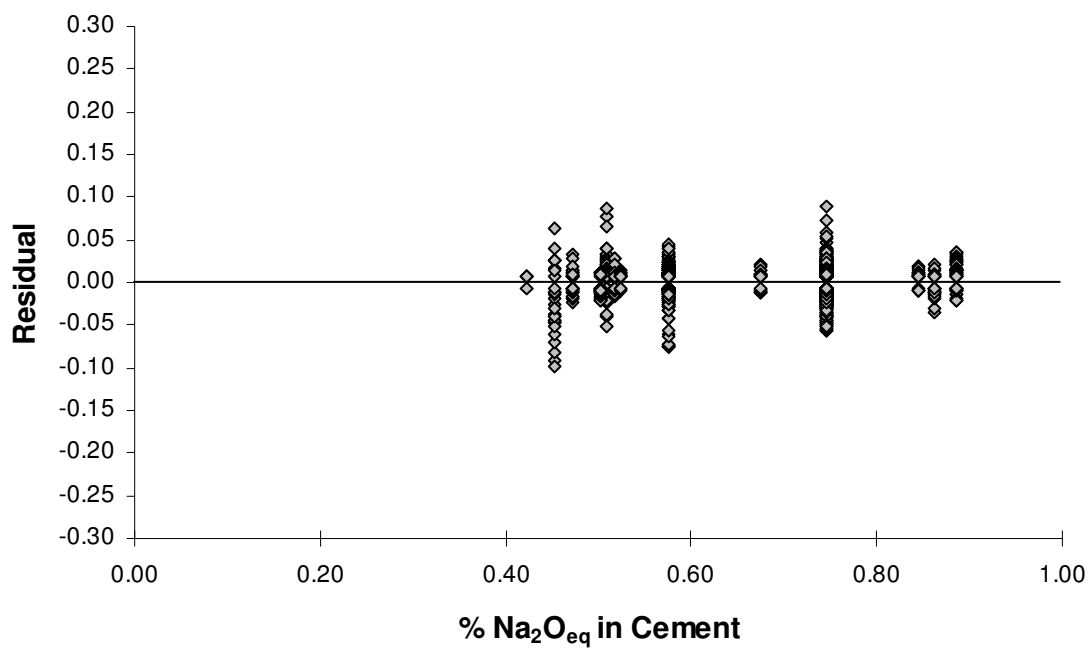


Figure D.28: Residuals v. % $\text{Na}_2\text{O}_{\text{eq}}$ ($\% \text{Na}_2\text{O} + 0.658 \times \text{K}_2\text{O}$) in Cement

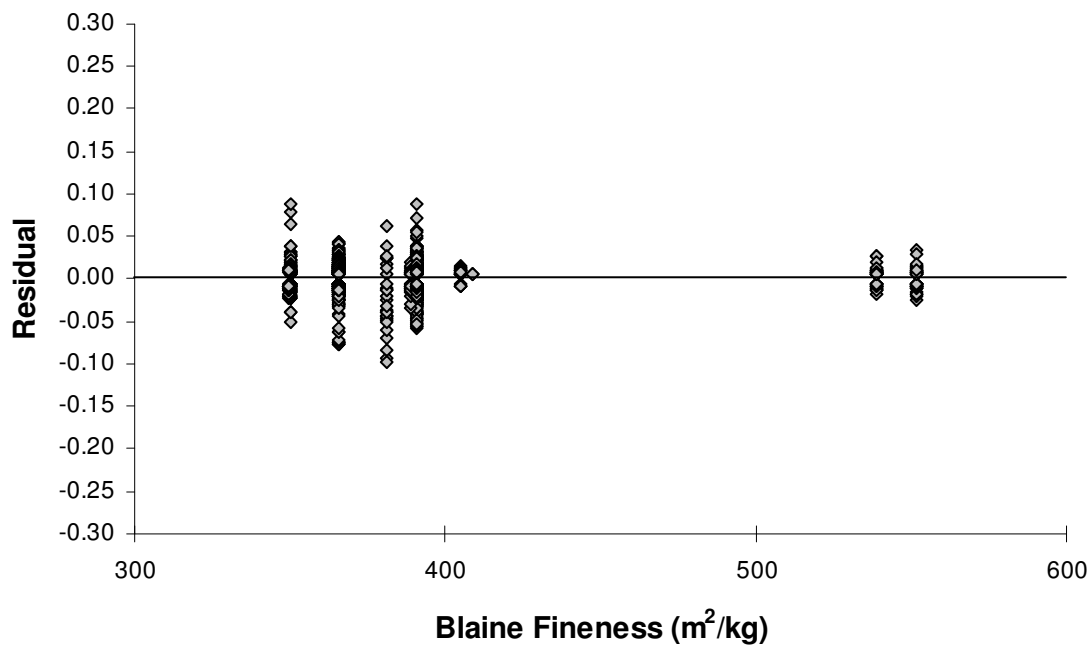


Figure D.29: Residuals v. Blaine Fineness of Cement

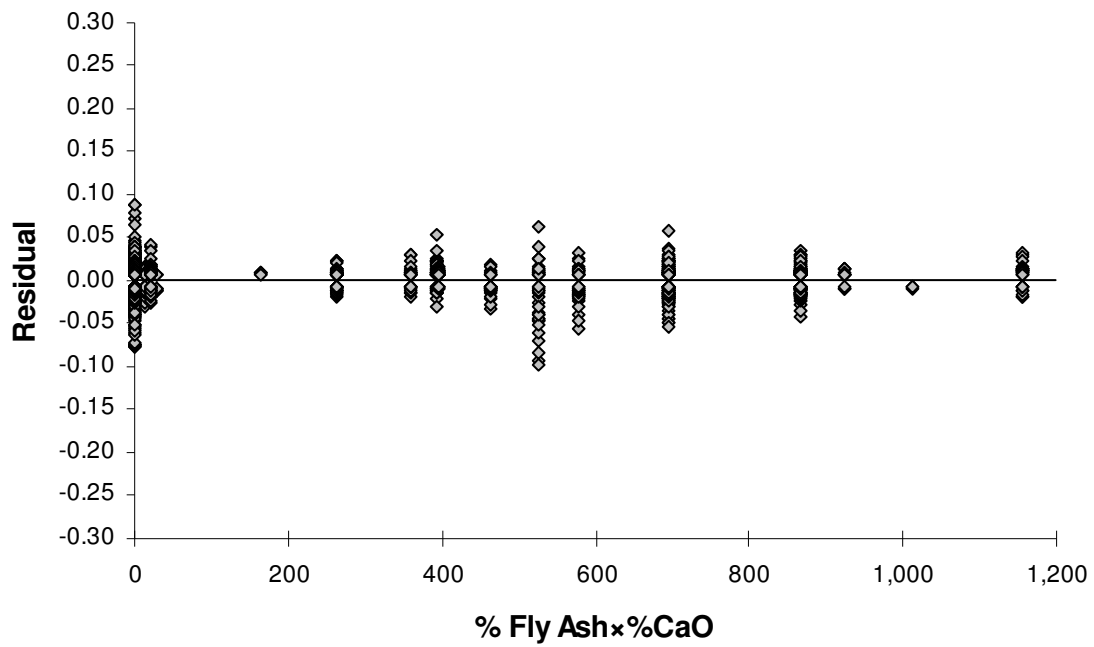


Figure D.30: Residuals v. % Fly Ash x % CaO in Fly Ash

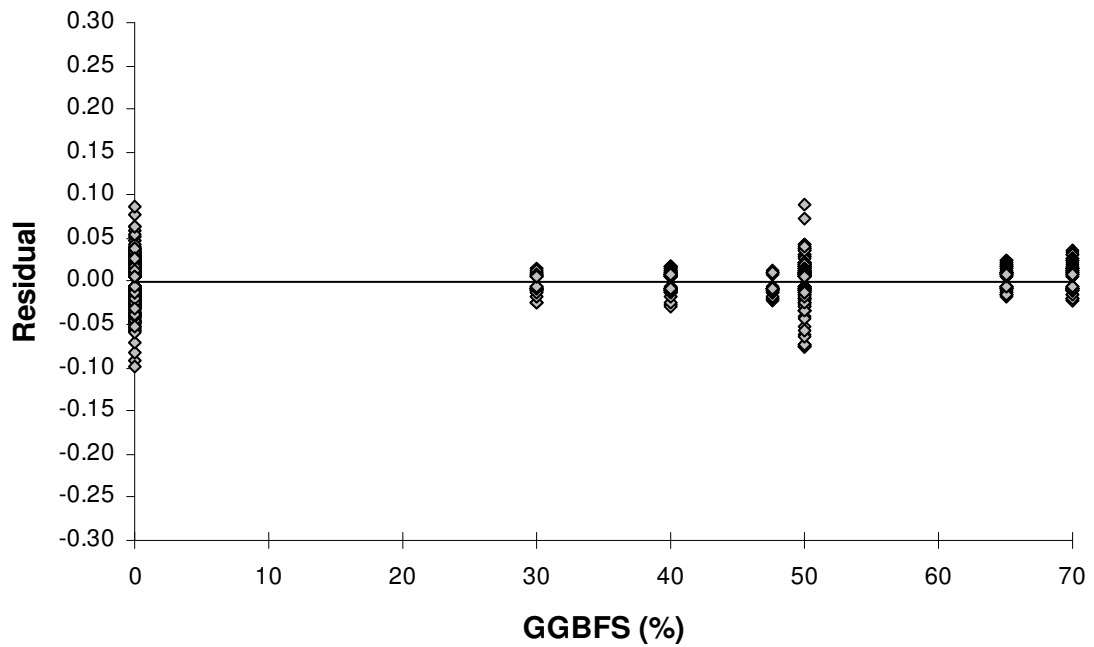


Figure D.31: Residuals v. % GGBFS in Mixture

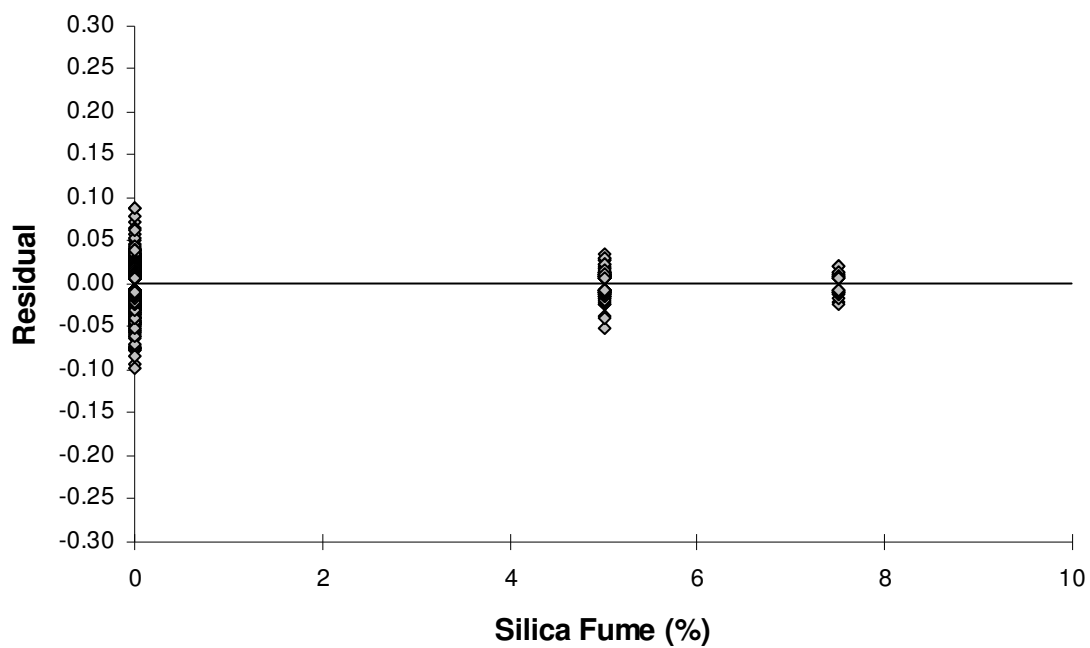


Figure D.32: Residuals v. % Silica Fume in Mixture

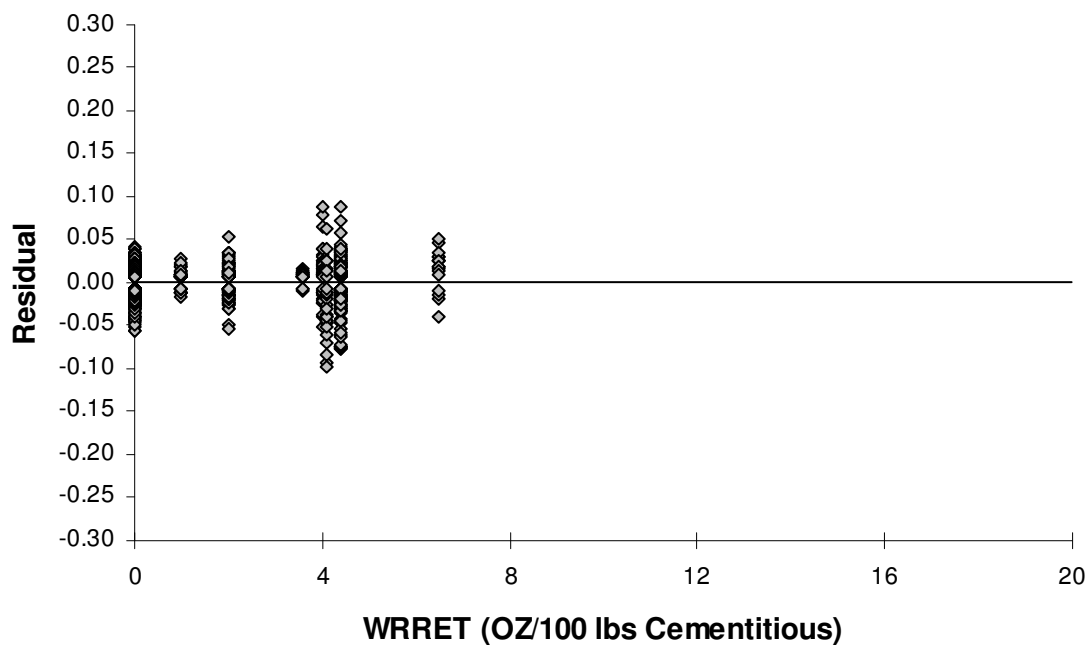


Figure D.33: Residuals v. WRRET Dosage (OZ/100 lbs Cementitious) in Mixture

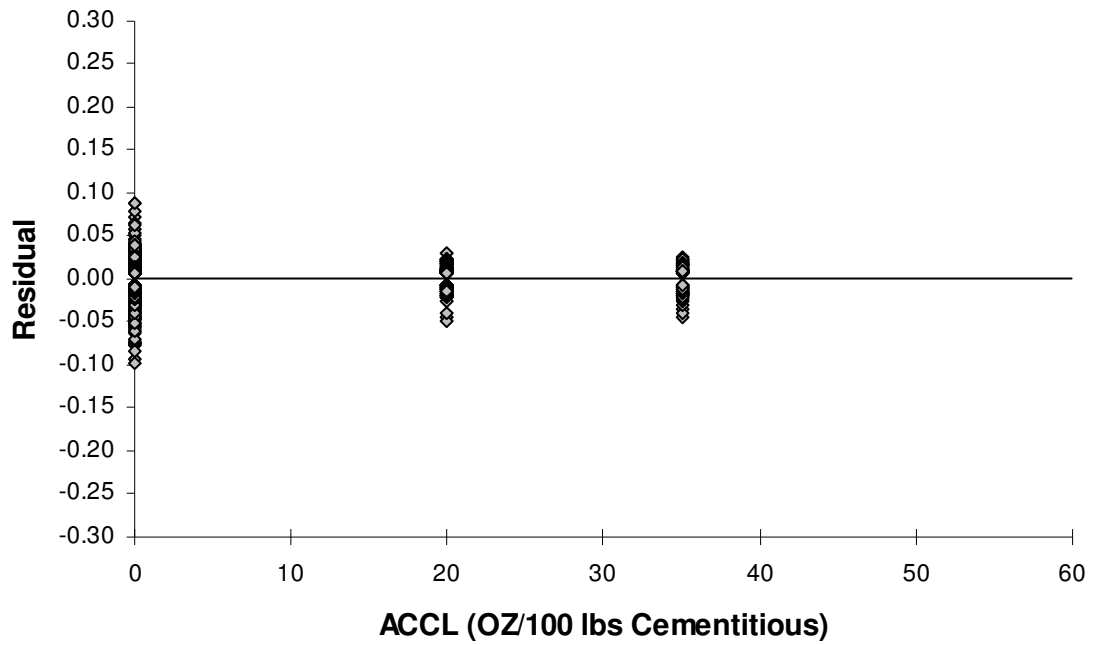


Figure D.34: Residuals v. ACCL Dosage (OZ/100 lbs Cementitious) in Mixture

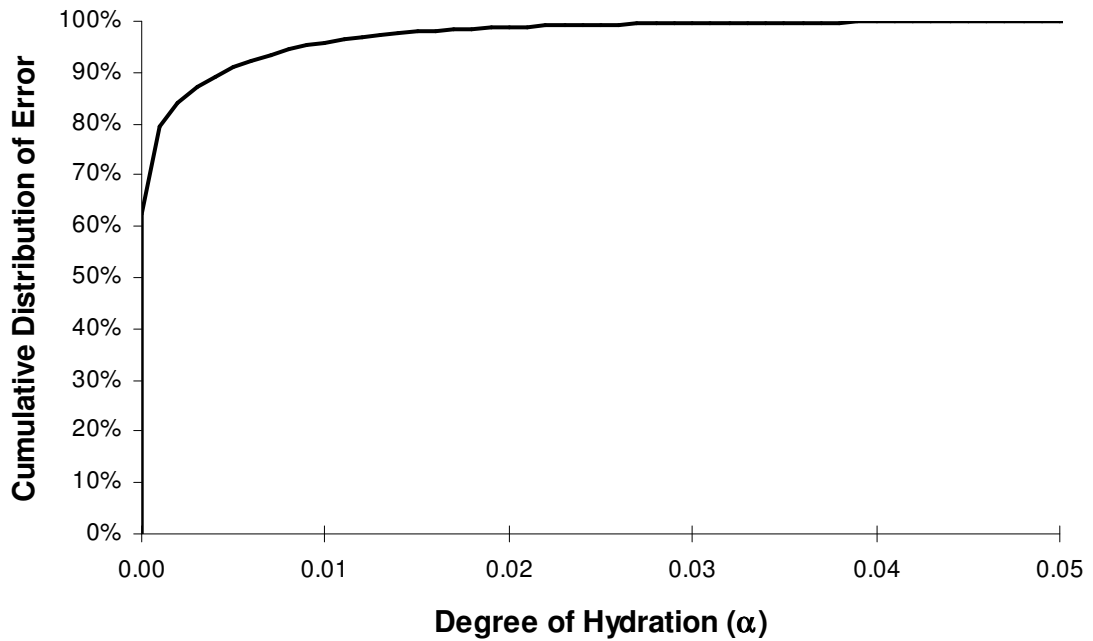


Figure D.35: Cumulative Error Distribution vs. Degree of Hydration

D.15. SAS CODE (V. 9.1.3) – BOGUE CALCULATIONS

```
data work.templ; set work.cement2;
lperC3S=log(perC3S);
lperC3A=log(perC3A);
lperC4AF=log(perC4AF);
lperC2S=log(perC2S);
lperGypsum=log(perGypsum);
lCemBlaine=log(CemBlaine);
lTotalNa2Oeq=log(TotalNa2Oeq);
lWRRET=log(WRRET);
lACCL=log(ACCL);
i1=WRRET*perC3A;
i2=WRRET*perSlag;
i3=WRRET*perCash;
i4=perCash*WRRET*pergypsum;
i5=c3a*TotalNa2Oeq*perCash;
i6=c3a*CemNa2Oeq*perCash;
i7=perCash*perC3A;
i8=perCash*perC3A*pergypsum;
i9=(perC3A+perC4AF)*pergypsum;
i10=perC3A*(perCash+perSlag);
i11=(perCash+perSlag)*perC3A*pergypsum;
i12=(perCash+perSlag)*WRRET*pergypsum;
i13=c3a*TotalNa2Oeq*(perCash+perSlag);
i14=c3a*CemNa2Oeq*(perCash+perSlag);
i15=HRWR+PCHRWR;
i16=(perCash)*TotalFACaO*pergypsum;
i17=(PerFA+PerUFFA)*TotalFACaO;
i18=(PerFA+PerUFFA)*TotalFACaO*perC3A;
i19=(PerFA+PerUFFA)*TotalFACaO*pergypsum;
i20=perFash*TotalFACaO;
i21=perCash*TotalFACaO;
i22=CemNa2Oeq*(100-perFA-PerUFFA-perSlag-PerSF)/100;
li1=log(i1);
li2=log(i2);
li3=log(i3);
li4=log(i4);
li5=log(i5);
li6=log(i6);
li7=log(i7);
li8=log(i8);
li9=log(i9);
li10=log(i10);
li11=log(i11);
li12=log(i12);
li13=log(i13);
li14=log(i14);
li15=log(i15);
li16=log(i16);
li17=log(i17);
li18=log(i18);
```

```

li19=log(i19);
li20=log(i20);
li21=log(i21);
lEaMeas=log(EaMeas);
ltau=log(tau);
run;
proc rsquare c;
model lEaMeas EaMeas= C3S C2S C3A C4AF MgO SO3 gypsum wc perFash
perCash perSF perC3S perC2S perC3A perC4AF perGypsum FreeCao CemBlaine
PerSlag CemNa2Oeq TotalNa2Oeq WRRET HRWR PCHRWR ACCL i1 i2 i3 i4 i5
i6 i7 i8 i9 i10 i11 i12 i13 i14 i15 i16 i17 i18 i19 i20 i21 i22
/select=30 stop=10;
run; quit;

proc glm;
proc glm; model lEameas Eameas = PerSlag PerSF CemBlaine CemNa2Oeq
WRRET ACCL i9 i17
output out=plotit p=pred r=resid;
run;
proc gplot; plot pred*lEameas resid*pred;
run;quit;

data work.alphapredict; set work.cement2;
i1=WRRET*perC3A;
i2=WRRET*perSlag;
i3=WRRET*perCash;
i4=perCash*WRRET*pergypsum;
i5=c3a*TotalNa2Oeq*perCash;
i6=c3a*CemNa2Oeq*perCash;
i7=perCash*perC3A;
i8=perCash*perC3A*pergypsum;
i9=(perC3A+perC4AF)*pergypsum;
i10=perC3A*(perCash+perSlag);
i11=(perCash+perSlag)*perC3A*pergypsum;
i12=(perCash+perSlag)*WRRET*pergypsum;
i13=c3a*TotalNa2Oeq*(perCash+perSlag);
i14=c3a*CemNa2Oeq*(perCash+perSlag);
i15=HRWR+PCHRWR;
i16=(perCash+perSlag)*TotalFACaO*pergypsum;
i17=(PerFA+PerUFFA)*TotalFACaO;
i18=(PerFA+PerUFFA)*TotalFACaO*perC3A;
i19=(PerFA+PerUFFA)*TotalFACaO*pergypsum;
i20=perFash*TotalFACaO;
i21=perCash*TotalFACaO;
lEaMeas=log(EaMeas);
ltau=log(tau);
lEaMeas=log(EaMeas);
run;
proc nlin;
parms C1=41230 C2=162.0 C3=-516 C4=-19.83 C5=-3469 C6=-2462 C7=-127.9
C8=83.28 C9=2.963;
EaMeas1=(C1+C2*PerSlag+C3*PerSF+C4*CemBlaine+C5*CemNa2Oeq+C6*WRRET+C7*A
CCL+C8*perCem*perCem*(C3A+C4AF)*Gypsum+C9*i17);
model alpha=exp(-(tau/(exp(EaMeas1/8.3144*(1/296-
1/(temp+273))))*time))**beta))*alphamax;
output out=good p=predict r=resid stdr=eresid;
run;

```

```
proc gplot;
plot alpha*predict resid*predict resid*alpha;
run; quit;
```

D.16. SAS CODE (V. 9.1.3) – RIETVELD ANALYSIS

```
data work.templ; set work.cement2;
lperC3S=log(perC3S);
lperalite=log(alite);
lperC3A=log(perC3A);
lperaluminate=log(aluminate);
lperC4AF=log(perC4AF);
lperferrite=log(ferrite);
lperC2S=log(perC2S);
lperbelite=log(belite);
lperGypsum=log(perGypsum);
lCemBlaine=log(CemBlaine);
lTotalNa2Oeq=log(TotalNa2Oeq);
lWRRET=log(WRRET);
lACCL=log(ACCL);
i1=WRRET*perC3A;
i2=WRRET*perSlag;
i3=WRRET*perCash;
i4=perCash*WRRET*pergypsum;
i5=c3a*TotalNa2Oeq*perCash;
i6=c3a*CemNa2Oeq*perCash;
i7=perCash*perC3A;
i8=perCash*perC3A*pergypsum;
i9=(perAluminate)*(pergypsumR+perHemihydrate+perAnhydrite+perK2SO4);
i10=perC3A*(perCash+perSlag);
i11=(perCash+perSlag)*perC3A*pergypsum;
i12=(perCash+perSlag)*WRRET*pergypsum;
i13=c3a*TotalNa2Oeq*(perCash+perSlag);
i14=c3a*CemNa2Oeq*(perCash+perSlag);
i15=HRWR+PCHRWR;
i16=(perCash)*TotalFACaO*pergypsum;
i17=(PerFA+PerUFFA)*TotalFACaO;
i18=(PerFA+PerUFFA)*TotalFACaO*perC3A;
i19=(PerFA+PerUFFA)*TotalFACaO*pergypsum;
i20=perFash*TotalFACaO;
i21=perCash*TotalFACaO;
i22=CemNa2Oeq*(100-perFA-PerUFFA-perSlag-PerSF)/100;
i23=(pergypsumR+perHemihydrate+perAnhydrite+perK2SO4);
li1=log(i1);
li2=log(i2);
li3=log(i3);
li4=log(i4);
li5=log(i5);
li6=log(i6);
li7=log(i7);
li8=log(i8);
li9=log(i9);
li10=log(i10);
li11=log(i11);
```



```

li12=log(i12);
li13=log(i13);
li14=log(i14);
li15=log(i15);
li16=log(i16);
li17=log(i17);
li18=log(i18);
li19=log(i19);
li20=log(i20);
li21=log(i21);
lEaMeas=log(EaMeas);
ltau=log(tau);
run;
proc rsquare c;
model lEaMeas EaMeas= alite belite aluminate ferrite periclase gypsumR
Hemihydrate Anhydrite K2SO4 wc perFash perCash perSF perAlite perBelite
perAluminate perFerrite Periclase perGypsumR perHemihydrate
perAnhydrite perK2SO4 FreeCao CemBlaine PerSlag CemNa2O CemK2O
TotalNa2Oeq WRRET HRWR PCHRWR ACCL i1 i2 i3 i4 i5 i6 i7 i8 i9 i10 i11
i12 i13 i14 i15 i16 i17 i18 i19 i20 i21 i22 /select=30 stop=10;
run; quit;

proc glm;
proc glm; model lEameas Eameas = PerSlag PerSF CemBlaine WRRET ACCL i9
i17;
output out=plotit p=pred r=resid;
run;
proc gplot; plot pred*lEameas resid*pred;
run; quit;

data work.alphapredict; set work.cement2;
lperC3S=log(perC3S);
lperalite=log(alite);
lperC3A=log(perC3A);
lperaluminate=log(aluminate);
lperC4AF=log(perC4AF);
lperferrite=log(ferrite);
lperC2S=log(perC2S);
lperbelite=log(belite);
lperGypsum=log(perGypsum);
lCemBlaine=log(CemBlaine);
lTotalNa2Oeq=log(TotalNa2Oeq);
lWRRET=log(WRRET);
lACCL=log(ACCL);
i1=WRRET*perC3A;
i2=WRRET*perSlag;
i3=WRRET*perCash;
i4=perCash*WRRET*pergypsum;
i5=c3a*TotalNa2Oeq*perCash;
i6=c3a*CemNa2Oeq*perCash;
i7=perCash*perC3A;
i8=perCash*perC3A*pergypsum;
i9=(perAluminate)*(pergypsumR+perHemihydrate+perAnhydrite+perK2SO4);
i10=perC3A*(perCash+perSlag);
i11=(perCash+perSlag)*perC3A*pergypsum;
i12=(perCash+perSlag)*WRRET*pergypsum;
i13=c3a*TotalNa2Oeq*(perCash+perSlag);

```

```

i14=c3a*CemNa2Oeq*(perCash+perSlag);
i15=HRWR+PCHRWR;
i16=(perCash)*TotalFACaO*pergypsum;
i17=(PerFA+PerUFFA)*TotalFACaO;
i18=(PerFA+PerUFFA)*TotalFACaO*perC3A;
i19=(PerFA+PerUFFA)*TotalFACaO*pergypsum;
i20=perFash*TotalFACaO;
i21=perCash*TotalFACaO;
i22=CemNa2Oeq*(100-perFA-PerUFFA-perSlag-PerSF)/100;
li1=log(i1);
li2=log(i2);
li3=log(i3);
li4=log(i4);
li5=log(i5);
li6=log(i6);
li7=log(i7);
li8=log(i8);
li9=log(i9);
li10=log(i10);
li11=log(i11);
li12=log(i12);
li13=log(i13);
li14=log(i14);
li15=log(i15);
li16=log(i16);
li17=log(i17);
li18=log(i18);
li19=log(i19);
li20=log(i20);
li21=log(i21);
lEaMeas=log(EaMeas);
ltau=log(tau);
run;
proc nlin;
parms C1=34808 C2=161 C3=-514 C4=-12.4 C5=-2378 C6=-131 C7=117 C8=3.15;
EaMeas1=(C1+C2*PerSlag+C3*PerSF+C4*CemBlaine+C5*WRRET+C6*ACCL+C7*i9+C8*
i17);
model alpha=exp(-(tau/(exp(EaMeas1/8.3144*(1/296-
1/(temp+273))))*time)**beta))*alphamax;
output out=good p=predict r=resid stdr=eresid;
run;
proc gplot;
plot alpha*predict resid*predict resid*alpha;
run;
quit;

/*An approximate R2 can be determined by 1-SSE/SST or 1-residual
SS/corrected total SS*/

```

APPENDIX E. ADDITIONAL SEMI-ADIABATIC TEST RESULTS FOR CHAPTER 7

The following results are presented as supplementary support for the conclusions presented in Chapter 7.

E.1. EFFECTS OF MRWR AND HRWR ON HYDRATION

Chapter 7 showed that the addition of a PCHRWR could slightly increase the peak height of the hydration curve, and the addition of a NHRWR could slightly delay the hydration. Also, it was stated that the addition of a high-range water reducer has little effect on the adiabatic temperature rise. This is supported by Figure E.1 and Figure E.2. However, the PCHRWR causes the peak height of the heat of hydration curve to increase with some of the mixtures. This translates into a slight increase in early temperature, which can be seen for cement C1 and C12. The NHRWR causes a slight delay at early ages with cement C2 and C12. Nevertheless, these effects are minor compared to the effects of WRRET. Figure E.3 shows the delay with the addition of a MRWR. Again, the final adiabatic temperature rise is not affected, but the early temperature development is retarded somewhat. Figure E.4 shows the rate of heat evolution with 70% cement C2 and 30% SCM FC2 and both NHRWR and PCHRWR. Interestingly, the admixtures have no effect on the rate of heat evolution for this mixture.

E.2. ADDITIONAL COMPARISONS OF EFFECTS OF ACCL AND AEA ON HYDRATION AND ADIABATIC TEMPERATURE RISE

Figure E.5 and Figure E.6 show the rate of heat evolution and the adiabatic temperature rise for Cement C6 with ACCL. Figure E.7 and Figure E.8 show the rate of

heat evolution and the adiabatic temperature rise for mixtures with air-entraining admixture. These results parallel the results that are shown in Chapter 7. They show that 1.30% ACCL will increase the slope of the accelerating portion of the hydration curve. Figure E.7 and Figure E.8 also show that AEA has very little effect on the rate of heat evolution and does not alter the adiabatic temperature rise.

E.3. EFFECTS OF CHEMICAL ADMIXTURES ON τ AND β

Figure E.9 shows that the time parameter, τ , is not significantly affected by the addition of NHRWR or PCHRWR. Figure E.11 shows that the MRWR causes τ to increase. Figure E.10 and Figure E.12 show that all of the mid-range and high-range admixtures increase β . Figure E.13 compares dosage of accelerator to the time parameter τ for mixtures of 100% cement C2 and C10. Increasing dosages will decrease τ , which was also shown in Chapter 7. However, the detail of the pure cement behavior was not clear, because of the scale of the graph. The effects of air entraining admixture on τ are shown in Figure E.15. The addition of AEA causes no change in τ . The effects of ACCL and AEA on the slope parameter, β , are shown in Figure E.14 and Figure E.16, respectively. The addition of these admixtures to a mixture produces little change in β . Figure E.17 shows the second derivative versus time of the rate of heat evolution for mixtures with 70% cement C1, 30% fly ash FF2, and WRRET. The first positive peak corresponds with the first inflection point in the hydration curve, which roughly correlates with initial set. The time at which this peak occurs also correlates with the time parameter, τ . Figure E.18 shows the relationship between admixture dosage, τ , and the time of first inflection point, and Figure E.19 shows the same relationship for the

slope parameter, β . The time of initial set appears to be exponentially related to the dosage of admixture, while the relationships between admixture dosage, τ , and β are either bilinear, linear, or exponential. Future multivariate regression will determine the most appropriate relationship. However, the amount of data here is not enough to suggest anything beyond the simple relationships discussed in Chapter 7.

E.4. EFFECTS OF ADMIXTURES ON α_u

Each of the admixtures in this study will alter the degree of hydration parameter, α_u , in different ways. The major trends are discussed in Chapter 7. Further discussion of the trends in α_u will be left until Chapter 8 when multivariate statistical analysis can be performed on all of the results to distill to variables that have the greatest effects. However, several of the minor trends will be highlighted here.

First, there does not appear to be any discernable trend in α_u with addition of LRWR to a mixture, as shown in Figure E.20. However, WRRET tends to reduce α_u , as shown in Figure E.21. Next, most of the results with NHRWR, PCHRWR, and MRWR tend to show that these admixtures cause a reduction in α_u , as shown in Figure E.22 through Figure E.24. The exception to this is the mixture with 100% cement C9 with MRWR, which causes a negligible change in α_u . Figure E.25 shows how α_u changes with the addition of ACCL. Figure E.26 shows this same trend with the cement only. α_u rises when paired with 100% C2 and C10, but tends to drop when paired with other mixtures with SCM's. The addition of AEA tends has little effect on α_u , as shown in Figure E.27.

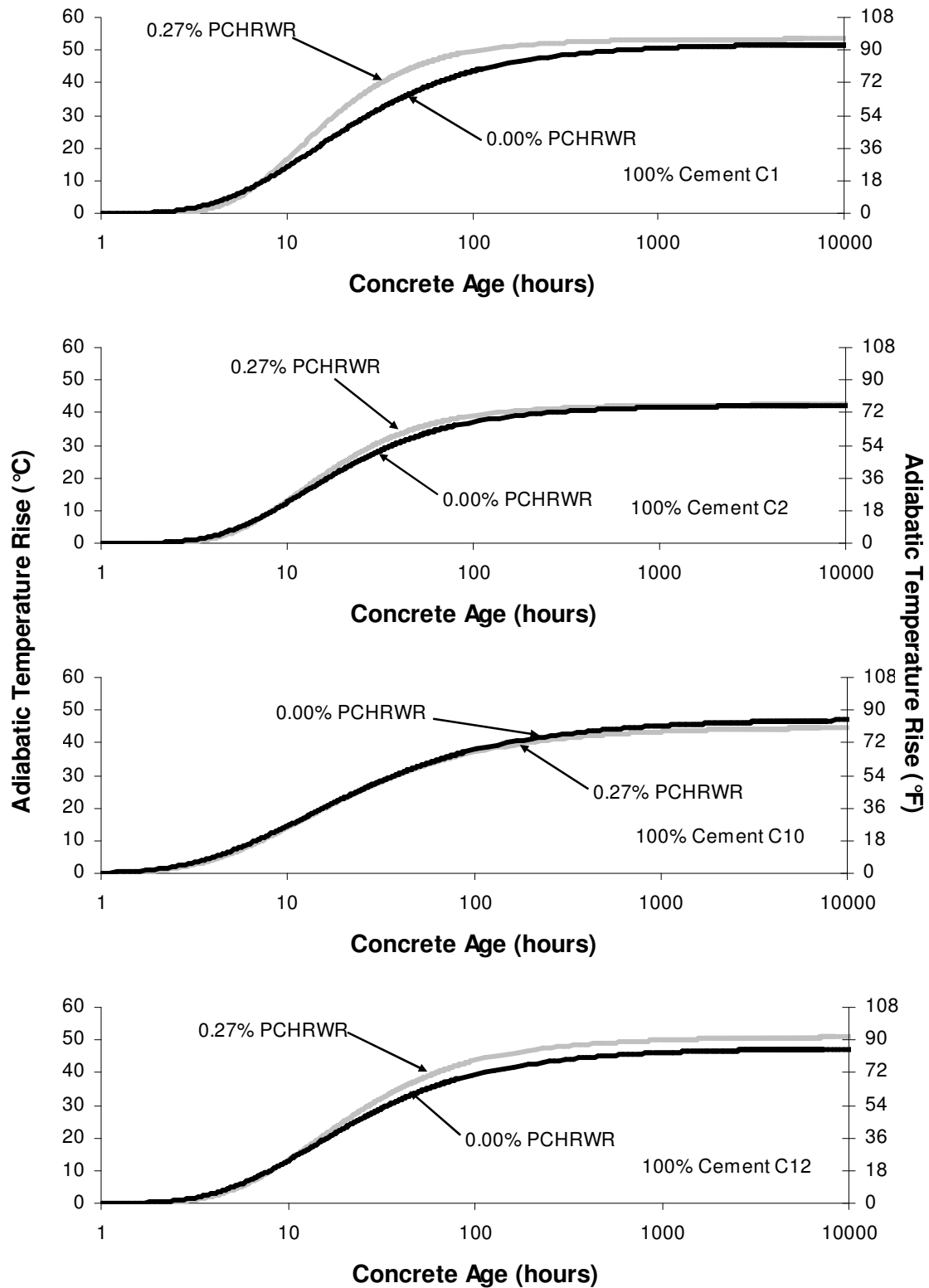


Figure E.1: Effects of Polycarboxylate-Based HRWR on Adiabatic Temperature Rise of Cement C1, C2, C10, and C12

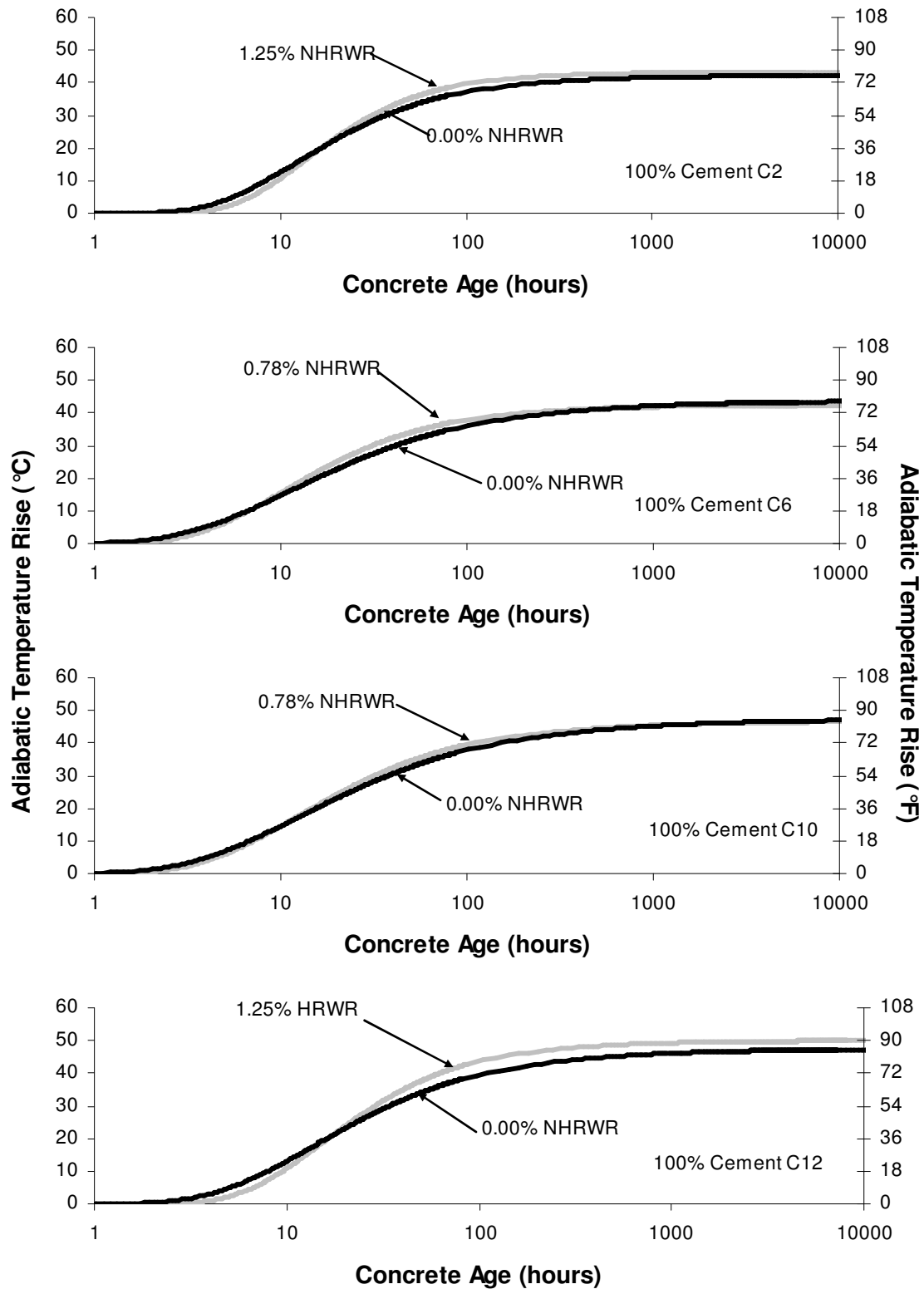


Figure E.2: Effects of Naphthalene-Based HRWR on Adiabatic Temperature Rise of Cement C2, C6, C10, and C12

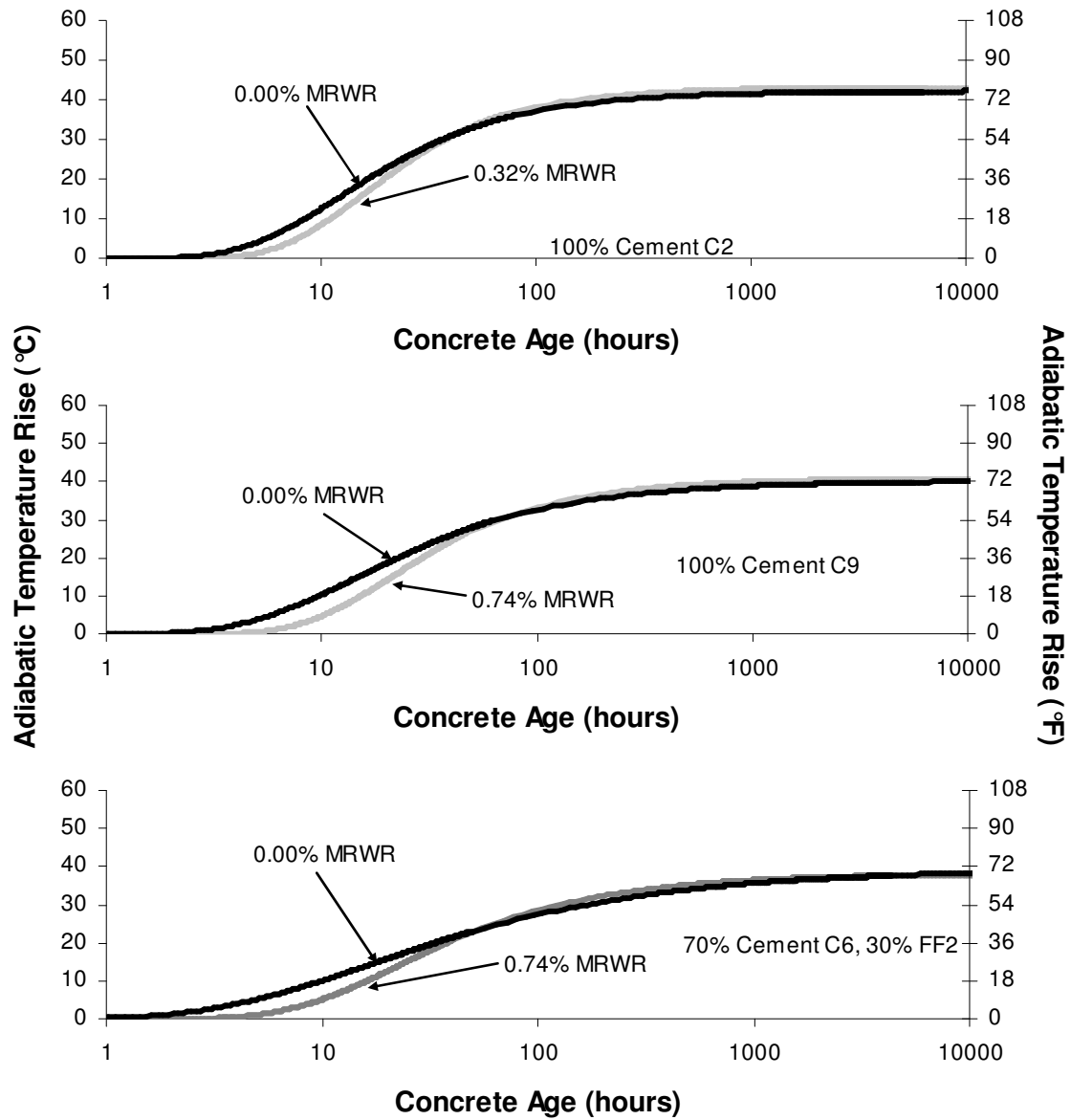


Figure E.3: Effects of MRWR on Adiabatic Temperature Rise

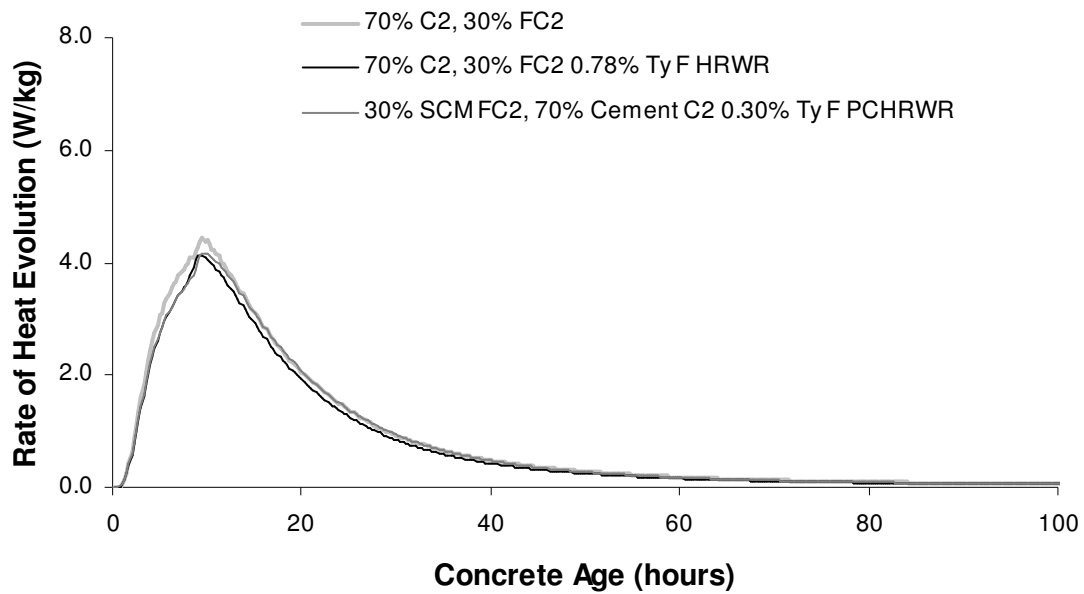


Figure E.4: Effects of Naphthalene and Polycarboxylate-Based HRWR on Rate of Heat Evolution of a Mixture of 70% Cement C2 and 30% SCM FC2

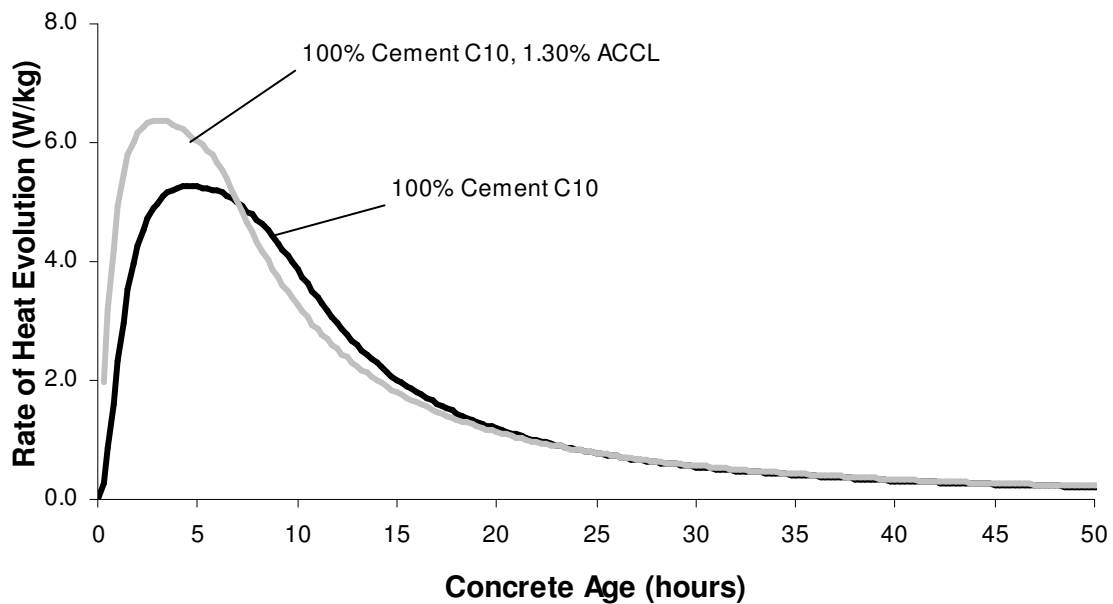


Figure E.5: Effects of Type C Non-Chloride Accelerator on Hydration of a Mixture of 100% Cement C6

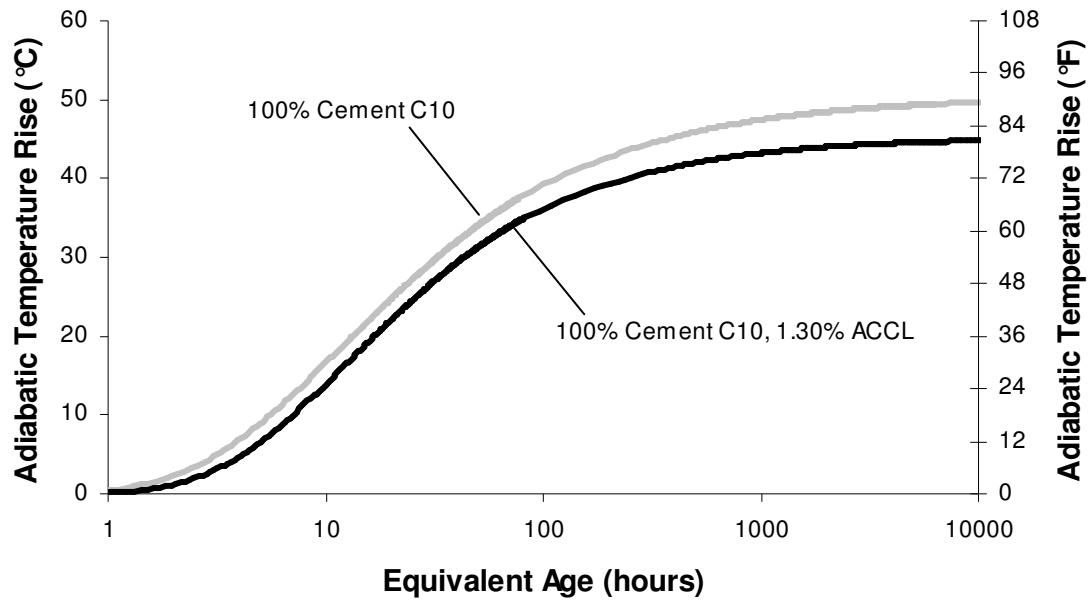


Figure E.6: Effects of Type C Non-Chloride Accelerator on Adiabatic Temperature Rise of a Mixture of 100% Cement C6

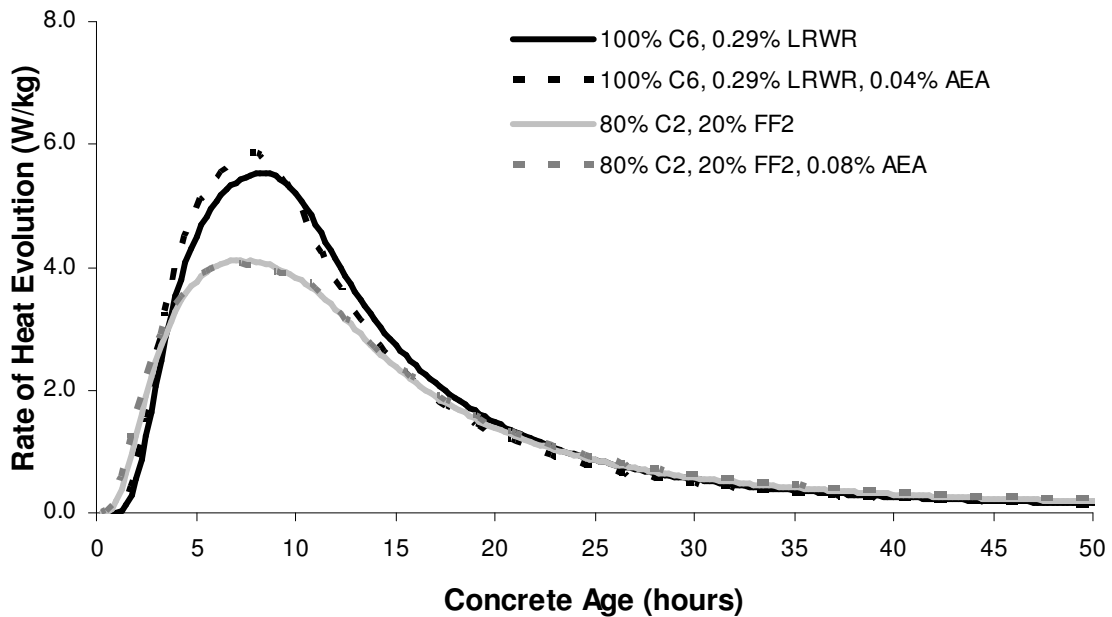


Figure E.7: Effects of Air Entraining Admixture on Hydration of a Mixture of 100% Cement C6 with LRWR and a Mixture of 80% Cement C2 and 20% Fly Ash FF2

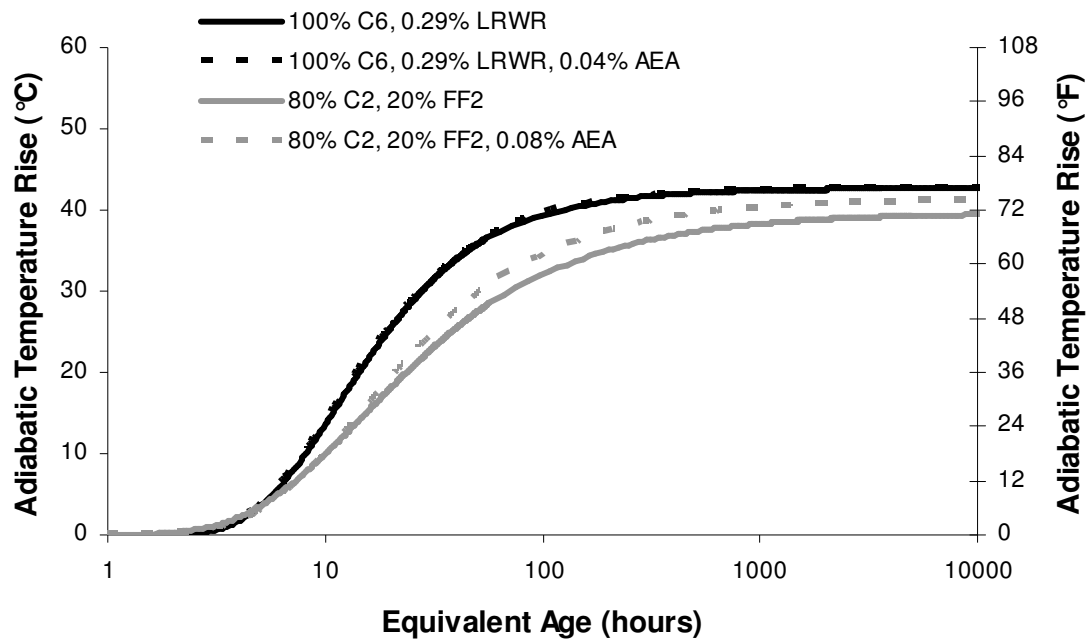


Figure E.8: Effects of Air Entraining Admixture on Adiabatic Temperature Rise of a Mixture of 100% Cement C6 with LRWR and a Mixture of 80% Cement C2 and 20% Fly Ash FF2

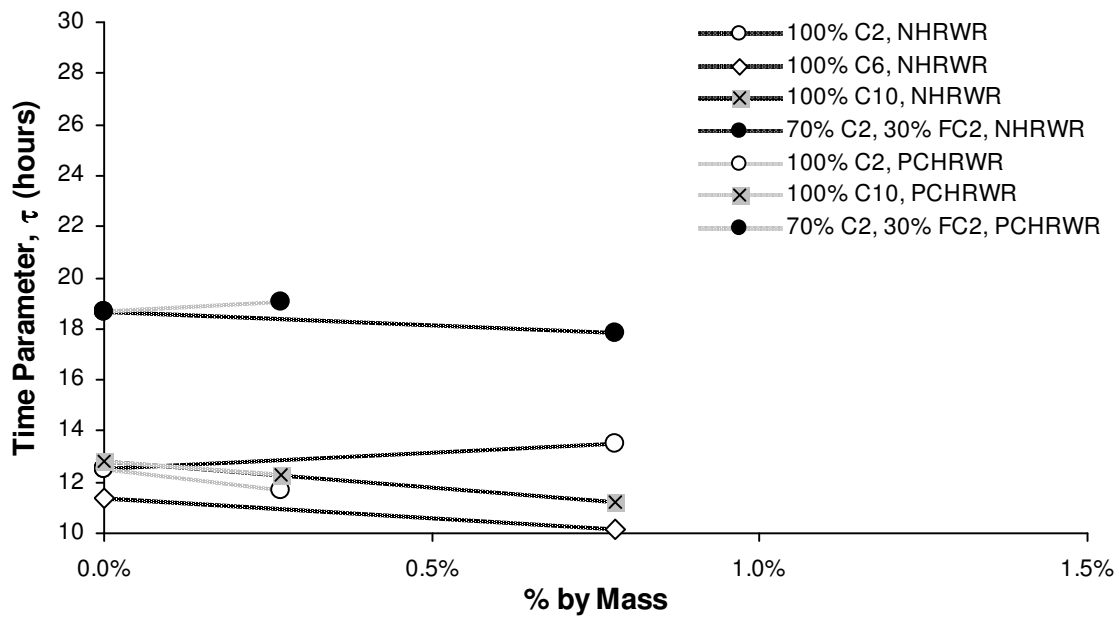


Figure E.9: Effects of Type F HRWR (N-Naphthalene, PC-Polycarboxylate) on Time Parameter (τ)

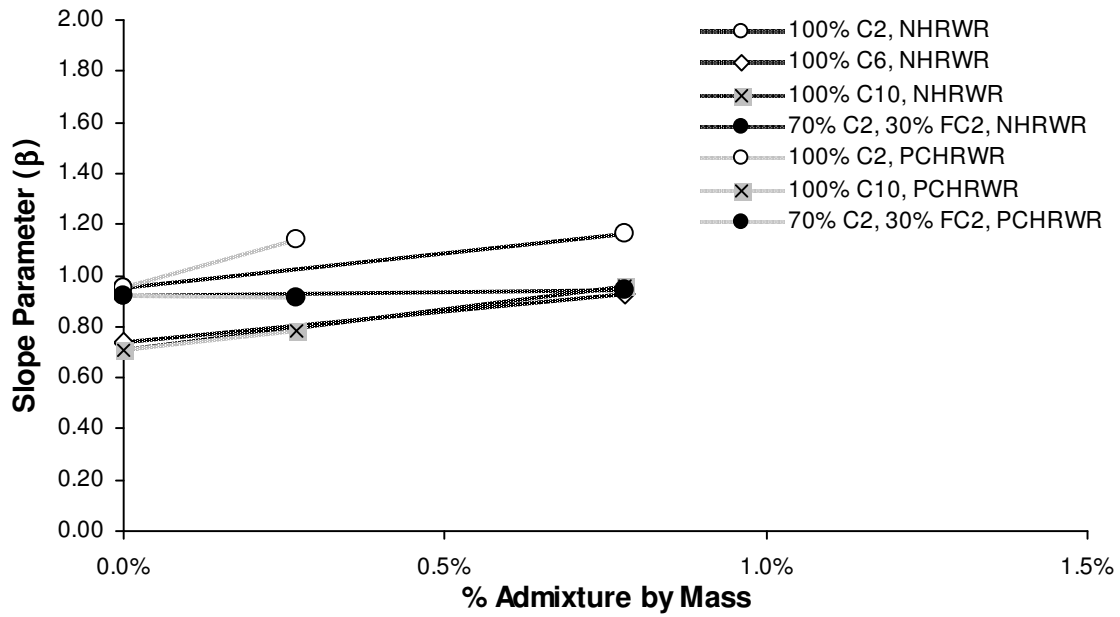


Figure E.10: Effects of Type F HRWR (N-Naphthalene, PC-Polycarboxylate) on Slope Parameter (β)

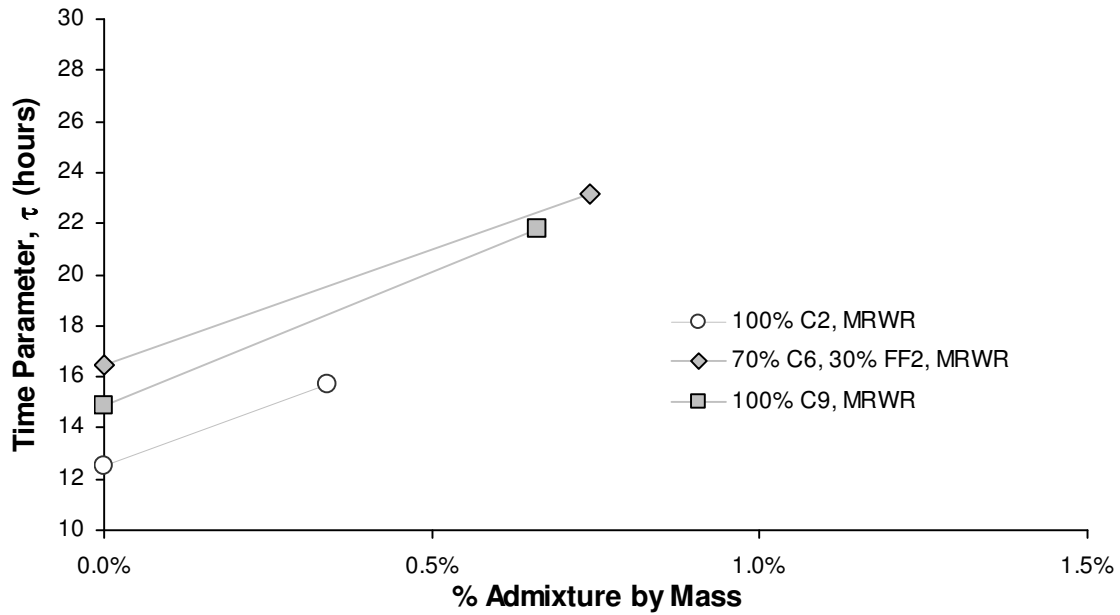


Figure E.11: Effects of Mid-Range Water Reducer (MRWR) on Time Parameter (τ)

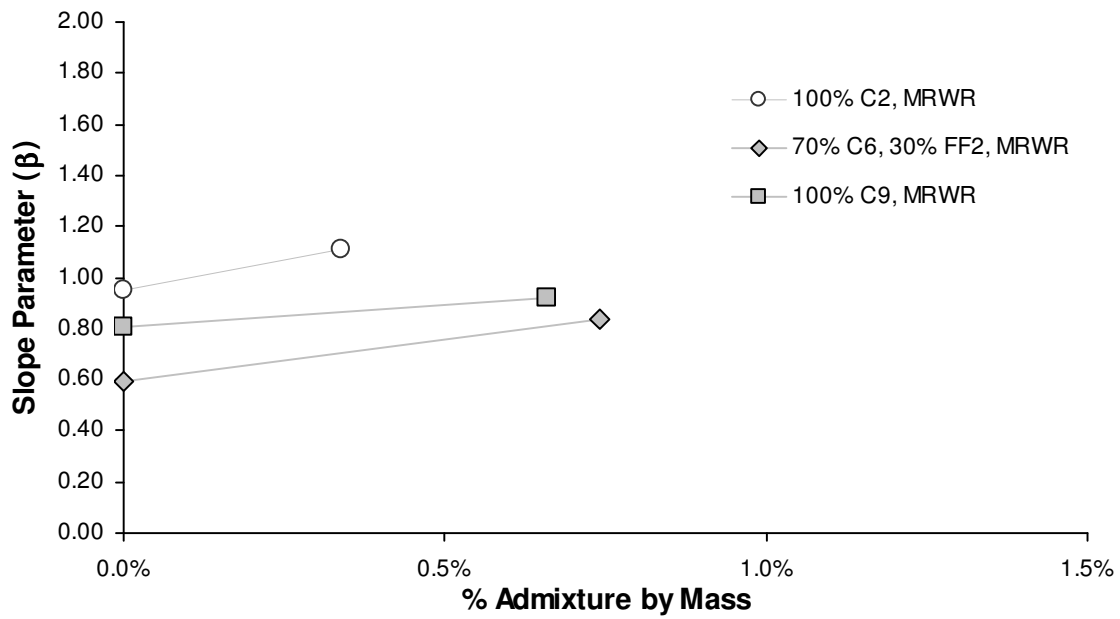


Figure E.12: Effects of MRWR on Slope Parameter (β)

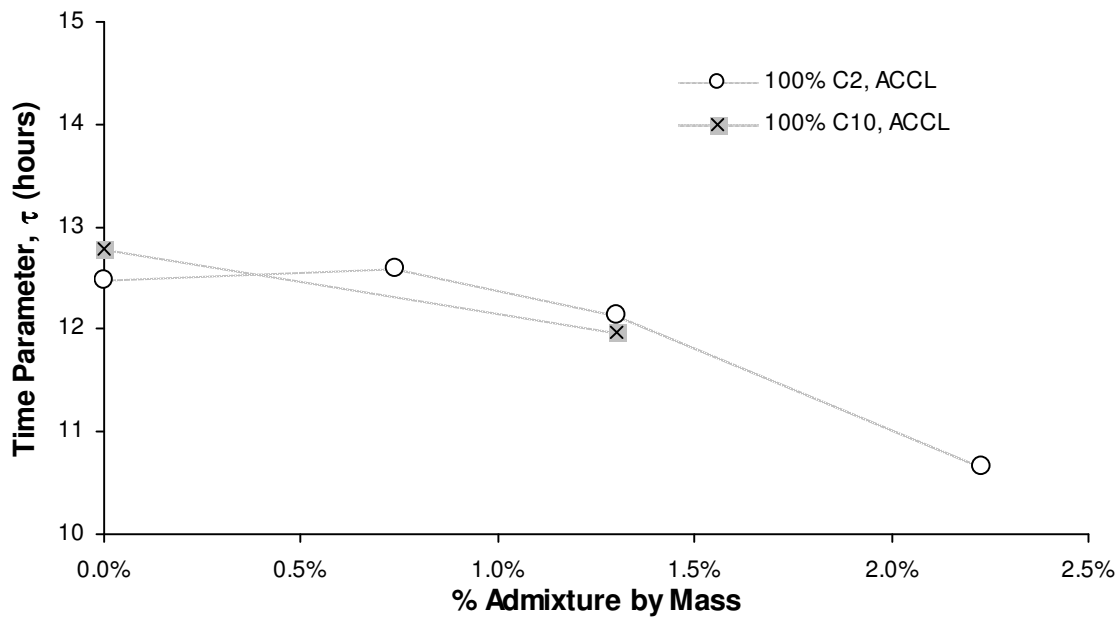


Figure E.13: Effects of Type C Accelerator (ACCL) on Time Parameter (τ) of 100% Cement

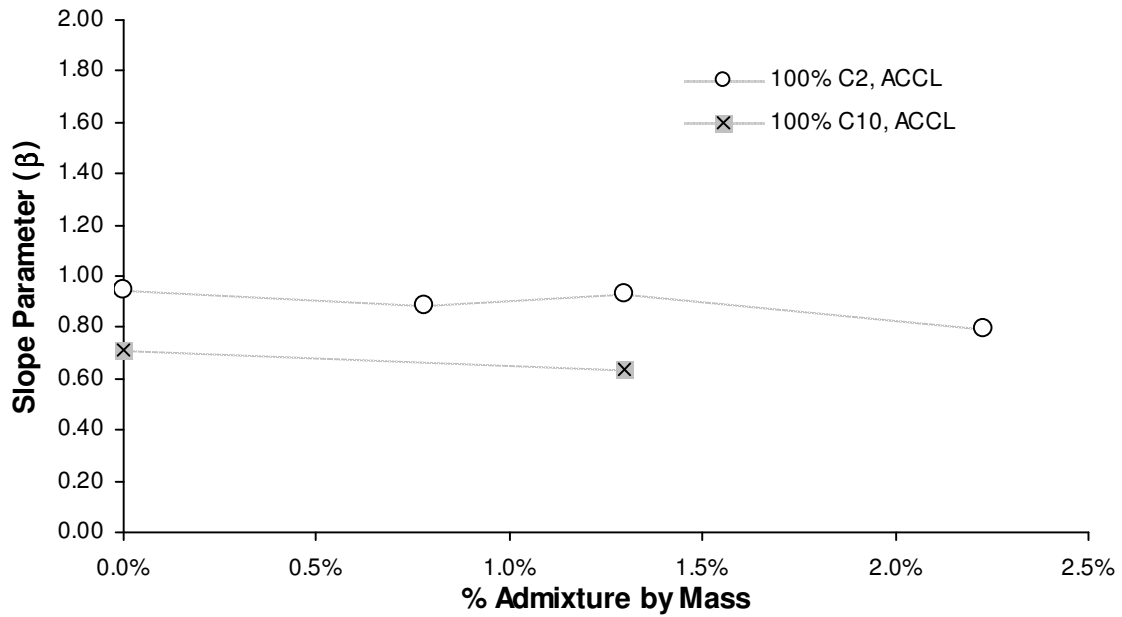


Figure E.14: Effects of Type C Accelerator (ACCL) on Slope Parameter (β) of 100% Cement

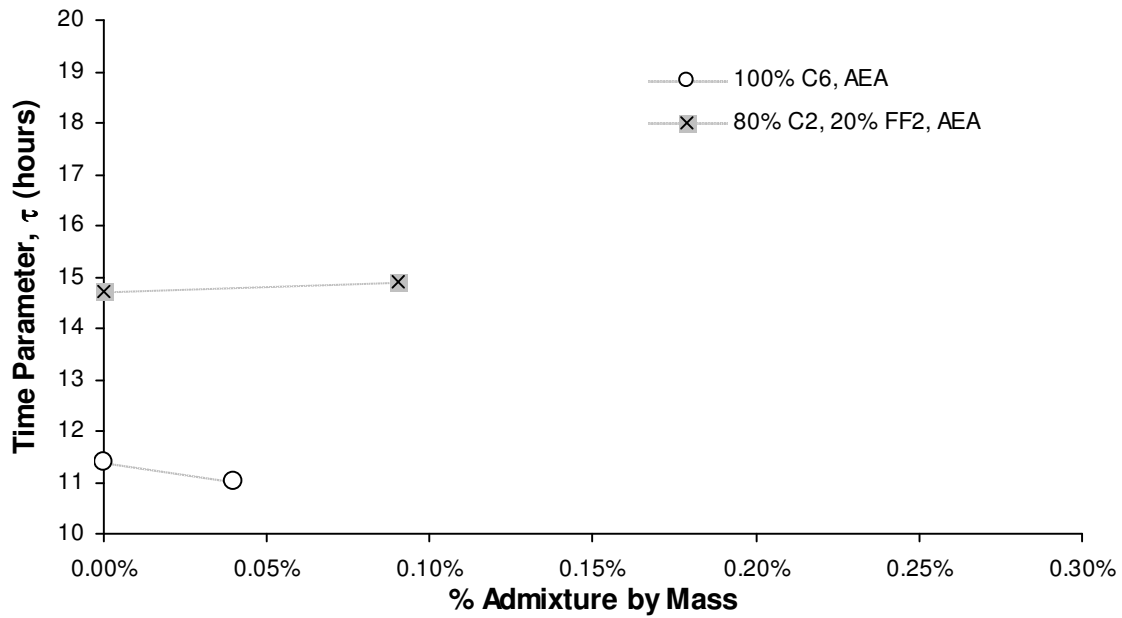


Figure E.15: Effects of Air Entraining Admixture (AEA) on Time Parameter (τ)

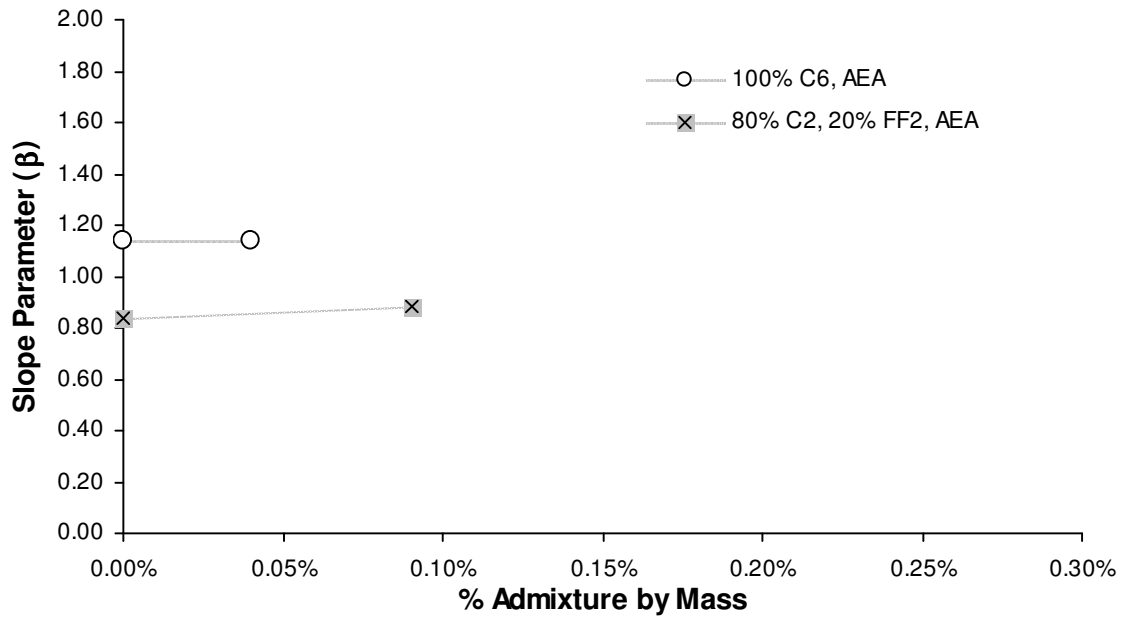


Figure E.16: Effects of Air Entraining Admixture (AEA) on Slope Parameter (β)

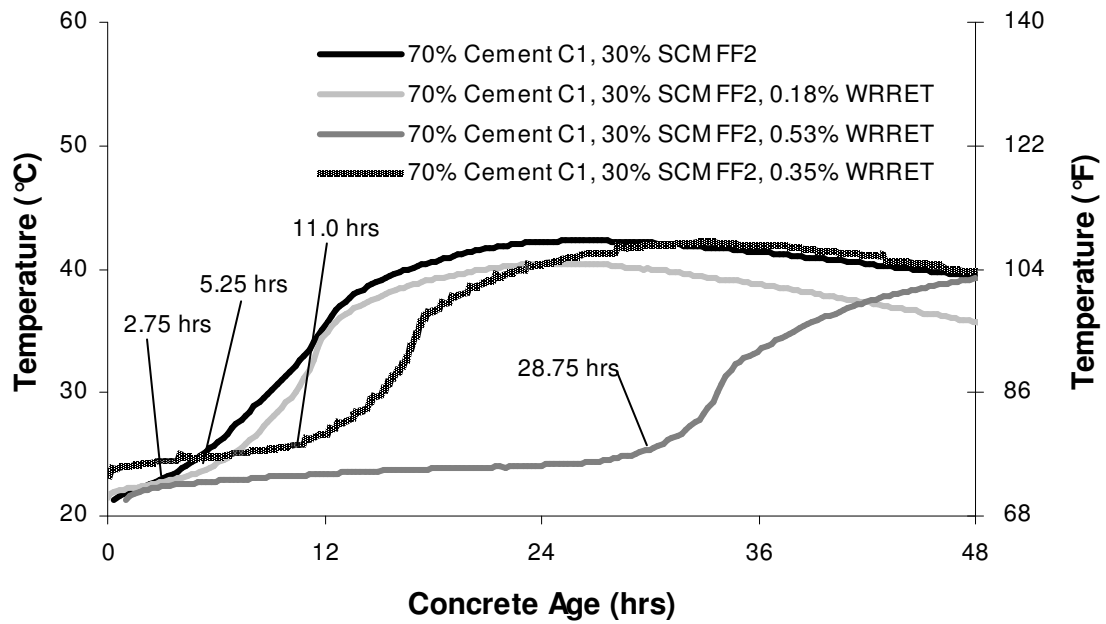


Figure E.17: Concrete Temperature for Mixtures of 70% C1, 30% FF2, and Different Dosages of WRRET

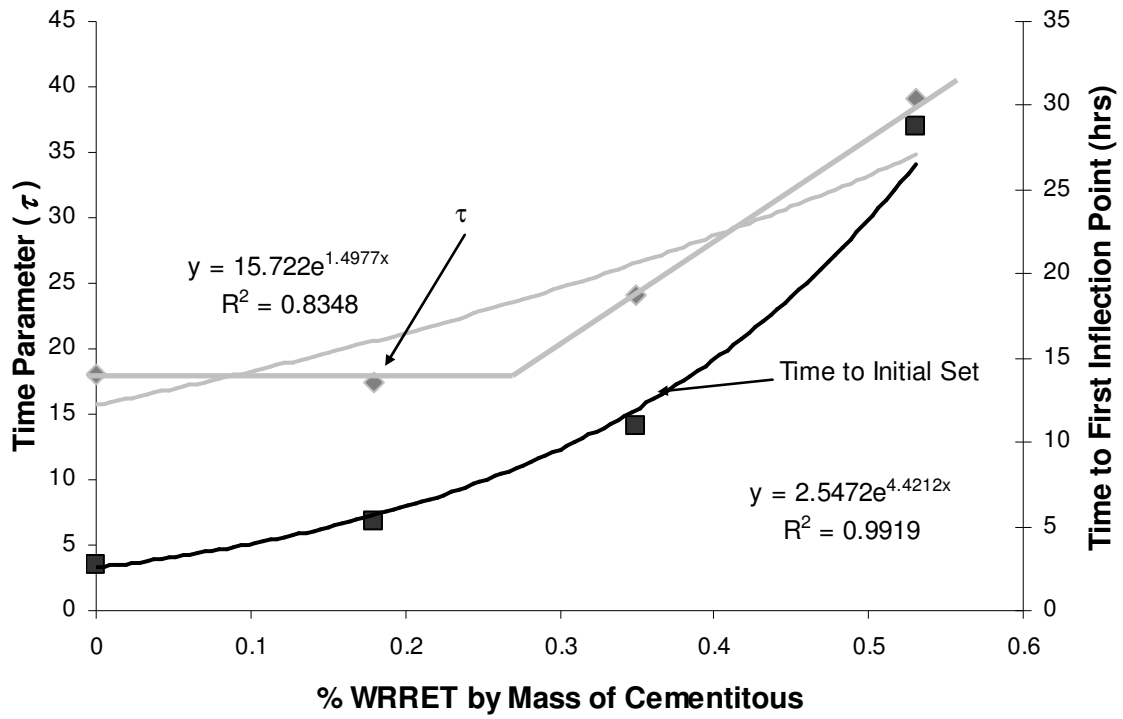


Figure E.18: Comparison Between Time of Set and Time Parameter (τ) for Mixtures of 70% C1, 30% FF2, and Different Dosages of WRRET

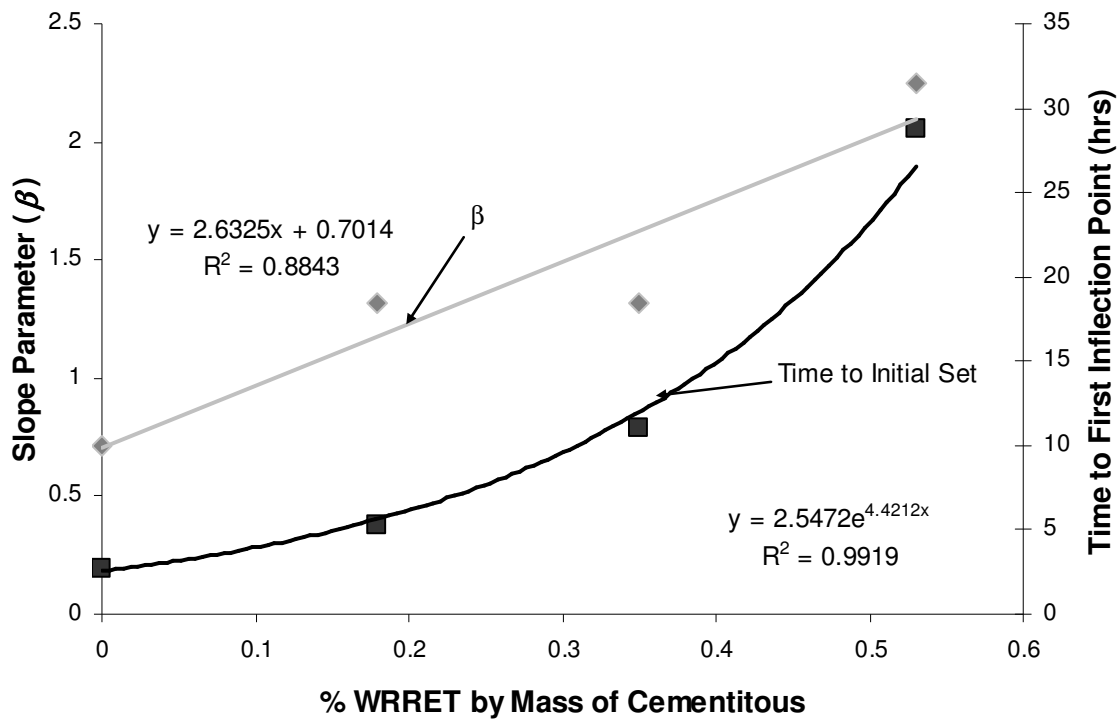


Figure E.19: Comparison Between Time of Set and Time Parameter (β) for Mixtures of 70% C1, 30% FF2, and Different Dosages of WRRET

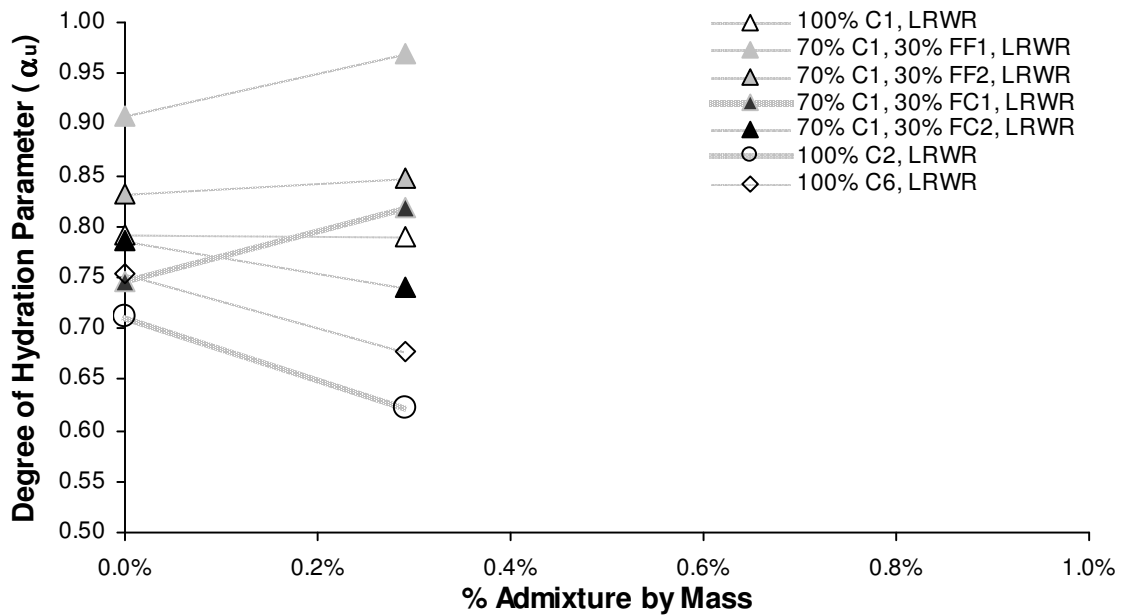


Figure E.20: Effects of Type A LRWR on Degree of Hydration Parameter (α_u)

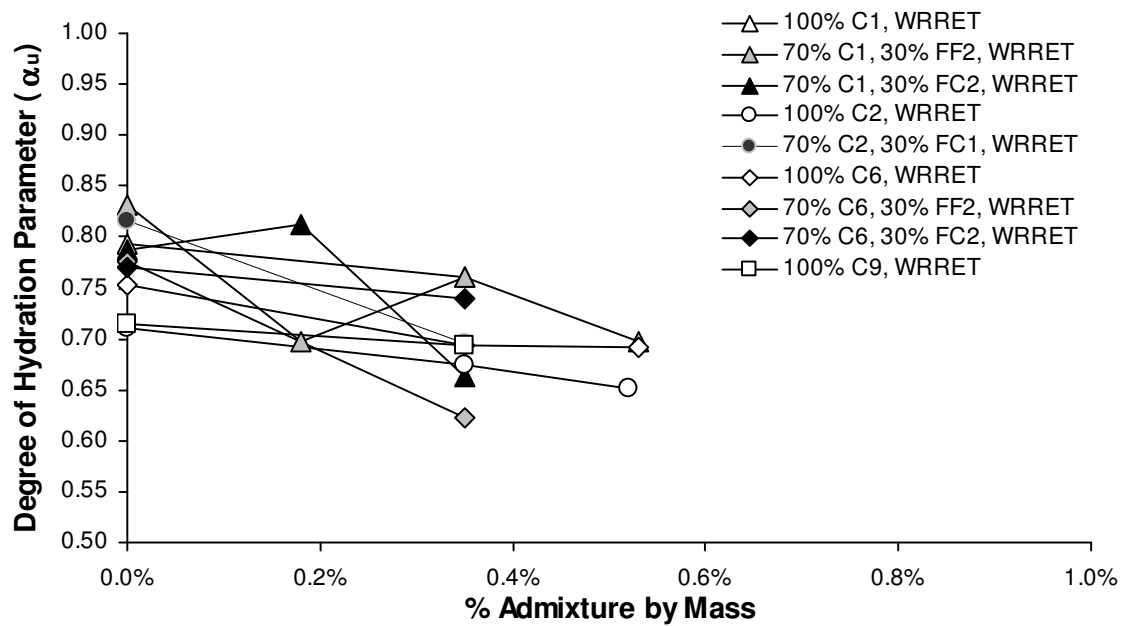


Figure E.21: Effects of Type B&D WRRET on Degree of Hydration Parameter (α_u)

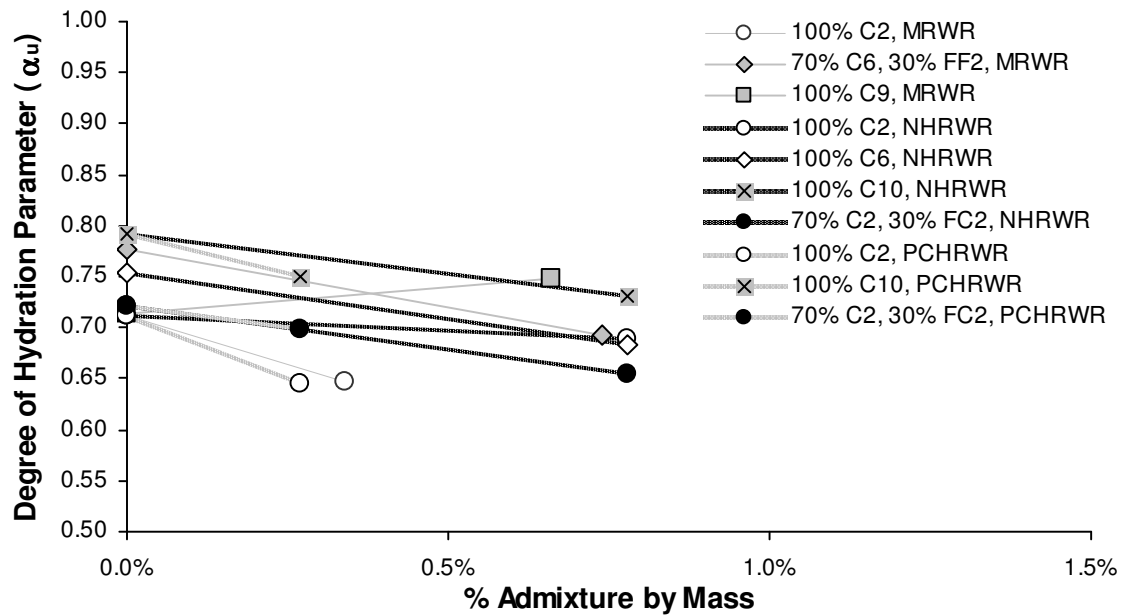


Figure E.22: Effects of Type F HRWR (N-Naphthalene, PC-Polycarboxylate, M-Mid-Range) on Degree of Hydration Parameter (α_u)

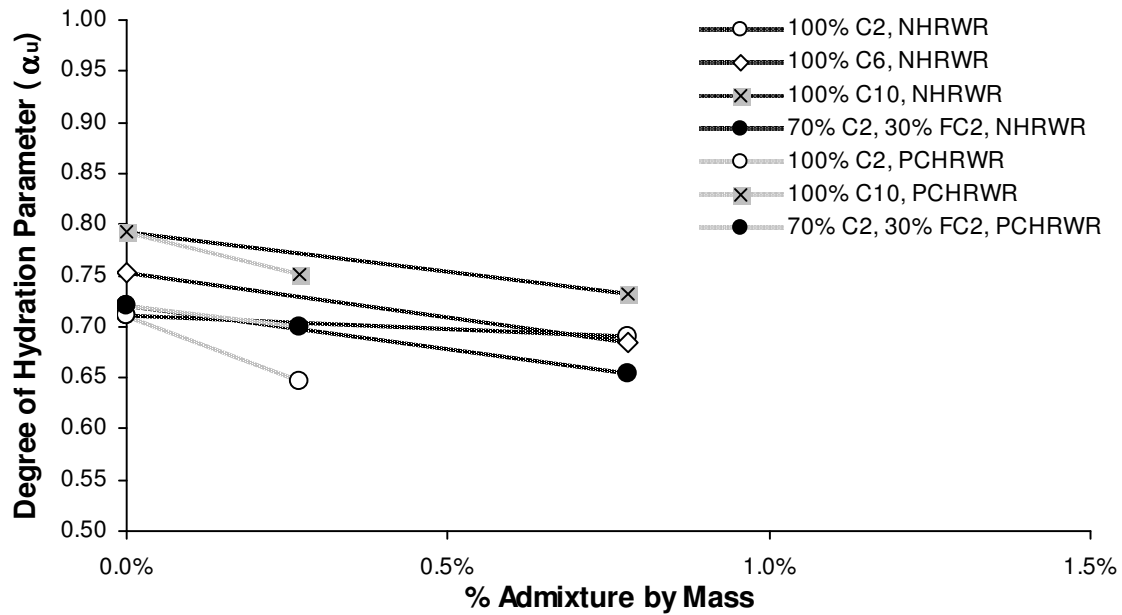


Figure E.23: Effects of Type F HRWR (N-Naphthalene, PC-Polycarboxylate) on Degree of Hydration Parameter (α_u)

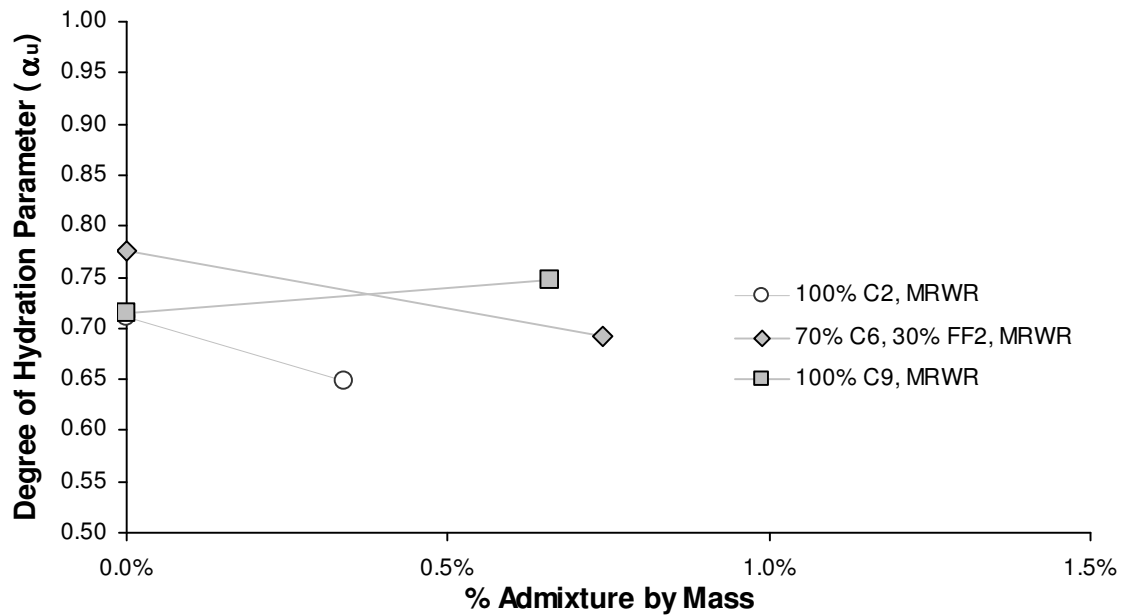


Figure E.24: Effects of MRWR on Degree of Hydration Parameter (α_u)

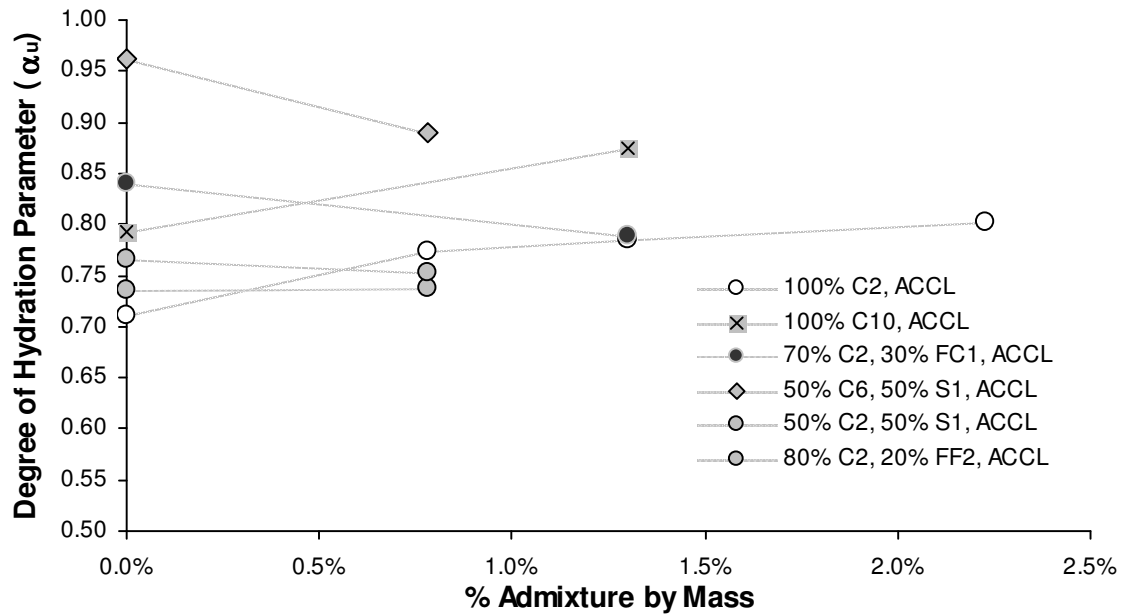


Figure E.25: Effects of Type C Accelerator (ACCL) on Degree of Hydration Parameter (α_u)

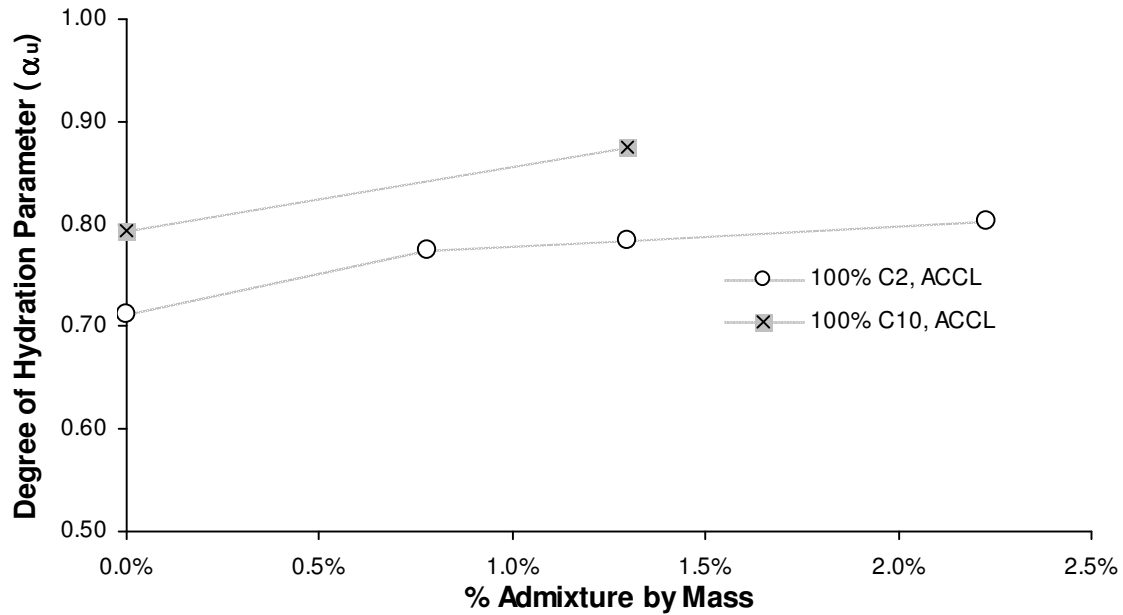


Figure E.26: Effect of Type C Accelerator (ACCL) on Degree of Hydration Parameter (α_u) for 100% Cement

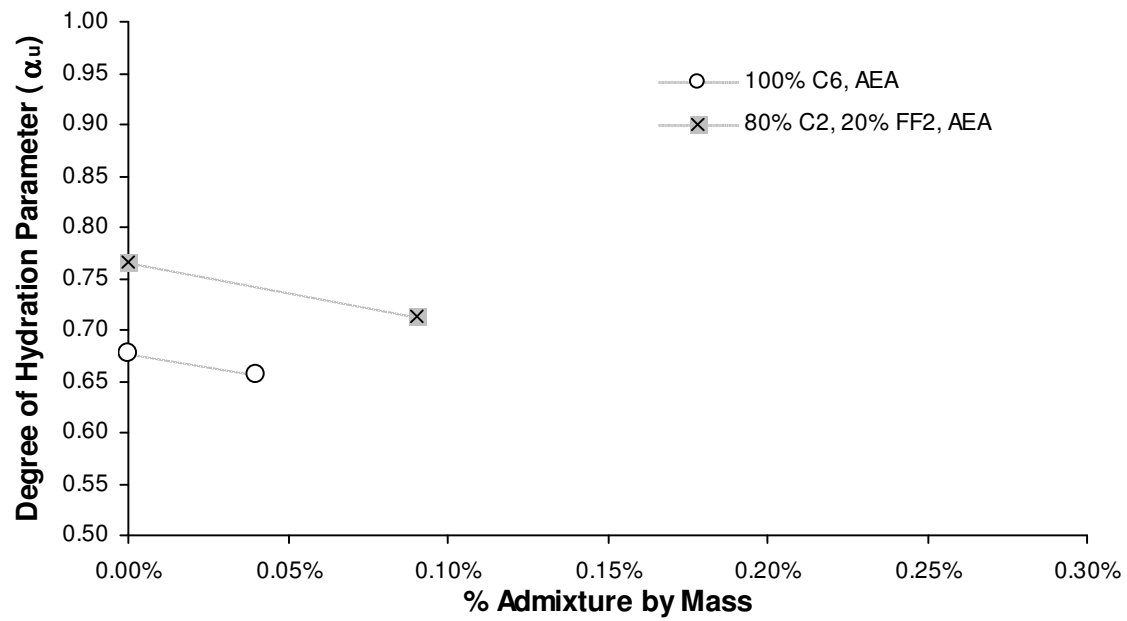


Figure E.27: Effects of Air Entraining Admixture (AEA) on Degree of Hydration Parameter (α_u)

APPENDIX F. ADDITIONAL SEMI-ADIABATIC CALORIMETER RESULTS FOR CHAPTER 8

The adiabatic temperature rise of a concrete mixture provides the best method to quantify the combined effects of different mixture constituents. The following plots show the adiabatic temperature rise for the mixtures in Chapter 7. These results provide background to the trends that are presented in this chapter.

F.1. ADIABATIC TEMPERATURE RISE OF MIXTURES WITH CLASS F FLY ASH

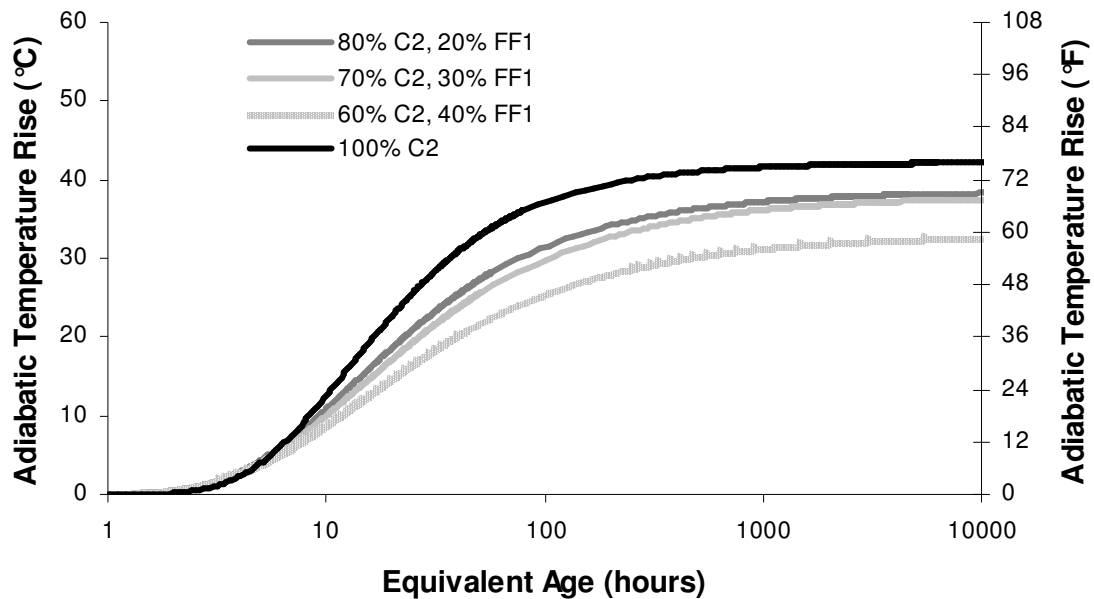


Figure F.1: Adiabatic Temperature Rise of Cement C2 with Fly Ash FF1

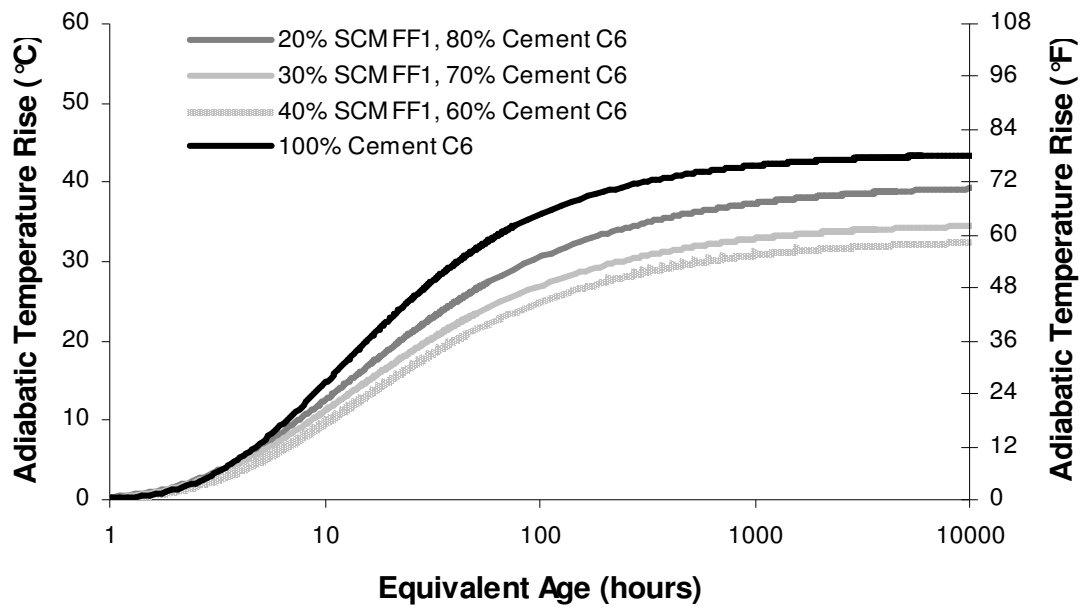


Figure F.2: Adiabatic Temperature Rise of Cement C6 with Fly Ash FF1

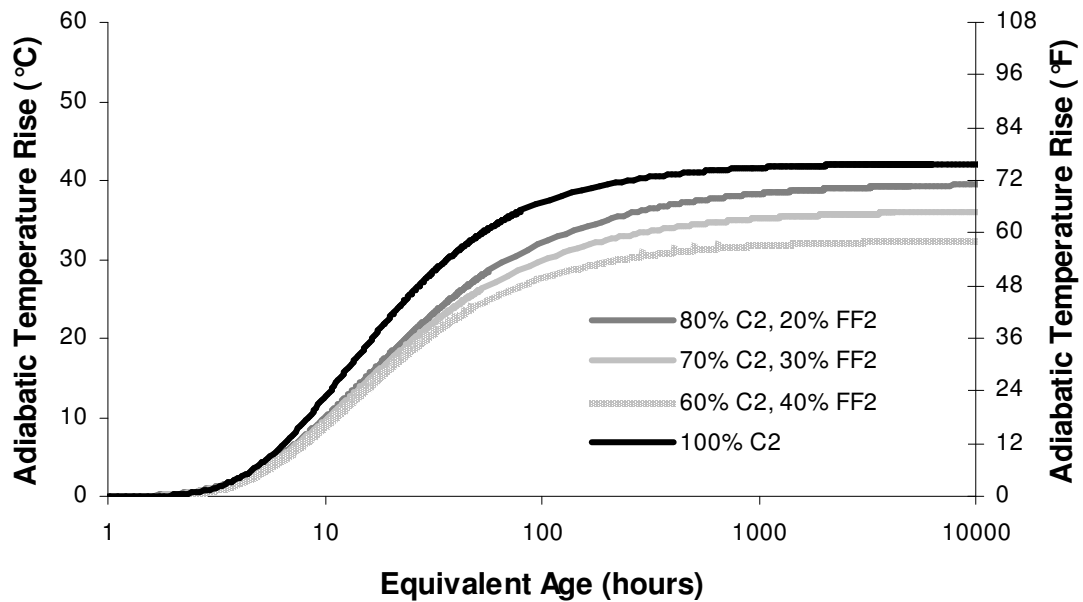


Figure F.3: Adiabatic Temperature Rise of Cement C2 with Fly Ash FF2

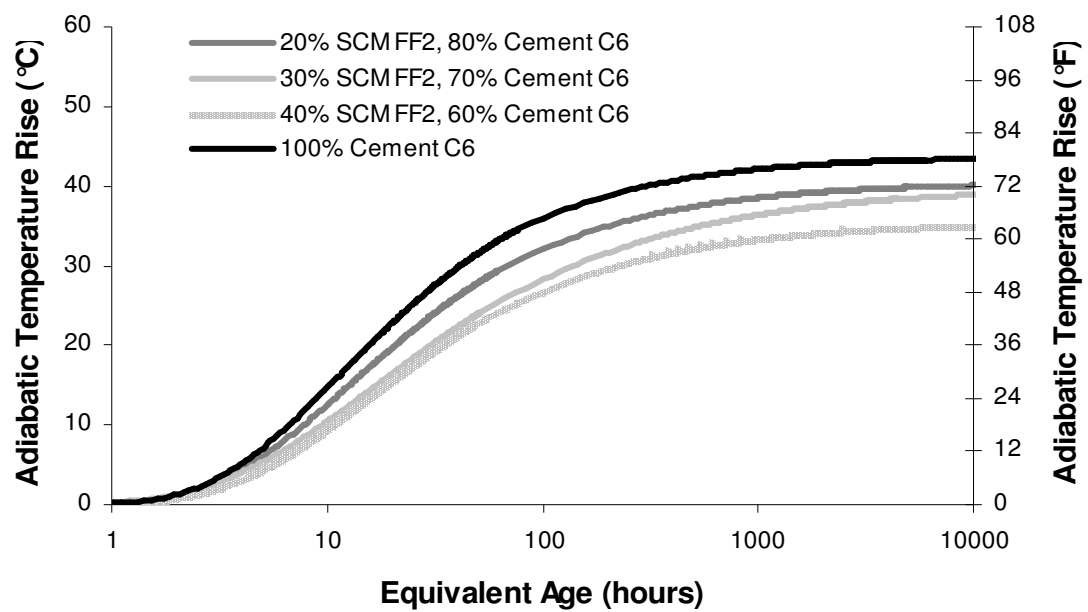


Figure F.4: Adiabatic Temperature Rise of Cement C6 with Fly Ash FF2

F.2. ADIABATIC TEMPERATURE RISE OF MIXTURES WITH CLASS C FLY ASH

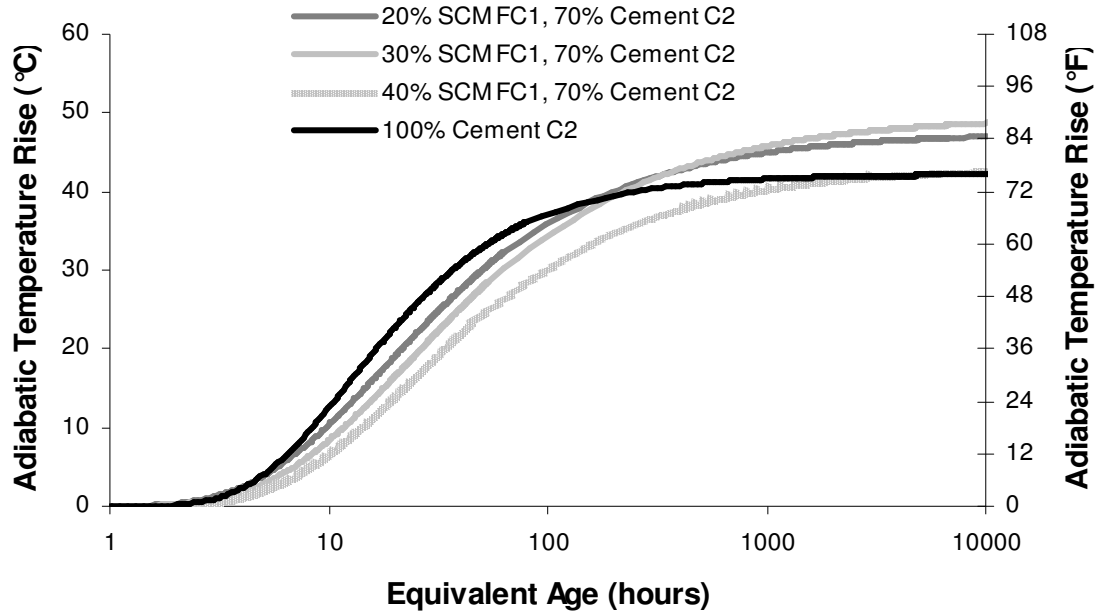


Figure F.5: Adiabatic Temperature Rise of Cement C2 with Fly Ash FC1

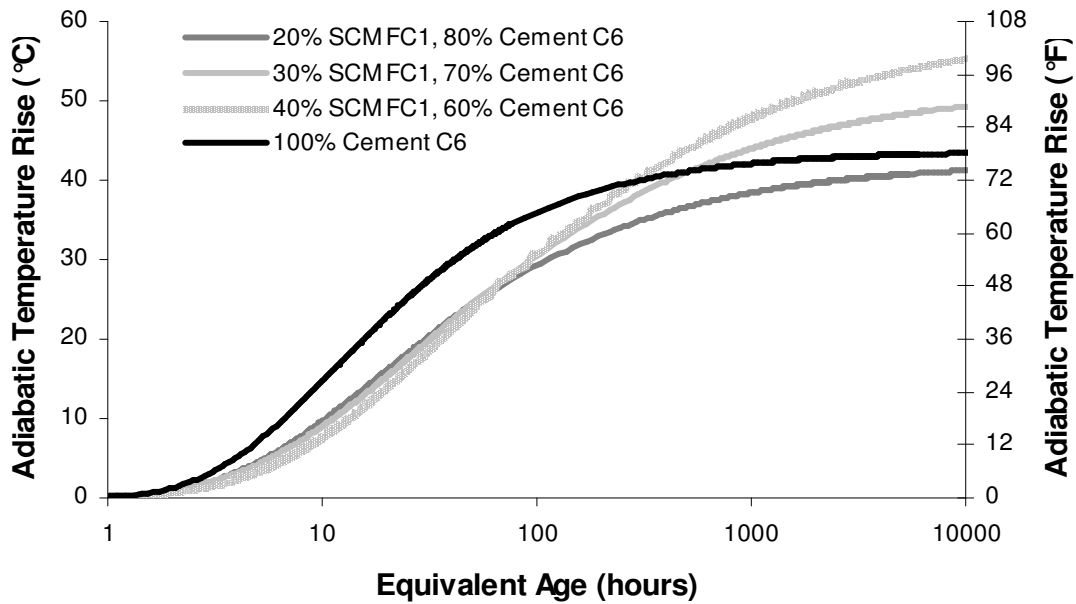


Figure F.6: Adiabatic Temperature Rise of Cement C6 with Fly Ash FC1

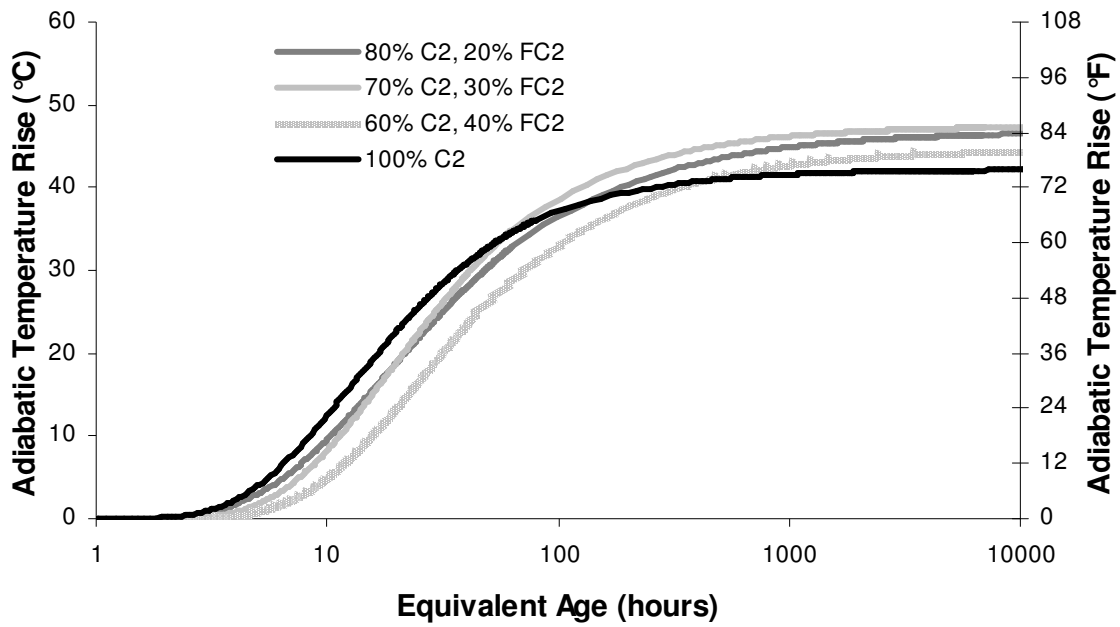


Figure F.7: Adiabatic Temperature Rise of Cement C2 with Fly Ash FC2

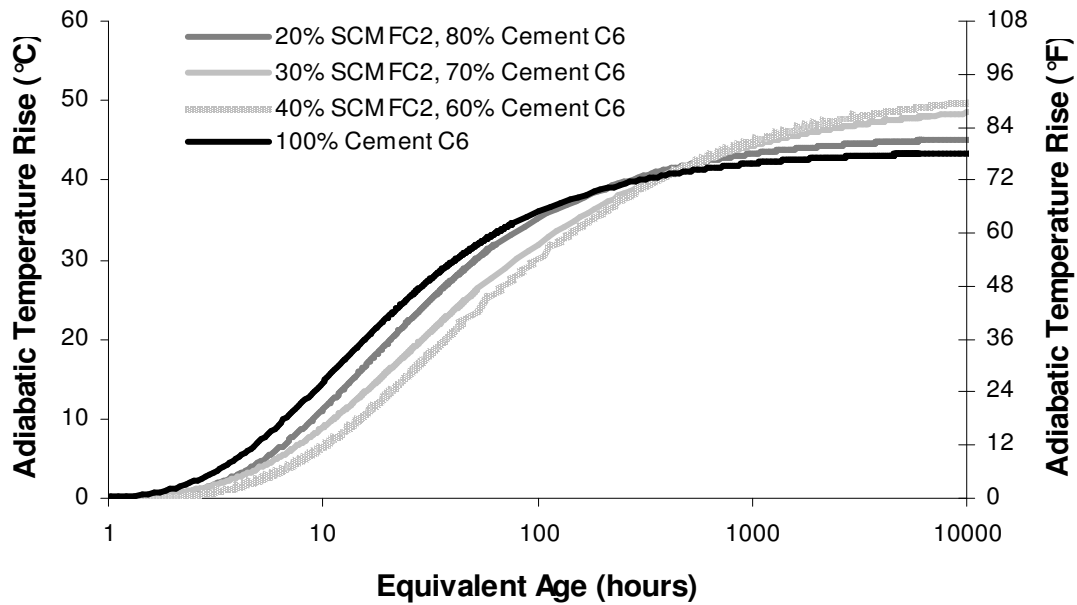


Figure F.8: Adiabatic Temperature Rise of Cement C6 with FC2

F.3. ADIABATIC TEMPERATURE RISE OF MIXTURES GGBF SLAG – S1

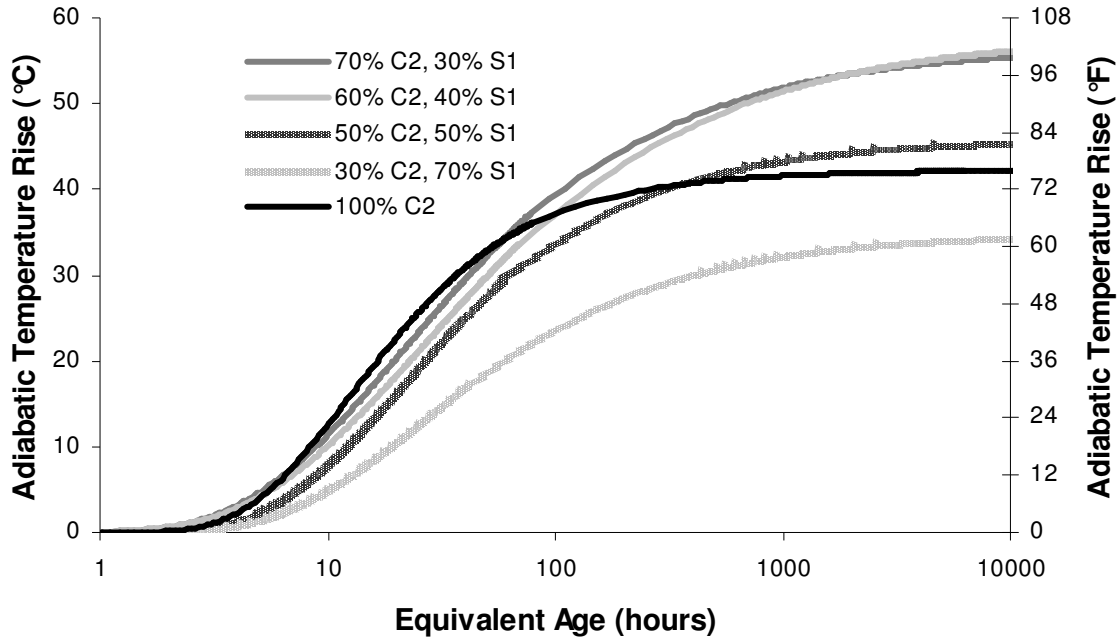


Figure F.9: Adiabatic Temperature Rise of Cement C2 with S1

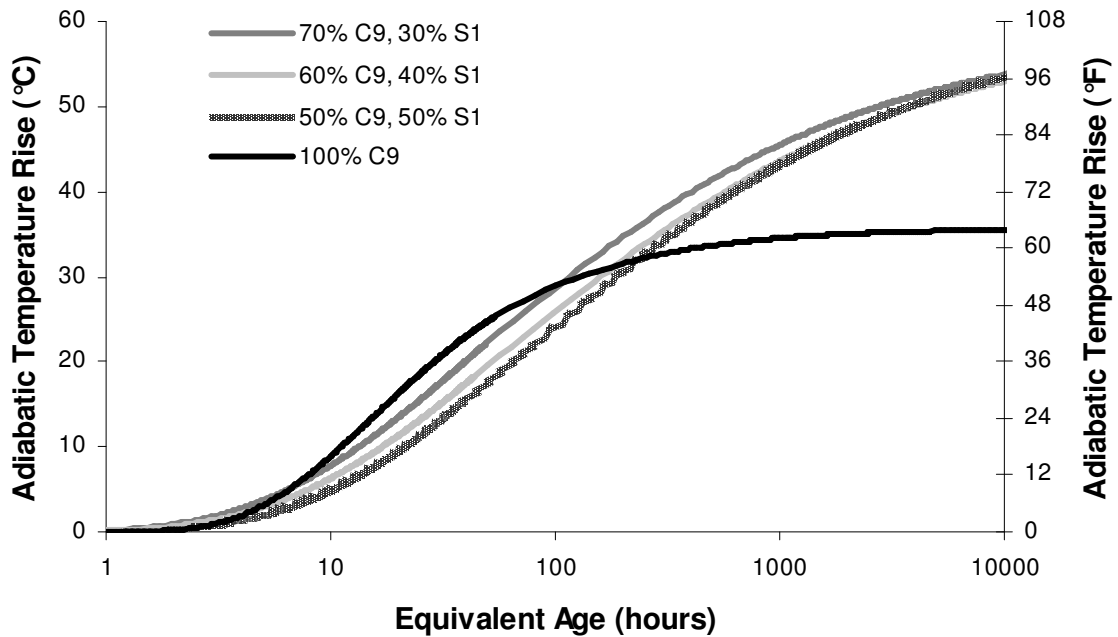


Figure F.10: Adiabatic Temperature Rise of Cement C6 with S1

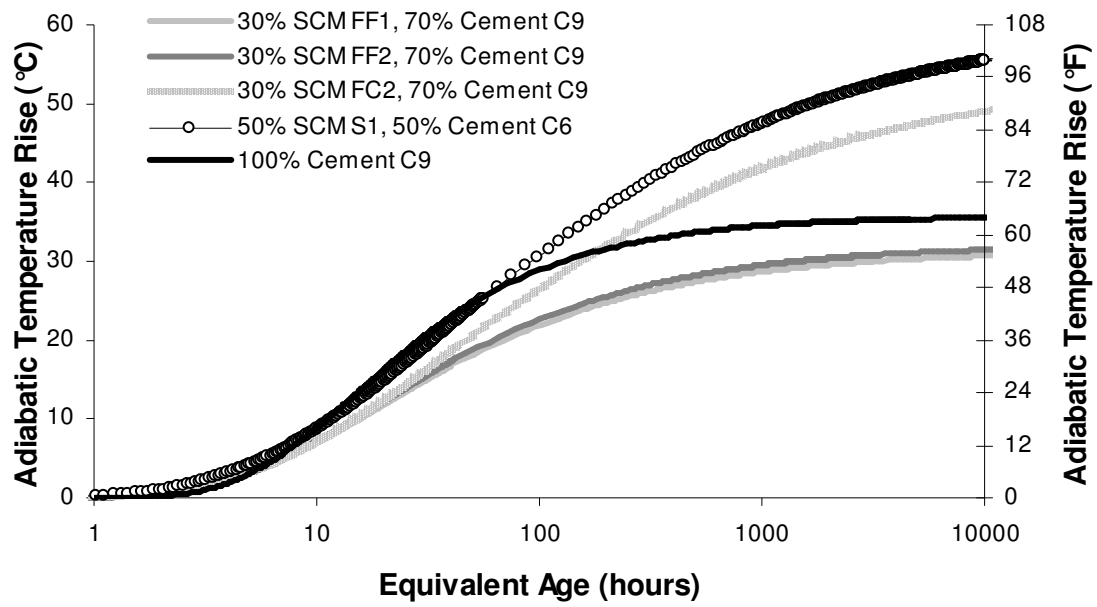


Figure F.11: Adiabatic Temperature Rise of Cement C9 with Different SCM's

F.4. ADIABATIC TEMPERATURE RISE OF MIXTURES WITH SILICA FUME

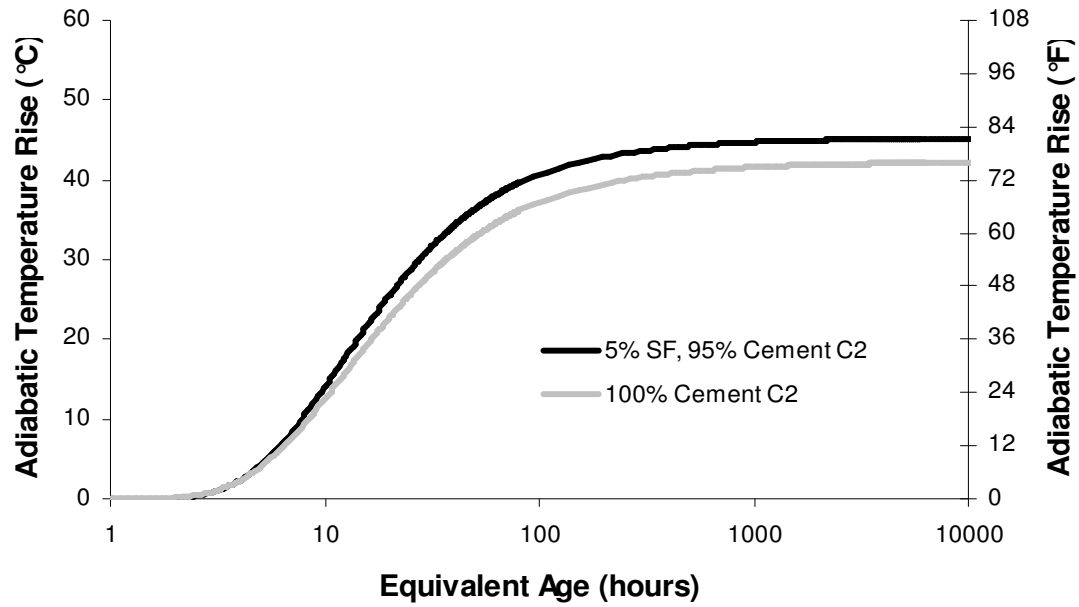


Figure F.12: Adiabatic Temperature Rise of Cement C2 with Silica Fume

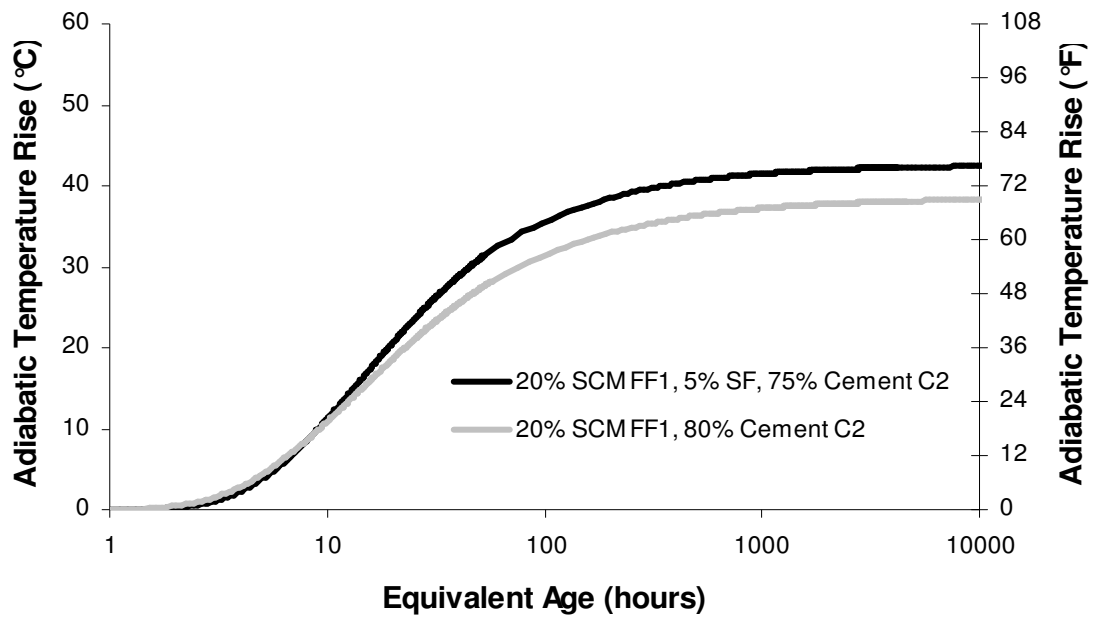


Figure F.13: Adiabatic Temperature Rise of Cement C2 and 20% FF1 with Silica Fume

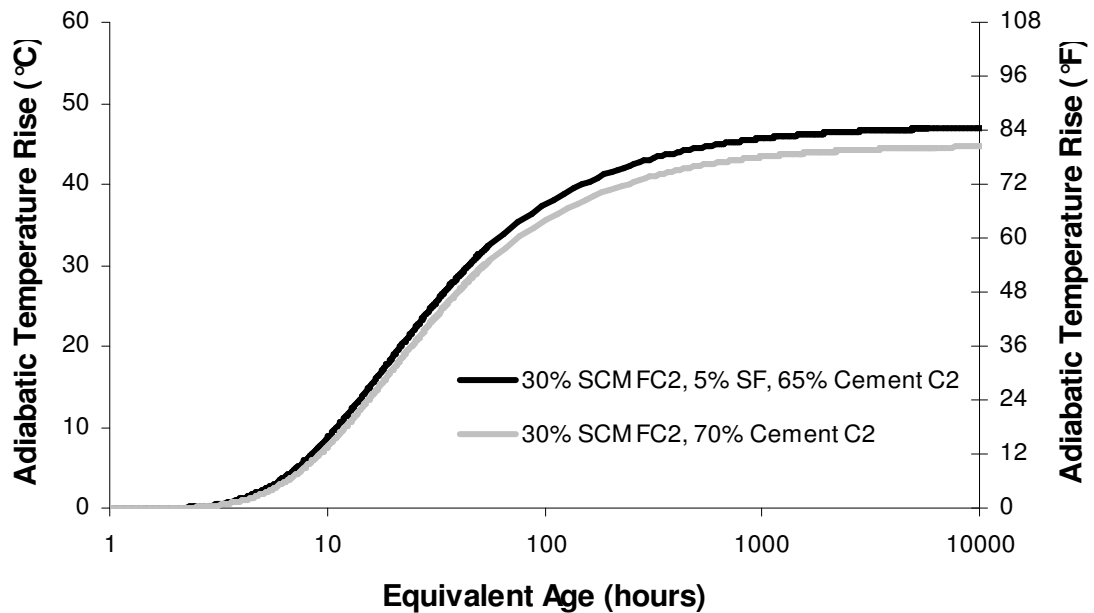


Figure F.14: Adiabatic Temperature Rise of Cement C2 and 30% FC2 with Silica Fume

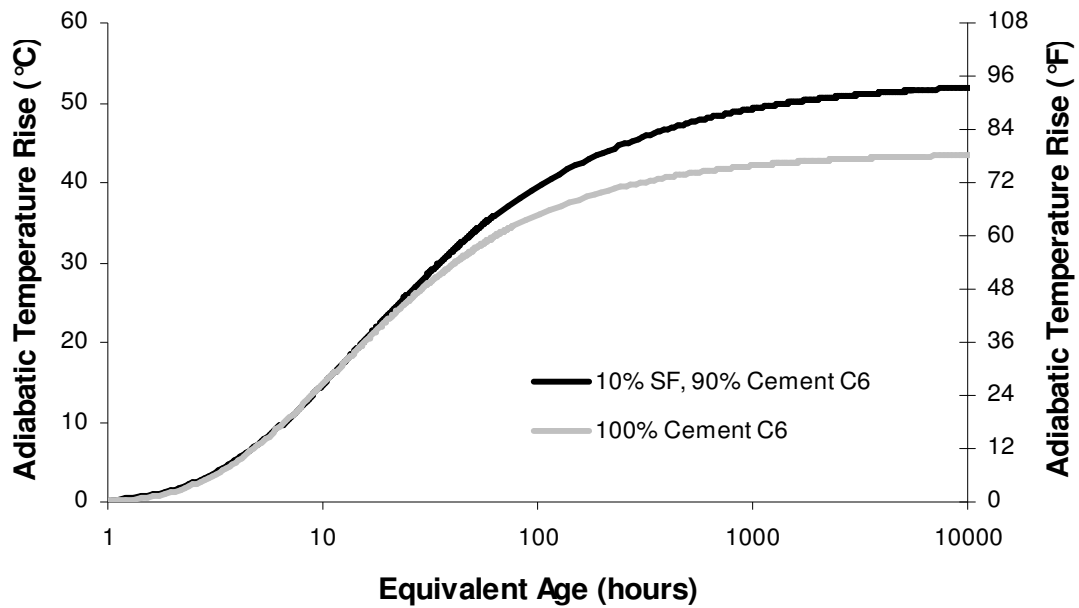


Figure F.15: Adiabatic Temperature Rise of Cement C6 with Silica Fume

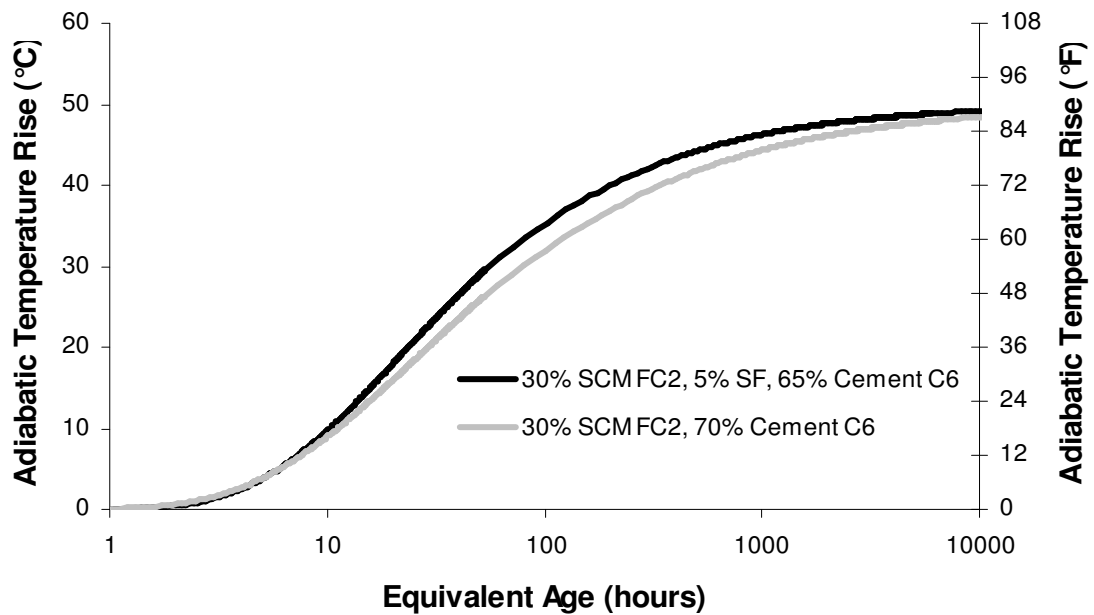


Figure F.16: Adiabatic Temperature Rise of Cement C6 and 30% Fly Ash FC2 with Silica Fume

F.5. RATE OF HEAT EVOLUTION FOR MIXTURES WITH CEMENT C6 AND FLY ASH

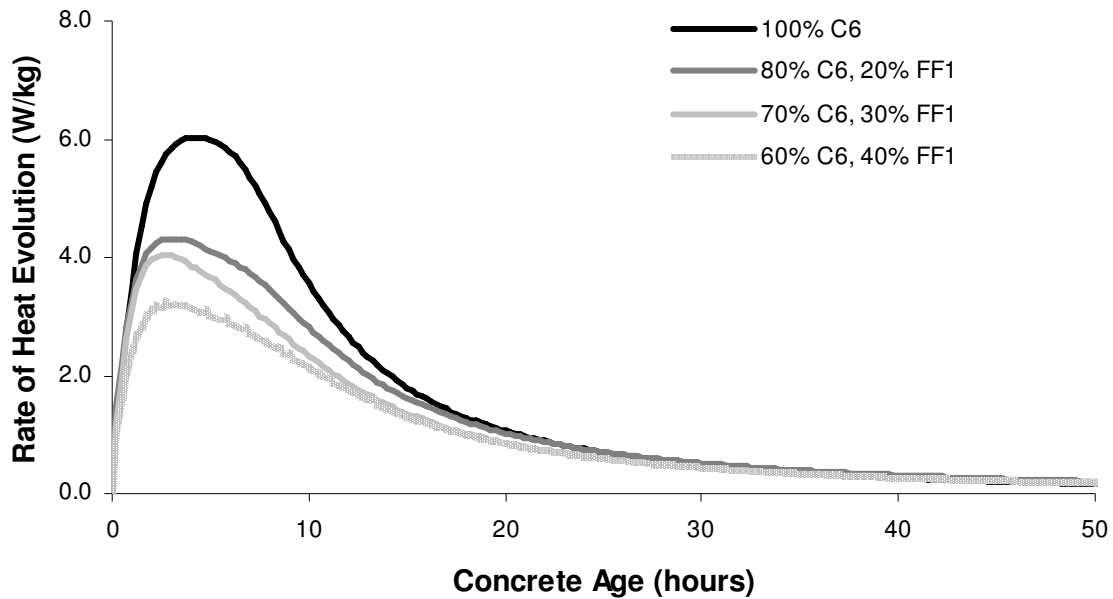


Figure F.17: Rate of Heat Evolution per Kilogram of Cementitious for Cement C6 with FF1, Normalized per Kilogram of Cementitious Material

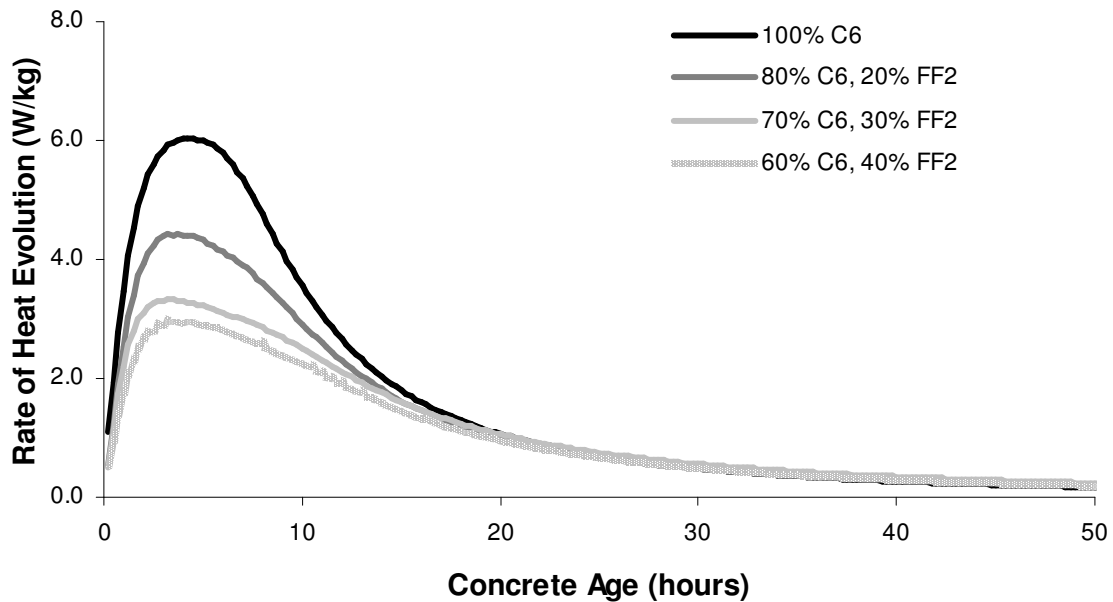


Figure F.18: Rate of Heat Evolution per Kilogram of Cementitious for Cement C6 with FF2, Normalized per Kilogram of Cementitious Material

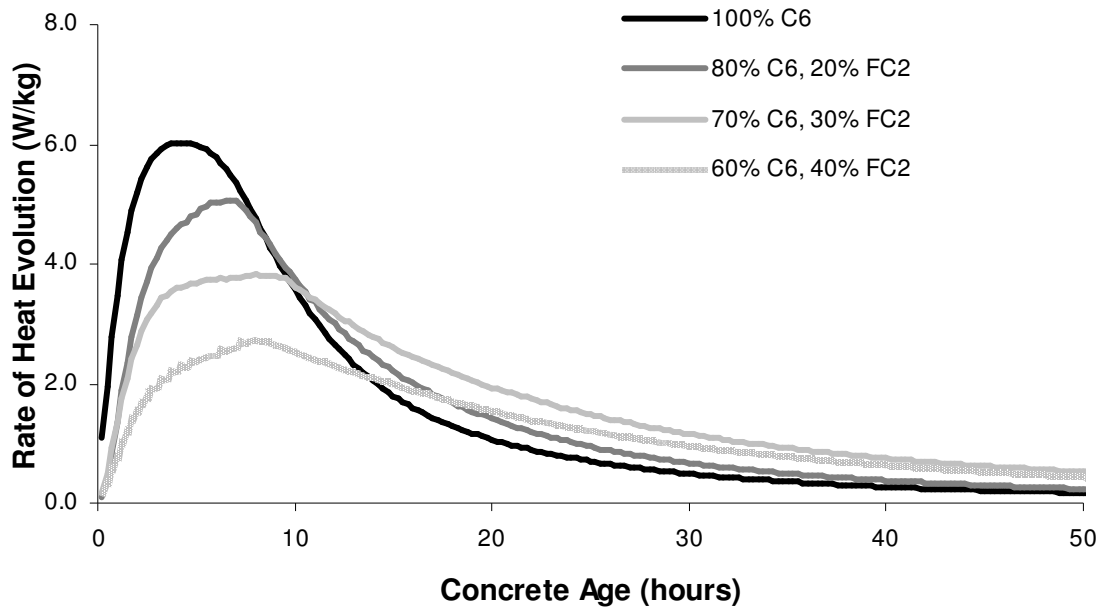


Figure F.19: Rate of Heat Evolution per Kilogram of Cementitious for Cement C6 with Fly Ash FC2, Normalized per Kilogram of Cementitious Material

F.6. RATE OF HEAT EVOLUTION NORMALIZED BY CEMENT CONTENT

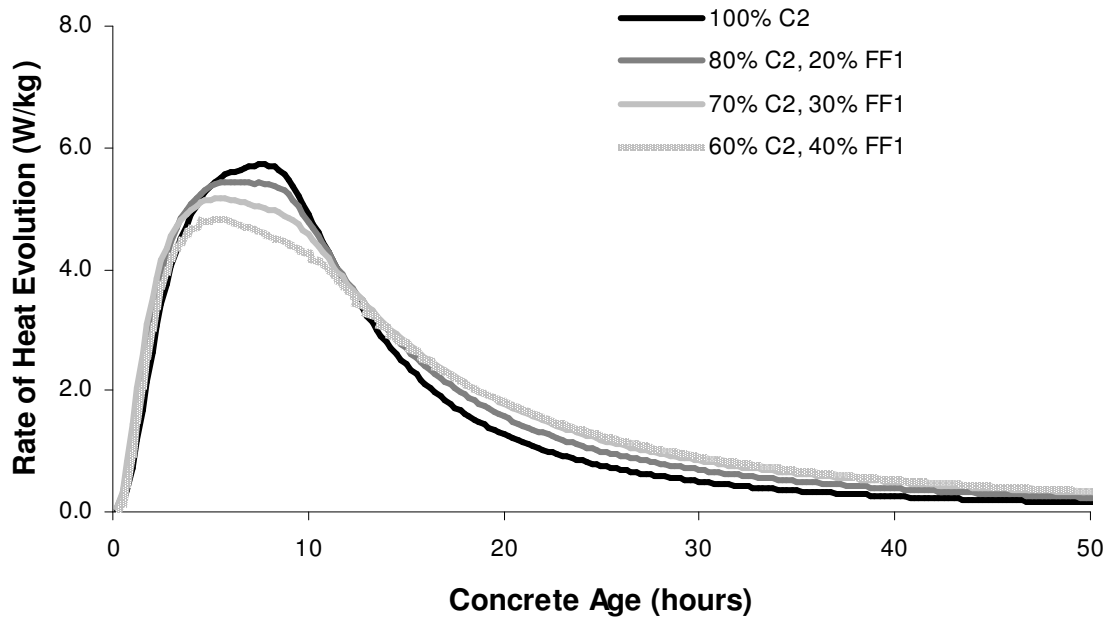


Figure F.20: Rate of Heat Evolution for Cement C2 with FF1, Normalized per Kilogram of Cement

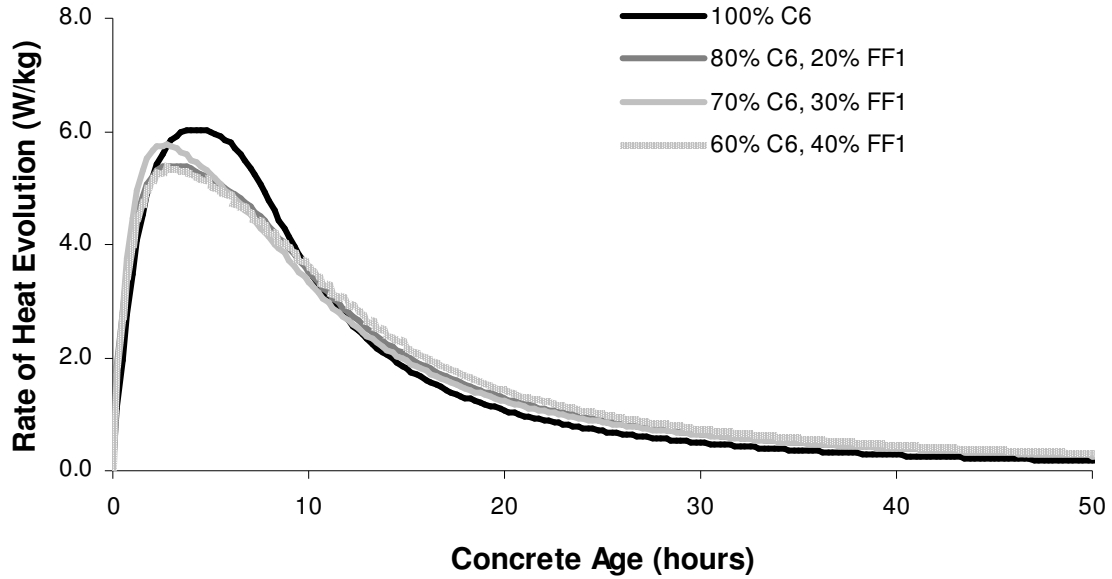


Figure F.21: Rate of Heat Evolution for Cement C6 with FF1, Normalized per Kilogram of Cement

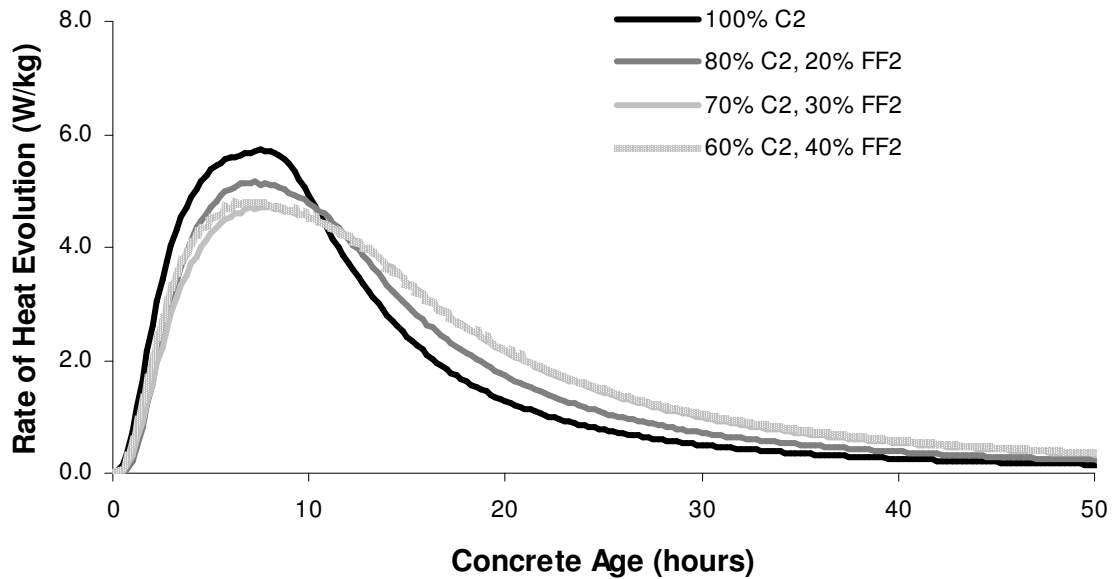


Figure F.22: Rate of Heat Evolution for Cement C2 with FF2, Normalized per Kilogram of Cement

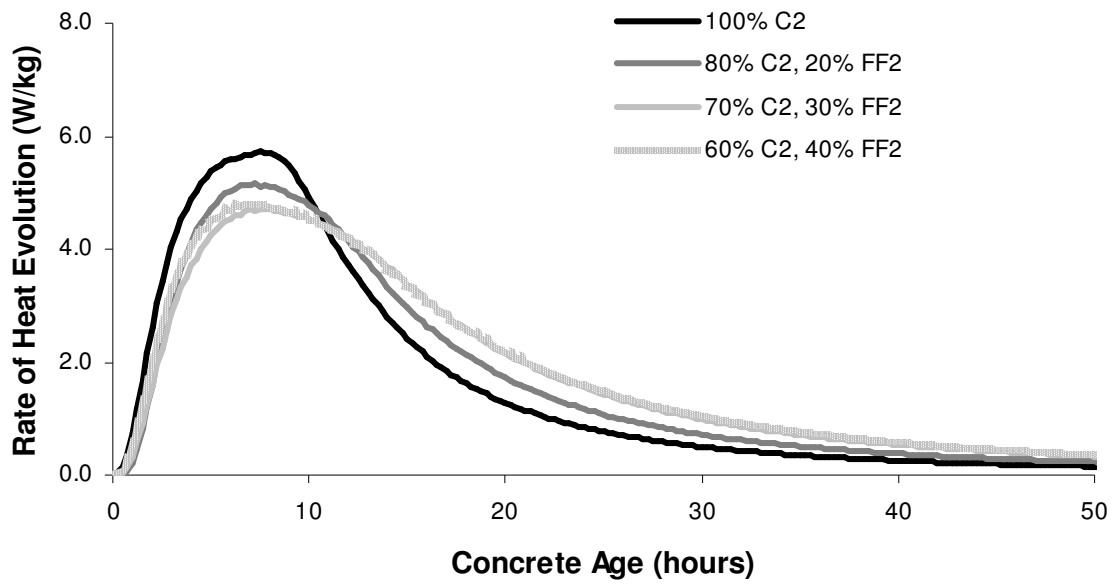


Figure F.23: Rate of Heat Evolution for Cement C6 with FF2, Normalized per Kilogram of Cement

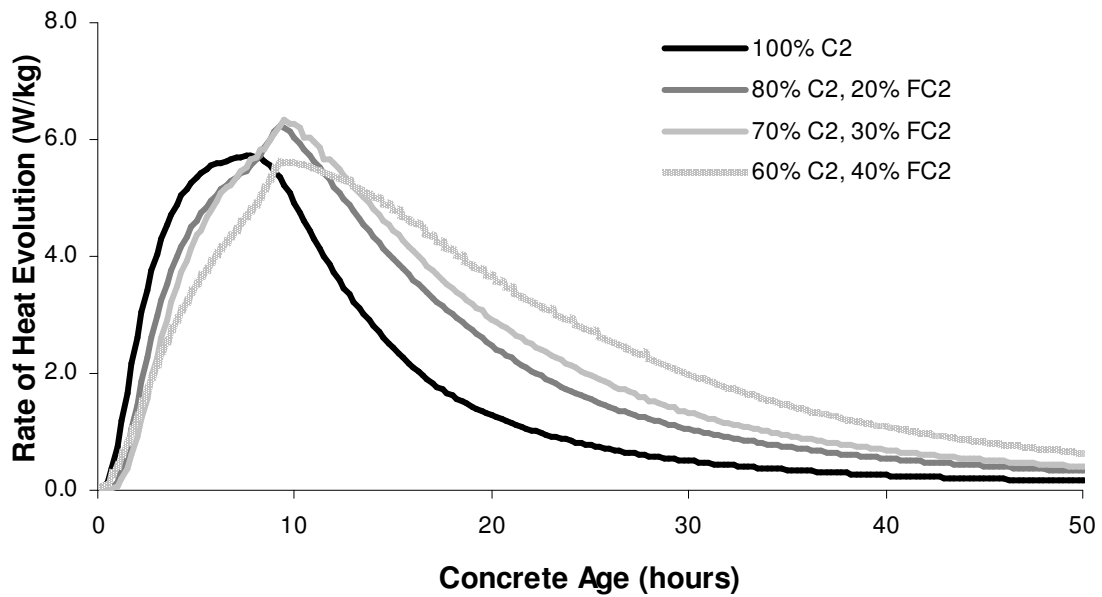


Figure F.24: Rate of Heat Evolution for Cement C2 with FC2, Normalized per Kilogram of Cement

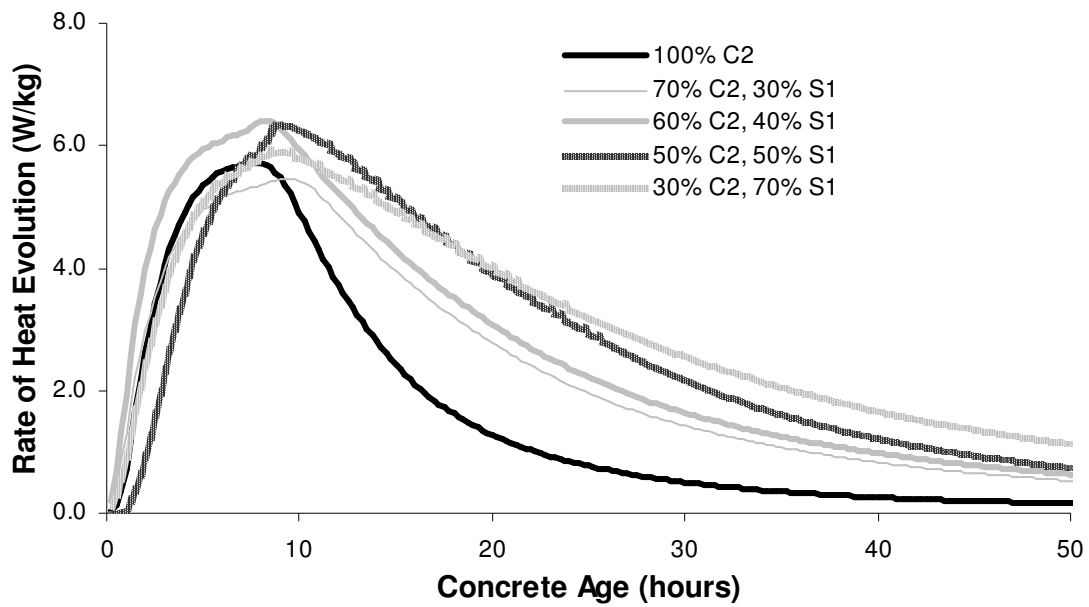


Figure F.25: Rate of Heat Evolution for Cement C2 with S1, Normalized per Kilogram of Cement

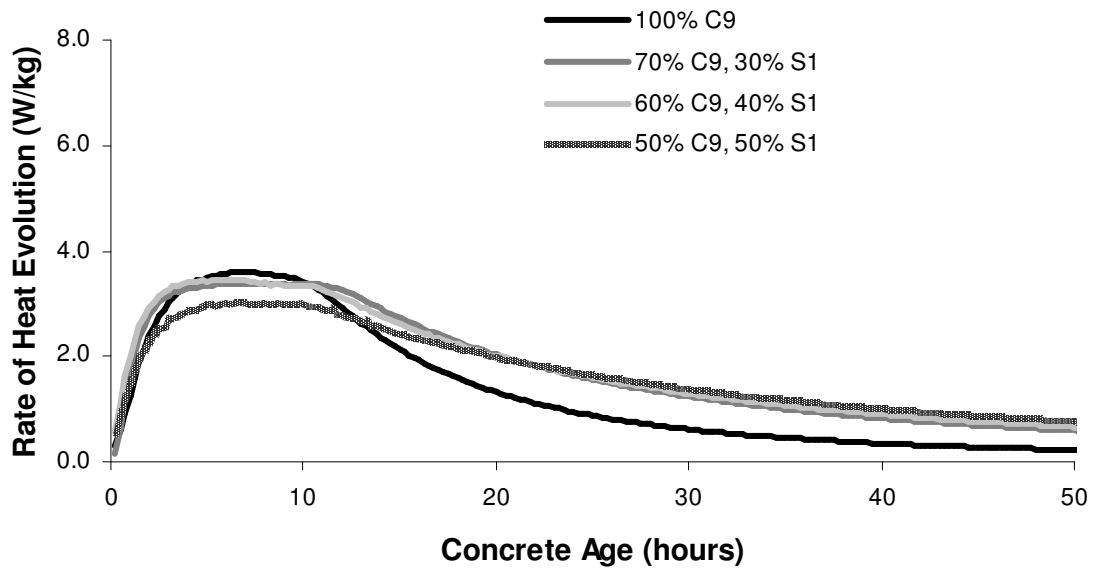


Figure F.26: Rate of Heat Evolution for Cement C9 with S1, Normalized per Kilogram of Cement

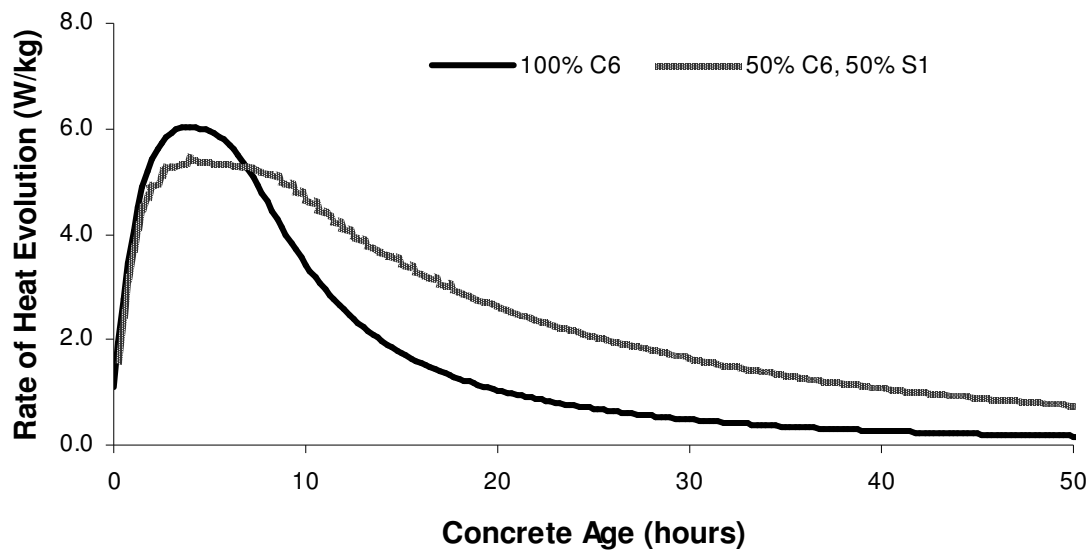


Figure F.27: Rate of Heat Evolution for Cement C6 with S1, Normalized per Kilogram of Cement

F.7. RATE OF HEAT EVOLUTION FOR MIXTURES WITH SILICA FUME

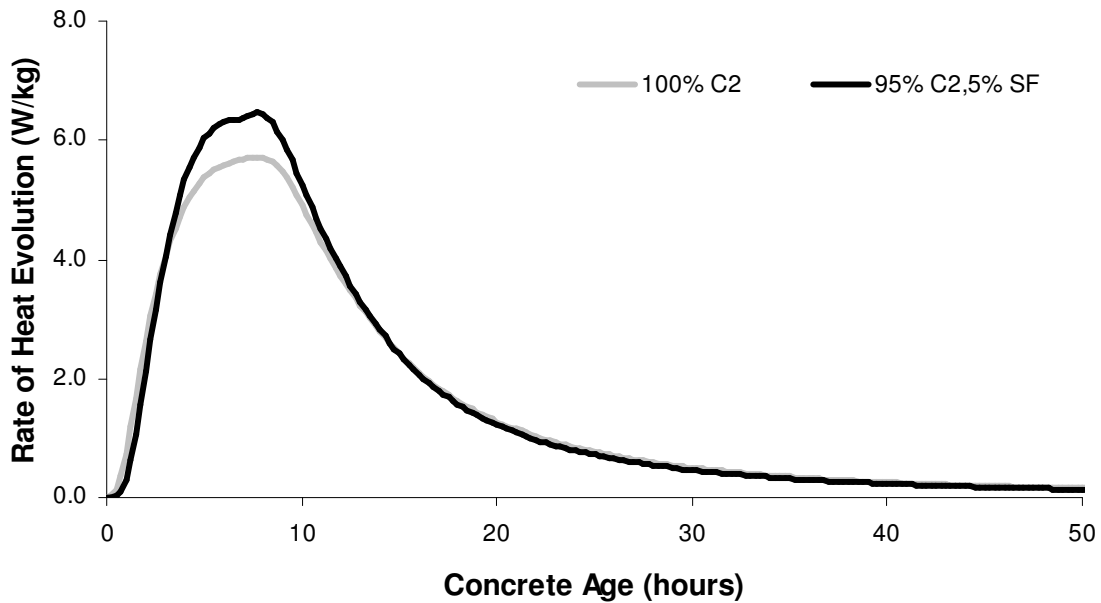


Figure F.28: Rate of Heat Evolution for Cement C2 with Silica Fume, Normalized per Kilogram of Cementitious Material

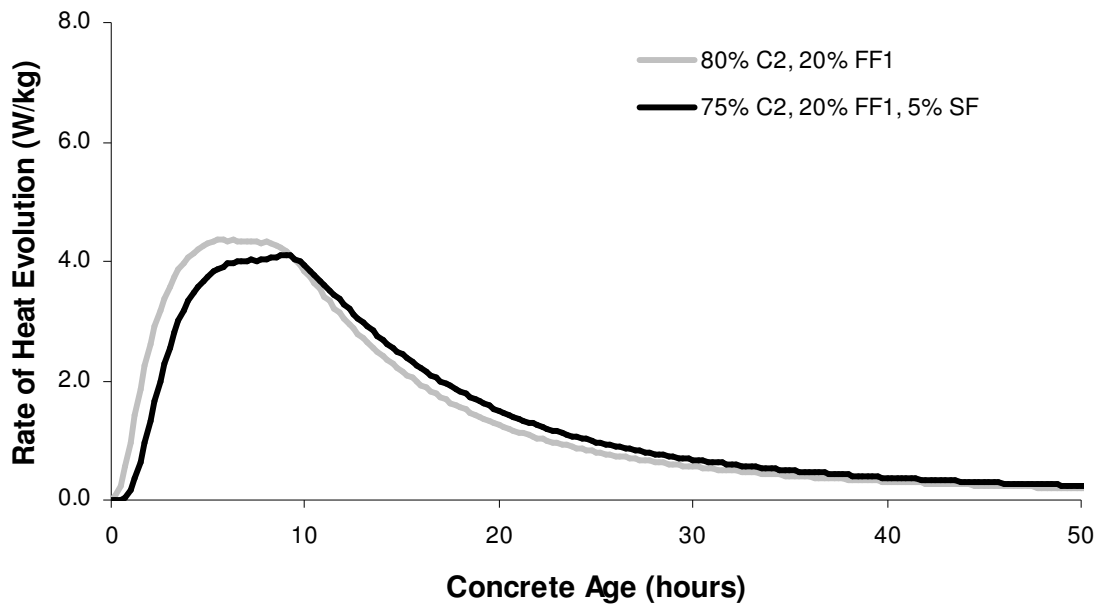


Figure F.29: Rate of Heat Evolution for Cement C2 and 20% Fly Ash FF1 with Silica Fume, Normalized per Kilogram of Cementitious Material

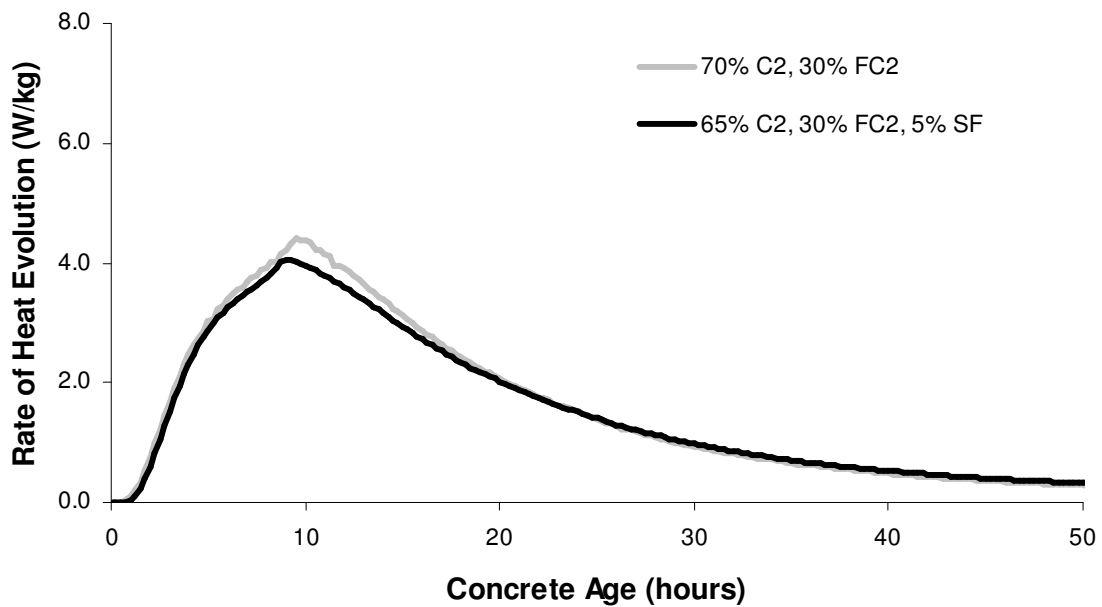


Figure F.30: Rate of Heat Evolution for Cement C2 and 30% Fly Ash FC2 with Silica Fume, Normalized per Kilogram of Cementitious Material

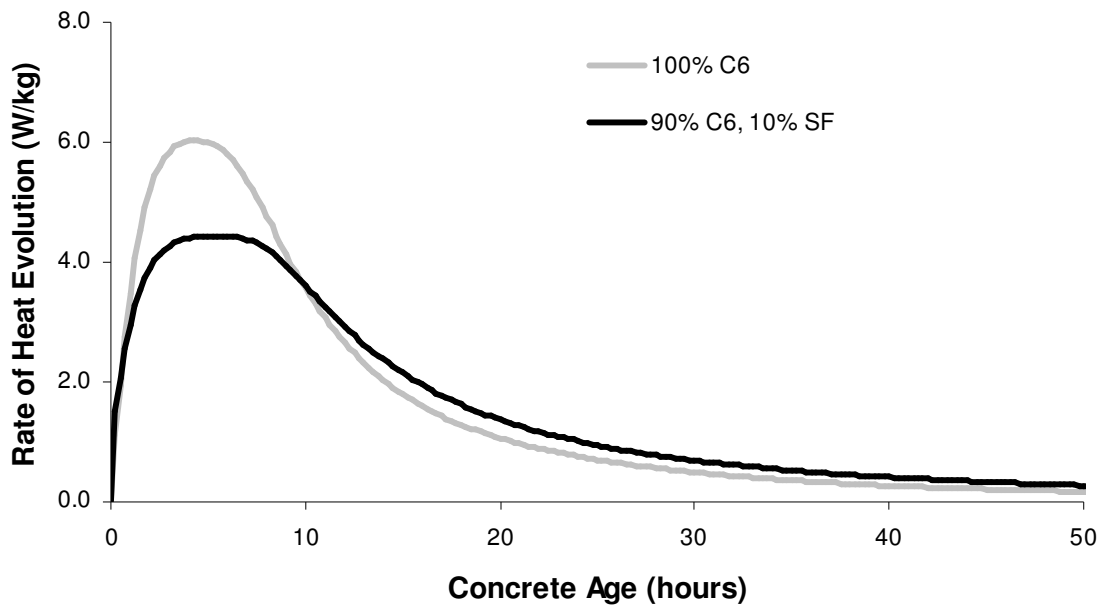


Figure F.31: Rate of Heat Evolution for Cement C6 with Silica Fume, Normalized per Kilogram of Cementitious Material

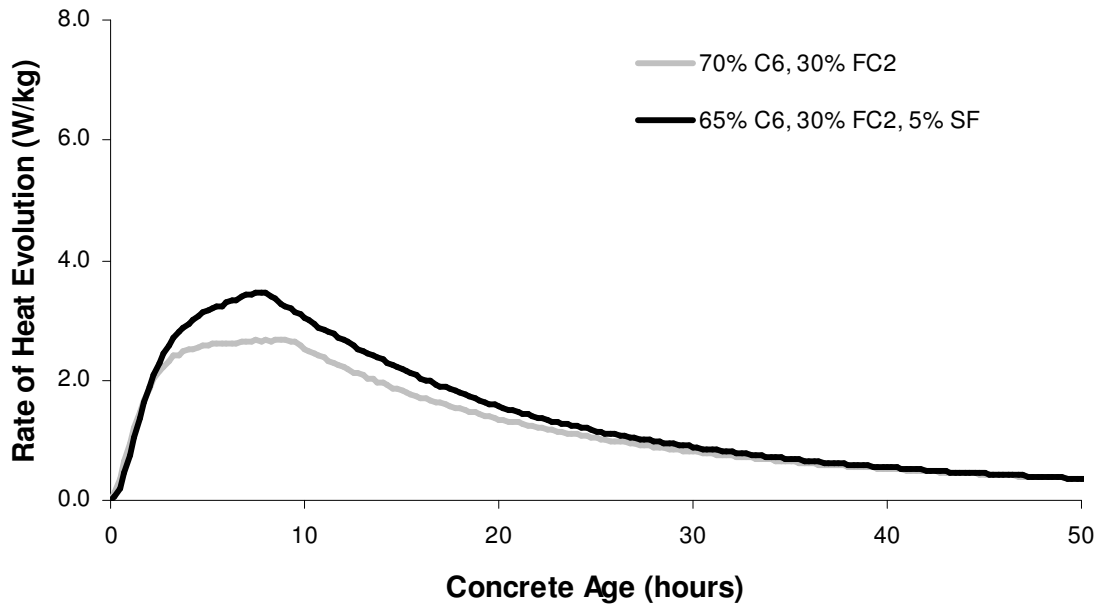


Figure F.32: Rate of Heat Evolution for Cement C2 and 30% Fly Ash FC2 with Silica Fume, Normalized per Kilogram of Cementitious Material

F.8. EFFECT OF LIMITING α_U TO 1.0

The following figures are intended to illustrate the problems associated with mixtures that evolve heat very slowly. A combination of Cement C9 (a Type V cement) with 50% GGBF slag should produce a very low amount of heat. However, the calculations produce unrealistic values for α_u . There are several possible reasons for this phenomenon.

First, the estimate of the contribution of GGBFS to H_u could be wrong. However, it is unlikely that slag would evolve 40% more heat than is predicted by the independent, fractional model for H_u . Also, mixtures with Cement C2 and C10 did not show the same increase in α_u as was seen with Cement C6 and C9. Cement C2 and C10 have a higher C_3A content than Cement C6 and C9, which leads to heat evolution occurring at a much earlier stage. However, the total amount of heat from each of these cements is relatively similar. The timing of this release of heat plays some role in the α_u value that is obtained from the test.

In many cases, the mixtures that have an α_u greater than or approaching 1.0 had this kind of retardation and have a very low rate of heat evolution. Figure F.33 through Figure F.36 show the sensitivity of the hydration model to α_u , τ , and β . It is possible that mixtures with low heat cements (such as C6 and C9), combined with relatively reactive SCM's, may evolve heat over a longer period than is covered by the test. Also, the slope of the decelerating portion of the hydration curve is much less with mixtures with very low heat evolution. These delays have a large impact on the model parameters.

In the middle of the range of tests for which the model was developed, the three parameter model gives acceptable, predictable results. However, these parameters are not

independent of the adiabatic temperature rise and the rate of heat evolution. For example, an increase in the rate of heat evolution does not necessarily directly translate into a higher α_u . Hypothetically, if hydration were to occur at very early ages, the rate of heat evolution could be increased by lowering β , as shown in Figure F.34. Conversely, a decrease in the rate of heat evolution may also be modeled by an increase in τ and a decrease in β with mixtures that have a very low rate of heat evolution and retardation. Figure F.36 shows that the effect of α_u on the rate of heat evolution is highly dependent on the amount of retardation of a mixture.

Several conclusions may be drawn from this sensitivity analysis. First, mixtures that evolve heat at a relatively high or early rate are modeled well by the three parameter model. Second, mixtures that are significantly retarded and have a very low rate of heat evolution may produce unrealistic hydration parameters. However, these parameters may be used to extrapolate information about a mixture within the first week of analysis. Extrapolation beyond this time should be done with caution, since these mixtures may not have as high an adiabatic temperature rise as predicted by the model. Finally, there appears to be a strong correlation between β and α_u , as shown in Figure F.37. When β drops, α_u tends to rise. Unfortunately, describing α_u using β as a dependent variable is a rather convoluted exercise that detaches the parameters from their physical meaning.

The problem may be managed rather simply by capping α_u at 1.0 during the analysis. The curve-fitting procedure attempts to match the measured temperature to the predicted temperature using least-squares regression. In cases where heat evolution is very low, this can lead to values for α_u much greater than 1.0. By capping α_u at 1.0, some accuracy is sacrificed in the curve fitting, but a much more realistic result is

generally produced when extrapolated beyond one week. Figure F.38 shows that capping α_u reduces the adiabatic temperature rise by 5.2 °C (9.4 °F) at approximately 2000 equivalent hours, which is about one week of test time. The difference increases at later ages. Therefore, extrapolation of adiabatic temperature rise beyond one week should be evaluated carefully. In very large elements, or in cases where significant amounts of heat may evolve after one week, a more detailed test procedure may be required. Figure F.39 shows that capping α_u has very little effect on the rate of heat evolution.

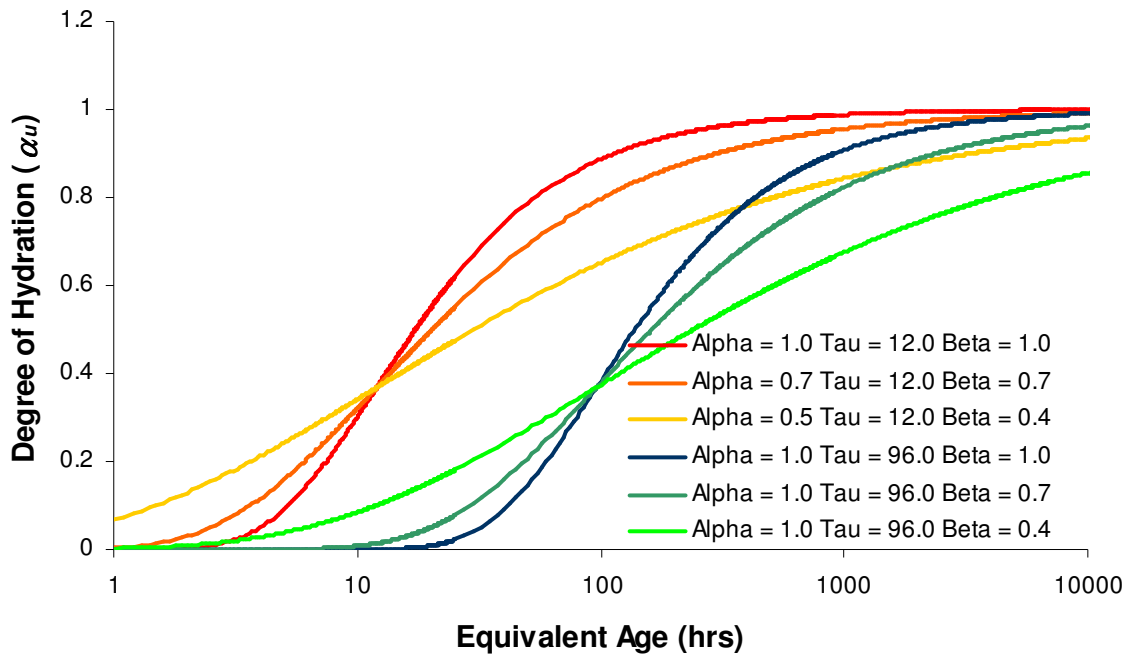


Figure F.33: Effect of β on Degree of Hydration

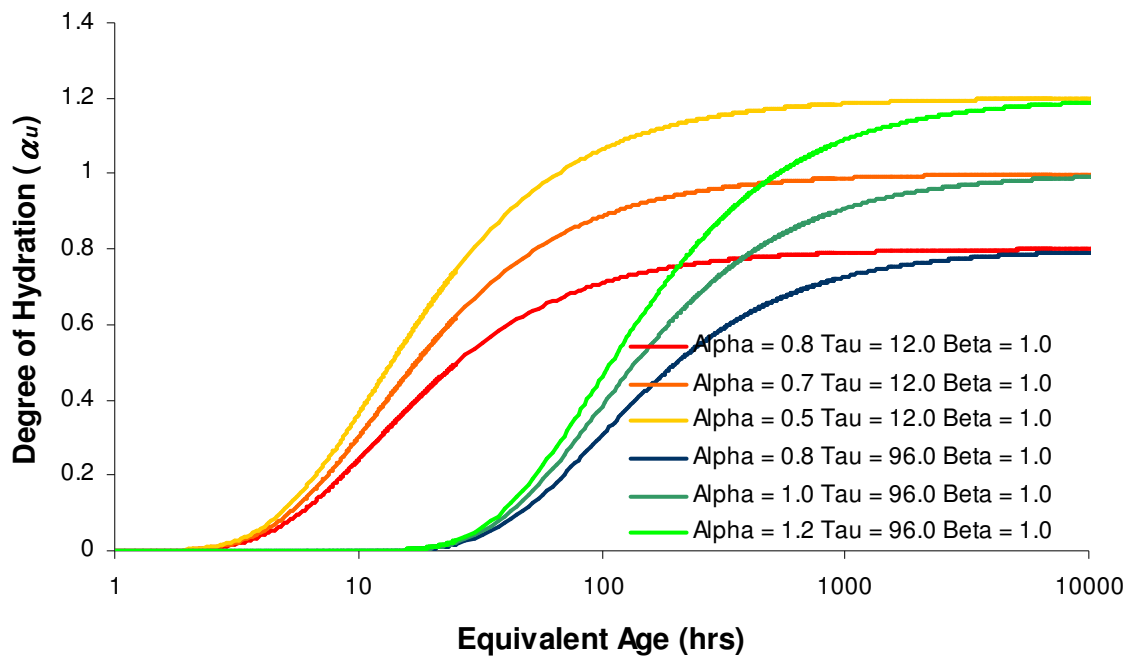


Figure F.34: Effect of α_u on Degree of Hydration

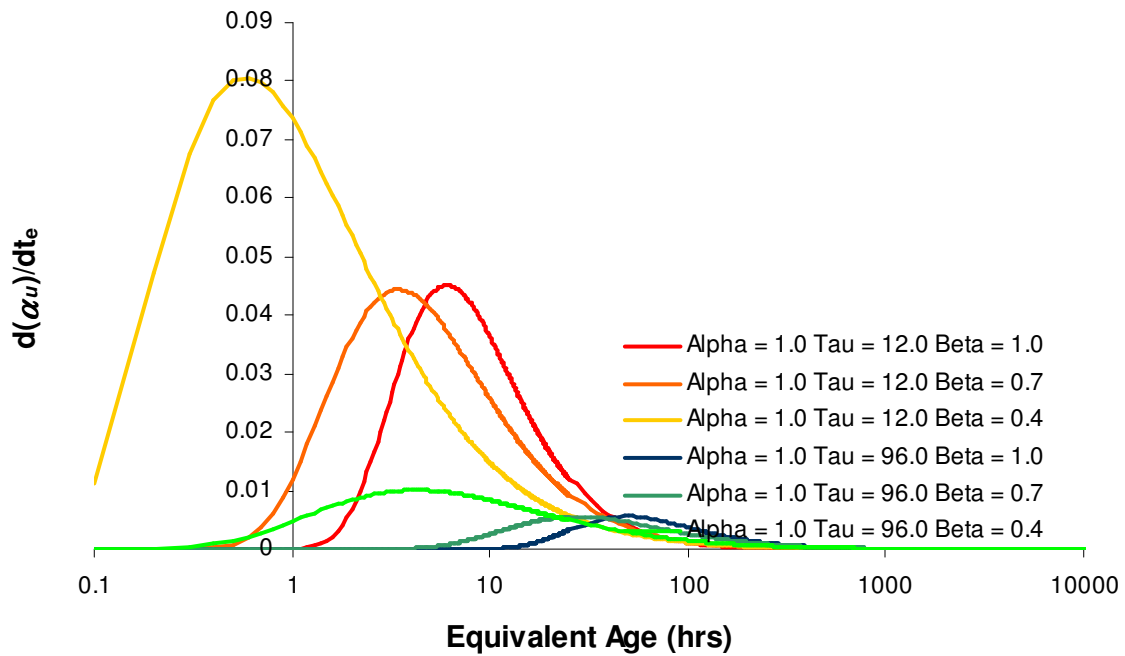


Figure F.35: Effect of β on Rate of Heat Evolution, as Measured by Change in Degree of Hydration

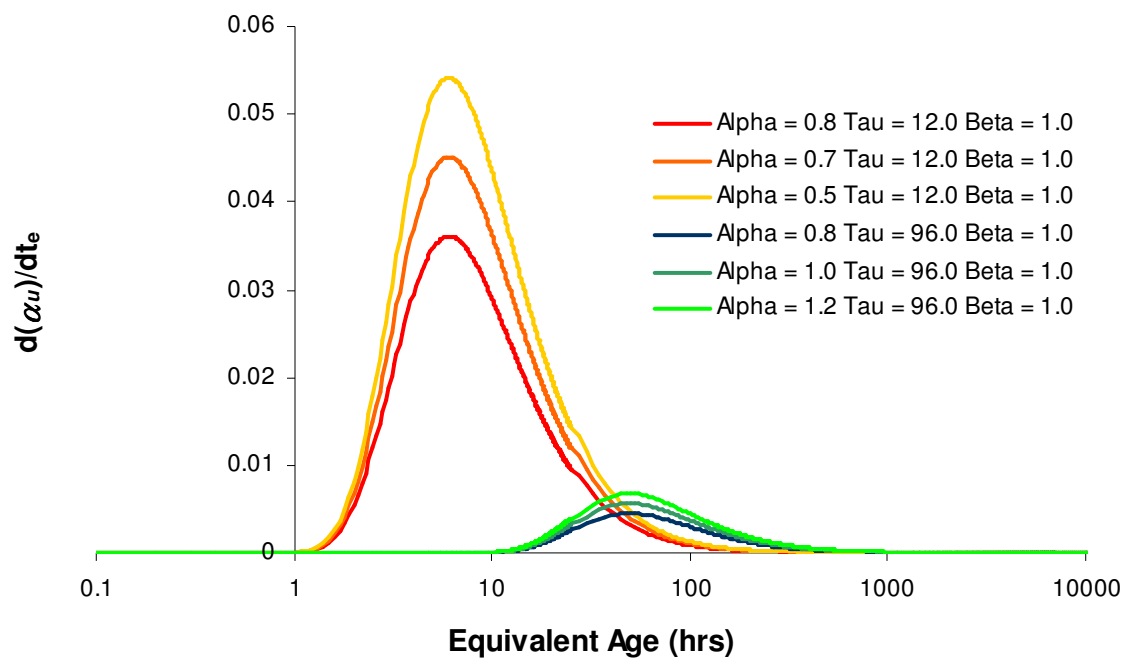


Figure F.36: Effect of α_u on Rate of Heat Evolution, as Measured by Change in Degree of Hydration

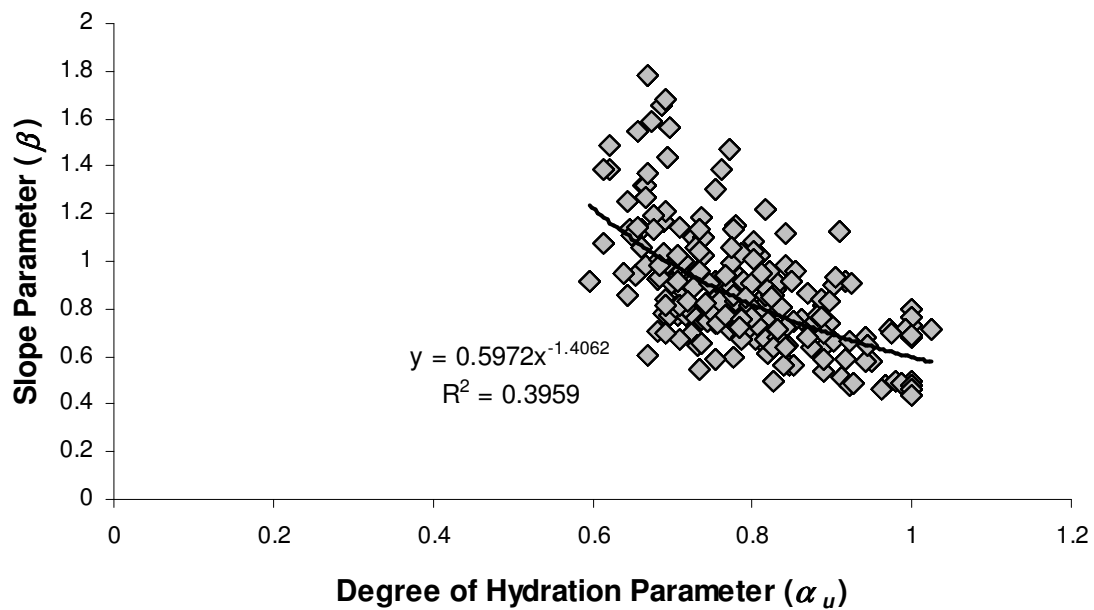


Figure F.37: Correlation Between Slope Parameter (β) and Degree of Hydration Parameter (α_u)

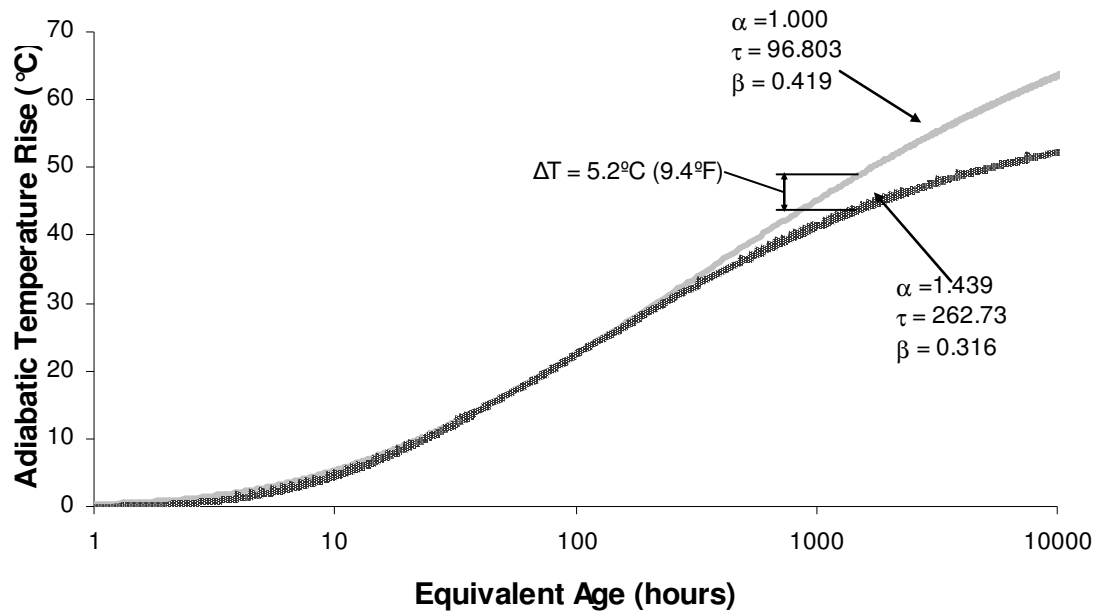


Figure F.38: Effect of Truncation of α_i on Adiabatic Temperature Rise

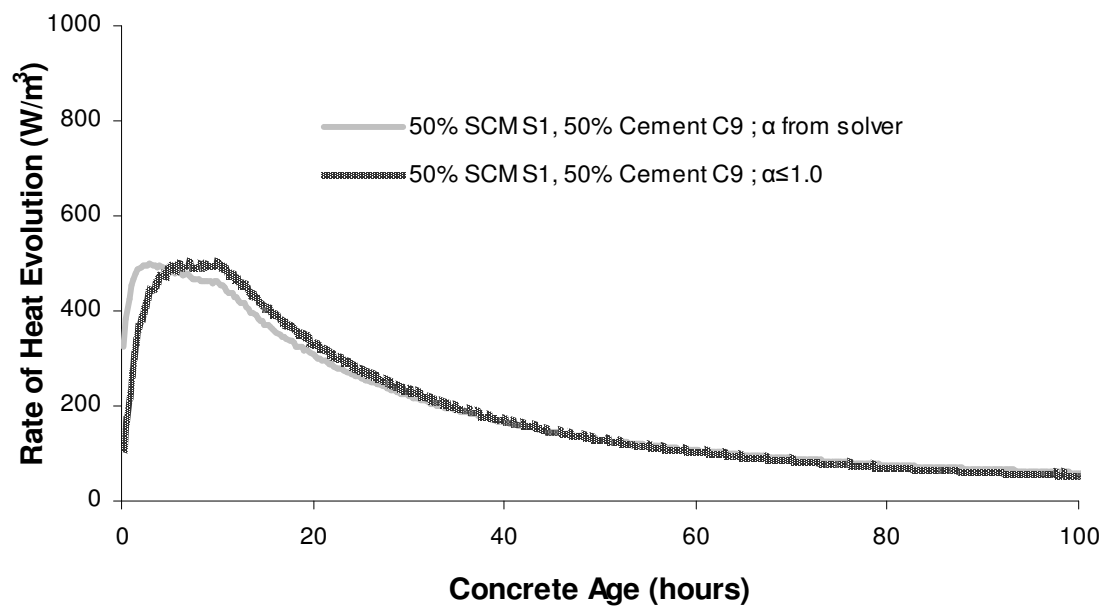


Figure F.39: Effect of Truncation of α_i on Rate of Heat Evolution

APPENDIX G. ADDITIONAL DISCUSSION OF MULTIVARIATE REGRESSION MODELING OF EXPONENTIAL MODEL PARAMETERS FOR CHAPTER 9

The procedure for modeling α_u , τ , and β from the three-parameter exponential parameter model is similar to the procedure outlined in Appendix D for activation energy (E_a). There are three differences that should be noted. First, α_u , τ , and β are determined for each mixture using the procedure outlined in Chapter 6. E_a is determined from the model developed in Chapter 5. For the present dataset, there is only one set of test data per mixture, unlike the modeling of E_a , where there were five tests at different temperatures for each mixture. Next, a number of tests were repeated to assess the confidence limits of the semi-adiabatic test method. The procedure is discussed in Chapter 6. Repeated tests were averaged so each unique mixture has only one set of data points. This prevents the regression analysis from assigning excessive weight to mixtures that are repeated. Finally, the procedure for modeling will include a dataset for regression analysis and a dataset for validation of the model. The predictive ability of the regression model in the present study may be assessed with these two datasets, because these datasets are independent of one another. The following sections will supplement the discussion of the selection of independent variables for the regression model in Chapter 9.

G.1. INDEPENDENT VARIABLES IN STUDY

Due to the computation speed necessary to investigate all of the variables at once, several iterations of the RSQUARE procedure were run to eliminate unlikely independent

variables. Based on several iterations of the RSQUARE procedure, the following variables were chosen to be investigated more thoroughly:

wc = water-cementitious materials ratio;

$PerFlash$ = % Class F fly ash in mixture;

$PerCash$ = % Class C fly ash in mixture;

$PerSF$ = % silica fume in mixture;

$perC3S$ = weighted % C_3S in cementitious system (accounts for dilution by SCM's) by ASTM C150 Bogue calculations;

$lperC3S$ = $\ln(perC3S)$;

$perAlite$ = weighted % C_3S and associated polymorphs (as determined by Rietveld analysis) in cementitious system (accounts for dilution by SCM's);

$perC2S$ = weighted % C_2S in cementitious system (accounts for dilution by SCM's) by ASTM C150 Bogue calculations;

$lperC2S$ = $\ln(perC2S)$;

$perBelite$ = weighted % C_2S and associated polymorphs (as determined by Rietveld analysis) in cementitious system (accounts for dilution by SCM's);

$perC3A$ = weighted % C_3A in cementitious system (accounts for dilution by SCM's) by ASTM C150 Bogue calculations;

$lperC3A$ = $\ln(perC3A)$;

$perAluminate$ = weighted % C_3A and associated polymorphs (as determined by Rietveld analysis) in cementitious system (accounts for dilution by SCM's);

$perC4AF$ = weighted % C_4AF in cementitious system (accounts for dilution by SCM's) by ASTM C150 Bogue calculations;

$lperC4AF = \ln (perC4AF);$

$perFerrite$ = weighted % C_4AF and associated polymorphs (as determined by Rietveld analysis) in cementitious system (accounts for dilution by SCM's);

$perGypsum$ = weighted % gypsum in cementitious system (accounts for dilution by SCM's) by ASTM C150 Bogue calculations;

$lperGypsum = \ln (perGypsum);$

$perGypsumR$ = weighted % $CaSO_4 - H_2O$ (gypsum) (as determined by Rietveld analysis) in cementitious system (accounts for dilution by SCM's);

$perHemihydrate$ = weighted % $CaSO_4 - \frac{1}{2} H_2O$ (Hemihydrate) (as determined by Rietveld analysis) in cementitious system (accounts for dilution by SCM's);

$perAnhydrite$ = weighted % $CaSO_4$ (as determined by Rietveld analysis) in cementitious system (accounts for dilution by SCM's);

$perK2SO4$ = weighted % K_2SO_4 (arcanite) (as determined by Rietveld analysis) in cementitious system (accounts for dilution by SCM's);

$FreeCaO$ = Free lime content in cement, as determined by Rietveld analysis;

$CemBlaine$ = Blaine fineness of cement;

$lCemBlaine = \ln (CemBlaine);$

$FABlaine$ = Blaine fineness of fly ash;

$SlagBlaine$ = Blaine fineness of ground granulated blast furnace (GGBF) slag;

$SFBlaine$ = Blaine fineness of silica fume;

$perSlag$ = % ground granulated blast furnace (GGBF) slag in mixture;

$CemNa2Oeq$ = % Na_2O_{eq} in cement ($0.658 \times \%K_2O + \%Na_2O$);

$lCemNa2Oeq = \ln (CemNa2Oeq);$

$TotalNa2O_{eq} = \% Na_2O_{eq}$ in all cementitious material in mixture ($0.658 \times \%K_2O + \%Na_2O$);

$lTotalNa2O_{eq} = \ln (TotalNa2O_{eq})$;

$CemNa2O = \%Na_2O$ in cement

$CemK2O = \%K_2O$ in cement

$WRRET =$ ASTM Ty A&D water reducer/retarder, OZ/100 lbs of cementitious material;

$lWRRET = \ln (WRRET)$;

$HRWR =$ ASTM Ty F naphthalene or melamine-based high range water reducer, OZ/100 lbs of cementitious material;

$lHRWR = \ln (HRWR)$;

$PCHRWR =$ ASTM F polycarboxylate-based high range water reducer, OZ/100 lbs of cementitious material;

$lPCHRWR = \ln (PCHRWR)$;

$ACCL =$ ASTM Ty C calcium-nitrate based accelerator, OZ/100 lbs of cementitious material;

$lACCL = \ln (ACCL)$;

$i5 = C3A \times TotalNa2O_{eq} \times perCash$;

$i6 = C3A \times CemNa2O_{eq} \times perCash$;

$i7 = perCash \times perC3A$;

$i8 = perCash \times perC3A \times perGypsum$;

$i9 = (perC3A + perC4AF) \times perGypsum$;

$i9R = (perAluminate) \times (perGypsum + perHemihydrate + perAnhydrite + perK2SO4)$;

$i10 = perC3A \times (perCash + perSlag)$;

$$\begin{aligned}
i11 &= (\text{perCash} + \text{perSlag}) \times \text{perC3A} \times \text{perGypsum}; \\
i13 &= \text{C3A} * \text{TotalNa2Oeq} \times (\text{perCash} + \text{perSlag}); \\
i14 &= \text{C3A} * \text{CemNa2Oeq} \times (\text{perCash} + \text{perSlag}); \\
i15 &= \text{HRWR} + \text{PCHRWR}; \\
i16 &= (\text{perCash} + \text{perSlag}) \times \text{TotalFACaO} \times \text{perGypsum}; \\
i17 &= (\text{PerFA} + \text{PerUFFA}) \times \text{TotalFACaO}; \\
i18 &= i17 \times \text{perAluminate} \times i10; \\
i19 &= i17 \times \text{perAluminate}; \\
i20 &= i17 \times \text{perAluminate} \times \text{WRRET}; \\
i21 &= \text{perFash} + \text{perUFFA}; \\
i22 &= \text{perCash} \times \text{TotalFACaO}; \\
i23 &= \text{perCemNa2Oeq} \times \text{perSlag}; \\
i24 &= \text{perCemNa2O} \times \text{perSlag}; \\
i25 &= \text{perCemNa2Oeq} \times \text{perSlag} \times i17;
\end{aligned}$$

Based on the work in Chapters 6 through 8, several possible variables were considered highly likely to have an effect on α_u , τ , and β . These variables were w_c , WRRET , HRWR and PCHRWR , perSlag , perC3A , perC4AF , or perC3S , $\text{perCash} \times \text{FACaO}$, perFash , perSF , ACCL , and CemBlaine . In addition, perAluminate , perFerrite , perAlite , perGypsumR , perAnhydrite , perHemihydrate , perK2SO4 , perPericlase , and perFreeCaO were considered. Possible interactions between these variables were also considered. Both linear and logarithmic relationships between the dependent variables α_u , τ , and β and the combinations of independent variables were

considered. The best fit of the data was obtained by using the natural log of the dependent variable.

Two models were made. The first model was based on crystalline compounds determined from oxide analysis and Bogue calculations. The strongest correlation with $\ln(\alpha_u)$ was found with *perCemNa2Oeq* ($R^2=0.209$), *wc* ($R^2=0.137$), and *perGypsum* ($R^2=0.133$). The strongest correlation with $\ln(\tau)$ was found with *perC3S* ($R^2=0.44$), *perGypsum* ($R^2=0.367$), and *perSlag* ($R^2=0.314$). The strongest correlation with $\ln(\beta)$ was found with *perC3A* ($R^2=0.340$), *perGypsum* ($R^2=0.327$), and *WRRET* ($R^2=0.276$). .

The second model was based on crystalline compounds determined from quantitative x-ray diffraction (QXRD) and Rietveld analysis. The strongest correlation with $\ln(\alpha_u)$ was found with *perAnhydrite* ($R^2=0.229$), *perCemNa2Oeq* ($R^2=0.209$), and *wc* ($R^2=0.137$). The strongest correlation with $\ln(\tau)$ was found with *perAlite* ($R^2=0.443$), and *perAnhydrite* ($R^2=0.364$), and *perSlag* ($R^2=0.314$). The strongest correlation with $\ln(\beta)$ was found with *perAluminate* ($R^2=0.306$), *perAlite* ($R^2=0.285$), and *WRRET* ($R^2=0.276$).

Figure G.1 through Figure G.20 shows the results from the RSQUARE procedure for the data with cement phases determined from both Bogue calculations and Rietveld analysis. R^2 was improved by taking the natural log of the variables, so only these results are shown. Combinations of one to nine variables were tested with this procedure, and those with covariance greater than 0.65 are highlighted in yellow. Figure G.21 through Figure G.23 show the correlation matrix for the independent variables that include Bogue compounds. Figure G.24 through Figure G.26 show the correlation matrix for the independent variables that include phases calculated from Rietveld analysis.

G.2. NUMBER OF VARIABLES

Just like the model for E_a , a model for α_u , τ , and β should describe as much of the variability as possible with as few dependent variables as possible, since incremental gains in accuracy may be offset by poor predictive ability of the model. A comparison of R^2 versus number of variables will provide an indication of the appropriate number of dependent variables to model. The relationship between the coefficient of determination (R^2) and the number of independent variables is shown in Figure G.33 and Figure G.34. The improvement in R^2 decreases as the number of variables increases. The data points in the figure represent the combination of variables with the highest R^2 value. A comparison between the R^2 for the data with phases determined from Rietveld analysis, which is shown in Figure G.33, and the data with phases from Bogue calculations, shown in Figure G.34, indicates that the results are relatively similar. Rietveld analysis and Bogue calculations gave roughly similar R^2 .

Based on the results from the RSQUARE procedure, several variables were chosen for further investigation for each of the dependent variables (α_u , τ , and β). *perFerrite*, *HRWR*, *PCHRWR*, *WRRET*, *PerSF*, *wc*, *perCemNa2Oeq*, and *perFA×FACaO* (*i17*) were selected for the independent variable $l\alpha_u$. *perAlite*, *WRRET*, *ACCL*, *PerSlag*, *perCemNa2O*, and *i17* were selected for the independent variable $l\tau$. *perAluminate*, *WRRET*, *LRWR*, *MRWR*, *HRWR*, *PCHRWR*, *PerSlag*, *perCemK2O*, and *i17* were selected for the independent variable $l\beta$.

G.3. ANOVA

An analysis of variance (ANOVA) was performed for the variables selected for non-linear analysis. Depending on the variable combination, it was possible to get a very

high R^2 . However, R^2 is not the only criteria for selecting a model. The complexity of the model should not be excessively complex given the scope of testing. Also, each variable chosen should be statistically significant. Variables with the probability of a Type I and Type III error higher than 5.0% were rejected as potential variables in the E_a model.

ANOVA gives the overall F test of significance for all of the variables investigated. Figure G.27 through Figure G.29 show the ANOVA for the dataset with Bogue calculations. The probability of Type I and Type III errors is below 0.01% for all of the variables investigated. Figure G.30 through Figure G.32 show the ANOVA for the dataset with Rietveld calculations. Again, the probability of Type I and Type III errors is below 0.01% for all variables, except for MRWR (4.7%). The t-test for each of the variables showed a high probability (>99.9%) of significance. Based on this testing, a combination of 6 variables for α_u , 5 variables for τ , and 9 variables for β were selected as combinations of variables to be used in the non-linear regression analysis.

Figure G.35, Figure G.36, and Figure G.37 show the results of linear regression analysis for α_u , τ , and β , respectively. R^2 was 0.504 for α_u , 0.736 for τ , and 0.801 for β for the data with Bogue calculations. R^2 was 0.503 for α_u , 0.736 for τ , and 0.798 for β for the data with Rietveld analysis, which is nearly identical.

G.4. NOTES FOR NON-LINEAR ANALYSIS

The procedure for non-linear analysis is included in Chapter 9 but is not repeated here. A number of different types of models were tried. For most of the independent variables, an exponential model effectively modeled their effects on the degree of hydration. However, the effects of w/c were modeled using a rational equation. The

effects of high dosages of water reducers on τ and β suggested that a power function might be appropriate, because the delays at high dosages were highly non-linear. Also, greater than 50% replacement of SCM in a mixture caused α_u to either drop or rise significantly. With 100% SCM, α_u should be 0. There was clearly an effect from both the curve fitting algorithm and from the cement type. Therefore, a parabolic shape for α_u was investigated. However, the improvements in R^2 were minimal. More testing is required to make judgments at the extremes of dosage ranges.

The residual plots of each of the independent variables are presented in Figure G.42 through Figure G.57. These results show that the distribution of error for all of the independent variables is random.

G.5. NOTES FOR SENSITIVITY ANALYSIS

A sensitivity analysis was performed for each of the variables included in the hydration model. Figure G.58 and Figure G.59 are two of the variables that had a relatively small effect on the degree of hydration. However, their inclusion in the model produced a much better fit of the data. They are included here for completeness.

G.6. SAS 9.1.3 CODE – BOGUE MODEL

```

data work.temp1; set work.cement;
lperC3S=log(perC3S);
lalite=log(alite);
lperalite=log(peralite);
lperC3A=log(perC3A);
laluminate=log(aluminate);
lperaluminate=log(peraluminate);
lperC4AF=log(perC4AF);
lferrite=log(ferrite);
lperferrite=log(perferrite);
lperC2S=log(perC2S);
lbelite=log(belite);
lperGypsum=log(perGypsum);
lCemBlaine=log(CemBlaine);
lTotalNa2Oeq=log(TotalNa2Oeq);
lACCL=log(ACCL);
lWRRET=log(WRRET);
i1=WRRET*perAlite;
i2=WRRET*perBelite;
i3=WRRET*Aluminate;
i4=perAluminate*WRRET*(GypsumR+Hemihydrate+Anhydrite+K2SO4);
i5=perAluminate*LRWR;
i6=(perAluminate+perFerrite)*(GypsumR+Hemihydrate+Anhydrite+K2SO4);
i7=(perAluminate)*(GypsumR+Hemihydrate+Anhydrite+K2SO4);
i8=WRRET*perAluminate;
i9=(perAluminate)*(perSlag+perFA*TotalFACaO);
i10=GypsumR+Hemihydrate+Anhydrite;
i11=(perAluminate)*(GypsumR+Hemihydrate+Anhydrite+K2SO4)*cemNa2Oeq;
i12=perSlag+perFA+perUFFA;
i17=(PerFA+PerUFFA)*TotalFACaO;
i18=i17*perAluminate*i10;
i19=i17*perAluminate;
i20=i17*perAluminate*WRRET;
i21=(perFash+perUFFA);
i22=perCash*TotalFACaO;
i23=perCemNa2Oeq*perSlag;
i24=perCemNa2O*perSlag;
i25=perCemNa2Oeq*(perSlag)*i17;
lalpha=log(alphamax);
ltau=log(tau);
lbeta=log(beta);
run;
proc rsquare c;
model alphamax lalpha tau ltau beta lbeta HOHcem HOHcemSCM HOHcemUlt
HOHcemSCMUlt= perAlite perBelite perAluminate perFerrite perPericlase
perGypsumR perHemihydrate perAnhydrite perK2SO4 perFreeCaO WRRET LRWR
MRWR HRWR PCHRWR ACCL AIR PerFA PerSlag PerSF PerUFFA wc PerAir
TotalFACaO /*perFash perCash*/ /*FABlaine*/ CemBlaine perCemNa2O
perCemK2O perCemNa2Oeq /*CemNa2Oeq TotalNa2Oeq /*i1 i2 i3 i4 i5*/ i10
/*i7 i8 i9 i11 i12*/ i17 /*i18 i19 i20*/i21 /*i22*/select=20 stop=15;
run; quit;

```

```

proc glm; model lalpha = perFerrite HRWR PCHRWR WRRET PerSF wc
perCemNa2Oeq i17/solution ;
output out=plotit p=pred r=resid;
run;
quit;
proc gplot;
plot lalpha*pred resid*pred resid*lalpha;
run; quit;

proc glm; model tau = /*i7 i9*/ perAlite WRRET ACCL PerSlag perCemNa2O
i17/solution ;
output out=plotit p=pred r=resid;
run;
quit;
proc gplot;
plot tau*pred resid*pred resid*tau;
run; quit;

proc glm; model lbeta = perAluminate WRRET LRWR MRWR HRWR PCHRWR
PerSlag /*perCemK2O*/ i17/solution ;
output out=plotit p=pred r=resid;
run;
quit;
proc gplot;
plot lbeta*pred resid*pred resid*lbeta;
run; quit;

proc glm; model HOHcem = perSlag i17 perSF/solution ;
output out=plotit p=pred r=resid;
run;
quit;
proc gplot;
plot HOHcem*pred resid*pred resid*HOHcem;
run; quit;

proc glm; model HOHcemUlt = perSlag i17 perSF/solution ;
output out=plotit p=pred r=resid;
run;quit;
proc gplot;
plot HOHcemUlt*pred resid*pred resid*HOHcemUlt;
run;quit;

data work.temp1; set work.cement;
lperC3S=log(perC3S);
lperC3A=log(perC3A);
lperC4AF=log(perC4AF);
lperC2S=log(perC2S);
lperGypsum=log(perGypsum);
lCemBlaine=log(CemBlaine);
lTotalNa2Oeq=log(TotalNa2Oeq);
lACCL=log(ACCL);
i1=WRRET*perAlite;
i2=WRRET*perBelite;
i3=WRRET*Aluminate;
i4=perAluminate*WRRET*(GypsumR+Hemihydrate+Anhydrite+K2SO4);
i5=perAluminate*LRWR;
i6=(perAluminate+perFerrite)*(GypsumR+Hemihydrate+Anhydrite+K2SO4);

```



```

i7=(perAluminate)*(GypsumR+Hemihydrate+Anhydrite+K2SO4);
i8=WRRET*perAluminate;
i9=(Aluminate)*(perSlag+perFA*TotalFACaO);
i10=GypsumR+Hemihydrate+Anhydrite;
i11=(perAluminate)*(GypsumR+Hemihydrate+Anhydrite+K2SO4)*cemNa2Oeq;
i12=perSlag+perFA+perUFFA;
i17=(PerFA+PerUFFA)*TotalFACaO;
i18=i17*perAluminate*i10;
run;
proc nlin;
parms c1=-0.4934 c2=0.0237 c3=0.0950 c4=0.0329 c5=0.0174 c6=-.00502
c8=0.0358 C9=0.00687 e1=2.6972 e2=-0.00518 e3=-0.00509 e4=0.670
e5=0.0161 e6=1.4281 e7=0.000531 f1=-0.33 f2=-0.00869 f4=-0.3803
f5=-0.0184 f6=-0.00769 f9=-0.00011;
betal=exp(c1+c2*perAluminate+C3*WRRET+c4*LRWR+c5*MRWR+c6*perSlag
+C8*PCHRWR+C9*HRWR);
taul=exp(e1+e2*perAlite+e3*ACCL+WRRET*e4+e5*perSlag+e6*perCemNa2O
+e7*i17);
alphamax1=1.031*wc/(0.194+wc)+exp(f1+f2*perFerrite+f4*perCemNa2Oeq
+f5*WRRET+f6*PCHRWR+i17*f9);
model alpha=exp(-(taul/time)**betal))*alphamax1;
output out=good p=predict r=resid stdr=eresid;
run;
proc gplot;
plot alpha*predict resid*predict resid*alpha;
run;quit;

```

G.7. SAS 9.1.3 CODE – RIETVELD MODEL

```

data work.temp1; set work.cement;
lperC3S=log(perC3S);
lalite=log(alite);
lperalite=log(peralite);
lperC3A=log(perC3A);
laluminate=log(aluminate);
lperaluminate=log(peraluminate);
lperC4AF=log(perC4AF);
lferrite=log(ferrite);
lperferrite=log(perferrite);
lperC2S=log(perC2S);
lbelite=log(belite);
lperGypsum=log(perGypsum);
lCemBlaine=log(CemBlaine);
lTotalNa2Oeq=log(TotalNa2Oeq);
lACCL=log(ACCL);
lWRRET=log(WRRET);
i1=WRRET*perAlite;
i2=WRRET*perBelite;
i3=WRRET*Aluminate;
i4=perAluminate*WRRET*(GypsumR+Hemihydrate+Anhydrite+K2SO4);
i5=perAluminate*LRWR;
i6=(perAluminate+perFerrite)*(GypsumR+Hemihydrate+Anhydrite+K2SO4);
i7=(perAluminate)*(GypsumR+Hemihydrate+Anhydrite+K2SO4);
i8=WRRET*perAluminate;
i9=(perAluminate)*(perSlag+perFA*TotalFACaO);
i10=GypsumR+Hemihydrate+Anhydrite;
i11=(perAluminate)*(GypsumR+Hemihydrate+Anhydrite+K2SO4)*cemNa2Oeq;
i12=perSlag+perFA+perUFFA;
i17=(PerFA+PerUFFA)*TotalFACaO;
i18=i17*perAluminate*i10;
i19=i17*perAluminate;
i20=i17*perAluminate*WRRET;
i21=(perFash+perUFFA);
i22=perCash*TotalFACaO;
i23=perCemNa2Oeq*perSlag;
i24=perCemNa2O*perSlag;
i25=perCemNa2Oeq*(perSlag)*i17;
lalpha=log(alphamax);
ltau=log(tau);
lbeta=log(beta);
run;
proc rsquare c;
model alphamax lalpha tau ltau beta lbeta HOHcem HOHcemSCM HOHcemUlt
HOHcemSCMUlt= perAlite perBelite perAluminate perFerrite perPericlase
perGypsumR perHemihydrate perAnhydrite perK2SO4 perFreeCaO WRRET LRWR
MRWR HRWR PCHRWR ACCL AIR PerFA PerSlag PerSF PerUFFA wc PerAir
TotalFACaO /*perFash perCash*/ /*FABlaine*/ CemBlaine perCemNa2O
perCemK2O perCemNa2Oeq /*CemNa2Oeq TotalNa2Oeq /*i1 i2 i3 i4 i5*/ i10
/*i7 i8 i9 i11 i12*/ i17 /*i18 i19 i20*/i21 /*i22*/select=20 stop=15;
run;quit;

```

```

proc glm; model lalpha = perFerrite HRWR PCHRWR WRRET PerSF wc
perCemNa2Oeq i17/solution ;
output out=plotit p=pred r=resid;
run;
quit;
proc gplot;
plot lalpha*pred resid*pred resid*lalpha;
run;quit;

proc glm; model tau = perAlite WRRET ACCL PerSlag perCemNa2O
i17/solution ;
output out=plotit p=pred r=resid;
run;
quit;
proc gplot;
plot tau*pred resid*pred resid*tau;
run; quit;

proc glm; model lbeta = perAluminate WRRET LRWR MRWR HRWR PCHRWR
PerSlag i17/solution ;
output out=plotit p=pred r=resid;
run;
quit;
proc gplot;
plot lbeta*pred resid*pred resid*lbeta;
run; quit;

proc glm; model HOHcem = perSlag i17 perSF/solution ;
output out=plotit p=pred r=resid;
run;
quit;
proc gplot;
plot HOHcem*pred resid*pred resid*HOHcem;
run; quit;

proc glm; model HOHcemUlt = perSlag i17 perSF/solution ;
output out=plotit p=pred r=resid;
run;
quit;
proc gplot;
plot HOHcemUlt*pred resid*pred resid*HOHcemUlt;
run; quit;

data work.temp1; set work.cement;
lperC3S=log(perC3S);
lperC3A=log(perC3A);
lperC4AF=log(perC4AF);
lperC2S=log(perC2S);
lperGypsum=log(perGypsum);
lCemBlaine=log(CemBlaine);
lTotalNa2Oeq=log(TotalNa2Oeq);
lACCL=log(ACCL);
i1=WRRET*perAlite;
i2=WRRET*perBelite;
i3=WRRET*Aluminate;
i4=perAluminate*WRRET*(GypsumR+Hemihydrate+Anhydrite+K2SO4);
i5=perAluminate*LRWR;

```

```

i6=(perAluminate+perFerrite)*(GypsumR+Hemihydrate+Anhydrite+K2SO4);
i7=(perAluminate)*(GypsumR+Hemihydrate+Anhydrite+K2SO4);
i8=WRRET*perAluminate;
i9=(Aluminate)*(perSlag+perFA*TotalFACaO);
i10=GypsumR+Hemihydrate+Anhydrite;
i11=(perAluminate)*(GypsumR+Hemihydrate+Anhydrite+K2SO4)*cemNa2Oeq;
i12=perSlag+perFA+perUFFA;
i17=(PerFA+PerUFFA)*TotalFACaO;
i18=i17*perAluminate*i10;
run;
proc nlin;
parms c1=-0.4934 c2=0.0237 c3=0.0950 c4=0.0329 c5=0.0174 c6=-.00502
c8=0.0358 C9=0.00687 e1=2.6972 e2=-0.00518 e3=-0.00509 e4=0.670
e5=0.0161 e6=1.4281 e7=0.000531 f1=-0.33 f2=-0.00869 f4=-0.3803
f5=-0.0184 f6=-0.00769 f9=-0.00011;
beta1=exp(c1+c2*perAluminate+C3*WRRET+c4*LRWR+c5*MRWR+c6*perSlag
+C8*PCHRWR+C9*HRWR);
tau1=exp(e1+e2*perAlite+e3*ACCL+WRRET*e4+e5*perSlag+e6*perCemNa2O
+e7*i17);
alphamax1=1.031*wc/(0.194+wc)+exp(f1+f2*perFerrite+f4*perCemNa2Oeq
+f5*WRRET+f6*PCHRWR+i17*f9);
model alpha=exp(-((tau1/time)**beta1))*alphamax1;
output out=good p=predict r=resid stdr=eresid;
run;
proc gplot;
plot alpha*predict resid*predict resid*alpha;
run; quit;

```

Table G-1: Chemical and Physical Properties of Cements

	Cement																	
	C1	C2	C3	C4	C5	C6	C7	C8	C9	C10	C11	C12	C13	C14	C15	C16	C17	C18
SiO ₂	20.45	19.18	20.25	21.29	20.6	20.77	19.72	19.82	21.63	21.03	20.35	19.38	20.49	20.58	20.12	20.57	21.25	21.27
Al ₂ O ₃	5.43	5.34	5.27	4.88	4.8	3.88	5.27	4.76	4.04	4.13	4.73	4.79	4.92	5.92	4.74	4.82	5.31	4.96
Fe ₂ O ₃	2.01	2.3	3.14	2.92	3.2	3.73	2.02	3.59	5.29	3.78	3.39	3.17	3.29	2.72	2.98	3.22	1.87	3.31
CaO	64.51	63.17	61.86	63.31	64.3	64.5	64.08	64.3	63.07	63.4	64.8	65.24	64.38	62.99	64.21	63.94	63.61	61.95
MgO	1.15	1.09	2.68	1.23	1.5	1.01	1.22	0.8	0.77	1.32	0.83	1.44	1.49	0.95	1.43	1.82	1.3	2.04
Na ₂ O	0.14	0.12	0.27	0.28	0.18	0.18	0.13	0.07	0.27	0.14	0.13	0.16	0.19	0.23	0.21	0.22	0.14	0.24
K ₂ O	0.56	0.95	0.90	0.4	0.37	0.6	0.52	0.68	0.23	0.55	0.65	0.36	0.4	0.76	0.46	0.54	0.56	0.42
Na ₂ O+0.658*K ₂ O	0.51	0.75	0.86	0.54	0.42	0.57	0.47	0.52	0.42	0.50	0.56	0.40	0.45	0.73	0.51	0.58	0.51	0.52
TiO ₂	0.27	0.26	0.22	0.2	0.32	0.17	0.25	0.19	0.19	0.19	0.21	0.19	0.21	0.28	0.18	0.2	0.24	0.27
MnO ₂	0.03	0.04	0.08	0.33	0.48	0.04	0.03	0.09	0.11	0.59	0.27	0.34	0.38	0.25	0.34	0.02	0.03	0.43
P ₂ O ₅	0.16	0.21	0.2	0.05	0.06	0.04	0.24	0.27	0.03	0.16	0.16	0.05	0.06	0.19	0.05	0.09	-	0.08
SrO	0.10	0.09	0.21	0.04	0.06	0.04	0.11	0.04	0.08	0.18	0.19	0.03	0.05	0.19	0.04	0.11	-	0.04
BaO	0.03	0.03	0.03	0.03	0.04	0.03	0.03	0.03	0.03	0.03	0.03	0.03	0.03	0.04	0.03	0	-	0.02
SO ₃	3.35	3.2	4.17	2.63	2.8	2.38	4.4	3.47	2.74	3.02	2.66	2.43	2.76	3.1	2.5	2.49	3.56	2.56
LOI	1.80	4.1	0.73	2.43	1.2	2.67	1.95	1.88	1.55	1.5	1.62	2.4	1.36	1.81	2.7	1.95	-	2.41
Free CaO	0.00	0	0.70	0	0	0	0.00	0.00	0	0	0	0.6	0.6	0	0.5	0.00	0.00	0.5
C ₃ S	58.29	63.11	46.15	51.47	60.40	66.54	60.16	64.13	49.85	56.51	64.93	68.75	60.74	47.52	65.25	59.88	48.96	45.19
C ₂ S	14.65	7.38	23.24	22.21	13.50	9.35	11.16	8.45	24.41	17.66	9.36	3.70	12.92	23.15	8.46	13.80	23.99	26.89
C ₃ A	10.99	10.26	8.65	7.99	7.31	3.97	10.55	6.54	1.76	4.55	6.80	7.33	7.47	11.09	7.52	7.32	10.91	7.54
C ₄ AF	6.12	7.00	9.56	8.80	9.74	11.35	6.15	10.92	16.10	11.50	10.32	9.56	10.01	8.28	9.07	9.80	5.69	10.07
Results from Rietveld Analysis																		
C ₃ S	61.20	61.00	57.20	56.60	55.50	55.70	64.60	54.00	49.00	64.00	64.50	67.60	62.90	54.00	57.40	55.70	58.80	58.50
C ₂ S	16.00	15.60	15.10	18.60	17.40	21.10	11.80	21.70	26.40	15.30	15.30	7.30	11.00	18.60	16.00	18.00	19.20	13.80
C ₃ A	13.10	9.60	5.30	6.40	6.80	4.00	12.40	5.70	4.40	5.10	4.40	5.40	6.70	9.90	6.30	5.00	11.40	6.20
C ₄ AF	3.50	6.00	9.60	8.60	10.70	10.70	4.00	10.20	12.10	11.00	10.80	10.10	10.10	6.60	10.10	10.50	2.20	10.00
CSH ₂ (gypsum)	5.70	5.44	7.09	4.47	4.76	4.05	7.48	5.90	4.66	5.13	4.52	4.13	4.69	5.27	4.25	4.23	6.05	4.35
Periclase	0	0	0.9	0.5	0.6	0	0	0	0	0	0	0.5	0.6	0	0.7	1.1	0.8	0.9
Gypsum	1.4	0.4	6.6	3.1	0.9	0	2.4	0	2.3	1.6	1.5	1.6	2.2	2.4	1.2	2.3	2.6	1.6
Hemihydrate	1.5	1.2	0.8	1.3	1.9	2.5	2.4	3.7	2	0.6	0.5	2.2	1.8	1.1	2.1	0.9	1.9	2.7
Anhydrite	0.6	0.7	0.4	0.6	0.9	0.7	0.6	0.6	0.4	0.6	0.6	0.4	0.6	0.5	0.5	0.6	0.8	0.5
K ₂ SO ₄	1.5	1	1.6	0.8	0.5	0.7	0.8	1.3	0.9	0	0.4	0.3	0	1.2	0.8	0.7	2	1.3
CaCO ₃	0.8	3.6	1.7	3.4	2.5	3.2	0.7	1.5	2.5	1	1.2	3.6	2.8	5.7	4	4.1	0	3.2
Blaine	350.0	390.9	388.9	413.2	404.9	365.4	552.0	539.0	409.0	349.3	353.5	393.0	380.8	363.5	393.0	330.0	330.0	330.0

Table G-2: Chemical and Physical Properties of Cements from Literature

Cement (AS-Schindler, 2002, Z - Ge, 2006)										
	AS1	AS2	AS3	AS4	AS5	AS6	AS7	AS8	AS9	Z1
SiO ₂	-	-	-	-	-	-	19.9	20.9	20.1	20.75
Al ₂ O ₃	-	-	-	-	-	-	5.7	5	5.3	4.49
Fe ₂ O ₃	-	-	-	-	-	-	2.9	1.8	3.2	3.45
CaO	-	-	-	-	-	-	63.6	65.4	65.5	62.32
MgO	0.95	3.77	0.98	2	1.2	3.72	1.3	1.4	0.6	2.88
Na ₂ O	-	-	-	-	-	-	-	-	-	0.09
K ₂ O	-	-	-	-	-	-	-	-	-	0.67
Na ₂ O+0.658*K ₂ O	0.57	0.50	0.63	0.55	0.46	0.49	0.69	0.52	0.67	0.531
SO ₃	2.81	2.33	3.36	2.79	3.2	2.27	3.5	2.9	3.3	2.75
LOI	-	-	-	-	-	-	1.9	1.44	1.2	0.1
Free CaO	0.77	0.77	2.3	2	1.02	0.7	2.9	1	0.8	-
C ₃ S	53	60	56	57	53	60	57	63	64	53.06
C ₂ S	23	14	16	18	21	14	14	12	9	19.46
C ₃ A	6	5.33	11	6	5	6	10	10	8	6.06
C ₄ AF	10	10	7	10	12	10	8	6	10	10.50
Blaine	374	362	342	350	350	362	358	354	367	373

Table G-3: Chemical and Physical Properties of SCM's

Supplementary Cementing Materials																
	FF1	FF2	FF3	FF4	FF5	FF6	FF7	FF8	FC1	FC2	FC3	FC4	UFFA	SF	S1	S2
SiO ₂	56.63	51.69	53.08	46.69	55.72	47.84	49.52	53.44	37.83	33.31	37.4	34.47	50.65	94.28	34.48	-
Al ₂ O ₃	30.68	24.81	28.3	19.69	19.42	18.05	17.63	19.96	19.83	18.39	17.74	20.35	26.64	0.04	11.35	-
Fe ₂ O ₃	4.94	4.22	8.14	5.09	4.23	5.03	5.51	7.24	6.17	5.4	5.89	5.65	4.66	0.06	0.67	-
CaO	0.69	13.12	1.33	18.35	13.14	19.93	19.53	12.24	23.13	28.91	25.93	26.50	10.85	0.51	41.73	-
MgO	0.73	2.29	0.98	2.97	2.94	3.32	2.8	2.79	4.62	5.25	5.24	4.70	2.23	0.57	7.32	-
Na ₂ O	0.12	0.18	0.52	1.77	0.82	0.82	0.55	0.5	1.74	1.64	1.63	1.76	0.41	0.06	0.14	-
K ₂ O	2.26	0.84	2.64	0.86	0.85	0.91	0.99	1.2	0.057	0.35	0.58	0.46	1.02	0.99	0.38	-
Na ₂ O+0.658*K ₂ O	1.607	0.733	2.257	2.336	1.379	1.419	1.201	1.290	1.778	1.870	2.012	2.063	1.081	0.711	0.390	-
SO ₃	0	0.46	0.03	0.82	0.47	1.21	1.1	0.63	1.5	2.27	1.8	1.71	1	0.16	1.88	0.35
LOI	2.1	0.23	2.81	0.4	-	0.54	0.43	0.17	0.67	0.34	0.5	0.25	0.39	3.1	0.83	-
Blaine	147.3	165.5	-	420.3	300	295.6	295.6	300.0	348.4	299.9	587.9	-	394.4	20000	331.6	552.0

Table G-4: Chemical and Physical Properties of SCM's from Literature

Supplementary Cementing Materials (AS-Schindler, 2002, ZG - Ge, 2006)															
	FF9 AS	FF10 AS	FF11 AS	FF12 ZG	FF13 ZG	FC5 AS	FC6 AS	FC7 AS	FC8 AS	FC9 ZG	FC10 ZG	S3 AS	S4 ZG	S5 ZG	S6 ZG
SiO ₂	57.3	58.2	54.1	46.92	45.33	32.7	39.6	32.4	35.6	31.83	32.62	-	37.18	35.68	37.32
Al ₂ O ₃	-	-	26.2	15.11	23.02	-	-	-	21.4	19.02	19.32	-	9.17	11.24	9
Fe ₂ O ₃	-	-	3	7.06	23.52	-	-	-	5.6	5.99	6.46	-	0.91	0.7	0.7
CaO	10.6	10.8	10.8	16.77	1.51	24.7	25.3	25.4	24.3	27.11	28.89	-	37.13	36.61	36.74
MgO	-	-	2.4	4.94	0.64	-	-	-	4.8	4.47	4.56	-	10.17	10.11	10.34
Na ₂ O	-	-	-	3.3	0.36	-	-	-	-	2.12	1.86	-	0.32	0.34	0.31
K ₂ O	-	-	-	2.17	1.76	-	-	-	-	0.27	0.35	-	0.43	0.41	0.37
Na ₂ O+0.658*K ₂ O	0.3	0.4	0.3	4.728	1.518	1.22	1.18	1.61	1.4	2.298	2.090	-	0.603	0.610	0.553
SO ₃	-	-	0.3	1.31	0.31	-	-	-	1.2	3.51	2.48	1.6	1.06	1.71	0.997
LOI	-	-	0.1	0.1	1.6	-	-	-	0.3	0.2	0.1	-	0	0	0
Blaine	-	-	-	-	-	-	-	-	-	-	-	506	-	-	-

Table G-5: Mixture Information and Semi-Adiabatic Calorimetry Results Summary – Model Dataset

Mixture Proportions								Chemical Admixture ASTM Designation								Hydration Parameters					Aggregate	
Cement	SCM 1		SCM2		Cement + SCM	Water	wc	B&D	A	MR	F-N	F-PC	C	AEA	Other	E _a	H _u	α	τ	β	CA	FA / (CA+FA)
					lb/ft ³	lb/ft ³																
					Note: LN=Liquid Nitrogen, CNI = Calcium Nitrite														J/mol			
C1	-	0%	-	0%	564	180	0.32	-	-	-	-	0.65%	-	-	-	40,650	481	0.664	15.581	1.318	SRG	0.40
C1	-	0%	-	0%	658	211	0.32	-	-	-	-	0.65%	-	-	-	40,650	481	0.643	13.001	1.249	SRG	0.40
C1	-	0%	-	0%	564	180	0.32	-	-	-	-	0.65%	-	-	-	40,650	481	0.710	12.780	1.147	SRG	0.40
C1	-	0%	-	0%	564	180	0.32	-	-	-	-	0.65%	-	-	-	40,650	481	0.714	13.371	0.997	SRG	0.40
C1	-	0%	-	0%	564	203	0.36	-	-	-	-	0.41%	-	-	-	40,650	481	0.661	12.214	1.059	SRG	0.40
C1	-	0%	-	0%	611	232	0.38	-	-	-	-	0.22%	-	-	-	40,650	481	0.775	12.476	1.059	SRG	0.40
C1	-	0%	-	0%	564	226	0.40	-	-	-	-	0.21%	-	-	-	40,650	481	0.728	12.741	1.060	SRG	0.40
C1	-	0%	-	0%	564	237	0.42	-	-	-	-	0.41%	-	-	-	40,650	481	0.801	12.285	1.041	LS	0.40
C1	-	0%	-	0%	564	237	0.42	0.35%	-	-	-	-	-	-	-	29,826	481	0.761	15.651	1.386	SRG	0.40
C1	-	0%	-	0%	470	197	0.42	-	0.29%	-	-	-	-	-	-	30,810	481	0.786	13.868	1.030	LS	0.40
C1	-	0%	-	0%	564	237	0.42	-	0.29%	-	-	-	-	-	-	30,810	481	0.786	12.748	1.133	SRG	0.40
C1	-	0%	-	0%	658	276	0.42	-	0.29%	-	-	-	-	-	-	30,810	481	0.735	11.665	1.136	SRG	0.40
C1	-	0%	-	0%	564	248	0.44	-	-	-	-	-	-	-	-	40,650	481	0.793	13.804	0.847	SRG	0.40
C1	-	0%	-	0%	517	248	0.48	-	-	-	-	-	-	-	-	40,650	481	0.896	15.164	0.831	SRG	0.40
C1	-	0%	-	0%	470	249	0.53	-	-	-	-	-	-	-	-	40,650	481	0.905	13.526	0.932	SRG	0.40
C2	-	0%	-	0%	564	248	0.44	-	-	-	-	-	-	-	-	38,725	482	0.712	11.924	0.959	SRG	0.45
C2	-	0%	-	0%	564	248	0.44	-	-	-	-	-	0.74%	-	-	36,165	482	0.774	12.597	0.887	SRG	0.45
C2	-	0%	-	0%	564	248	0.44	-	-	-	-	-	1.30%	-	-	34,245	482	0.785	12.144	0.929	SRG	0.45
C2	-	0%	-	0%	564	248	0.44	-	-	-	-	-	2.23%	-	-	31,045	482	0.803	10.653	0.793	SRG	0.45
C2	-	0%	-	0%	564	214	0.38	-	-	-	-	0.27%	-	-	-	38,725	482	0.694	12.117	0.994	SRG	0.45
C2	-	0%	-	0%	564	214	0.38	-	-	-	-	0.27%	-	-	CNI	38,725	482	0.662	13.080	1.131	SRG	0.45
C2	-	0%	-	0%	564	226	0.40	0.35%	-	-	-	-	-	-	-	27,901	482	0.687	17.587	1.652	SRG	0.46
C2	-	0%	-	0%	564	237	0.42	-	-	0.33%	-	-	-	-	-	38,725	482	0.648	15.732	1.109	LS	0.40
C2	-	0%	-	0%	564	248	0.44	0.35%	-	-	-	-	-	-	-	27,901	482	0.674	19.300	1.592	SRG	0.45
C2	-	0%	-	0%	534	235	0.44	-	-	-	1.25%	-	-	-	-	38,725	482	0.690	13.474	1.165	SRG	0.45
C2	-	0%	-	0%	564	248	0.44	-	-	-	-	0.27%	-	-	-	38,725	482	0.645	11.682	1.138	SRG	0.45
C3	-	0%	-	0%	658	290	0.44	-	-	-	-	-	-	-	-	41,290	463	0.721	14.340	0.897	SRG	0.45
C3	-	0%	-	0%	564	282	0.50	-	-	-	-	-	-	-	-	41,290	463	0.775	14.159	0.991	SRG	0.45
C6	-	0%	-	0%	564	237	0.42	-	0.29%	-	-	-	-	-	-	27,325	463	0.677	11.383	1.137	SRG	0.40
C6	-	0%	-	0%	564	237	0.42	-	0.29%	-	-	-	-	0.04%	-	27,325	463	0.656	11.010	1.140	SRG	0.40
C6	-	0%	-	0%	564	248	0.44	-	-	-	-	-	-	-	-	37,165	463	0.753	11.399	0.737	SRG	0.45
C6	-	0%	-	0%	564	248	0.44	0.35%	-	-	-	-	-	-	-	26,341	463	0.693	14.902	1.208	SRG	0.45

Table G-6: Mixture Information and Semi-Adiabatic Calorimetry Results Summary – Model Dataset

Mixture Proportions								Chemical Admixture ASTM Designation									Hydration Parameters					Aggregate	
Cement	SCM 1		SCM2		Cement + SCM	Water	w/c	B&D	A	MR	F-N	F-PC	C	AEA	Other	E _a	H _u	α	τ	β	CA	FA / (CA+FA)	
					lb/ft ³	lb/ft ³																	
					Note: LN=Liquid Nitrogen, CNI = Calcium Nitrite											J/mol	J/g	hrs					
C6	-	0%	-	0%	564	248	0.44	0.52%	-	-	-	-	-	-	-	25,000	463	0.691	23.341	1.680	SRG	0.45	
C6	-	0%	-	0%	564	248	0.44	-	-	-	0.78%	-	-	-	-	37,165	463	0.684	10.147	0.929	SRG	0.45	
C6	-	0%	-	0%	564	274	0.49	-	-	-	-	-	-	-	-	37,165	463	0.689	10.189	0.784	SRG	0.44	
C6	-	0%	-	0%	547	292	0.53	-	-	-	-	-	-	-	-	37,165	463	0.716	11.362	0.765	SRG	0.45	
C7	-	0%	-	0%	658	211	0.32	0.32%	-	-	1.25%	-	-	-	-	29,224	485	0.657	13.389	1.543	SRG	0.40	
C7	-	0%	-	0%	658	211	0.32	-	-	-	-	0.69%	-	-	-	39,064	485	0.614	11.186	1.387	SRG	0.40	
C8	-	0%	-	0%	658	211	0.32	-	-	-	-	0.69%	-	-	-	37,344	474	0.614	10.293	1.073	SRG	0.40	
C8	-	0%	-	0%	564	248	0.44	-	-	-	-	-	-	-	-	37,344	474	0.726	9.351	0.893	SRG	0.45	
C9	-	0%	-	0%	564	248	0.44	-	-	-	-	-	-	-	-	38,597	419	0.714	14.864	0.807	SRG	0.44	
C9	-	0%	-	0%	564	248	0.44	0.35%	-	-	-	-	-	-	-	27,773	419	0.694	27.220	1.436	SRG	0.45	
C9	-	0%	-	0%	560	247	0.44	-	-	0.66%	-	-	-	-	-	38,597	419	0.790	20.784	0.919	SRG	0.45	
C10	-	0%	-	0%	564	248	0.44	-	-	-	-	-	-	-	-	39,437	446	0.793	12.778	0.709	SRG	0.45	
C10	-	0%	-	0%	564	248	0.44	0.24%	-	-	-	-	-	-	-	32,057	446	0.678	15.014	1.191	SRG	0.45	
C10	-	0%	-	0%	564	248	0.44	0.35%	-	-	-	-	-	-	-	28,613	446	0.738	18.191	1.186	SRG	0.45	
C10	-	0%	-	0%	564	248	0.44	-	-	-	0.78%	-	-	-	-	39,437	446	0.731	11.221	0.955	SRG	0.45	
C10	-	0%	-	0%	564	248	0.44	-	-	-	-	0.27%	-	-	-	39,437	446	0.750	12.294	0.783	SRG	0.45	
C10	-	0%	-	0%	564	248	0.44	-	-	-	-	-	1.30%	-	-	34,957	446	0.875	11.968	0.638	SRG	0.45	
C12	-	0%	-	0%	552	248	0.45	-	-	-	-	-	-	-	-	37,882	462	0.811	13.008	0.803	SRG	0.45	
C12	-	0%	-	0%	564	248	0.44	-	-	-	-	-	-	-	LN	37,882	462	0.778	13.754	0.830	SRG	0.45	
C12	-	0%	-	0%	564	248	0.44	0.24%	-	-	-	-	-	-	-	30,502	462	0.843	14.859	0.987	SRG	0.45	
C12	-	0%	-	0%	564	248	0.44	0.24%	-	-	-	-	-	-	LN	30,502	462	0.780	16.288	1.155	SRG	0.45	
C12	-	0%	-	0%	564	248	0.44	-	0.44%	-	-	-	-	-	-	23,122	462	0.816	13.966	1.215	SRG	0.45	
C12	-	0%	-	0%	564	248	0.44	-	0.44%	-	-	-	-	-	LN	23,122	462	0.754	16.432	1.307	SRG	0.45	
C12	-	0%	-	0%	564	248	0.44	-	-	-	-	0.50%	-	-	-	37,882	462	0.827	13.982	0.922	SRG	0.45	
C12	-	0%	-	0%	564	248	0.44	-	-	-	-	0.50%	-	-	LN	37,882	462	0.816	14.762	0.858	SRG	0.45	
C12	-	0%	-	0%	564	248	0.44	-	-	-	0.70%	-	-	-	-	37,882	462	0.799	14.865	0.906	SRG	0.45	
C12	-	0%	-	0%	564	248	0.44	-	-	-	0.70%	-	-	-	LN	37,882	462	0.829	16.227	0.883	SRG	0.45	
C12	-	0%	-	0%	564	248	0.44	-	-	-	1.25%	-	-	-	-	37,882	462	0.767	14.271	0.944	SRG	0.45	
C12	-	0%	-	0%	564	248	0.44	-	-	-	1.25%	-	-	-	LN	37,882	462	0.809	15.271	1.025	SRG	0.45	
C12	-	0%	-	0%	564	248	0.44	-	-	-	-	0.41%	-	0.03%	-	37,882	462	0.824	13.462	0.857	SRG	0.45	
C12	-	0%	-	0%	564	248	0.44	-	-	-	-	0.41%	-	0.03%	LN	37,882	462	0.831	13.684	0.907	SRG	0.45	
C12	-	0%	-	0%	500	263	0.53	-	-	-	-	-	-	-	-	37,882	462	0.890	15.417	0.700	SRG	0.45	

Table G-7: Mixture Information and Semi-Adiabatic Calorimetry Results Summary – Model Dataset

Mixture Proportions								Chemical Admixture ASTM Designation								Hydration Parameters					Aggregate	
Cement	SCM 1		SCM2		Cement + SCM	Water	w/c	B&D	A	MR	F-N	F-PC	C	AEA	Other	E _a	H _u	α	τ	β	CA	FA / (CA+FA)
					Note: LN=Liquid Nitrogen, CNI = Calcium Nitrite																J/mol	J/g
C14	-	0%	-	0%	564	248	0.44	-	-	-	-	-	-	-	-	39,999	456	0.788	11.582	0.801	SRG	0.40
C16	-	0%	-	0%	517	217	0.42	-	0.22%	-	-	-	-	0.04%	-	31,357	471	0.734	17.875	0.960	SRG	0.40
C17	-	0%	-	0%	564	237	0.42	-	-	-	-	-	-	-	-	41,294	459	0.837	13.971	0.884	SRG	0.40
C1	FF1	20%	-	0%	564	237	0.42	-	0.29%	-	-	-	-	-	-	27,930	387	0.903	16.634	0.897	SRG	0.40
C1	FF1	30%	-	0%	564	237	0.42	-	0.29%	-	-	-	-	-	-	26,733	340	0.970	16.300	0.876	SRG	0.40
C1	FF1	30%	-	0%	564	248	0.44	-	-	-	-	-	-	-	-	36,573	340	0.908	15.551	0.731	SRG	0.40
C2	FF1	20%	-	0%	564	248	0.44	-	-	-	-	-	-	-	-	35,951	388	0.803	13.142	0.815	SRG	0.44
C2	FF1	30%	-	0%	564	248	0.44	-	-	-	-	-	-	-	-	34,798	341	0.889	14.032	0.817	SRG	0.44
C2	FF1	40%	-	0%	564	248	0.44	-	-	-	-	-	-	-	-	33,802	294	0.896	14.236	0.741	SRG	0.44
C6	FF1	20%	-	0%	564	248	0.44	-	-	-	-	-	-	-	-	35,347	372	0.845	12.340	0.651	SRG	0.44
C6	FF1	30%	-	0%	564	248	0.44	-	-	-	-	-	-	-	-	34,592	327	0.836	11.920	0.655	SRG	0.44
C6	FF1	30%	-	0%	564	237	0.42	0.35%	-	-	-	-	-	-	-	25,000	327	0.668	22.983	1.369	SRG	0.40
C6	FF1	40%	-	0%	564	248	0.44	-	-	-	-	-	-	-	-	33,942	282	0.902	13.310	0.665	SRG	0.45
C9	FF1	30%	-	0%	564	248	0.44	-	-	-	-	-	-	-	-	35,125	297	0.794	15.315	0.707	SRG	0.45
C10	FF1	30%	-	0%	564	248	0.44	-	-	-	-	-	-	-	-	35,997	316	0.788	13.123	0.676	SRG	0.44
C1	FF2	20%	-	0%	564	237	0.42	-	0.29%	-	-	-	-	-	-	28,666	432	0.854	16.789	0.962	SRG	0.40
C1	FF2	30%	-	0%	564	237	0.42	-	0.29%	-	-	-	-	-	-	27,837	408	0.850	18.524	0.891	SRG	0.40
C1	FF2	30%	-	0%	564	237	0.42	-	0.29%	-	-	-	-	-	-	27,837	408	0.886	19.407	0.843	SRG	0.40
C1	FF2	30%	-	0%	564	237	0.42	-	0.29%	-	-	-	-	-	-	27,837	408	0.801	19.473	1.010	SRG	0.40
C1	FF2	30%	-	0%	564	237	0.42	-	0.29%	-	-	-	-	-	-	27,837	408	0.822	15.221	0.954	SRG	0.40
C1	FF2	30%	-	0%	564	248	0.44	-	-	-	-	-	-	-	-	37,677	408	0.832	18.076	0.710	SRG	0.40
C1	FF2	30%	-	0%	564	237	0.42	0.35%	-	-	-	-	-	-	-	26,853	408	0.761	24.152	1.314	SRG	0.40
C2	FF2	20%	-	0%	564	299	0.53	-	-	-	-	-	-	-	-	36,687	433	0.851	16.263	0.744	SRG	0.40
C2	FF2	20%	-	0%	564	248	0.44	-	-	-	-	-	-	-	-	36,687	433	0.681	13.186	0.926	SRG	0.44
C2	FF2	20%	-	0%	564	248	0.44	-	-	-	-	-	0.74%	-	-	34,127	433	0.753	16.396	0.915	SRG	0.44
C2	FF2	21%	-	0%	543	236	0.44	-	-	-	-	-	-	0.08%	-	36,687	431	0.713	14.901	0.883	SRG	0.45
C2	FF2	30%	-	0%	560	336	0.60	0.08%	-	-	-	-	-	-	-	39,233	410	0.862	16.736	0.758	SRG	0.40
C2	FF2	30%	-	0%	564	254	0.45	-	-	-	-	-	-	-	-	35,902	408	0.710	13.854	0.872	SRG	0.42
C2	FF2	40%	-	0%	564	248	0.44	-	-	-	-	-	-	-	-	35,274	384	0.701	16.104	0.834	SRG	0.44
C6	FF2	20%	-	0%	564	248	0.44	-	-	-	-	-	-	-	-	36,082	417	0.725	12.671	0.699	SRG	0.45
C6	FF2	30%	-	0%	564	248	0.44	-	-	-	-	-	-	-	-	35,696	395	0.776	16.492	0.593	SRG	0.44
C6	FF2	30%	-	0%	564	237	0.42	0.35%	-	-	-	-	-	-	-	25,000	395	0.622	24.308	1.386	SRG	0.44

Table G-8: Mixture Information and Semi-Adiabatic Calorimetry Results Summary – Model Dataset

Mixture Proportions								Chemical Admixture ASTM Designation								Hydration Parameters					Aggregate	
Cement	SCM 1		SCM2		Cement + SCM	Water	w/c	B&D	A	MR	F-N	F-PC	C	AEA	Other	E _a	H _u	α	τ	β	CA	FA / (CA+FA)
					Note: LN=Liquid Nitrogen, CNI = Calcium Nitrite												J/mol	J/g	hrs			
C6	FF2	30%	-	0%	564	214	0.38	-	-	0.75%	-	-	-	-	-	35,696	395	0.692	23.180	0.839	SRG	0.44
C6	FF2	40%	-	0%	564	248	0.44	-	-	-	-	-	-	-	-	35,413	372	0.709	15.394	0.670	SRG	0.44
C8	FF2	20%	-	0%	658	211	0.32	-	-	-	-	0.41%	-	-	-	35,031	426	0.684	10.724	0.987	SRG	0.40
C9	FF2	30%	-	0%	564	248	0.44	-	-	-	-	-	-	-	-	36,229	364	0.691	16.590	0.695	SRG	0.44
C10	FF2	30%	-	0%	564	248	0.44	-	-	-	-	-	-	-	-	37,101	383	0.682	15.024	0.707	SRG	0.45
C9	FF3	30%	-	0%	564	248	0.44	-	-	-	-	-	-	-	-	35,182	301	0.826	17.171	0.637	SRG	0.45
C12	FF3	30%	-	0%	564	248	0.44	-	-	-	-	0.27%	-	-	-	35,037	331	0.879	16.844	0.745	SRG	0.43
C12	FF3	50%	-	0%	491	258	0.53	-	-	-	-	-	-	-	-	33,721	243	1.000	15.418	0.800	SRG	0.44
C12	FF3	50%	-	0%	564	248	0.44	-	-	-	-	-	-	-	-	33,721	243	1.000	16.137	0.735	SRG	0.44
C12	FF3	50%	-	0%	564	248	0.44	-	-	-	-	-	-	-	LN	33,721	243	1.000	17.133	0.768	SRG	0.44
C12	FF3	50%	-	0%	564	248	0.44	-	-	-	-	0.27%	-	-	-	33,721	243	1.000	17.778	0.677	SRG	0.44
C15	FF3	30%	-	0%	564	237	0.42	-	-	-	-	0.27%	-	0.03%	-	34,665	347	0.870	17.314	0.682	SRG	0.44
C15	FF3	30%	-	0%	564	237	0.42	-	-	-	-	0.27%	-	0.03%	LN	34,665	347	0.797	17.672	0.812	SRG	0.44
C13	FF4	29%	-	0%	591	207	0.35	0.33%	-	0.22%	-	-	-	0.10%	-	27,069	438	0.726	15.401	1.104	SRG	0.38
C13	FF4	31%	-	0%	611	214	0.35	0.19%	-	0.33%	-	-	-	0.08%	-	31,155	434	0.820	19.217	0.886	SRG	0.38
C13	FF4	40%	-	0%	564	248	0.44	-	-	-	-	-	-	-	-	36,750	421	0.815	15.594	0.656	SRG	0.45
C16	FF5	20%	-	0%	517	217	0.42	-	0.22%	-	-	-	-	0.04%	-	29,962	424	0.685	20.650	0.842	LS	0.40
C16	FF5	35%	-	0%	517	200	0.39	-	0.22%	-	-	-	-	0.02%	-	28,399	338	0.768	23.335	0.897	LS	0.40
C16	FF5	35%	-	0%	517	217	0.42	-	0.22%	-	-	-	-	0.04%	-	29,232	389	0.708	23.641	0.818	LS	0.40
C16	FF5	35%	-	0%	517	202	0.39	-	0.22%	-	-	-	-	-	-	29,232	389	0.738	29.213	0.658	LS	0.40
C11	FF6	44%	-	0%	506	175	0.35	-	0.36%	-	0.78%	-	-	0.05%	-	24,928	423	0.807	18.280	0.735	SRG	0.41
C11	FF6	55%	-	0%	557	187	0.34	-	0.20%	-	0.42%	-	-	0.04%	-	30,204	411	0.732	21.578	0.651	SRG	0.41
C11	FF6	55%	-	0%	557	212	0.38	-	0.74%	-	-	-	-	-	-	25,000	411	0.717	27.537	0.774	SRG	0.41
C11	FF6	55%	-	0%	557	212	0.38	-	0.74%	-	-	-	-	-	-	25,000	411	0.640	21.453	0.947	SRG	0.41
C2	FF7	20%	-	0%	530	209	0.40	-	0.27%	-	-	-	-	0.26%	-	28,196	456	0.645	15.589	0.855	SRG	0.45
C5	FF7	20%	-	0%	530	209	0.40	0.29%	-	-	-	-	-	-	-	28,359	447	0.725	19.329	0.784	LS	0.45
C1	FC1	20%	-	0%	564	237	0.42	-	0.29%	-	-	-	-	-	-	29,258	468	0.903	16.634	0.897	SRG	0.40
C1	FC1	30%	-	0%	564	248	0.44	-	-	-	-	-	-	-	-	38,566	462	0.747	16.782	0.904	LS	0.40
C1	FC1	30%	-	0%	564	237	0.42	0.35%	-	-	-	-	-	-	-	27,742	462	0.770	29.576	1.121	SRG	0.40
C2	FC1	20%	-	0%	564	248	0.44	-	-	-	-	-	-	-	-	37,279	469	0.817	17.357	0.760	SRG	0.44
C2	FC1	30%	-	0%	564	248	0.44	-	-	-	-	-	-	-	-	36,791	462	0.841	22.172	0.724	SRG	0.44
C2	FC1	30%	-	0%	564	248	0.44	-	-	-	-	-	1.30%	-	-	32,311	462	0.790	15.946	0.919	SRG	0.44

Table G-9: Mixture Information and Semi-Adiabatic Calorimetry Results Summary – Model Dataset

Mixture Proportions								Chemical Admixture ASTM Designation									Hydration Parameters					Aggregate	
Cement	SCM 1		SCM2		Cement + SCM	Water	wc	B&D	A	MR	F-N	F-PC	C	AEA	Other	E _a	H _u	α	τ	β	CA	FA / (CA+FA)	
																			lb/ft ³				lb/ft ³
					Note: LN=Liquid Nitrogen, CNI = Calcium Nitrite											J/mol	J/g						
C2	FC1	30%	-	0%	564	248	0.44	0.35%	-	-	-	-	-	-	-	25,967	462	0.696	28.086	1.560	SRG	0.44	
C2	FC1	40%	-	0%	564	248	0.44	-	-	-	-	-	-	-	-	36,459	456	0.742	22.936	0.765	SRG	0.44	
C6	FC1	20%	-	0%	564	248	0.44	-	-	-	-	-	-	-	-	36,675	453	0.670	19.161	0.605	SRG	0.40	
C6	FC1	30%	-	0%	564	248	0.44	-	-	-	-	-	-	-	-	36,585	449	0.911	29.493	0.525	SRG	0.45	
C6	FC1	40%	-	0%	564	248	0.44	-	-	-	-	-	-	-	-	36,598	444	1.000	43.451	0.495	SRG	0.44	
C8	FC1	30%	-	0%	658	211	0.32	-	-	-	-	0.41%	-	-	-	35,021	456	0.596	13.786	0.919	SRG	0.40	
C10	FC1	30%	-	0%	564	248	0.44	-	-	-	-	-	-	-	-	37,990	437	0.839	23.940	0.561	SRG	0.45	
C11	FC1	40%	-	0%	564	248	0.44	-	-	-	-	-	-	-	-	37,355	451	0.847	26.128	0.564	SRG	0.44	
C15	FC1	30%	-	0%	564	248	0.44	-	-	-	-	0.27%	-	0.02%	-	36,601	464	0.828	27.312	0.857	SRG	0.44	
C1	FC2	20%	-	0%	564	237	0.42	-	0.29%	-	-	-	-	-	-	29,600	489	0.803	19.815	1.087	SRG	0.40	
C1	FC2	30%	-	0%	564	248	0.44	-	-	-	-	-	-	-	-	39,079	493	0.787	22.711	0.753	SRG	0.40	
C1	FC2	30%	-	0%	564	237	0.42	0.18%	-	-	-	-	-	-	-	33,667	493	0.812	26.436	0.951	SRG	0.40	
C1	FC2	30%	-	0%	564	237	0.42	-	0.29%	-	-	-	-	-	-	29,239	493	0.740	21.418	1.028	SRG	0.40	
C1	FC2	30%	-	0%	564	237	0.42	0.35%	-	-	-	-	-	-	-	28,255	493	0.662	32.018	1.324	SRG	0.40	
C2	FC2	20%	-	0%	564	248	0.44	-	-	-	-	-	-	-	-	37,621	490	0.764	17.377	0.823	SRG	0.45	
C2	FC2	30%	-	0%	564	248	0.44	-	-	-	-	-	-	-	-	37,304	494	0.721	18.649	0.917	SRG	0.45	
C2	FC2	30%	-	0%	564	214	0.38	-	-	-	-	0.27%	-	-	-	37,304	494	0.699	19.031	0.913	SRG	0.45	
C2	FC2	30%	-	0%	564	214	0.38	-	-	-	0.78%	-	-	-	-	37,304	494	0.655	17.808	0.941	SRG	0.45	
C2	FC2	40%	-	0%	564	248	0.44	-	-	-	-	-	-	-	-	37,143	497	0.714	23.678	0.915	SRG	0.45	
C6	FC2	20%	-	0%	564	248	0.44	-	-	-	-	-	-	-	-	37,017	474	0.767	15.740	0.731	SRG	0.45	
C6	FC2	30%	-	0%	564	237	0.42	0.35%	-	-	-	-	-	-	-	26,274	480	0.739	34.268	1.103	SRG	0.45	
C6	FC2	30%	-	0%	564	248	0.44	-	-	-	-	-	-	-	-	37,098	480	0.770	27.678	0.566	SRG	0.40	
C6	FC2	40%	-	0%	564	248	0.44	-	-	-	-	-	-	-	-	37,283	486	0.819	32.424	0.610	SRG	0.44	
C9	FC2	30%	-	0%	564	248	0.44	-	-	-	-	-	-	-	-	37,631	450	0.923	41.159	0.480	SRG	0.44	
C9	FC2	30%	-	0%	564	249	0.44	-	-	-	-	-	-	-	-	37,631	450	0.926	43.866	0.490	SRG	0.45	
C10	FC2	30%	-	0%	564	248	0.44	-	-	-	-	-	-	-	-	38,503	468	0.852	26.859	0.566	SRG	0.45	
C10	FC2	30%	-	0%	564	248	0.44	-	-	-	0.78%	-	-	-	-	38,503	468	0.746	19.205	0.770	SRG	0.45	
C14	FC3	20%	-	0%	532	210	0.40	-	0.29%	-	-	-	-	0.04%	-	28,682	458	0.837	16.520	0.808	SRG	0.40	
C12	FC4	30%	-	0%	564	248	0.44	-	-	-	-	0.21%	-	-	-	36,973	448	0.936	29.916	0.695	SRG	0.44	
C12	FC4	30%	-	0%	564	248	0.44	-	-	-	-	-	-	-	-	36,973	448	1.000	31.324	0.642	SRG	0.44	
C15	FC4	30%	-	0%	564	248	0.44	-	-	-	-	0.21%	-	-	LN	36,601	464	0.850	26.053	0.769	SRG	0.44	
C15	FC4	30%	-	0%	564	248	0.44	-	-	-	-	-	-	-	LN	36,601	464	0.908	29.247	0.682	SRG	0.44	

Table G-10: Mixture Information and Semi-Adiabatic Calorimetry Results Summary – Model Dataset

Mixture Proportions								Chemical Admixture ASTM Designation									Hydration Parameters					Aggregate	
Cement	SCM 1		SCM2		Cement + SCM	Water	w/c	B&D	A	MR	F-N	F-PC	C	AEA	Other	E _a	H _u	α	τ	β	CA	FA / (CA+FA)	
					lb/ft ³	lb/ft ³																	
					Note: LN=Liquid Nitrogen, CNI = Calcium Nitrite											J/mol	J/g	hrs					
C1	S1	30%	-	0%	564	237	0.42	-	0.29%	-	-	-	-	-	-	31,532	475	1.000	22.135	0.750	SRG	0.40	
C1	S1	50%	-	0%	564	237	0.42	-	0.29%	-	-	-	-	-	-	32,824	471	0.921	28.367	0.664	SRG	0.40	
C1	S1	50%	-	0%	564	237	0.42	0.18%	-	-	-	-	-	-	-	37,252	471	0.797	26.549	0.694	SRG	0.40	
C1	S1	50%	-	0%	564	237	0.42	0.35%	-	-	-	-	-	-	-	31,840	471	0.699	26.202	1.094	SRG	0.40	
C2	S1	30%	-	0%	564	248	0.44	-	-	-	-	-	-	-	-	39,597	476	0.889	21.291	0.638	SRG	0.45	
C2	S1	40%	-	0%	564	248	0.44	-	-	-	-	-	-	-	-	40,200	474	0.918	26.057	0.592	SRG	0.45	
C2	S1	50%	-	0%	564	248	0.44	-	-	-	-	-	-	-	-	40,960	472	0.735	21.698	0.757	SRG	0.45	
C2	S1	50%	-	0%	564	248	0.44	-	-	-	-	-	0.74%	-	-	38,400	472	0.737	23.750	0.780	SRG	0.45	
C6	S1	50%	-	0%	564	248	0.44	-	-	-	-	-	-	-	-	41,392	462	0.961	42.531	0.461	SRG	0.45	
C6	S1	50%	-	0%	564	248	0.44	-	-	-	-	-	0.74%	-	-	38,832	462	0.890	30.283	0.592	SRG	0.45	
C9	S1	40%	-	0%	705	248	0.35	-	-	-	0.78%	-	-	-	-	40,644	436	0.911	43.825	0.510	SRG	0.45	
C9	S1	40%	-	0%	564	248	0.44	-	-	-	-	-	-	-	-	40,644	436	1.000	47.914	0.478	SRG	0.45	
C9	S1	40%	-	0%	564	248	0.44	-	-	-	-	-	-	-	-	40,644	436	1.000	53.192	0.465	SRG	0.45	
C9	S1	50%	-	0%	564	248	0.44	-	-	-	-	-	-	-	-	41,502	440	1.000	81.595	0.439	SRG	0.45	
C10	S1	48%	-	0%	584	258	0.44	-	-	0.41%	-	-	-	0.02%	-	42,168	453	0.986	39.731	0.485	SRG	0.43	
C10	S1	48%	-	0%	583	238	0.41	-	-	0.78%	-	-	-	0.05%	-	42,176	453	0.942	42.580	0.580	SRG	0.44	
C11	S1	30%	-	0%	564	248	0.44	-	-	-	-	-	-	-	-	40,315	471	0.966	27.479	0.482	SRG	0.45	
C11	S1	40%	-	0%	564	248	0.44	-	-	-	-	-	-	-	-	41,097	469	0.978	28.729	0.498	SRG	0.45	
C11	S1	50%	-	0%	564	248	0.44	-	-	-	-	-	-	-	-	42,008	468	1.000	39.858	0.460	SRG	0.45	
C12	S1	50%	-	0%	564	248	0.44	-	-	-	-	0.21%	-	-	-	41,624	461	0.949	32.809	0.583	SRG	0.44	
C12	S1	50%	-	0%	564	248	0.44	-	-	-	-	0.34%	-	-	-	41,624	461	0.843	28.876	0.639	SRG	0.44	
C16	S2	35%	-	0%	517	208	0.40	-	0.22%	-	-	-	-	-	-	33,541	467	0.718	24.992	0.830	LS	0.40	
C2	SF	5%	-	0%	564	248	0.44	-	-	-	-	-	-	-	-	35,383	458	0.739	11.772	1.024	SRG	0.45	
C6	SF	10%	-	0%	564	248	0.44	-	-	-	-	-	-	-	-	31,024	416	0.944	14.812	0.643	SRG	0.45	
C9	SF	10%	-	0%	560	190	0.34	0.24%	-	-	1.25%	-	-	-	-	24,741	377	0.973	18.412	0.717	SRG	0.45	
C6	UFFA	15%	-	0%	564	248	0.44	-	-	-	-	-	-	-	-	36,213	422	0.786	14.907	0.679	SRG	0.45	
C6	FF2	15%	UFFA	15%	564	248	0.44	-	-	-	-	-	-	-	-	35,595	388	0.803	15.513	0.670	SRG	0.45	
C11	FF6	24%	UFFA	9%	557	187	0.34	-	0.20%	-	0.54%	-	-	0.04%	-	30,061	422	0.783	16.195	0.724	SRG	0.41	
C11	FF6	38%	UFFA	5%	495	160	0.32	-	0.24%	-	0.56%	-	-	0.04%	-	28,909	416	0.700	17.334	0.905	SRG	0.41	
C11	FF6	45%	UFFA	9%	557	187	0.34	-	0.20%	-	0.47%	-	-	0.04%	-	30,012	398	0.696	18.348	0.771	SRG	0.41	
C2	FC2	30%	UFFA	8%	564	180	0.32	-	-	-	-	0.69%	-	-	-	36,735	471	0.660	24.864	1.047	SRG	0.44	
C2	FC2	30%	UFFA	12%	564	180	0.32	-	-	-	-	0.58%	-	-	-	36,488	459	0.678	23.600	1.072	SRG	0.44	

Table G-11: Mixture Information and Semi-Adiabatic Calorimetry Results Summary – Model Dataset

Mixture Proportions								Chemical Admixture ASTM Designation								Hydration Parameters					Aggregate	
Cement	SCM 1		SCM2		Cement + SCM	Water	wc	B&D	A	MR	F-N	F-PC	C	AEA	Other	E _a	H _u	α	τ	β	CA	FA / (CA+FA)
					Note: LN=Liquid Nitrogen, CNI = Calcium Nitrite																	
C2	FC3	30%	UFFA	8%	564	180	0.32	0.35%	-	-	1.25%	-	-	-	-	25,258	430	0.773	38.680	1.468	SRG	0.44
C2	FF1	20%	SF	5%	564	248	0.44	0.06%	-	-	-	-	-	-	-	30,797	364	0.870	14.041	0.868	SRG	0.44
C2	FC2	30%	SF	5%	564	248	0.44	-	-	-	-	-	-	-	-	34,196	470	0.758	18.734	0.861	SRG	0.44
C2	FC2	30%	SF	5%	564	180	0.32	-	-	-	-	0.69%	-	-	-	34,196	470	0.690	20.264	1.034	SRG	0.44
C2	FC2	35%	SF	5%	564	248	0.44	-	-	-	-	-	-	-	-	34,135	471	0.736	19.732	0.923	SRG	0.44
C6	FC2	30%	SF	5%	564	248	0.44	-	-	-	-	-	-	-	-	34,170	457	0.817	21.175	0.669	SRG	0.45
C2	FC3	30%	SF	5%	564	180	0.32	-	-	-	1.25%	-	-	-	-	33,931	453	0.748	22.162	0.803	SRG	0.44
C16	FF5	15%	S2	35%	517	226	0.44	-	0.22%	-	-	-	-	-	-	33,083	432	0.766	28.149	0.774	LS	0.40

Table G-12: Mixture Information and Semi-Adiabatic Calorimetry Results Summary – Validation Dataset

Mixture Proportions									Chemical Admixture ASTM Designation							Hydration Parameters					Aggregate	
Cement	SCM 1		SCM2		Cement + SCM	Water	wc	Field Site?	B&D	A	MR	F-N	F-PC	C	AEA	Ea	H _u	α	τ	β	CA	FA / (CA+FA)
					lb/ft ³	lb/ft ³										J/mol	J/g		hrs			
C5	FF7	20%	-	0%	530	225	0.42	Y	-	0.27%	-	-	-	-	0.21%	28,359	447	0.679	14.604	0.868	LS	0.45
C5	FF7	20%	-	0%	531	225	0.42	Y	-	0.27%	-	-	-	-	0.21%	28,362	447	0.747	17.200	0.809	LS	0.45
C13	FF4	29%	-	0%	591	207	0.35	Y	-	0.20%	0.34%	-	-	-	0.10%	30,513	438	0.804	13.502	0.884	SRG	0.38
C14	FC3	20%	-	0%	532	210	0.40	Y	-	0.29%	-	-	-	-	0.04%	28,623	458	0.835	15.870	0.867	G	0.40
C5	FF7	26%	-	0%	555	260	0.47	Y	0.07%	0.20%	-	-	-	-	0.10%	28,057	440	0.888	22.155	0.836	LS	0.45
C5	FF7	26%	-	0%	682	279	0.41	Y	0.06%	0.23%	-	-	-	-	0.09%	27,583	440	0.867	23.245	0.865	LS	0.44
C11	FF6	44%	-	0%	506	175	0.35	Y	-	0.36%	-	0.78%	-	-	0.05%	25,000	423	0.666	21.988	0.672	SRG	0.40
C13	FF4	31%	-	0%	611	214	0.35	Y	-	0.18%	0.33%	-	-	-	0.11%	31,153	434	0.780	22.745	0.802	SRG	0.42
C10	S1	48%	-	0%	583	234	0.40	Y	-	-	0.78%	-	-	-	0.04%	42,176	453	1.000	38.444	0.532	LS	0.38
AS1	FF9-AS	16%	-	0%	494	193	0.39	Y	0.18%	-	-	-	-	-	0.10%	36,848	409	0.725	15.500	1.010	LS	0.44
AS2	FC5-AS	21%	-	0%	536	238	0.44	Y	0.22%	-	-	-	-	-	0.04%	36,636	476	0.841	31.050	0.818	LS	0.37
AS3	-	0%	-	0%	470	217	0.46	Y	0.18%	-	-	-	-	-	0.02%	45,712	489	0.729	13.390	0.935	LS	0.36
AS4	FC6-AS	32%	-	0%	539	220	0.41	Y	0.24%	-	-	-	-	-	0.06%	35,341	475	0.857	28.350	0.720	LS	0.41
AS5	FF10-AS	18%	-	0%	458	229	0.50	Y	0.36%	-	-	-	-	-	0.05%	39,310	405	0.788	17.890	0.681	LS	0.41
AS6	FC7-AS	22%	-	0%	585	238	0.41	Y	0.19%	-	-	-	-	-	0.08%	38,375	480	0.850	35.950	0.573	LS	0.39
AS7	FC8-AS	30%	-	0%	517	207	0.40	N	0.12%	-	-	-	-	-	0.03%	40,304	465	0.884	23.810	0.674	LS	0.42
AS7	-	0%	-	0%	564	207	0.37	N	0.11%	-	-	-	-	-	0.03%	45,991	477	0.689	13.690	0.905	LS	0.43
AS7	FC8-AS	13%	-	0%	553	207	0.37	N	0.12%	-	-	-	-	-	0.03%	43,148	471	0.713	13.810	0.874	LS	0.41
AS7	FC8-AS	23%	-	0%	546	207	0.38	N	0.12%	-	-	-	-	-	0.03%	41,252	468	0.793	23.280	0.772	LS	0.41
AS7	FC8-AS	32%	-	0%	539	207	0.38	N	0.12%	-	-	-	-	-	0.03%	39,357	464	0.893	29.430	0.716	LS	0.41
AS7	FC8-AS	42%	-	0%	532	207	0.39	N	0.12%	-	-	-	-	-	0.03%	37,461	460	0.849	36.660	0.724	LS	0.41
AS7	FF11-AS	12%	-	0%	542	207	0.38	N	0.12%	-	-	-	-	-	0.03%	40,703	444	0.797	15.970	0.825	LS	0.41
AS7	FF11-AS	20%	-	0%	527	207	0.39	N	0.12%	-	-	-	-	-	0.03%	37,178	421	0.831	18.300	0.786	LS	0.41
AS7	FF11-AS	28%	-	0%	513	207	0.40	N	0.12%	-	-	-	-	-	0.03%	33,653	396	0.838	19.080	0.809	LS	0.41
AS7	FF11-AS	38%	-	0%	498	207	0.42	N	0.13%	-	-	-	-	-	0.03%	30,127	370	0.894	21.730	0.774	LS	0.41
AS7	S3-AS	28%	-	0%	551	207	0.38	N	0.12%	-	-	-	-	-	0.03%	51,510	472	0.822	25.220	0.625	LS	0.41
AS7	S3-AS	48%	-	0%	543	207	0.38	N	0.12%	-	-	-	-	-	0.03%	55,189	469	0.854	38.220	0.554	LS	0.41
AS8	-	0%	-	0%	517	259	0.50	N	0.12%	-	-	-	-	-	0.03%	41,977	513	0.887	16.880	0.719	LS	0.41
AS9	-	0%	-	0%	517	259	0.50	N	0.12%	-	-	-	-	-	0.03%	46,269	492	0.882	16.320	0.727	LS	0.41
C1	FF2	30%	-	0%	564	235	0.42	N	0.18%	-	-	-	-	-	-	32,265	408	0.726	17.499	1.321	SRG	0.40
C1	FF2	30%	-	0%	564	237	0.42	N	0.53%	-	-	-	-	-	-	25,000	408	0.700	39.675	2.147	SRG	0.40
C2	FC2	30%	-	0%	564	237	0.42	N	0.35%	-	-	-	-	-	-	26,480	493	0.668	36.796	1.735	SRG	0.40

Table G-13: Mixture Information and Semi-Adiabatic Calorimetry Results Summary – Validation Dataset

Mixture Proportions								Chemical Admixture ASTM Designation								Hydration Parameters					Aggregate	
Cement	SCM 1		SCM 2		Cement + SCM	Water	wc	Field Site?	B&D	A	MR	F-N	F-PC	C	AEA	Ea	Hu	α	τ	β	CA	FA / (CA+FA)
					lb/ft ³	lb/ft ³										J/mol	J/g		hrs			
C16	S2	50%	-	0%	517	217	0.42	N	0.24%	-	-	-	-	-	-	34,929	466	0.694	28.080	0.830	LS	0.41
C18	FF8	25%	-	0%	588	263	0.45	N	0.23%	-	-	-	-	-	0.02%	29,634	353	0.800	18.249	0.766	SRG	0.40
Z1	-	0%	-	0%	564	225	0.40	N	-	0.30%	-	-	-	-	0.04%	36,489	471	0.740	14.784	0.897	LS	0.44
Z1	-	0%	-	0%	564	225	0.40	N	-	0.30%	-	-	-	-	0.04%	36,489	471	0.760	16.269	0.890	LS	0.44
Z1	FC9-ZG	15%	-	0%	564	225	0.40	N	-	0.30%	-	-	-	-	0.04%	35,903	473	0.800	21.648	0.826	LS	0.44
Z1	FC9-ZG	30%	-	0%	564	225	0.40	N	-	0.00%	-	-	-	-	0.04%	35,607	476	0.820	27.000	0.721	LS	0.44
Z1	FC9-ZG	45%	-	0%	564	225	0.40	N	-	0.00%	-	-	-	-	0.04%	35,602	479	0.870	33.639	0.647	LS	0.44
Z1	FC9-ZG	60%	-	0%	564	225	0.40	N	-	0.00%	-	-	-	-	0.04%	35,886	481	0.900	50.328	0.575	LS	0.44
Z1	S3-ZG	15%	-	0%	564	225	0.40	N	-	0.30%	-	-	-	-	0.04%	37,129	470	0.780	19.379	0.753	LS	0.44
Z1	S3-ZG	30%	-	0%	564	225	0.40	N	-	0.30%	-	-	-	-	0.04%	38,060	468	0.860	30.093	0.579	LS	0.44
Z1	S3-ZG	45%	-	0%	564	225	0.40	N	-	0.30%	-	-	-	-	0.04%	39,281	467	0.930	49.334	0.499	LS	0.44
Z1	FC9-ZG	4%	S4-ZG	11%	564	225	0.40	N	-	0.30%	-	-	-	-	0.04%	36,823	470	0.820	23.251	0.728	LS	0.44
Z1	FC9-ZG	8%	S4-ZG	23%	564	225	0.40	N	-	0.30%	-	-	-	-	0.04%	37,447	470	0.850	32.728	0.647	LS	0.44
Z1	FC9-ZG	11%	S4-ZG	34%	564	225	0.40	N	-	0.30%	-	-	-	-	0.04%	38,361	470	0.890	42.166	0.501	LS	0.44
Z1	FC9-ZG	15%	S4-ZG	45%	564	225	0.40	N	-	0.30%	-	-	-	-	0.04%	39,565	469	0.950	80.048	0.429	LS	0.44
Z1	FC9-ZG	11%	S4-ZG	4%	564	225	0.40	N	-	0.30%	-	-	-	-	0.04%	36,209	472	0.800	18.790	0.790	LS	0.44
Z1	FC9-ZG	23%	S4-ZG	8%	564	225	0.40	N	-	0.30%	-	-	-	-	0.04%	36,220	474	0.820	24.972	0.673	LS	0.44
Z1	FC9-ZG	34%	S4-ZG	11%	564	225	0.40	N	-	0.00%	-	-	-	-	0.04%	36,521	476	0.830	35.487	0.588	LS	0.44
Z1	FC9-ZG	45%	S4-ZG	15%	564	225	0.40	N	-	0.00%	-	-	-	-	0.04%	37,113	477	0.950	61.246	0.497	LS	0.44
Z1	FF12-ZG	30%	-	0%	564	225	0.40	N	-	0.00%	-	-	-	-	0.04%	34,689	420	0.810	24.677	0.773	LS	0.44
Z1	FF13-ZG	30%	-	0%	564	225	0.40	N	-	0.00%	-	-	-	-	0.04%	33,334	338	0.830	16.120	0.788	LS	0.44
Z1	FC10-ZG	30%	-	0%	564	225	0.40	N	-	0.00%	-	-	-	-	0.04%	35,765	486	0.840	35.469	0.800	LS	0.44
Z1	S5-ZG	30%	-	0%	564	225	0.40	N	-	0.30%	-	-	-	-	0.04%	38,060	468	0.950	29.752	0.701	LS	0.44
Z1	S6-ZG	30%	-	0%	564	225	0.40	N	-	0.30%	-	-	-	-	0.04%	38,060	468	0.870	30.047	0.588	LS	0.44

Bogue - 1 Variable

IAlpha		ITau		IBeta	
R ²	Variables	R ²	Variables	R ²	Variables
	1		1		1
0.180	perCemNa2Oeq	0.433	perC3S	0.343	perC3A
0.178	wc	0.358	perGypsum	0.328	perGypsum
0.104	perGypsum	0.318	PerSlag	0.252	perC3S
0.087	WRRET	0.303	perCemNa2Oeq	0.246	WRRET
0.067	perFreeCaO	0.254	perC3A	0.220	perCemNa2Oeq
0.066	perC3S	0.212	perMgO	0.201	PerSlag
0.052	PCHRWR	0.078	i17	0.155	perMgO
0.047	perC3A	0.061	TotalFACaO	0.082	wc
0.039	PerAir	0.041	WRRET	0.051	PCHRWR
0.038	PerSlag	0.034	perC4AF	0.040	PerAir
0.020	CemBlaine	0.031	PCHRWR	0.022	LRWR
0.016	AIR	0.025	perCemNa2O	0.016	HRWR
0.014	i17	0.021	MRWR	0.010	CemBlaine
0.014	perMgO	0.015	CemBlaine	0.010	perCemNa2O
0.013	HRWR	0.015	ACCL	0.006	perC2S

Figure G.1: Results from PROC RSQUARE , Bogue Calculations, One Variable**Rietveld - 1 Variable**

IAlpha		ITau		IBeta	
R ²	Variables	R ²	Variables	R ²	Variables
	1		1		1
0.180	perCemNa2Oeq	0.435	perAlite	0.302	perAluminate
0.178	wc	0.318	PerSlag	0.284	perAlite
0.087	WRRET	0.303	perCemNa2Oeq	0.246	WRRET
0.086	perBelite	0.175	perAluminate	0.201	PerSlag
0.067	perFreeCaO	0.078	i17	0.082	wc
0.052	PCHRWR	0.063	perBelite	0.051	PCHRWR
0.051	i10	0.061	TotalFACaO	0.040	PerAir
0.042	perAlite	0.041	WRRET	0.028	perBelite
0.039	PerAir	0.031	PCHRWR	0.022	LRWR
0.038	PerSlag	0.027	perFerrite	0.016	HRWR
0.035	perAluminate	0.025	perCemNa2O	0.010	CemBlaine
0.029	i21	0.021	MRWR	0.010	perCemNa2O
0.020	CemBlaine	0.015	CemBlaine	0.008	perFerrite
0.016	AIR	0.015	ACCL	0.004	i17
0.015	perPericlase	0.010	perFreeCaO	0.003	TotalFACaO

Figure G.2: Results from PROC RSQUARE , Rietveld Calculations, One Variable

Bogue - 2 Variables								
IAlpha			ITau			IBeta		
R ²	Variables		R ²	Variables		R ²	Variables	
	1	2		1	2		1	2
0.383	wc	perCemNa2Oeq	0.518	perC3S	PerSlag	0.590	perC3A	WRRET
0.268	perC3S	wc	0.509	PerSlag	i17	0.557	perGypsum	WRRET
0.262	perGypsum	wc	0.491	perGypsum	PerSlag	0.476	perC3S	WRRET
0.258	WRRET	perCemNa2Oeq	0.487	perC3S	WRRET	0.448	WRRET	perCemNa2Oeq
0.253	WRRET	wc	0.484	PerSlag	TotalFACaO	0.440	WRRET	PerSlag
0.227	perCemNa2Oeq	i17	0.479	perC3S	perGypsum	0.425	perC3A	PerSlag
0.225	PCHRWR	perCemNa2Oeq	0.472	perC3S	perC3A	0.400	perC3S	perC3A
0.219	perFreeCaO	perCemNa2Oeq	0.467	perC3S	perCemNa2Oeq	0.392	perC3A	wc
0.212	perMgO	wc	0.454	perC3S	perC4AF	0.391	perGypsum	PerSlag
0.211	perFreeCaO	wc	0.453	PerSlag	perCemNa2Oeq	0.387	perC2S	perGypsum
0.210	TotalFACaO	perCemNa2Oeq	0.451	perC3S	perCemNa2O	0.386	perGypsum	wc
0.209	PerAir	perCemNa2Oeq	0.447	perC3S	LRWR	0.382	perC3A	perC4AF
0.207	PerSlag	wc	0.445	perC3S	perFreeCaO	0.381	perC3A	perGypsum
0.207	perC3A	wc	0.441	perC3S	MRWR	0.371	perGypsum	PerAir
0.197	AIR	perCemNa2Oeq	0.440	perC3A	PerSlag	0.366	perC3S	wc

Figure G.3: Results from PROC RSQUARE, Bogue Calculations, Two Variables

Rietveld - 2 Variables								
IAlpha			ITau			IBeta		
R ²	Variables		R ²	Variables		R ²	Variables	
	1	2		1	2		1	2
0.383	wc	perCemNa2Oeq	0.526	perAlite	PerSlag	0.543	perAluminate	WRRET
0.268	perBelite	wc	0.509	PerSlag	i17	0.515	perAlite	WRRET
0.258	WRRET	perCemNa2Oeq	0.485	perAlite	WRRET	0.440	WRRET	PerSlag
0.253	WRRET	wc	0.484	PerSlag	TotalFACaO	0.405	perAluminate	PerSlag
0.234	perAlite	wc	0.471	perAlite	perCemNa2Oeq	0.392	perAlite	wc
0.227	perCemNa2Oeq	i17	0.454	perAlite	perCemNa2O	0.378	perAlite	perAluminate
0.225	PCHRWR	perCemNa2Oeq	0.454	perAlite	perFreeCaO	0.367	perAlite	perFerrite
0.223	wc	i10	0.453	PerSlag	perCemNa2Oeq	0.360	perAluminate	perFerrite
0.219	perFreeCaO	perCemNa2Oeq	0.450	perAlite	i10	0.346	perAluminate	PerAir
0.211	perFreeCaO	wc	0.449	perAlite	perPericlase	0.345	perAluminate	wc
0.210	TotalFACaO	perCemNa2Oeq	0.445	perAlite	MRWR	0.345	WRRET	PCHRWR
0.209	PerAir	perCemNa2Oeq	0.443	perAlite	LRWR	0.340	perAlite	PerSlag
0.207	PerSlag	wc	0.442	perAlite	perBelite	0.323	perAluminate	HRWR
0.199	wc	i21	0.441	perAlite	i21	0.320	perAluminate	perFreeCaO
0.197	AIR	perCemNa2Oeq	0.440	perAlite	CemBlaine	0.319	perAluminate	perPericlase

Figure G.4: Results from PROC RSQUARE, Rietveld Calculations, Two Variables

Bogue - 3 and 4 Variables								
Alpha								
R ²	Variables			R ²	Variables			
	1	2	3		1	2	3	4
0.449	WRRET	wc	perCemNa2Oeq	0.468	perC3A	WRRET	wc	perCemNa2Oeq
0.406	perC3A	wc	perCemNa2Oeq	0.468	WRRET	wc	perCemNa2Oeq	i17
0.397	wc	perCemNa2Oeq	i17	0.462	WRRET	wc	TotalFACaO	perCemNa2Oeq
0.395	perFreeCaO	wc	perCemNa2Oeq	0.456	perFreeCaO	WRRET	wc	perCemNa2Oeq
0.393	wc	TotalFACaO	perCemNa2Oeq	0.455	WRRET	ACCL	wc	perCemNa2Oeq
0.392	ACCL	wc	perCemNa2Oeq	0.454	perC2S	WRRET	wc	perCemNa2Oeq
0.389	perC4AF	wc	perCemNa2Oeq	0.454	perMgO	WRRET	wc	perCemNa2Oeq
0.389	wc	PerAir	perCemNa2Oeq	0.454	perGypsum	WRRET	wc	perCemNa2Oeq
0.388	perGypsum	wc	perCemNa2Oeq	0.453	WRRET	wc	perCemNa2O	perCemNa2Oeq
0.386	perC2S	wc	perCemNa2Oeq	0.452	perC4AF	WRRET	wc	perCemNa2Oeq
0.385	AIR	wc	perCemNa2Oeq	0.452	WRRET	wc	CemBlaine	perCemNa2Oeq
0.385	PerSF	wc	perCemNa2Oeq	0.452	WRRET	AIR	wc	perCemNa2Oeq
0.385	perMgO	wc	perCemNa2Oeq	0.451	WRRET	PCHRWR	wc	perCemNa2Oeq
0.384	wc	perCemNa2O	perCemNa2Oeq	0.450	WRRET	LRWR	wc	perCemNa2Oeq
0.384	perC3S	wc	perCemNa2Oeq	0.449	perC3S	WRRET	wc	perCemNa2Oeq

Figure G.5: Results from PROC RSQUARE, Bogue Calculations, Three and Four Variables, $\ln(\alpha_i)$

ITau								
R ²	Variables			R ²	Variables			
	1	2	3		1	2	3	4
0.573	perC3A	PerSlag	i17	0.630	perC3A	WRRET	PerSlag	i17
0.571	perC3S	WRRET	PerSlag	0.622	WRRET	PerSlag	perCemNa2Oeq	i17
0.568	WRRET	PerSlag	i17	0.620	perC3S	PerSlag	perCemNa2O	i17
0.563	perC3A	PerSlag	TotalFACaO	0.619	perGypsum	WRRET	PerSlag	i17
0.563	PerSlag	perCemNa2O	i17	0.618	perGypsum	PerSlag	perCemNa2O	i17
0.562	PerSlag	perCemNa2Oeq	i17	0.618	perC3S	WRRET	PerSlag	i17
0.561	perGypsum	PerSlag	i17	0.616	perC3A	WRRET	PerSlag	TotalFACaO
0.559	perC3S	PerSlag	i17	0.616	PerSlag	perCemNa2O	perCemNa2Oeq	i17
0.555	perGypsum	PerSlag	TotalFACaO	0.612	perC2S	perGypsum	PerSlag	i17
0.553	perC3S	PerSlag	TotalFACaO	0.612	WRRET	PerSlag	perCemNa2O	i17
0.553	PerSlag	TotalFACaO	perCemNa2Oeq	0.611	WRRET	PerSlag	TotalFACaO	perCemNa2Oeq
0.552	perC3S	perGypsum	PerSlag	0.610	perGypsum	WRRET	PerSlag	TotalFACaO
0.548	perC3S	perC3A	PerSlag	0.610	perC3S	WRRET	PerSlag	TotalFACaO
0.541	perGypsum	WRRET	PerSlag	0.606	perC3S	perGypsum	WRRET	PerSlag
0.540	perC3S	PerSlag	perCemNa2Oeq	0.604	perC2S	perGypsum	PerSlag	TotalFACaO

Figure G.6: Results from PROC RSQUARE, Bogue Calculations, Three and Four Variables, $\ln(\tau)$

lBeta								
R ²	Variables			R ²	Variables			
	1	2	3		1	2	3	4
0.667	perC3A	WRRET	PerSlag	0.715	perC2S	perGypsum	WRRET	LRWR
0.640	perC2S	perGypsum	WRRET	0.702	perC3A	WRRET	PerSlag	wc
0.635	perC3S	perC3A	WRRET	0.699	perC3A	WRRET	LRWR	PerSlag
0.628	perC3A	WRRET	wc	0.694	perC3A	WRRET	PCHRWR	PerSlag
0.628	perGypsum	WRRET	LRWR	0.692	perC3S	perC3A	WRRET	wc
0.627	perC3A	WRRET	LRWR	0.687	perC3S	perC3A	WRRET	LRWR
0.620	perGypsum	WRRET	PerSlag	0.687	perC2S	perGypsum	WRRET	PerSlag
0.619	perC3A	WRRET	PCHRWR	0.686	perC3A	WRRET	PerSlag	CemBlaine
0.619	perC3A	perGypsum	WRRET	0.685	perGypsum	WRRET	LRWR	PCHRWR
0.618	perC3A	perC4AF	WRRET	0.683	perC2S	perGypsum	WRRET	wc
0.613	perC3A	WRRET	CemBlaine	0.680	perC3S	perC3A	WRRET	PerSlag
0.605	perGypsum	WRRET	wc	0.678	perC3A	perGypsum	WRRET	PerSlag
0.602	perC3A	WRRET	perCemNa2Oeq	0.678	perC3A	WRRET	MRWR	PerSlag
0.601	perC3A	WRRET	HRWR	0.677	perGypsum	WRRET	LRWR	PerSlag
0.596	perC3A	WRRET	MRWR	0.675	perC3A	WRRET	HRWR	PerSlag

Figure G.7: Results from PROC RSQUARE, Bogue Calculations, Three and Four Variables, $\ln(\beta)$

Rietveld - 3 and 4 Variables								
IAlpha								
R ²	Variables			R ²	Variables			
	1	2	3		1	2	3	4
0.449	WRRET	wc	perCemNa2Oeq	0.468	WRRET	wc	perCemNa2Oeq	i17
0.399	perAluminate	wc	perCemNa2Oeq	0.464	perAluminate	WRRET	wc	perCemNa2Oeq
0.397	wc	perCemNa2Oeq	i17	0.462	WRRET	wc	TotalFACaO	perCemNa2Oeq
0.395	perFreeCaO	wc	perCemNa2Oeq	0.460	WRRET	wc	perCemNa2Oeq	i10
0.393	wc	TotalFACaO	perCemNa2Oeq	0.456	perFreeCaO	WRRET	wc	perCemNa2Oeq
0.393	wc	perCemNa2Oeq	i10	0.455	perFerrite	WRRET	wc	perCemNa2Oeq
0.392	ACCL	wc	perCemNa2Oeq	0.455	WRRET	ACCL	wc	perCemNa2Oeq
0.392	perFerrite	wc	perCemNa2Oeq	0.454	perPericlase	WRRET	wc	perCemNa2Oeq
0.391	perBelite	wc	perCemNa2Oeq	0.453	WRRET	wc	perCemNa2O	perCemNa2Oeq
0.389	wc	PerAir	perCemNa2Oeq	0.453	perBelite	WRRET	wc	perCemNa2Oeq
0.385	perAlite	wc	perCemNa2Oeq	0.452	WRRET	wc	CemBlaine	perCemNa2Oeq
0.385	AIR	wc	perCemNa2Oeq	0.452	WRRET	AIR	wc	perCemNa2Oeq
0.385	PerSF	wc	perCemNa2Oeq	0.451	perAlite	WRRET	wc	perCemNa2Oeq
0.384	wc	perCemNa2O	perCemNa2Oeq	0.451	WRRET	PCHRWR	wc	perCemNa2Oeq
0.384	wc	perCemNa2Oeq	i21	0.450	WRRET	LRWR	wc	perCemNa2Oeq

Figure G.8: Results from PROC RSQUARE, Rietveld Calculations, Three and Four Variables, $\ln(\alpha_i)$

ITau								
R ²	Variables			R ²				
	1	2	3		1	2	3	4
0.576	perAlite	WRRET	PerSlag	0.629	perAlite	PerSlag	perCemNa2O	i17
0.568	WRRET	PerSlag	i17	0.622	WRRET	PerSlag	perCemNa2Oeq	i17
0.565	perAlite	PerSlag	i17	0.622	perAlite	WRRET	PerSlag	i17
0.563	PerSlag	perCemNa2O	i17	0.616	PerSlag	perCemNa2O	perCemNa2Oeq	i17
0.562	PerSlag	perCemNa2Oeq	i17	0.614	perAlite	WRRET	PerSlag	TotalFACaO
0.559	perAlite	PerSlag	TotalFACaO	0.612	WRRET	PerSlag	perCemNa2O	i17
0.553	PerSlag	TotalFACaO	perCemNa2Oeq	0.611	perAlite	PerSlag	TotalFACaO	perCemNa2O
0.549	perAlite	PerSlag	perCemNa2O	0.611	WRRET	PerSlag	TotalFACaO	perCemNa2Oeq
0.548	perAlite	PerSlag	perCemNa2Oeq	0.603	WRRET	PerSlag	i10	i17
0.544	PerSlag	i10	i17	0.601	perAluminate	WRRET	PerSlag	i17
0.543	perAluminate	PerSlag	i17	0.599	perAlite	WRRET	PerSlag	perCemNa2Oeq
0.541	perAlite	perFreeCaO	PerSlag	0.598	perAlite	perFreeCaO	WRRET	PerSlag
0.540	WRRET	PerSlag	TotalFACaO	0.594	PerSlag	TotalFACaO	perCemNa2O	perCemNa2Oeq
0.539	perAlite	perPericlase	PerSlag	0.593	perAlite	PerSlag	i10	i17
0.537	perAlite	PerSlag	i10	0.592	perAlite	WRRET	PerSlag	perCemNa2O

Figure G.9: Results from PROC RSQUARE, Rietveld Calculations, Three and Four Variables, $\ln(\tau)$

lBeta								
R ²	Variables			R ²				
	1	2	3		1	2	3	4
0.643	perAluminate	WRRET	PerSlag	0.674	perAluminate	WRRET	PCHRWR	PerSlag
0.613	perAlite	perFerrite	WRRET	0.674	perAluminate	WRRET	PerSlag	wc
0.612	perAlite	perAluminate	WRRET	0.673	perAlite	perFerrite	WRRET	PerSlag
0.607	perAlite	WRRET	wc	0.673	perAlite	perFerrite	WRRET	wc
0.586	perAluminate	perFerrite	WRRET	0.671	perAluminate	WRRET	LRWR	PerSlag
0.582	perAlite	WRRET	LRWR	0.669	perAlite	perAluminate	WRRET	wc
0.579	perAluminate	WRRET	PCHRWR	0.668	perAluminate	WRRET	PerSlag	CemBlaine
0.578	perAluminate	perFreeCaO	WRRET	0.666	perAlite	perAluminate	WRRET	PerSlag
0.578	perAluminate	WRRET	LRWR	0.662	perAluminate	perFreeCaO	WRRET	PerSlag
0.577	perAluminate	WRRET	wc	0.659	perAlite	perAluminate	WRRET	LRWR
0.575	perAluminate	WRRET	CemBlaine	0.656	perAlite	perFerrite	WRRET	LRWR
0.570	perAlite	WRRET	PerSlag	0.656	perAluminate	WRRET	HRWR	PerSlag
0.562	perAluminate	WRRET	HRWR	0.653	perAluminate	WRRET	PerSlag	PerAir
0.558	perAlite	WRRET	PCHRWR	0.651	perAluminate	perFerrite	WRRET	PerSlag
0.557	perAlite	WRRET	i17	0.650	perAluminate	WRRET	MRWR	PerSlag

Figure G.10: Results from PROC RSQUARE, Rietveld Calculations, Three and Four Variables, $\ln(\beta)$

Bogue - 5 Variables

IAlpha					
R ²	Variables				
	1	2	3	4	5
0.485	perC3A	WRRET	wc	perCemNa2Oeq	i17
0.481	perC3A	WRRET	wc	TotalFACaO	perCemNa2Oeq
0.480	perC4AF	WRRET	wc	perCemNa2Oeq	i17
0.480	perC4AF	WRRET	wc	perCemNa2O	perCemNa2Oeq
0.478	perC3A	WRRET	wc	perCemNa2O	perCemNa2Oeq
0.475	perC2S	perC3A	WRRET	wc	perCemNa2Oeq
0.475	perC3A	WRRET	PCHRWR	wc	perCemNa2Oeq
0.474	perC3A	WRRET	ACCL	wc	perCemNa2Oeq
0.473	WRRET	wc	CemBlaine	perCemNa2Oeq	i17
0.473	WRRET	PCHRWR	wc	perCemNa2Oeq	i17

ITau					
R ²	Variables				
	1	2	3	4	5
0.669	perC3S	WRRET	PerSlag	perCemNa2O	i17
0.667	WRRET	PerSlag	perCemNa2O	perCemNa2Oeq	i17
0.666	perGypsum	WRRET	PerSlag	perCemNa2O	i17
0.661	perC2S	perGypsum	WRRET	PerSlag	i17
0.656	perC3S	perC4AF	WRRET	PerSlag	i17
0.656	perMgO	WRRET	PerSlag	perCemNa2O	i17
0.651	perC2S	perGypsum	WRRET	PerSlag	TotalFACaO
0.651	perC3S	WRRET	PerSlag	TotalFACaO	perCemNa2O
0.650	perC3A	WRRET	PerSlag	perCemNa2O	i17
0.649	perC3S	perC3A	WRRET	PerSlag	i17

IBeta					
R ²	Variables				
	1	2	3	4	5
0.751	perC2S	perGypsum	WRRET	LRWR	PerSlag
0.751	perC2S	perGypsum	WRRET	LRWR	PCHRWR
0.742	perC3A	WRRET	LRWR	PCHRWR	PerSlag
0.737	perC2S	perGypsum	WRRET	LRWR	wc
0.732	perGypsum	WRRET	LRWR	PCHRWR	PerSlag
0.732	perC3A	WRRET	LRWR	PerSlag	CemBlaine
0.728	perC3S	perC3A	WRRET	LRWR	PCHRWR
0.728	perC3S	perC3A	WRRET	PerSlag	wc
0.728	perC2S	perGypsum	WRRET	PerSlag	wc
0.727	perC3S	perC3A	WRRET	LRWR	wc

Figure G.11: Results from PROC RSQUARE, Bogue Calculations, Five Variables

Rietveld - 5 Variables

IAlpha					
R ²	Variables				
	1	2	3	4	5
0.481	perFerrite	WRRET	wc	perCemNa2Oeq	i17
0.478	perAluminate	WRRET	wc	perCemNa2Oeq	i17
0.477	perBelite	WRRET	wc	perCemNa2Oeq	i17
0.475	perFerrite	WRRET	wc	perCemNa2O	perCemNa2Oeq
0.475	perFerrite	WRRET	wc	perCemNa2Oeq	i10
0.475	perAluminate	WRRET	wc	TotalFACaO	perCemNa2Oeq
0.474	perFerrite	WRRET	wc	TotalFACaO	perCemNa2Oeq
0.473	perAluminate	WRRET	wc	perCemNa2Oeq	i10
0.473	WRRET	wc	CemBlaine	perCemNa2Oeq	i17
0.473	WRRET	PCHRWR	wc	perCemNa2Oeq	i17

ITau					
R ²	Variables				
	1	2	3	4	5
0.675	perAlite	WRRET	PerSlag	perCemNa2O	i17
0.656	perAlite	WRRET	PerSlag	TotalFACaO	perCemNa2O
0.650	perAlite	WRRET	PerSlag	i10	i17
0.642	perAlite	perFreeCaO	WRRET	PerSlag	i17
0.638	perAlite	perBelite	PerSlag	perCemNa2O	i17
0.637	perAlite	WRRET	PerSlag	TotalFACaO	i10
0.636	perAlite	perFreeCaO	WRRET	PerSlag	TotalFACaO
0.635	perAlite	perFerrite	WRRET	PerSlag	i17
0.634	perAlite	LRWR	PerSlag	perCemNa2O	i17
0.633	perAlite	ACCL	PerSlag	perCemNa2O	i17

IBeta					
R ²	Variables				
	1	2	3	4	5
0.721	perAlite	perFerrite	WRRET	PerSlag	wc
0.719	perAluminate	WRRET	LRWR	PCHRWR	PerSlag
0.713	perAlite	perAluminate	WRRET	PerSlag	wc
0.711	perAluminate	WRRET	LRWR	PerSlag	CemBlaine
0.706	perAlite	perFerrite	WRRET	LRWR	PerSlag
0.705	perAlite	perAluminate	WRRET	LRWR	PCHRWR
0.704	perAluminate	perFreeCaO	WRRET	PerSlag	wc
0.703	perAlite	perAluminate	WRRET	LRWR	PerSlag
0.703	perAlite	perFerrite	WRRET	LRWR	CemBlaine
0.703	perAlite	perFerrite	WRRET	LRWR	PCHRWR

Figure G.12: Results from PROC RSQUARE, Rietveld Calculations, Five Variables

Bogue - 6 Variables

IAlpha						
R ²	Variables					
	1	2	3	4	5	6
0.500	perC4AF	WRRET	wc	perCemNa2O	perCemNa2Oeq	i17
0.496	perC3S	perC3A	WRRET	wc	perCemNa2Oeq	i17
0.496	perC3A	WRRET	PCHRWR	wc	perCemNa2Oeq	i17
0.495	perC4AF	WRRET	wc	TotalFACaO	perCemNa2O	perCemNa2Oeq
0.491	perC3A	WRRET	PCHRWR	wc	TotalFACaO	perCemNa2Oeq
0.490	perC3A	WRRET	ACCL	wc	perCemNa2Oeq	i17
0.490	perC3S	perC3A	WRRET	wc	TotalFACaO	perCemNa2Oeq
0.490*	perC4AF	WRRET	PerSlag	wc	perCemNa2Oeq	i17
0.489	perC3A	perGypsum	WRRET	wc	perCemNa2Oeq	i17
0.489	perC3S	perC3A	WRRET	wc	perCemNa2O	perCemNa2Oeq

*Final Model

ITau						
R ²	Variables					
	1	2	3	4	5	6
0.690	perC3S	perGypsum	WRRET	PerSlag	perCemNa2O	i17
0.690	perC3S	WRRET	PerSlag	perCemNa2O	perCemNa2Oeq	i17
0.689	perC3S	perC2S	WRRET	PerSlag	perCemNa2O	i17
0.687	perMgO	WRRET	PerSlag	perCemNa2O	perCemNa2Oeq	i17
0.683	perC3S	perMgO	WRRET	PerSlag	perCemNa2O	i17
0.680	perC3S	perC3A	WRRET	PerSlag	perCemNa2O	i17
0.679	perMgO	perGypsum	WRRET	PerSlag	perCemNa2O	i17
0.679	perMgO	perFreeCaO	WRRET	PerSlag	perCemNa2O	i17
0.678	perC3S	perGypsum	WRRET	PerSlag	TotalFACaO	perCemNa2O
0.678	perGypsum	WRRET	PerSlag	perCemNa2O	perCemNa2Oeq	i17
0.672*	perC3S	ACCL	WRRET	perCemNa2O	PerSlag	i17

*Final Model

IBeta						
R ²	Variables					
	1	2	3	4	5	6
0.786	perC2S	perGypsum	WRRET	LRWR	PCHRWR	PerSlag
0.773	perC2S	perGypsum	WRRET	LRWR	PerSlag	wc
0.764	perC3A	WRRET	LRWR	PCHRWR	PerSlag	perCemNa2Oeq
0.762	perC3S	perC3A	WRRET	LRWR	PCHRWR	PerSlag
0.761	perC3A	perGypsum	WRRET	LRWR	PCHRWR	PerSlag
0.761	perC3A	WRRET	LRWR	PCHRWR	PerSlag	CemBlaine
0.760	perC2S	perGypsum	WRRET	LRWR	MRWR	PerSlag
0.759	perC2S	perGypsum	WRRET	LRWR	PCHRWR	i17
0.758	perC2S	perGypsum	WRRET	LRWR	HRWR	PCHRWR
0.758	perC2S	perGypsum	WRRET	LRWR	MRWR	PCHRWR

Figure G.13: Results from PROC RSQUARE, Bogue Calculations, Six Variables

Rietveld - 6 Variables

IAlpha						
R ²	Variables					
	1	2	3	4	5	6
0.494	perFerrite	perFreeCaO	WRRET	wc	perCemNa2Oeq	i17
0.491	perFerrite	WRRET	wc	perCemNa2O	perCemNa2Oeq	i17
0.490	perFerrite	WRRET	wc	perCemNa2Oeq	i10	i17
0.490	perFerrite	perPericlase	WRRET	wc	perCemNa2Oeq	i17
0.489	perFerrite	WRRET	PerSlag	wc	perCemNa2Oeq	i17
0.488	perFerrite	perFreeCaO	WRRET	wc	TotalFACaO	perCemNa2Oeq
0.487	perBelite	perFerrite	WRRET	wc	perCemNa2O	perCemNa2Oeq
0.487	perFerrite	WRRET	wc	TotalFACaO	perCemNa2O	perCemNa2Oeq
0.487	perAluminate	WRRET	PCHRWR	wc	perCemNa2Oeq	i17
0.486	perFerrite	WRRET	wc	TotalFACaO	perCemNa2Oeq	i10
0.486*	perFerrite	PCHRWR	WRRET	wc	perCemNa2Oeq	i17

*Final Model

ITau						
R ²	Variables					
	1	2	3	4	5	6
0.685	perAlite	perBelite	WRRET	PerSlag	perCemNa2O	i17
0.683	perAlite	perFreeCaO	WRRET	PerSlag	perCemNa2O	i17
0.681	perAlite	WRRET	MRWR	PerSlag	perCemNa2O	i17
0.677*	perAlite	WRRET	ACCL	PerSlag	perCemNa2O	i17
0.677	perAlite	WRRET	AIR	PerSlag	perCemNa2O	i17
0.676	perAlite	WRRET	PerSlag	PerAir	perCemNa2O	i17
0.676	perAlite	WRRET	LRWR	PerSlag	perCemNa2O	i17
0.676	perAlite	WRRET	PerSlag	perCemNa2O	i10	i17
0.676	perAlite	WRRET	PerSlag	wc	perCemNa2O	i17
0.675	perAlite	WRRET	PerSlag	PerSF	perCemNa2O	i17

*Final Model

IBeta						
R ²	Variables					
	1	2	3	4	5	6
0.750	perAlite	perFerrite	WRRET	LRWR	PCHRWR	PerSlag
0.749	perAlite	perFerrite	WRRET	LRWR	PerSlag	CemBlaine
0.747	perAlite	perAluminate	WRRET	LRWR	PCHRWR	PerSlag
0.742	perAlite	perFerrite	WRRET	LRWR	PerSlag	wc
0.742	perAluminate	WRRET	LRWR	PCHRWR	PerSlag	CemBlaine
0.740	perAluminate	WRRET	LRWR	HRWR	PCHRWR	PerSlag
0.739	perAlite	perAluminate	WRRET	LRWR	PerSlag	CemBlaine
0.737	perAlite	perAluminate	WRRET	LRWR	PerSlag	wc
0.735	perAlite	perFerrite	WRRET	PerSlag	wc	CemBlaine
0.733	perAluminate	perFerrite	WRRET	LRWR	PCHRWR	PerSlag

Figure G.14: Results from PROC RSQUARE, Rietveld Calculations, Six Variables

Bogue - 7 Variables

IAlpha							
R ²	Variables						
	1	2	3	4	5	6	7
0.508	perC3S	perC3A	WRRET	PerSlag	wc	perCemNa2Oeq	i17
0.507	perC4AF	WRRET	ACCL	wc	perCemNa2O	perCemNa2Oeq	i17
0.507	perC4AF	WRRET	PCHRWR	wc	perCemNa2O	perCemNa2Oeq	i17
0.506	perC4AF	WRRET	PerSlag	wc	perCemNa2O	perCemNa2Oeq	i17
0.506	perC3S	perC3A	perFreeCaO	WRRET	wc	perCemNa2Oeq	i17
0.506	perC2S	perC3A	perGypsum	WRRET	wc	perCemNa2Oeq	i17
0.505	perC2S	perC4AF	perFreeCaO	WRRET	wc	perCemNa2Oeq	i17
0.504	perC3S	perC3A	WRRET	wc	perCemNa2O	perCemNa2Oeq	i17
0.504	perC3A	WRRET	LRWR	PCHRWR	wc	perCemNa2Oeq	i17
0.503	perC3S	perC3A	WRRET	PCHRWR	wc	perCemNa2Oeq	i17

Figure G.15: Results from PROC RSQUARE, Bogue Calculations, Seven Variables, $\ln(\alpha_i)$

ITau							
R ²	Variables						
	1	2	3	4	5	6	7
0.706	perC3S	perMgO	perFreeCaO	WRRET	PerSlag	perCemNa2O	i17
0.700	perC3S	perC2S	perMgO	WRRET	PerSlag	perCemNa2O	i17
0.699	perC3S	perC2S	WRRET	PerSlag	perCemNa2O	perCemNa2Oeq	i17
0.699	perC3S	perMgO	WRRET	PerSlag	perCemNa2O	perCemNa2Oeq	i17
0.697	perC3S	perMgO	perFreeCaO	WRRET	PerSlag	TotalFACaO	perCemNa2O
0.696	perC3S	perGypsum	WRRET	PerSlag	perCemNa2O	perCemNa2Oeq	i17
0.696	perC3S	WRRET	LRWR	PerSlag	perCemNa2O	perCemNa2Oeq	i17
0.695	perC3S	perMgO	perGypsum	WRRET	PerSlag	perCemNa2O	i17
0.695	perC3S	perGypsum	WRRET	MRWR	PerSlag	perCemNa2O	i17
0.695	perC3S	perC2S	WRRET	MRWR	PerSlag	perCemNa2O	i17

Figure G.16: Results from PROC RSQUARE, Bogue Calculations, Seven Variables, $\ln(\tau)$

IBeta							
R ²	Variables						
	1	2	3	4	5	6	7
0.797	perC2S	perGypsum	WRRET	LRWR	MRWR	PCHRWR	PerSlag
0.792	perC2S	perGypsum	WRRET	LRWR	HRWR	PCHRWR	PerSlag
0.789	perC2S	perGypsum	WRRET	LRWR	PCHRWR	PerSlag	perCemNa2Oeq
0.789	perC2S	perC3A	perGypsum	WRRET	LRWR	PCHRWR	PerSlag
0.789	perC2S	perGypsum	WRRET	LRWR	PCHRWR	PerSlag	wc
0.788	perC2S	perC4AF	perGypsum	WRRET	LRWR	PCHRWR	PerSlag
0.787	perC2S	perMgO	perGypsum	WRRET	LRWR	PCHRWR	PerSlag
0.787	perC3S	perC2S	perGypsum	WRRET	LRWR	PCHRWR	PerSlag
0.787	perC2S	perGypsum	WRRET	LRWR	PCHRWR	PerSlag	CemBlaine
0.787	perC2S	perGypsum	WRRET	LRWR	PCHRWR	PerSlag	PerSF
0.772*	perC3A	WRRET	LRWR	MRWR	HRWR	PCHRWR	PerSlag

*Final Model

Figure G.17: Results from PROC RSQUARE, Bogue Calculations, Seven Variables, $\ln(\beta)$

Rietveld - 7 Variables							
IAlpha							
R ²	Variables						
	1	2	3	4	5	6	7
0.506	perFerrite	perFreeCaO	WRRET	PCHRWR	wc	perCemNa2Oeq	i17
0.505	perBelite	perFerrite	WRRET	wc	perCemNa2O	perCemNa2Oeq	i17
0.502	perFerrite	perFreeCaO	WRRET	wc	perCemNa2O	perCemNa2Oeq	i17
0.500	perBelite	perFerrite	WRRET	wc	TotalFACaO	perCemNa2O	perCemNa2Oeq
0.500	perFerrite	perFreeCaO	WRRET	ACCL	wc	perCemNa2Oeq	i17
0.499	perFerrite	perFreeCaO	WRRET	PerSlag	wc	perCemNa2Oeq	i17
0.499	perFerrite	perFreeCaO	WRRET	wc	CemBlaine	perCemNa2Oeq	i17
0.499	perFerrite	perFreeCaO	WRRET	PCHRWR	wc	TotalFACaO	perCemNa2Oeq
0.498	perAluminate	perFreeCaO	WRRET	PCHRWR	wc	perCemNa2Oeq	i17
0.498	perAlite	perAluminate	perFreeCaO	WRRET	wc	perCemNa2Oeq	i17

Figure G.18: Results from PROC RSQUARE, Rietveld Calculations, Seven Variables, $\ln(\alpha_i)$

ITau							
R ²	Variables						
	1	2	3	4	5	6	7
0.692	perAlite	perBelite	perPericlase	WRRET	PerSlag	perCemNa2O	i17
0.692	perAlite	perBelite	WRRET	MRWR	PerSlag	perCemNa2O	i17
0.689	perAlite	perFreeCaO	WRRET	MRWR	PerSlag	perCemNa2O	i17
0.689	perAlite	perBelite	WRRET	AIR	PerSlag	perCemNa2O	i17
0.689	perAlite	perPericlase	perFreeCaO	WRRET	PerSlag	perCemNa2O	i17
0.688	perAlite	perBelite	WRRET	PerSlag	PerAir	perCemNa2O	i17
0.687	perAlite	perBelite	WRRET	LRWR	PerSlag	perCemNa2O	i17
0.687	perAlite	perBelite	WRRET	ACCL	PerSlag	perCemNa2O	i17
0.686	perAlite	perBelite	WRRET	PerSlag	PerSF	perCemNa2O	i17
0.686	perAlite	perBelite	perAluminate	WRRET	PerSlag	perCemNa2O	i17

Figure G.19: Results from PROC RSQUARE, Rietveld Calculations, Seven Variables, $\ln(\tau)$

IBeta							
R ²	Variables						
	1	2	3	4	5	6	7
0.775	perAlite	perFerrite	WRRET	LRWR	PCHRWR	PerSlag	CemBlaine
0.768	perAlite	perFerrite	WRRET	LRWR	PerSlag	wc	CemBlaine
0.767	perAlite	perAluminate	WRRET	LRWR	PCHRWR	PerSlag	CemBlaine
0.761	perAlite	perAluminate	WRRET	LRWR	HRWR	PCHRWR	PerSlag
0.761	perAlite	perFerrite	WRRET	LRWR	MRWR	PCHRWR	PerSlag
0.760	perAlite	perFerrite	WRRET	LRWR	HRWR	PCHRWR	PerSlag
0.760	perAlite	perFerrite	WRRET	LRWR	MRWR	PerSlag	CemBlaine
0.758	perAlite	perAluminate	WRRET	LRWR	PerSlag	wc	CemBlaine
0.756	perAlite	perFerrite	WRRET	LRWR	PCHRWR	PerSlag	wc
0.756	perAluminate	WRRET	LRWR	HRWR	PCHRWR	PerSlag	CemBlaine
0.751*	perAluminate	WRRET	LRWR	MRWR	HRWR	PCHRWR	PerSlag

*Final Model

Figure G.20: Results from PROC RSQUARE, Rietveld Calculations, Seven Variables, $\ln(\beta)$

Variable	perC3S	perC2S	perC3A	perC4AF	perMgO	perGypsum	perFreeCaO	WRRET	LRWR	MRWR	HRWR	PCHRWR
perC3S	1.00	0.02	0.50	0.44	0.65	0.66	0.30	0.07	-0.12	-0.08	0.08	0.19
perC2S	0.02	1.00	0.05	0.47	0.25	0.50	-0.26	0.08	-0.02	0.07	-0.05	-0.07
perC3A	0.50	0.05	1.00	-0.39	0.50	0.75	0.06	0.00	0.07	-0.15	-0.01	0.25
perC4AF	0.44	0.47	-0.39	1.00	0.27	0.19	0.16	0.07	-0.19	0.09	0.09	-0.06
perMgO	0.65	0.25	0.50	0.27	1.00	0.62	0.57	0.05	-0.05	-0.06	0.02	0.13
perGypsum	0.66	0.50	0.75	0.19	0.62	1.00	-0.03	0.07	-0.09	-0.07	0.04	0.22
perFreeCaO	0.30	-0.26	0.06	0.16	0.57	-0.03	1.00	-0.03	-0.08	-0.02	0.09	0.14
WRRET	0.07	0.08	0.00	0.07	0.05	0.07	-0.03	1.00	-0.16	0.00	0.07	-0.15
LRWR	-0.12	-0.02	0.07	-0.19	-0.05	-0.09	-0.08	-0.16	1.00	-0.07	-0.03	-0.17
MRWR	-0.08	0.07	-0.15	0.09	-0.06	-0.07	-0.02	0.00	-0.07	1.00	-0.05	-0.07
HRWR	0.08	-0.05	-0.01	0.09	0.02	0.04	0.09	0.07	-0.03	-0.05	1.00	-0.12
PCHRWR	0.19	-0.07	0.25	-0.06	0.13	0.22	0.14	-0.15	-0.17	-0.07	-0.12	1.00
ACCL	0.08	-0.04	0.11	-0.02	0.03	0.11	-0.08	-0.07	-0.08	-0.03	-0.05	-0.07
AIR	-0.07	-0.07	-0.02	-0.06	0.00	-0.10	0.06	0.01	0.23	0.16	0.01	-0.04
PerFA	-0.58	-0.34	-0.32	-0.41	-0.46	-0.57	-0.09	-0.05	0.17	-0.05	-0.04	-0.11
PerSlag	-0.46	-0.11	-0.29	-0.20	-0.33	-0.38	-0.10	-0.05	-0.04	0.14	-0.07	-0.09
PerSF	-0.01	-0.01	-0.06	0.05	-0.09	-0.02	-0.09	0.02	-0.08	-0.03	0.19	-0.01
PerUFFA	-0.08	-0.12	-0.11	-0.05	-0.15	-0.14	-0.08	-0.02	0.01	-0.03	0.12	0.10
wc	0.12	-0.02	-0.11	0.18	0.15	-0.08	0.19	-0.09	-0.19	-0.08	-0.29	-0.48
PerAir	0.07	-0.11	0.11	-0.06	0.18	-0.02	0.11	0.12	0.25	0.14	0.02	0.07
TotalFACaO	-0.40	-0.22	-0.16	-0.33	-0.34	-0.34	-0.17	0.01	0.09	-0.05	0.02	-0.07
CemBlaine	0.15	-0.14	-0.03	0.22	-0.07	0.20	0.15	0.00	-0.28	-0.02	0.14	0.29
perCemNa2O	0.40	0.65	-0.09	0.79	0.51	0.34	0.27	0.08	-0.10	0.04	0.02	-0.07
perCemK2O	0.50	-0.03	0.66	-0.14	0.33	0.63	-0.24	0.01	-0.12	-0.09	-0.01	0.06
perCemNa2Oeq	0.62	0.19	0.61	0.13	0.49	0.73	-0.15	0.03	-0.15	-0.07	-0.01	0.04
CemNa2Oeq	-0.03	-0.18	0.32	-0.36	-0.04	0.16	-0.38	-0.04	-0.08	-0.06	-0.04	-0.09
i10	0.01	0.46	-0.12	0.40	0.41	0.15	0.51	0.02	-0.03	0.01	-0.01	0.08
i17	-0.45	-0.26	-0.21	-0.35	-0.40	-0.40	-0.16	0.00	0.15	-0.05	0.06	-0.05
i21	-0.04	-0.09	-0.11	-0.01	-0.11	-0.12	-0.07	-0.02	-0.01	-0.03	0.08	0.06
i22	-0.45	-0.26	-0.21	-0.35	-0.40	-0.40	-0.16	0.00	0.15	-0.05	0.06	-0.05
alphamax	-0.33	-0.08	-0.24	-0.11	-0.18	-0.37	0.22	-0.23	-0.06	0.03	-0.08	-0.21
lalpha	-0.32	-0.08	-0.23	-0.11	-0.16	-0.36	0.23	-0.24	-0.05	0.03	-0.07	-0.23
tau	-0.59	-0.06	-0.48	-0.12	-0.44	-0.53	-0.11	0.11	-0.04	0.14	-0.02	-0.14
ltau	-0.66	-0.12	-0.48	-0.21	-0.46	-0.61	-0.09	0.17	0.00	0.15	-0.02	-0.17
beta	0.47	0.08	0.53	-0.02	0.35	0.55	0.01	0.60	0.11	-0.05	0.11	0.21
lbeta	0.50	0.07	0.58	-0.04	0.40	0.57	0.04	0.53	0.14	-0.05	0.11	0.22
HOHcem	-0.67	-0.41	-0.20	-0.63	-0.50	-0.58	-0.05	-0.08	0.15	0.05	-0.03	-0.11

Figure G.21: Correlation Matrix from PROC RSQUARE – Bogue Calculations - Variables in Yellow Have a Covariance >0.65

	ACCL	AIR	PerFA	PerSlag	PerSF	PerUFFA	wc	PerAir	TotalFACaO	CemBlaine	perCemNa2O	perCemK2O	perCemNa2Oeq
perC3S	0.08	-0.07	-0.58	-0.46	-0.01	-0.08	0.12	0.07	-0.40	0.15	0.40	0.50	0.62
perC2S	-0.04	-0.07	-0.34	-0.11	-0.01	-0.12	-0.02	-0.11	-0.22	-0.14	0.65	-0.03	0.19
perC3A	0.11	-0.02	-0.32	-0.29	-0.06	-0.11	-0.11	0.11	-0.16	-0.03	-0.09	0.66	0.61
perC4AF	-0.02	-0.06	-0.41	-0.20	0.05	-0.05	0.18	-0.06	-0.33	0.22	0.79	-0.14	0.13
perMgO	0.03	0.00	-0.46	-0.33	-0.09	-0.15	0.15	0.18	-0.34	-0.07	0.51	0.33	0.49
perGypsum	0.11	-0.10	-0.57	-0.38	-0.02	-0.14	-0.08	-0.02	-0.34	0.20	0.34	0.63	0.73
perFreeCaO	-0.08	0.06	-0.09	-0.10	-0.09	-0.08	0.19	0.11	-0.17	0.15	0.27	-0.24	-0.15
WRRET	-0.07	0.01	-0.05	-0.05	0.02	-0.02	-0.09	0.12	0.01	0.00	0.08	0.01	0.03
LRWR	-0.08	0.23	0.17	-0.04	-0.08	0.01	-0.19	0.25	0.09	-0.28	-0.10	-0.12	-0.15
MRWR	-0.03	0.16	-0.05	0.14	-0.03	-0.03	-0.08	0.14	-0.05	-0.02	0.04	-0.09	-0.07
HRWR	-0.05	0.01	-0.04	-0.07	0.19	0.12	-0.29	0.02	0.02	0.14	0.02	-0.01	-0.01
PCHRWR	-0.07	-0.04	-0.11	-0.09	-0.01	0.10	-0.48	0.07	-0.07	0.29	-0.07	0.06	0.04
ACCL	1.00	-0.05	-0.11	0.04	-0.04	-0.03	0.07	-0.01	-0.07	0.02	-0.07	0.25	0.22
AIR	-0.05	1.00	0.13	-0.04	-0.05	0.04	-0.20	0.53	0.12	-0.06	-0.04	0.00	-0.02
PerFA	-0.11	0.13	1.00	-0.34	0.00	0.07	-0.10	-0.03	0.69	-0.07	-0.44	-0.29	-0.43
PerSlag	0.04	-0.04	-0.34	1.00	-0.07	-0.07	0.05	0.00	-0.27	-0.05	-0.23	-0.30	-0.37
PerSF	-0.04	-0.05	0.00	-0.07	1.00	-0.04	-0.11	-0.01	0.08	0.05	0.03	0.06	0.07
PerUFFA	-0.03	0.04	0.07	-0.07	-0.04	1.00	-0.23	-0.03	0.14	-0.04	-0.11	0.00	-0.04
wc	0.07	-0.20	-0.10	0.05	-0.11	-0.23	1.00	-0.22	-0.16	-0.18	0.20	0.01	0.08
PerAir	-0.01	0.53	-0.03	0.00	-0.01	-0.03	-0.22	1.00	-0.01	-0.08	0.00	0.06	0.06
TotalFACaO	-0.07	0.12	0.69	-0.27	0.08	0.14	-0.16	-0.01	1.00	-0.05	-0.34	-0.08	-0.19
CemBlaine	0.02	-0.06	-0.07	-0.05	0.05	-0.04	-0.18	-0.08	-0.05	1.00	-0.01	0.07	0.07
perCemNa2O	-0.07	-0.04	-0.44	-0.23	0.03	-0.11	0.20	0.00	-0.34	-0.01	1.00	-0.10	0.24
perCemK2O	0.25	0.00	-0.29	-0.30	0.06	0.00	0.01	0.06	-0.08	0.07	-0.10	1.00	0.94
perCemNa2Oeq	0.22	-0.02	-0.43	-0.37	0.07	-0.04	0.08	0.06	-0.19	0.07	0.24	0.94	1.00
CemNa2Oeq	0.21	0.06	0.08	-0.07	0.13	0.11	0.00	0.04	0.21	-0.01	-0.29	0.80	0.68
i10	-0.19	-0.05	-0.17	0.00	-0.09	-0.14	0.02	-0.08	-0.24	0.25	0.61	-0.47	-0.26
i17	-0.08	0.11	0.75	-0.27	0.07	0.20	-0.23	-0.02	0.95	-0.07	-0.39	-0.12	-0.25
i21	-0.03	0.02	0.03	-0.06	-0.03	0.94	-0.16	-0.04	0.11	-0.04	-0.06	0.01	-0.02
i22	-0.08	0.11	0.75	-0.26	0.07	0.18	-0.23	-0.01	0.95	-0.07	-0.39	-0.12	-0.25
alphanax	0.02	-0.12	0.07	0.36	0.09	-0.09	0.35	-0.18	-0.12	-0.14	-0.06	-0.46	-0.47
lalpha	0.03	-0.13	0.07	0.34	0.09	-0.09	0.37	-0.18	-0.11	-0.16	-0.05	-0.45	-0.46
tau	-0.09	-0.03	0.12	0.59	-0.05	0.01	-0.01	-0.03	0.25	-0.06	-0.13	-0.47	-0.50
ltau	-0.12	-0.01	0.23	0.56	-0.03	0.02	-0.03	0.01	0.36	-0.13	-0.18	-0.50	-0.55
beta	-0.05	-0.02	-0.20	-0.37	-0.05	0.00	-0.29	0.18	-0.11	0.11	0.09	0.42	0.44
lbeta	-0.03	0.00	-0.18	-0.44	-0.04	0.00	-0.28	0.20	-0.09	0.10	0.09	0.45	0.47
HOHcem	0.03	0.00	0.27	0.64	0.03	0.06	-0.03	-0.01	0.36	-0.17	-0.61	-0.32	-0.51

Figure G.22: Correlation Matrix from PROC RSQUARE – Bogue Calculations - Variables in Yellow Have a Covariance >0.65

	CemNa2Oeq	i10	i17	i21	i22	alphamax	alpha	tau	ltau	beta	lbeta	HOHcem
perC3S	-0.03	0.01	-0.45	-0.04	-0.45	-0.33	-0.32	-0.59	-0.66	0.47	0.50	-0.67
perC2S	-0.18	0.46	-0.26	-0.09	-0.26	-0.08	-0.08	-0.06	-0.12	0.08	0.07	-0.41
perC3A	0.32	-0.12	-0.21	-0.11	-0.21	-0.24	-0.23	-0.48	-0.48	0.53	0.58	-0.20
perC4AF	-0.36	0.40	-0.35	-0.01	-0.35	-0.11	-0.11	-0.12	-0.21	-0.02	-0.04	-0.63
perMgO	-0.04	0.41	-0.40	-0.11	-0.40	-0.18	-0.16	-0.44	-0.46	0.35	0.40	-0.50
perGypsum	0.16	0.15	-0.40	-0.12	-0.40	-0.37	-0.36	-0.53	-0.61	0.55	0.57	-0.58
perFreeCaO	-0.38	0.51	-0.16	-0.07	-0.16	0.22	0.23	-0.11	-0.09	0.01	0.04	-0.05
WRRET	-0.04	0.02	0.00	-0.02	0.00	-0.23	-0.24	0.11	0.17	0.60	0.53	-0.08
LRWR	-0.08	-0.03	0.15	-0.01	0.15	-0.06	-0.05	-0.04	0.00	0.11	0.14	0.15
MRWR	-0.06	0.01	-0.05	-0.03	-0.05	0.03	0.03	0.14	0.15	-0.05	-0.05	0.05
HRWR	-0.04	-0.01	0.06	0.08	0.06	-0.08	-0.07	-0.02	-0.02	0.11	0.11	-0.03
PCHRWR	-0.09	0.08	-0.05	0.06	-0.05	-0.21	-0.23	-0.14	-0.17	0.21	0.22	-0.11
ACCL	0.21	-0.19	-0.08	-0.03	-0.08	0.02	0.03	-0.09	-0.12	-0.05	-0.03	0.03
AIR	0.06	-0.05	0.11	0.02	0.11	-0.12	-0.13	-0.03	-0.01	-0.02	0.00	0.00
PerFA	0.08	-0.17	0.75	0.03	0.75	0.07	0.07	0.12	0.23	-0.20	-0.18	0.27
PerSlag	-0.07	0.00	-0.27	-0.06	-0.26	0.36	0.34	0.59	0.56	-0.37	-0.44	0.64
PerSF	0.13	-0.09	0.07	-0.03	0.07	0.09	0.09	-0.05	-0.03	-0.05	-0.04	0.03
PerUFFA	0.11	-0.14	0.20	0.94	0.18	-0.09	-0.09	0.01	0.02	0.00	0.00	0.06
wc	0.00	0.02	-0.23	-0.16	-0.23	0.35	0.37	-0.01	-0.03	-0.29	-0.28	-0.03
PerAir	0.04	-0.08	-0.02	-0.04	-0.01	-0.18	-0.18	-0.03	0.01	0.18	0.20	-0.01
TotalFACaO	0.21	-0.24	0.95	0.11	0.95	-0.12	-0.11	0.25	0.36	-0.11	-0.09	0.36
CemBlaine	-0.01	0.25	-0.07	-0.04	-0.07	-0.14	-0.16	-0.06	-0.13	0.11	0.10	-0.17
perCemNa2O	-0.29	0.61	-0.39	-0.06	-0.39	-0.06	-0.05	-0.13	-0.18	0.09	0.09	-0.61
perCemK2O	0.80	-0.47	-0.12	0.01	-0.12	-0.46	-0.45	-0.47	-0.50	0.42	0.45	-0.32
perCemNa2Oeq	0.68	-0.26	-0.25	-0.02	-0.25	-0.47	-0.46	-0.50	-0.55	0.44	0.47	-0.51
CemNa2Oeq	1.00	-0.59	0.20	0.08	0.20	-0.35	-0.34	-0.15	-0.12	0.15	0.17	0.07
i10	-0.59	1.00	-0.27	-0.11	-0.27	0.19	0.19	0.08	0.03	-0.04	-0.05	-0.21
i17	0.20	-0.27	1.00	0.14	1.00	-0.13	-0.13	0.27	0.39	-0.11	-0.10	0.41
i21	0.08	-0.11	0.14	1.00	0.11	-0.07	-0.06	-0.01	0.00	-0.02	-0.02	0.03
i22	0.20	-0.27	1.00	0.11	1.00	-0.13	-0.13	0.27	0.39	-0.11	-0.10	0.42
alphamax	-0.35	0.19	-0.13	-0.07	-0.13	1.00	1.00	0.42	0.41	-0.60	-0.64	0.43
alpha	-0.34	0.19	-0.13	-0.06	-0.13	1.00	1.00	0.41	0.39	-0.61	-0.64	0.43
tau	-0.15	0.08	0.27	-0.01	0.27	0.42	0.41	1.00	0.96	-0.35	-0.46	0.56
ltau	-0.12	0.03	0.39	0.00	0.39	0.41	0.39	0.96	1.00	-0.32	-0.43	0.65
beta	0.15	-0.04	-0.11	-0.02	-0.11	-0.60	-0.61	-0.35	-0.32	1.00	0.98	-0.36
lbeta	0.17	-0.05	-0.10	-0.02	-0.10	-0.64	-0.64	-0.46	-0.43	0.98	1.00	-0.38
HOHcem	0.07	-0.21	0.41	0.03	0.42	0.43	0.43	0.56	0.65	-0.36	-0.38	1.00

Figure G.23: Correlation Matrix from PROC RSQUARE – Bogue Calculations - Variables in Yellow Have a Covariance >0.65

Variable	perAlite	perBelite	perAluminate	perFerrite	perPericlase	perGypsumF	Hemihydrate	perAnhydrite	perK2SO4	perFreeCaO	WRRET	LRWR	MRWR
perAlite	1.00	0.25	0.56	0.31	0.19	0.31	0.45	0.65	0.32	0.34	0.07	-0.08	-0.07
perBelite	0.25	1.00	0.17	0.36	-0.27	0.07	0.43	0.57	0.50	-0.47	0.08	-0.12	0.03
perAluminate	0.56	0.17	1.00	-0.55	-0.16	0.17	0.05	0.55	0.80	-0.17	0.05	0.06	-0.11
perFerrite	0.31	0.36	-0.55	1.00	0.29	0.19	0.48	0.05	-0.43	0.37	0.05	-0.18	0.08
perPericlase	0.19	-0.27	-0.16	0.29	1.00	0.53	0.13	-0.18	-0.12	0.70	-0.05	0.06	-0.04
perGypsumR	0.31	0.07	0.17	0.19	0.53	1.00	-0.05	-0.17	0.20	0.43	-0.02	0.07	0.02
perHemihydrate	0.45	0.43	0.05	0.48	0.13	-0.05	1.00	0.31	0.23	0.30	0.09	-0.19	-0.04
perAnhydrite	0.65	0.57	0.55	0.05	-0.18	-0.17	0.31	1.00	0.50	-0.33	0.12	-0.11	-0.05
perK2SO4	0.32	0.50	0.80	-0.43	-0.12	0.20	0.23	0.50	1.00	-0.28	0.00	0.05	-0.12
perFreeCaO	0.34	-0.47	-0.17	0.37	0.70	0.43	0.30	-0.33	-0.28	1.00	-0.03	-0.08	-0.02
WRRET	0.07	0.08	0.05	0.05	-0.05	-0.02	0.09	0.12	0.00	-0.03	1.00	-0.16	0.00
LRWR	-0.08	-0.12	0.06	-0.18	0.06	0.07	-0.19	-0.11	0.05	-0.08	-0.16	1.00	-0.07
MRWR	-0.07	0.03	-0.11	0.08	-0.04	0.02	-0.04	-0.05	-0.12	-0.02	0.00	-0.07	1.00
HRWR	0.10	-0.07	-0.05	0.11	0.00	0.06	0.01	-0.03	-0.14	0.09	0.07	-0.03	-0.05
PCHRWR	0.20	-0.05	0.23	-0.06	0.05	0.03	0.21	0.05	0.15	0.14	-0.15	-0.17	-0.07
ACCL	0.09	0.03	0.08	-0.02	-0.09	-0.09	-0.09	0.16	0.01	-0.08	-0.07	-0.08	-0.03
AIR	-0.07	-0.11	-0.09	0.01	0.13	0.01	-0.13	-0.05	-0.13	0.06	0.01	0.23	0.16
PerFA	-0.62	-0.40	-0.34	-0.29	-0.06	-0.27	-0.37	-0.45	-0.30	-0.09	-0.05	0.17	-0.05
PerSlag	-0.44	-0.23	-0.24	-0.18	-0.07	-0.06	-0.28	-0.40	-0.20	-0.10	-0.05	-0.04	0.14
PerSF	-0.05	0.10	-0.04	0.03	-0.10	-0.09	0.01	0.04	0.01	-0.09	0.02	-0.08	-0.03
PerUFFA	-0.12	-0.04	-0.13	-0.01	-0.09	-0.13	-0.07	-0.03	-0.09	-0.08	-0.02	0.01	-0.03
wc	0.08	0.02	-0.14	0.21	0.10	0.00	0.07	0.01	-0.11	0.19	-0.09	-0.19	-0.08
PerAir	0.06	-0.13	-0.01	0.06	0.33	0.04	-0.15	0.05	-0.12	0.11	0.12	0.25	0.14
TotalFACaO	-0.43	-0.22	-0.16	-0.26	-0.13	-0.26	-0.28	-0.20	-0.15	-0.17	0.01	0.09	-0.05
CemBlaine	0.06	0.09	-0.07	0.21	-0.07	-0.03	0.46	-0.05	-0.01	0.15	0.00	-0.28	-0.02
perCemNa2O	0.41	0.61	-0.02	0.65	0.35	0.59	0.45	0.15	0.18	0.27	0.08	-0.10	0.04
perCemK2O	0.49	0.28	0.52	-0.15	-0.20	-0.15	-0.02	0.78	0.46	-0.24	0.01	-0.12	-0.09
perCemNa2Oeq	0.61	0.47	0.50	0.07	-0.08	0.05	0.14	0.81	0.51	-0.15	0.03	-0.15	-0.07
i10	0.10	0.13	-0.09	0.31	0.54	0.75	0.42	-0.32	0.14	0.51	0.02	-0.03	0.01
i17	-0.47	-0.28	-0.22	-0.27	-0.14	-0.26	-0.34	-0.27	-0.20	-0.16	0.00	0.15	-0.05
i21	-0.09	0.00	-0.12	0.02	-0.08	-0.13	-0.02	0.01	-0.07	-0.07	-0.02	-0.01	-0.03
alphamax	-0.28	-0.32	-0.21	-0.08	0.10	0.08	-0.14	-0.49	-0.22	0.22	-0.23	-0.06	0.03
lalpha	-0.26	-0.32	-0.20	-0.08	0.11	0.09	-0.15	-0.48	-0.21	0.23	-0.24	-0.05	0.03
tau	-0.60	-0.18	-0.39	-0.11	-0.05	-0.05	-0.30	-0.54	-0.28	-0.11	0.11	-0.04	0.14
ltau	-0.67	-0.28	-0.41	-0.17	-0.01	-0.07	-0.39	-0.60	-0.32	-0.09	0.17	0.00	0.15
lbeta	0.50	0.17	0.52	-0.09	-0.02	0.08	0.23	0.46	0.39	0.01	0.60	0.11	-0.05
lbeta	0.53	0.15	0.55	-0.10	0.02	0.09	0.23	0.48	0.42	0.04	0.53	0.14	-0.05
HOHcem	-0.64	-0.61	-0.21	-0.52	-0.10	-0.22	-0.52	-0.56	-0.26	-0.05	-0.08	0.15	0.05
HOHcemUlt	-0.70	-0.51	-0.35	-0.38	-0.10	-0.19	-0.48	-0.62	-0.34	-0.07	-0.15	0.08	0.09

Figure G.24: Correlation Matrix from PROC RSQUARE – Rietveld Calculations - Variables in Yellow Have a Covariance >0.65

Variable	HRWR	PCHRWR	ACCL	AIR	PerFA	PerSlag	PerSF	PerUFFA	wc	PerAir	TotalFACaO	CemBlaine	perCemNa2O
perAlite	0.10	0.20	0.09	-0.07	-0.62	-0.44	-0.05	-0.12	0.08	0.06	-0.43	0.06	0.41
perBelite	-0.07	-0.05	0.03	-0.11	-0.40	-0.23	0.10	-0.04	0.02	-0.13	-0.22	0.09	0.61
perAluminate	-0.05	0.23	0.08	-0.09	-0.34	-0.24	-0.04	-0.13	-0.14	-0.01	-0.16	-0.07	-0.02
perFerrite	0.11	-0.06	-0.02	0.01	-0.29	-0.18	0.03	-0.01	0.21	0.06	-0.26	0.21	0.65
perPericlase	0.00	0.05	-0.09	0.13	-0.06	-0.07	-0.10	-0.09	0.10	0.33	-0.13	-0.07	0.35
perGypsumR	0.06	0.03	-0.09	0.01	-0.27	-0.06	-0.09	-0.13	0.00	0.04	-0.26	-0.03	0.59
perHemihydrate	0.01	0.21	-0.09	-0.13	-0.37	-0.28	0.01	-0.07	0.07	-0.15	-0.28	0.46	0.45
perAnhydrite	-0.03	0.05	0.16	-0.05	-0.45	-0.40	0.04	-0.03	0.01	0.05	-0.20	-0.05	0.15
perK2SO4	-0.14	0.15	0.01	-0.13	-0.30	-0.20	0.01	-0.09	-0.11	-0.12	-0.15	-0.01	0.18
perFreeCaO	0.09	0.14	-0.08	0.06	-0.09	-0.10	-0.09	-0.08	0.19	0.11	-0.17	0.15	0.27
WRRET	0.07	-0.15	-0.07	0.01	-0.05	-0.05	0.02	-0.02	-0.09	0.12	0.01	0.00	0.08
LRWR	-0.03	-0.17	-0.08	0.23	0.17	-0.04	-0.08	0.01	-0.19	0.25	0.09	-0.28	-0.10
MRWR	-0.05	-0.07	-0.03	0.16	-0.05	0.14	-0.03	-0.03	-0.08	0.14	-0.05	-0.02	0.04
HRWR	1.00	-0.12	-0.05	0.01	-0.04	-0.07	0.19	0.12	-0.29	0.02	0.02	0.14	0.02
PCHRWR	-0.12	1.00	-0.07	-0.04	-0.11	-0.09	-0.01	0.10	-0.48	0.07	-0.07	0.29	-0.07
ACCL	-0.05	-0.07	1.00	-0.05	-0.11	0.04	-0.04	-0.03	0.07	-0.01	-0.07	0.02	-0.07
AIR	0.01	-0.04	-0.05	1.00	0.13	-0.04	-0.05	0.04	-0.20	0.53	0.12	-0.06	-0.04
PerFA	-0.04	-0.11	-0.11	0.13	1.00	-0.34	0.00	0.07	-0.10	-0.03	0.69	-0.07	-0.44
PerSlag	-0.07	-0.09	0.04	-0.04	-0.34	1.00	-0.07	-0.07	0.05	0.00	-0.27	-0.05	-0.23
PerSF	0.19	-0.01	-0.04	-0.05	0.00	-0.07	1.00	-0.04	-0.11	-0.01	0.08	0.05	0.03
PerUFFA	0.12	0.10	-0.03	0.04	0.07	-0.07	-0.04	1.00	-0.23	-0.03	0.14	-0.04	-0.11
wc	-0.29	-0.48	0.07	-0.20	-0.10	0.05	-0.11	-0.23	1.00	-0.22	-0.16	-0.18	0.20
PerAir	0.02	0.07	-0.01	0.53	-0.03	0.00	-0.01	-0.03	-0.22	1.00	-0.01	-0.08	0.00
TotalFACaO	0.02	-0.07	-0.07	0.12	0.69	-0.27	0.08	0.14	-0.16	-0.01	1.00	-0.05	-0.34
CemBlaine	0.14	0.29	0.02	-0.06	-0.07	-0.05	0.05	-0.04	-0.18	-0.08	-0.05	1.00	-0.01
perCemNa2O	0.02	-0.07	-0.07	-0.04	-0.44	-0.23	0.03	-0.11	0.20	0.00	-0.34	-0.01	1.00
perCemK2O	-0.01	0.06	0.25	0.00	-0.29	-0.30	0.06	0.00	0.01	0.06	-0.08	0.07	-0.10
perCemNa2Oeq	-0.01	0.04	0.22	-0.02	-0.43	-0.37	0.07	-0.04	0.08	0.06	-0.19	0.07	0.24
i10	-0.01	0.08	-0.19	-0.05	-0.17	0.00	-0.09	-0.14	0.02	-0.08	-0.24	0.25	0.61
i17	0.06	-0.05	-0.08	0.11	0.75	-0.27	0.07	0.20	-0.23	-0.02	0.95	-0.07	-0.39
i21	0.08	0.06	-0.03	0.02	0.03	-0.06	-0.03	0.94	-0.16	-0.04	0.11	-0.04	-0.06
alphamax	-0.08	-0.21	0.02	-0.12	0.07	0.36	0.09	-0.09	0.35	-0.18	-0.12	-0.14	-0.06
lalpha	-0.07	-0.23	0.03	-0.13	0.07	0.34	0.09	-0.09	0.37	-0.18	-0.11	-0.16	-0.05
tau	-0.02	-0.14	-0.09	-0.03	0.12	0.59	-0.05	0.01	-0.01	-0.03	0.25	-0.06	-0.13
ltau	-0.02	-0.17	-0.12	-0.01	0.23	0.56	-0.03	0.02	-0.03	0.01	0.36	-0.13	-0.18
beta	0.11	0.21	-0.05	-0.02	-0.20	-0.37	-0.05	0.00	-0.29	0.18	-0.11	0.11	0.09
lbeta	0.11	0.22	-0.03	0.00	-0.18	-0.44	-0.04	0.00	-0.28	0.20	-0.09	0.10	0.09
HOHcem	-0.03	-0.11	0.03	0.00	0.27	0.64	0.03	0.06	-0.03	-0.01	0.36	-0.17	-0.61
HOHcemUlt	-0.05	-0.15	0.01	0.00	0.21	0.74	0.02	0.03	0.02	-0.05	0.28	-0.14	-0.50

Figure G.25: Correlation Matrix from PROC RSQUARE – Rietveld Calculations - Variables in Yellow Have a Covariance >0.65

Variable	perCemK2O	perCemNa2Oeq	i10	i17	i21	alphamax	lalpha	tau	ltau	beta	lbeta	HOHcem	HOHcemUlt
perAlite	0.49	0.61	0.10	-0.47	-0.09	-0.28	-0.26	-0.60	-0.67	0.50	0.53	-0.64	-0.70
perBelite	0.28	0.47	0.13	-0.28	0.00	-0.32	-0.32	-0.18	-0.28	0.17	0.15	-0.61	-0.51
perAluminate	0.52	0.50	-0.09	-0.22	-0.12	-0.21	-0.20	-0.39	-0.41	0.52	0.55	-0.21	-0.35
perFerrite	-0.15	0.07	0.31	-0.27	0.02	-0.08	-0.08	-0.11	-0.17	-0.09	-0.10	-0.52	-0.38
perPericlase	-0.20	-0.08	0.54	-0.14	-0.08	0.10	0.11	-0.05	-0.01	-0.02	0.02	-0.10	-0.10
perGypsumR	-0.15	0.05	0.75	-0.26	-0.13	0.08	0.09	-0.05	-0.07	0.08	0.09	-0.22	-0.19
perHemihydrate	-0.02	0.14	0.42	-0.34	-0.02	-0.14	-0.15	-0.30	-0.39	0.23	0.23	-0.52	-0.48
perAnhydrite	0.78	0.81	-0.32	-0.27	0.01	-0.49	-0.48	-0.54	-0.60	0.46	0.48	-0.56	-0.62
perK2SO4	0.46	0.51	0.14	-0.20	-0.07	-0.22	-0.21	-0.28	-0.32	0.39	0.42	-0.26	-0.34
perFreeCaO	-0.24	-0.15	0.51	-0.16	-0.07	0.22	0.23	-0.11	-0.09	0.01	0.04	-0.05	-0.07
WRRET	0.01	0.03	0.02	0.00	-0.02	-0.23	-0.24	0.11	0.17	0.60	0.53	-0.08	-0.15
LRWR	-0.12	-0.15	-0.03	0.15	-0.01	-0.06	-0.05	-0.04	0.00	0.11	0.14	0.15	0.08
MRWR	-0.09	-0.07	0.01	-0.05	-0.03	0.03	0.03	0.14	0.15	-0.05	-0.05	0.05	0.09
HRWR	-0.01	-0.01	-0.01	0.06	0.08	-0.08	-0.07	-0.02	-0.02	0.11	0.11	-0.03	-0.05
PCHRWR	0.06	0.04	0.08	-0.05	0.06	-0.21	-0.23	-0.14	-0.17	0.21	0.22	-0.11	-0.15
ACCL	0.25	0.22	-0.19	-0.08	-0.03	0.02	0.03	-0.09	-0.12	-0.05	-0.03	0.03	0.01
AIR	0.00	-0.02	-0.05	0.11	0.02	-0.12	-0.13	-0.03	-0.01	-0.02	0.00	0.00	0.00
PerFA	-0.29	-0.43	-0.17	0.75	0.03	0.07	0.07	0.12	0.23	-0.20	-0.18	0.27	0.21
PerSlag	-0.30	-0.37	0.00	-0.27	-0.06	0.36	0.34	0.59	0.56	-0.37	-0.44	0.64	0.74
PerSF	0.06	0.07	-0.09	0.07	-0.03	0.09	0.09	-0.05	-0.03	-0.05	-0.04	0.03	0.02
PerUFFA	0.00	-0.04	-0.14	0.20	0.94	-0.09	-0.09	0.01	0.02	0.00	0.00	0.06	0.03
wc	0.01	0.08	0.02	-0.23	-0.16	0.35	0.37	-0.01	-0.03	-0.29	-0.28	-0.03	0.02
PerAir	0.06	0.06	-0.08	-0.02	-0.04	-0.18	-0.18	-0.03	0.01	0.18	0.20	-0.01	-0.05
TotalFACaO	-0.08	-0.19	-0.24	0.95	0.11	-0.12	-0.11	0.25	0.36	-0.11	-0.09	0.36	0.28
CemBlaine	0.07	0.07	0.25	-0.07	-0.04	-0.14	-0.16	-0.06	-0.13	0.11	0.10	-0.17	-0.14
perCemNa2O	-0.10	0.24	0.61	-0.39	-0.06	-0.06	-0.05	-0.13	-0.18	0.09	0.09	-0.61	-0.50
perCemK2O	1.00	0.94	-0.47	-0.12	0.01	-0.46	-0.45	-0.47	-0.50	0.42	0.45	-0.32	-0.43
perCemNa2Oeq	0.94	1.00	-0.26	-0.25	-0.02	-0.47	-0.46	-0.50	-0.55	0.44	0.47	-0.51	-0.58
i10	-0.47	-0.26	1.00	-0.27	-0.11	0.19	0.19	0.08	0.03	-0.04	-0.05	-0.21	-0.12
i17	-0.12	-0.25	-0.27	1.00	0.14	-0.13	-0.13	0.27	0.39	-0.11	-0.10	0.41	0.34
i21	0.01	-0.02	-0.11	0.14	1.00	-0.07	-0.06	-0.01	0.00	-0.02	-0.02	0.03	0.01
alphamax	-0.46	-0.47	0.19	-0.13	-0.07	1.00	1.00	0.42	0.41	-0.60	-0.64	0.43	0.56
lalpha	-0.45	-0.46	0.19	-0.13	-0.06	1.00	1.00	0.41	0.39	-0.61	-0.64	0.43	0.55
tau	-0.47	-0.50	0.08	0.27	-0.01	0.42	0.41	1.00	0.96	-0.35	-0.46	0.56	0.73
ltau	-0.50	-0.55	0.03	0.39	0.00	0.41	0.39	0.96	1.00	-0.32	-0.43	0.65	0.77
beta	0.42	0.44	-0.04	-0.11	-0.02	-0.60	-0.61	-0.35	-0.32	1.00	0.98	-0.36	-0.55
lbeta	0.45	0.47	-0.05	-0.10	-0.02	-0.64	-0.64	-0.46	-0.43	0.98	1.00	-0.38	-0.60
HOHcem	-0.32	-0.51	-0.21	0.41	0.03	0.43	0.43	0.56	0.65	-0.36	-0.38	1.00	0.94
HOHcemUlt	-0.43	-0.58	-0.12	0.34	0.01	0.56	0.55	0.73	0.77	-0.55	-0.60	0.94	1.00

Figure G.26: Correlation Matrix from PROC RSQUARE – Rietveld Calculations - Variables in Yellow Have a Covariance >0.65

PROC GLM - lalpha - BOGUE

The SAS System

Dependent Variable: lalpha

Source	DF	Σ Squares	Mean Square	F Value	Pr>F
Model	6	2.527E+01	4.212E+00	577.99	<.0001
Error	3665	2.671E+01	7.287E-03		
Corrected Total	3671	5.198E+01			

R^2	C.V.	Root MSE	IEaMeas Mean
0.486	-33.986	0.09	-0.25

Type I F Test

Source	DF	Type I SS Mean	Mean Square	F Value	Pr>F
perC4AF	1	1.568E-01	1.568E-01	21.52	<.0001
WRRET	1	4.460E+00	4.460E+00	612.01	<.0001
PCHRWR	1	4.229E+00	4.229E+00	580.35	<.0001
wc	1	5.401E+00	5.401E+00	741.12	<.0001
perCemNa2Oeq	1	9.373E+00	9.373E+00	1286.28	<.0001
i17	1	1.652E+00	1.652E+00	226.67	<.0001

Type III F Test

Source	DF	Type III SS Mean	Mean Square	F Value	Pr>F
perC4AF	1	6.796E-01	6.796E-01	93.25	<.0001
WRRET	1	3.826E+00	3.826E+00	525.01	<.0001
PCHRWR	1	3.025E-01	3.025E-01	41.51	<.0001
wc	1	4.723E+00	4.723E+00	648.14	<.0001
perCemNa2Oeq	1	1.040E+01	1.040E+01	1426.73	<.0001
i17	1	1.652E+00	1.652E+00	226.67	<.0001

t Test and Parameter Estimate

Parameter	Estimate	Standard Error	t Value	Pr> t
Intercept	-0.44	0.02	-23.28	<.0001
perC4AF	-0.01	0.00	-9.66	<.0001
WRRET	-0.02	0.00	-22.91	<.0001
PerSF	0.00	0.00	-6.44	<.0001
wc	1.04	0.04	25.46	<.0001
perCemNa2Oeq	-0.40	0.01	-37.77	<.0001
i17	0.00	0.00	-15.06	<.0001

Figure G.27: Results for PROC GLM for Six (6) Variables - Bogue Calculations, $\ln(\alpha_i)$

PROC GLM - Itau - BOGUE

The SAS System

Dependent Variable: Itau

Source	DF	Σ Squares	Mean Square	F Value	Pr>F
Model	6	3.673E+02	6.122E+01	1249.54	<.0001
Error	3665	1.796E+02	4.899E-02		
Corrected Total	3671	5.468E+02			

R^2	C.V.	Root MSE	IEaMeas Mean
0.672	7.592	0.22	2.92

Type I F Test

Source	DF	Type I SS Mean	Mean Square	F Value	Pr>F
perC3S	1	2.367E+02	2.367E+02	4831.8	<.0001
ACCL	1	2.432E+00	2.432E+00	49.64	<.0001
WRRET	1	2.838E+01	2.838E+01	579.24	<.0001
PerSlag	1	4.787E+01	4.787E+01	977.17	<.0001
perCemNa2O	1	7.371E+00	7.371E+00	150.45	<.0001
i17	1	4.453E+01	4.453E+01	908.94	<.0001

Type III F Test

Source	DF	Type III SS Mean	Mean Square	F Value	Pr>F
perC3S	1	2.933E+01	2.933E+01	598.74	<.0001
ACCL	1	1.538E+00	1.538E+00	31.39	<.0001
WRRET	1	2.546E+01	2.546E+01	519.62	<.0001
PerSlag	1	9.210E+01	9.210E+01	1880.04	<.0001
perCemNa2O	1	2.629E+01	2.629E+01	536.60	<.0001
i17	1	4.453E+01	4.453E+01	908.94	<.0001

t Test and Parameter Estimate

Parameter	Estimate	Standard Error	t Value	Pr> t
Intercept	2.93	0.03	102.15	<.0001
perC3S	-0.01	0.00	-24.47	<.0001
ACCL	0.00	0.00	-5.60	<.0001
WRRET	0.06	0.00	22.80	<.0001
PerSlag	0.02	0.00	43.36	<.0001
perCemNa2O	2.39	0.10	23.16	<.0001
i17	0.00	0.00	30.15	<.0001

Figure G.28: Results for PROC GLM for Five (5) Variables - Bogue Calculations, $\ln(\eta)$

PROC GLM - lbeta - BOGUE

The SAS System

Dependent Variable: lbeta

Source	DF	Σ Squares	Mean Square	F Value	Pr>F
Model	7	2.184E+02	3.120E+01	1778.63	<.0001
Error	3664	6.427E+01	1.754E-02		
Corrected Total	3671	2.827E+02			

R^2	C.V.	Root MSE	EaMeas Mean
0.773	-74.013	0.13	-0.18

Type I F Test

Source	DF	Type I SS Mean	Mean Square	F Value	Pr>F
perC3A	1	9.706E+01	9.706E+01	5533.13	<.0001
WRRET	1	6.966E+01	6.966E+01	3971.2	<.0001
LRWR	1	1.060E+01	1.060E+01	604.54	<.0001
MRWR	1	1.902E+00	1.902E+00	108.44	<.0001
HRWR	1	3.583E+00	3.583E+00	204.24	<.0001
PCHRWR	1	1.629E+01	1.629E+01	928.78	<.0001
PerSlag	1	1.930E+01	1.930E+01	1100.07	<.0001

Type III F Test

Source	DF	Type III SS Mean	Mean Square	F Value	Pr>F
perC3A	1	4.652E+01	4.652E+01	2652.26	<.0001
WRRET	1	8.755E+01	8.755E+01	4991.26	<.0001
LRWR	1	1.449E+01	1.449E+01	825.89	<.0001
MRWR	1	4.411E+00	4.411E+00	251.44	<.0001
HRWR	1	4.617E+00	4.617E+00	263.21	<.0001
PCHRWR	1	1.499E+01	1.499E+01	854.82	<.0001
PerSlag	1	1.930E+01	1.930E+01	1100.07	<.0001

t Test and Parameter Estimate

Parameter	Estimate	Standard Error	t Value	Pr> t
Intercept	-0.55	0.01	-93.24	<.0001
perC3A	0.04	0.00	51.50	<.0001
WRRET	0.11	0.00	70.65	<.0001
LRWR	0.04	0.00	28.74	<.0001
MRWR	0.03	0.00	15.86	<.0001
HRWR	0.01	0.00	16.22	<.0001
PCHRWR	0.03	0.00	29.24	<.0001
PerSlag	-0.01	0.00	-33.17	<.0001

Figure G.29: Results for PROC GLM for Nine (9) Variables - Bogue Calculations, $\ln(\beta)$

PROC GLM - lalpha - RIETVELD

The SAS System

Dependent Variable: lalpha

Source	DF	Σ Squares	Mean Square	F Value	Pr>F
Model	6	2.526E+01	4.210E+00	577.36	<.0001
Error	3665	2.672E+01	7.291E-03		
Corrected Total	3671	5.198E+01			

R^2	C.V.	Root MSE	EaMeas Mean
0.486	-33.995	0.09	-0.25

Type I F Test

Source	DF	Type I SS Mean	Mean Square	F Value	Pr>F
perFerrite	1	5.458E-02	5.458E-02	7.49	0.0062
PCHRWR	1	2.768E+00	2.768E+00	379.64	<.0001
WRRET	1	5.939E+00	5.939E+00	814.58	<.0001
wc	1	5.348E+00	5.348E+00	733.46	<.0001
perCemNa2Oeq	1	9.640E+00	9.640E+00	1322.09	<.0001
i17	1	1.509E+00	1.509E+00	206.9	<.0001

Type III F Test

Source	DF	Type III SS Mean	Mean Square	F Value	Pr>F
perFerrite	1	6.653E-01	6.653E-01	91.25	<.0001
PCHRWR	1	2.729E-01	2.729E-01	37.43	<.0001
WRRET	1	3.753E+00	3.753E+00	514.79	<.0001
wc	1	4.874E+00	4.874E+00	668.46	<.0001
perCemNa2Oeq	1	1.074E+01	1.074E+01	1473.1	<.0001
i17	1	1.509E+00	1.509E+00	206.9	<.0001

t Test and Parameter Estimate

Parameter	Estimate	Standard Error	t Value	Pr> t
Intercept	-0.46	0.02	-24.50	<.0001
perFerrite	-0.01	0.00	-9.55	<.0001
PCHRWR	0.00	0.00	-6.12	<.0001
WRRET	-0.02	0.00	-22.69	<.0001
wc	1.06	0.04	25.85	<.0001
perCemNa2Oeq	-0.41	0.01	-38.38	<.0001
i17	0.00	0.00	-14.38	<.0001

Figure G.30: Results for PROC GLM for Six (6) Variables - Rietveld Calculations, $\ln(\alpha_i)$

PROC GLM - Itau - RIETVELD

The SAS System

Dependent Variable: Itau

Source	DF	Σ Squares	Mean Square	F Value	Pr>F
Model	6	3.703E+02	6.171E+01	1281.07	<.0001
Error	3665	1.766E+02	4.817E-02		
Corrected Total	3671	5.468E+02			

R^2	C.V.	Root MSE	EaMeas Mean
0.677	7.528	0.22	2.92

Type I F Test

Source	DF	Type I SS Mean	Mean Square	F Value	Pr>F
perAlite	1	2.380E+02	2.380E+02	4939.95	<.0001
WRRET	1	2.696E+01	2.696E+01	559.64	<.0001
ACCL	1	1.143E+00	1.143E+00	23.73	<.0001
PerSlag	1	5.172E+01	5.172E+01	1073.53	<.0001
perCemNa2O	1	8.070E+00	8.070E+00	167.51	<.0001
i17	1	4.442E+01	4.442E+01	922.04	<.0001

Type III F Test

Source	DF	Type III SS Mean	Mean Square	F Value	Pr>F
perAlite	1	3.232E+01	3.232E+01	670.99	<.0001
WRRET	1	2.414E+01	2.414E+01	501.15	<.0001
ACCL	1	1.414E+00	1.414E+00	29.34	<.0001
PerSlag	1	9.635E+01	9.635E+01	1999.95	<.0001
perCemNa2O	1	2.726E+01	2.726E+01	565.93	<.0001
i17	1	4.442E+01	4.442E+01	922.04	<.0001

t Test and Parameter Estimate

Parameter	Estimate	Standard Error	t Value	Pr> t
Intercept	2.93	0.03	106.30	<.0001
perAlite	-0.01	0.00	-25.90	<.0001
WRRET	0.06	0.00	22.39	<.0001
ACCL	0.00	0.00	-5.42	<.0001
PerSlag	0.02	0.00	44.72	<.0001
perCemNa2O	2.44	0.10	23.79	<.0001
i17	0.00	0.00	30.37	<.0001

Figure G.31: Results for PROC GLM for Five (5) Variables - Rietveld Calculations, $\ln(\eta)$

PROC GLM - lbeta - RIETVELD

The SAS System

Dependent Variable: lbeta

Source	DF	Σ Squares	Mean Square	F Value	Pr>F
Model	7	2.123E+02	3.033E+01	1579.74	<.0001
Error	3664	7.035E+01	1.920E-02		
Corrected Total	3671	2.827E+02			

R^2	C.V.	Root MSE	EaMeas Mean
0.751	-77.433	0.14	-0.18

Type I F Test

Source	DF	Type I SS Mean	Mean Square	F Value	Pr>F
perAluminate	1	8.525E+01	8.525E+01	4440.25	<.0001
WRRET	1	6.834E+01	6.834E+01	3559.15	<.0001
LRWR	1	9.660E+00	9.660E+00	503.13	<.0001
MRWR	1	7.238E-01	7.238E-01	37.7	<.0001
HRWR	1	5.519E+00	5.519E+00	287.44	<.0001
PCHRWR	1	1.889E+01	1.889E+01	984.03	<.0001
PerSlag	1	2.393E+01	2.393E+01	1246.48	<.0001

Type III F Test

Source	DF	Type III SS Mean	Mean Square	F Value	Pr>F
perAluminate	1	4.045E+01	4.045E+01	2106.56	<.0001
WRRET	1	8.606E+01	8.606E+01	4482.38	<.0001
LRWR	1	1.364E+01	1.364E+01	710.27	<.0001
MRWR	1	3.259E+00	3.259E+00	169.75	<.0001
HRWR	1	6.196E+00	6.196E+00	322.69	<.0001
PCHRWR	1	16.6685746	16.6685746	868.15	<.0001
PerSlag	1	2.393E+01	2.393E+01	1246.48	<.0001

t Test and Parameter Estimate

Parameter	Estimate	Standard Error	t Value	Pr> t
Intercept	-0.50	0.01	-89.69	<.0001
perAluminate	0.04	0.00	45.90	<.0001
WRRET	0.11	0.00	66.95	<.0001
LRWR	0.04	0.00	26.65	<.0001
MRWR	0.03	0.00	13.03	<.0001
HRWR	0.01	0.00	17.96	<.0001
PCHRWR	0.03	0.00	29.46	<.0001
PerSlag	-0.01	0.00	-35.31	<.0001

Figure G.32: Results for PROC GLM for Nine (9) Variables - Rietveld Calculations, $\ln(\beta)$

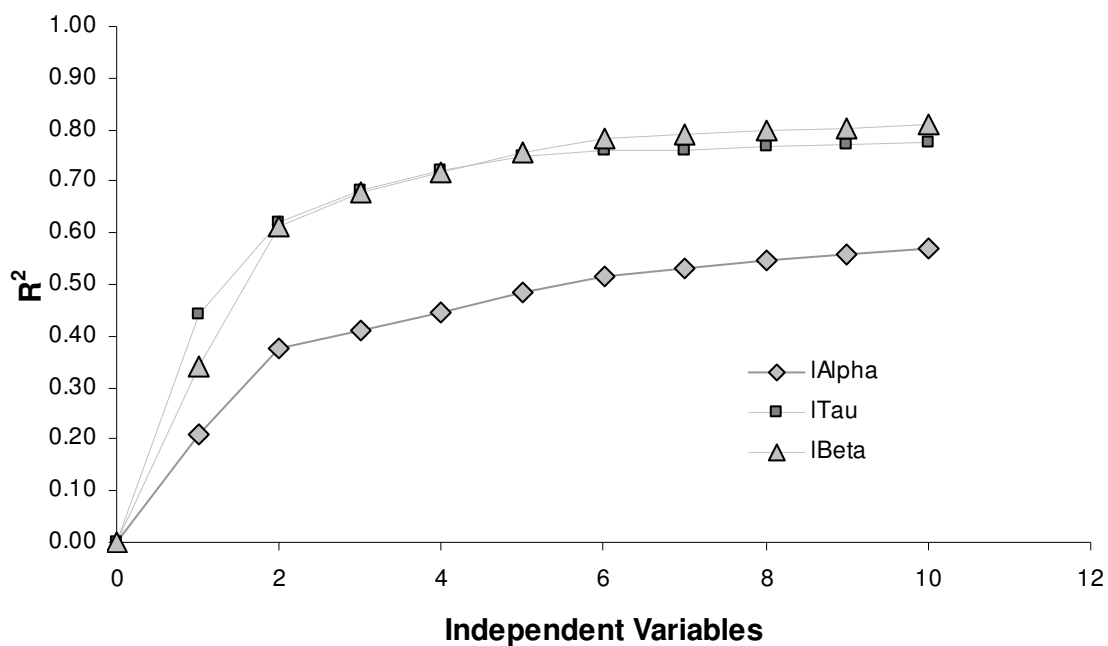


Figure G.33: Coefficient of Determination vs. Number of Independent Variables for Bogue Calculations

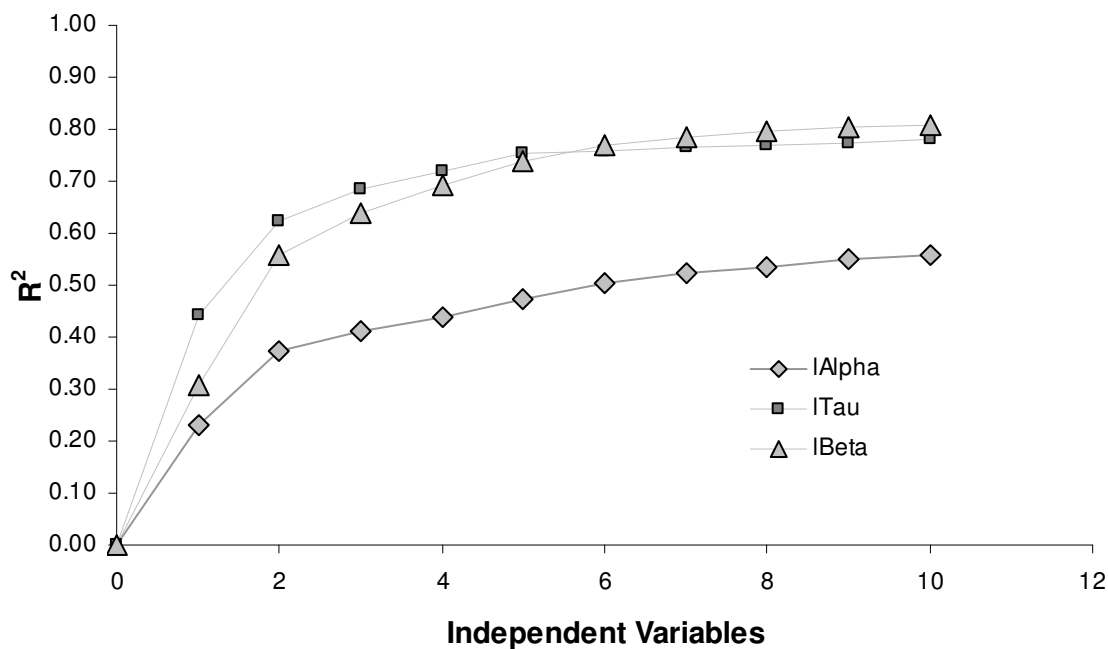


Figure G.34: Coefficient of Determination vs. Number of Independent Variables for Rietveld Calculations

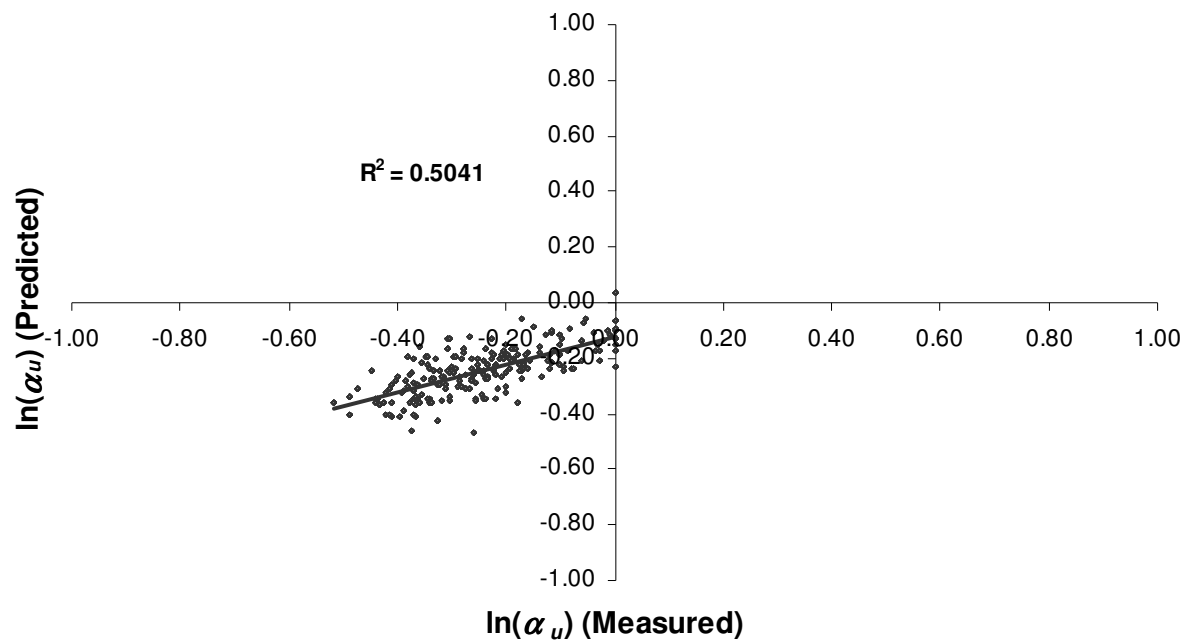


Figure G.35: Proc GLM Results for Degree of Hydration Parameter (α_u)

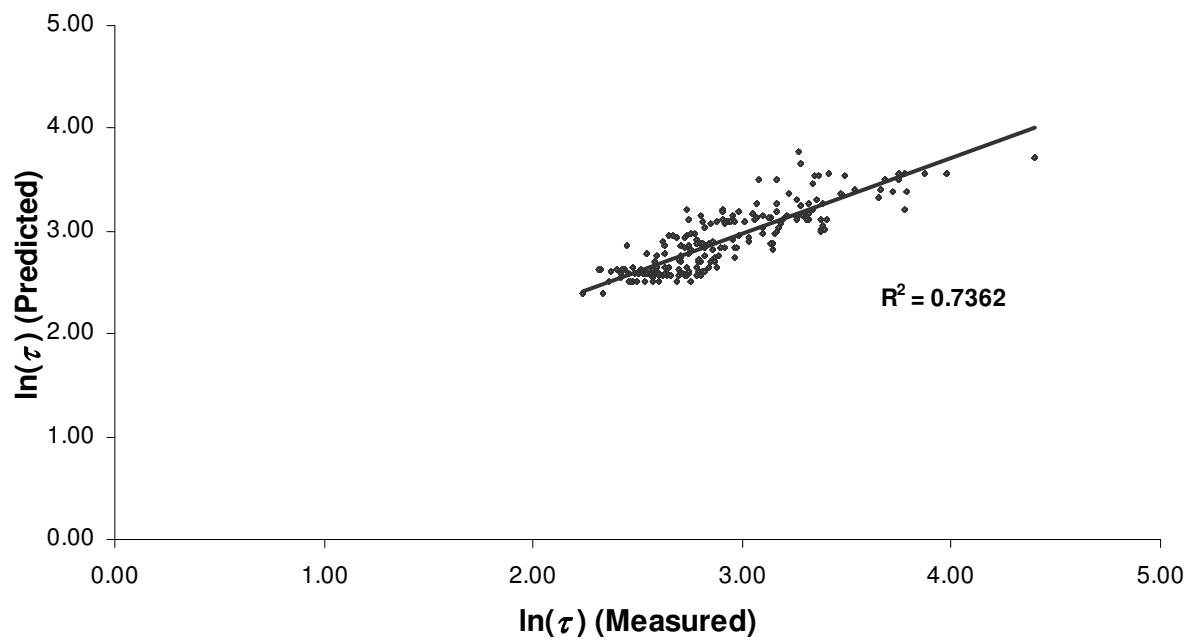


Figure G.36: Proc GLM Results for Time Parameter (τ)

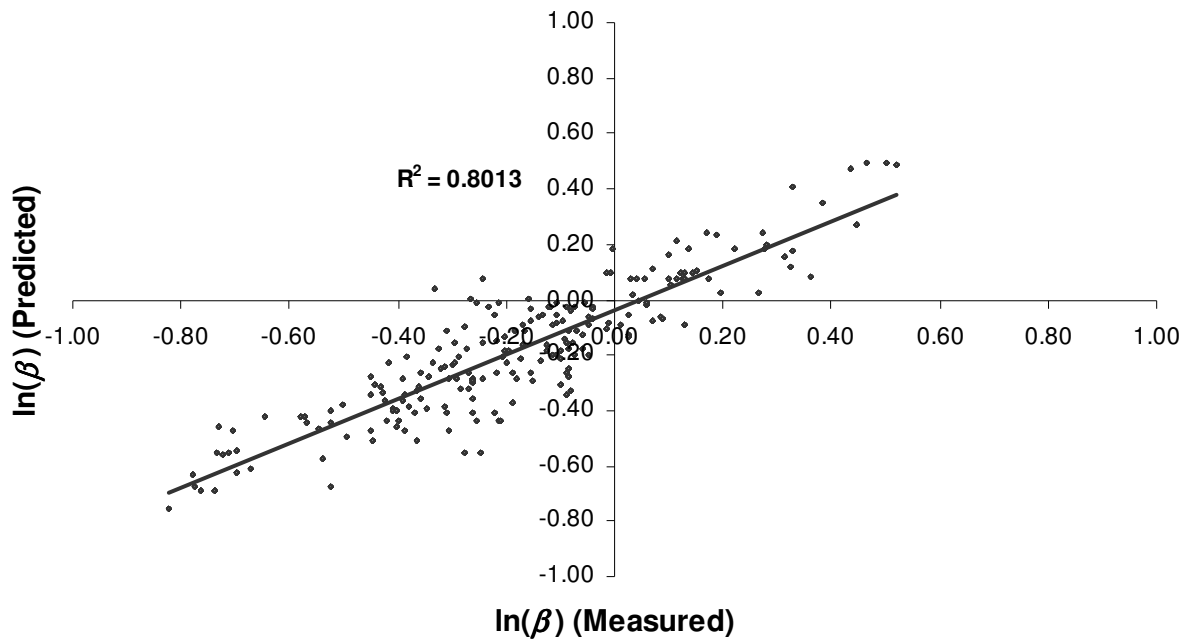


Figure G.37: Proc GLM Results for Slope Parameter (β)

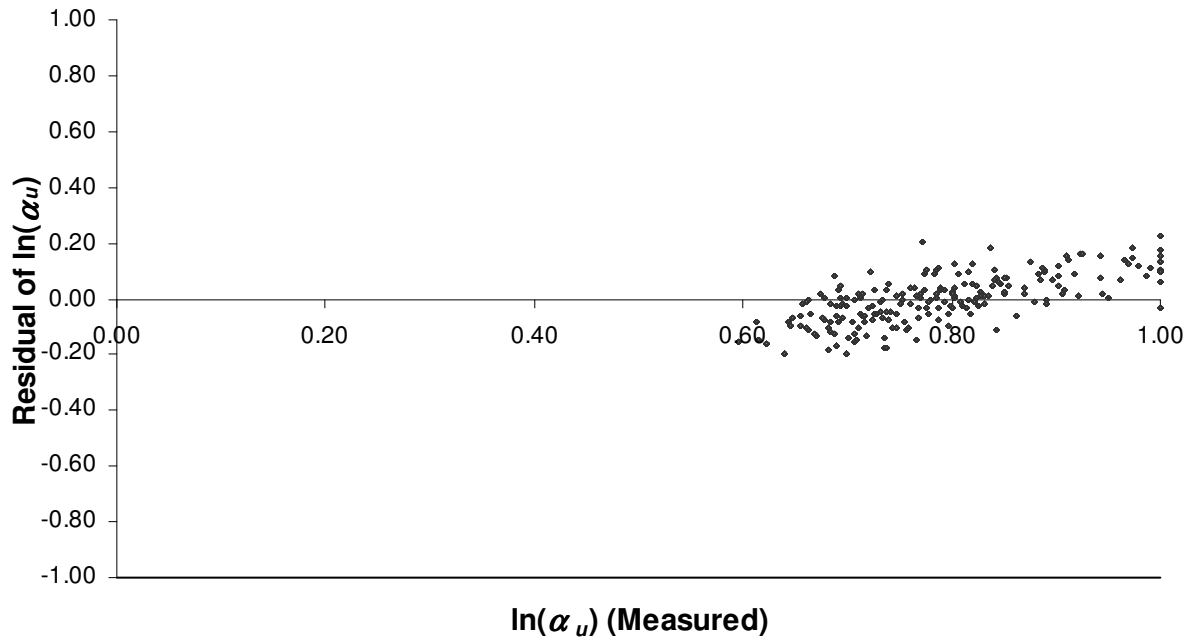


Figure G.38: Residual Plot for Degree of Hydration Parameter (α_u)

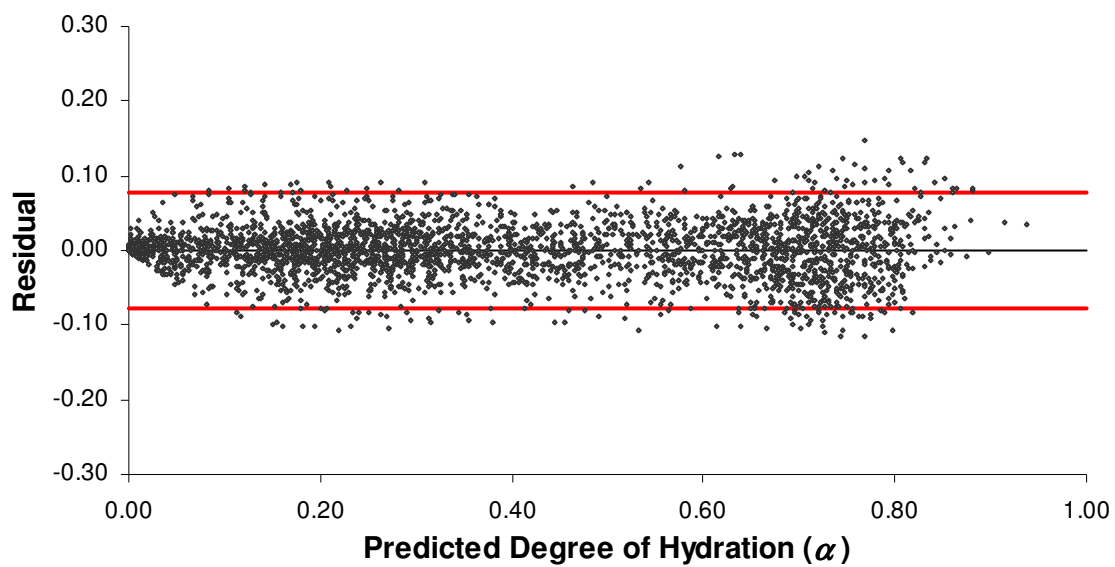


Figure G.39: Residual Plot for Hydration Model

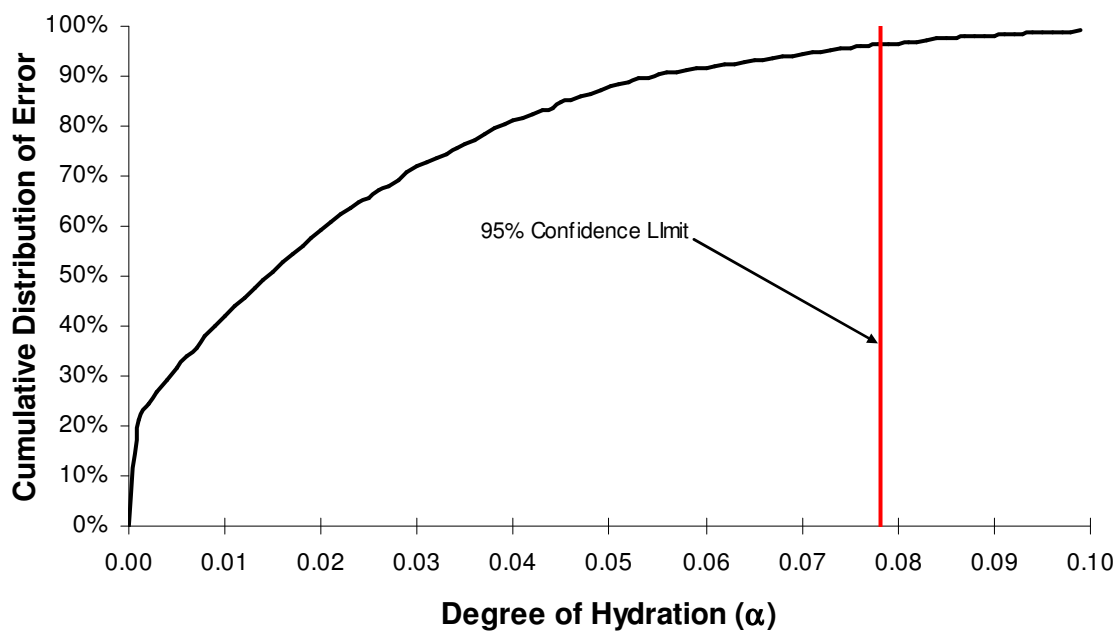


Figure G.40: Cumulative Distribution of Error for Rietveld Model

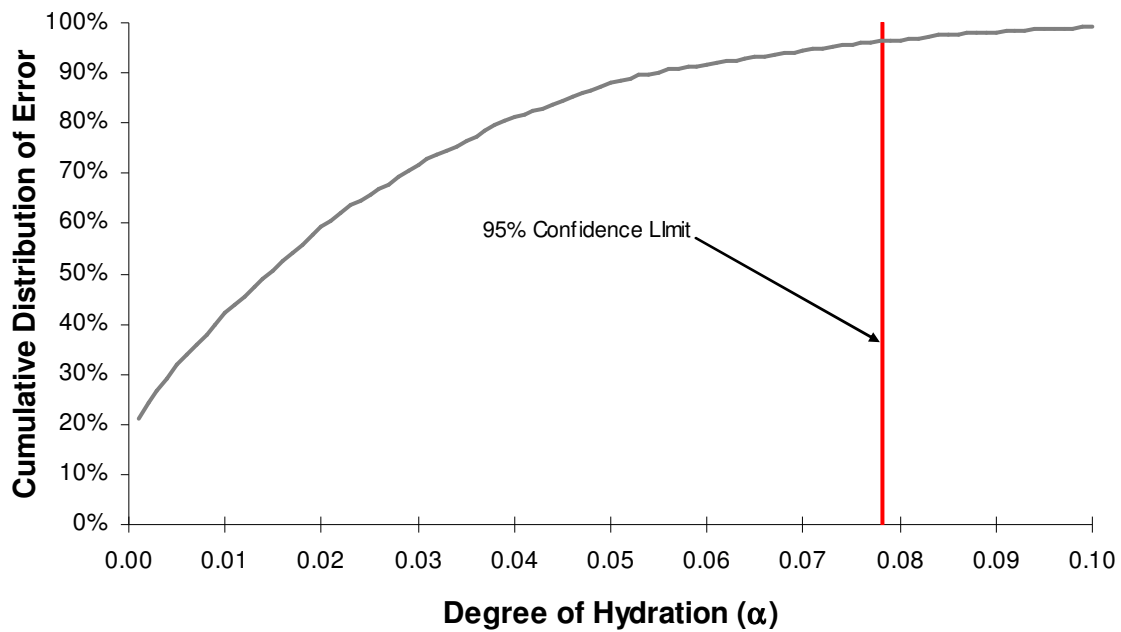


Figure G.41: Cumulative Distribution of Error for Bogue Model

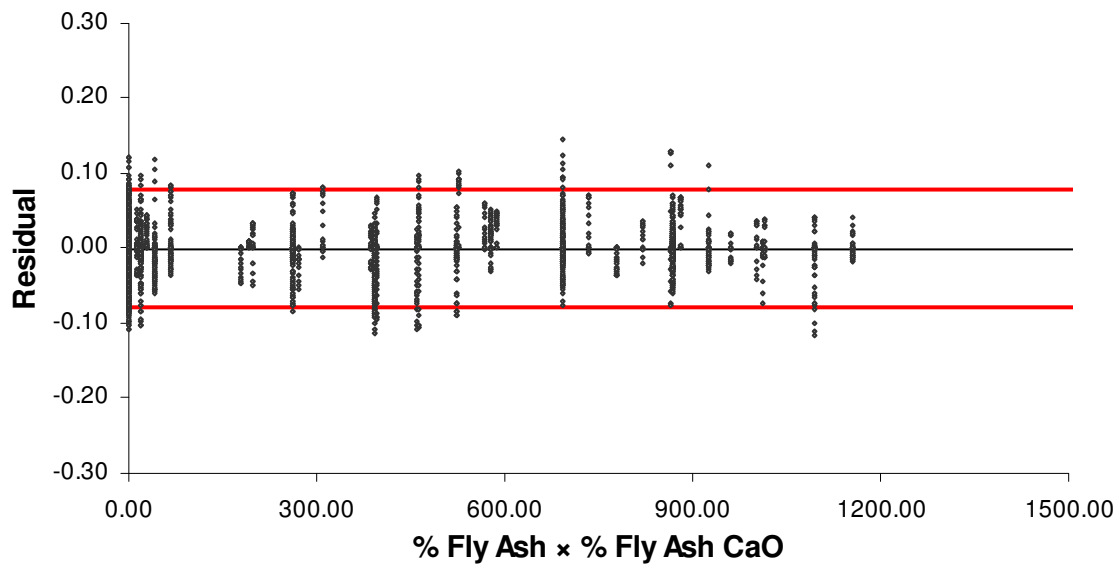


Figure G.42: Residual Plot for i17 (% Fly Ash \times % Fly Ash CaO)

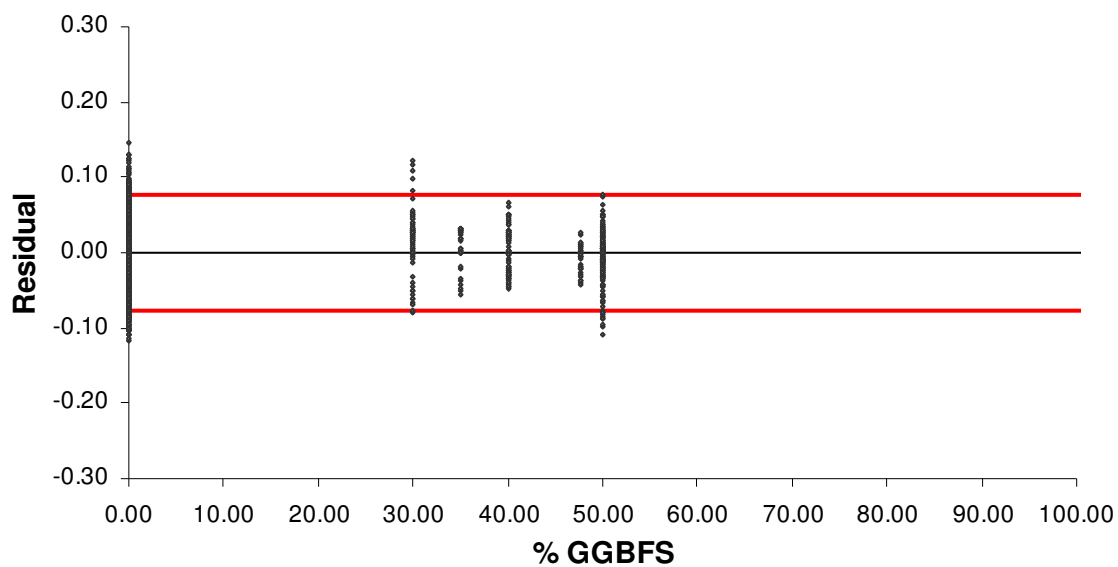


Figure G.43: Residual Plot for % GGBF Slag

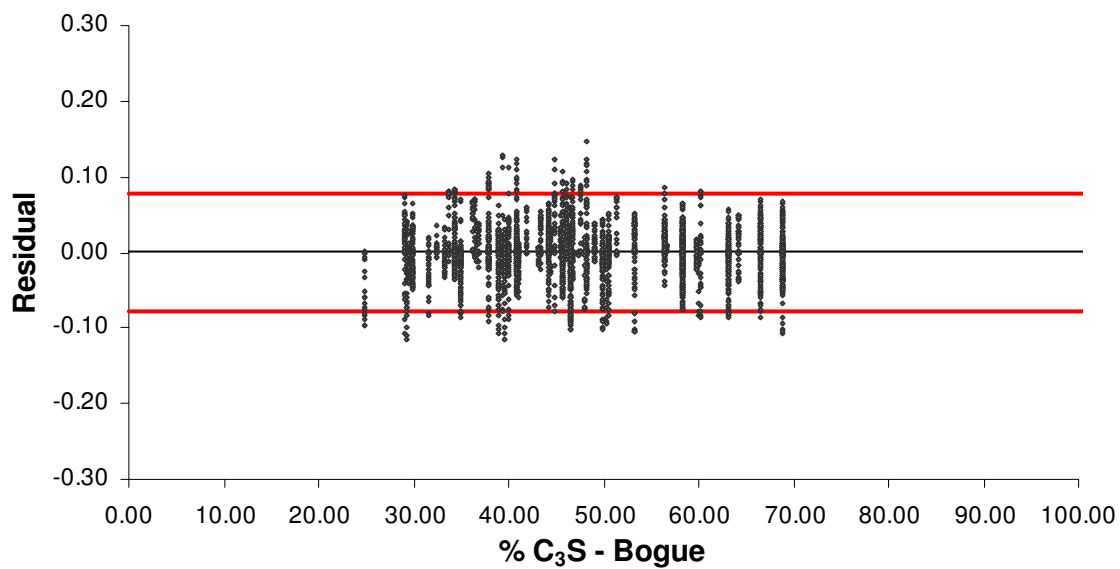


Figure G.44: Residual Plot for % C₃S, as Determined by Bogue Calculations

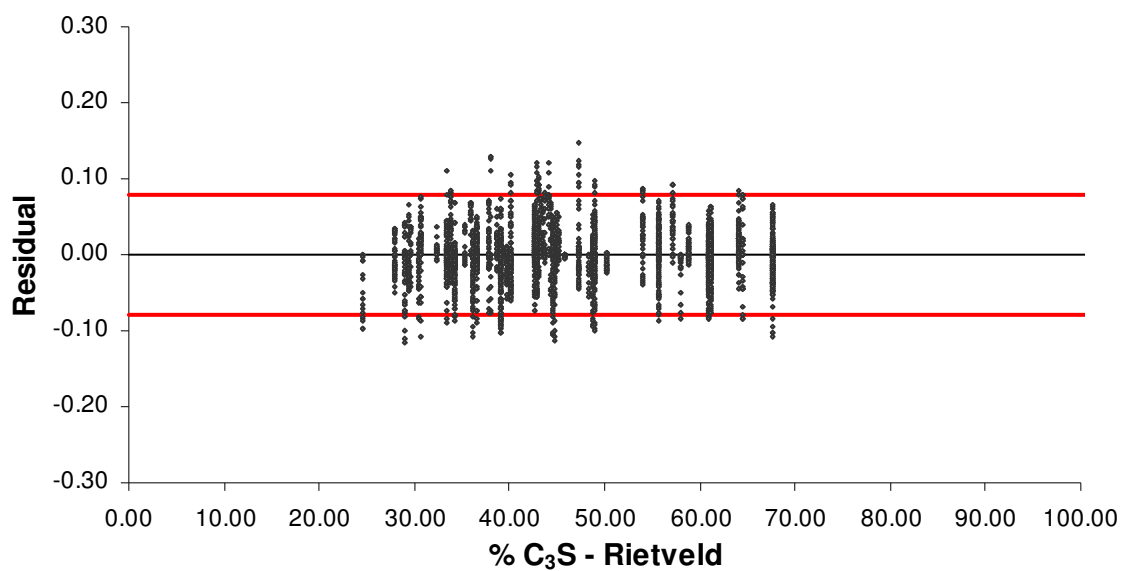


Figure G.45: Residual Plot for $\% \text{C}_3\text{S}$, as Determined by Rietveld Analysis

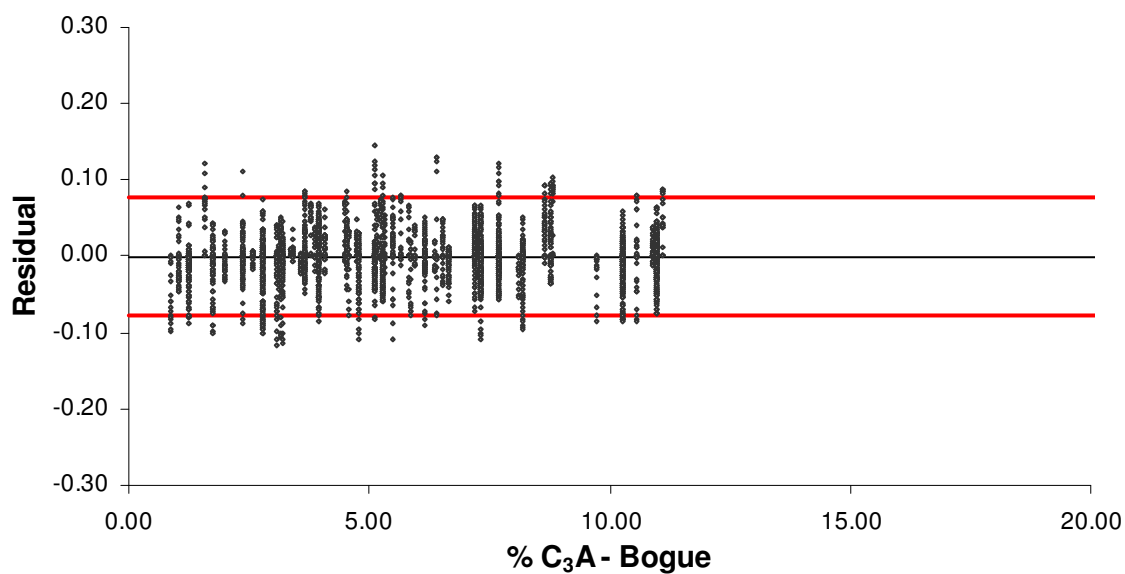


Figure G.46: Residual Plot for $\% \text{C}_3\text{A}$, as Determined by Bogue Calculations

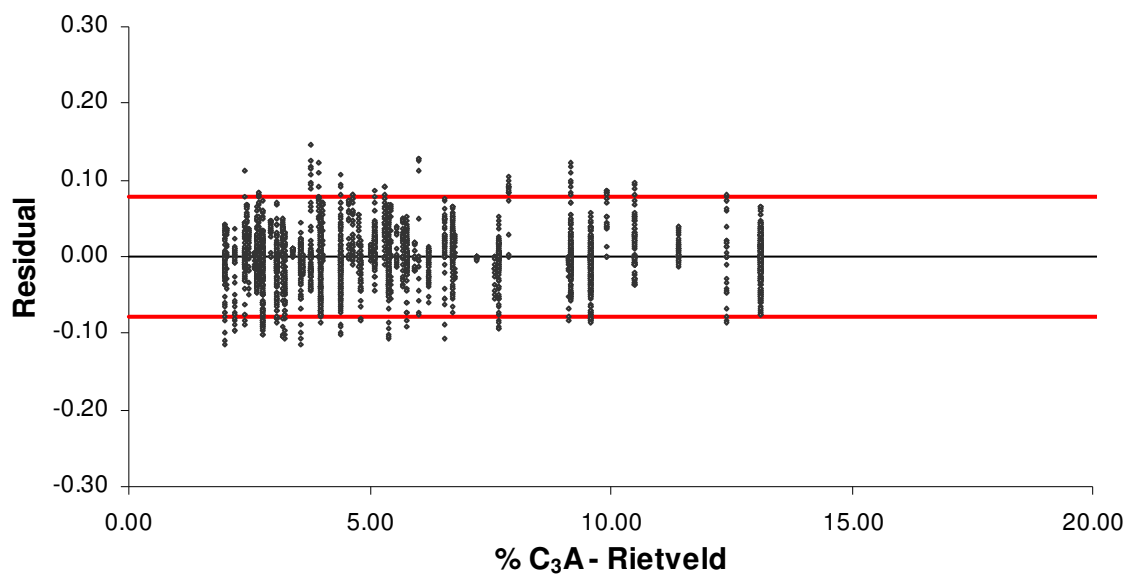


Figure G.47: Residual Plot for % C_3A , as Determined by Rietveld Analysis

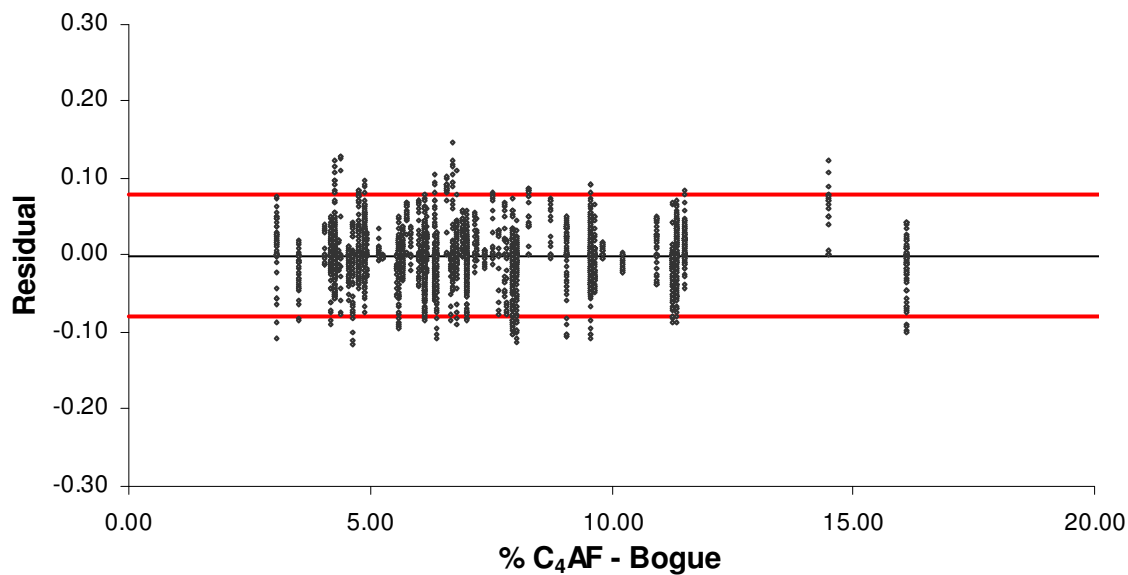


Figure G.48: Residual Plot for % C_4AF , as Determined by Bogue Calculations

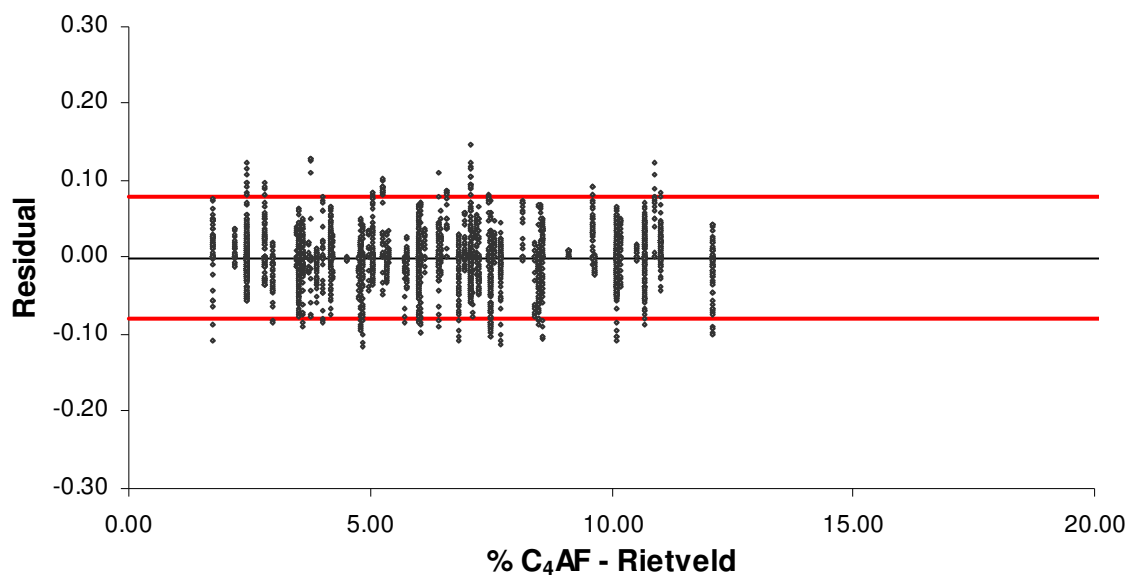


Figure G.49: Residual Plot for % C₄AF, as Determined by Rietveld Analysis

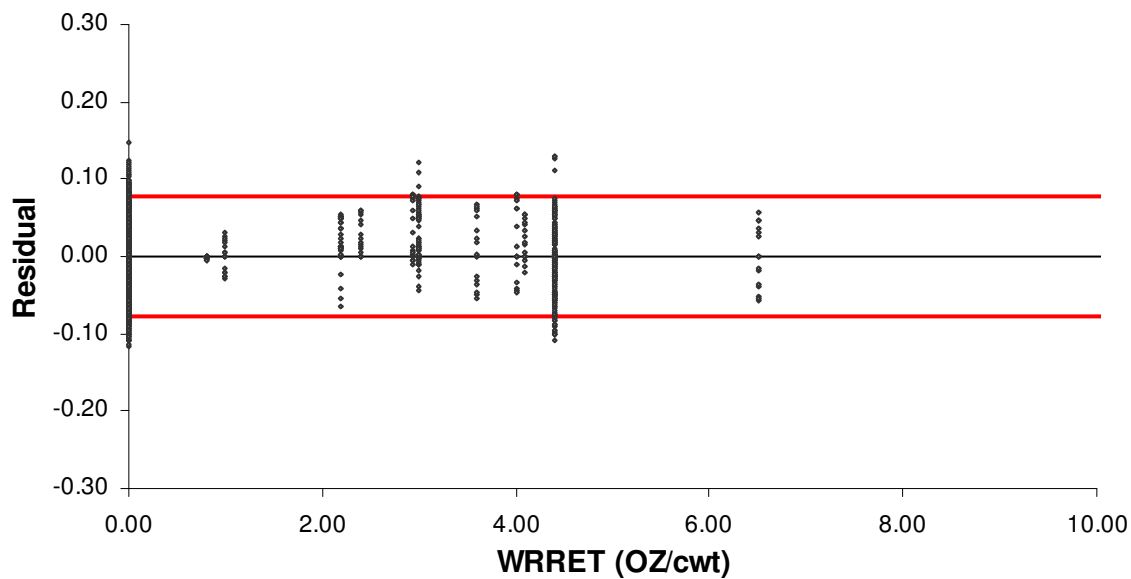


Figure G.50: Residual Plot for ASTM Type B&D Water Reducer/Retarder

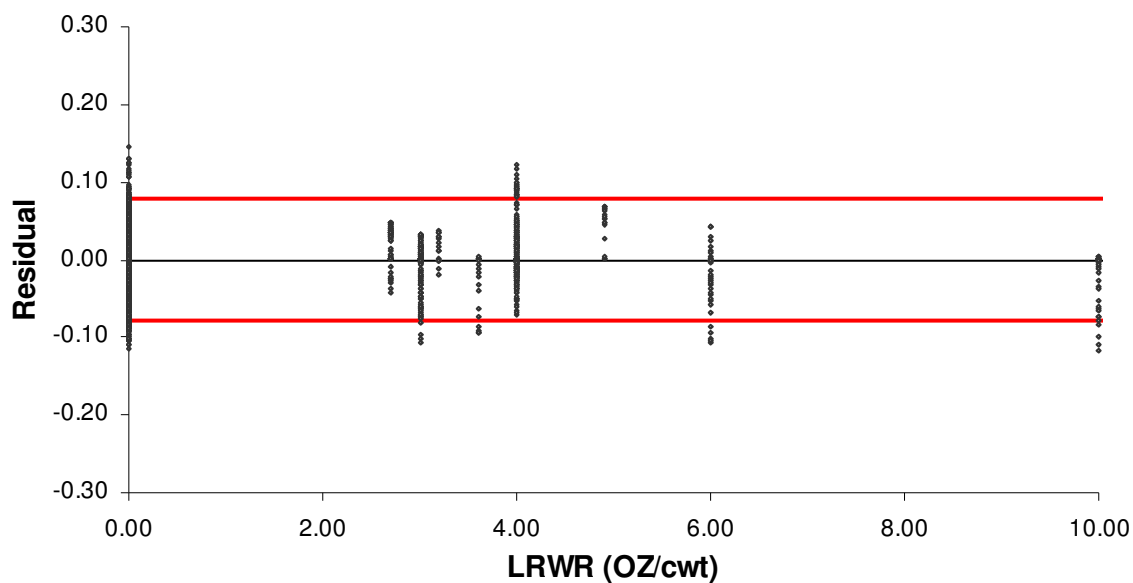


Figure G.51: Residual Plot for ASTM Type A Low Range Water Reducer

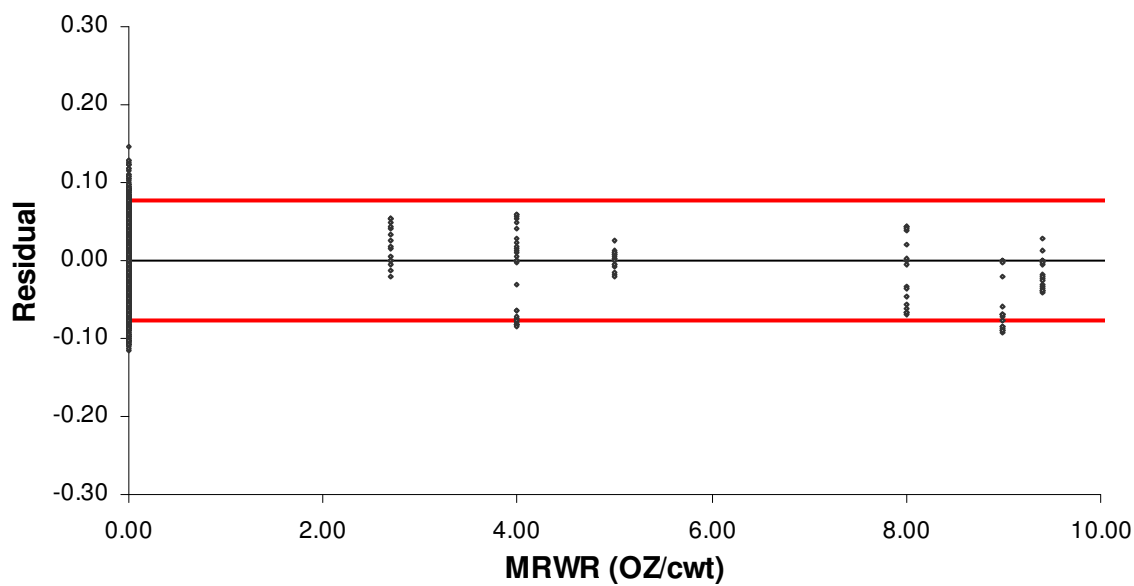


Figure G.52: Residual Plot for Mid Range Water Reducer

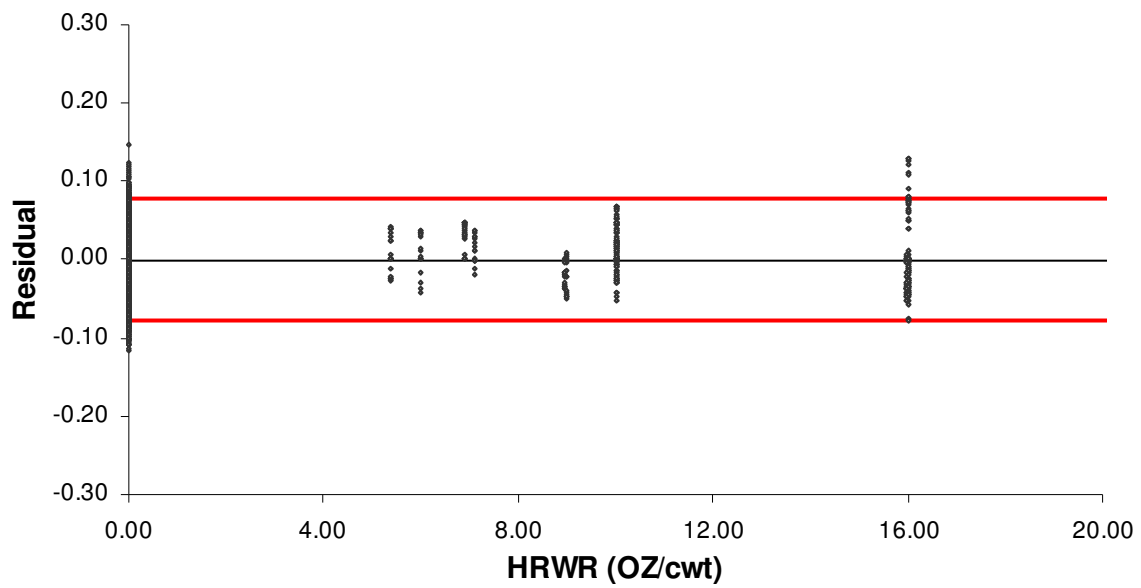


Figure G.53: Residual Plot for ASTM Type F Naphthalene-Sulfonate-Based High Range Water Reducer

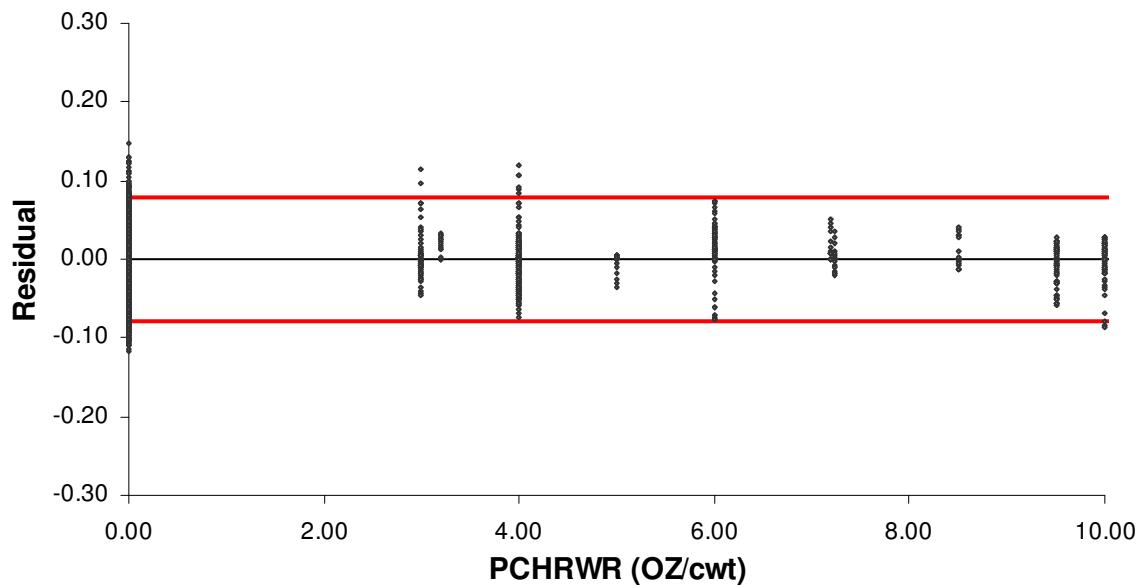


Figure G.54: Residual Plot for ASTM Type F Polycarboxylate-Based High Range Water Reducer

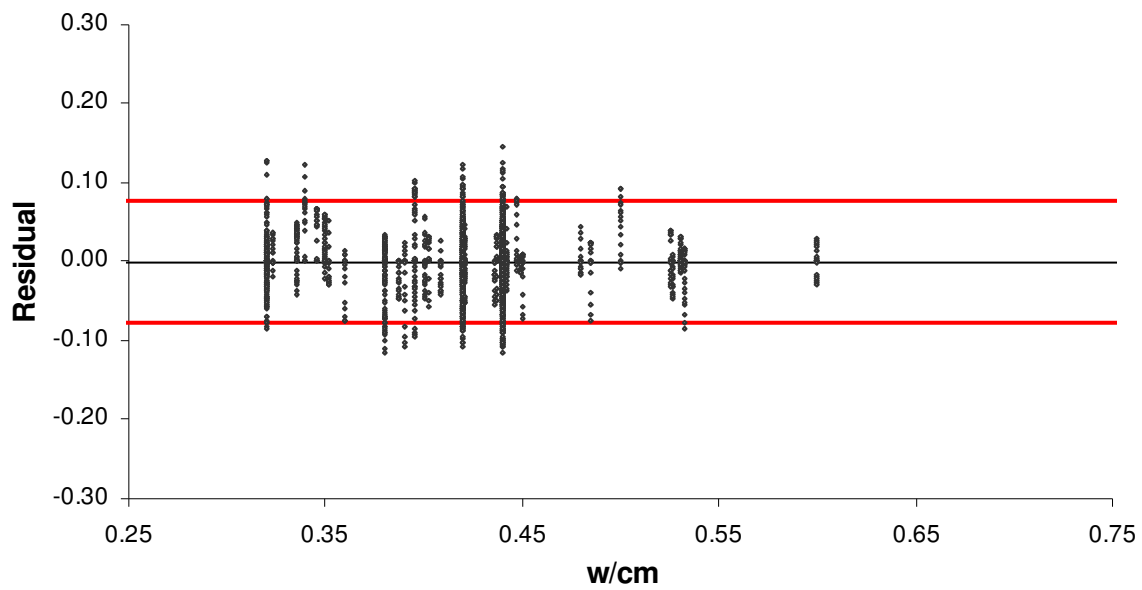


Figure G.55: Residual Plot for w/cm

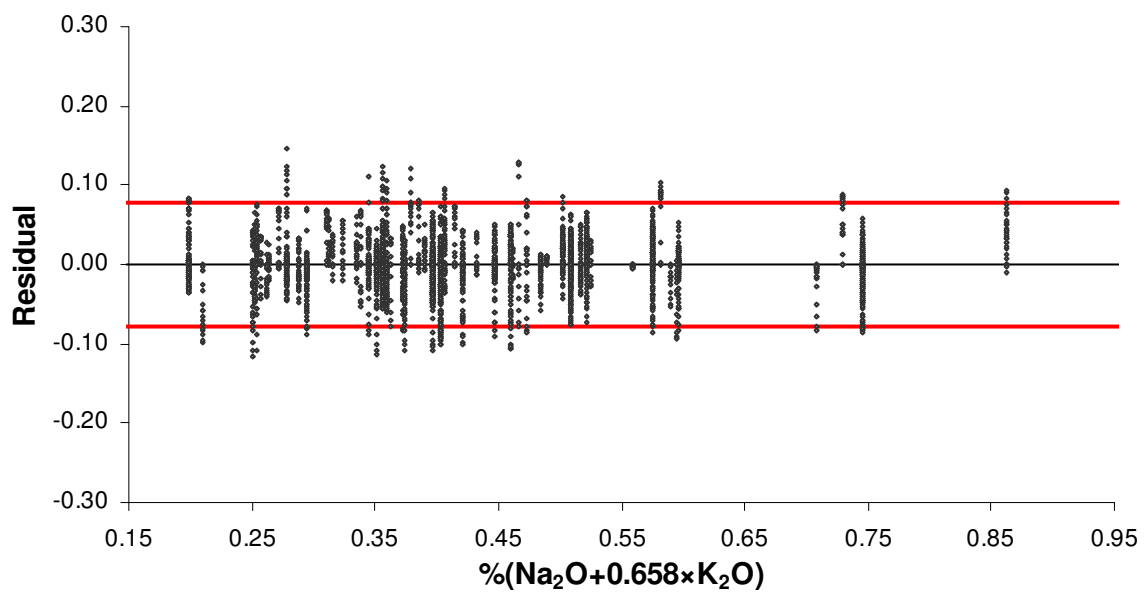


Figure G.56: Residual Plot for Total Alkalies in Cement

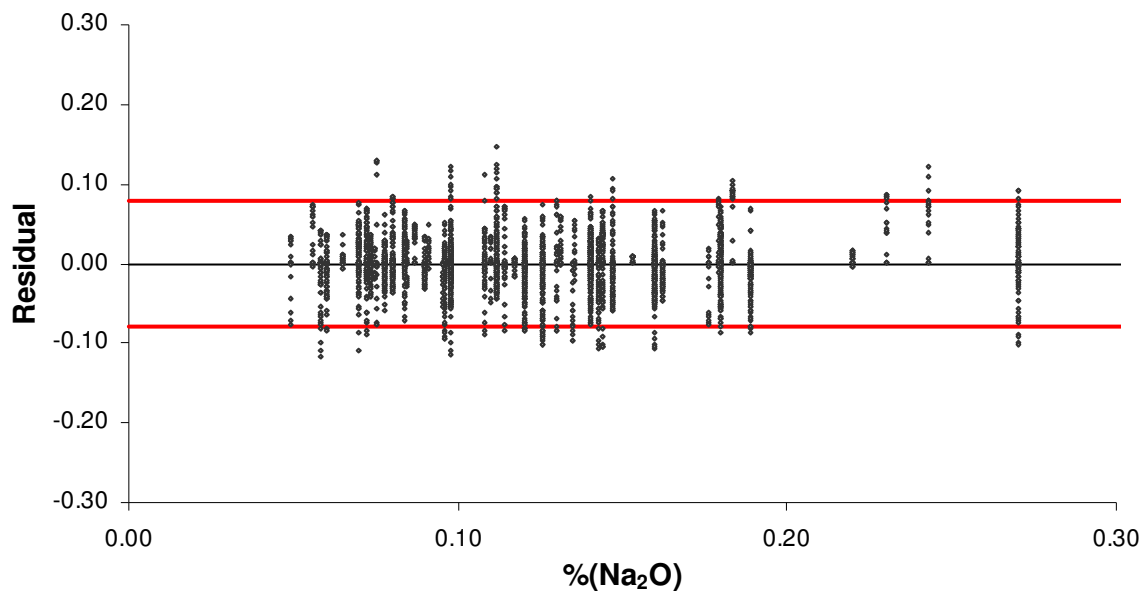


Figure G.57: Residual Plot for Na₂O in Cement

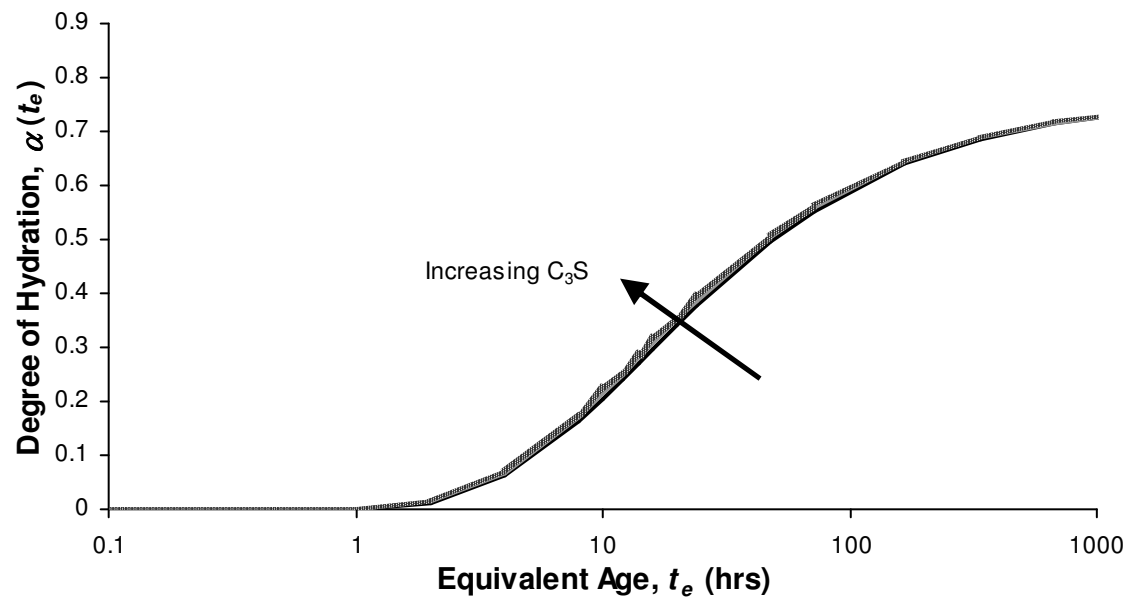


Figure G.58: Effect of C₃S on Degree of Hydration

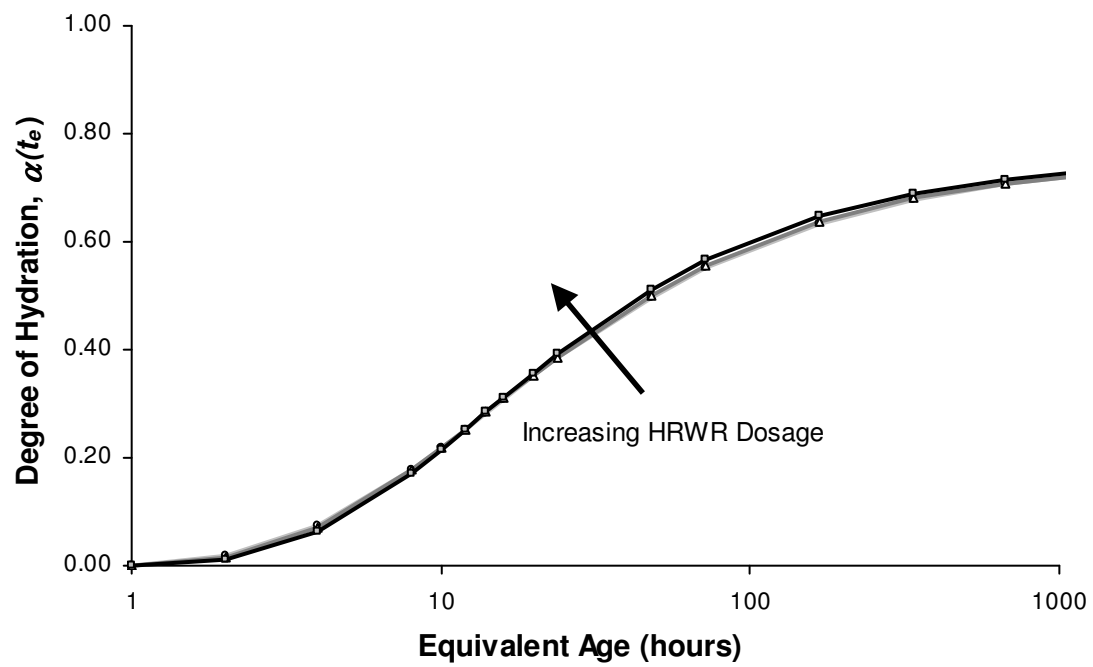


Figure G.59: Effect of HRWR (Naphthalene or Polycarboxylate-based) on Degree of Hydration

REFERENCES

1. ACI Committee 207, “Guide to Mass Concrete”, ACI 207.1R-05, American Concrete Institute, Farmington Hills, Michigan, 2005.
2. ACI Committee 207, “Effect of Restraint, Volume Change, and Reinforcement on Cracking of Mass Concrete”, ACI 207.2R-05, American Concrete Institute, Farmington Hills, Michigan, 2005.
3. ACI Committee 232, “Use of Fly Ash in Concrete”, ACI 232.2R-03, American Concrete Institute, Farmington Hills, Michigan, 2003.
4. ACI Committee 233, “Ground Granulated Blast-Furnace Slag as a Cementitious Constituent in Concrete”, ACI 233 R-00, American Concrete Institute, Farmington Hills, Michigan, 2000.
5. ACI Committee 234, “Guide for the Use of Silica Fume in Concrete”, ACI 234R-06, American Concrete Institute, Farmington Hills, Michigan, 2006.
6. ASTM C 33, “Standard Specification for Concrete Aggregates” Annual Book of ASTM Standards, V. 04.01., ASTM International, West Conshohocken, PA., 2003, 11 pp.
7. ASTM C 114, ”Standard Test Methods for Chemical Analysis of Hydraulic Cement” Annual Book of ASTM Standards, Vol 04.01., ASTM International, West Conshohocken, PA., 2005, 31 pp.
8. ASTM C 150, “Standard Specification for Portland Cement,” Annual Book of ASTM Standards, Vol 04.01., ASTM International, West Conshohocken, PA., 2002, 8 pp.

9. ASTM C 192, “Standard for Making and Curing Concrete Test Specimens in the Laboratory,” Annual Book of ASTM Standards, Vol 04.01., ASTM International, West Conshohocken, PA, 2006, 8 pp.
10. ASTM C 186, ”Standard Test Method for Heat of Hydration of Hydraulic Cement” Annual Book of ASTM Standards, Vol 04.01., ASTM International, West Conshohocken, PA., 2005, 7 pp.
11. ASTM C 494, “Standard Specification for Chemical Admixtures for Concrete,” Annual Book of ASTM Standards, V. 04.01., ASTM International, West Conshohocken, PA., 2005, 10 pp.
12. ASTM C 618, “Standard Specification for Coal Ash and Raw or Calcined Natural Pozzolans for Use in Concrete,” Annual Book of ASTM Standards, V. 04.01., ASTM International, West Conshohocken, PA., 2003, 3 pp.
13. ASTM C 670, “Preparing Precision and Bias Statements for Test Methods for Construction Materials,” Annual Book of ASTM Standards, Vol 04.01., ASTM International, West Conshohocken, PA, 2003, 9 pp.
14. ASTM C 989, “Standard Specification for Ground Granulated Blast-Furnace Slag for Use in Concrete and Mortars,” Annual Book of ASTM Standards, V. 04.01., ASTM International, West Conshohocken, PA., 2005, 5 pp.
15. ASTM C 1074, “Standard Practice for Estimating Concrete Strength by the Maturity Method,” ASTM International, West Conshohocken, PA, 1998, 8 pp.
16. ASTM C 1240, “Standard Specification for Silica Fume Used in Cementitious Mixtures” Annual Book of ASTM Standards, V. 04.01., ASTM International, West Conshohocken, PA., 2005, 7 pp.

17. Barnett, S.J., M.N. Soustos, S.G. Millard, and J.H. Bungey, "Strength Development of Mortars Containing Ground Granulated Blast Furnace Slag: Effect of Curing Temperature and Determination of Apparent Activation Energies" *Cement and Concrete Research*, V. 36, 2005, pp. 434-440.
18. Bhatti, J.I., "A Review of the Application of Thermal Analysis to Cement-Admixture Systems," *Thermochimica Acta*, V. 189, 1991, pp. 313-350.
19. Chandra, S., "Properties of Concrete with Mineral and Chemical Admixtures", *Structure and Performance of Cements*, 2nd ed., J. Bensted and P. Barnes, eds, 2002, pp 140-185.
20. Chanvillard, G., and L. D'Aloia, "Concrete Strength Estimation at Early Ages: Modification of the Method of Equivalent Age," *ACI Materials Journal*, V. 94, No. 6, Nov.-Dec. 1997, pp. 520-530.
21. Chini, A.R., L.C. Muszynski, L. Acquaye, and S. Tarkhan, Determination of the Maximum Placement and Curing Temperatures in Mass Concrete to Avoid Durability Problems and DEF, FDOT Contract BC 354-29. Comp. Lucy Acquaye, et al. Vers. Final Report. Feb. 2003.
22. Copeland, L.E., Kantro, D.L., Verbeck, G., "Part IV-3 Chemistry of Hydration of Portland Cement," 4th International Symposium of the Chemistry of Cement, Washington, D.C., 1960, pp. 429-465.
23. D'Aloia, L., and G. Chanvillard, "Determining the "Apparent" Activation Energy of Concrete; E_a – Numerical Simulations of the Heat of Hydration of Cement," *Cement and Concrete Research*, V. 32, 2002, pp. 1277-1289.

24. De Schutter, G., and Taerwe, L., "Degree of Hydration-Based Description of Mechanical Properties of Early-Age Concrete," *Materials and Structures*, Vol. 29, No. 7, 1996, pp. 335-344.
25. Devore, Jay L., *Probability and Statistics for Engineering and the Sciences*, 4th ed. Duxbury Press, New York, 743 p, 1995.
26. Diamond, S., "Alkali-Silica Reactions – Some Paradoxes," *Cement and Concrete Composites*, V.19, 1997, pp. 391-401.
27. Edmeades, R.M. and P.C. Hewlett, "Cement Admixtures," Lea's Chemistry of Cement and Concrete, 4th ed., ed. P.C. Hewlett, Arnold Publishers, New York, 1998, p 837-901.
28. Freiesleben Hansen, P., and E.J. Pedersen, "Maturity computer for controlling curing and hardening of concrete," *Nordisk Betong*, V. 1, No. 19, 1977, pp. 21-25.
29. Freiesleben Hansen, P. and Pederson, E. J., "Curing of Concrete Structures," Draft DEB-Guide to Durable Concrete Structures, Appendix 1, Comité Euro-International Du Béton, Switzerland, 1985.
30. Gartner, E.M., J.F. Young, D.A. Damidot, and I. Jawed, "Hydration of Portland Cement", *Structure and Performance of Cements*, 2nd ed., J. Bensted and P. Barnes, eds, 2002, pp 57-113.
31. Ge, Zhi, "Predicting Temperature and Strength Development of the Field Concrete", PhD Dissertation, Iowa State University, 2006.
32. Glasstone, S., K.J. Laidler, and H. Eyring, *The Theory of Rate Processes: The Kinetics of Chemical Reactions, Viscosity, Diffusion, and Electrochemical Phenomena*. McGraw-Hill Book Company, Inc. New York, 1941, 611 pp.

33. Haider, A. ,”The Benefits of Installing an Online Free Lime Analyzer to Control the Clinkering Process,” PCA Fall Technical Session, Oak Brook, IL, September 1999.
34. Hewlett, P. C., *Lea’s Chemistry of Cement and Concrete*, 4th ed. Arnold Publishers, New York, 1998.
35. Hsu, J.C. *Multiple Comparisons, Theory and Methods*, 1st ed. Chapman & Hall/CRC, Boca Raton, FL, 1996.
36. Jackson, P.J., “Portland Cement: Classification and Manufacture” Lea’s Chemistry of Cement and Concrete, 4th ed., ed. P.C. Hewlett, Arnold Publishers, New York, 1998, p 25-94.
37. Juenger, M.C.G. and H.M. Jennings, “New Insights into the Effects of Sugar on the Hydration and Microstructure of Cement Pastes,” *Cement and Concrete Research*, V. 32, 2002, pp 393-399.
38. Juenger, M.C.G., P.J.M. Monteiro, E.M. Gartner, and G.P. Denbeaux, “A Soft X-Ray Microscope Investigation Into the Effects of Calcium Chloride on Tricalcium Silicate Hydration,” *Cement and Concrete Research*, V. 35, 2005, pp 19-25.
39. Kada-Benameur, H., E. Wirquin, and B. Duthoit, "Determination of Apparent Activation Energy of Concrete by Isothermal Calorimetry," *Cement and Concrete Research*, V. 30, 2000, pp. 301-305.
40. Kjellsen, K.O., and R.J. Detwiler, “Later-Age Strength Prediction by a Modified Maturity Model,” *ACI Materials Journal*, V. 90, No. 3, May-June, 1993, pp. 220-227.

41. Lang, E. "Blast Furnace Cements", Structure and Performance of Cements, 2nd ed. eds. J. Bensted and P. Barnes, Spon Press, New York, 2002, p 310-325.
42. Lawrence, C.D., "The Constitution and Specification of Portland Cements" Lea's Chemistry of Cement and Concrete, 4th ed., ed. P.C. Hewlett, Arnold Publishers, New York, 1998, p 131-193.
43. Lerch, W., and R.H. Bogue, "The Heat of Hydration of Portland Cement" Portland Cement Association Fellowship, National Bureau of Standards, Paper no. 26, May, 1934 30 pp.
44. Lerch, W., "The Influence of Gypsum on the Hydration and Properties of Portland Cement Paste," Proceedings of the American Society for Testing Materials, V. 46, 1946.
45. Lerch, W. and Ford, C. L., "Long-Term Study of Cement Performance in Concrete: Chapter 3 – Chemical and Physical Tests of the Cements," *ACI Journal*, Proceedings V. 44, No. 8, 1948, pp. 745-795.
46. Ma, W., D. Sample, R. Martin, and P.W. Brown, "Calorimetric Study of Cement Blends Containing Fly Ash, Silica Fume, and Slag at Elevated Temperatures." *Cement, Concrete, and Aggregates*, V. 16, 1994, pp. 93-99.
47. Maekawa, K., R. Chaube, and T. Kishi, Modelling of Concrete Performance: Hydration, Microstructure Formation, and Mass Transport, E&FN Spon, London, 1999.
48. Massazza, F., "Pozzolana and Pozzolanic Cements" Lea's Chemistry of Cement and Concrete, 4th ed., ed. P.C. Hewlett, Arnold Publishers, New York, 1998, p 471-631.

49. Mills, R.H. "Factors Influencing Cessation of hydration in Water Cured Cement Pastes." Special Report 90: Symposium on Structure of Portland Cement Paste and Concrete. Washington, D.C.: Highway Research Board, 1966. 406-424.
50. Moranville – Regourd, M., "Cements Made From Blastfurnace Slag," Lea's Chemistry of Cement and Concrete, 4th ed., ed. P.C. Hewlett, Arnold Publishers, New York, 1998, p 633-674.
51. Morabito, P., "Methods to Determine the Heat of Hydration of Concrete", Prevention of Thermal Cracking in Concrete at Early Ages, RILEM Report 15, E & FN Spon, London 1998.
52. NT Build 480, "Cement: Heat of Hydration," NORDTEST, Espoo, Finland, 1997, 6 pp.
53. Nave, C.R., "HyperPhysics", Department of Physics and Astronomy, Georgia State University, Atlanta, GA, 2005, <<http://hyperphysics.phy-astr.gsu.edu>> (1 June 2006).
54. Odler, I., and R. Wonnemann, "Effect of Alkalis on Portland Cement Hydration: I. Alkali Oxides Incorporated into the Crystalline Lattice of Clinker Minerals," *Cement and Concrete Research*, V. 13, No. 4, 1983, pp 477-482.
55. Ogawa, K, H. Uchikawa, K. Takemoto, and I. Yasui, "The Mechanism of the Hydration in the System C₃S Pozzolanas" *Cement and Concrete Research*, V. 10, No. 5, 1980, pp 683-696.
56. Pane, I., and W. Hansen, "Concrete Hydration and Mechanical Properties under Nonisothermal Conditions," *ACI Materials Journal*, V. 99, No. 6, Nov.-Dec, 2002, pp. 534-542.

57. Poole, J.L., “Methods of Activation Energy Calculation for Portland Cement,” Master’s Thesis, The University of Texas at Austin, 2004, 75 pp.
58. Poole, J.L., K.A. Riding, K.J. Folliard, M.G.C. Juenger, and A.K. Schindler “Methods of Activation Energy Calculation for Portland Cement,” *ACI Materials Journal*, V. 104, No. 1, Jan.-Feb., 2007, pp. 303-311.
59. Poole, J.L., “The Effects of Cement Chemistry and Water-Cement Ratio on Activation Energy,” PhD Dissertation, Chapter 2, The University of Texas at Austin, Austin, TX, 2007, pp 6-38.
60. Poole, J.L., “The Effects of Chemical Admixtures on Activation Energy of Cementitious Materials,” PhD Dissertation, Chapter 3, The University of Texas at Austin, Austin, TX, 2007, pp 39-69.
61. Poole, J.L., “The Effects of Supplementary Cementing Materials on Activation Energy,” PhD Dissertation, Chapter 4, The University of Texas at Austin, Austin, TX, 2007, pp 70-110.
62. Poole, J.L., “A Model for Estimating the Activation Energy of Cementitious Systems,” PhD Dissertation, Chapter 5, The University of Texas at Austin, Austin, TX, 2007, pp 111-142.
63. Poole, J.L., “Hydration Study of Cementitious Materials Using Semi-Adiabatic Calorimetry,” PhD Dissertation, Chapter 6, The University of Texas at Austin, Austin, TX, 2007, pp 143-173.
64. Poole, J.L., “Study of the Effects of Chemical Admixtures on Hydration,” PhD Dissertation, Chapter 7, The University of Texas at Austin, Austin, TX, 2007, pp 174-217.

65. Poole, J.L., "Hydration Study of Supplementary Cementing Materials Using Semi-Adiabatic Calorimetry," PhD Dissertation, Chapter 8, The University of Texas at Austin, Austin, TX, 2007, pp 219-263.
66. Poole, T.S., "Changes in ASTM Type II Portland Cement from 1940 to 1994", *Cement and Concrete Aggregates*, CCAGDP, Vol. 20, No. 1, June 1998, pp. 157-162.
67. Powers, T.C., and T.L. Brownyard. "Studies of the Physical Properties of Hardened Portland Cement Paste", *Journal of the American Concrete Institute*, Volume 18, no. 2-8, October 1946-April 1947.
68. RILEM 119-TCE, "Adiabatic and Semi-Adiabatic Calorimetry to Determine the Temperature Increase in Concrete due to Hydration Heat of Cement," RILEM Report 15, R. Springenschmid, ed., E&FN Spon, London, 1999, pp. 315-330.
69. Roberts, L.R. and P.C. Taylor, "Understanding Cement-SCM-Admixture Interaction Issues" *Concrete International*, V. 29, No. 1, 2007 pp 33-41.
70. Samet, B. and S.L. Sarkar, "The Influence of Calcium Sulfate Form on the Initial Hydration of Clinkers Containing Different Alkali Combinations", *Cement and Concrete Research*, V. 27, No. 3, 1997, pp. 369-380.
71. Sandberg, P. and Roberts, L., "Cement-Admixture Interactions Related to Aluminate Control", *Journal of ASTM International*, V. 2, No. 6, June 2005, pp.6-13.
72. Schindler, A.K., "Concrete Hydration, Temperature Development, and Setting at Early-Ages," Ph.D. Dissertation, University of Texas at Austin, Austin, TX, 531 pp.

73. Schindler, A.K., "Effect of Temperature on Hydration of Cementitious Materials", *ACI Materials Journal*, V. 101, No. 1, Jan.-Feb., 2004, pp. 72-81.
74. Schindler, A.K., "Prediction of Concrete Setting", RILEM International Symposium on "Advances in Concrete Through Science and Engineering", Evanston, Illinois, March 22-24, 2004.
75. Schindler, A.K., and K.J. Folliard, "Heat of Hydration Models for Cementitious Materials", *ACI Materials Journal*, V. 102, No. 1, Jan.-Feb., 2005, pp. 24-33.
76. Scrivener, K.L., T. Füllmann, E. Gallucci, G. Walenta, and E. Bermejo, "Quantitative Study of Portland Cement Hydration by X-Ray Diffraction/Rietveld Analysis and Independent Methods", *Cement and Concrete Research*, V. 34, 2004, pp 1541-1547.
77. Springenschmid, R. and Breitenbücher, R., "Influence of Constituents, Mix Proportions, and Temperature on Cracking Sensitivity of Concrete", *Prevention of Thermal Cracking in Concrete at Early Ages*, RILEM Report 15, E & FN Spon, London 1998.
78. Tank, R.C., and N.J. Carino, "Rate Constant Functions for Strength Development of Concrete" *ACI Materials Journal*, V. 88, No. 1, Jan.-Feb., 1991, pp. 74-83.
79. Taylor, H.F.W., Cement Chemistry, 1st ed. Academic Press Limited, London, 1990, 475 pp.
80. Thomas, N.L. and J.D. Birchall, "The Retardation Action of Sugars on Cement Hydration," *Cement and Concrete Research*, V. 13, No. 6, 1983, pp. 830-842.

81. Uchikawa, H., S. Hanehara, and D. Sawaki, "The Role of Steric Repulsive Force in the Dispersion of Cement Particles in Fresh Paste Prepared with Organic Admixture" *Cement and Concrete Research*, V. 27, No. 1, 1997, pp. 37-50.
82. Van Breugel, K., "Prediction of Temperature Development in Hardening Concrete", *Prevention of Thermal Cracking in Concrete at Early Ages*, RILEM Report 15, E & FN Spon, London 1998.
83. Verbeck, G., and Forster, C.W. "Long-Time Study of Cement Performance in Concrete. Chapter 6 – The Heats of Hydration of the Cement," Proceedings of the American Society for Testing Materials, Vol. 50, 1950, pp. 1235-1262.
84. Wadsö, L., "An Experimental Comparison Between Isothermal Calorimetry, Semi-Adiabatic Calorimetry and Solution Calorimetry for the Study of Cement Hydration." Nordtest Report TR 522, Nordtest, Espoo, Finland, 2003.
85. Young, J.F. "A Review of the Mechanisms of Set Retardation in Portland Cement Pastes Containing Organic Admixtures", *Cement and Concrete Research*, V. 2, No. 4, 1972, pp. 415-433.

VITA

Jonathan Larkin Poole was born in Greenville, South Carolina on April 19, 1977, the son of Marian Dotson Poole and Dr. Toy Spotswood Poole. He graduated from Vicksburg High School in Vicksburg, Mississippi in 1995. He then enrolled in the University of Texas at Austin, where he received the degree of Bachelor of Science in Civil Engineering. From 2000 to 2002, he was employed as a field engineer and estimator for Gilbert Texas Construction, L.P. (a subsidiary of Peter Kiewit Sons', Inc.). In September, 2002, he entered The Graduate School at University of Texas, where he worked as a graduate research assistant to Dr. Kevin Folliard and Dr. Maria Juenger at the Construction Materials Research Group until May, 2007. He received an M.S. from The University of Texas in August, 2004.

Permanent address: 4157 Hawthorne Ave Dallas, TX 75219

This dissertation was typed by the author.